http://waikato.researchgateway.ac.nz/

Research Commons at the University of Waikato

Copyright Statement:

The digital copy of this thesis is protected by the Copyright Act 1994 (New Zealand).

The thesis may be consulted by you, provided you comply with the provisions of the Act and the following conditions of use:

- Any use you make of these documents or images must be for research or private study purposes only, and you may not make them available to any other person.
- Authors control the copyright of their thesis. You will recognise the author's right to be identified as the author of the thesis, and due acknowledgement will be made to the author where appropriate.
- You will obtain the author's permission before publishing any material from the thesis.

Catastrophic Tsunamis in the Indonesian Archipelago

A thesis submitted in fulfillment of the requirements

for the Degree of

Doctor of Philosophy

In Earth and Ocean Sciences

by

Gegar Sapta Prasetya

2010

Abstract

Tsunamis are not rare events for the Indonesian Archipelago as a consequence of four major plate boundaries that meet and collide, and producing highly active seismic zone that is mostly located under the sea. The 'tsunami season' within this region started in 1992 at Hading Bay, Flores Island, with casualties of more than 2000 people, followed almost every two years with the 1994 East Java Tsunami, 1996 Tonggolobibi Sulawesi Tsunami, 1996 Biak Tsunamis, 1998 Papua New Guinea Tsunami, and the Banggai Tsunami in 2000. These represent the tsunami season for the eastern part of the Archipelago, since the western part of Archipelago was mostly quiet until the 26 December 2004 Great Sumatra Earthquake and Tsunami, which occurred at a place that never been thought before on the western-most part of the Archipelago. This earthquake and accompanying tsunamis not only a starting point of tsunami season for the western part of the Indonesian Archipelago, but also as a defining moment for the people who lived in the region in looking at the constellation of the archipelago, that changed the development paradigm into natural hazards based development program.

The 26 December 2004 event (Mw > 9.0) is a turning point for the tsunamigenic earthquake studies along the subduction zone. Intensive research of this event provides a new insight into tsunami dynamics and characteristics as reflected by the erosional and deposition patterns of the coastal areas, wave run-up height, flow depth and inundation, wave front and bore formation, wave-structure interactions, coastal protection and management of the low-lying areas, and the importance of consistent education and local knowledge about natural hazards (earthquake and tsunamis). The following event on 28 March 2005 (Mw = 8.5), occurred only 250 km distant from the 26 December 2004 event, and continued further south to Java Island on 17 July 2006 (Mw = 7.6) and 12 September 2007 (Mw = 8.4) on southwest Sumatra Island (Bengkulu) along the Java Trench. Field surveys results, and analysis of the source mechanism and distribution of the resulting tsunami waves along the coast, shows that each near-field tsunami generated within the subduction zone is unique and complex. Scientists have urged the public and policy makers to consider all subduction-type tectonic boundaries to be "locked, loaded and dangerous" zones that possess potential tsunami threats. Reliable and comprehensive databases for past and recent events and subsequent scientific analysis are needed in mitigating the tsunami hazards.

Fourteen (14) segments of potential catastrophic tsunamigenic earthquake and 21 volcanogenic tsunami sources were identified based on seismotectonic assessment, historical record, paleotsunami deposits and micro-atoll studies, as well as volcanic type and activities. Most of the volcanogenic tsunamis sources are located in the eastern archipelago around the Banda Arc and the Molluca Sea. Tsunamis from volcanic sources had different characteristic to tsunamis generated by an earthquake mechanism, both in the near field and also far field as revealed by numerical modelling assessment. A numerical modeling of tsunami based on scenarios developed, shows the region is very susceptible to tsunamis with elevation at the shoreline greater than 8 m. With this elevation, there is no structural mitigation that is economically feasible to protect long a coastline based on the assessment of the 26 December 2004 event. The non-structural mitigation measures such as mangroves and coastal forest or in combination with other soft options such as sand dunes, provides protection to some extent. However, further research needs to be carried out in defining appropriate mitigation measures. These high hazard zones require 'sacrifice zone' of at least 1 km from the shoreline, and vertical evacuation is needed to save lives.

Detailed assessment of tsunami inundation based on the 26 December 2004 event revealed that the distributions of the flow depths are not always inline with distribution of the flow speed. The areas that experienced the deepest flooding does not necessarily experience the fastest flows, while the damage within urban and rural areas mostly coincided with the flow speed distribution rather than runup and inundation depth distribution. Consequently, in assessing the tsunami hazards, especially when making inundation maps, the overland flow speed should be taken into account or incorporated into the inundation map. However, the problem is that not all coastal areas have nearshore bathymetry and topography data at a resolution needed to represent the nearshore and overland flow dynamics.

Results from assessment of the tsunami field survey and damage data from recent events provide the necessity information to derive the hazards level that correlate the tsunami elevation at a shoreline with destruction scale inland. This provides enough information to permit the construction of hazard maps for the region where detailed nearshore bathymetry and topography data are not available. The tsunami elevation at the shoreline can be derived from numerical models.

As demonstrated during the 26 December 2004 event, the impacts of tsunamis on the coastal areas include not only the destruction of the infrastructure, buildings, housing, coastal landforms as well as a massive casualties, but also the resulting waste and debris that mixes with other flotsam during wave runup and backwash. This may create another huge problem that leads to serious long term adverse environmental consequences. Debris dispersal modelling is applied to the Banda Aceh region based on that event, and shows that understanding the pathway and distribution of the suspended materials and flotsam caused by tsunamis is important for proper hazard mitigation planning and waste management action.

In assessing the potential future events, there is uncertainty and some disagreement from results of the tsunamigenic earthquake recurrence interval based on the empirical formula used. These need to be refined with more data such as from continuous Global Position System measurements. Likewise for volcanogenic tsunamis sources, which are better defined by their location but difficult to determine which processes are dominant to generate catastrophic tsunamis for the next events. The rule of thumb of the sea receding as a sign for impending tsunamis from the subduction zone earthquake source is not applicable for most of the volcanogenic tsunamis. For a tsunami generated by volcanic eruption, the warning is the eruption itself, which could be several days before a tsunami event. More research is required to better understand the characteristic of volcanogenic tsunamis.

In general, the arrival time of tsunamis along the subduction zone within the Indonesian Archipelago is within 10 – 30 minutes. The best lesson learned is from the people in Simeulue, who recognized a simple messaged, if a significant ground shaking was felt, and the sea recedes; then evacuate to higher ground. This type of community warning and self-evacuation are a challenge for modern life style in the city. Integration of life-long efforts to educate the population about the hazards and preparedness for an extreme event is needed. The most favorable way is to include earthquake and tsunami hazards, and preparedness as part of educational curricula taught at schools.

Acknowledgements

It was my Father who passed away just one day before I departed to pursue my study in New Zealand that introduced me for the first time about a tsunami that struck our home Island when I was a kid, on 19 August 1977 in the afternoon. The feelings that brought me to my career and a series of a field surveys on a tsunami since then (Flores 1992, East Java 1994, Tonggolobibi 1996, Biak 1996, 26 December 2004, 28 March 2005 and 17 July 2006 South Java) to understand the nature of this hazard and make a safer place for people who lived along the coast as he always reminds me. I would like to thank him, and also to my mother that always pray for me to be a good son and a good father and husband to my wife (Poedjihastoeti) and daughters (Amanda, Ardina and Tiara), and be useful to the community and society.

My thesis supervisors, Prof Terry Healy, Dr. Willem de Lange and Dr. Kerry Black for their guidance's, assistance, passion, motivation, critics and comments, and all supported by any means available to them that I owe to and hope that I could return their effort one day. Dr. Dave Campbell, chair of the Department of Earth and Ocean Sciences, Prof. Cam Nelson and Dr. Vicky Moon, Dr. Karyn Bryan, Mrs. Sydney Wright, Ms Felicia Goudie, the Postgraduate studies office and International Office for all advice and assistance during my study period.

Thanks to my colleague and friend, Dr. Jose Borrero, for his time and discussion and friendship since back in 1998, and to all the International Tsunami Survey Team (ITST) Community. All crew of the ASR office in Raglan: Joseph, Shaw, Moira, Hetty, Shawn, Cyprien, Andrew, Dougal, and James for all modelling work, jokes and laughs. Dirk, Kyle, Peter, Brad, Zoe, Bryna, Debra, Glen, Dave, Natalie, Clarrise, Ali, Branigan, N Cowie, Alex and all fellow students at the Coastal Marine Group at Ruakura Campus are thanked to be such good friends. The security that always visits Ruakura during my night shift and the Ruakura Campus staff are thanked for their friendly support.

Education New Zealand through the New Zealand International Doctoral Research Scholarships supported this study, and thanks to Ms. Camilla Swan a scholarship manager of Education New Zealand for her support and assistance. Environment Waikato provided support for specific research on this study through research contract arranged by Prof. Terry Healy of Coastal Marine Group Department of Earth and Ocean Sciences University of Waikato - UNIlink, and thanks to Dr. Peter Singleton and Dr. Vernon Pickett for their valuable support and discussions, and all staff of the Resource Information Group of Environment Waikato.

Thanks to my family that accompanied me during this study, and showed their love and patient with all conditions that we faced. I strongly believe that those experiences make us stronger and wiser, and acknowledge that there is no such peaceful place but home. Life is a wonderful thing when individuals appreciate each other's, what ever they are. Peace on earth.

Preface

This thesis comprises of six (6) chapters, and is structured to achieve the major objectives of the research, focuses upon the characteristic of major (catastrophic) tsunami events in the Indonesian Archipelago, and the assessment of the potential future tsunami hazard with the underlying aim to provide information to be used for hazard mitigation. Publications at peer-reviewed scientific journal and conference proceedings (published, submitted - in review), conference and workshop presentations and technical reports that form and relate to each chapter at the time of submission include:

Chapter 1 and 2:
Presentation title: *The two earthquakes and tsunamis that change the perspective of Indonesian People,* Oral Presentation at 100th Anniversay earthquake Conference, Commemorating the 1906 San Fransisco earthquake; Managing Risk in Earthquake Country, April 18 -21, 2006, Moscone Center, San Fransisco. USA.

Presentation title: *The tsunami experience in Indian Ocean in the recent decades: Tsunami is not a rare event*, Oral presentation at the 1st International Workshop on Tsunami Modelling. European Commision Joint Research Center, Institute for the Protection and Security of the Citizen, JRC Ispra, 5-6 October 2006. ITALY.

Chapter 3:
Prasetya, G., Black, K.P., De Lange, W., Borrero, J., Healy, T.R. in review (2009). *Debris Dispersal Modelling for the Great Sumatra Tsunamis on Banda Aceh and Surrounding Waters.* Journal of Natural Hazard (NHAZ 899).

Prasetya, G., Borrero, J., De Lange, W., Black, K.P., Healy, T.R. in review (2008). *Modelling of Inundation Dynamic on Banda Aceh, Indonesia during the Great Sumatra Tsunamis 26 December 2004.* Journal of Natural Hazard (NHAZ 613)

Prasetya, G., Healy, T.R., De Lange, W. (2008). *Hydrodynamic Modelling of Tsunami Overwash of Whitianga Township and Harbour*. Technical Report prepared for Environment Waikato. 92 p.

Borrero, J.C., Bosserelle, C., Prasetya, G., and Black, K.P (2007), Using 3DD to model tsunami inundation , *Proceedings of the Australasian Coast and Port Conference*. July 2007, Melbourne Australia. Paper 96, 6 p.

Chapter 4:
Prasetya, G.S., Healy, T.R., de Lange, W.P (2008). *Extreme tsunami runup and inundation flow at Banda Aceh, Indonesia: Are there any solution to this type of coastal disaster?* in Wallendorf, L., Jones, C., Eing, L., Jaffe, B (eds): Solution to Coastal Disaster 2008 Tsunamis, ASCE, pp.13-26.
Paper presented during the Solution to Coastal Disasters Conference 2008, April 13-16, 2008. Turtle Bay, Oahu. Hawaii.

Chapter 5:
Prasetya, G.S. (2008). Short movie on Sumatra Tsunami – a lesson learnt from Great Sumatra Tsunami on 26 December 2004 on Banda Aceh. Coastal Marine Group. Department of Earth and Ocean Science, The University of Waikato, 10 minutes duration. This short movie (CD-ROM attached in Appendix 4) is presented and being used during the Tsunami Simulation Drill in Banda Aceh, 1-2 November 2008, INDONESIA.

The research work is undertaken with the supervision of Prof. Terry Healy, Dr. Willem De Lange (Department of Earth and Ocean Sciences, University of Waikato, New Zealand), and Dr. Kerry Black (ASR Ltd Marine Consulting and Research, New Zealand).

Table of Contents

List of Figures

List of Table

List of Abbreviations

ADCIRC	Advanced Circulation Model for oceanic , coastal and estuarine waters
Bakosurtanal	Badan Koordinasi Survey dan Pemetaan Nasional
BMG	Badan Meteorologi dan Geofisika
BPPT	Badan Pengkajian dan Penerapan Teknologi
BRR	Badan Rekonstruksi dan Rehabilitasi
CNES	Centre National d'Etudes Spatiales
COMMIT	Community MOST Model Interface
CULWAVE	Cornell University Long and Intermediate Wave Modelling Package
COMCOT	Cornell Multi-grid Coupled Tsunami Model
DART	Deep-Ocean Assessment and Reporting of Tsunamis
GEBCO	General Bathymetric of The Ocean
GPS	Global Positioning System
ICG/IOTWS	Intergovernmental
IOC	Intergovernmental Oceanographic Commission
ITDB/PAC2004	Intergrated Tsunami Data Base for Pacific 2004
ITST	International Tsunami Survey Team
LIPI	Lembaga Ilmu Pengetahuan Indonesia
MOST	Method of Splitting Tsunamis
NOAA	National Oceanographic and Atmospheric Administration
NSW	Nonlinear Shallow Water
NZIDRS	New Zealand International Doctoral Research Scholarships
RANET	Radio Network
SERTIT	Service Regional de Traitement d'image et de Teledetection
SOP	Standard Operating Procedure
SRTM	Space Radar Topography Mission
TUNAMI	Tohoku University's Numerical Analysis Model for Investigation of tsunami
TIME	Tsunami Inundation and Modelling Exchange
USGS	United States Geological Survey
UNOSAT	is the United Nation Insitute for Training and Research (UNITAR) Operational Satellite Applications Program
UNESCO	United Nation
VPN-MPLS	Virtual Private Network – Multiprotocol Label Switching
VSAT	Very Small Aperture Terminal

List of Appendices

Chapter 1
Catastrophic Tsunamis in the Indonesian Archipelago

1.1. Introduction

Tsunamis, or seismic sea waves, are progressive sea waves with long wavelengths and periods generated by a disturbance of the sea surface associated with various geologic processes. Most of the processes are associated with submarine faulting, slides and slumps accompanying earthquakes; submarine and or island volcanism; sub-aerial or underwater landslides; atmospheric forcing; meteorite impact; or a combination of these generating mechanisms. Tsunami impacts are often forgotten and hence are underrated compared to other natural hazards, such as an earthquake or storm, due to their infrequent occurrence. The size and effect of a tsunami on a coastal area are a consequence of several factors: the amplitude and shape of the wave at the source, which is primarily controlled by the size and geometry of the source; the response of the coastal features, such as bays and harbours (which are capable of resonance, thereby amplifying selected wave frequencies) to the tsunami wave; and the nonlinear hydrodynamics of the breaking wave as well as fast moving flows as it inundates the coastal area.

The historical record indicates that more than 183 tsunamis occurred in the Indonesian Archipelago for the period 400 – 2007 AD as a consequence of the convergence of the Eurasian, Indo-Australian, Caroline and Philipines plates through the archipelago (Figure 1.1 and Figure 1.2). Prasetya et al. (2001) noted that 18 major tsunamis with clear evidence had been generated since 1900; 14 of them occurred in the eastern part of the Indonesian Archipelago. Since 2002, 4 tsunamis had been generated, three in the western Sunda Arc: the 26 December 2004 M_w = 9.3 Sumatra - Andaman earthquake and tsunamis, the 28 March 2005 M_w = 8.6 Nias earthquake and tsunamis, and Bengkulu earthquake and tsunami on 14 September 2007 M_w = 8.4 of the west coast of Sumatra Island. The remaining one was on the south coast of Central Java Island on17 July 2006 M_w = 7.6 - 7.7.

M_w is a moment magnitude scale that assigns a magnitude to the earthquake based on seismic moment (M_o) that measures the size of earthquake. M_o is computed based on the area of fault rupture, the average amount of slip and earth crust rigidity (shear modulus).

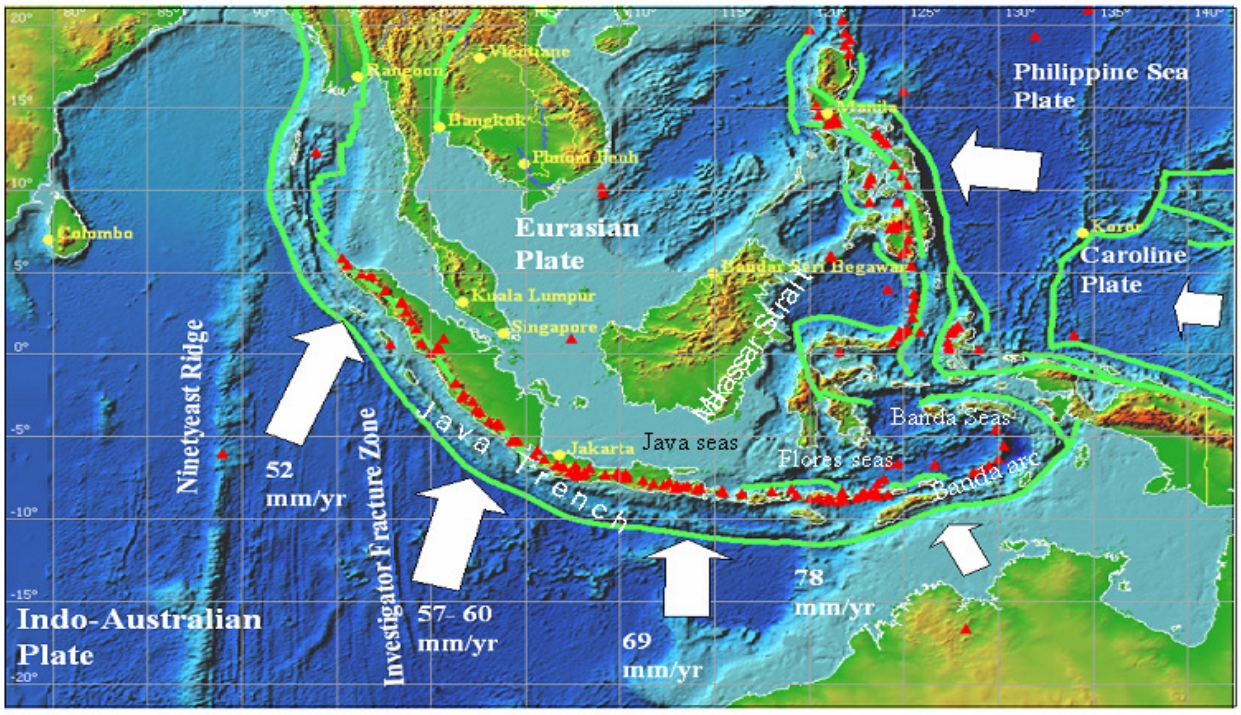

Figure 1.1. The tectonic setting of the Indonesian Archipelago showing the major subduction zones and faults (green line). White arrows show the direction and notes of plate motion. Red triangles are the active volcanoes. (Data source: Newcomb and McCann, 1987; Prasetya et al., 2001; Natawidjaya, 2003; ITDB/PAC 2004).

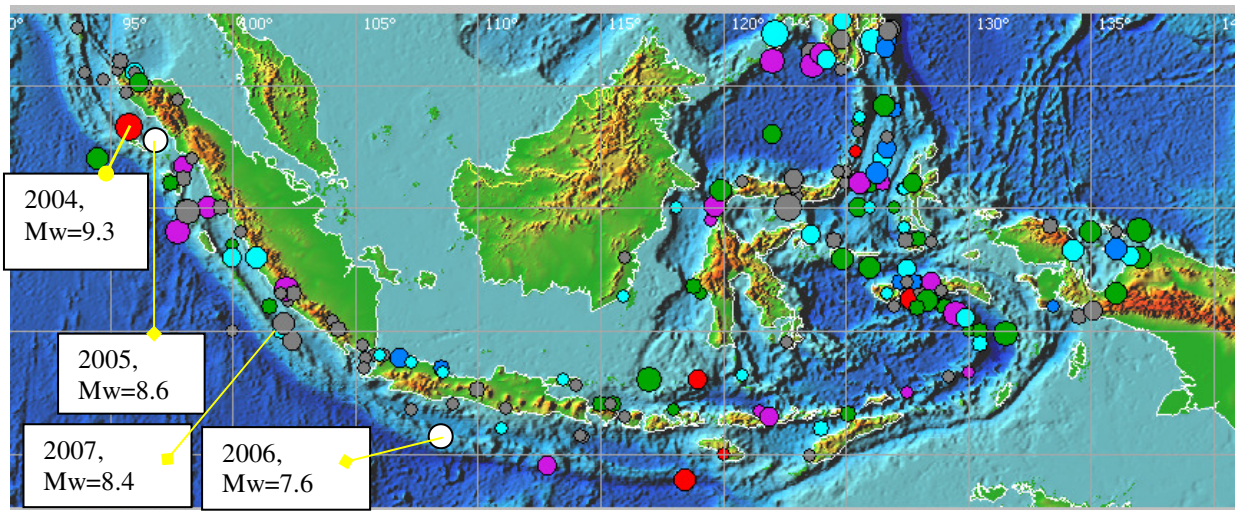

Figure 1.2. 183 tsunamis are listed in the Indonesian Archipelagos for the period 400 – 2007 AD as consequences of the convergence of the Eurasian, Indo-Australian, Caroline and Philipines plates along the subduction zone. The most recent 4 tsunamis were generated along the Java trench in the Indian Ocean:(Updated from ITDB/PAC 2004).

1.2. Catastrophic Tsunamis

The historical data obviously show that the tsunamis were not a rare event for the Indonesian Archipelago. Each tsunami had a different characteristic, size and impact on coastal areas. Eight tsunamis that occurred between 1992 (Flores earthquake and tsunami) and the Bengkulu event on 14 September 2007, have been well surveyed and documented by International Tsunami Survey Teams, confirming the uniqueness of each tsunami event (Tsuji et al., 1994; Imamura et al., 1995; Pelinovsky et al., 1997; Matsutomi et al., 2001; Yalciner et al., 2005; Jaffe et al., 2006; Borero et al., 2006). The December 26th, 2004 Sumatra-Andaman earthquake was the biggest event in the last 100 years in terms of size and extent, damage and fatalities, and involved the second largest tsunami after the 1883 Krakatau event. These two catastrophic events clearly show the region's high potential to generate a catastrophic tsunami, and tragically demonstrate the regional need for tsunami-hazard assessment, tsunami education, mitigation and planning and community preparedness. The global propagation of these two events can be seen in Figure 1.3 and Figure 1.4.

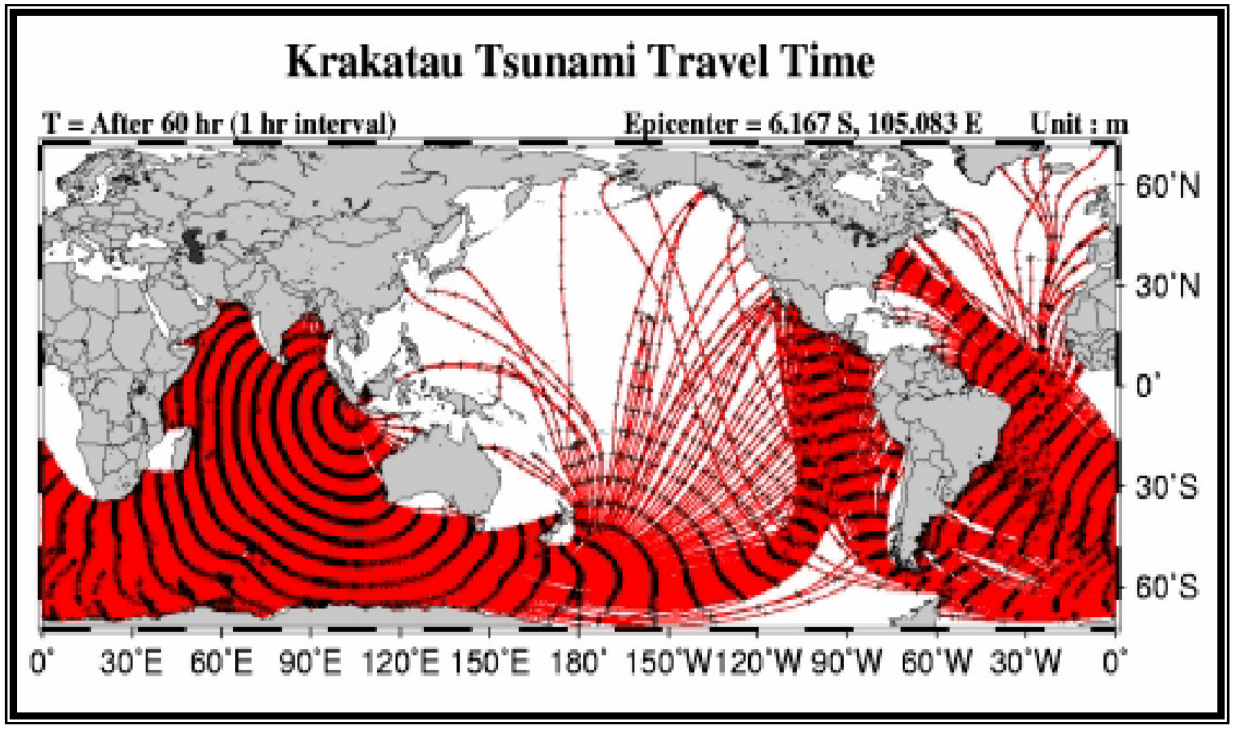

Figure 1.3. The tsunami from Krakatau volcanic eruptions affected the whole Indian Ocean, and continued to Pacific and Atlantic Oceans. (Source: Choi et al., 2003).

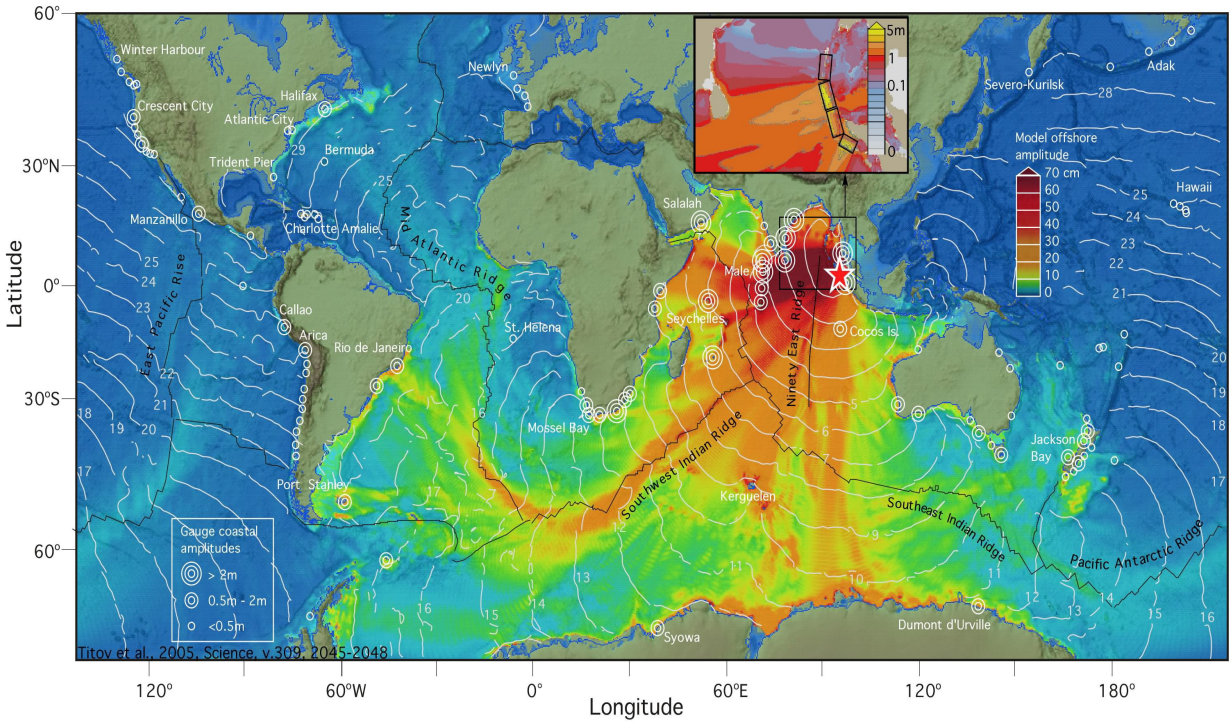

Figure 1.4. The propagation model of tsunami from the Sumatra-Andaman Earthquake on 26 December 200, (Mw=9.3) show the tsunamis affecting the Indian Ocean, and continuing into the Atlantic and Pacific Oceans. (Source: Vasily et al., 2005). Note the effect of mid-ocean ridges on tsunami propagation.

The 1883 eruption of Krakatau has been very well documented and most interpretations of the Krakatau event rest on the work of RDM Verbeek (Simkin and Fiske, 1983). Geology and geophysical, as well as modeling studies of this volcano are still continuing (Self and Rampino, 1981, 1982; Sigurdsson et al., 1991a, b; Deplus et al., 1995; Carey et al., 1996; Mandeville et al., 1996; Nomambhoy and Satake, 1997; Prasetya et al., 2000, Freundt, 2003; Spicak et al., 2002; Choi et al., 2003; Mader and Gittings, 2006). The new born 'Anak Krakatau' that first erupted in 1927, show that this volcanic complex is still active and there is a need for better understanding and assessment to mitigate any future event. Impact of the tsunamis during the 1883 Krakatau event within the Sunda Straits is illustrated in Figure.1.5. On the west coast of Java Island (Anjer) in Sunda Straits, tsunamis destroyed all villages and inundated the Labuhan area to the south as far as 3 km inland. 600 tonne blocks of coral were transported inland as far as 100 m from the coastline. Meanwhile on the southeast coast of Sumatra Island, the tsunamis reached the Teluk Betung City Council building (3 km from the coast) with a runup of about 15 m. More than 36,000 people who lived at the coastal area surround the Sunda Straits died and

tsunami flow depth and runup according to the eyewitnesses varied from 5 m to 40 m (Simkin and Fiske, 1983).

Figure.1.5. Damage due to catastrophic tsunamis produced by the 1883 Krakatau Eruption. More than 36,000 people died and tsunami runup and flow depth varied from 15 m to 35 m, with maximum 8 km inundation through the jungle. (Source: Simkin and Fiske, 1983).

The December 26th, 2004 event is the first great earthquake (M_w > 9) observed by the modern instruments of a global seismic network equipped with broadband frequencies, as well as geodetic observations using Satellite Global Positioning System (GPS), and the

first definitive measurements of deep ocean tsunamis by Satellite Altimetry during their propagation (Okal, 2005). More than 250,000 people died or were reported missing throughout the Indian Ocean countries. Of that total, 167,000 casualties or ~ 66.8% (BRR and Partners, 2006) were in Banda Aceh and other cities on the west coast of Sumatra Island. The tsunami inundated the Banda Aceh City up to 6 km inland with the flow depth and runup varying from 3 m to 25 m (Jaffe et al., 2006) as illustrated in Figure 1.6.

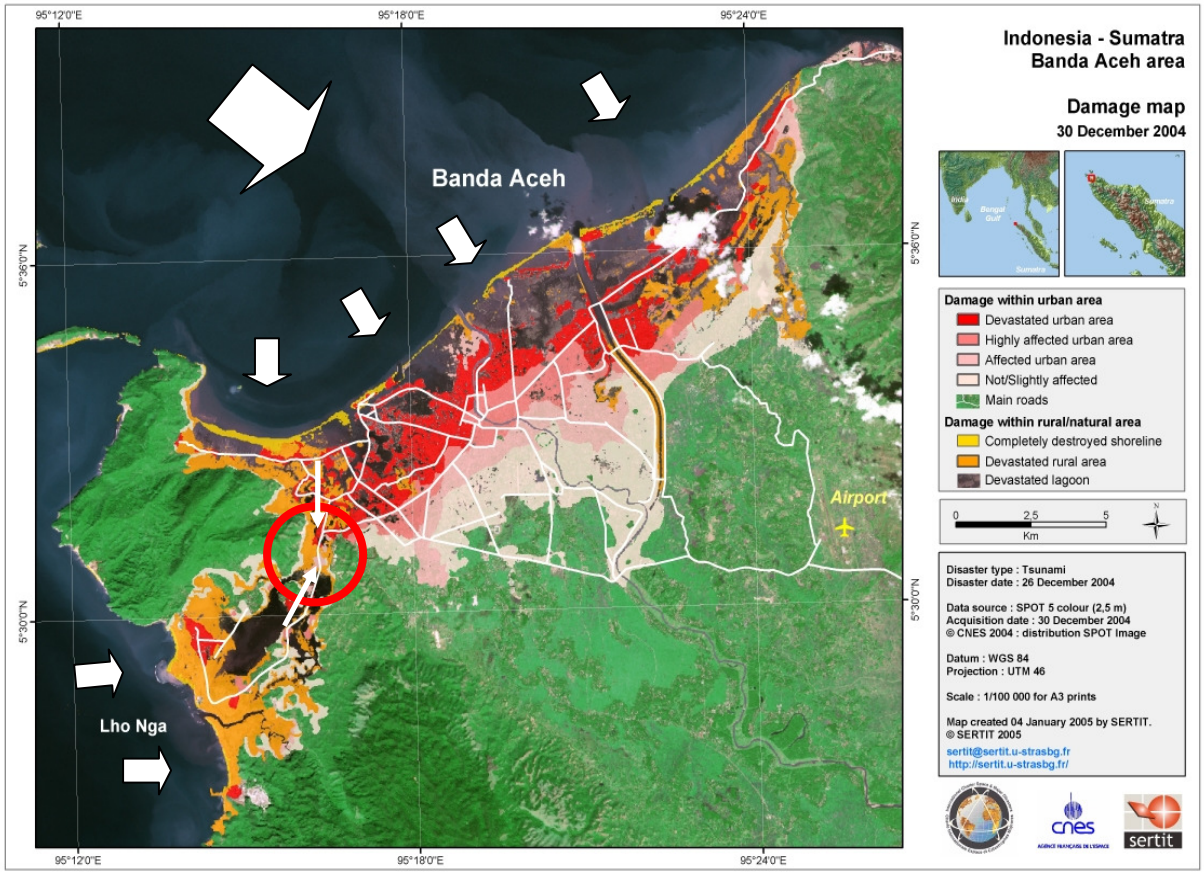

Figure 1.6. Damage map derived from satellite images showing the impact of tsunamis on the Banda Aceh region. The flow came from two directions; the waves from the southwest (Indian Ocean) penetrated to Banda Aceh from Lhok Nga and collided with the waves from Banda Aceh at Lampisang (red circle) about 6 km inland. (Map source: UNOSAT).

Results of the field surveys carried out on Sumatra and coastal areas of the Indian Ocean soon after the event (Figure 1.7), allowed a new insight into tsunami dynamics and characteristics as reflected by the erosional and deposition patterns of the coastal areas, wave runup height, flow depth and inundation, wave front and bore formation, wave-structure interactions, coastal protection and management of the low-lying areas, and the importance of consistent education and local knowledge about natural hazards (earthquake

and tsunamis). These led to scientific investigation of the processes, and development of protocols for coastal zone management.

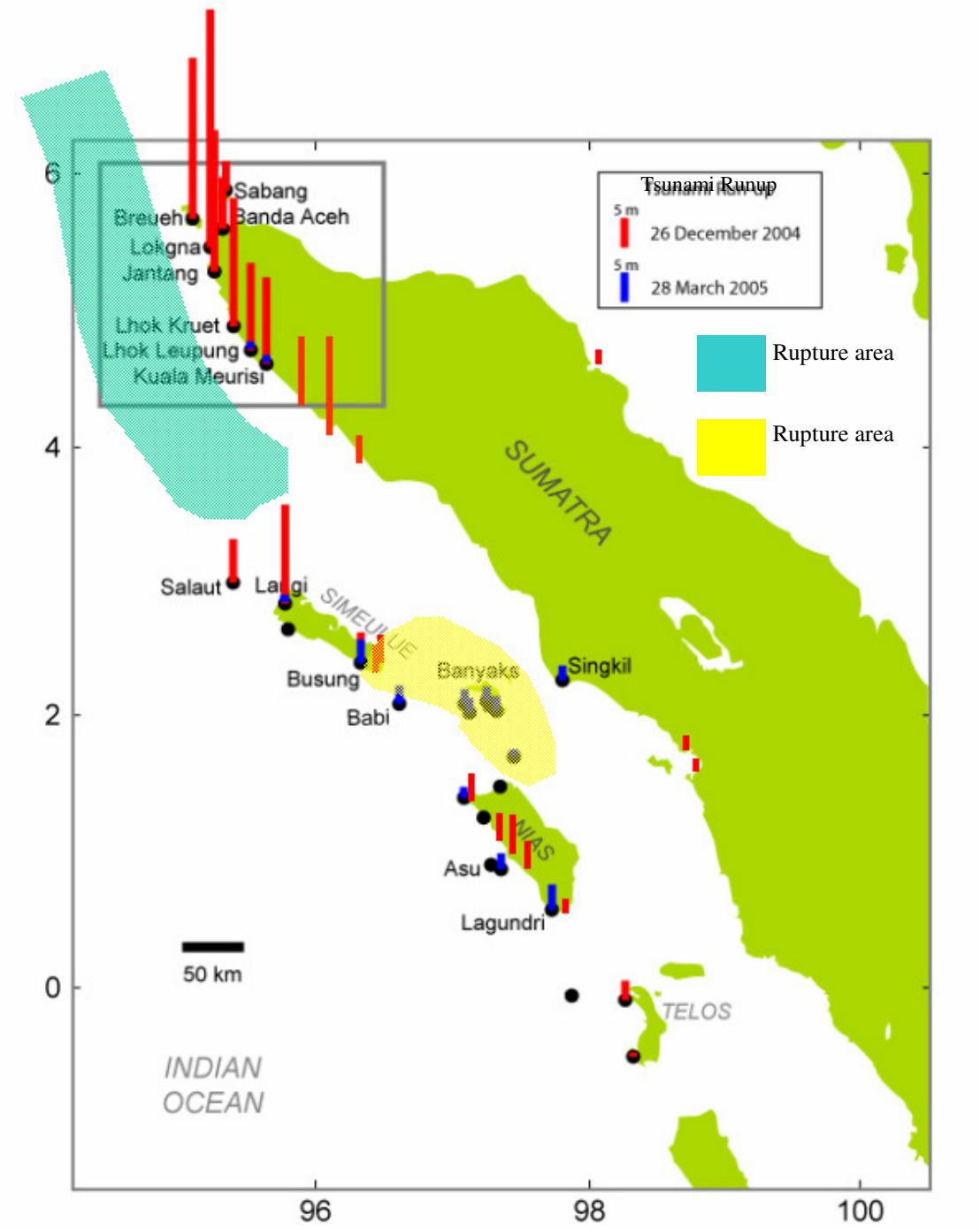

Figure 1.7. Results of tsunami runup survey carried out by the International Tsunami Survey Team along the west and north Coast of Sumatra and offshore Islands for 26 December 2004 (red bar) and 28 March 2005 (blue bar) events. The earthquake magnitude from the two events were almost similar (M_w >9 and 8.6) and located almost at the same depth, but produced dramatically different tsunamis (updated from Yalciner et al., 2005, and Jaffe et al., 2006).

From the historical record, southeastward of the Sumatra subduction zone where the 26 December 2004 Sumatra- Andaman took place, there were 4 great historical earthquakes which occurred in 1797, 1833, 1861, and 1907 that produced catastrophic tsunamis (Newcomb and McCann, 1987). Paleoseismic data suggest that a great earthquake recur about every 200 to 240 years along the adjacent section of the Sunda megathrust (Sieh, 2006), and the average interval between great tsunamigenic earthquakes, or couplets such as 1797 and 1833 ranges from 130 to 300 years and is nearly equal to the current dormant period. Rupture by the recent events in 2004 and 2005 have brought this section nearly to failure (Borero et al., 2006).

Further east along the Java trench (Sunda arc) south of Java – Bali and Nusa Tenggara Islands, there are no major tsunamis that could be categorized as a catastrophic event in the historical record. The same is true along the Banda arc, Makassar straits, Java and Flores seas region, except during the 1815 Tambora Volcano eruption that generated tsunamis in the Java and Flores seas and one event in Banda Sea in 1674. However, as the 26 December 2004 event occurred in the area that had not been active until the 1980s (Newcomb and McCann, 1987), most of the subduction zone should be considered as capable of generating catastrophic tsunamis, since most of the historical records are not long enough to cover the return period of such a large event.

1.3. Study Area

Most of the active seismic zone within the Indonesian Archipelago is located under the sea, and produces large shallow earthquakes that possess a high tsunamigenic potential within a range of 100- 300 km from the shore (Figure 1.8.a). The historical record indicates that more than 183 tsunamis have occurred in this region since AD 400. They can be divided into 5 source zones as illustrated in Figure 1.8.b: the Andaman Seas – Northern Sumatra subduction zone (zone I); the Central Sumatra subduction zone (Zone II); the South Sumatra-West Java subduction zone (zone III); the Central Java-Nusa Tenggara subduction zone (Zone IV); and the Banda-Flores Seas -Makassar Straits zone (Zone V).

Until 1980s, zones I and II, especially Sumatra, were characterized as relatively aseismic as inferred from the lack of great earthquakes in the instrumental record. Meanwhile Java and lesser Sunda (regions III and IV) had major (M_s>6) earthquakes in the historic record, but none are of the same magnitude as the great events from the subduction

M_s is a moment magnitude scale based on measuring the surface wave amplitude of surface waves with a period of 20 seconds.

zone near Sumatra to the northwest (Newcomb and McCann, 1987). However, since AD 2000, an earthquake with M_w = 7.8 occurred at the southern end of the Sumatra subduction zone at Enggano Island (boundary zone II and III), and continued at Simeulue Island (boundary zone I and II) in 2002 with Mw = 7.4. No tsunamis were generated since the epicenters of the earthquakes were located on land, and little disturbance of the sea surface occurred.

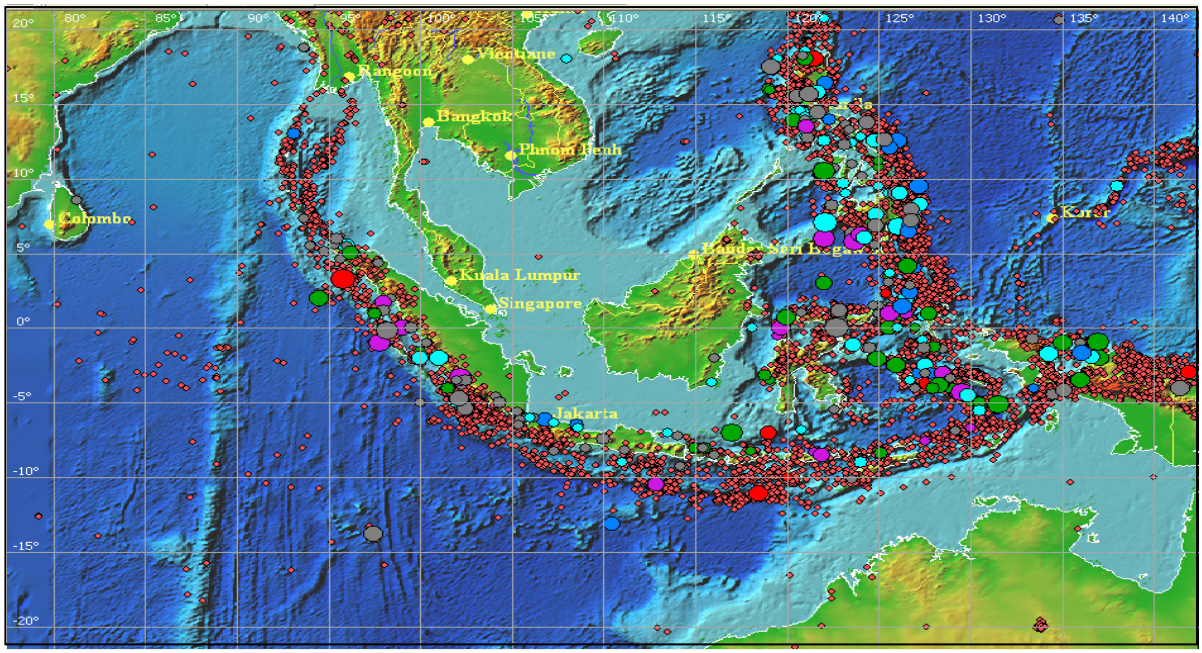

Figure 1.8.a. Distribution of shallow earthquakes within the Indonesian Archipelago (depth < 50 km) along the subduction zone (red small dot) overlain with the distribution of the tsunami events (larger dots with various colors) generated between 1700 and 2004 (Base map and Data source: ITDB/PAC 2004).

The Great Sumatra-Andaman Earthquakes and tsunami on 26 December 2004 (M_w = 9.3) was followed by the Nias Earthquake and tsunami on 28 March 2005 (M_w = 8.6) to the south. The earthquake sources apparently continued southeastward along the subduction zone, where an earthquake with M_w = 7.7 offshore from central Java generated tsunamis affecting the coastal area along the west and central Java island (zone III). This event was followed by a M_w = 8.4 earthquake on 14 September 2007 offshore from Bengkulu (zone II), which also generated tsunamis along the Bengkulu coast.

Field surveys and analysis of the source mechanism and distribution of the resulting tsunami waves along the coast, reveal that each near-field tsunami generated within the subduction zone is unique and complex, with the runup variability along the coast in relation to tsunami source parameter independent of seismic moment (Satake and Tanioka,

1999; Geist, 2002). Future event scenarios for possible catastrophic tsunamis will be assessed for each of the 5 zones based on historical events and seismic gap analysis.

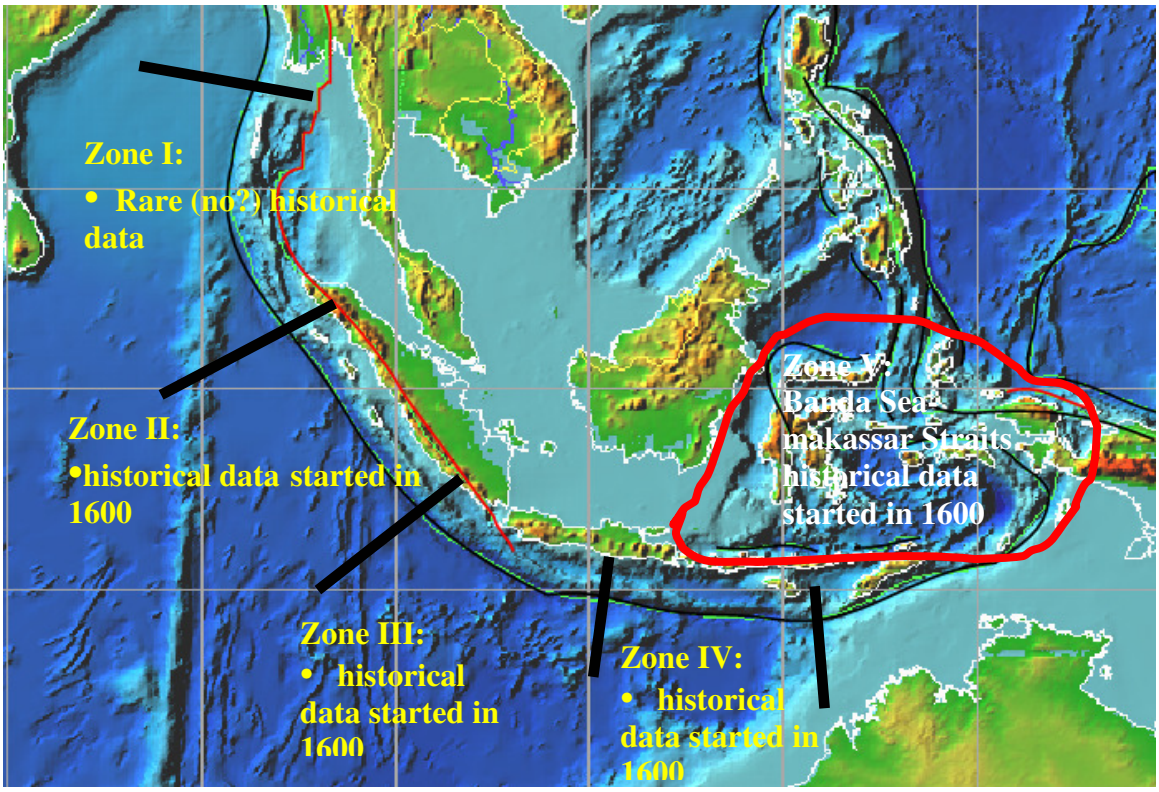

Figure 1.8.b. The tsunamigenic area of the Indonesian Archipelagos can be divided into 5 zones: I- Andaman Seas – Northern Sumatra subduction zone; II- Central Sumatra subduction zone; III- South Sumatra-West Java subduction zone; IV- Central Java-Nusa Tenggara subduction zone, and V- Banda-Flores Seas -Makassar Straits zone. Event scenarios with the sources along the subduction zone in the Indian Ocean will be assessed for each zones based on the historical and seismic gap analysis.

1.4. Aims and Objectives

This research focusses upon the characteristic of major (catastrophic) tsunami events in the Indonesian region, with the underlying aim and the assessment of the future tsunami hazard to provide information to be used for hazard mitigation.

The specific objectives of the research are:

1. to investigate the tsunagenic potential of earthquakes and volcanic sources within the Indonesian Archiplego based on the historical record, and assess the potential for future events;

2. to advance our understanding of tsunami processes that cause significant coastal damage and destruction, including runup and run down, and the geomorphic effects of tsunami erosion and deposition based on field data and numerical models; and
3. to develop and model tsunami scenarios for all potential Indonesian sources in order to quantify the associated hazards, in order to assess the risk.

These will be achieved through:

- Compilation of all the known historical tsunamis impacting upon Indonesia as well as assessment of potential sources not included by the historical record.
- Utilizing numerical modelling tools to assess the tsunami generation, propagation and inundation for historical, recent and potential catastrophic events from earthquakes and volcano sources. Benchmark the models with standards based on the 3rd International Long Wave Runup Workshop on June 17-18, 2004. Utilize data from the December 26th 2004 and March 28th 2005 events to verify the model (predicted) results against measurements and eyewitnesses accounts of tsunami runup height and inundation levels, and tsunami debris behaviour and deposition characteristics.
- Develop risk assessment and hazard maps for potential tsunami events based upon return intervals and assessment of sesmic gaps of the region

1.5. Structure of the Thesis

This research study is structured to achieve the major objectives of the research as follows:

Chapter 1 Outlines the background, the nature of catastrophic tsunamis within the Indonesian Archipelago, the region of interest for this research, and states the aim and objectives of the study.

Chapter 2 Defines the tsunamigenic region within the Indonesian Archipelago through assesment of the tectonic setting, identifies previous tsunamigenic earthquakes and volcanogenic tsunamis based on the historical record,

identifies potential sources that do not appears in the historical record, and identifies scenarios for possible future events.

Chapter 3 Discusses the 3DD mathematical model capabilities for tsunami generation, propagation, runup and inundation, debris dispersal model and benchmarking the model using the 3rd International Long Wave Runup Workshop of June 17-18, 2004 data set. Emphasis will be on utilizing the hydrodynamic and dispersal model for simulating the 26 December 2004 catastrophic events, and testing the model using high-resolution topography (LIDAR=light detecting and ranging) and accurate multi-beam soundings for nearshore bathymetry.

Chapter 4 Presents the results and discussion of numerical simulations based on scenarios defined in Chapter 2, and evaluates their significance for future re-development and coastal hazard management along the Indonesian coast.

Chapter 5 Develops hazards map based on numerical modelling results in chapter 4, and discuss an education outreach programs, and an appropriate tsunami warning systems

Chapter 6: Major research finding and some ideas for future research.

1.6. References:

Borero J, Sieh K, Chlleh M, and Synolakis C.: 2006, Tsunami inundation modeling for western Sumatra. *Proceedings of the National Academy of Sciences of the United States of America*,**103**, pp. 1-4.

Borrero, J.C., Synolakis, C.E. and Fritz, H.: 2006, Northern Sumatra field survey after the December 2004 Great Sumatra Earthquake and Indian Ocean Tsunami", *Earthquake Spectra, Special Issue III*, **22**, pp. 93-104.

Carey, S., Sigurdsson., Mandeville, C.,and Bronto, S.: 1996, Pyroclastic flows and surges over water: an example from the 1883 Krakatau eruption, *Bulletin Volcanology*, **57**, pp. 493-511.

Choi B.H., Pelinovsky E., Kim K.O, and Lee J.S.: 2003, Simulation of the trans-oceanic tsunami propagation due to the 1883 Krakatau volcanic eruption. *Natural Hazards and Earth System Science*, **3**, pp. 321-332.

Deplus, C., Bonvalot, S.,Dahrin, D., Diament, m., Harjono, H., and Dubois, J.: 1995, Inner structure of the Krakatau volcanic complex (Indonesia) from gravity and bathymetry data, *Journal of Volcanology and Geothermal Research*, **64**, pp. 23-52.

Freundt A.: 2003, Entrance of hot pyroclastic flows into the sea: experimental observations. *Bulletin of Volcanology*, **65**: pp. 144-164.

Geist, E.L.: 2002, Complex earthquake rupture and local tsunamis, *Journal of Geophysical Research*, **107**, ESE pp. 2 1-15.

Hamzah, L., Puspito, N., and Imamura, F.: 2000, Tsunami catalog and zones in Indonesia. *Journal of Natural Disaster Serv*ice, **22**, pp. 25-43.

Imamura, F., Gica, E., Takahashi, T., and Shuto, N.: 1995, Numerical simulation of the 1992 Flores tsunami: Interpretation of tsunami phenomena in northeastern Flores Island and damage at Babi Island. *Pure and Applied Geophysics*, **144**, pp. 555 - 568.

Jaffe B, Borero J., Prasetya G. S., Peters R., McAdoo B., Gelfenbaum G., morton R., Ruggeiro P., Higmann B., Dengler L., Hidayat R., Kingsley E., Widjokonko., Lukianto., moore A., Titov V., Yulianto E.: 2006, The December 2004 Indian Ocean Tsunami in Northwest Sumatera and Offshore Island. *Earthquake Spectra,* **22.No.S3**, I-XXXX. Earthquake Engineering Research Institute, USA.

Mader C, L., and Gittings m, L.: 2006, Numerical model for the Krakatau Hydrovolcanic Explosion and Tsunami, *Science of Tsunami Hazards*, **24 (3)**, pp. 174 - 182.

Mandeville, C.W., Carey, S., and Sigurdsson, H.: 1996, Sedimentology of the Krakatau 1883 submarine pyroclastic deposits, *Bulletin Volcanology*, **57**, pp. 512 - 529.

Matsutomi, H., Shuto, N., Imamura, F., and Takahashi, T.: 2001, Field survey of the 1996 Irian Jaya Earthquake tsunami in Biak Island., *Journal of Natural Hazards*, **24**, pp. 199 - 212.

Natawidjaja, D.H.: 2003, Neotectonic of the Sumatran Fault and Paleogeodesy of the Sumatran Subduction Zone, Ph.D. Thesis, California Institute of Technology, Pasadena.USA.289 p.

Newcomb, K. R, and McCann, W.R.: 1987, Seismic history and Seismotectonic of the Sunda Arc, *Journal Geophysical Research*, **92**, B1, pp. 421-439.

Nomambhoy, N. and Satake, K.: 1995, Generation mechanism of tsunamis from the 1883 Krakatau eruption, *Geophysical Research Letters*, **22(4)**, pp. 509 - 512.

Okal , E.: 2005, The Indian Ocean Tsunami Disaster: A lesson to Geophysicists, Paper presented at *Tsunami Deposit Workshops June 12- June 18 2005*. University of Washington Seattle Washington.USA

Pelinovsky E, Yuliadi D**,** Prasetya G.S, Hidayat R.: 1997, The 1996 Sulawesi tsunamis, *Journal of Natural Hazards*, **16**, pp. 29 – 38.

Prasetya G.S., De Lange, W.P., and Healy, T.R.: 2000, Volcanic tsunami generations mechanism based on Krakatau event 1883 and future mitigations in *Regional Report on Tsunami Research*, Shuto. F (ed), Japan, pp. 1-14.

Prasetya, G.S., De Lange, W.P., and Healy, T.R.: 2001, The Makassar Strait, tsunamigenic region, Indonesia. *Journal of Natural Hazard*, **24**, pp. 295 - 307.

Rynn, J.: 2002, A preliminary assessment of tsunami hazard and risk in the Indonesian region, *Science of Tsunami Hazards*, **20**, pp. 193 - 215.

Satake, K., and Tanioka, Y.: 1999, Source of tsunami and tsunamigenic earthquake in subduction zones, *Pure and Applied Geophysics*, **154**, pp. 467 - 463.

Sieh, K.: 2006, Sumatran Megathrust – from science to saving lives, *Philosophyical Transaction of Royal Society London A*, **364**, pp. 1947 - 1963.

Spicak A., Hanus V., and Vanek J.: 2002, Seismic activity around and under Krakatau volcano, Sunda Arc: constraints to the source region of island arc volcanism, *Studies on Geophysics and Geodesy*, **46**, pp. 545 - 565.

[a]Sigurdsson, H., Carey, S., Mandeville, C., and Bronto, S.: 1991, Pyroclastic flows of the 1883 Krakatau eruption., *EOS Transaction American Geophysical Union*, **72 (3)**, pp. 377 - 392.

[b]Sigurdsson, H., Carey, S., and Mandeville, C.: 1991, Krakatau., *National Geographic Research & Exploration*, **7(3)**, pp. 310 - 327

Simkin, T., and Fiske, R.: 1983, Krakatau, 1883 - the volcanic eruption and its effects, *Smithsonian Institutions Press*, Washington D.C, 464 p.

Self, S., and Rampino, M.R.: 1981, The 1883 eruption of Krakatau, *Nature* **294**, pp. 699 - 704.

Self, S., and Rampino, M.R.: 1982, Discussion: Comments on A Geophyisical interpretation of the 1883 Krkatau eruption by I. Yokoyama, *Journal of Volcanology and Geothermal Research* **13**, pp. 379 - 386.

Tsuji, Y., Imamura, F., Matsutomi, H., Synolakis, C.E., Nanang, T.P., Jumadi, Harada, S., Han, S.S., Arai, K., and Cook, B.: 1995, Field survey of the East Java earthquake and tsunami of June 3, 1994, *Pure and Applied Geophysics* **144**, pp. 839 - 854.

Vasily T., Rabinovich A.B., mofjeld H.O., Thomson R.E., and Gonzalez F.I.: 2005, The global reach of the 26 December 2004 Sumatra Tsunami, *SCIENCE* **309**, pp. 2045 - 2048.

Yalciner. A.C., Perincek. D., Ersoy. S., Prasetya. G., Hidayat. R., McAdoo. B.: 2005, Report on December 26, 2004, Indian Ocean Tsunami, Field Survey on Jan 21-31 at North of Sumatra, by ITST of UNESCO IOC. 18 p.

_____, ITDB/PAC.: 2004, Integrated Tsunami Databases for the Pacific. Version 5.11 of July 2004. CD-ROM *Tsunami Laboratory*. IcmmG,SD RAS. Novosibirsks, Russia.

_____**,** Badan Rekonstruksi dan Rehabilittasi (BRR) and Partners.: 2006, Aceh and Nias: *Two years after the tsunami*, *Progress Report*. 110 p.

Chapter 2

Tsunamigenic Regions of Indonesian Archipelago

2.1. Introduction

The convergence of the Eurasian, Indo-Australian, Caroline and Philippines Sea tectonic plates within the Indonesian Archipelago produces an active seismic zone. These plate convergences form a complex region containing a subduction-zone, collision zone, fault zone, forearc basin, backarc thrusting and spreading zone, and a volcanic chain along an island arc (Hamilton, 1979; Katili, 1989; Puspito and Shimazaki, 1995) as illustrated in Figure 2.1. Most of these active zones are located under the sea and produce large shallow earthquakes that posses a high tsunamigenic potential.

Since AD1600 there is a considerable record of tsunami occurrences. More than 183 mostly near-field tsunamis have been generated due to submarine earthquakes, volcanic eruptions and associated processes (Hamzah et al., 2000; Prasetya et al., 2001; Rynn, 2002; ITDB/PAC2004). Recently, a series of tsunamis occurred within this region following the great Sumatra Earthquake (M_w>9) on December 26, 2004, including the Nias Earthquake and tsunami on 28 March 2005, South Java Tsunami (M_w = 7.7) on 24 July 2006, and Bengkulu Tsunami (M_w = 8.4) on 12 September 2007. These recent events clearly showed the uniqueness of each near-field tsunami, as every tsunami had its own characteristic and site-specific impacts.

The Great Sumatra Earthquake and Tsunamis on 26 December 2004, was a turning point in studying subduction earthquake generated tsunamis (Synolakis and Bernard, 2006; Geist et al., 2007). Since this event, scientists have urged the public and policy makers to consider all subduction-type tectonic boundaries to be locked, loaded and dangerous zones that possess potential tsunami threats. Reliable and comprehensive databases for past and recent events, and subsequent scientific analysis are needed for mitigating the tsunami hazards.

2.2. Tectonic Setting

The Indonesian Archipelago is a chain of island Arcs (Figure 2.1) composed of oceanic trenches, non-volcanic and volcanic arcs, and forearc and backarc systems as a result of complex convergence of the Eurasian, Indo-Australian, Caroline and Philippines Sea tectonic plates, and several minor plates (Hamilton, 1979). The Indo-Australian Plate is moving northward relative to the Eurasian Plate and the convergence zone occurs along the Java Trench, and Timor and Seram Trough. The Philippines Sea Plate is moving west-northwestward relative to the Eurasian Plate, with the convergence zone along the Philippines Trench. Meanwhile the Caroline Plate is moving west-northwestward relative to the Philippines Sea Plate near the Yap Trench (Hamilton, 1989).

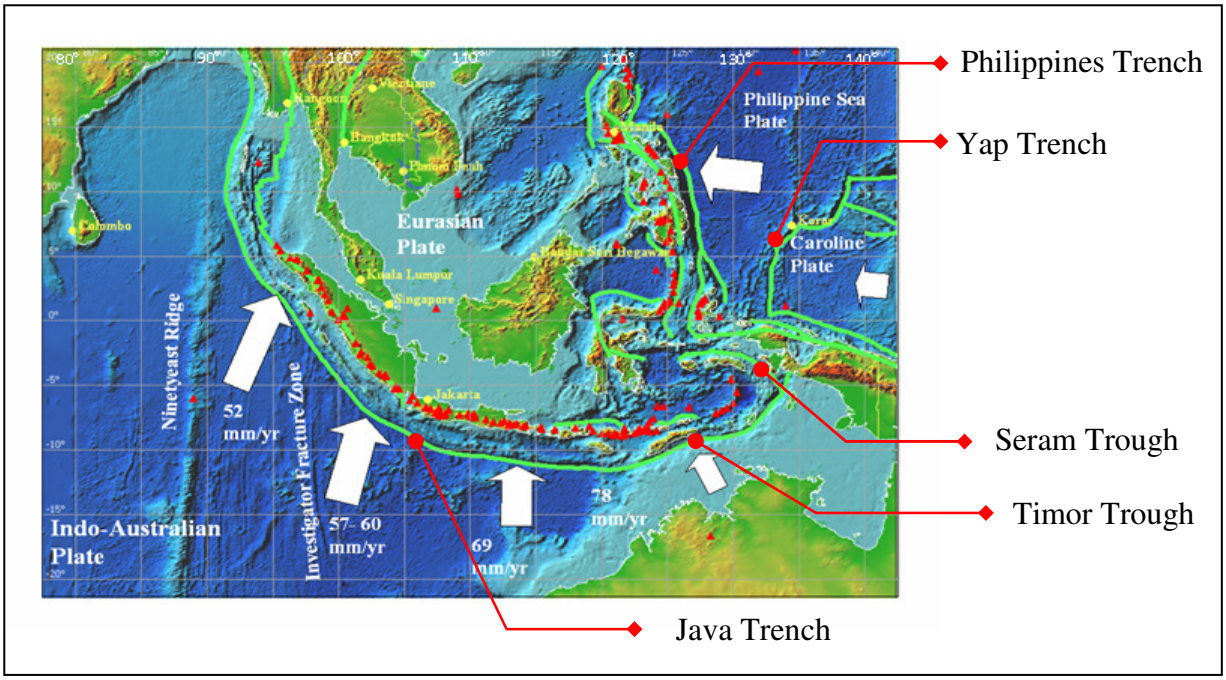

Figure 2.1. Tectonic setting of Indonesian Archipelago as a result of complex convergence of the Eurasian, Indo-Australian, Caroline and Philippines Sea Plates and several minor plates. It is composed of oceanic trenches, non-volcanic and volcanic arcs, and fore-arc and back-arc systems. (Base map: ITDB/PAC2004).

Convergence between the Indo-Australian and Eurasian Plates formed the Sunda Arc along the Java Trench, and Banda Arc along the Timor and Seram Troughs. The Sunda Arc extends westward from Sumba over 6000 km, passing through Sumbawa, Lombok, Bali, Java and Sumatra to the Andaman Islands in the northwest. The Banda Arc extends to the east from Sumba, passing through Tanimbar

and Aru islands and curves sharply in a counterclockwise direction to a westward trend to the north, through Seram and Buru Islands. The arc-trench system changes along strike from oceanic off Sumatra, through transitional off Java, to continental in the eastern Sunda Arc (Hamilton, 1989). This means that the Sunda and Banda convergent margin includes the transition from subduction of oceanic lithosphere of the Indian Ocean at the Java trench approximately west of 120E, to subduction of the Scott Plateau (possible thinned continental crust), to collision of thick crust of the Australian continent with the Banda Arc (McCaffrey, 1988). More complex tectonic systems exist at the edge of Sunda Arc in the west (Andaman Islands) and Banda Arc in the East (McCann et al., 1979; McCaffrey, 1989; Widiantoro and Hilst, 1997).

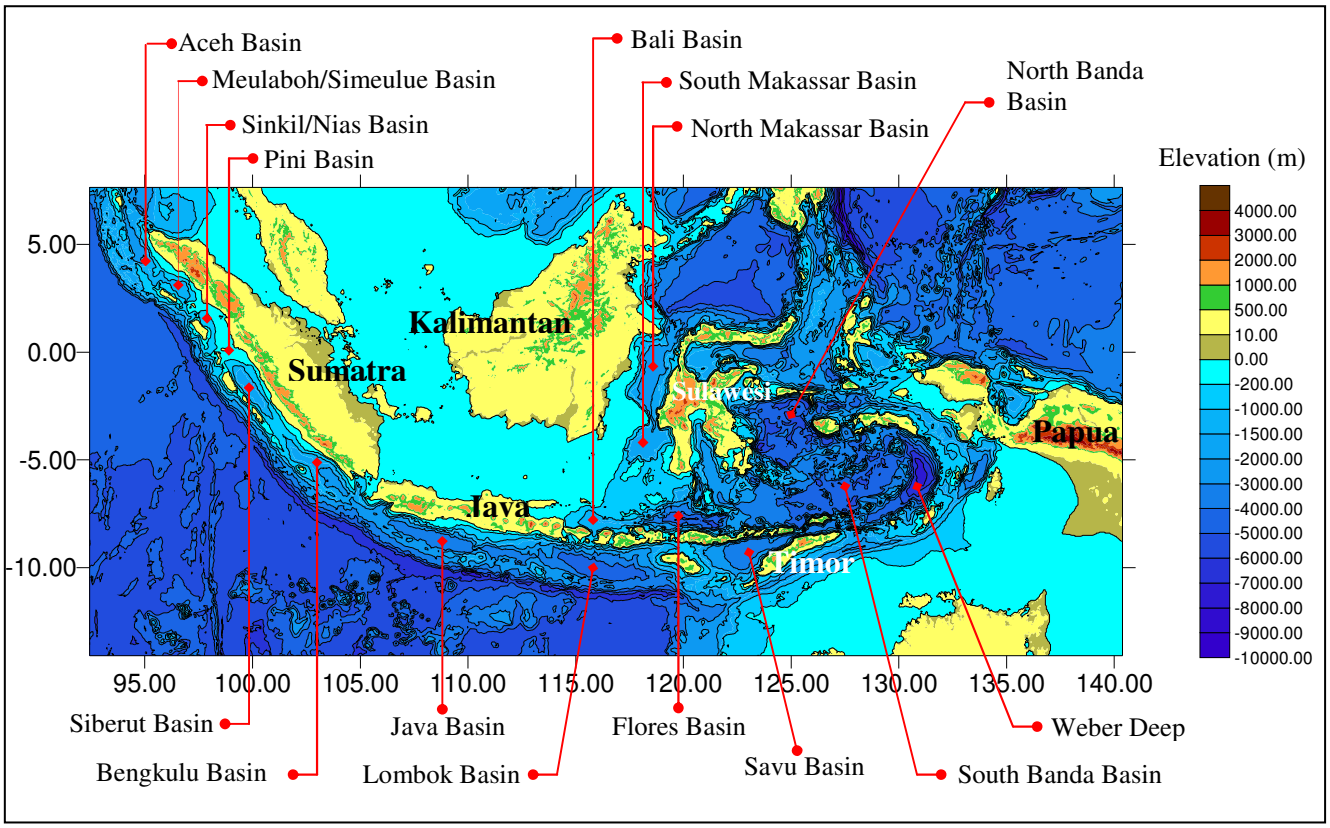

Figure 2.2. A series of fore-arc basins 50 to 100 km wide and a few hundred kilometers long, separated by transverse highs occur between the magmatic arc and outer-arc ridge within the Indonesian Archipelago. Back-arc basins are also indicated (Base map data from: GEBCO).

A series of forearc basins, 50 to 100 km wide and a few hundred kilometers long separated by transverse highs are identified along the Sunda Arc between the magmatic arc and outer-arc ridge and also at Banda Arc (van der Werff, 1996) as illustrated in Figure 2.2. From north-west to south-east, those basins have been identified respectively as: the Aceh, Meulaboh/Simeulue, Singkil/Nias and Pini basins

off Western North Sumatra, the Siberut and Bengkulu Basins off South Sumatra, the Java and Lombok Basins off the islands of Java, Bali, Lombok and Sumbawa, and the Savu Basin at the western margin of the Banda Arc to the south of Flores Island.

The backarc basins of the eastern Indonesia Archipelago are: Bali Basin to the north of Bali and Lombok islands, Flores Basin to the north of the island of Flores, and Banda Basin consisting of North Banda Basin and South Banda Basin surrounded by the Banda arc margin. Another basin is the Makassar Basin that has formed due to the spreading of the sea floor between the island of Kalimantan and Sulawesi during the Quaternary (McCaffrey, 1988; van der Werff, 1996).

Sunda Arc

Kinematics plate boundary studies along the Sunda Arc identified that the subduction occurs with a relatively simple style, where the oceanic crust is subducted beneath the continental platform. Further, the interplate motion is normal to the arc along Java and the Lesser Sunda Island (Java subduction-zone), and becomes oblique from Sunda Strait to Nicobar-Andaman Islands in the northwest (Sumatra Subduction-zone). This behavior is a consequence of the partitioning of the convergent motion into thrust and strike-slip faulting along the arc with the true direction of convergence close to North-South. The rate of plate convergence along the Sunda Arc varies from 78 mm/year near Sumba, 69 mm/year near Java to 57 mm/year at central Sumatra and 52 mm/year close to the tip of Sumatra Island in the northwest (Newcomb and McCann, 1987; Malod et al., 1995; Natawidjaja, 2003; Kopp et al., 2006) as illustrated in Figure 2.3.

Forearc geometry (the depth of the Forearc basins, trench slope break, and trench) of the Sunda Arc also varies systematically, and increases from west to the east (from Sumatra to Java) as the sediment thickness on the subducted plate decreases. Meanwhile the thickness and age of the subducted oceanic crust increases from 49-96 Ma below Sumatra to 96-134 Ma below Java. The increasing dip and depth of penetration of the Wadati-Benioff zone reflect this change from 250 km depth beneath Sumatra to 670 km below Java (Newcomb and McCann, 1987).

The Java trench, from Sumba to Sunda Strait has depths of more than 6000 m and sediment thickness in the trench varies markedly along a strike ranging from 200 to 900 m (van der Werff, 1996), which is less than sediment thickness in the Sumatra subduction zone (1000 – 2000 m). From Sunda Strait to the west of North Sumatra,

the trench gradually shoals from about 6000 m to approximately 5000 m and widens to a broad floor. Within the forearc region two major dextral strike-slip fault zones, the Sumatra and Mentawai fault zones, are aligned parallel to the trench and accommodate the obliquity of the convergence. The Sumatra fault system, which is located along the volcanic arc, connects the Sunda Strait in the south with the Andaman Sea in the north. The Mentawai Fault Zone (MFZ) separates the outer-arc ridge from the forearc basin. It extends from the Sunda Strait to the island of Nias and offshore Simeulue. The Investigator Fracture Zone (IFZ) exhibits 1000-1500 m of relief that intersects the forearc and underlying continental margin, and significantly the IFZ acted as major sediment dam to along strike sediment flow in the trench (Newcomb and McCann, 1987).

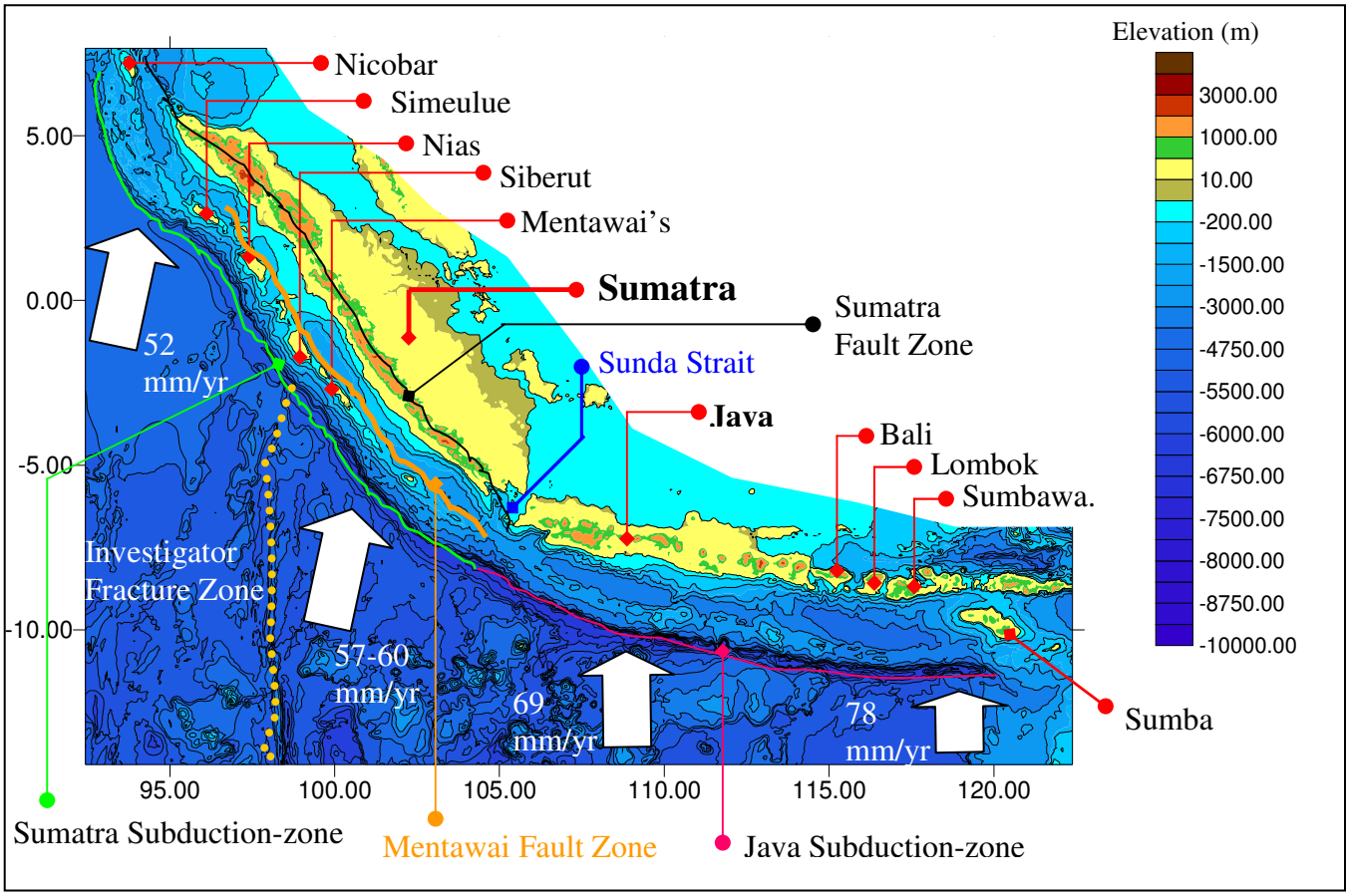

Figure 2.3. The Sunda Arc extends westward from Sumba over 6000 km, passing through Sumbawa, Lombok, Bali, Java and Sumatra to the Nicobar - Andaman Islands. The oceanic crust is subducted beneath the continental platform. The interplate motion is normal to the arc along Java and the Lesser Sunda Island (Java subduction-zone) and becomes oblique from Sunda Strait to Nicobar-Andaman Islands in the northwest (Sumatra Subduction-zone).

The Sunda Strait is located in a transitional zone between two different modes of subduction along the Sunda Arc; the normal (frontal) Java and Sumatra oblique subduction zones (Figure 2.4). This strait is a tensional tectonic regime as a result of clockwise rotation along the continental margin and northward movement of the Sumatra sliver plate along the Semangko fault zone (Schluter et al., 2002), and is disturbed by the Krakatau volcanic complex that lies in the middle of the Strait at the intersection of two graben zones and a north-south active shallow seismic belt (Nishimura et al., 1992).

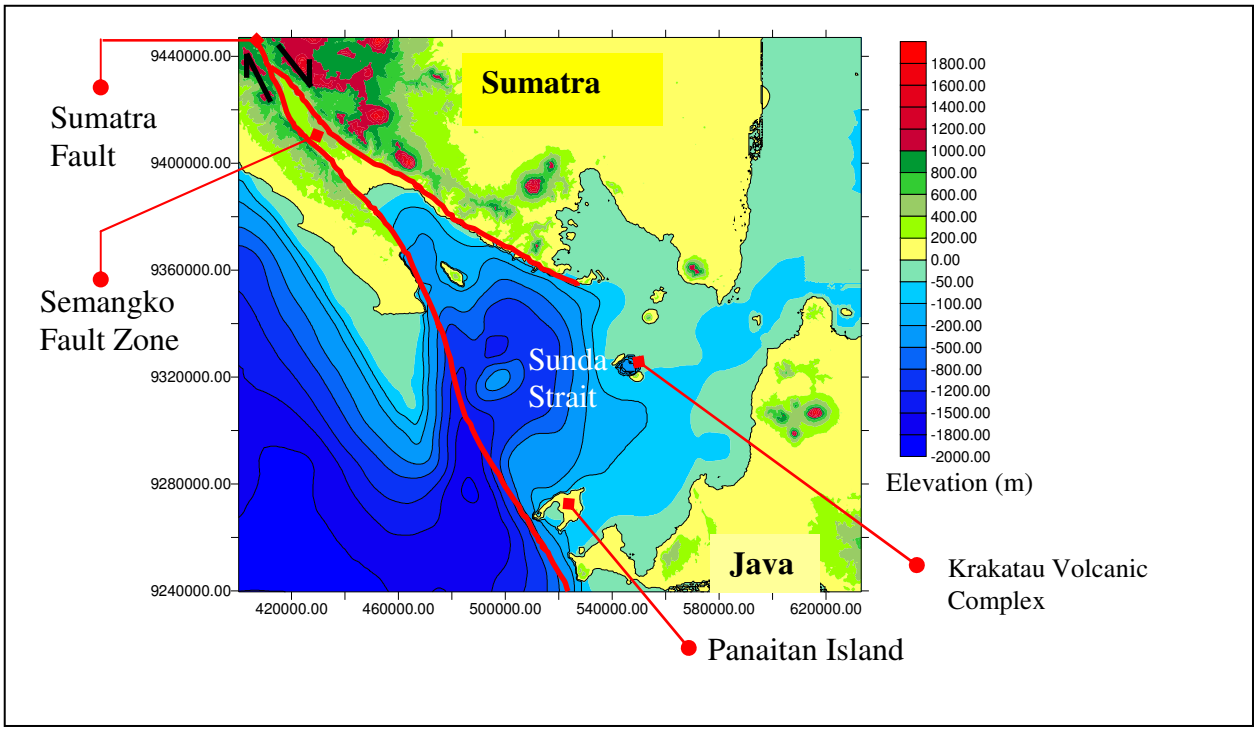

Figure 2.4. The Sunda Strait is located between Island of Sumatra and Java and transition between two different modes of subduction along Sunda Arc. The Krakatau Volcanic complex lies in the middle of the Strait.

The Banda Arc

A more complex tectonic system exists in the eastern part of the Indonesian Archipelago known as the Banda Arc tectonic system as illustrated in Figure 2.5. Fault plane solutions for shallow earthquakes show that the collision of the Australian continent with the Banda Arc shortens the overriding Indonesian Plate in the convergence direction (north-south direction), and elongates it in the east-west direction by a combination of strike-slip and thrust faulting beneath the forearc and backarc basins over the area between the Timor Trough and northern Banda

(McCaffrey, 1988, 1989). This phenomenon may explain the curvature of Banda Arc in the context of continent-island-arc collision.

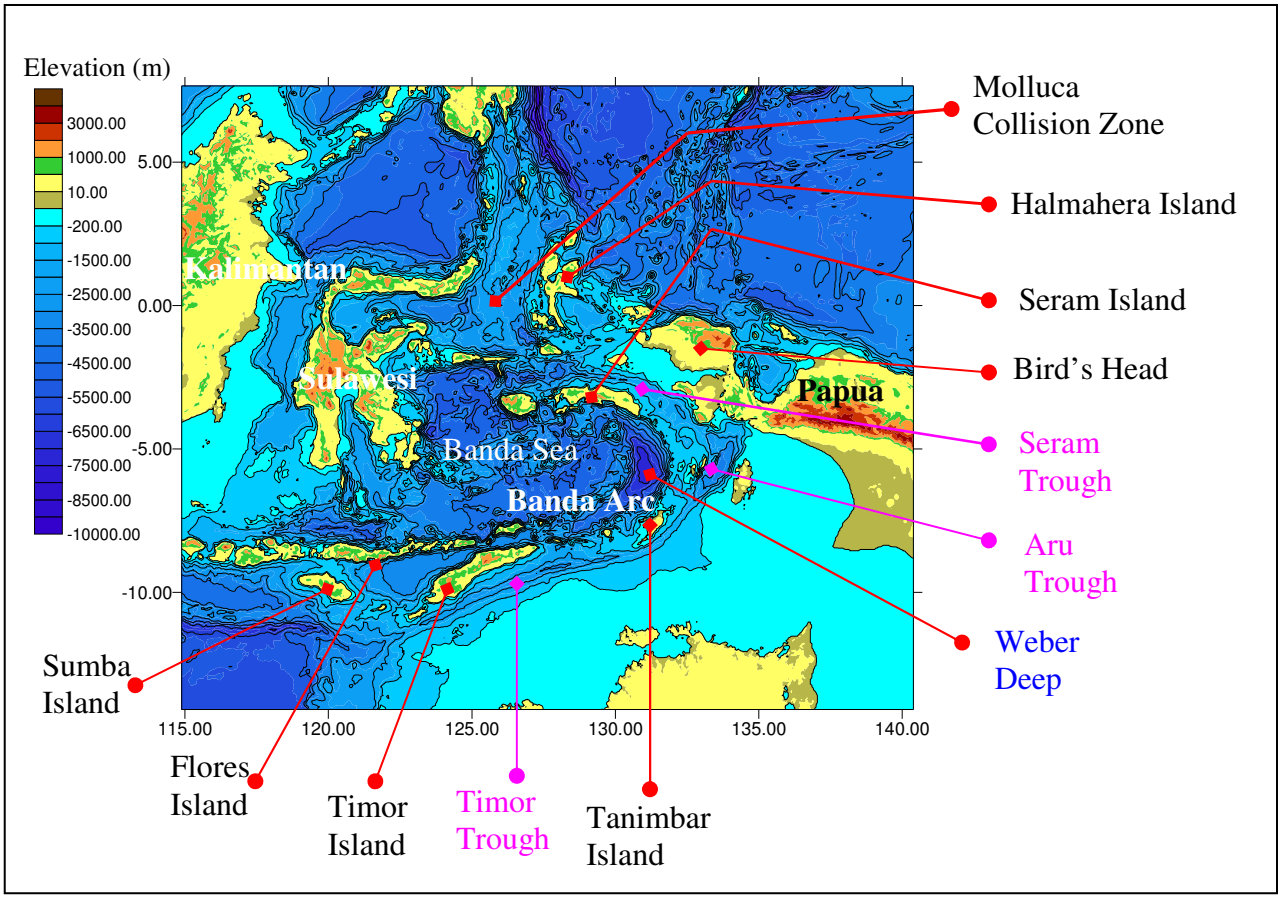

Figure 2.5. Multifaceted tectonic settings were identified within the Banda Arc region extending from the Island of Sumba in a counterclockwise direction through Timor Trough, Tanimbar Islands, Aru Trough and Seram Trough and to the Molluca Collision zone in the north. Two plates subduct beneath the Banda Arc: the Australian- Indian Ocean Plate along the Java trench, Timor Trough, and Aru Troughs, and the Bird's Head southwestward along the Seram Trough. This produces deep basins known as North Banda Basin, South Banda Basin and Weber Deep.

Shallow tectonics and the distribution of deep earthquakes beneath the Banda basin indicate that two plates subduct beneath the Banda Arc (McCaffrey, 1989); the Australian-Indian Ocean plate northward along the Java Trench, Timor Trough, and Aru Trough, and the Bird's Head micro-plate southwestward along the Seram Trough. The counterclockwise rotation (the curvature of Banda Arc) may have formed the narrow Weber Deep region in the Banda Sea with depth more than 8000 m, which is assumed to be oceanic crust trapped by the surrounding younger arcs.

To the north of the Banda Sea, there is the Molluca collision zone where the structure is more complex, with two oppositely dipping slabs associated with the

subducted Molluca Sea Plate. This is related to the active arc-arc collision between Halmahera and Sangihe. The dips of the two slab segments are significantly different (Widiantoro and van der Hilst, 1997).

The Makassar Strait.

This strait has been identified as an important boundary between the western and eastern Indonesian Archipelago from geotectonic synthesis of available geophysical data. It is a marginal basin occupying the continental shelf slope and rise area between Kalimantan and Sulawesi. The spreading of the sea floor between Kalimantan and Sulawesi is still poorly understood. However, according to Katili (1978), the opening of the Strait during the Quartenary formed the marginal basin. The spreading is concentrated along the Paternoster (or Pasternoster (Katili, 1978)) and Palu-Koro Transform Faults. The Palu-Koro fault zone connects with the North Sulawesi Trench, and separates the Sulawesi Sea from Makassar Basin (Katili, 1978; Silver et al., 1983; Hamilton, 1988). The Paternoster Fault divides the Makassar Basin into the North and South Makassar sub-basins (Figure 2.6). The north Makassar sub-basin is bounded by the Sulawesi Sea and it is deeper than the south sub-basin, which is bounded by the Java Sea.

The bathymetry map of Makassar Strait clearly shows two lineaments of steep gradient representing the Paternoster and Palu-Koro Transform Faults, forming the southern and northern boundary of the Makassar Trough respectively. Examination of the 1000 m isobaths closing the deep-water portion of Makassar Strait indicates that is possible to fit southern and central Sulawesi against the Kalimantan shelf by restoring the presumed east and south-southeasterly movement of this region (Katili, 1978), as illustrated in Figure 2.6.

The younger spreading of the Sulawesi Sea moved Sulawesi to the south-southeast along the Palu-Koro Transform Fault and created the southeast subduction-zone to the northwest of Sulawesi (Silver et al., 1983). This movement destroyed the spreading centers of the Makassar Trough. In the south, the spreading of sea floor of the Makassar Trough along the Paternoster Fault was accommodated by a small east-dipping subduction-zone (Katili, 1978).

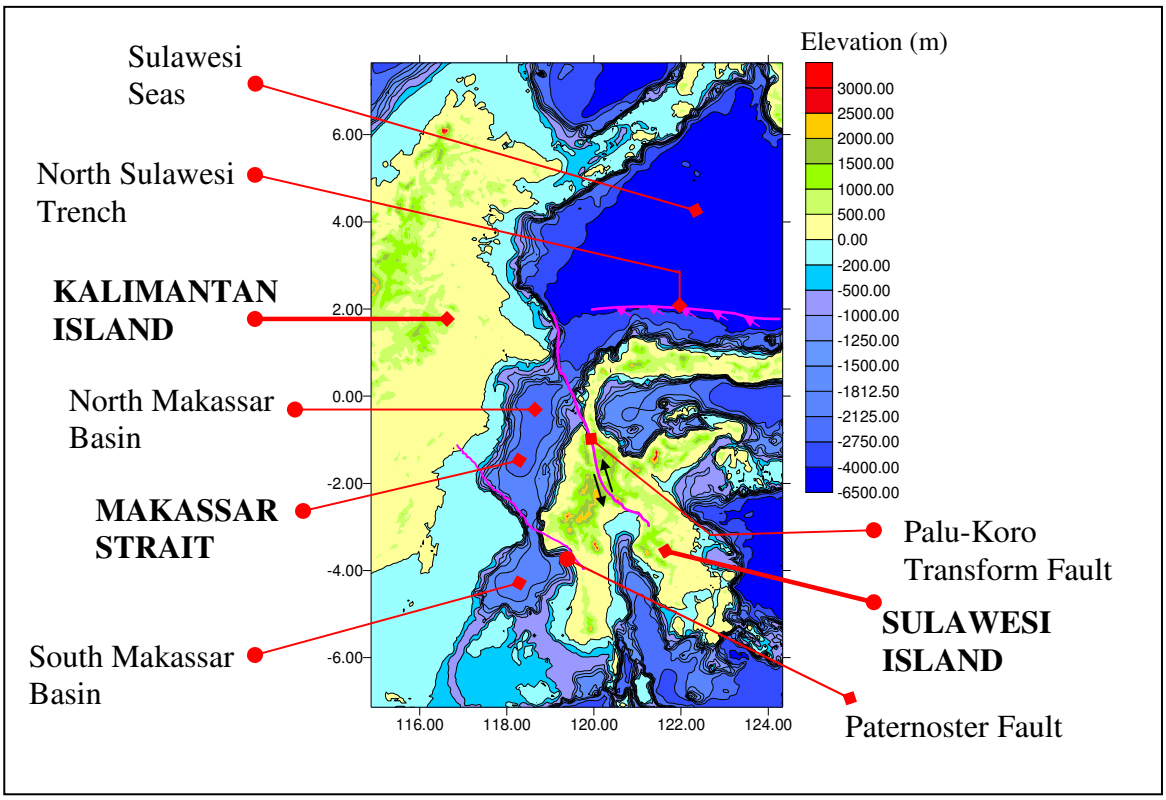

Figure 2.6. The Makassar Straits are located between Kalimantan and Sulawesi Island and known as a geologically important boundary between the west and eastern Indonesian archipelago. The Palu-Koro fault zone connects with the North Sulawesi trench, and separates the Sulawesi Sea from Makassar Basin. The Paternoster or Pasternoster (Katili, 1978) fault divides the Makassar basin into the North and South Makassar sub-basins as shown on the bathymetry map.

2.3. Tsunamigenic Earthquakes.

The seismic history of the Indonesian Archipelago can be divided into two periods: before the time of early instrumental recording (i.e. before 1900); and after. It is difficult to assess the full extent of seismic events for data sets before 1900, since the data depend upon the population density of the affected regions.

2.3.1. Pre-1900 events.

Newcomb and McCann (1987) analyzed the data sets of the Sunda Arc region for the period before AD 1900. Approximately, 60 intensity maps enabled them to characterize events that clearly had an inland epicenter, and events of submarine origin. The data sets from AD 1600 - 1900 indicated that the majority of large shocks were reported from Sumatra, even though it was less densely settled than neighboring islands such as Java. This implies that long-term levels of seismic activity from large earthquake are higher in Sumatra than Java. The International Tsunami Data Bases

(ITDB/PAC2004) listed 102 earthquakes events of submarine origin. Sixty-one (61) events occurred in the Banda Arc region, and 41 events along the Sunda Arc (Figure 2.7).

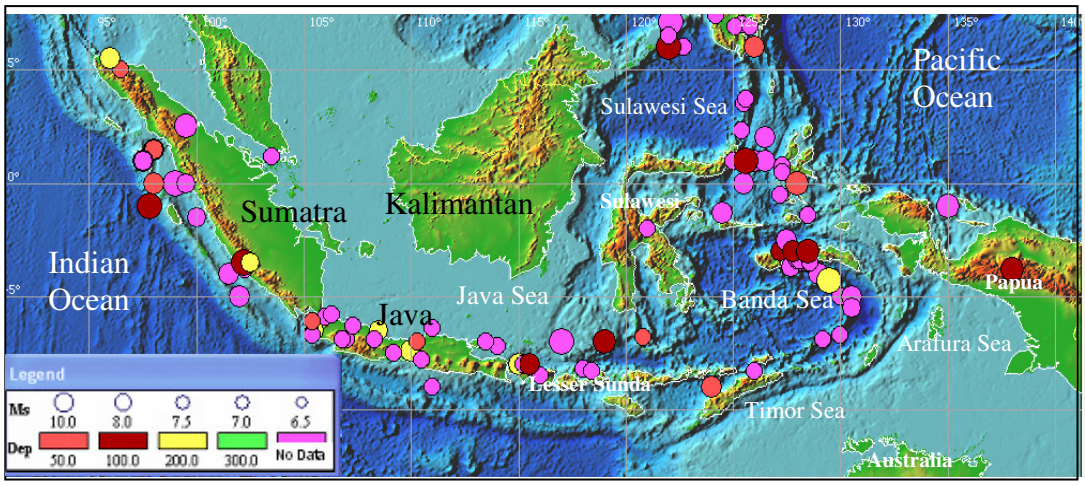

Figure 2.7. Earthquake distribution of the Indonesian Archipelago for the period AD 1000-1900 showing that the majority of large shallow shocks reported from Sumatra were of submarine origin. The central and eastern archipelagos lack great shallow depth earthquakes. Ms is unit scale of surface wave magnitude of the earthquake represented by the size of the circle from 6.5 to 10. The color bar (Dep) is the focal depth in km. The circle of the purple color mean there is no depth data. (Data source from: Newcomb and McCann, 1987, and ITDB/PAC2004).

The datasets show the absence of great submarine thrust earthquakes at shallow depths in eastern of Indonesia. This may be related to the contortions of the dipping slab as it bends around the eastern Banda Sea, and to the interference of the Australian continental shelf, Christmas Island ridge, and other bathymetric features with the subduction process (McCann et al., 1979; Newcomb and McCann, 1987). However, it should be kept in mind that the datasets are probably incomplete due to a poor record.

The Sunda Arc

For the Sumatra region, 17 large submarine earthquakes were recorded before AD 1900. The 1833, 1861 and 1907 events were the largest historical events for this region, and all 3 generated devastating tsunamis. Based on Newcomb and McCann (1987), three active locations that produce large shallow earthquakes associated with damaging tsunamis are identified along the Sumatra segment of the Sunda Arc as follows (Figure 2.8):

- Northwestern Region – the area northwest of Simeulue Islands up to Nicobar Island, which had a quiescent period between AD 1600-1900.

- Central Region – the area of central Sumatra from Simeulue Island up to Nias Island, which experienced the 1843, 1852, series of 1861, and 1907 large earthquakes and tsunami events.
- Southeastern Region – the area southeast of Batu Islands through Siberut and Enggano Islands, which had large historical earthquakes associated with tsunami events in 1681, 1797 and 1833.

The data sets from ITDB/PAC2004 and Newcomb and McCann (1987) show the locations of the epicenters of the all tsunamigenic earthquakes at the southern end of the region affected. This indicates that the nucleation of large earthquakes such as 1833, 1861 and 1907 started from the southeast with rupture propagating to the northwest, which possibly follows the direction of the Indo-Australian Plate movement. The magnitude and extend of damage area (red shading) of earthquake and tsunamis events shows that large submarine earthquakes do not always generate large tsunamis. The behavior is very site specific as illustrated in Figure 2.9. The Northwestern Region in particular shows a poor correlation between earthquake and tsunami magnitudes.

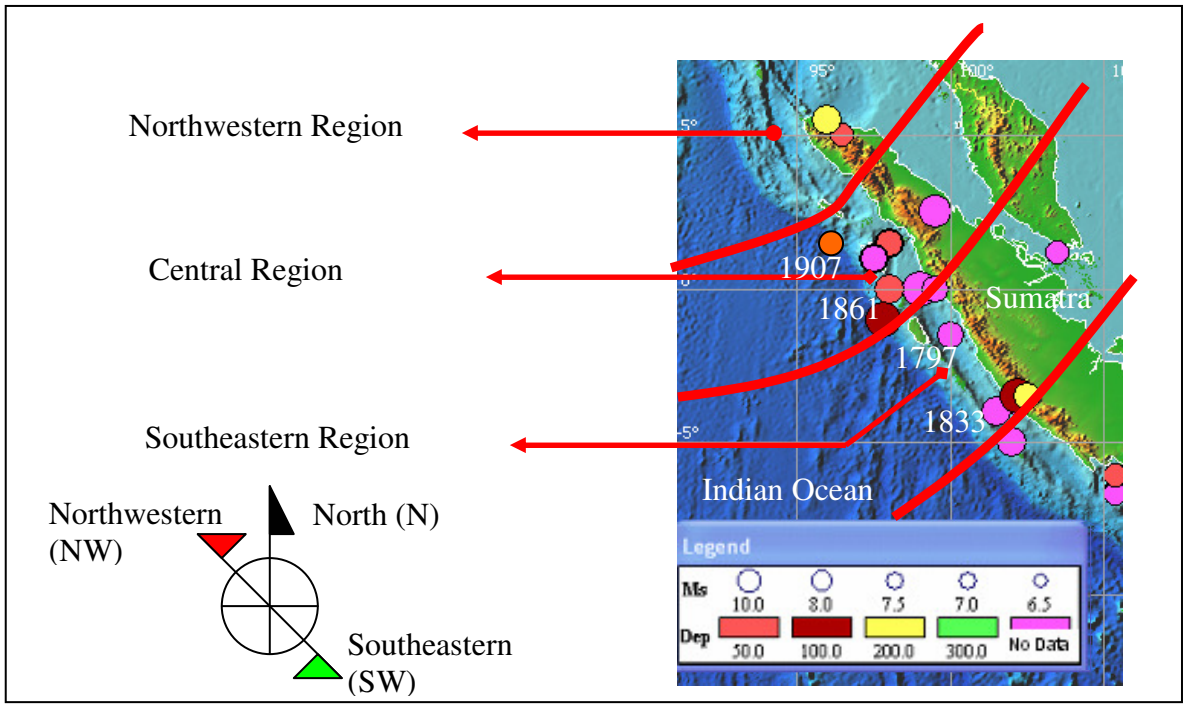

Figure 2.8. Three seismically active locations along the Sumatra subduction zone and on island of Sumatra produced large shallow earthquake and generate tsunamis such as the 1797, 1833, 1861 and 1907. Ms is unit scale of surface wave magnitude of the earthquake represented by the size of the circle from 6.5 to 10. The color bar (Dep) is the focal depth in km where the purple color mean there is no depth data. (Base map: ITDB/PAC2004).

From Sunda Straits towards Sumba Island, more than 30 events were reported before 1903. Five (5) major events had been reported in Java, with 3 events suggesting a submarine origin off Java Island in the Indian Ocean where two of them generated tsunamis (4 January 1840, 20 October 1859). The 1903 event with magnitude M_s=7.9 was from submarine origin and located seaward of westernmost Java but did not generate tsunamis. According to Newcomb and McCann (1987) this event was not an interplate thrust because its location was approximately 200 km south of the position determined by Richter (1958) and is in an intraplate setting (Figure 2.10). However, the earthquakes that generated tsunamis in Java were not always in an interplate setting. The event of 1921 was intraplate, with the epicenter located at the Roo Rise, seaward of the trench.

In comparison with the Sumatra Subduction-zone, where most of the large submarine origin earthquakes were interplate, the Java subduction-zone had both interplate and intraplate earthquakes events, but generally of low to moderate magnitude. The intraplate events within the Java region are located in the immediate vicinity of a plate boundary, involving rupture of the lithosphere seaward of the trench in a zone where it undergoes bending just prior to subduction (Okal, 1983). Hence, intraplate events along the Java subduction-zone involve older oceanic plate bending under continental plate with frontal/normal type of subduction, in contrast to the younger oceanic plate of the Sumatra subduction-zone with an oblique type of subduction. The dataset between AD 1600 -1900 indicates that the offshore area (the Java forearc to the east of lesser Sunda) lacked of moderate to large earthquakes. Hence, it has a low seismic potential; only the area between 109E to 112E was more active in the past, but lacked of shallow events (Newcomb and McCann, 1987). The January 4, 1840 and October 20 1859 events were interplate events and September 11, 1921 was an intraplate event (Figure 2.11). This historical data shows that a relatively low magnitude, inter and intraplate earthquakes events were the characteristic of the tsunamigenic earthquakes of the southern Java subduction zone.

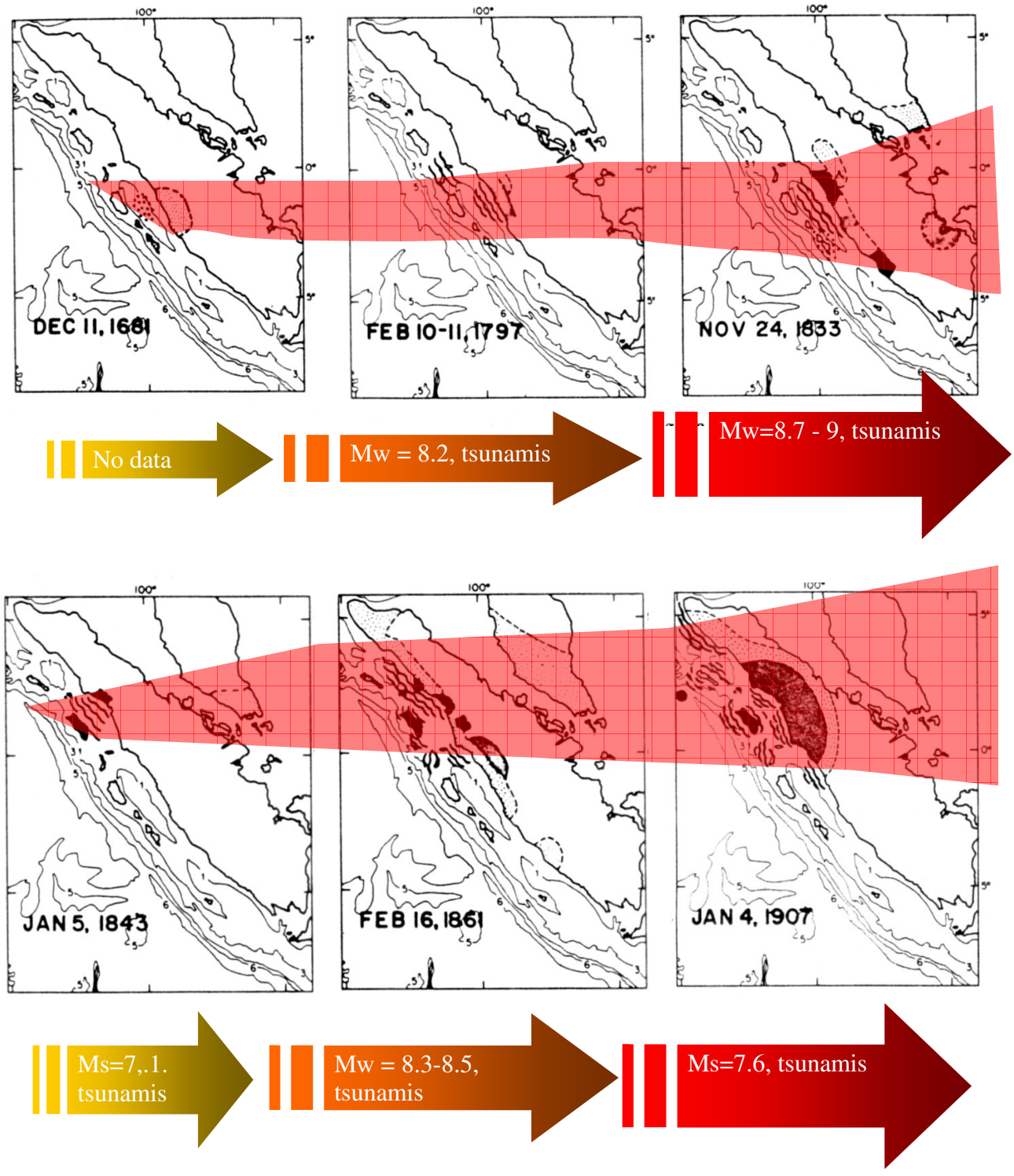

Figure 2.9. The magnitude and extent of damage area (red hatching) of earthquake and tsunami events in the Central and Southeastern regions had linear correlations where larger earthquakes generate larger tsunamis. However, in the Northeastern region (lower panels), the earthquake magnitude and the extent of tsunamis impact doesn't have a linear correlation, which means a great earthquake does not always generate large tsunamis. Data source: Newcomb and McCann (1987).

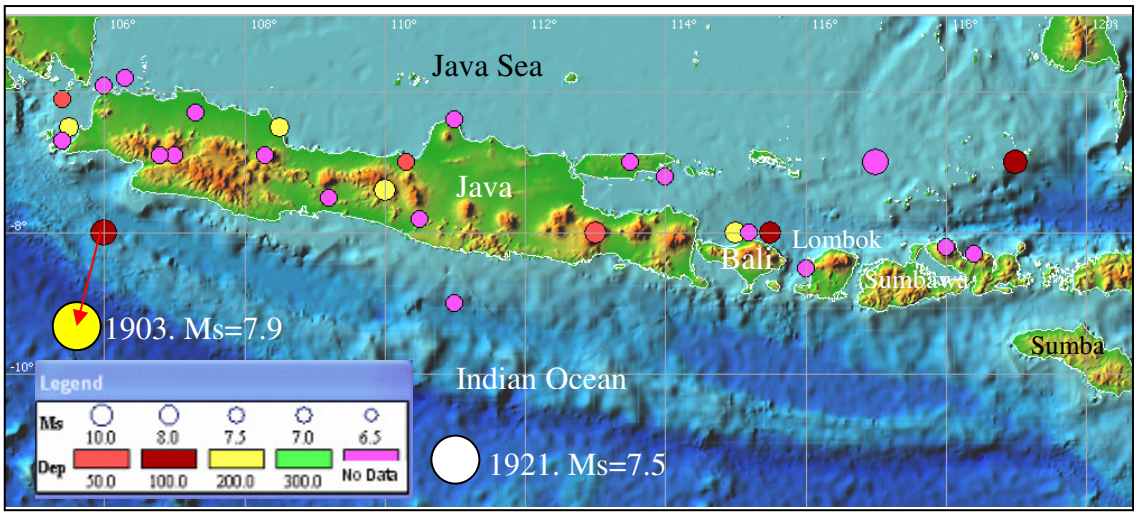

Figure 2.10. Earthquakes on Java and lesser Sunda do not include moderate and large shallow earthquake. Tsunamigenic earthquakes within this region were not always by an interplate events (1840 and 1859), but also include intraplate sources (1903 and 1921). The arrow shows the corrected position for the 1903 events (dark brown to yellow). Ms is unit scale of surface wave magnitude of the earthquake represented by the size of the circle from 6.5 to 10. The color bar (Dep) is the focal depth in km, where the purple color indicates there is no depth data. Data source: Newcomb and McCann 1987 and base map: ITDB/PAC2004.

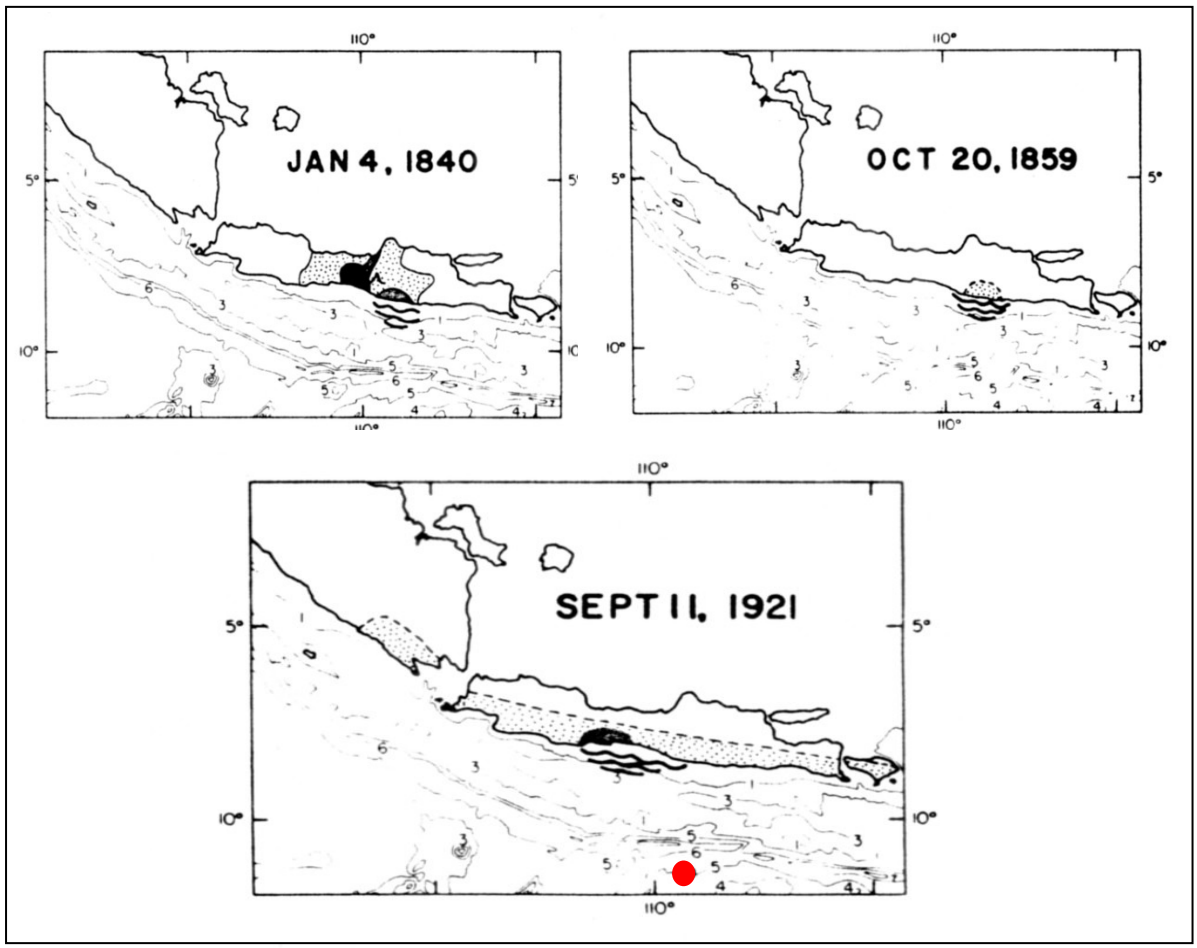

Figure 2.11. The interplate and intraplate earthquake events that generated tsunamis in the Java region. The red circle is the epicenter location of the intraplate event. Data Source: Newcomb and McCann (1987).

The Banda Arc

A tectonic map of the Banda Arc is illustrated in Figure 2. 12. A total of 61 large earthquakes with magnitude Ms > 6.5 have been identified, and 56 of them are suggested to be of submarine origin, with 35 events generating tsunamis (Figure 2.13 and 2.14). The highest intensity occurred along the ridge at the edge of the Banda Arc in the Banda Sea region with 17 events, while to the north at the Molluca Sea Collision Zone there were 9 events. Three earthquakes in the backarc (north of Lombok, Sumbawa and Flores islands) were of submarine origin and may have generated tsunamis. Meanwhile to the north of the Molluca Sea Collision Zone, along the ridge of north Sulawesi, two events have been identified, and at the margin of Sulawesi Sea one event. Due to limitation and uncertainties of the historical report for the period before AD 1900 on this region, the extent of damage and impact of earthquakes and tsunami cannot be defined clearly.

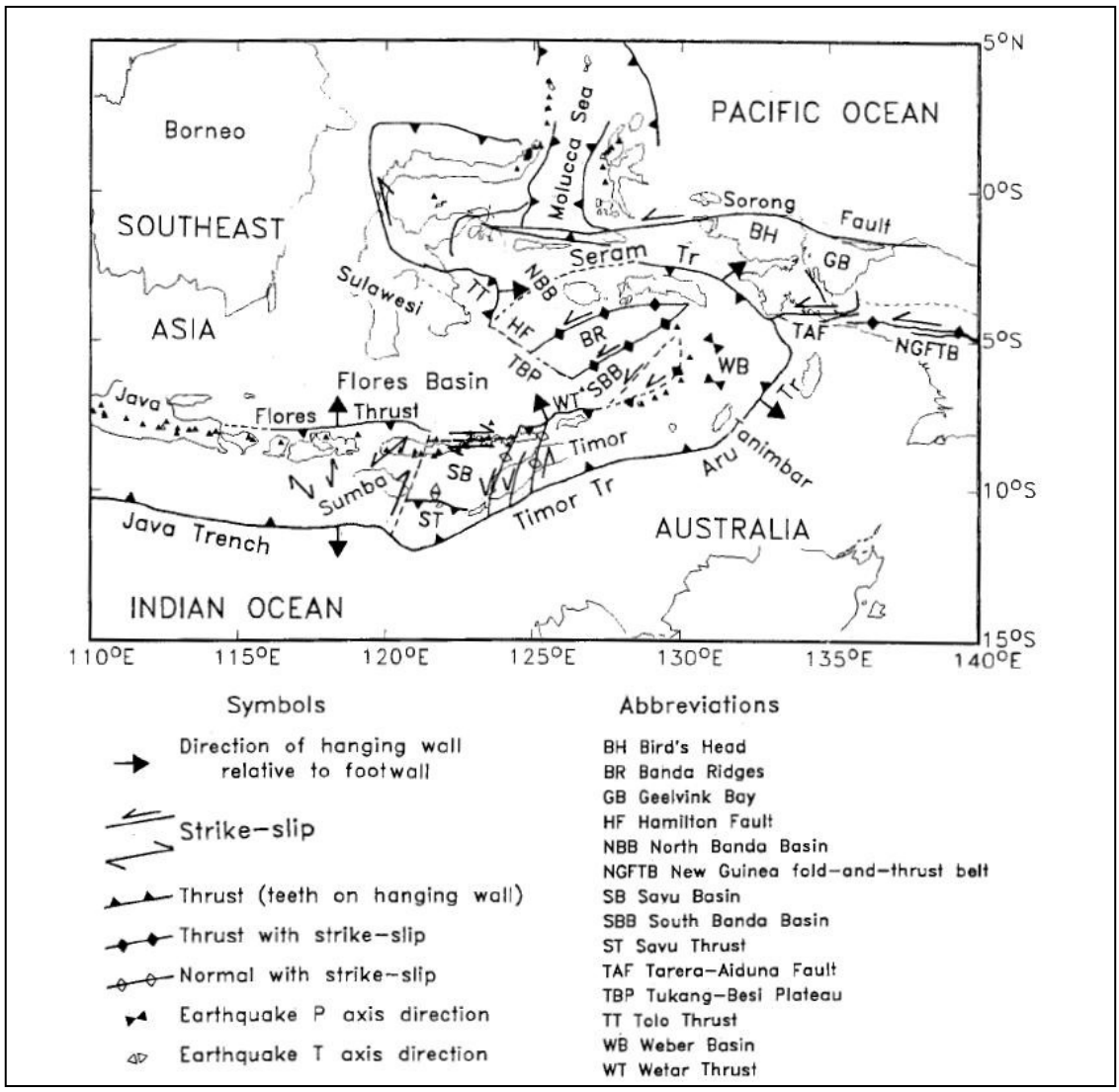

Figure 2.12. The tectonic map of the Banda Arc shows the major faults and subduction-zones as a result of the collision of the three major tectonic plates of Indo-Australia, Eurasia and Pacific. (Map source: McCaffrey, 1988).

The largest event for this region occurred in 1674, between Buru and Seram Island in the Banda Sea (Figure 2.13) with a magnitude M_s = 8.0. According to the historical data (ITDB/PAC2004), this earthquake generated tsunamis with H_{max} = 80 m, which is improbable. However, more recent events have more reliable data, such as the 1852 event with magnitude M_s = 8.2 at the margin of the South Banda Basin south of Seram Island that generated tsunamis with H_{max} = 8 m. Another event occurred in 1820 located at the backarc north of Sumbawa Island at the edge of Flores Basin, with M_s=7.5 that generated tsunamis with H_{max} =24 m.

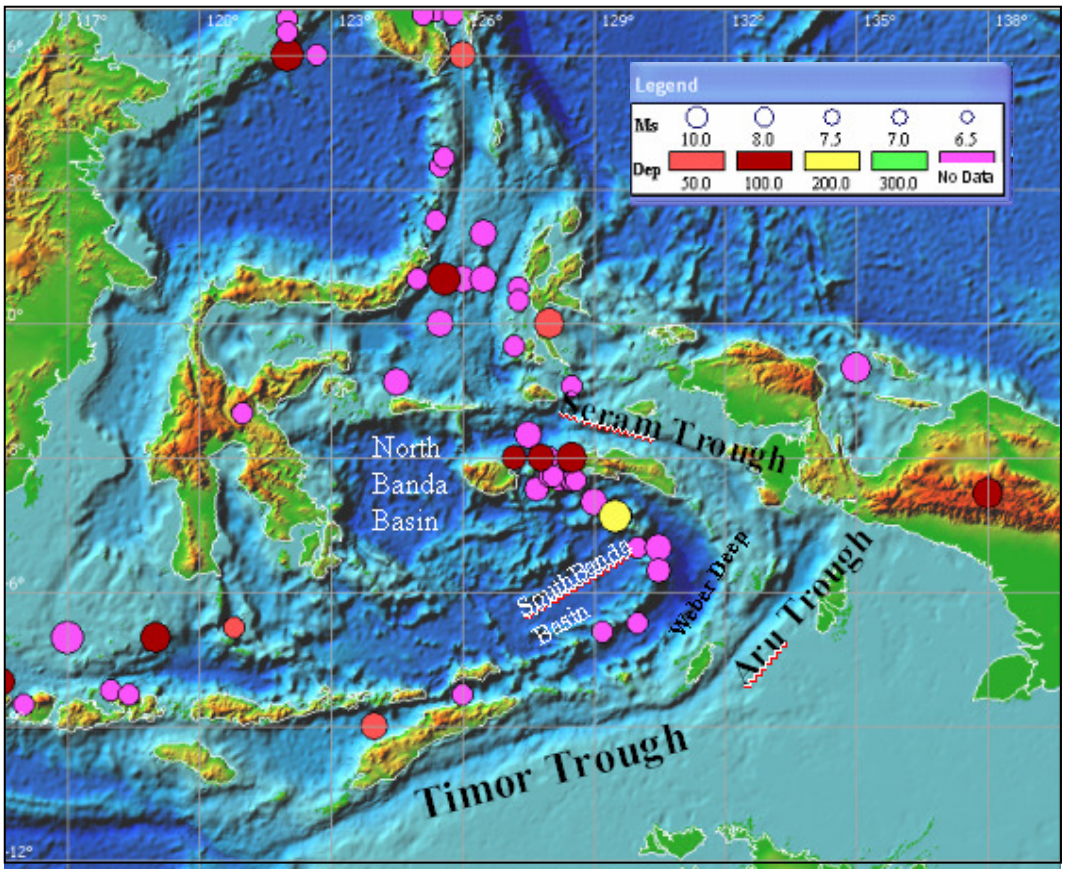

Figure 2.13. The earthquake distribution in Banda Arc region follows the island arc from west to the east and bending to the north in a counterclockwise direction. Most of the epicenters are located behind the Weber Deep. The majority of the earthquakes are submarine events and most of them have generated tsunamis. Ms is unit scale of surface wave magnitude of the earthquake represented by the size of the circle from 6.5 to 10. The color bar (Dep) is the focal depth in km where the purple color means there is no depth data. Data source; ITDB/PAC2004

To the north of Banda Arc, at the Molluca Collision Zone, there was one great earthquake in 1889 with magnitude M_s = 8.0, that generated tsunamis with H_{max} = 15 m (ITDB/PAC 2004). At the northern margin of Sulawesi Seas in 1897, an earthquake with M_s = 8.5 generated tsunamis with H_{max} = 6 m. An event in 1674 where the wave height (H_{max}) reached 80 m at a nearby island needs to be reassessed and confirmed.

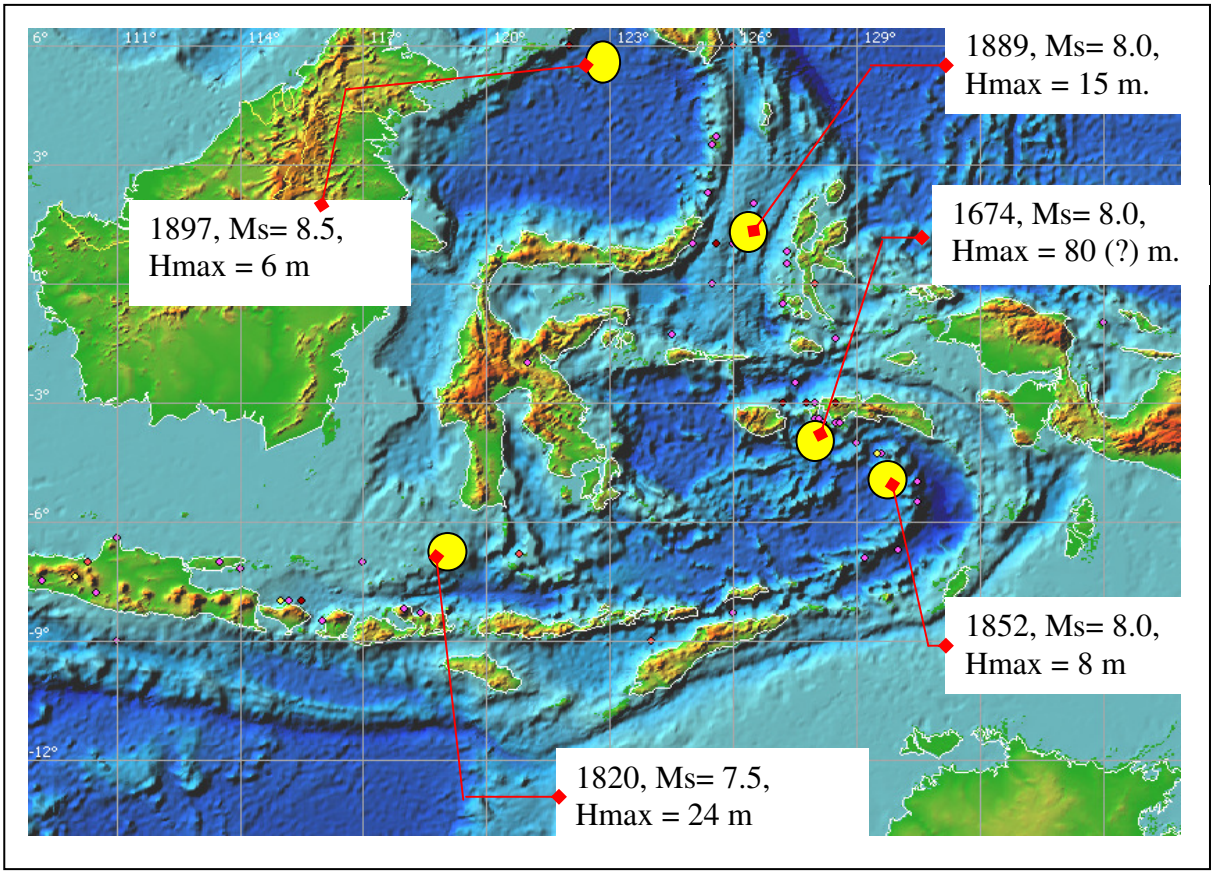

Figure 2.14. Great earthquake events within the Banda Arc showing that each seismic zone is capable of generating great earthquakes and tsunamis (Base map and data source: ITDB/PAC2004).

2.3.2. Post – 1900 events.

Instrumentally recorded earthquakes have significantly improved the seismotectonic understanding of the region. The distribution of earthquakes from AD 1900 to 2004 can be seen in Figures 2.15 to 2.17 for magnitudes greater than M_s =5. Within the Sumatra region, most of the earthquakes occurred between the Sumatra Subduction-Zone and the Sumatra Fault Zone, with depths ranging from 0 – 200 km (red, dark brown and yellow dots). To the east, starting from the subduction-zone area in the Indian Ocean, to the backarc area on the Java sea behind the Java and Nusa Tenggara Islands up to the Banda Sea, the lateral earthquake distribution had maximum depth around 700 km (purple dots). The same distribution is also found for the Sulawesi Seas to the north of Sulawesi Island. However, within this region (Banda Arc to the North), a more complicated earthquake distribution occurred from these complex tectonic settings.

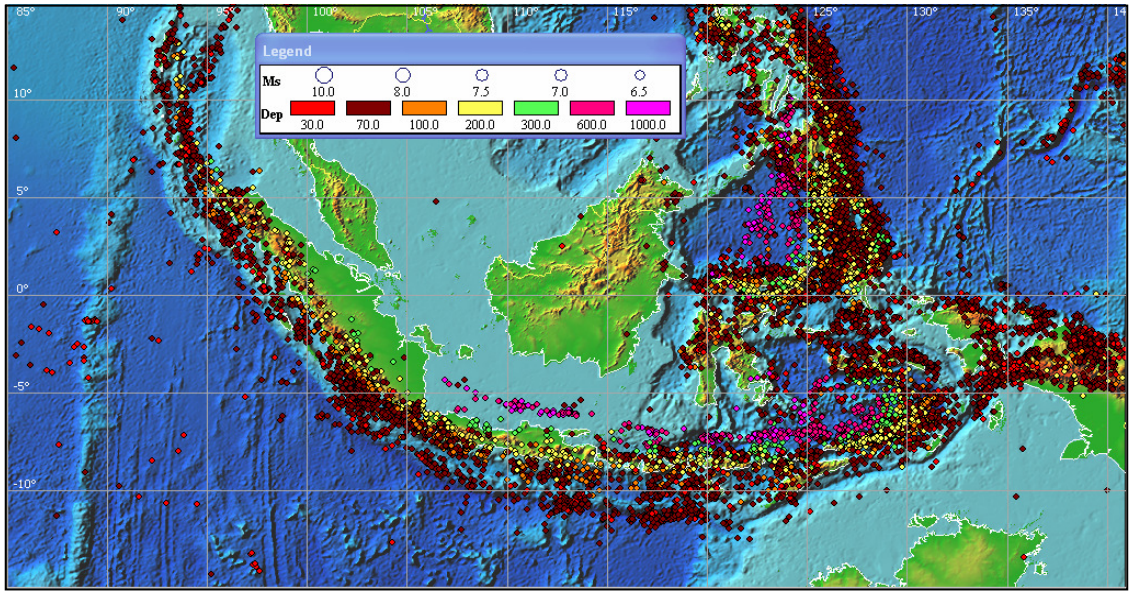

Figure 2.15. The total earthquake distribution with magnitude > 5.0 M_s from AD 1900 until 2004 for the Indonesian Archipelago. Earthquake depths range from 0 –200 km in western Sunda Arc along the Sumatra Island, to 0 - 700 km in the East. (Source: ITDB/PAC2004).

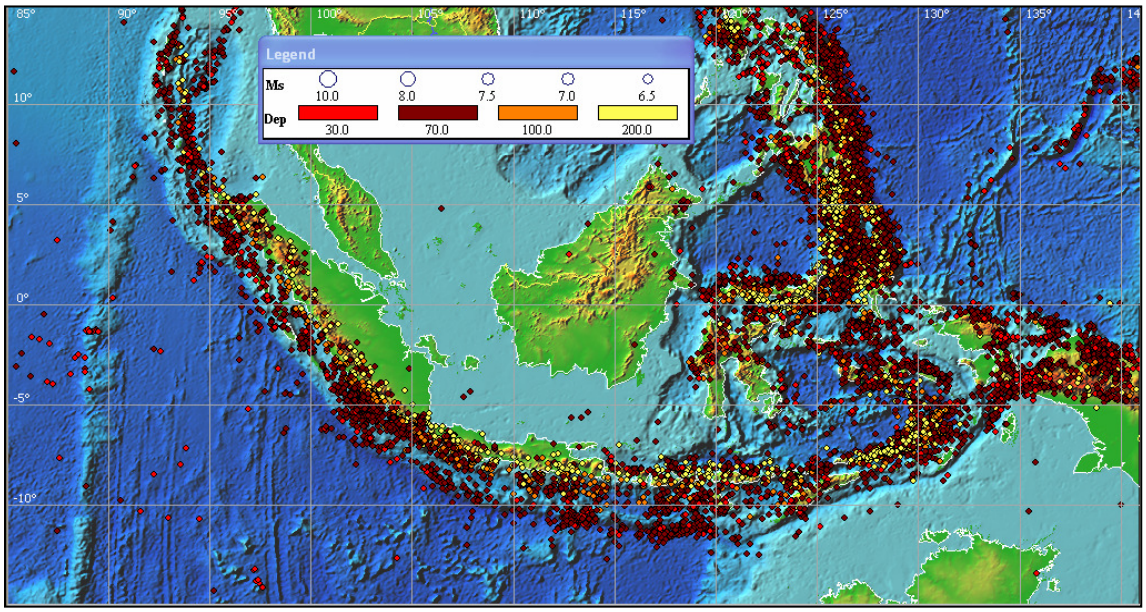

Figure 2.16. Shallow earthquakes with magnitude >5.0 M_s and depths <230 km from AD 1900 until 2004 for the Indonesian Archipelago. (Source: ITDB/PAC2004).

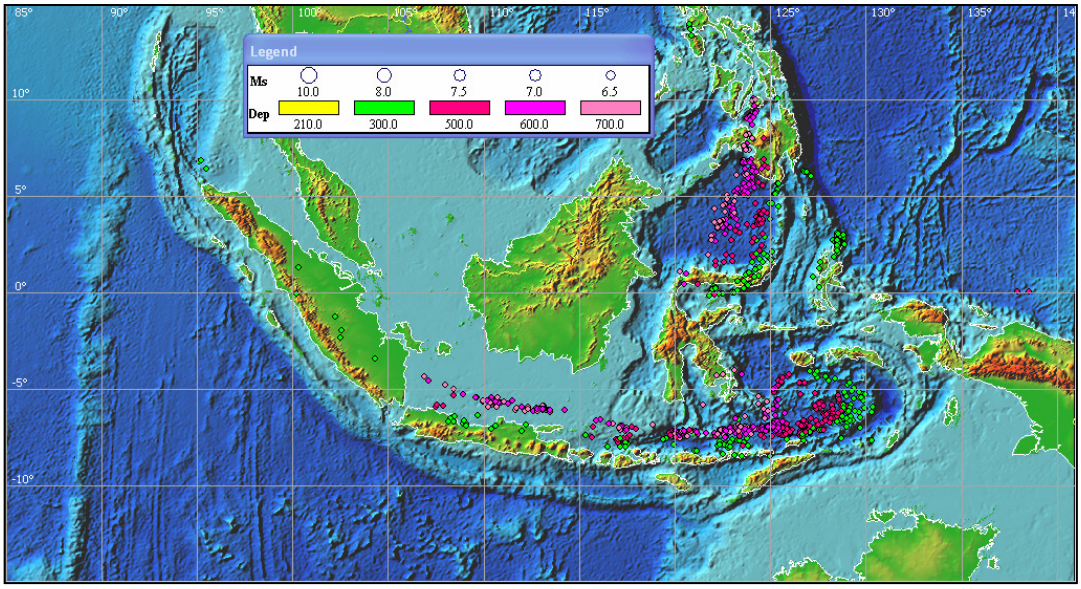

Figure 2.17. Deep earthquakes from 200 - 700 km with magnitudes >5.0 M_s from AD 1900 - 2004 for the Indonesian Archipelago. These data show that deeper earthquakes occur in the back-arc from Java eastward. (Source: ITDB/PAC2004).

2.4. Seismicity and Slab Geometry of Subducted Plates

With the availability of earthquake datasets since AD 1900, the slab geometry of the subducted plate was identified. Vertical cross-sections of seismicity projected perpendicular to the strike of the trench showed the maximum depth of seismic events and hence the slab geometry of the subducted plate. Deep (>300 km) and intermediate (70 km – 300 km) earthquakes form the Wadati-Benioff zone, which at some places extends to > 700 km. The focal mechanisms vary with depth. Those shallower than 300 km generally show down-dip tension, and those below 300 km generally show down-dip compression.

The Wadati-Benioff zone earthquakes illustrate that material cold enough to fail seismically (rather than flow) is being subducted, which gives the best information about the geometry and mechanics of slabs (Stein and Wysession, 2002). Near the surface, the slab is extended by its own weight (down-dip tension), whereas at depth, it encounters stronger lower mantle material, causing down-dip compression. There are also mineral phase changes that occur at different depths in the cold slab than in the surrounding mantle. A thermal model shows that a younger slab will have a slower speed, a hotter temperature and dip at a low angle and producing relatively shallow earthquakes, whereas an older slab will have faster speed, colder temperatures and produce deep earthquakes.

The Sunda Arc

For the Sumatra region, the greatest depth of earthquake events is approximately 250 km, and seismicity indicates a low dip angle for the subducted oceanic plate beneath the continental plate of Sumatra Island. The maximum dip of the slab is about 30°. Further to the east along the Sunda Arc, the maximum earthquake depth increases to > 650 km and the dip angle of the subducted plate also increases. There is a discontinuity in seismicity at a depth range of 220 – 500 km by Java Island. The reason for this is unclear, although a similar case was identified in the Tonga area, where the slab seems to be continuous in the depth range where a discontinuity exits (Puspito and Shimazaki, 1995). This suggests there is no break in the slab under Java.

Figure 2.18 shows the profile of seismicity at the northwestern tip of Sumatra, where the maximum depth of the earthquake is 229 km. Most of the earthquakes occur at depths ranging from 10 km to 100 km and are located beneath the accretionary wedge. The slab dips at a low angle initially, but close to the trench axis it becomes more vertical, suggesting complex deformation occurs in the Nicobar-Andaman Islands. From the bathymetric profile, most of the earthquakes are located close to the continental margin (Figure 2.18), leading to the possibility of major slope failure and mass movement during a large earthquake, and contributing to catastrophic tsunamis.

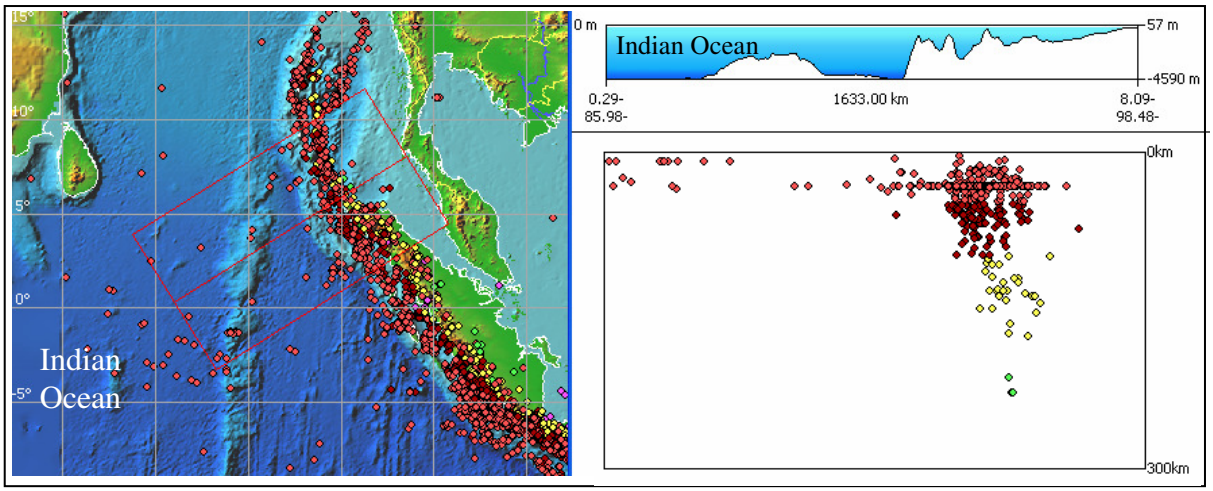

Figure 2.18. Cross-section of sesimicity at the northwestern tip of Sumatra. The red dot represent a shallow earthquake up to 100 km depth, yellow up to 200 km, and green up to 300 km (Source: ITDB/PAC2004).

The seismicity profile for central Sumatra (Figure 2.19) shows that the maximum depth of the earthquake is about 290 km (deeper than the northwestern tip ~229 km). The slab dips beneath the continental crust at about 10-15 degrees. The maximum depth and dip slab angle increases towards the southeastern end of the Sumatra, where the maximum depth of the earthquakes approximately 294 km (Figure 2.20).

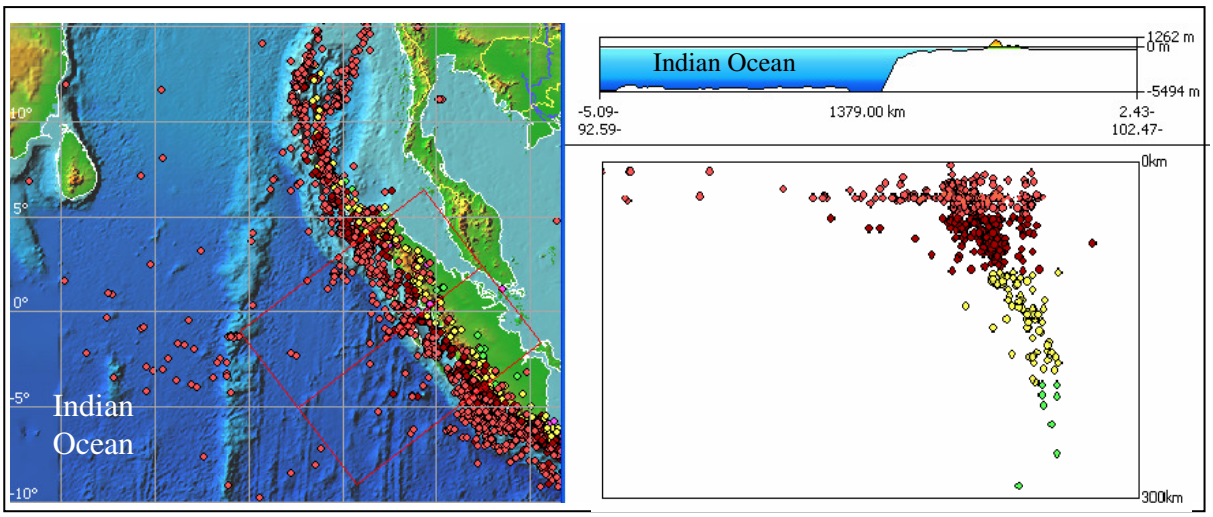

Figure 2.19. Cross-section of seismicity for central Sumatra. The red dot represent a shallow earthquake up to 100 km depth, yellow up to 200 km, and green up to 300 km (Source: ITDB/PAC2004).

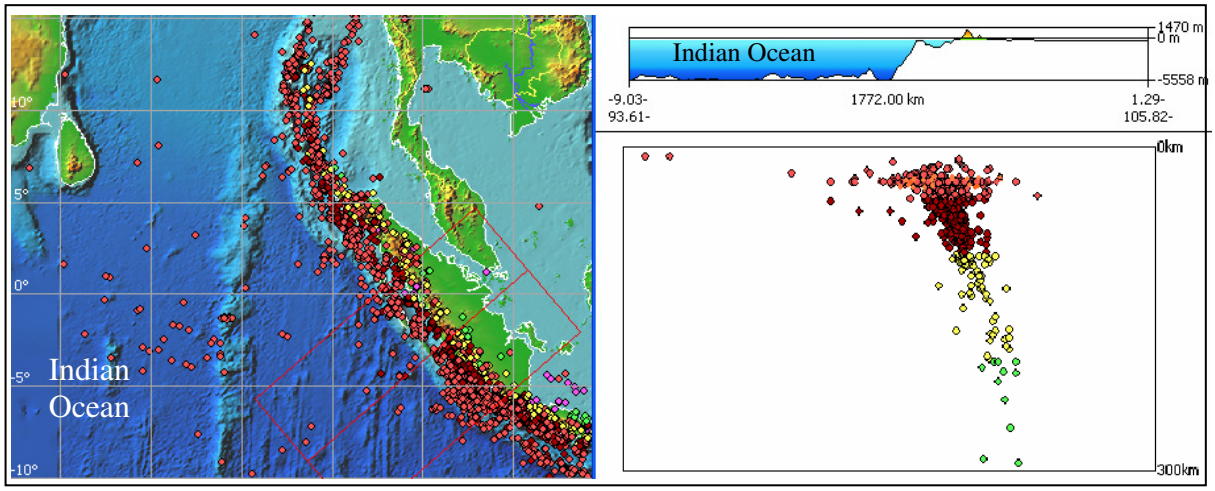

Figure 2.20. Cross-section of seismicity for the southeastern end of Sumatra. The red dot represent a shallow earthquake up to 100 km depth, yellow up to 200 km, and green up to 300 km (Source: ITDB/PAC2004).

Further southeastward along the Java subduction-zone, Figure 2.21 shows the discontinuity of events at depths of 220 – 500 km by Java Island. At the end of the

Sunda Arc (Figure 2.22), the cross section of seismicity shows the dip slab angle increases relative to the western part of the Sunda Arc. The deepest earthquakes were up to 647 km.

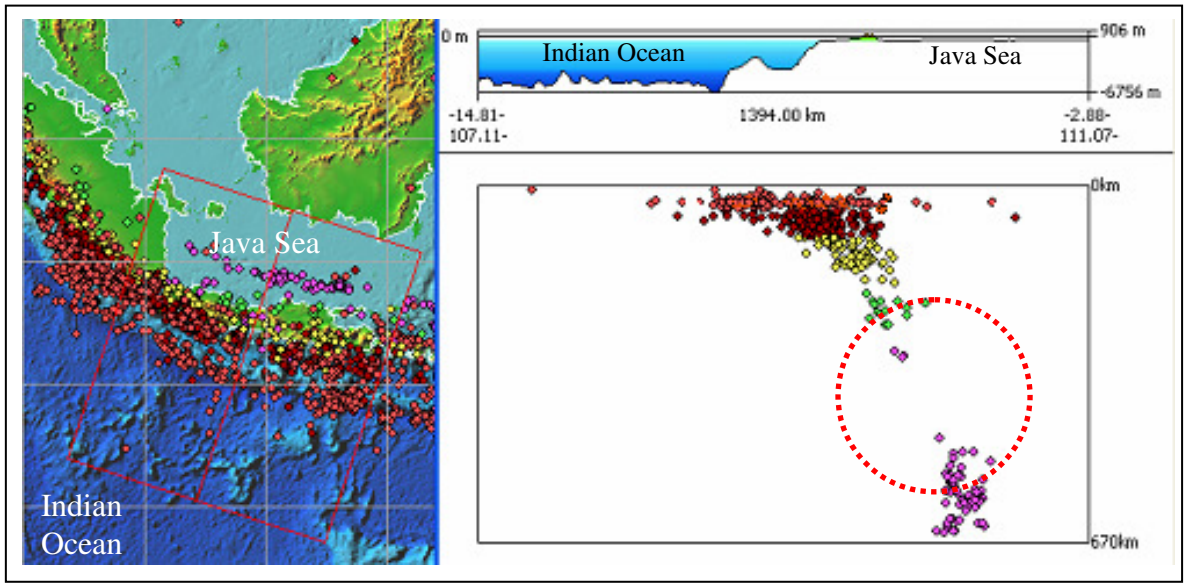

Figure 2.21. Cross-section of seismicity across the Java subduction-zone. A discontinuity occurs at depth of 220-500 km as shown by the red dotted circle. The red dot represent a shallow earthquake up to 100 km depth, yellow up to 200 km, and green up to 300 km, purple up to 700 km (Source: ITDB/PAC2004).

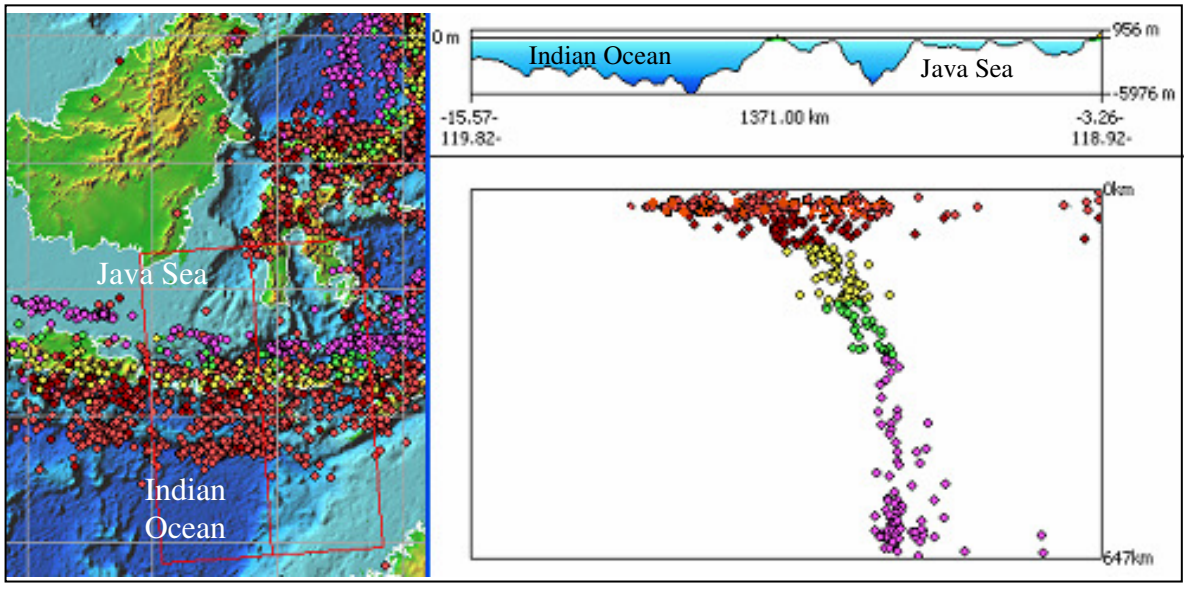

Figure 2.22. Cross-section of seismicity at the eastern end of Sunda Arc across the Nusa Tenggara islands The red dot represent a shallow earthquake up to 100 km depth, yellow up to 200 km, and green up to 300 km, purple up to 700 km (Source: ITDB/PAC2004).

The Banda Arc

The cross section of seismicity projected perpendicular to the strike of the trench for the Banda Arc region is divided into three major areas due to the subduction of the continental plate into the island arc off Timor, Tanimbar and Seram islands, and the westward movement of the Pacific Plate relative to the Eurasian Plate. This intersection region of three major plates, Eurasia, Indo-Australia, and Pacific, is one of the most complex tectonic areas in the world (Das, 2004).

The Australian Plate subducts northwards at a velocity of 8 cm/year, while the westward motion of the Pacific Plate relative to the Eurasian Plate, at a velocity of ~9 cm/year, is accommodated by west-southwestward subduction along the Seram Trough (Das, 2004 and Bock et al., 2003). As a result, the Banda subduction-zone has one of the highest curvatures of any major subduction-zone on Earth. This is reflected in the seismicity from the surface down to ~650 km depth, although the seismicity is very non-uniform, both along the arc and with depth (Das, 2004). Several discontinuities occur at 100 – 450 km and 350 to 670 km depths at different portions of the arc, as illustrated in Figures 2.23-25. Milsom (2001) reported that the shallow earthquake distribution (less than 25 km) is confused or scattered compared to deeper earthquakes confirmed and concluded this a two slab model of Banda Arc subduction. Figures 2.24 and 2.25 shows the seismicity becomes shallower from west to east. The distribution at Seram is also sparse (fewer events) than for Timor and Tanimbar

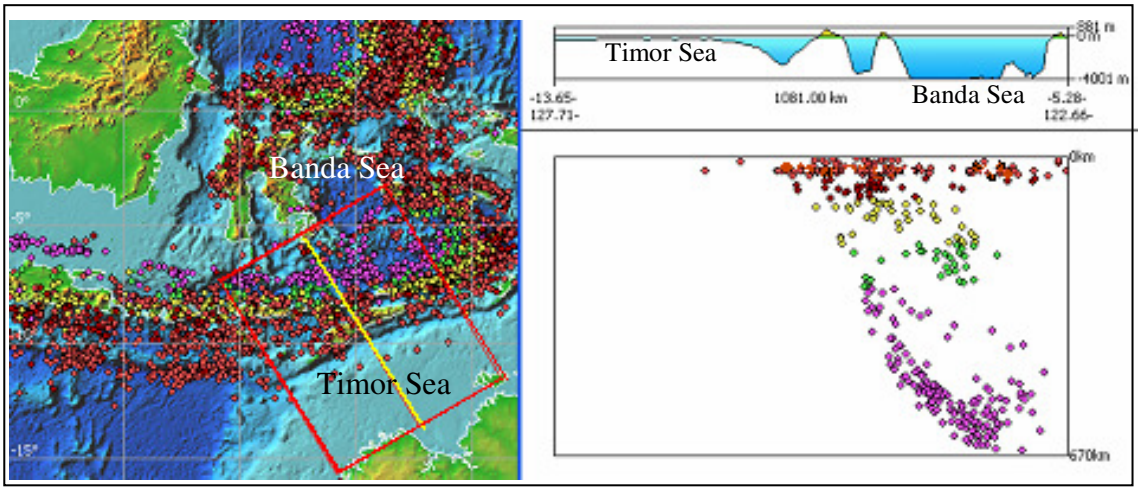

Figure 2.23. Cross-section of seismicity for the Timor Trough that reaching 670 km depth. The red dot represent a shallow earthquake up to 100 km depth, yellow up to 200 km, and green up to 300 km, purple up to 700 km (Source: ITDB/PAC2004).

Two opposing subducted slabs are clearly identified through the east-west cross-section of the Molluca sea collision zone (Figure 2.26). The westward-subducting slab dips more steeply than the eastward, as inferred from high-resolution tomographic-imaging (Widiantoro and Hills, 1997). The distributions of the shallow earthquakes are almost uniform throughout the region, and mostly involve thrust earthquakes that have a high tsunamigenic potential.

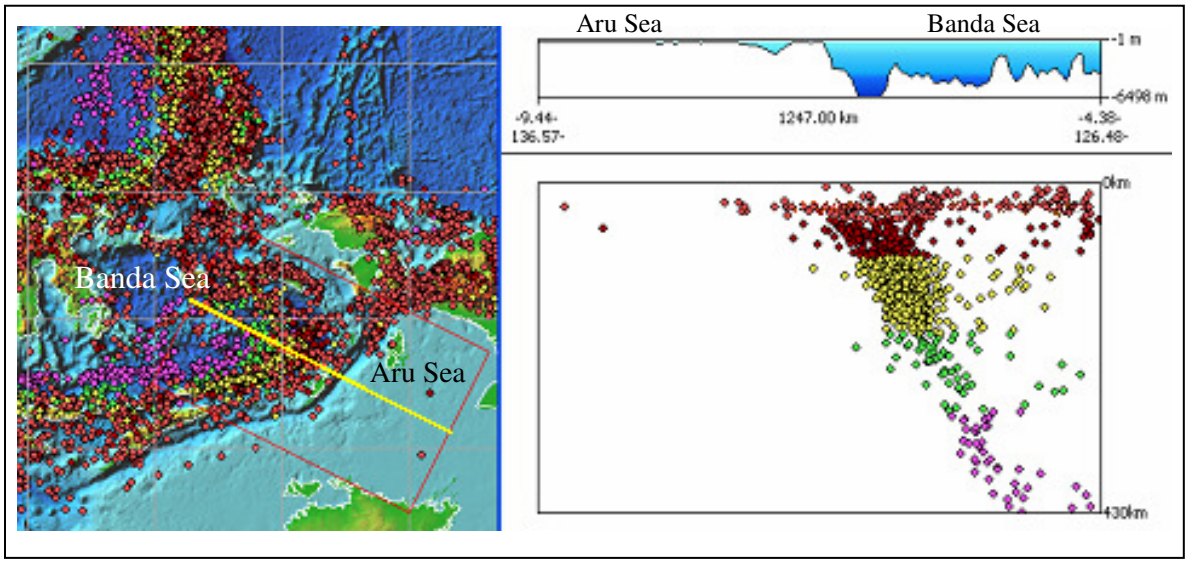

Figure 2.24. Cross-section of seismicity for Tanimbar Island areas. The maximum earthquake depths are less than for the Timor trough. The red dot represent a shallow earthquake up to 100 km depth, yellow up to 200 km, and green up to 300 km, purple up to 700 km (Source: ITDB/PAC2004).

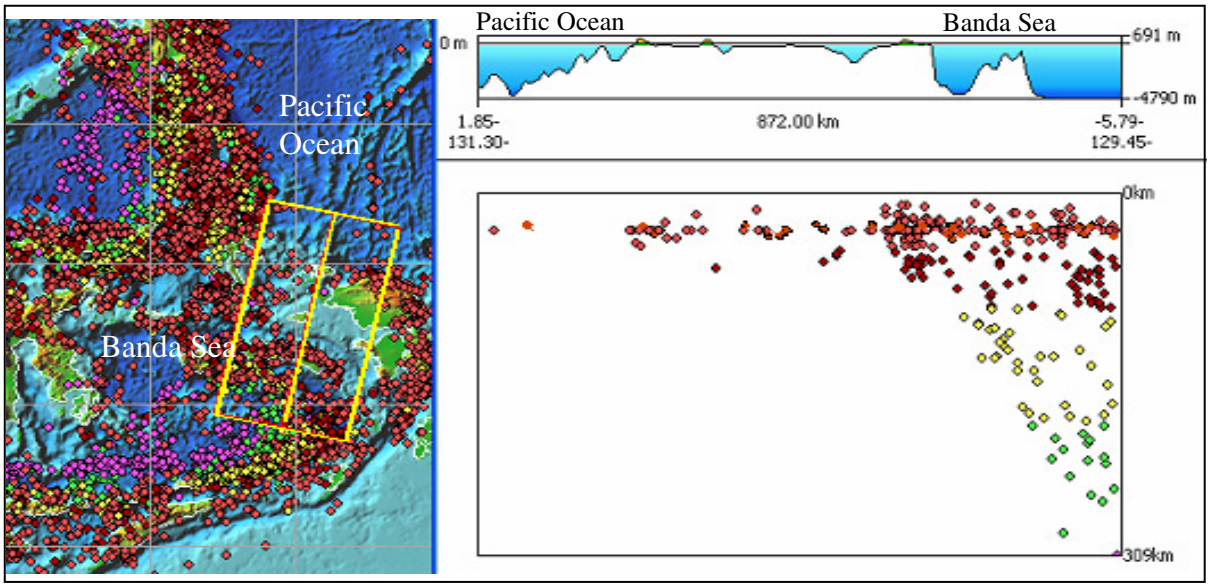

Figure 2.25. Cross-section of seismicity for at Seram Island areas. The hypocenters are shallower than for Timor and Tanimbar. The red dot represent a shallow earthquake up to 100 km depth, yellow up to 200 km, and green up to 300 km, purple up to 700 km (Source: ITDB/PAC2004).

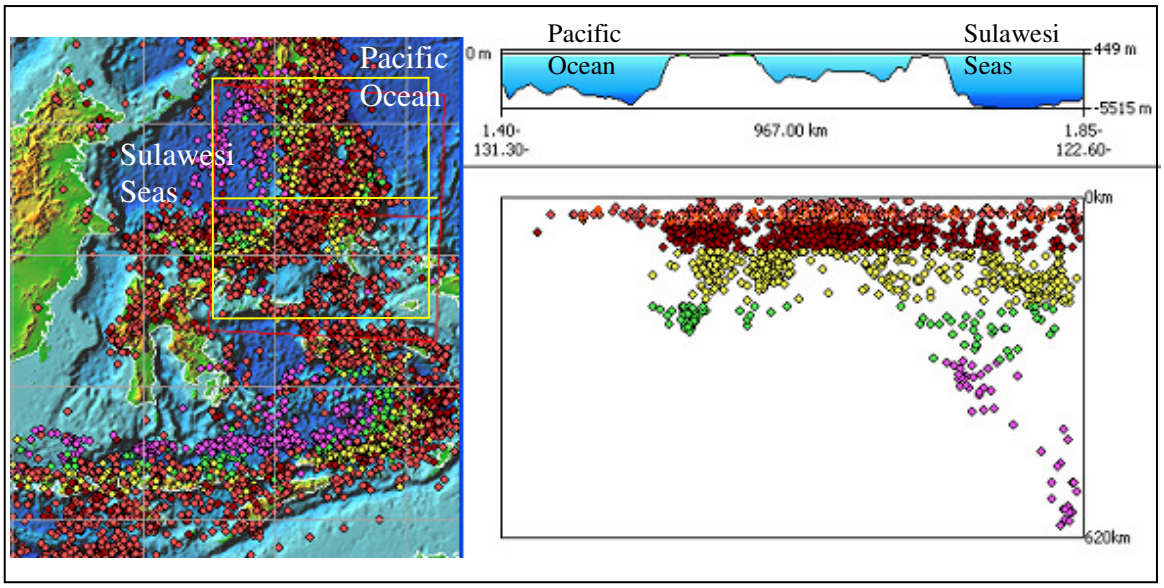

Figure 2.26. Cross-section of seismicity for the Molluca Collision Zone that reaching 620 km depth. The red dot represent a shallow earthquake up to 100 km depth, yellow up to 200 km, and green up to 300 km, purple up to 700 km (Source: ITDB/PAC2004).

Northern Sulawesi Island.

The northern arm of the Sulawesi Island seismicity cross-section (Figure 2.27) shows the earthquake distribution from the Celebes Sea (Sulawesi Sea) to Tomini Bay. This subduction-zone mostly produces shallow thrust earthquakes. The pattern and orientation of shallow earthquake stresses are perpendicular to the structural trend of Sulawesi Island (Puspito, 1995). The low dip angle of the subducted plate and sparse distribution of the earthquakes with depth are evident, as well as concentration of the intermediate earthquakes at a depth of ~210 km.

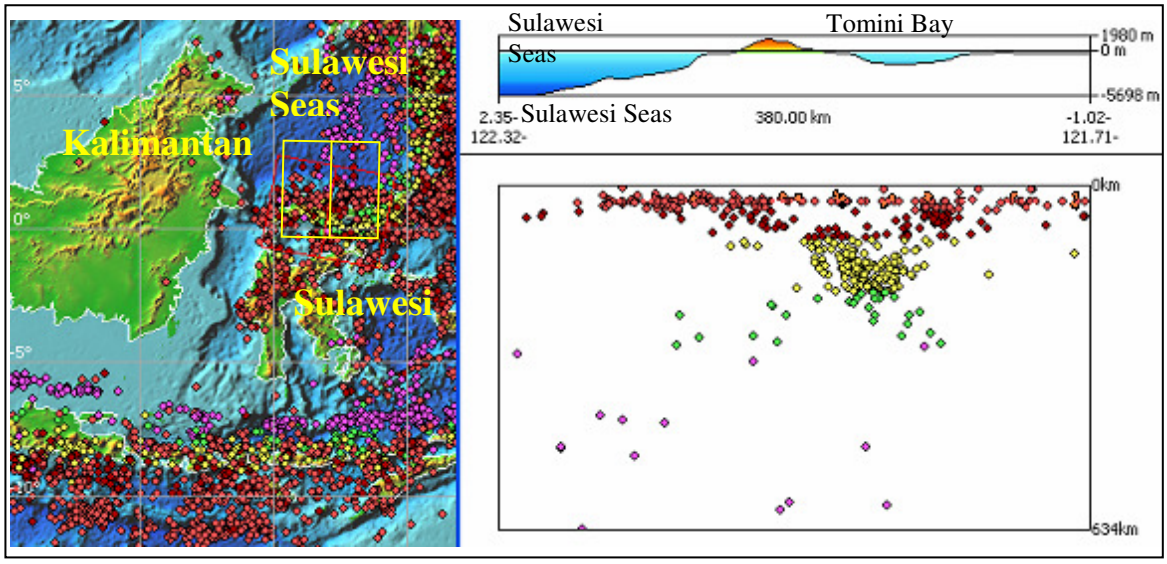

Figure 2.27. Cross-section of seismicity for Northern Sulawesi Island. Note the concentration of intermediate depth earthquakes at a depth of ~ 150 km. The red dot represent a shallow earthquake up to 100 km depth, yellow up to 200 km, and green up to 300 km, purple up to 700 km (Source: ITDB/PAC2004).

Makassar Straits

Unlike the rest of Indonesia, where seismic activity is triggered by a subduction-zone system, the movement of two major fault zones that cross Makassar Strait dominates this region. Most earthquakes have occurred close to the western coast of Sulawesi Island, where the transform faults (Paternoster and Palu-Koro) start to cross the Makassar Strait towards Kalimantan. The focal mechanisms of large shallow earthquakes are dominated by thrusting and strike-slip movements, which are produced by these two fault zones (Puspito, 1995). The compression (P) and tension (T) axes for shallow earthquakes within the backarc rift of the Makassar Strait and the northern Sulawesi subduction-zone are generally perpendicular to the structural trend of Sulawesi Island. The fault slip distribution is also similar to the compression axes pattern, which means that it is likely that Makassar Strait will continue to experience the same type of thrust and strike-slip earthquakes as observed in the past (Puspito and Triyoso, 1994). The cross section of seismicity is illustrated in Figure 2.28, where the deepest hypocenter reaches 130 km below the surface and events are sparse.

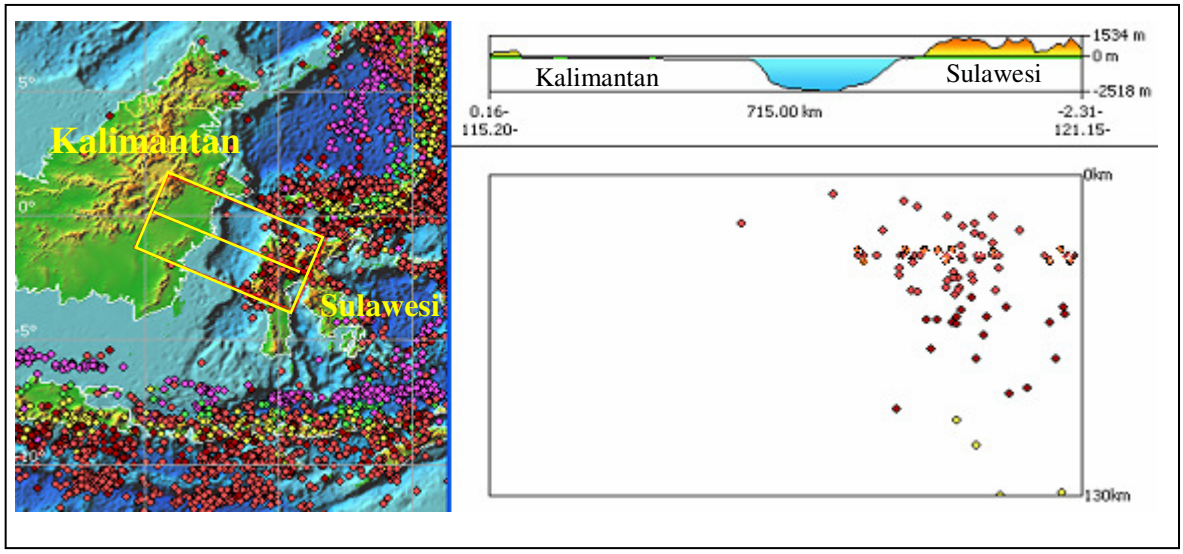

Figure 2.28. Cross-section of seismicity for Northern Sulawesi Island that reaching 130 km depth. The red dot represent a shallow earthquake up to 100 km depth, yellow up to 200 km (Source: ITDB/PAC2004).

2.5. Past Seismic Tsunami events

Based on available tsunami record (ITDB/PAC2004; Rynn, 2002; Prasetya et al., 2001; Hamzah et al., 2000), most Indonesian tsunami have been generated by earthquakes (90%), with the remainder due to volcanic eruption (8%), landslides (1%)

or un-identified processes (1%). Rynn (2002) and Hamzah et al. (2000) noted that a total of 105 tsunamis had been generated for the period of 1600 – 1999 while the ITDB/PAC2004 databases shows a total of 181 events up to 2004 including the great Sumatra earthquake and tsunamis on 26 December 2004 and the Nias earthquake and tsunamis on 28 March 2005. The last two events in 2006 (South Java tsunami) and 2007 (Bengkulu tsunami) made a total number of tsunamis of 183 up to 2007. Prasetya et al. (2001) analyzed the data set from 1900 to 2000 and noted that only 18 tsunamis with clear evidence had been generated. Fourteen (14) of them occurred in the eastern part of the Indonesian Archipelago (from Makassar Strait to the Banda Arc). Eight (8) of the 14 events occurred in the Makassar Strait, and involved secondary submarine slumping/landslides as secondary generating mechanism as occurred during the Flores 1992 and Biak 1996.

Therefore it is necessary to further investigate historical tsunamigenic earthquakes to determine whether a secondary generating mechanism was involved. In particular it is important to identify any event whose tsunamis are significantly larger than expected from the seismic magnitude. The distribution of historical earthquake tsunamis with clear evidence since 1900 is illustrated in Figure 2.29a. Figure 2.29b, divides these events into zones based on the inferred primary and secondary mechanism.

Based on the historical record, tsunamis from the earthquakes sources since AD 1600 along the Sumatra segment of the Sunda trench (subduction zone) have been produced by large or mega-thrust earthquakes with magnitudes ranging from 7.9 (the 1907 event) to $M_w > 9.0$ (the 26 December 2004 event). In contrast, the Java segment is characterized by tsunami earthquakes (Okal and Synolakis, 2008), with two interplate events (2 June 1994 and 17 July 2007), and 1 intraplate event (11 September 1921). All events had magnitudes less than M_w=8. The last segment of the Sunda Arc along the Lesser Sunda from Bali to Sumba had one event since 1900 (19 August 1977) associated with normal faulting with $M_w = 8.0$. There is a gap along the Sunda Arc between the Sumatra and Java segment where there is no historical record of large tsunamigenic earthquakes.

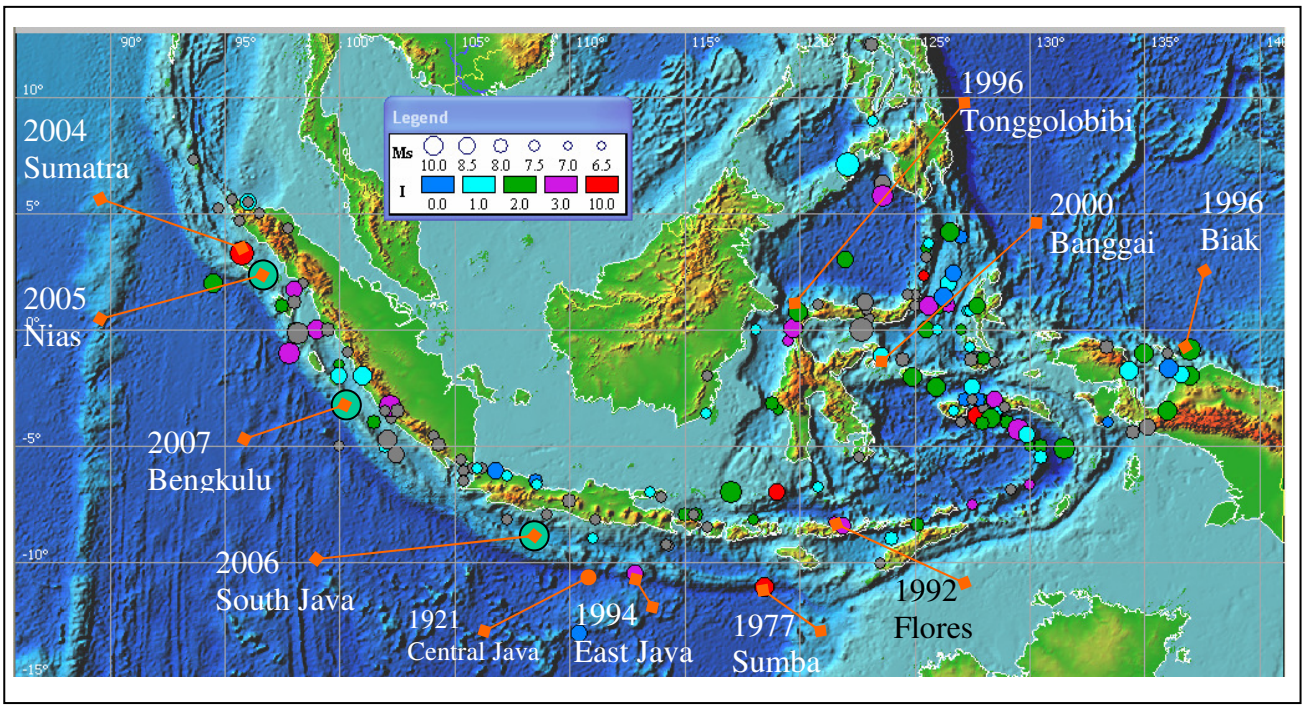

Figure 2.29a. The distribution of major earthquake and tsunamis with clear evidence since 1900. Since 1992, tsunamis are more frequent, either due to increase seismicity or better communication such as TV, Radio or newspaper. (Base map source: ITDB/PAC2004).

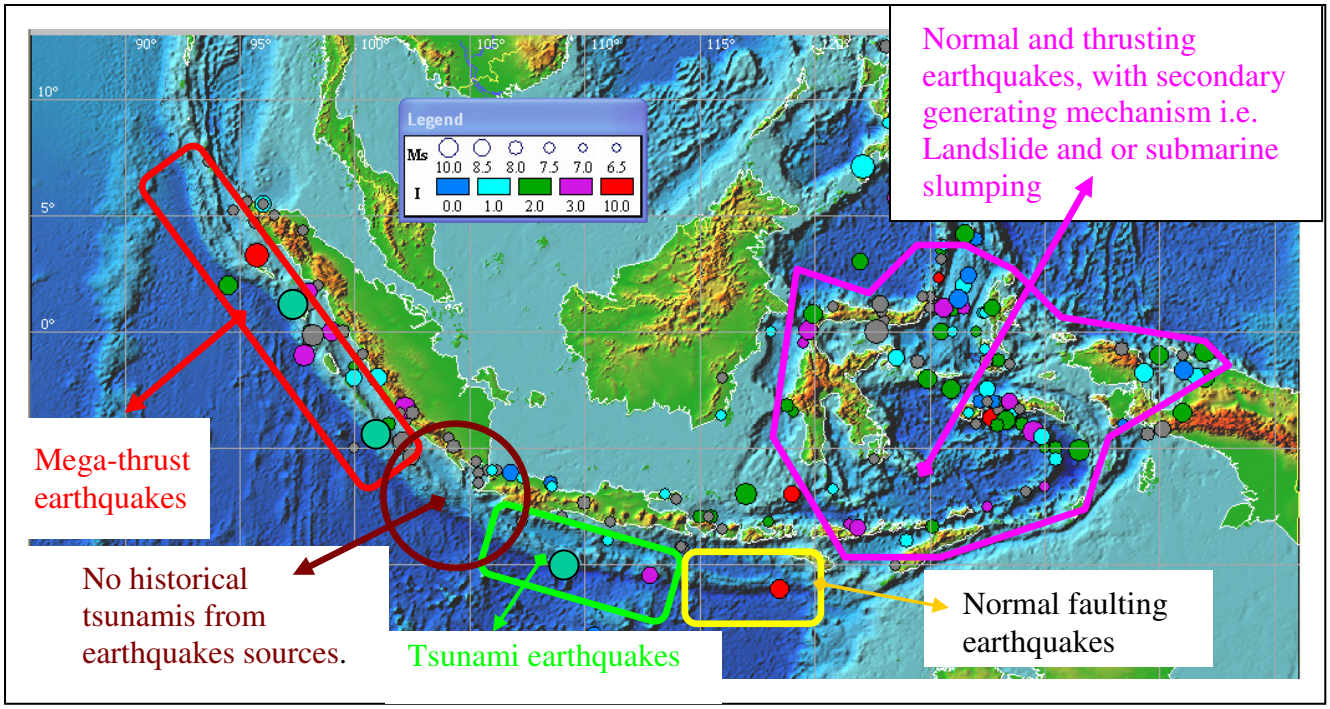

Figure 2.29b. Tsunami source zones, showing the variety of mechanisms of tsunamigenic earthquake from mega-thrust earthquakes at the western end of the archipelago to mixed mechanisms in the east (Base map source: ITDB/PAC2004).

2.6. Volcanogenic Tsunamis

A major volcanic arc occurs along the Indonesian Archipelago from west (Sunda Arc) to the east (Banda Arc) as illustrated in Figure 2.30. Some of these volcanoes are associated with multiple tsunami events as recorded by historical data.

Figure 2.30. Active volcanoes along the Indonesian Archipelago, including sub-aerial and submarine volcanoes (Source: USGS).

At least 9 tsunamis have been linked directly to volcanic eruptions in the Indonesian Archipelago (Prasetya, 1998; Hamzah, 2000); Krakatau Island in 416 AD and 1883, Tambora on Sumbawa Island in 1815, Rokatinda on Flores Island in 1928, Ruang Island in 1889, Awu Island in 1856 and 1892, Gamkonora Island in 1673, and Gamalama Island in 1871. More events are highly possible, especially from the volcanic Arc surrounding the Banda Sea such as Bandi Api, Serua, Nila and Teon, Halmahera (Makian) and Sangihe (Karangetang) including the north Sulawesi volcanic island of Una-Una in Tomini Bay. Weh Island at the tip of Sumatra, offshore Banda Aceh has been suspected of generating a tsunami during a Pleistocene eruption that resulted in the partial collapse of an older center that was then breached and filled by the sea. The distributions of historical volcanic tsunamis and possible sources for

future events are illustrated in Figure 2.31. Most of the volcanoes that are likely to generate tsunamis based on the historical record, are located at the eastern end of Sunda Arc (Flores Island) and along the Banda Arc, and Halmahera and Sangihe volcanic arcs as part of Molluca collision zone. The Sunda Arc is represented by Weh Island located at the northern-tip of Sumatra, the Krakatau volcanic complex in Sunda Strait, and Tambora Volcano on Sumbawa Island.

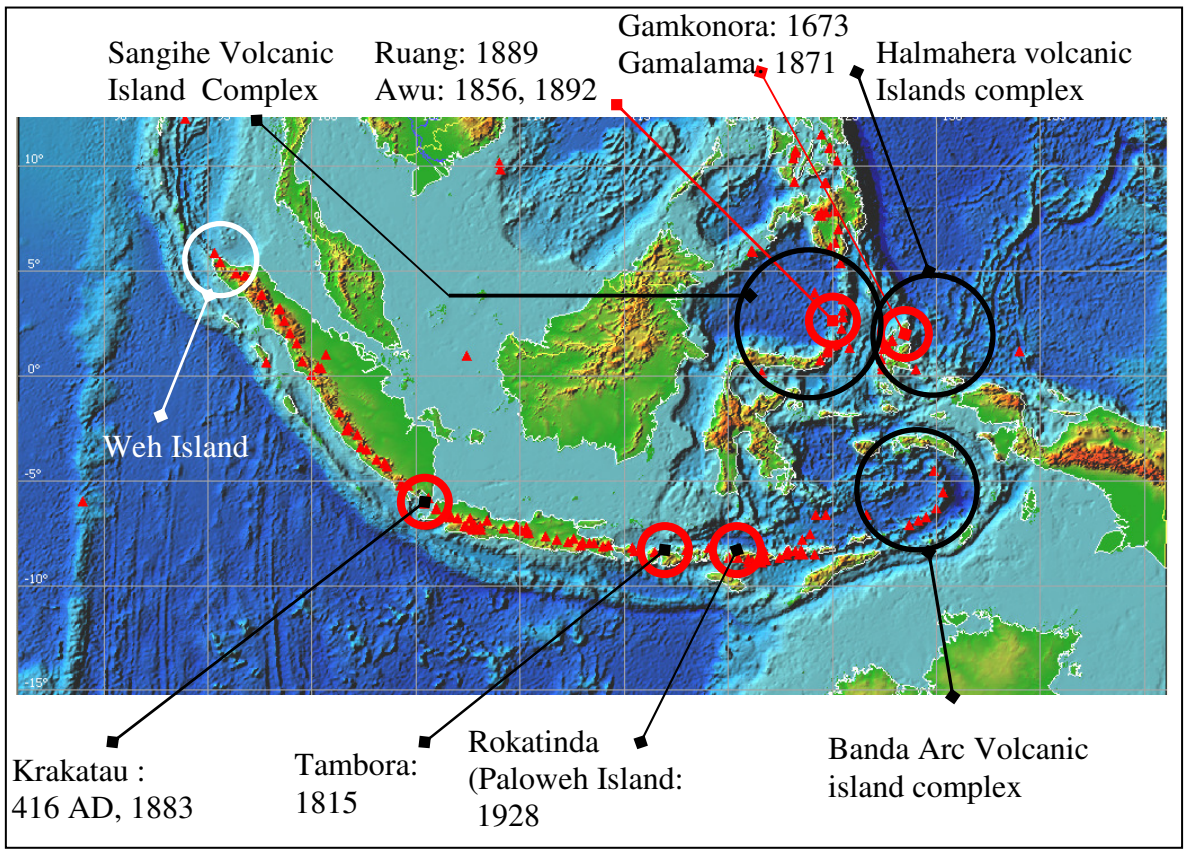

Figure 2.31. Historical volcanic tsunamis (red circles), volcanic island complexes (black circles), and potential Weh Island source (Base map source: ITDB/PAC 2004).

Accounts of volcanic activitiy for this region are mainly from the Catalog of Active Volcanoes (Newmann van Padang, 1951), Data Gunung Api Indonesia (catalogue of Indonesian Volcanoes with eruptions in historical time) by Kusumadinata, (1979), and the electronic database of the Global Volcanism Program, Smithsonian National Museum of Natural History (http://160.111.247.173/world) .

2.6.1. Volcanic Tsunami sources along the Sunda Arc

Weh Volcanic Island

Weh Island is located offshore of the northern part of Banda Aceh Province at the northwestern end of Sumatra Island in the Andaman Seas (Figure 2.32). It has been interpreted as the remains of a partially collapsed or remnant of an older center that has been breached to the northwest and filled by the sea during the Pleistocene that might be able to cause tsunamis (Kusumadinata, 1979).

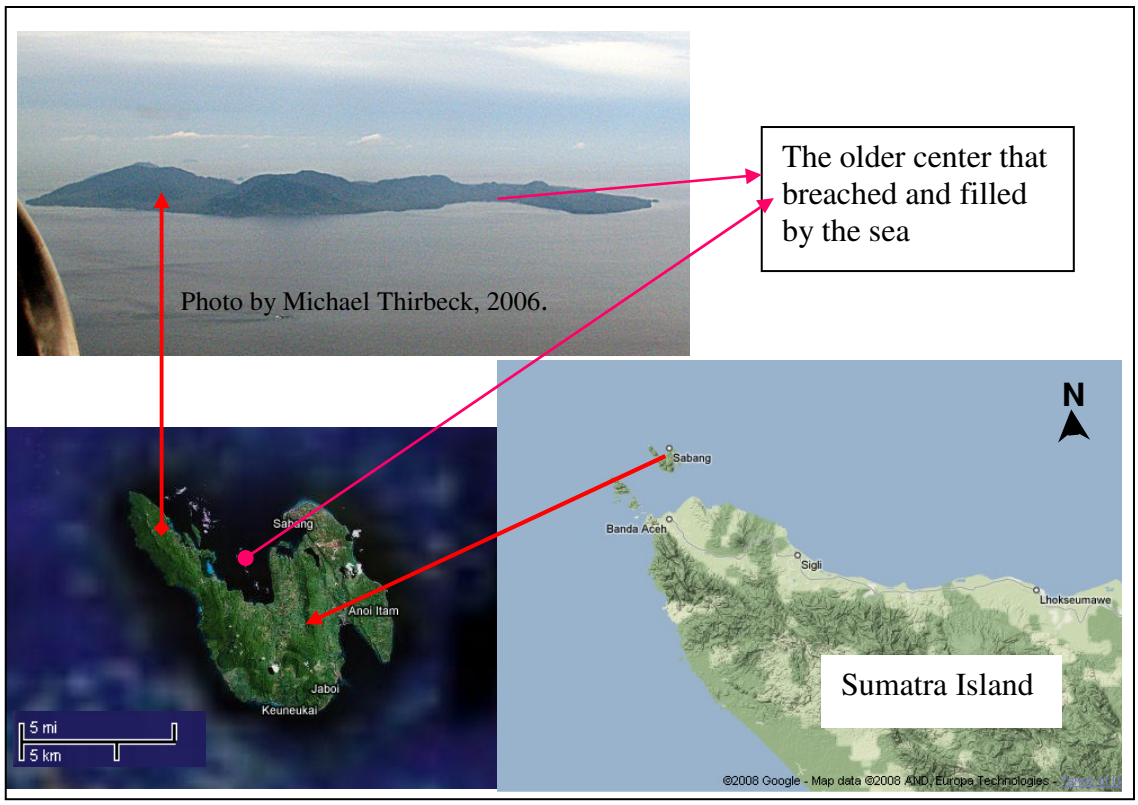

Figure 2.32. Location of Weh Volcanic Island at the tip of northwestern Sumatra Island (Banda Aceh Province, Indonesia). Above is the aerial photo looking down from the northwest to the southwest. Below (left) is the satellite image showing the older center. (Image and map: Google earth and Google map).

Krakatau Island

The Krakatau Island volcanic complex is located in the Sunda Strait between Java and Sumatra Islands (Figure 2.33). The largest tsunami event in recorded history was the Krakatau eruption in 1883, which caused a death toll of 36,000 people. It was followed by the Tambora explosion in 1815 that generated tsunamis in the Java and Flores seas.

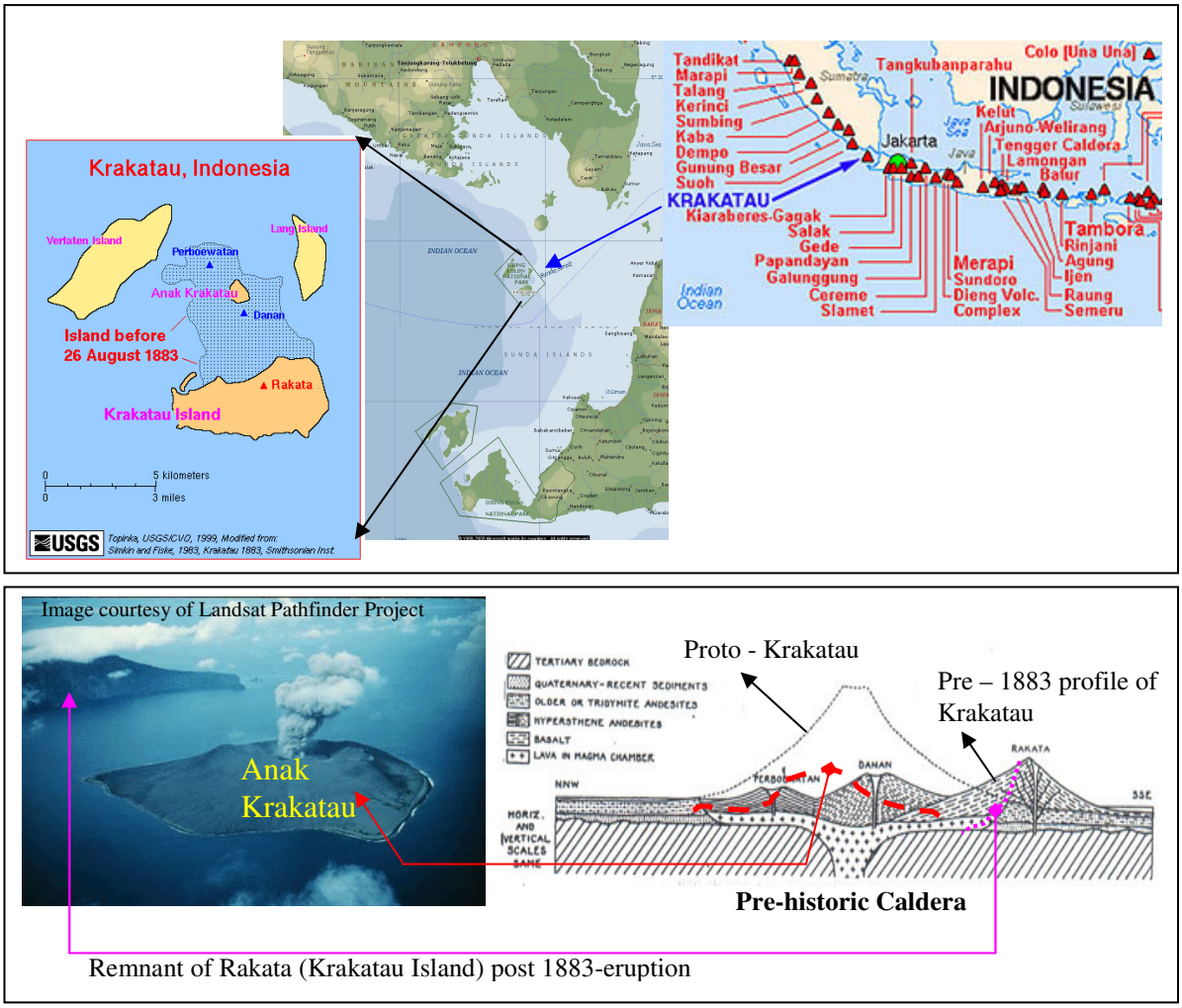

Figure 2.33. The location of Krakatau Volcano in Sunda Straits (above), and the sequence of eruptions from the proto-Krakatau before 1883, after 1883, and the newborn volcano with position in between former Perboewatan and Danan crater (below). Figure modified from Simkin and Fiske (1983).

The Krakatau eruption in 1883 and its impacts are well documented (Simkin and Fiske, 1983). The event has been extensively researched to understand the processes of the eruptions and tsunami generating mechanisms (Latter, 1981; Self and Rampino, 1981, 1982; Sigurdsson et al., 1991a, b; Deplus et al., 1995; Carey et al., 1996; Mandeville et al., 1996; Nomambhoy and Satake, 1997; Prasetya et al., 2000; Freundt, 2003; Spicak et al., 2002; Choi et al., 2003; Mader and Gittings, 2006). Krakatau has erupted sequentially since 416 AD, when a major event destroyed the ancient Krakatau and formed a caldera 7 km wide. The eruption in 1883 left almost the same size of the caldera, and subsequently a new volcano has formed in 1928, which has frequently erupted since then. Four mechanisms had been proposed for tsunami generation during the Krakatau 1883 events: the submarine explosions, caldera

collapse, pyroclastic flows and flank collapse/debris avalanche. Prasetya (1998) based on physical and numerical modeling experiment suggested that the pyroclastic flow is the main generating mechanism for the largest tsunamis during the 1883 event.

Tambora Volcano

Tambora is a stratovolcano, occupying the whole Sanggar Peninsula of Sumbawa Island (Figure 2.34). Its eruption in 1815 was one of the largest eruptions in recorded history and produced global climate effects (Stothers, 1984; Sigurdsson and Carey, 1992). The pyroclastic flows produced by the eruption reached the seas on all sides of peninsula, and generated tsunamis in the Java and Flores Seas. However, there is no record of the impact of tsunamis along the coasts of Java and the Flores Seas. The salt-water lake on Satonda Island north of Tambora Volcano is suggested to have originated from the tsunamis that overtopped the Island during the event. The summit elevation is 2850 above sea level and the known eruption after 1815 was in 1967 (Kusumadinata, 1979).

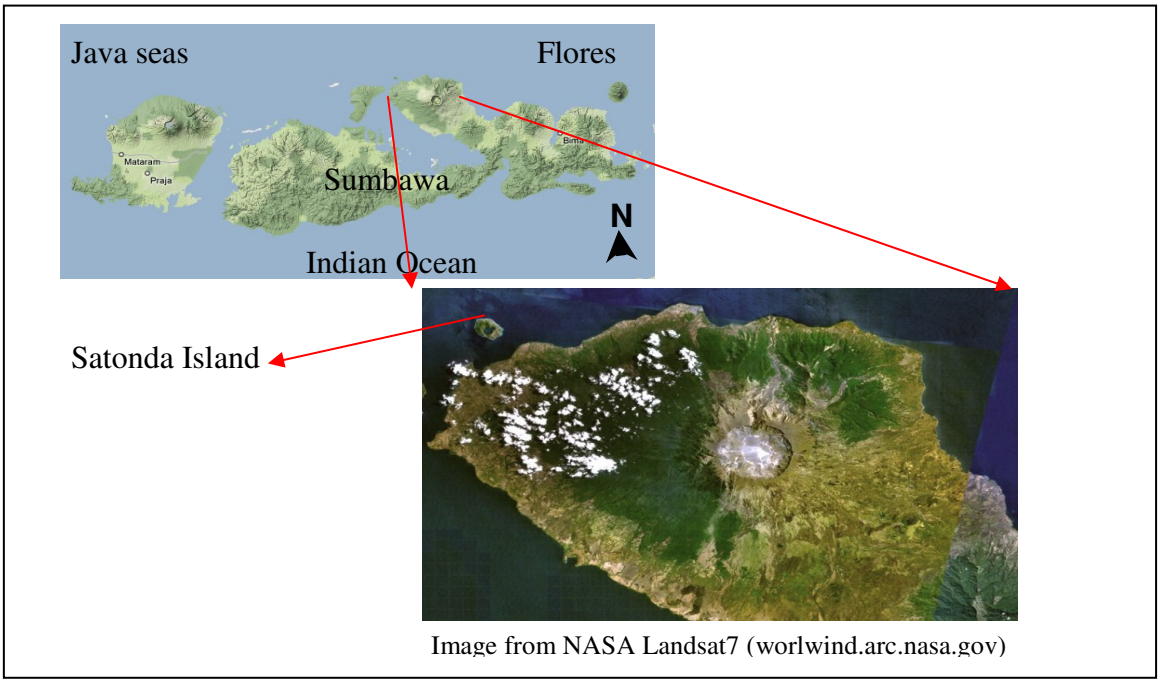

Figure 2.34. The Tambora Volcano located at Sanngar Peninsula, Sumbawa Island. The white circular structure on the Landsat 7 image (NASA) is the caldera. (Image and map: Google earth and Google map).

Sangeang Api Volcanic Island

Sangeang Api Volcano is stratovolcano and forms a small 13 km wide island to the northeast of Sumbawa Island (Figure 2.32). It has two large trachybasaltic-to-

tranchyandesitic volcanic cones ~ 1949 m high Doro Api at the center and 1795 m high Doro Manoti on the eastern rim (Kusumadinata, 1979). Flank vents occur on the south side of Doro Mantoi and near the northern coast. Historically, eruptions have been recorded since 1512; however, there is no data about the eruption processes.

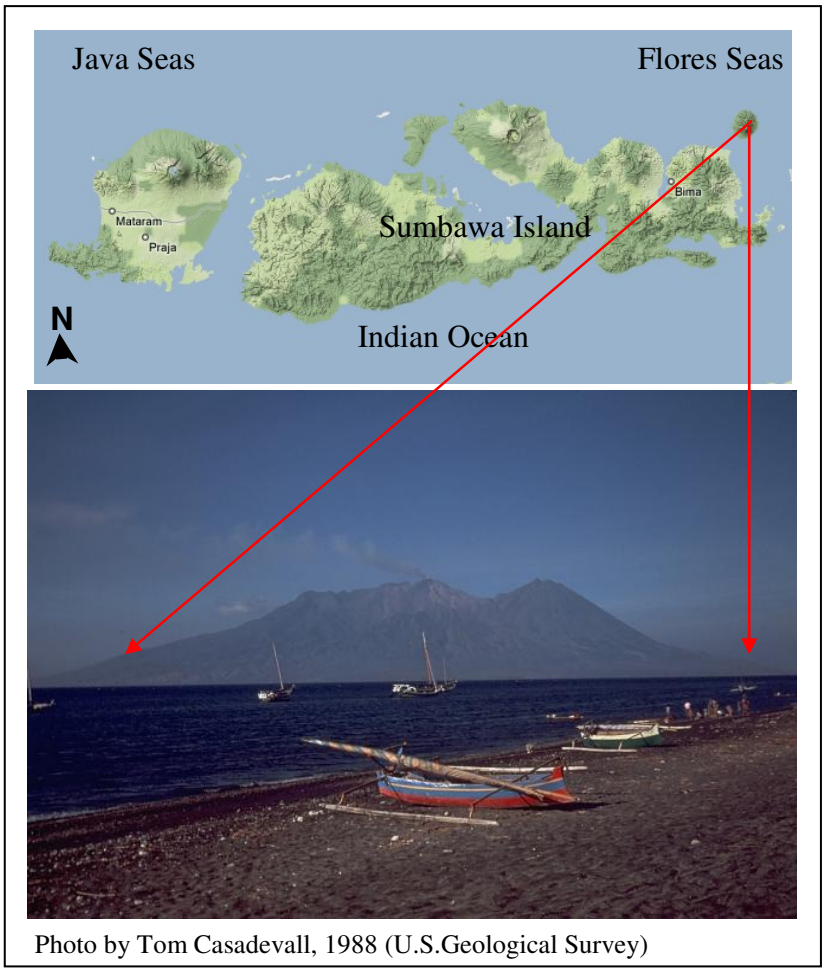

Figure 2.35. The location of Sangiang Api Volcano ~ 11 km from the shoreline of Sumbawa Island in the Flores Sea. (Image and map: Google earth and Google map).

Iya Volcano

Iya Volcano is stratovolcano, located on a small peninsula south of the city of Ende on Central Flores Island, facing the Savu Sea (Figure 2.36). It is the southernmost of a group of three volcanoes, where the cones to the north, Rooja and Pui, appear to be slightly older than Iya (Kusumadinata, 1979). The southern side of Iya drops steeply to the sea (Savu Sea). It has had numerous moderate explosive eruptions during historical times; however, there are no data in relation to the eruptions and associated processes.

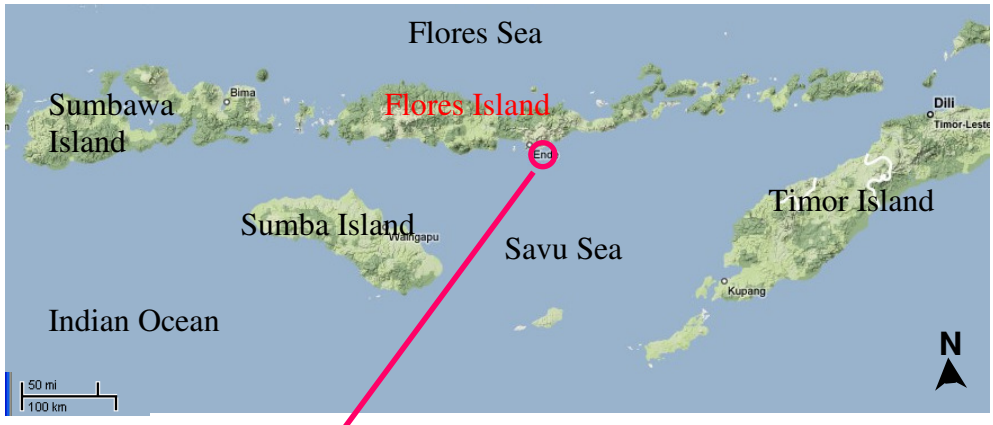

Photo by Ruska Hadian, 1985 (Volcanological Survey of Indonesia)

Figure 2.36. The location of Iya Volcano at the tip of a small peninsula, south of Ende City, Flores Island. (Image and map: Google earth and Google map).

Rokatinda (Paluweh) Volcano

Rokatinda Volcano is stratovolcano that forms an 8 km wide island, and about 22 km from offshore Flores Island in the Flores Sea (Figure 2.37). The volcano rises about 3000 m above the sea floor, and the summit is about 875 m above sea level. The broad irregular summit region contains overlapping craters up to 900 m wide and several lava domes. Several flank vents occur along a NW-trending fissure (Kusumadinata, 1979). The largest historical eruption of Rokatinda occurred in 1928, when a strong explosive eruption was accompanied by landslide-induced tsunamis and lava dome emplacement. The last known eruption was in 1985 (Volcanology Survey of Indonesia Annual report, 1986).

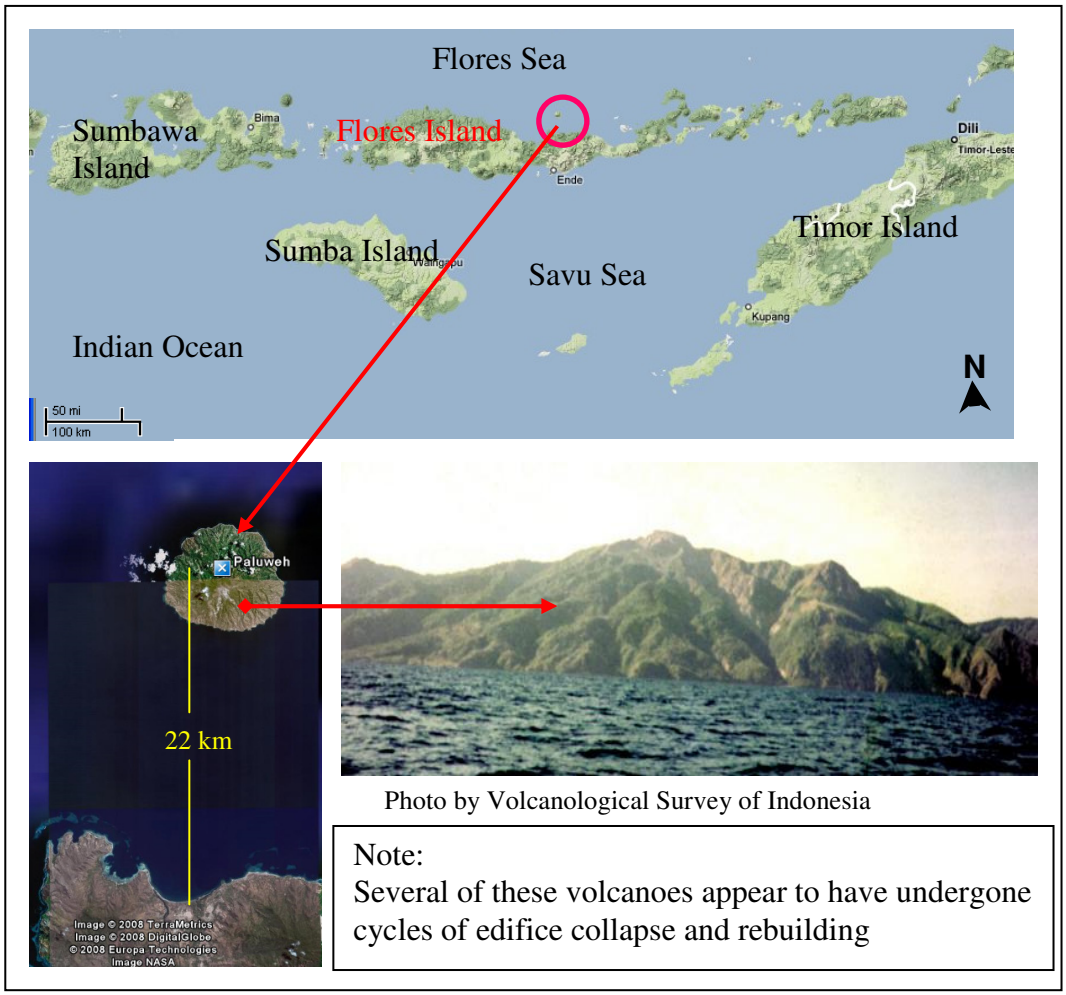

Figure 2.37. The location of Rokatinda volcanic island, 22 km offshore of Flores Island. (Image and map: Google earth and Google map).

Lewotolo Volcano

Lewotolo is a symmetrical stratovolcano as viewed from the north and east and rises to 1423 m (Figure 2.38). A small cone with a 130-m-wide crater constructed at the southeast side of a larger crater forms the volcano's high point (Kusumadinata, 1979). Many lava flows have reached the coastline. Historical eruptions, recorded since 1660, have consisted of explosive activity from the summit crater. There are no documented reports about tsunamis from this source even though it is clear that this volcano is able to cause tsunamis within the Flores Sea.

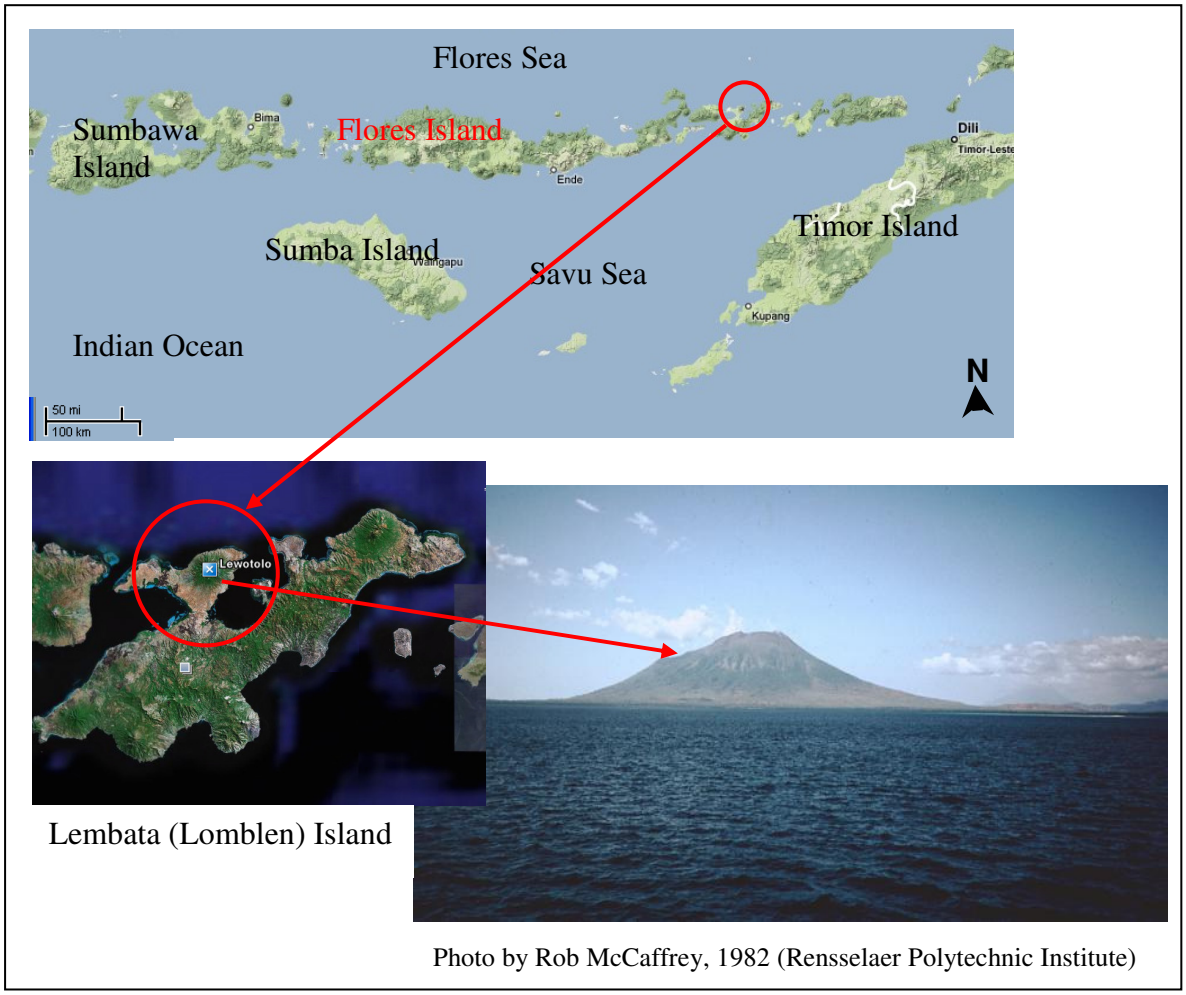

Figure 2.38. The location of Lewotolo volcano on the northern part of Lembata Island. (Image and map: Google earth and Google map).

Batutara Volcano

Batu Tara volcano is a small isolated island in the Flores Sea about 50 km north of Lembata (fomerly Lomblen) Island, which has the local name Komba Island (Figure 2.39). It contains a scarp on the eastern side, similar to the Sciara del Fuoco of Italy's Stromboli volcano (Kusumadinata, 1979). Vegetation covers the flanks of Batu Tara to within 50 m of the 748-m-high summit. Batu Tara lies north of the main volcanic arc and is noted for its potassic leucite-bearing basanitic and tephritic rocks. The first historical eruption from Batu Tara, during 1847-52, produced explosions and lava flows (Kusumadinata, 1979); however during those eruptions there was no observation on tsunami generation.

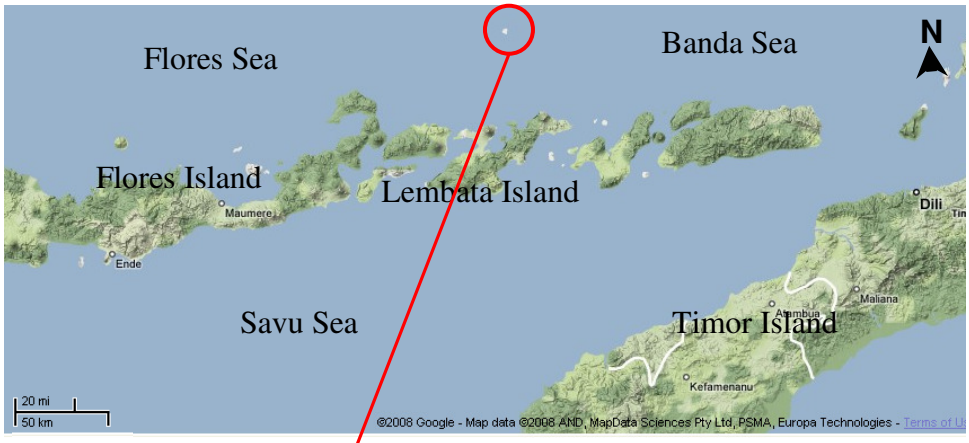

Photo by O. Rukman, 1981 (Volcanological Survey of Indonesia)

Figure 2.39. The location of Batutara volcano on the northern coast of Lembata Island, 50 km offshore in the Flores Sea. (Image and map: Google earth and Google map).

2.6.2. The Banda Sea Volcanic Island Arc complex

With a complex tectonic structure, there are subaerial volcanoes and a series of submarine volcanoes such as Emperor of China and Nieuwerkerk. The Catalog of active volcanoes of the world (Van Padang, 1951) described the Emperor of China, which is located in western part of Banda Sea, as erupting in 1893 and in 1927. However, it is uncertain if they existed, as these submarine volcanoes would have to receive their magma-supply from very great depth (greater than 500 km) whereas usually the offshore volcanoes east of Flores have magma sources near 50 to 250 km depth (Hedervari and Papp, 1981).

Wurlali Volcano

Wurlali is a stratovolcano, forming part of Damar Island, and it is the southwestern-most of the historically active volcano in the Banda Arc (Figure 2.40). The 868-m-high andesitic stratovolcano formed at the northern end of a 5-km-wide caldera on the eastern side of Damar Island in the Banda Sea. An explosive eruption in 1892 is the only known historic activity (Van Padang, 1951; Jezek and Hutchison, 1978; Kusumadinata, 1979).

Figure 2.40. The location of Wurlali Volcano in the Banda Sea. (Image and map: Google earth and Google map).

Teon Volcano

Teon Volcano is a stratovolcano, which is also known as Serawerna, the name of its active crater. Another smaller crater is located north-northeast of Serawerna as illustrated in Figure 2.41 Explosive eruptions have been recorded from the andesitic Teon Volcano since the 17th century. The largest historical eruption, in 1660, produced pyroclastic flows and surges and caused damage and fatalities (Kusumadinata, 1979). The horse-shoe crater on top of the Volcano shows a clear

evidence of edifice failure, as is also identified at White Island, New Zealand (Moon et al., 2008).

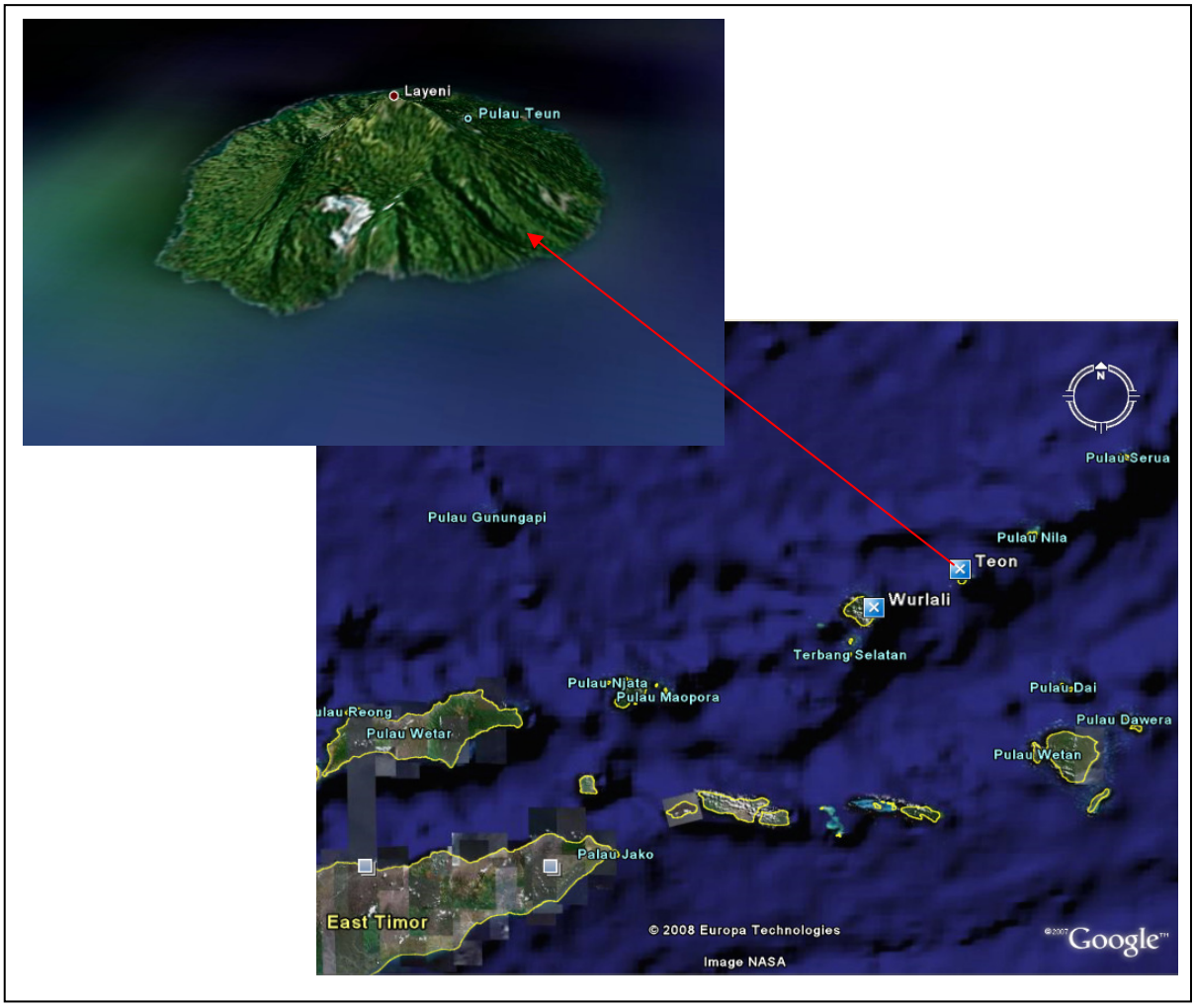

Figure 2.41. The location of Teon volcanic island between Wurlali and Nila Island in the Banda Sea. (Image and map: Google earth and Google map).

Nila Volcano

Nila Volcano is a 5 x 6 km volcanic island in the Banda Sea comprised of a low-rimmed caldera (Figure 2.42). The stratovolcano rim is breached at sea level to the south and east and contains a 781 m-high youthful forested cone. Phreatic eruptions from the dominantly andesitic Nila, also known as Laworkawra, have occurred from summit vents and flank fissures in historical time. A 1932 eruption from a fissure that extended from the summit to the southeast coast produced heavy ash fall that forced abandonment of Rumadai Village (Kusumadinata, 1979).

Photo by Ruska Hadian, 1975 (Volcanological Survey of Indonesia)

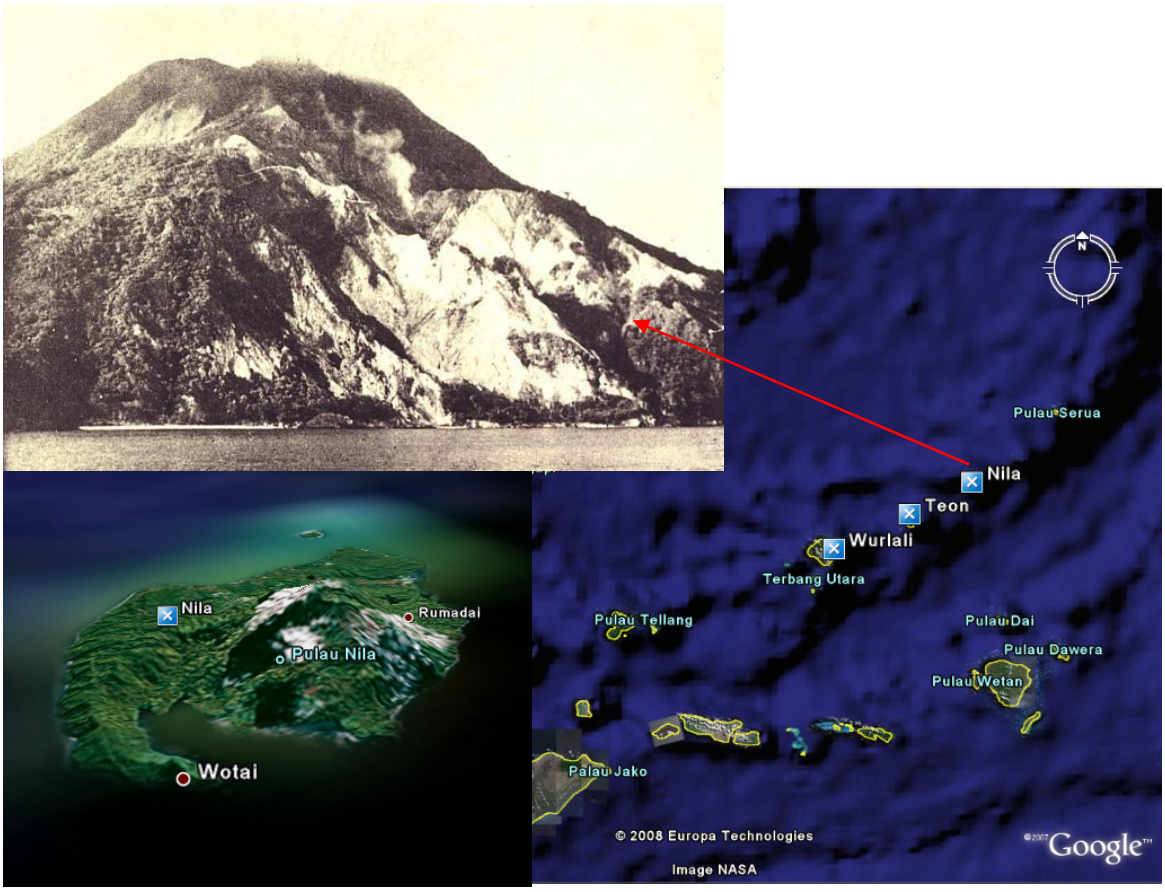

Figure 2.42. The location of Nila volcanic island in the Banda Sea. The photo shows the scarp on the volcano, and below (left) is view from Google earth shows the geometry of the island and the Rumadai villages. (Image and map: Google earth and Google map).

Serua Volcano

Serua Volcano is small volcanic island about 2 x 4 km with an emergent summit rising 3600 m above the Banda Sea floor (Figure 2.43). A truncated central cone surrounded by an old somma wall is capped by the 641-m-high Wuarlapna lava volcano. The andesitic Serua volcano, also known as Legatal, lies near the center of the Banda Arc and is one of the most active of the Banda Sea volcanoes, with many eruptions since the 17th century (Kusumadinata, 1979).

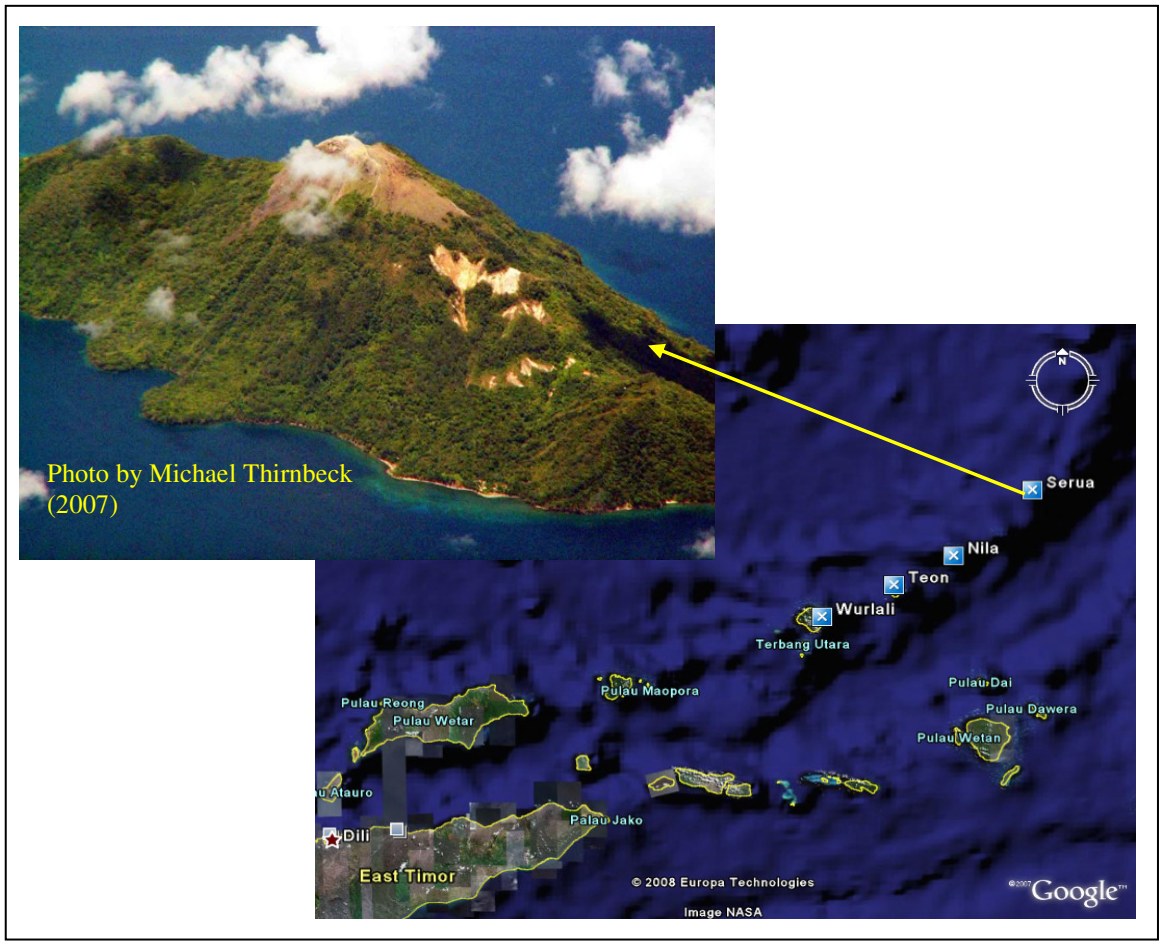

Figure 2.43. The location of Serua Volcano in the Banda Sea. This volcano has steep slopes on both sites. (Image and map: Google earth and Google map).

Manuk Volcano

Manuk Volcano is a small steep-sided island located at the easternmost-end of the Arcuate Banda volcanic arc. The 282-m-high truncated andesitic cone rises 3000 m from the sea floor (Figure 2.44). No confirmed historical eruptions are known from this uninhabitated island, although there was a report that a member of the 1874 Challenger Expedition saw smoke rising from the crater of Manuk (Global Volcanism Program, http://160.111.247.173/world)

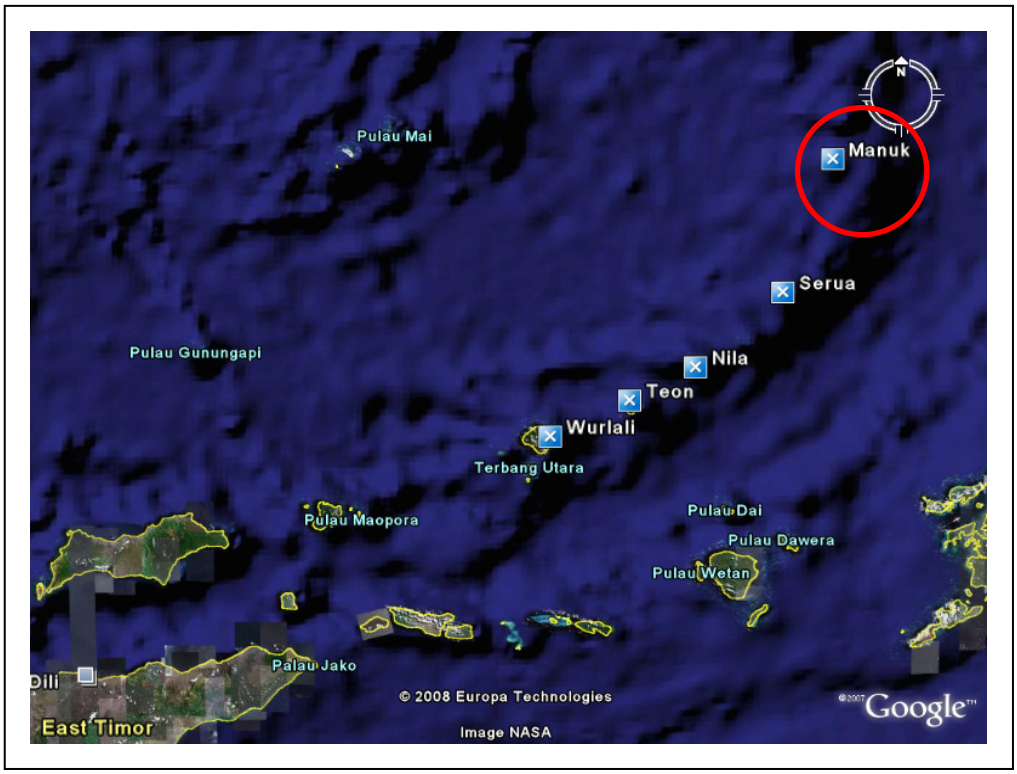

Figure 2.44. The location of Manuk Volcano in the Banda Sea. This volcanic island is small but is considered active by the Global Volcanism Program (http://160.111.247.173/world). (Image and map: Google earth and Google map).

Banda Api Volcano

The Banda Api Volcano is a small island volcano that was the northeasternmost volcano in the Sunda–Banda Arc (Figure 2.45). It has had a long period of historical observation because of its key location close to the thriving Portuguese and Dutch spice trade. The basaltic-to-rhyodactic Banda Api is located in the southwest corner of a 7 km wide mostly submerged caldera that comprises the northern most of a chain of volcanic islands in the Banda Sea (Kusumadinata, 1979). At least two episodes, of caldera formation are thought to have occurred, with the Arcuate islands of Lonthor and Neira considered to be the remnants of the pre-caldera volcanoes. Banda Api forms a conical peak rising to 640 m at the center of the 3 km wide Banda Api Island. Eruptions have been recorded since 1568, mostly consisting of strombolian eruptions from the summit crater. However, larger explosive eruptions have occurred, and occasional lava flows have reached the coast. There are no reports of tsunamis.

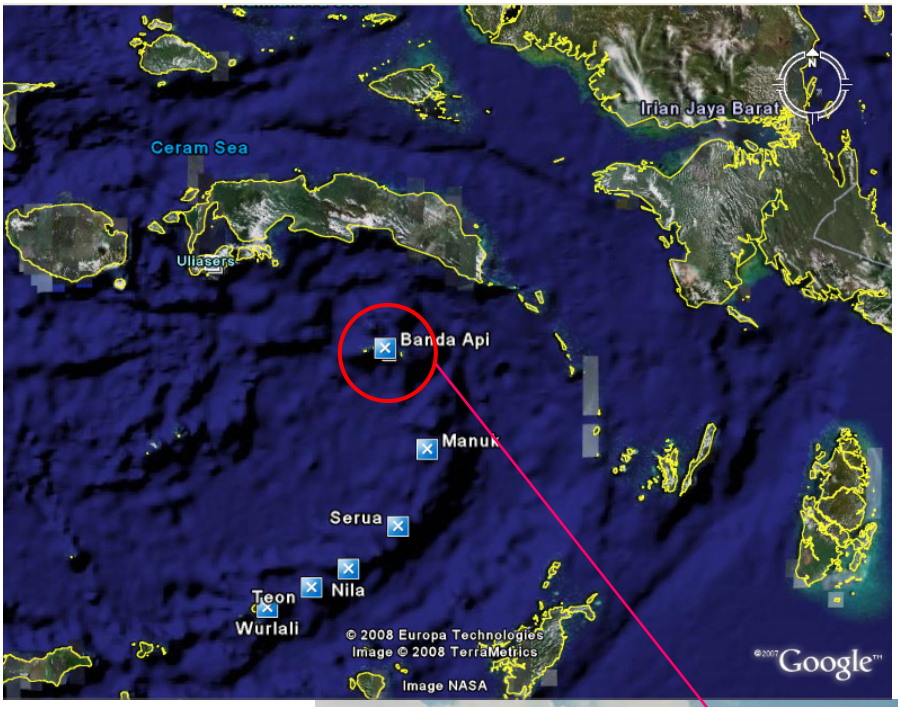

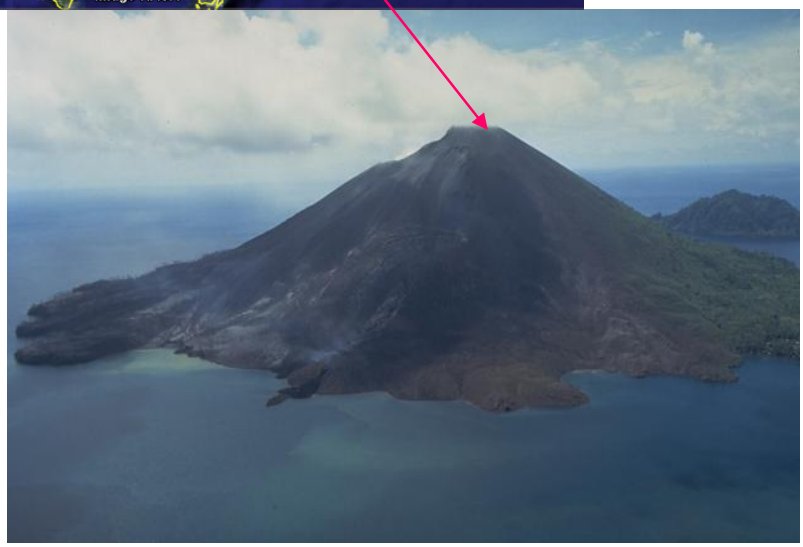

Photo by Tom Casadevall, 1988 (U.S.Geological Survey)

Figure 2.45. The location of Banda Api volcano in the Banda Sea. It has a long period of historical observation because of its key location close to the thriving Portuguese and Dutch spice trade. (Image and map: Google earth and Google map).

2.6.3. The Halmahera Volcanic complex

Gamkonora Volcano

Gamkonora Volcano is located on the west coast of Halmera Island (Figure 2.46). The shifting of eruption centers on Gamkonora, at 1635 m the highest peak of Halmahera, has produced an elongated series of summit craters along a north-south trending rift. Since its first recorded eruption in the 16th Century, Gamkonora has typically

produced small-to-moderate explosive eruptions. Its largest eruption, in 1673, was accompanied by tsunamis that inundated villages (Hamzah et al., 2000).

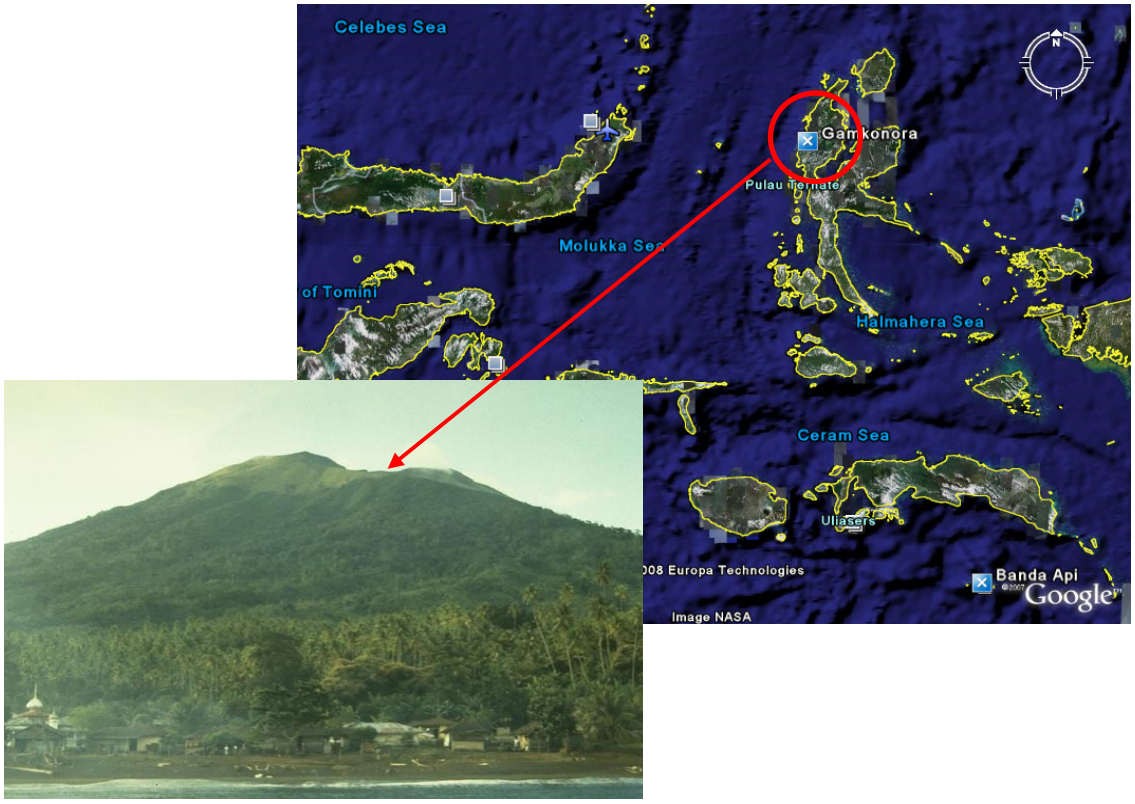

Photo by A. Solihin, 1984 (Volcanological Survey of Indonesia)

Figure 2.46. The location of Gamkonora Volcano on the Halmera mainland. During the 1673 eruption, tsunamis were generated that inundate the surrounded coastal areas. (Image and map: Google earth and Google map).

Gamalama Volcano

Gamalama (Peak of Ternate) is a near-conical stratovolcano that comprises the entire island of Ternate off the western coast of Halmahera (Figure 2.2.47), and is one of Indonesia's most active volcanoes (Kusumadinata, 1979). The island of Ternate was a major regional center in the Portuguese and Dutch spice trade for several centuries, which contributed to the thorough documentation of Gamalama's historical activity. Three cones, progressively younger to the north, form the summit of Gamalama, which reaches 1715 m. Several maars and vents define a rift zone, parallel to the Halmahera Island Arc that cuts through the volcano. Eruptions, recorded frequently since the 16th century, typically originated from summit craters, although flank eruptions have occurred in 1763, 1770, 1775, and 1962-63. There was an eruption in 1871 that caused tsunamis (Hamzah et al., 2000).

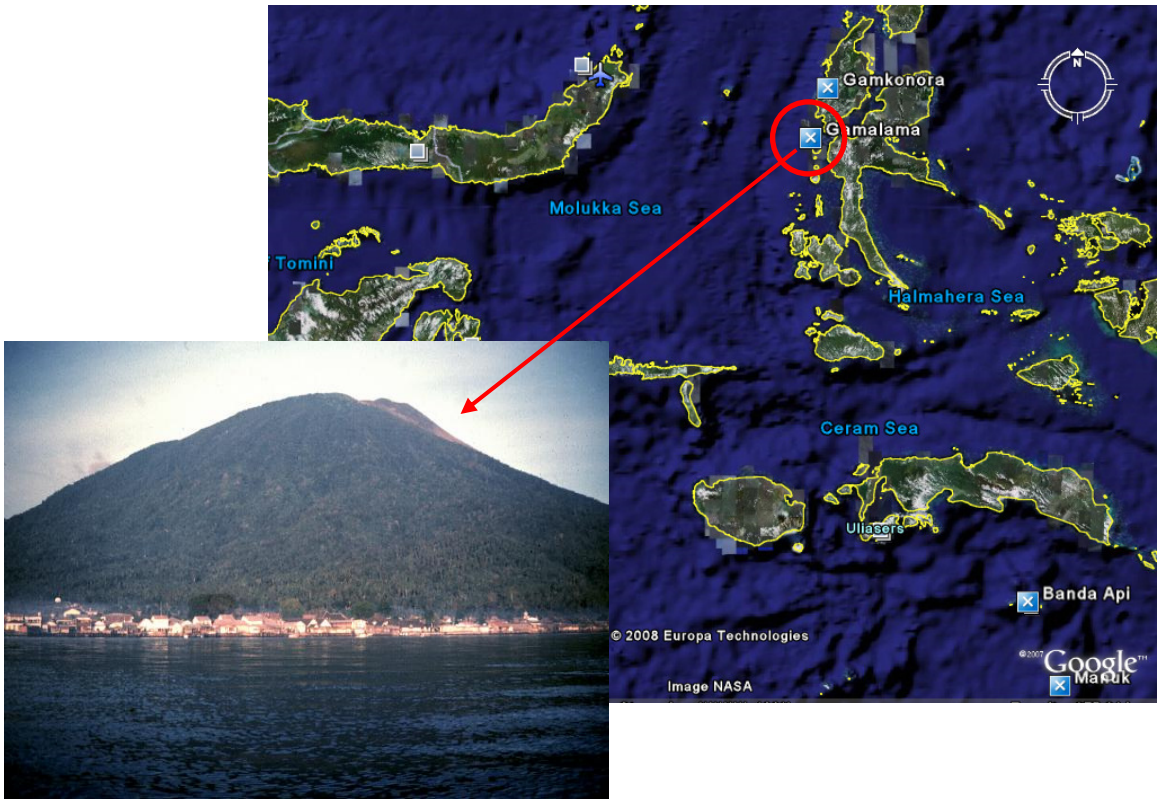

Photo by Jack Lockwood, 1980 (U.S.Geological Survey)

Figure 2.47. The location of Gamalama Volcano in the Molluca Sea. The eruptions in 1871 cause tsunamis. (Image and map: Google earth and Google map).

Tidore Volcanic Island

The Tidore volcanic complex consists of two dramatically different volcanic structures (Figure 2.48). The beautifully conical 1730 m high Kiematabu peak on the south end of Tidore Island is the highest volcano of the North Maluku Island chain west of Halmahera. The broad, lower Sabale volcano on the north side of the island is a caldera containing two cones. Maitara Island, 1 km off the northwest coast, forms another volcanic event. Tidore was mapped as Holocene in age by Apandi and Sudana (1980).

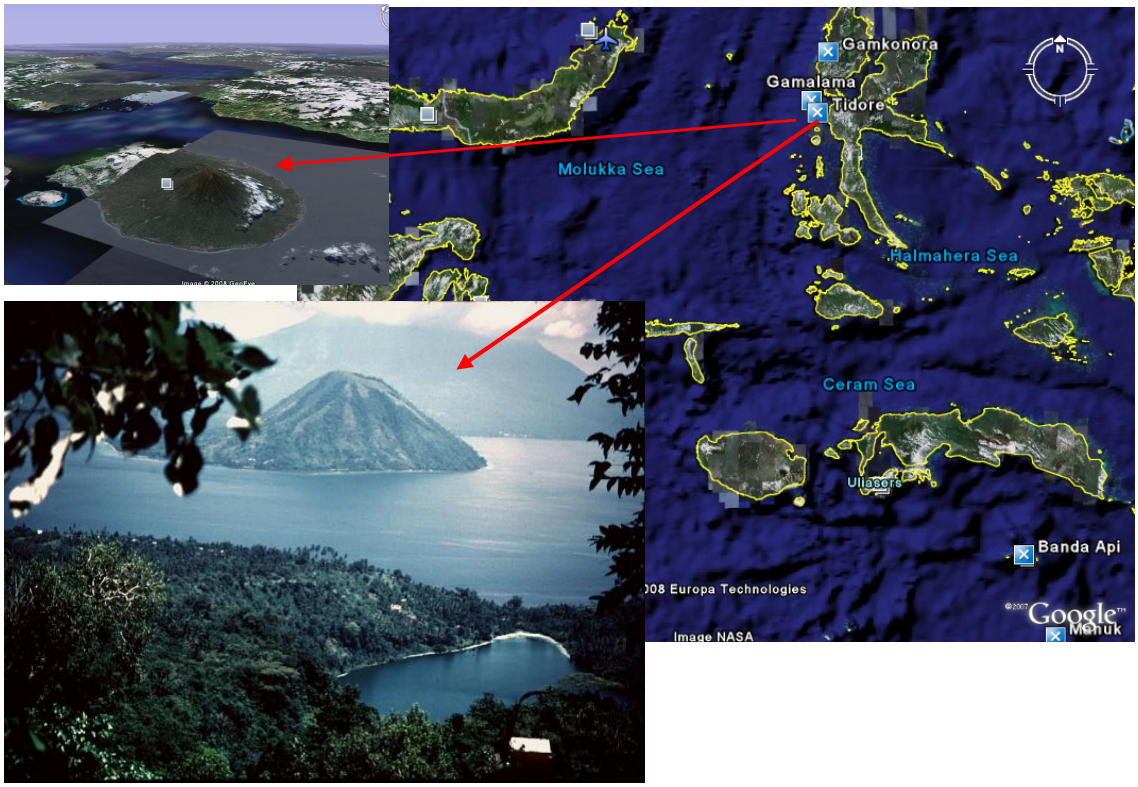

Photo by Jack Lockwood, 1980 (U.S.Geological Survey)

Figure 2.48. The location of Tidore Volcanic complex in the Molluca Sea. (Image and map: Google earth and Google map).

Makian Volcano

Makian volcano forms a 10-km-wide island near the southern end of a chain of volcanic islands off the west coast of Halmahera (Figure 2.49). It has been the source of infrequent, but violent eruptions that have devastated villages on the island. The large 1.5 km wide summit crater, containing a small lake on the northeast side, gives the 1357 m high peak a flat-topped profile. Two prominent valleys extend to the coast from the summit crater on the north and east sides. Four parasitic cones are found on the western flanks. Eruptions have been recorded since 1550; major eruptions in 1646, 1760-61, 1861-62, 1890, and 1988 caused extensive damage and many fatalities (Kusumadinata, 1979).

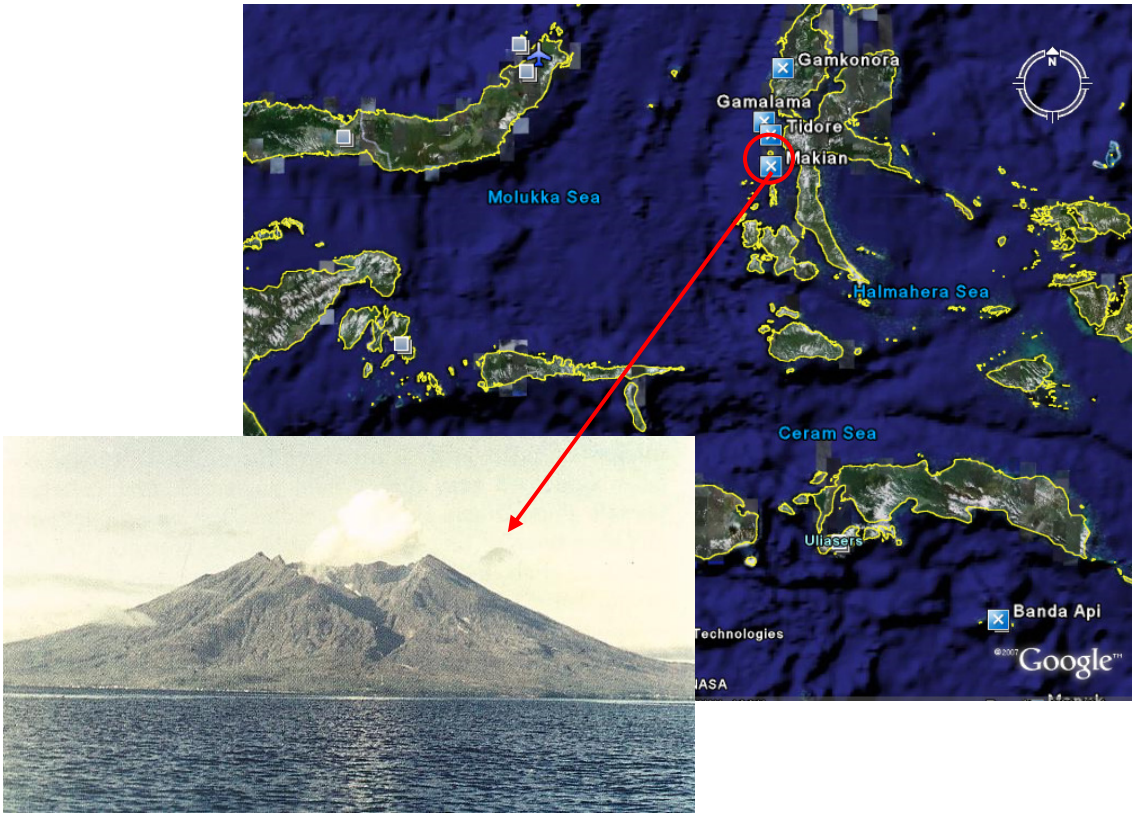

Photo by Sumaryono (Volcanological Survey of Indonesia)

Figure 2.49. The location of Makian Volcano in the Molluca Sea. This volcanic island is very active and caused extensive damage and casualties in the past. Possibly tsunamis were generated during one of the previous major eruptions (Image and map: Google earth and Google map).

2.6.4. Sangihe Volcanic Island Arc Complex

Three active volcanoes within the Sangihe Volcanic Complex are considered capable of generating tsunamis, while the others are too recent, or are deeply dissected and possibly inactive as identified by Moorice et al. (1983).

Ruang Volcano

Ruang Volcano in the Sangihe Volcanic Complex is the southernmost volcano of the system (Figure 2.50). The 4 x 5 km volcano rises to 722 m above sea level and 1700 m above the ocean floor. The summit of Ruang volcano contains a crater partially filled by a lava dome initially emplaced in 1904 and partially filled with the 1949 lava dome. Explosive eruptions recorded since 1808 have often been accompanied by lava dome formation and pyroclastic flows that have damaged inhabited areas. An eruption in 1889 has been reported to generate tsunamis (Hamzah et al. 2000).

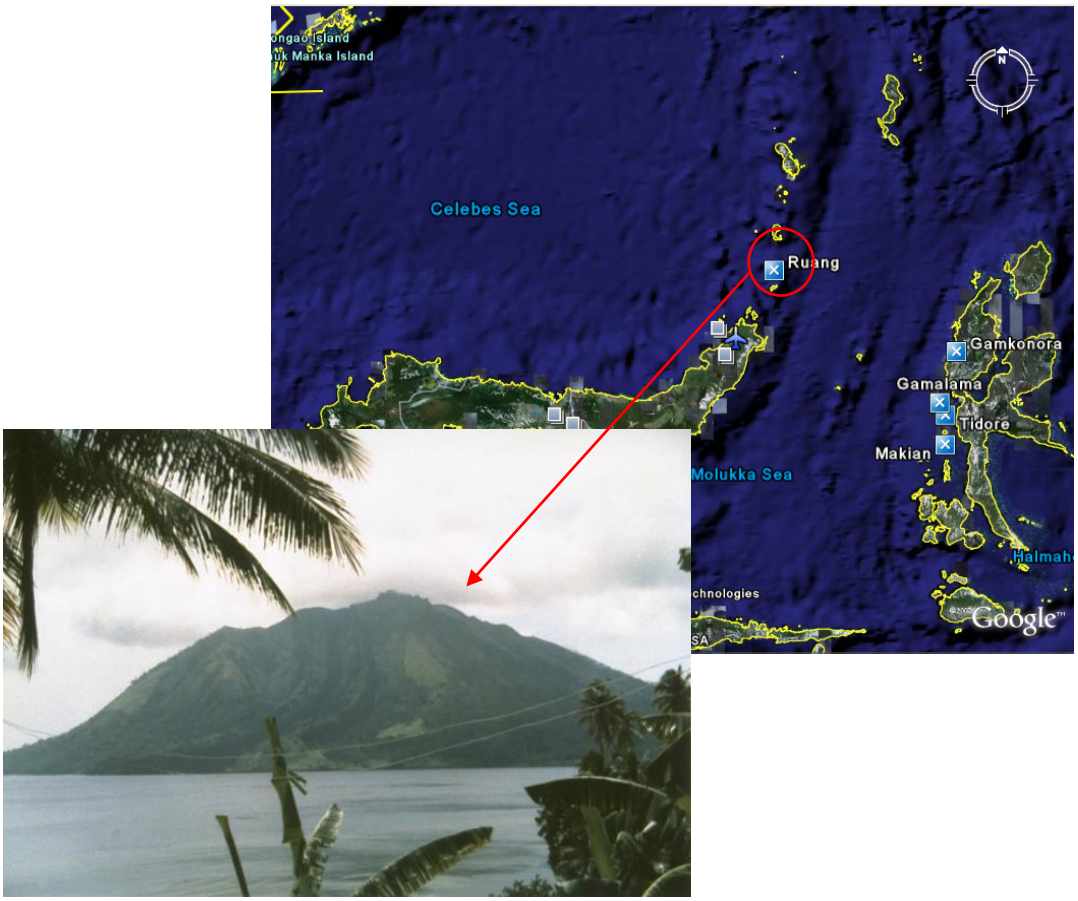

Figure 2.50. The location of Ruang Volcano at the edge of Celebes Sea. This volcanic island has generated tsunami during one of the major eruption in the past. (Image and map: Google earth and Google map).

Karangetang Volcano

The Karangetang (Api siau) stratovolcano lies at the northern end of the island of Siu, north Sulawesi, rising 1784 m above sea level and 2700 m above the ocean floor (Figure 2.51). It contains five summit craters along a North-South line, and is one of the most active volcanoes in Indonesia, with more than 40 eruptions recorded since 1675, and many additional eruptions that were not documented.

Photo by Volcanological Survey of Indonesia

Figure 2.51. The location of Karangetang Volcano Island at the edge of the Celebes Sea, 50 km northern ward of Ruang Volcano. This volcanic island is still active and has had major eruption in the past. (Image and map: Google earth and Google map).

Twentieth Century eruptions have included frequent explosive activity, sometimes accompanied by pyroclastic flows and lahars. Lava dome growth has occurred in the summit craters; and collapse of lava flow fronts has also produced pyroclastic flows.

Awu Volcano

The massive Awu stratovolcano occupies the northern end of Great Sangihe Island, the largest of the Sangihe Arc (Figure 2.52). Deep valleys that form passageways from lahars, dissect the flanks of the 1320 m high volcano (above sea level), which was constructed within a 4.5 km wide caldera. Awu is one of Indonesia's deadliest volcanoes with 15 eruptions since 1640; powerful explosive eruptions in 1711, 1812, 1856, 1892, and 1966 produced devastating pyroclastic flows and lahars that caused more than 8000 cumulative fatalities (Kusumadinata, 1979). Its eruptions in 1856 and 1892 generated tsunamis (Hamzah et al., 2000). Awu contained a summit crater lake that was 1 km wide and 172 m deep in 1922, but was largely ejected during the 1966 eruption.

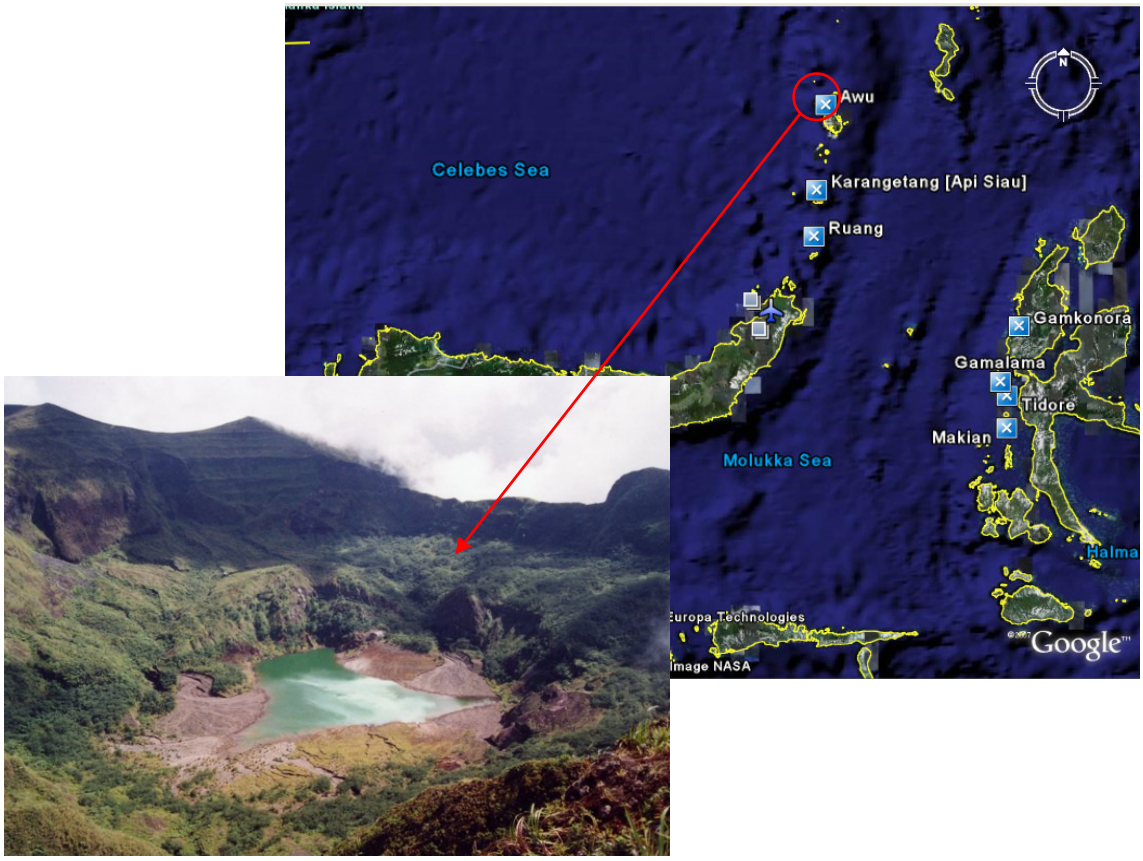

Photo by Kristianto, 1995 (Centre of Volcanology & Geology Hazard Mitigation, Volcanological Survey of Indonesia)

Figure 2.52. The location of Awu Volcano at the northern most end of the Sangihe volcanic island chain. Its eruption in the past has generated tsunamis. (Image and map: Google earth and Google map).

2.7. Discussion

The tsunamigenic regions of the Indonesian Archipelago are located along the subduction-zone, collision zone, fault zone, backarc thrusting and spreading zone, as well as along volcanic island arcs, as the result of the convergence of the Eurasian, Indo-Australian, Caroline and Philippines Sea plates. Two main tsunami sources are identified; submarine earthquakes, and volcanic eruptions with associated processes such as landslides, caldera collapse, pyroclastic flows, underwater explosions and debris avalanches.

2.7.1. Earthquake sources

The tsunamigenic earthquake regions have been identified along the Sumatra and Java subduction-zone (Sunda Arc), Banda Arc, Molluca Collusion Zone, northern Sulawesi subduction-zone, Palu-Koro transform fault in Makassar Strait and the subduction-zone of northern Irian Jaya. The earthquake magnitude, the size of the rupture zone, and the extent of tsunami impact based on the historical record (McCann et al., 1979; Hamzah et al., 2000; Prasetya et al., 2001; Rynn, 2002; ITDB/PAC2004), and from the recent events after the Boxing Day Tsunami 2004 (M_w >9), Nias earthquake and tsunami (M_w = 8.5) on 28 March 2005 (Jaffe et al., 2006), South Java earthquake and tsunami (M_w = 7.6) (Fritz et al., 2007), and Bengkulu earthquake and tsunami (M_w = 8.4) (Borrero et al., 2008), revealed that tsunamis due to subduction zone thrust earthquakes along the Sumatra segment were greater than any tsunamis generated by the earthquakes elsewhere in Indonesia Archipelago.

Geist et al. (2007), pointed out the tectonic aspects of the 26 December 2004 event, and noted that prior to the event, it was generally unclear whether M>9 earthquakes could occur in highly oblique subduction-zones. Okal and Synolakis (2008) identified that the Ruff & Kanamori (1980) model that combine the age of the subducting lithospheric plate and kinematic rate of convergence at the trench to predict the maximum size of the relevant subduction earthquake, was not a reliable estimation for the event. They identified that the length over which a fault system extends continuously along a convergent plate boundary is the *prima facie* indicator of the potential for a mega-earthquake capable of generating a destructive tsunami especially in the far field. The increasing obliquity of convergence from the south (Java) to the north (Sumatra-Andaman) that causes an increase in the thickness of sediment entering the subduction-zone with the possibility of increases in pore pressure (Karig et al., 1980; More et al., 1980; van der Werff, 1996; Prawirodirdjo et al., 1997) is another factor that contributes to large earthquakes associated with tsunami. Newcomb and McCann (1987) identified this for a series of great earthquakes associated with tsunamis that occurred in 1797, 1833, 1861 and 1907 along the Sumatra subduction zone.

Fuller et al. (2006) used recent observations of an association between forearc basins and slip during subduction-zone thrust earthquakes to suggest a link between

processes controlling upper plate structure and seismic coupling on the subduction-zone thrust fault. Their numerical simulation is illustrated in Figure 2.53 (taken from Figure 2 and 3 of Fuller et al., 2006) and demonstrates that sedimentation stabilizes the underlying wedge, preventing internal deformation beneath the basin, and maximum slip during great-thrust earthquakes tends to occur where sedimentary basins stabilize the overlying wedge. Fuller et al. (2006) also explain a mechanism allowing two large earthquakes close to each other (couplet), such as a series of events in 1833, 1861; 1907, 1908; 2004 and 2005. Their results shows that due to the lack of deformation in stable sedimentary basins, there is an increased likelihood of thermal pressurization of the subduction thrust, which allows the fault to load faster, and allows greater healing of the fault between rupture events. The evidence that the sediment thickness increases from the Java subduction-zone to Sumatra subduction-zone (Newcomb and McCann, 1987; van der Werf, 1996) is clear, and is the likely cause of the great thrust subduction earthquakes.

These results imply that east of central Java, there are less great earthquake generating tsunamis, as well as relatively long return periods, due to less sediment thickness compared to the western part. From central Java towards the east, Koop et al. (2006) indicated that subduction erosive processes are the dominant mode of mass transfer, which means that sediment thickness decreases. Newcomb and McCann (1987) recognized that the contact zone between adjoining plates where great interplate earthquakes occur in Sumatra is broader than for Java. Gravemeyer and Tiwari (2006) also recognized this from the analysis of the gravity anomaly, seismic profile and temperature distribution. This implies that the shallow portion of the Benioff zone dip is shallower in Sumatra and steeper in Java. Hence, moderately long rupture zones (>150 km) occur in Java compared to extremely long rupture zones (>450 km) on shallowly dipping slabs with a wide zone of contact in Sumatra.

Even though, in general, the sediment thicknesses are increased from south (Java) to the north (Sumatra), tsunami hazard analysis needs to be done sector by sector along the trench. As an example, the Investigator Fracture Zone (IFZ) at 99E exhibits 1000-1500 m of relief that intersects the forearc and underneath the continental margin. This acts as a major sediment dam to along strike sediment flow in the trench causing a local increase in sediment thickness (Newcomb and McCann, 1987). This

information is very important in designing the rupture zones for initial conditions for tsunami forecasting and modeling. For example, contrast the behavior of two recent great earthquakes and tsunamis: the 26 December 2004 with Mw>9 and 28 March 2005 with M_w=8.5. The 26 December 2004 local tsunami intensity was similar to other tsunamigenic earthquakes with comparable magnitude, while the 28 March 2005 was deficient relative to its earthquake magnitude (Geist et al., 2006).

Along the Java trench (south of Java island), historical records showed that most tsunami occurred in eastern Java. The last event on June 4, 1994 (east Java tsunami) was located close to the previous tsunamis of January 4, 1840 and October 20, 1859. Most events involved interplate earthquakes. However, there is an anomalous source located at Roo Rise, seaward of the trench, such as the intraplate event on September 1921. Like IFZ on the Sumatra subduction zone, the Roo Rise apparently contributed to tsunami events that occurred mostly to the east of Java Island. The south Java tsunami that occurred on July 17, 2006 was located at the area west of the Roo Rise where there was no previous record. Therefore not all tsunamigenic earthquakes along the Java Trench are necessarily interplate thrust events as indicated by Newcomb and McCann (1987).

Gravemeyer and Tiwari (2006) showed that Bougier gravity anomalies correlate well with the occurrence of large megathrust earthquakes along the Sunda subduction zone (Sunda Arc), where a negative anomaly marks segments characterized by larger earthquakes, while positive anomalies indicate lower seismic potential (Figure 2.54). Futhermore, the thermal models and structural constraints derived from seismic and gravity data are used to explain the seismogenic behavior. Moving from Java to Sumatra, the oblique subduction of young oceanic crust is shifted trench ward, increasing the width of the locked megathrust. This result, in a shallow mantle wedge underlying the forearc basin off Java, is causing a prominent positive gravity anomaly. This serpentinized mantle wedge limits the width of the coupling off Java to 30-40 km, compared to > 120 km offshore Sumatra (Gravemeyer and Tiwari, 2006).

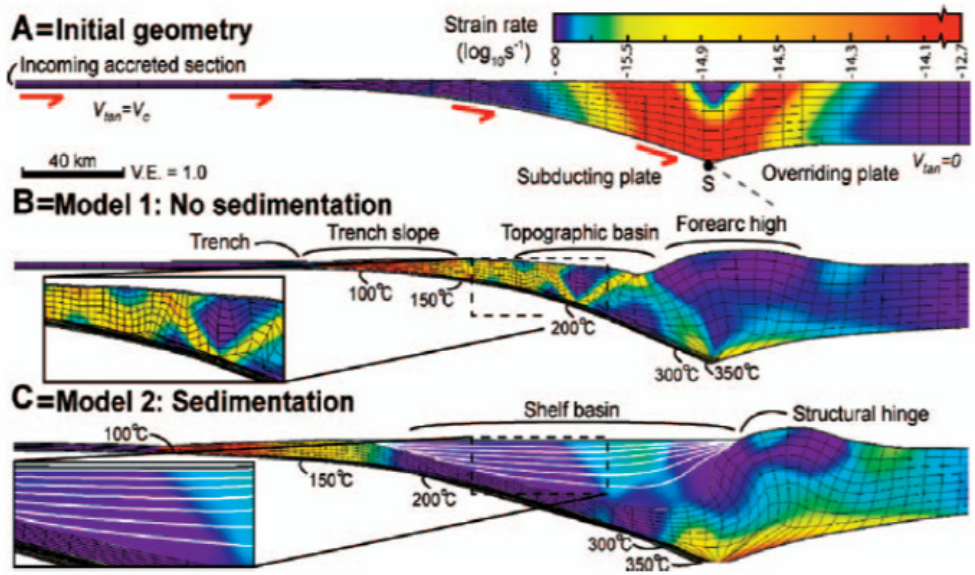

Figure 2. Numerical models for plane-strain, viscous-plastic deformation of a subduction wedge driven by basal traction and sediment accretion (see material in Data Repository [see footnote 1]). Color field shows strain rate (second invariant of strain rate tensor), and Lagrangian mesh shows integrated deformation. A: Model immediately after start of convergence representing a continental margin prior to initiation of subduction. B: Model 1 (no sedimentation) at 5 m.y. Lagrangian mesh and strain rate show active deformation throughout wedge, from trench to forearc high. Wedge deformation is primarily plastic as indicated by localizations in strain-rate field. (See Fig. DR2 and Video DR1 in Data Repository for additional details.) C: Model 2 (sedimentation) shown at 5 m.y. with parameterization identical to Model 1 except that topographic basin is filled with sediment with material properties identical to rest of the wedge. Strain rate, Lagrangian mesh, and synthetic stratigraphy of the basin (white lines) indicate little deformation of forearc basin or underlying wedge. (See Fig. DR3 and Video DR2 in Data Repository for additional details.)

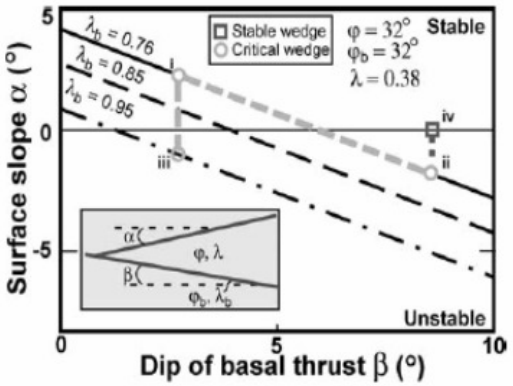

Figure 3. Relationship between surface slope α and subduction thrust dip β for a minimum-taper critical Coulomb wedge. Solution is given for 3 values of fluid pressure ratio λ_b on the subduction thrust, with other variables held constant: wedge friction φ = 32°, subduction thrust φ_b = 32°, wedge fluid pressure ratio λ = 0.38. Path i to ii represents the surface slope of a critically tapered wedge with a thrust that increases in dip landward. Landward increase in fluid pressure on the basal thrust also results in a landward decrease in surface slope (i to iii). Path ii to iv illustrates influence of sedimentation. Filling of topographic depression results in an increase of α to zero, which stabilizes the wedge beneath the basin. We refer to these basins as negative-α basins.

Figure 2.53. The numerical simulation results of plane-strain, viscous-plastic deformation for a subduction wedge driven by basal traction and sediment accretion of Fuller et al. (2006).

A number of significant tsunamis have been generated in the past within the Banda Arc subduction-zone, Molluca collision zone, and northern Sulawesi subduction-zone. However, the database also shows that no tsunamis have been generated since the last big events in 1674 for south Ceram Island (M_s= 8 and H_{max}= 80 m (questionable)), 1889 in the Molluca collision zone (M_s=8.0 and H_{max}=15m), and 1852 at Banda Sea (M_s= 8.0, H_{max} = 8 m). Earthquake databases show that several large earthquakes have occurred close to those areas, such as the 1938 earthquake (Okal and Raymond, 2003). However, no tsunamis were reported, probably because the hypocenter was 60 km. Hence is too deep to generate a tsunami. Recent tsunami events around the perimeter of the region are the 1992 Flores tsunami at Hading Bay Flores Sea, the 1996 Tonggolobibi tsunami generated from the earthquake source on the northern Sulawesi subduction-zone and Palu-Koro transform fault system, and the 1996 Biak tsunami. The Flores tsunamis in 1992 involved a landslide as a secondary generating mechanism, as did the 1996 tsunamis in Biak. It is probable that most tsunami occurring in the eastern part of Indonesia involve the landslides as a secondary generating mechanism, instead of an earthquake mechanism directly. The last event for this region occurred in 2000 and hit the Banggai region, eastern Sulawesi Island.

2.7.2. Seismic gaps and potential large earthquakes

The term "seismic gap" following McCann et al. (1979) refers to any region along an active plate boundary that has not experienced a large thrust or strike-slip earthquake for more than 30 years, and is considered likely to produce a large earthquake during the next few decades. McCann et al. (1979), after Kelleher and McCann (1976), identified that east of the Sunda Strait, Java and the Lesser Sunda Islands lack historic great earthquakes associated with tsunamis, whereas to the west, in Sumatra, the historical record indicates frequent great earthquakes and extensive damage by tsunamis. Newcomb and McCann (1987) concluded that the entire length of Sumatra has the potential to produce great thrust earthquakes; its seismic potential should be considered high (as there has been no recurrence of the great events of 1833 (M_w = 8.7-8.8) and 1861 (M_w = 8.3-8.5). In contrast, no such events have been reported off Java and the Lesser Sunda Islands.

A series of large earthquakes associated with tsunamis starting with the great Sumatra earthquake and tsunamis in 2004, showed the potential of large earthquakes associated with damaging tsunami along the Sumatra segments as identified by McCann et al. (1979) and Newcomb and McCann (1987). Moreover, McCloskey et al. (2005) computed the Coulomb stress after the 26 December 2004 event, and identified a Coulomb stress transfer to the southeast to where the March 28, 2005 M_w = 8.5 event occurred. Natawidjaja (2003), based on coral studies on Mentawai Island, showed a pattern of large earthquakes cycles and the evidences of 1600s, 1797 (M_w = 8.2-8.3) and the 1833 (M_w = 8.7-8.8) events. Paleoseismic data (Sieh, 2006) suggest that great earthquakes recur about every 200 to 240 years along the adjacent section of the Sunda megathrust. With the last event in 1797 and 1833, a great earthquake is due now. The March 28, 2005 (M_w = 8.5) event has been suggested as a repeat of the 1861 (M_w = 8.3-8.5) event but with less tsunami impact. It is not clear if the recent Bengkulu event on 12 September 2007 (M_w = 8.4) was the repeat of the 1833 event since its rupture zone, magnitude and tsunami impact were smaller than in 1833 (M_w = 8.7-8.8). It is obvious now, that one of the seismic gaps that is highly possible to rupture in the near future involves a repeat of the 1797 event, since both sides of this segment have already ruptured (March 28, 2005 ~ Nias Earthquake and Tsunamis M_w = 8.5 and 12 September 2007~ Bengkulu earthquake and tsunamis M_w = 8.4). Recent data from GPS measurements (Natawidjaja, pers.comm., 2008) show that the preconditions for a repeat of the 1797 event already occur, and there is an accumulation of stress under Mentawai Island.

The rupture propagation (aftershock distribution) from the recent large subduction-zone earthquakes of 26 December 2004 and 12 September 2007 started from the southeast and propagated to the northwest. This is consistent with the direction of the Indo-Australian plate movement along the oblique subduction zone (Figure 2.55a). This implies that any earthquake at the southeastern end of the segment boundary, such as the 1797 event, is a warning for the possible generation of damaging tsunamis. This rupture propagation to the northwestward is consistent with historical events as indicated previously.

In contrast, the rupture distributions of the 28 March 2005 and 1935 events were equally distributed to the northwest and southeast of the epicenter. The Mentawai Fault zone possibly contributes to the distribution of the aftershock of those two events. Based on this pattern, the locations of the 1861 and 1907 rupture zone were better determined and reconstructed (Figure 2.55b).

A quiescent period, as identified by McCann et al. (1979), found to the east of Sunda Straits along the Sunda Arc based on pre-1975 data, vanished when the 1977 Sumba earthquakes and tsunamis (M_w = 7.7; revised by USGS as M_w = 8.2-8.3), East Java tsunamis in 1994 (M_w = 7.8) and south Java tsunami in 2006 (M_w = 7.7) occurred. However, another gap that still retains potential to generate catastrophic tsunamis is identified between Enggano Island and the western Java forearc, with the Sunda Strait in the center of the gap where there is no historical record of shallow large earthquake since 1800. In addition, there is the gap that lies between the South Java 2006 event, and the east Java 1994 event, with the last seismic gap between the 1994 east Java tsunami and 1977 Sumba tsunami.

In contrast with the Sunda Arc, the seismic gaps for the Banda Arc and most of the eastern Indonesian Archipelago are difficult to assess, as the tectonic structures are very complex and still poorly understood. However, the historical record provides some insights. No large tsunamigenic earthquakes have occurred within the same segment within the Banda Arc, and to the north within the Molluca Collision Zone. All recent tsunamis have been from different segments, such as in 1996 at Tonggolobibi as part of the Palu-Koro Transform fault and north Sulawesi Subduction zone, and the Banggai Tsunami in 2000 at the boundary of Banda Arc and Molluca Collision Zone. This suggests that all segments are potentially seismic gaps, except those with event in the last 30 years.

Combining the seismic gap concept (McCann et al., 1979), with the length over which the fault system extends continuously along a convergent plate boundary (Okal and Synolakis, 2008) and the basin boundaries, potential tsunamigenic earthquake events can

be estimated using the McCaffrey (2008) methods. This has been done along the Sunda and Banda Arc and the Halmahera and Molluca Collision Zone as well as the northern Sulawesi Subduction Zone and Makassar Strait as illustrated in Figures 2.56a and 2.56b, and Table 2.1. These scenarios also take into account the strong variability and unpredictability of the fragmentation of rupture during major earthquakes along a given subduction zone, as indicated by Okal and Synolakis (2008). McCaffrey (2008) estimated the maximum earthquake magnitude (the seismic moment of M_o^{max}) from the longest possible subduction zone rupture length (L) as

$$M_o^{max} = \mu\, u_{av}\, L\, Z_{max} / \text{Sin}\, \delta,$$

where μ is the shear modulus, Z_{max} is the maximum depth of dip (in metre), δ is the average fault dip angle derived from earthquake mechanism (in degree), and u_{av} is the average slip in the earthquake which is estimated from the rupture length (in metre) by

$$u_{av} \sim 2.5 \times 10^{-5}\, L.$$

Finally, the maximum moment magnitude (M_w^{max}) is estimated from the seismic moment using equation

$$M_w^{max} = 2/3 \log Mo - 6.07, \text{ Mo in Nm.}$$

The recurrence time for a large event can be estimated from the relationships of

$$T = u_{av}/f\chi\nu,$$

where ν is the plate motion rate, f is the fraction of the total seismic moment represented by large earthquakes and χ is the fraction of slip on the boundary that occurs seismically. For large earthquakes the sum of f and χ is equal to 1 with f varied from 0.32 to 0.45 for the subduction zone (McCaffrey, 2008). The fault characteristics calculated for the Indonesian Archipelago subduction zones (possible seismic gap and maximum fault length) is summarized in Table 2.1.

2.7.3. The Volcanic sources

From the historical record, at least 9 volcanic tsunamis were identified with two events, Krakatau 1883 and Tambora 1815, categorized as catastrophic events. The Krakatau 1883 event was the first large-scale natural disaster that became worldwide news, and it was well documented due to its location in relation to the inhabited areas of Sunda Strait.

More than 36,000 people were killed by the tsunamis and associated processes. The geographic distributions of the volcanogenic sources clearly show that many are close to populations areas. Also for some, a repeat of the Krakatau 1883 and Tambora 1815 events will affect a large number of coastal communities.

Along the Sumatra Subduction Zone, most volcanoes are located away from the coast on the main island. The exception is Weh Island, which erupted during the Pleistocene, and possibly generated tsunamis. On the contrary, for the eastern part of the Archipelago, the Banda Arc, and Molluca Collision Zone form a volcanic island arc. There are 18 volcanic islands that potentially can generate tsunamis. Some of them have generated tsunamis in the past. However, there is no threat of volcanogenic tsunamis for Java Island, except for a repeat of the Krakatau 1883 eruption (from Anak Krakatau), and possible refraction and diffraction of waves from a repeat of the Tambora 1815 event.

2.8. Summary

- The historical record within the Indonesian Archipelago shows that the region is very susceptible to tsunamis from subduction zone earthquakes and volcanic eruptions. Most of the catastrophic tsunamis have occurred along the Sunda Arc subduction zone up to Lesser Sunda, including the Krakatau volcano. Fewer events have occurred in the eastern part of the Archipelago along the Banda Arc, Halmahera and Molluca Colission Zones, northern Sulawesi Islands, and the Makassar Straits.

- Along the Sunda Arc, the potential for large destructive earthquakes and tsunamis is much larger in Sumatra than Java and lesser Sunda. Geological and geophysical data demonstrated that the Sumatra subduction zone is the most likely location for future megathrust earthquakes. In the Banda Arc and most of the eastern part of the Archipelago, the size and extent of the earthquakes and associated tsunami impacts were less but more frequent due to the complex tectonic structure. Within this region, volcanic tsunamis are more likely (18 volcanic tsunamis sources) than

the western part of the Archipelago (2 volcanic tsunamis sources: Anak Krakatau (active) and Tambora (in-active)).

- The 26 December 2004 mega-thrust earthquake (M_w > 9) and tsunamis that occurred along the northern Sumatra-Nicobar-Andaman trench had a 1200 km rupture zone. This event was previously been considered unlikely to occur within a highly oblique subduction zone, even though the historical record indicated that this area was a seismic gap from events in 1881 (two event in Nicobar Islands), 1841 in Andaman, and southern Simuelue Island in 1907. The Simeulue Island earthquake in 2002 (M_w = 7.8) could have been the pre-shock for the 26 December 2004 megathrust earthquake and tsunamis (Natawidjaja, pers.comm.).

- A series of large earthquakes and tsunamis occurred along the Sunda Arc after the megathrust earthquake of 26 December 2004. These were the 28 March 2005 event (M_w = 8.5), South Java earthquake and tsunami on 17 July 2006 (M_w = 7.7), and Bengkulu earthquake and tsunami on 12 September 2007 (M_w = 8.4). This has left a seismic gap for the region affected by the 1797 and 1833 events identified by coral micro-atoll studies (Natawidjaja, 2003). At the end of the Sumatra segment, the gap was identified between the Enggano Island, offshore of the south end of Sumatra Island, and the location where the South Java tsunamis occurred on 17 July 2006. There is no historical record for this gap, which is similar to the 2004 megathrust earthquake before the event. Further east along the Java and Lesser Sunda Arc, two seismic gap areas are identified: a gap between the 2006 (South Java) event and the 1994 (east Java event), and the gap between the 4 June 1994 East Java earthquake and tsunamis and the August 19, 1977 Sumba earthquake and tsunamis.

- For the Banda Arc and eastern Indonesia Archipelago, scenarios for potential large tsunamigenic earthquakes are difficult to assess using a seismic gap approach, given that the tectonic structure is very complex and still poorly understood. Further, historical data did not show any trend allowing identification

of seismic gaps. Therefore, potential tsunamigenic areas for this region were derived and identified based on major active thrusting fault and the nature of the subduction zone as reported by McCaffrey (1988), and their possible maximum ruptures were determined following McCaffrey (2008).

- Given the historical record, it is an important to assess volcanic tsunamis as it is for the subduction-zone earthquakes, and their secondary processes. The assessment can be done through numerical modeling by developing a range of scenarios for each volcano or other tsunami sources. The source parameters need to be considered carefully, and should be based on reliable field data sets. Highly accurate bathymetry and topography data sets are required in modeling a propagation of tsunami into the coastal areas and during runup and inundation on land.

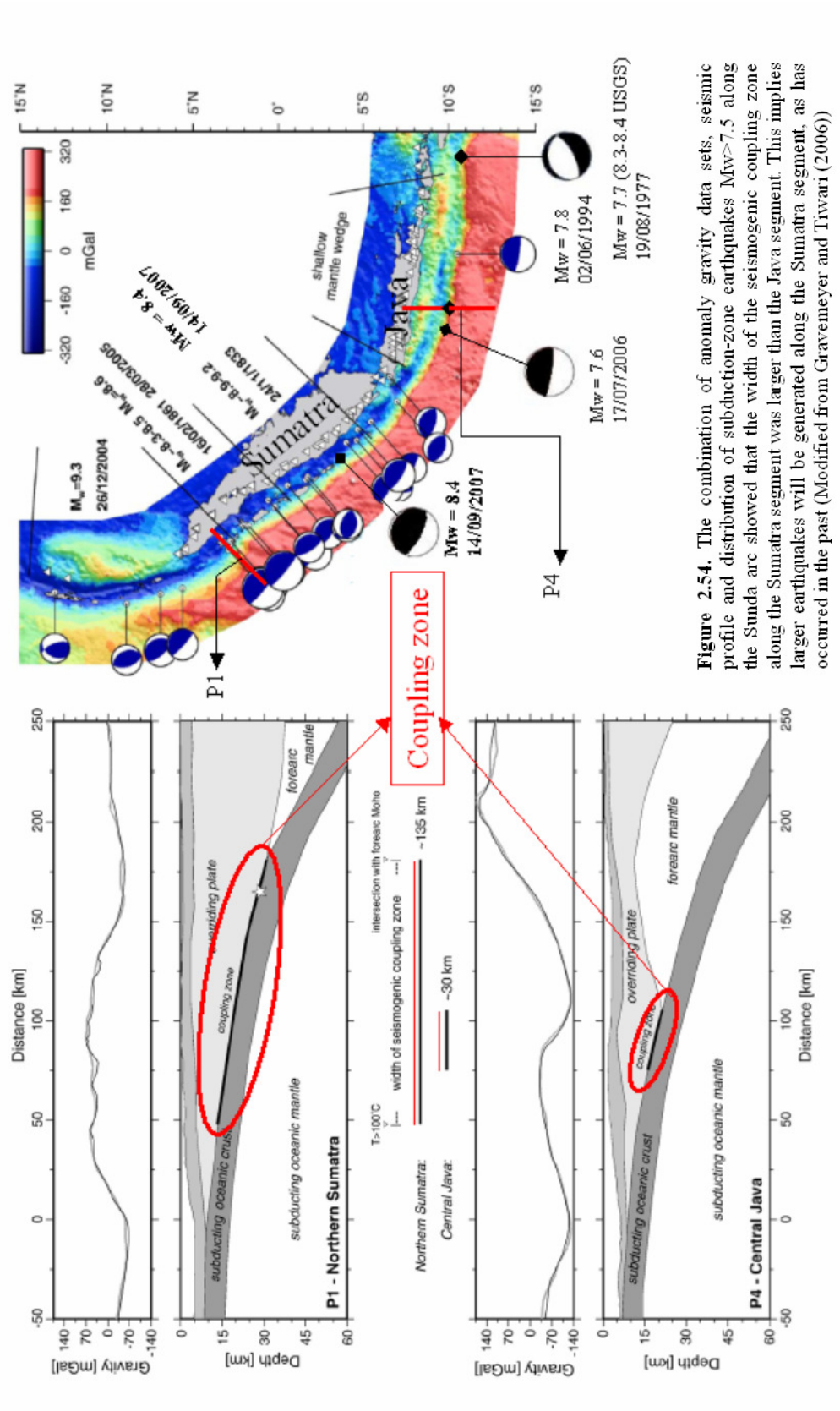

Figure 2.54. The combination of anomaly gravity data sets, seismic profile and distribution of subduction-zone earthquakes Mw>7.5 along the Sunda arc showed that the width of the seismogenic coupling zone along the Sumatra segment was larger than the Java segment. This implies larger earthquakes will be generated along the Sumatra segment, as has occurred in the past (Modified from Gravemeyer and Tiwari (2006))

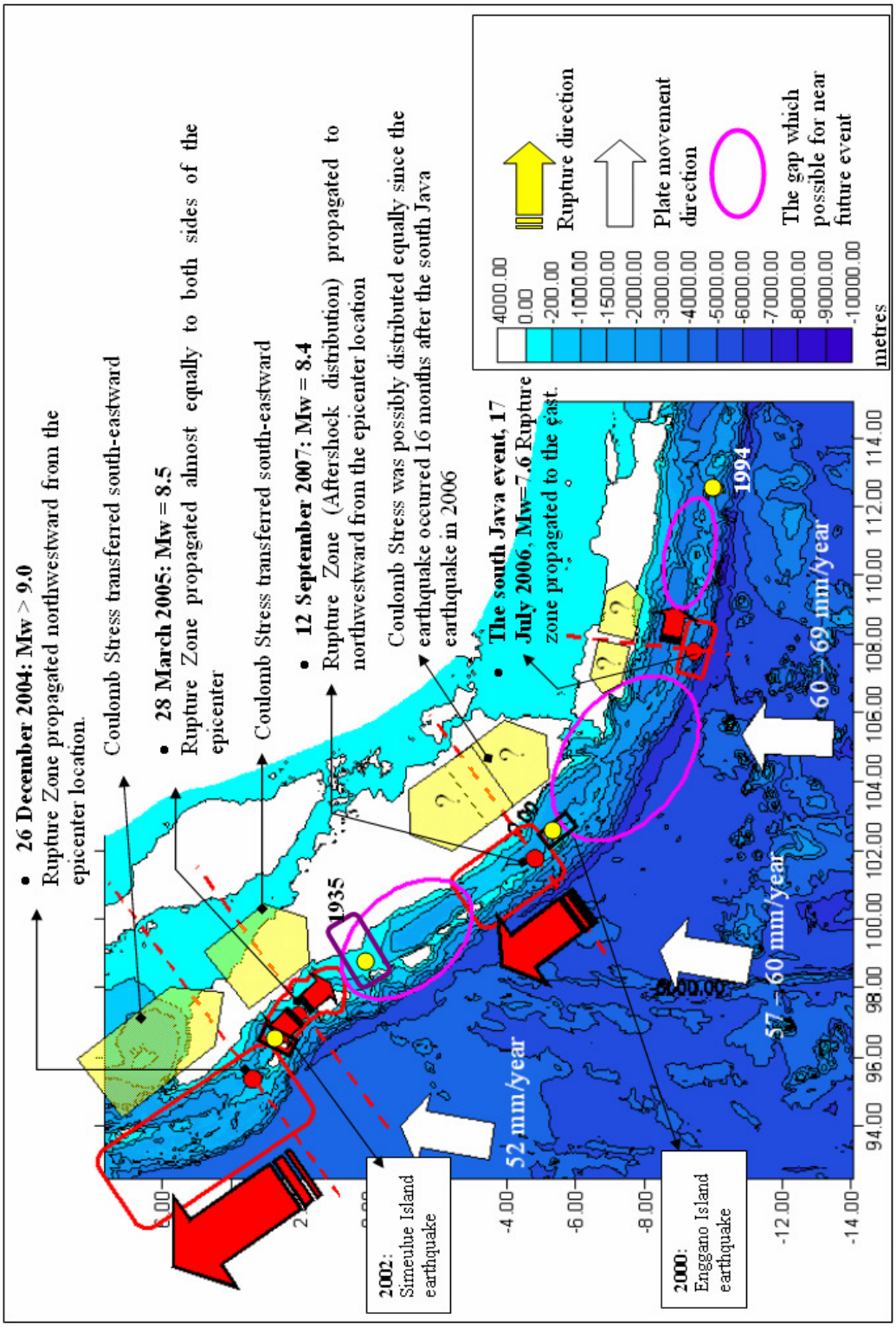

Figure 2.55a. The Coulomb stress of the 26 December 2004 apparently propagated to the southeast, and triggered a series of earthquakes along the Sunda Arc, leaving a gap that is highly likely to generate a large earthquake in the near future. Most rupture propagation (red arrows) of the large tsunamigenic earthquakes nucleated close to the trench is to the north-westward along the Sumatra segment (e.g., the 26 December 2004 and 12 September 2007). For those earthquakes, which are generated further away from the trench along the Mentawai Fault Zone such as the March 28, 2005 (and also the 2002 and 1935), their aftershocks were distributed equally on both side of the epicentre. Along the Java segment, the recent south Java 2006 event shows the ruptures were propagated to the east.

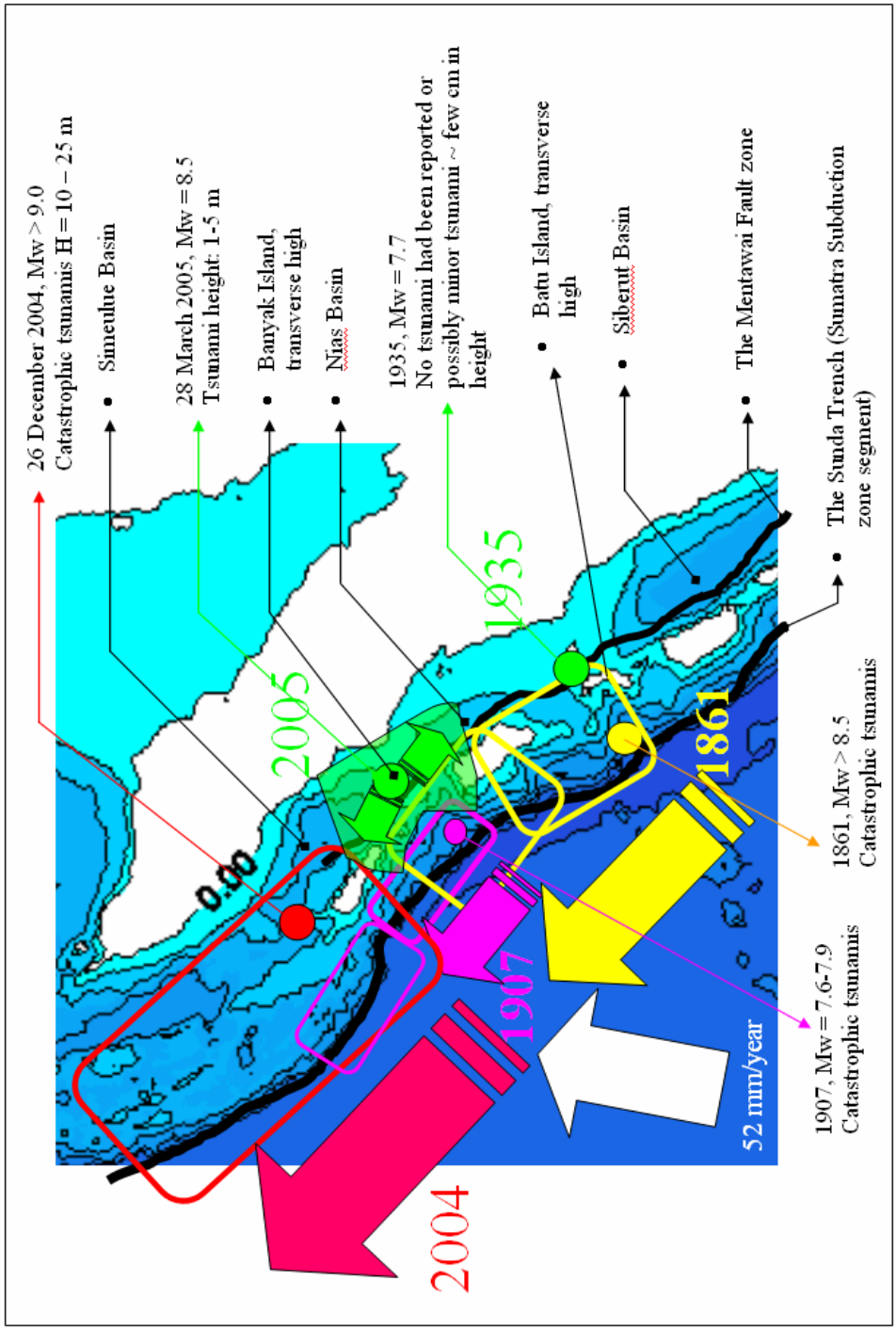

Figure 2.55b. Directionality of the rupture propagation for those earthquakes associated with damaging tsunamis, which occurred close to the trench along the Sumatra segment (2004, 1907 and 1861), is consistently to the north-westward. This directionality occurs possibly as a consequence of the Indian Ocean plate movement that moves to the north along the Southeast-Northwest lineaments of the collision zone which then transfers most the energy and rupture propagation to the northwest (the 1861(as well as the 1797 and 1833; see figure 2.56a), 1907, and 2004 events). Earthquakes further from the trench (along the Mentawai Fault Zone) rupture in two directions (e.g. epicentre is in the middle of the rupture zone).

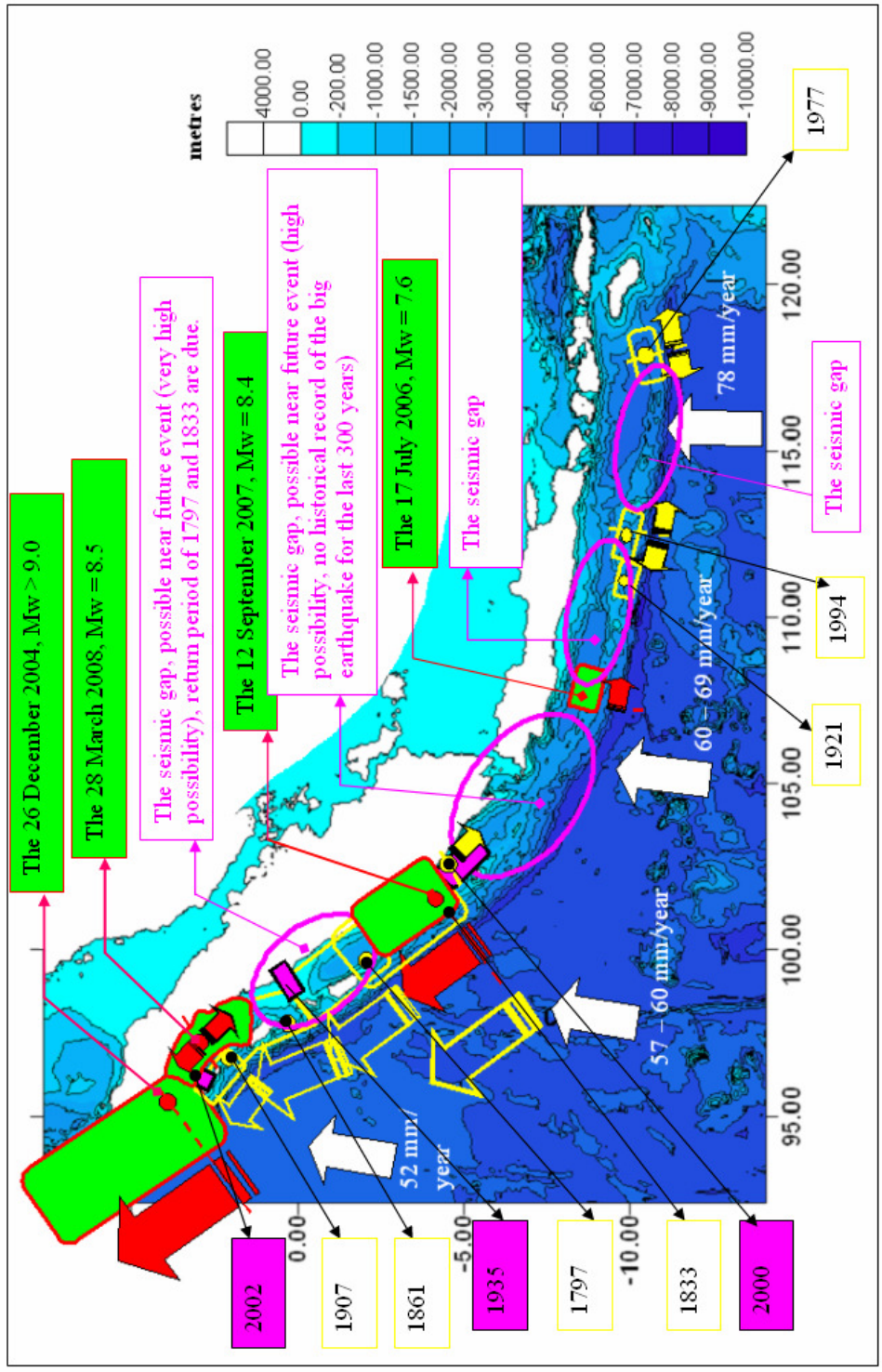

Figure 2.56a The seismic gap analysis shows that the area between the March 28, 2005 and 12 September 2007 events has a high potential to fail in the near future. This is consistent with the return period of the 1797 event based on micro atoll studies. The gap between 17 July 2006 and 12 September 2007 (also the 2000) events has had no historical record of large earthquakes for the last 300 years. Another two gaps are identified further east, between the 17 July 2006 and 1994 events, and between 1994 East Java and 1977 Sumba events. The red arrows showed the propagation of the recent ruptures and the yellow arrows show the historical earthquake and tsunami events rupture propagation direction. There are three large earthquakes which have not generated tsunami. The Sumatra segment is divided into three regions; the 2002 Simeulue earthquake at the northern end, the 2000 Enggano earthquake at the southern end and the 1935 Batu island earthquake. The 2002 Simeulue event has been suggested as pre-shock for the 26 December 2004 earthquake (Natawidjaja 2008 pers.comm.).

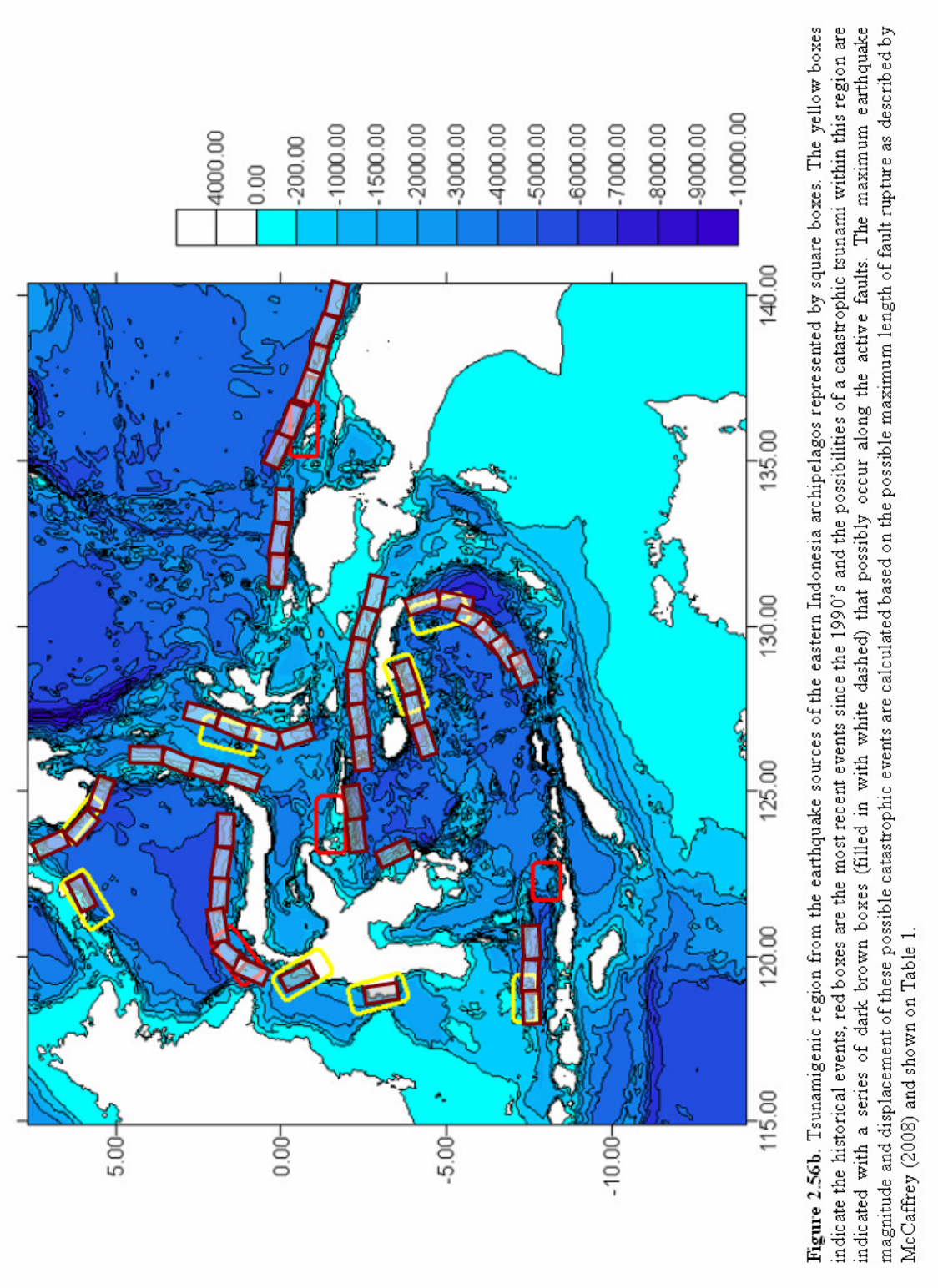

Figure 2.56b. Tsunamigenic region from the earthquake sources of the eastern Indonesia archipelagos represented by square boxes. The yellow boxes indicate the historical events, red boxes are the most recent events since the 1990's and the possibilities of a catastrophic tsunami within this region are indicated with a series of dark brown boxes (filled in with white dashed) that possibly occur along the active faults. The maximum earthquake magnitude and displacement of these possible catastrophic events are calculated based on the possible maximum length of fault rupture as described by McCaffrey (2008) and shown on Table 1.

Table 2.1. Calculation of fault parameter and moment magnitude for past catastrophic events, and possible maximum magnitude and rupture for a future event along the subduction zone within Indonesian Archipelago based on McCaffrey (2008) methods.

FAULT SEGMENT	SEGMENT		TOTAL LENGTH	SLIP(Uav)	Zmax	dip angle	Mo	M_{wmax}	Con. Rate (mm/year)		Ret. period (years)			Std
	(km)	(m)	(km)	(m)	(m)	(degree)	(Nm)	(Nm)	Min	Max	Min	Max	Avrg	(years)
1907	360.80	360800	360.80	9.02	10000	8	5.62243E+21	8.43	40	52	225.50	173.46	196.08	25.06
1861	400.28	400280	400.28	10.1	10000	10	6.9202E+21	8.49	40	52	250.18	192.44	217.54	27.80
1797	179.54	179543	389.57	9.74	10000	10	6.55491E+21	8.48	40	60	243.48	162.32	194.79	27.05
	210.03	210029												
1833	116.31	116308	356.82	8.92	10000	10	5.49913E+21	8.42	40	60	223.01	148.68	178.41	24.78
	163.42	163417												
	77.10	77097												
SUNDA GAP	153.01	153012	624.04	15.60	10000	10	1.68198E+22	8.75	50	66.9	312.02	233.20	266.91	28.37
	178.50	178504												
	292.53	292528												
West-Central JAVA GAP	446.85	446854	446.85	11.17	15000	20	6.56798E+21	8.48	40	69	279.28	161.90	204.98	31.03
East JAVA GAP	279.85	279854	279.85	7.00	15000	20	2.57611E+21	8.20	40	69	174.91	101.40	128.37	19.43
SUMBA GAP	504.02	504023	504.02	12.60	10000	10	1.09722E+22	8.62	40	78	315.01	161.55	213.57	35.00
BANDA ARC	189.64	189638	390.17	9.75	20000	10	1.31498E+22	8.68	20	50	487.71	195.08	278.69	97.54
	115.32	115316												
	85.21	85212												
SERAM FAULT	244.47	244471	797.82	19.95	15000	15	2.76671E+22	8.89	20	50	997.27	398.91	569.87	199.45
	250.05	250047												
	303.30	303299												
MOLLUCA	132.23	132233	534.86	13.37	10000	10	1.23556E+22	8.66	20	50	668.57	267.43	382.04	133.71
	254.78	254776												
	147.85	147847												
SANGIHE	261.16	261158	591.50	14.79	10000	10	1.51113E+22	8.72	20	50	739.38	295.75	422.50	147.88
	330.34	330342												
NORTH SULAWESI	422.66	422662	422.66	10.57	15000	10	1.15736E+22	8.64	20	50	528.33	211.33	301.90	105.67
NORTH SUMBAWA	340.38	340375	340.38	8.51	15000	20	3.8108E+21	8.32	20	50	425.47	170.19	243.13	85.09

Seismic moment (Mo) and maximum moment magnitude (M_{wmax}) calculation based on McCaffrey (2008).
Con Rate: convergence rates taken from Rangin et al. 1999, Ret. Period = Return Period, Std = standard deviation +/-, Zmax = the focal depth, Avrg = average.

2.9. References.

Bennett, J.J., Bridge, D.M., Cameron, N.R., Djunuddin, A., Ghazali, S.A., Jeffery, D.H., Keats, W., Rock, N.M.S., Thompson, S.J., Whandoyo, R.: 1981, Geologic map of the Banda Aceh quadrangle, North Sumatra. *Geology Research Development Center*, Indonesia. 1:250.000 scale.

Bock, Y.L., Prawirodirdjo, L., Genrich, J.F., Stevens, C.W., McCaffrey, C., Subarya, C., Puntodewo, S.S.O., and Calais, E.: 2003, Crustal motion in Indonesia from Global Positioning System measurements, *Journal of Geophysical Research* **108(B8)**, pp**.** 2367.

Borrero, J.C., Weiss, R., Hidayat, R., suranto., Bosserelle, C., Okal, E.A.: 2008, Field survey and detailed numerical modeling of the tsunami from the Bengkulu earthquake of 12 September 2007, *Geophysical Research Abstracts* **10**, EGU2008 – A - 11494.

Das, S.: 2004, Seismicity gaps and the shape of the seismic zone in the Banda Sea region from relocated hypocenters, *Journal of Geophysical Research* **109**, B12303, pp. 1-18.

Fritz, H.M., Kongko, W., Moore, A., McAdoo, B., Goff, J., Harbitz, C., Uslu, B., Kalligeris, N., Suteja, B., Kalsum, K., Titov, V., Gusman, A., Latief, H., Santoso, E., Sujoko, S., Djulkarnaen, D., Sunendar, H., Synolakis, C.: 2007, Extreme runup from the 17 July 2006 Java tsunami, *Geophysical Research Letters* **34**, L12602, pp. 1 - 5.

Fuller, W.C., Willett, S.D., Brandon, M.T.: 2006. Formation of forearc basins and their influence on subduction zone earthquakes, *Geology* **34** (2), pp.65-68.

Geist, E.L.: 2002, Complex earthquake rupture and local tsunamis, *Journal of Geophysical Research* **107** (B5), pp. 2-1 – 2-15

Geist, E.L., Bilek, S.K., Arcas, D., and Titov, V.V.: 2006, Difference in tsunami generation between the December 26, 2004 and March 28, 2005 Sumatra Earthquakes, *Earth Planet Space* **58**, pp. 185 - 193.

Geist, E.L., Bilek, S.L., Arcas, D., Titov, V.V.: 2006, Differences in tsunami generation between the December 26, 2004 and March 28, 2005 Sumatra earthquakes, *Earth Planet Space* **58**, pp. 185 - 193.

Geist, E.L., Titov, V.V., Arcas, D., Pollitz, F.F., and Billek, S.L.: 2007, Implications of the 26 December 2004 Sumatra –Andaman earthquake on tsunami forecast and assessment model for great subduction-zone earthquakes, *Bulletin of the Seismological Society of America* **97** (1A), pp. S249-S270.

Gravemeyer, I, and Tiwari, V.I.: 2006, Overriding plate controls spatial distribution of megathrust earthquakes in the Sunda-Andaman subduction zone, *Earth and Planetary Science Letters* (251), pp. 199 - 208.

Hamzah, L., Puspito, N., and Imamura, F.: 2000, Tsunami catalog and zones in Indonesia. *Journal of Natural Disaster Serv*ice, **22**, pp. 25-43.

Hamilton, W.B.: 1988, Plate tectonics and island Arcs, *Bulletin of Geology Society of America* **100**, pp. 1503 - 1527.

Hamilton, W.: 1989, Convergent-plate tectonics viewed from the Indonesian region. In: A.Sudrajat, H.D.Tjia, S.Asikin and A.N.Katili (Eds), *J.A.Katili Commenmorative Volume*, Geology Indonesia, Indonesia Association of Geology, 35 - 88.

Hamilton, W.: 1979, Tectonic of the Indonesian region. *U.S.Geological Survey Prof.Pap*.**1078**, 345 p.

Hedervari, P., and Papp, Z.: 1981, Seismicity maps of the Indonesian region, Tectonophysics **76**, pp. 131-148.

Jaffe, B.E, C. Borrero, J.C., Prasetya, G.S., Peters, P., McAdoo, B., Gelfenbaum, G., Morton, R., Ruggiero, P., Higman, B., Dengler, L., Hidayat, R., Kingsley, E., Widjo Kongko, Lukijanto, Moore, A., Titov, V., and Yulianto, E.: 2006, The December 26, 2004 Indian Ocean tsunami in Northwest Sumatra and Offshore Islands, *Earthquake Spectra, Special Issue III* **22**, pp. s105-s135.

Jezek, P.A., and Hutchison, C.S.: 1978, Banda Arc of Eastern Indonesia: petrology and geochemistry of volcanic rocks, *Bulletin Volcanology* **41**, pp. 586-608.

Katili, J.A.: 1978, Past and present geotectonic position of Sulawesi, Indonesia, *Tectonophysic* **45**, pp. 289 - 322.

Katili, J.A.: 1989, Review of past and present geotectonic concepts of eastern Indonesia, *Netherlands Journal of Sea Research* **24** (2/3), pp. 103 - 129.

Kopp, H., Flueh, E.R., Petersen, C.J., Weinrebe, W., Wittwer, A., Meramex Scientists.: 2006, The Java margin revisited: Evidence for subduction erosion off Java, *Earth and Planetary Science Letters* **242**, pp. 130-142.

Kusumadinanta, K.: 1979,Data dasar Gunung api Indonesia. Bandung, *Volcanological Survey of* Indonesia, 820 p. (In Indonesian)

Latter, J.H.: 1981, Tsunamis of volcanic origin: summary of causes, with particular reference to Krakatoa, 1883, *Bulletin Volcanologique* **44**, pp. 467 - 490.

Malod, J.A., Karta, K., Beslier, M.O., and Zen Jr, M.T.: 1995, From normal to oblique subduction: Tectonic relationships between Java and Sumatra, *Journal of Southeast Asian Earth Sciences* **12** (1/2), pp. 85 - 93

McCloskey, J., Nalbant, S.S., and Steacey, S.: 2005, Earthquake risk from co-seismic stress, *Nature* **434**, pp. 291.

McCaffrey, R.: 1988, Active tectonics of the Eastern Sunda and Banda Arcs, *Journal of Geophysical Research* **93** (B12), pp. 15, 163 - 15,182.

McCaffrey, R.: 1989, Seismological constraints and speculations on Banda Arc tectonics, *Netherland Journal of Sea Research* **24**, pp. 141-152.

McCaffrey, R.: 2008, Global frequency of magnitude 9 earthqukaes, *Geology* **36** (3), pp. 263-266. *The Geological Society of America*

McCann, W.R., Nishenko, S.P., Sykes, L.R, and Krause, J.: 1979, Seismic gaps and plate tectonics: Seismic potential for Major Boundaries, *Pure and Applied Geophysics* **117**, pp. 1082-1147.

Milsom, J.: 2001, Subduction in eastern Indonesia: how many slabs?, *Tectonophysics* **338**, pp. 167-178.

Moon, V., Bradshaw, J., de Lange, W.:2008, Geomorphic development of White Island Volcano based on slope stability modeling, Engineering Geology, doi:10.1016/j.enggeo.2008.08.003.

More, G.F., Curray, J.R., Moore, D.G., and Karig, D.E.: 1980, Variations in geologic structure along the Sunda fore Arc, northeastern Indian Ocean, in The Tectonic and Geologic Evolution of Southeast Asian Seas and Island, D.E.Hayes (Eds), *American Geophysical Monograph* **23**, pp. 145-160.

Morrice, M.G., Jezek, P.A., Gill, J.B., Whitford, D.J., and Monoarfa, M.: 1983, An introduction to the Sangihe Arc: Volcanism accompanying Arc-Arc collision in the Molluca Sea, Indonesia, *Journal of Volcanology and Geothermal Research* **10**, pp. 135 - 165.

Natawidjaja, D.H.: 2003, Neotectonics of the Sumatran Fault and Paleogeodesy of the Sumatran subduction zone, Ph.D. thesis, *California Institute of Technology*., Pasadena. USA.

Newcomb, K.R., and McCann.: 1987, Seismic history and seismotectonic of the Sunda Arc, *Journal of Geophysical Research* **92** (B1), pp. 421 - 439.

Nishimura, S., Harjono, H., Suparka, S.: 1992, The Krakatau Islands: The Geotectonic Setting, *GeoJournal* **28.2**, pp. 87-98.

Okal, E.A., and Raymond, D.: 2003, The mechanism of great Banda Sea earthquake of 1 February 1938: applying the method of preliminary determination of focal mechanism to a historical event, *Earth and Planetary Science Letters* **216**, pp. 1 - 15.

Okal, E.A., and Synolaki. C.E.: 2008, Far-field tsunami hazard from mega-thrust earthquakes in the Indian Ocean, *Geophysical Journal International* **172**, pp. 995 - 1015.

Prasetya G.S., De Lange, W.P., and Healy, T.R.: 2000, Volcanic tsunami generations mechanism based on Krakatau event 1883 and future mitigations in *Regional Report on Tsunami Research*, Shuto. F (ed), Japan, pp. 1-14.

Prasetya, G.S., De Lange, W.P., and Healy, T.R.: 2001, The Makassar Strait, tsunamigenic region, Indonesia. *Journal of Natural Hazard*, **24**, pp. 295 - 307.

Prasetya, G.S.: 1998. Modelling of Volcanic Tsunamis. MSc. Thesis. Department of Earth Sciences. 300.p.

Puspito, N., and Shimazaki, K.: 1995, Mantle structure and seismotectonics of the Sunda and Banda Arcs, *Tectonophysics* **251**(1-4), pp. 215 - 228.

Puspito, N.T.: 1995, General Seismological features of tsunamis in Indonesia. *Proceeding Workshop on Tsunami 1995*, LPTP-BPP Teknologi, Jakarta. 25 p.

Puspito, N.T. and Triyoso, W.: 1994, Aspek kegempaan tsunami di Indonesia: suatu tinjauan awal, *Seminar sehari masalah tsunami di Indonesia dan aspek-aspeknya. Bandung*, pp. 167-175 (in Bahasa Indonesia).

Prawirodirdjo, L., Bock, Y., McCaffrey, R., Genrich, J.F., Calais, E., Stevens, S.W., Puntodewo,S.S.O., Subarya, C., Rais, J., Zwick, P.C and Fauzi, R.M.: 1997, Geodetic observations of interseismic strain segmentation at the Sumatra Subduction zone, *Geophysical Research Letter* **24**, pp. 2601 - 2604.

Richter, C.F.: 1958, Elementary Seismology, 768 p. W.H. Freeman. San Fransisco. California.

Ruff, L.J., and Kanamori, H.: 1980, Seismicity and the subduction process, *Journal of Physics Earth Planet International* **23**, pp. 240 – 252.

Silver, E.A., McCaffrey, R., and Smith, R.B.: 1983, Collision, rotation, and the initiation of subduction in the evolution of Sulawesi, Indonesia, *Journal of Geophysical Research* **88** (B11), pp. 9407-9418.

Stein, S., and Wysession, M.: 2002, Introduction to seismology, earthquakes and earth structure, 498 p.*Wiley Blackwell*. London.

Synolakis, C.E., and Bernard, E.: 2006, Tsunami Science before and beyond Boxing Day 2004. *Philosphical Transactions of The Royal Society A* **364**, pp. 2231 - 2265.

Rangin, C., Le Pichon, X., Mazzotti, S., Pubellier, M., Chamot-Rooke, N., Aurelio, M., Walpersdorf, A., and Quebral, R.: 1999, Plate convergence measured by GPS across the SUndaland/Philippine Sea Plate deformed boundary: The Philippines and eastern Indonesia, *Geophysical Journal International* **139**, pp. 296 - 316.

Rynn, J.: 2002, A preliminary assessment of tsunami hazard and risk in the Indonesian region, *Science of Tsunami Hazards* **20**, pp. 193 - 215.

Schulter, H.U., Gaedicke, C., Roeser, H.A., Schreckenberger, B., Meyer, B., Reichert, C., Djajadihardja, Y., and Prexl, A.: 2002, Tectonic features of the southern Sumatra-western Java Forearc of Indonesia, *Tectonics* **21** (5), pp. 11 - 15.

Sigurdsson, H., and Carey, S.: 1992, Eruptive history of Tambora volcano, Indonesia. In: Degens, E.T, Wong, H.K, Zen, M.T, (eds). The Sea off Mount Tambora, *Mitteilschen Geol-Paleont Inst Univ Hamburg* **70**, pp. 187 - 206.

Slothers, R.B.: 1984, The great Tambora eruption in 1815 and its aftermath, *Science* **224**, pp. 1191-1198.

Van Padang, N.: 1951, Indonesia. Catalog of Active Volcanoes of the World and Solfatara Fields. Rome: *IAVCEI* **1**, pp. 1-271.

Van Padang, N.: 1959, Change in theop of Mount Ruang (Indonesia), *Geol end Mijnbouw* **21**, pp. 113-118.

Van der Werff, W.: 1996, Variation in Forearc basin development along the Sunda Arc, Indonesia, *Journal of Southeast Asian Earth Sciences* **14** (5), pp. 331-349.

Widiantoro, S., and van der Hilst, R.: 1997, Mantle structure beneath Indonesia inferred from high-resolution tomographic imaging, *Geophysical Journal International* **130**, pp. 167 - 182.

_____, ITDB/PAC.: 2004, Integrated Tsunami Databases for the Pacific. Version 5.11 of July 2004. CD-ROM *Tsunami Laboratory*. IcmmG,SD RAS. Novosibirsks, Russia.

_____, Volcanology Survey of Indonesia: 1986, *Annual Report of the Volcanological Survey* 1984-1985.

Chapter 3

Tsunami Model, Benchmark Test, and the Boxing Day Event Simulated

3.1. Introduction

The progress towards a more realistic understanding of the entire tsunami evolution process from generation to runup started in the early 1990's. Coordinated field data collection following events, as well as large-scale laboratory and numerical model research were undertaken, and become available following the September 2, 1992 Nicaraguan tsunamis (Figure 3.1).

Figure 3.1. A decade of tsunami events in the 1990s provided an opportunity for a more realistic understanding of the entire tsunami evolution process from generation to runup. (Source image: Gonzales 1999).

During this decade, an advance in understanding of tsunami generation, propagation and runup, and the importance of landslide-triggered tsunamis, as observed during the Flores event in 1992 and Papua New Guinea in 1998 (Synolakis and Bernard, 2006), was achieved. Numerical models of tsunamis were tested with benchmark cases developed from laboratory experiments, as well as field measurements, through a series of international workshops on long wave runup models (Liu et al. 1991; Yeh et al. 1996). Models used different equations and numerical solution techniques, and some had included inundation models as well as generation and propagation code. These models are TUNAMI N1, N2 and N3 developed by the Disaster Control Research Center, Tohoku University (Imamura et al. 1988, Imamura 1996) for the purpose of creating an early warning system. They were derived from the Goto and Shuto (1983) model and implemented in Japan. The models have been transferred to other tsunami prone countries through the TIME Project (Tsunami Inundation and Modelling Exchange) of IOC – UNESCO.

Another important model is MOST (Method of Splitting tsunamis) from NOAA, which was originally developed by Vasily Titov and Costas Synolakis at the University of Southern California (Titov and Synolakis, 1998). After the Boxing Day 2004 tsunami, this model was implemented through most Indian Ocean countries, and is now known as the Community MOST Model Interface (COMMIT). Less commonly used models include: COMCOT (Cornell Multi-grid Coupled Tsunami Model) developed by a researcher at Cornell university (Liu et al. 1995); CULWAVE (Cornell University Long and Intermediate Wave Modeling Package) developed by Lynett and Liu (2002); and FUNWAVE developed by Kennedy et al. 2000.

TUNAMI, MOST and COMCOT are used nonlinear shallow-water (NSW) equations with different finite-difference algorithms. In contrast CULWAVE and FUNWAVE utilize several high-order depth integrated wave hydrodynamics models (Boussinesq-type models) to represent the highly non-linear behaviour of tsunami waves during inundation, and the dispersivity of tsunami generated by landslide processes. Some other models use a finite element solution for tsunami modeling, such as the Kawahara model (Kawahara et al, 1978) and ADCIRC (Priest et al. 1997).

Since the 2004 Boxing Day mega-tsunami, interest in the numerical modelling of tsunamis has grown substantially. With many researchers worldwide, the development of new models and algorithms is ongoing. Synolakis and Bernard (2006)

reviewed the state-of-knowledge before the Boxing Day 2004 event, and identified key aspects for future research. These are:

- Validated inundation models need to be developed and improved through benchmark testing and instrumental tsunameter measurements. Standards for operational codes need to be established.
- A methodology is needed to better quantify short-duration impact forces on structures.
- The mapping of vulnerable continental margins to identify unrecognized hazards must proceed expeditiously, along with paleotsunami research to establish repeat intervals.
- Models of the coupling between deforming seafloor motions and propagation model initializations need further refinement.
- Comprehensive educational efforts on tsunami hazard mitigation are necessary worldwide.

3.2. The 3DD numerical model

The numerical model known as 3DD modeling suites (Black 2001) consists of a series of coupled numerical models that simulate physical and biological processes in marine and freshwater environments. In this research, two modules were used, the 3DD hydrodynamic module to simulate the behaviour of tsunami waves, and POL3DD to simulate debris dispersal caused by tsunamis. 3DD is a 3-dimensional-baroclinic model based on the nonlinear shallow water equations (NSW), that uses a fully explicit time stepping solution (Black 2001). The model has been applied at scales from micro-scale circulation over sand beds (Black and Vincent, 2001) to continental scale circulation (Middleton and Black, 1994). The common application of the model is for estuaries with large inter-tidal zones, where flooding and drying processes are important. The 3DD flooding and drying scheme was designed to allow smooth transitions between dry and flooded conditions, without developing instabilities or "spikes" in the currents that frequently occurs in modeling of a large intertidal zone due to inappropriate numerical solutions. POL3DD is a Lagrangian 3-dimensional dispersal model that links to 3DD. The model has broad capabilities for modelling transport of dissolved, passive and active material such as larvae, effluent, bacteria or sediment in a homogenous or stratified ocean, on continental shelf or

shallow water environments. The model solves the Lagrangian form of the transport/dispersion equations using a particle tracking technique (Black 1996, 2001).

3.2.1. The Governing Equations

The momentum and mass conservation equation

3DD solves the momentum and mass conservation equation in 3-dimensions given by:

$$\frac{\partial u}{\partial t}+u\frac{\partial u}{\partial x}+v\frac{\partial u}{\partial y}+w\frac{\partial u}{\partial z}-fv=-g\frac{\partial \varsigma}{\partial x}-\frac{1}{\rho}\frac{\partial P}{\partial x}+A_H\left(\frac{\partial^2 u}{\partial x}+\frac{\partial^2 u}{\partial y}\right)+\frac{\partial}{\partial z}\left(N_Z\frac{\partial u}{\partial z}\right) \quad 3.1$$

$$\frac{\partial v}{\partial t}+u\frac{\partial v}{\partial x}+v\frac{\partial v}{\partial y}+w\frac{\partial v}{\partial z}+fu=-g\frac{\partial \varsigma}{\partial y}-\frac{1}{\rho}\frac{\partial P}{\partial y}+A_H\left(\frac{\partial^2 v}{\partial x}+\frac{\partial^2 v}{\partial y}\right)+\frac{\partial}{\partial z}\left(N_Z\frac{\partial v}{\partial z}\right) \quad 3.2$$

$$w=-\frac{\partial}{\partial x}\int_{-h}^{z}u dz-\frac{\partial}{\partial y}\int_{-h}^{z}v dz \quad 3.3$$

t is the time in second, u, v are horizontal velocities in the x, y directions respectively (ms^{-1}), w the vertical velocity (positive upward) (ms^{-1}), h the depth (m), g the gravitational acceleration (ms^{-2}), ζ the sea level above a horizontal datum (m), f the coriolis parameter, P the baroclinic component of the pressure (Pa), A_H the horizontal eddy viscosity coefficient (m^2s^{-1}), and N_z the vertical eddy viscosity coefficient (m^2s^{-1}). All units are in metric sytem (meters, kilograms, and seconds).

The advection/diffusion equation

The Eulerian governing equation of POL3DD for advection/diffusion is:

$$\frac{\partial C}{\partial t}=\frac{\partial}{\partial x}\left(E_x\frac{\partial C}{\partial x}-uC\right)+\frac{\partial}{\partial y}\left(E_y\frac{\partial C}{\partial y}-vC\right)+\frac{\partial}{\partial z}\left(E_z\frac{\partial C}{\partial z}+\psi_s C-wC\right)-kC+S_s \quad 3.4$$

where C is the concentration, t is time, x,y,z are orthogonal spatial coordinates, E_x, E_y, and E_z are coefficients of eddy diffusivity, ψ_s is the still water fall velocity under gravity, and u,v,w are horizontal and vertical components of the fluid velocity, k is the decay coefficient for a non-conservative tracer (e.g. $k = 2.3/T_{90}$ for faecal indicator bacteria) and S_s is the tracer/effluent source term. Currents and sea level from the 3DD model results are used to specify the circulation in POL3DD. Currents derived

from a hydrodynamic model firstly advect particles, while diffusion is modeled as a random walk, with position increments proportional to horizontal and vertical eddy diffusivity (Black, 2001).

Conservative water-borne transport is often simulated to examine pollutant pathways, destination and residence times. Particles can be tracked until they leave the model region and their interactions with the environment are simulated. Chemical pollutants react according to their own signatures, while E coli and faecal coliform concentration depends on solar radiation levels and water clarity. Oil spills have many unique characteristics, including density of the oil, leakages, evaporations rates and vertical mixing into the water column, which are considered inside the model. To investigate the distribution of a range of pollutants based from identified sources, four types of sub-models are used within POL3DD: conservative, chemical pollutants, E.Coli and oil spills. Details of the equations, treatment, and solutions used by the sub-models are presented in Black (2001).

In shallow water, all forces acting on the water column must be considered to accurately model tsunami inundation. During inundation, the wavelength of the incident tsunami becomes shorter while the amplitude, steepness and curvature of water level increase. Factors such as the Coriolis force, the baroclinic component of the pressure, and the inertia force caused by the vertical acceleration of the water can be ignored. However, the convective inertia force and bottom friction become increasingly important. The treatment of these parameters within the model is discussed below.

Bed Friction and Eddy Viscosity

At the sea bed, z = -h, and the horizontal bottom stresses represented by the last term in equations 3.1 and 3.2 become respectively:

$$\rho N_z \frac{\partial u}{\partial z} = \tau_x^h \qquad \rho N_z \frac{\partial v}{\partial z} = \tau_y^h \tag{3.5}$$

where τ_x^s and τ_y^s denote the components of bottom stress :

$$\tau_x^h = \frac{\rho g u_h \left(u_h^2 + v_h^2\right)^{0.5}}{C^2} \qquad \tau_y^h = \frac{\rho g v_h \left(u_h^2 + v_h^2\right)^{0.5}}{C^2} \tag{3.6}$$

with u_h and v_h being the bottom currents and C is Chezy's coefficient which varies according to the bed type and depth.

This can be expressed as:

$$C = 18 \log_{10}(0.37\ h/z_o)\ , \qquad 3.7$$

where z_o is the roughness length as defined by the Karman-Prandtl vertical velocity profile. Typical values of z_o are in the order of 0.001 m for simulating the tidal hydrodynamics in estuaries, 0.01 m for rough irregular beds, and 0.08 m over very rough beds such as coral reefs (Black 2001). To calibrate the model, these values need to be adjusted according to the type of land cover. For our inundation modeling, we varied the bed friction throughout the model domain according to the roughness length, which represented different surface topography or land cover types as suggested by Black (2001) for modeling large intertidal areas, estuaries or over rough bed or boulders.

The horizontal eddy viscosity coefficient A_H is used to represent the formation of small-scale vortices ('eddies') in the flow. This value should be set with care, as excessive values will smooth out small-scale features in the flow. We assumed a value of 1 for offshore propagation and 5 for overland flows.

Flooding and Drying

The 3DD flooding and drying scheme is designed to allow smooth transitions and reduce instabilities by avoiding sudden jumps in the current velocity during the drying and wetting processes. The model uses two parameters to control these: the *effective depth value* and *drying height*. The effective depth is used in the bed friction term to prevent this value from becoming too large near zero depths. The drying height is the depth when the model considers a cell to be 'dry' in flooding and drying zones. The necessary value for these two parameters to control the tsunami overland flow was obtained through model calibration. For this case, it was found that standard values of 0.3 m for the effective depth and 0.05 m for the drying height were acceptable.

3.2.2. Benchmark testing and validation

Benchmark testing and validation of the model was carried out by Borrero et al. (2007) to introduce the tsunami modeling capabilities of 3DD. The model was used to specifically replicate benchmark problem #2, from the 3rd International workshop on Long Wave Runup Model held on June 17-18 2004, on Catalina Island at the

Wrigley Marine Science Center (Figure 3.2). The objective of the benchmark problem is to calibrate a numerical model to accurately reproduce the runup behaviour of a simulated tsunami in a laboratory experiment. The experiment was a simulation of the 1993 Okushiri tsunami as it affected an area near the village of Monai on Okushiri Island. In the real event, the highest runup of 32 m was recorded here where the tsunami runup mark was noted in a narrow gulley.

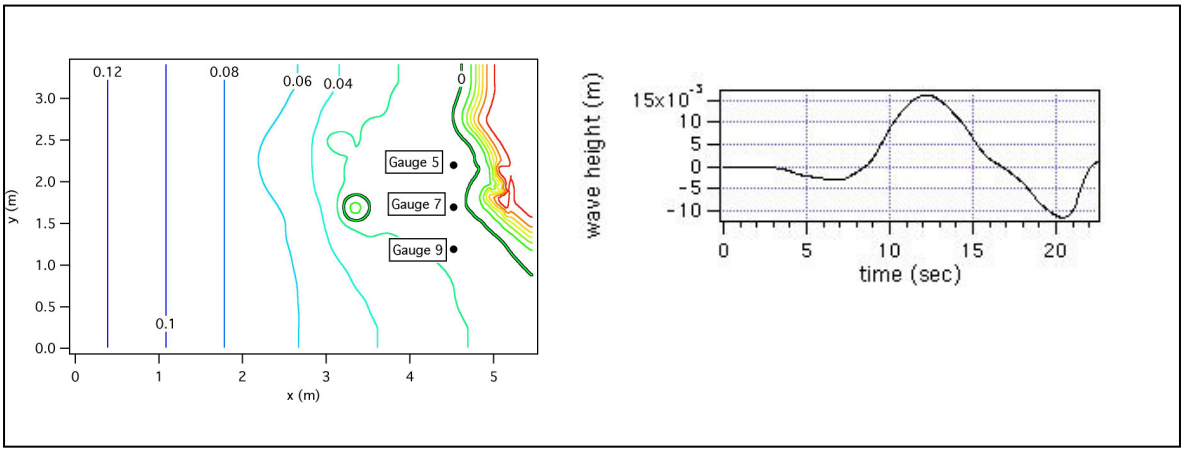

Figure 3.2. Model bathymetry and input time series as provided for the benchmark problem (Borrero et al. 2007).

Model Setup

Two models were setup to replicate the benchmark problem due to the coding structures of 3DD where the dimensions of the computational domain are limited to data values with a length scale precision of .01 m. One model used a scale factor of 9 (3DD x9) and the other was scaled up 100 times (3DD x100). The time dimension was scaled by the square root of the overall scale factor; i.e. 3 or 10 respectively.

Four parameters that affect the waves propagation and inundation in 3DD were as follows: the effective depth, drying height, roughness length and eddy viscosity. The effective depth value is added to the actual depth in bed friction terms in depth-averaged simulations to prevent the terms becoming too large in shallow (depth near zero) water. The drying height is the depth when the model considers a cell wall to be dry in an inter-tidal zone. Roughness length is used in the calculation of the seabed friction through the Chezy formula given by equation 3.7.

The eddy viscosity term is used to simulate small-scale *vortices* (or *eddies*) in the flow by applying a larger scale parameter that characterizes the transport and dissipation of energy in the smaller scale flow. At the laboratory scale where

roughness was not known, the seabed friction was obtained from model calibration. The model parameters are listed in Table 3.1 below.

Table 3.1: Model settings for 3DD to replicate tsunami benchmark case #2.

	Effective depth (m)	Drying height (m)	Roughness length (m)	Eddy viscosity (m^2s^{-1})
Model x100	0.2	0.01	0.0001	0.1
Model x9	0.02	0.01	0.0001	0.01

Results

Comparison of the numerical model output at a grid node near the western boundary to the original input data is illustrated in Figure 3.3. The model results shows that the input wave in the two models is exactly the same as the initial input. The scale changes were proportional and did not affect the initial wave shape. Further, time series of water surface elevation were extracted from three locations that corresponded to wave gauge locations in the experimental set up as illustrated in Figure 3.4 (a-c).

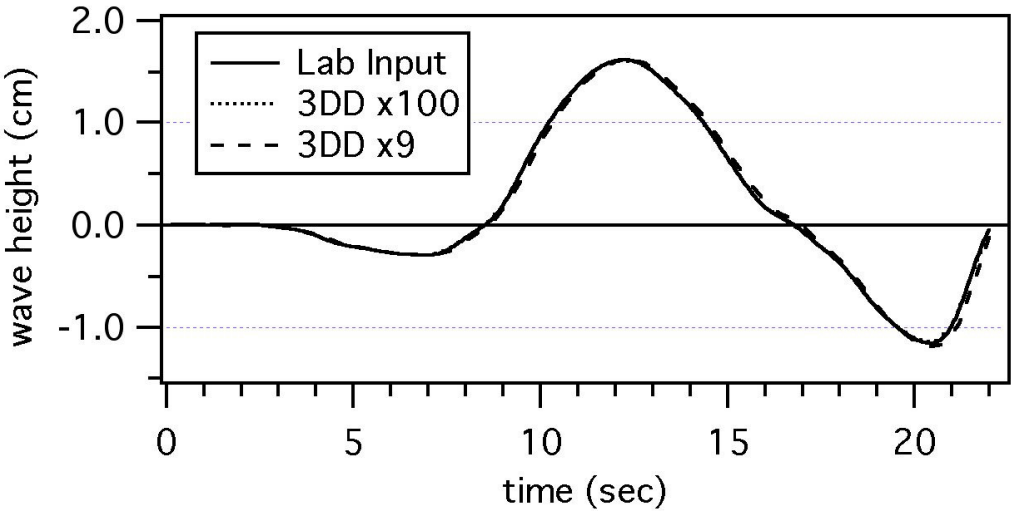

Figure 3.3. Comparing laboratory input data to model results from a grid node close to the western boundary (Borrero et al. 2007).

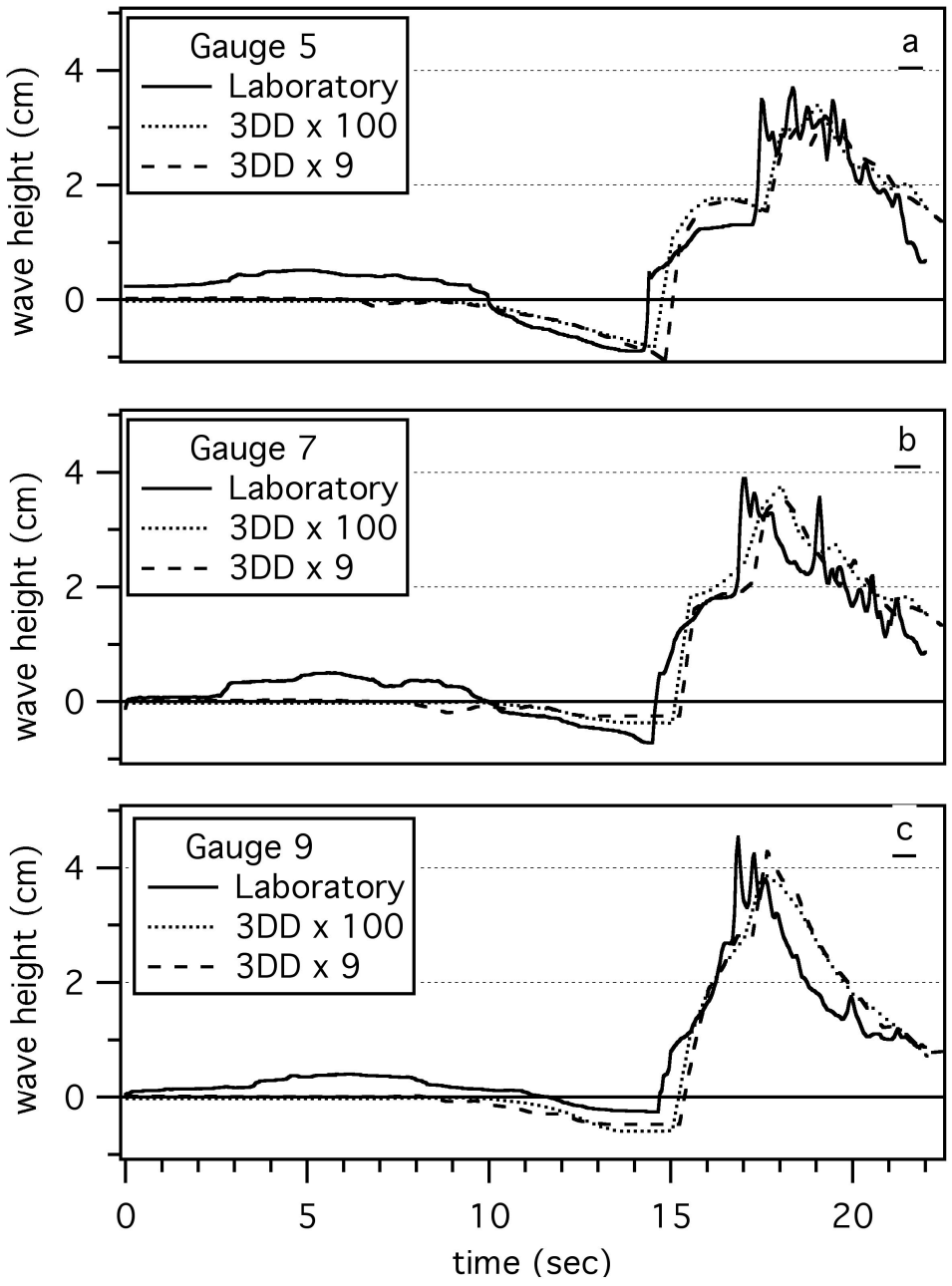

Figure 3.4 (a-c). Comparisons of the model output to the experimental data at three locations (Borrero et al. 2007).

For all three gauges, the model showed a time lag of about 0.5 s and the high frequency oscillations in the laboratory data are not perfectly reproduced in the model. This is likely due to the fact that the oscillations correspond to surface fluctuations as the wave nears breaking, something that is not accounted for in the long wave, depth averaged model. Although there is some discrepancy between the model and the measured data on the wave lead in phase, the wave height compares very well overall

to the laboratory data. Borerro et al. (2007) noted that the model output from 3DD is virtually identical (phase lag included) to results obtained by Chawla et al. (2005) using the popular MOST models for the same benchmark study.

For the runup, the maximum runup of 6.45 m is observed in the cove for the 3DD x 100 models as illustrated in Figure 3.5. Recalculated to the Okushuri coast scale (4 times larger) this corresponds to a runup of 25.8 m. For the 3DD x 9 cases, the maximum run up is 0.715 m. When expanded to full scale (44.4 times larger), this corresponds to runup of 31.8 m, compared to the measured value of 32 m (Borerro et al. 2007).

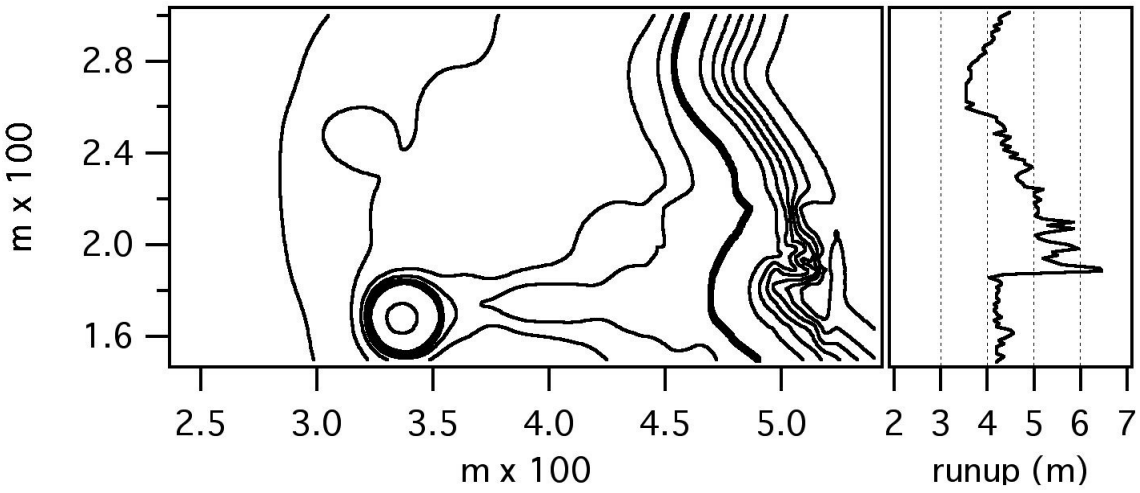

Figure 3.5. Plotting of the wave runup along the eastern boundary for the 3DD x100 case (Borrero et al. 2007).

3.2.3. Model Performance Statistics

Model performance statistics are utilized to ensure that performance of numerical models can quantitatively assess (Aida, 1978; Sutherland et al., 2004) as an addition to the normally qualitative assessment ranking such as "poor", "good" and "excellent" or "compares very well". Various model performance measures include bias, accuracy (Mean Absolute Error (MAE), Root Mean Squared Error (RMSE)), and skill (Brier Skill Score (BSS)) (Sutherland et al., 2004), and correction factor (K) and fluctuation measures (k) of Aida (1978).

Results of the model performance statistics applied for Gauges 5, 7, and 9 (Table 3.2) indicate that the model had a tendency of consistently slightly under predicting with low bias values (in cm) of -0.68, -0.29 and -0.58 respectively. The accuracies are shown by low values of RMSE and MAE, which are 1.65 cm and 1.32

cm for Gauge 5; 1.35 and 1.06 for Gauge 7, and 1.39 and 1.10 for Gauge 9. The skill score (BSS) that had a value of between 0 – 1 (perfect agreement gives a skill score of 1) shows that Gauges 7 and 9 had skill scores of 0.91 and 0.96 respectively, and Gauge 5 had 0.89. These numbers suggest that the model had a skill to reproduce 90-95% of comparable wave height. This also supported by the K and k factor of Aida (1978) that gave correction factor values of 0.89 to 0.97 and fluctuation factor of 0.07 to 0.12 respectively.

Table 3.2 Model Performance Statistic Results.

Score	Gauge 5	Gauge 7	Gauge 9
Bias	-0.68	-0.29	-0.58
RMSE (Root Mean Squared Error)	1.65	1.35	1.39
MAE (Mean Absolute Error)	1.32	1.06	1.10
BSS (0 – 1) (Brier Skill Score)	0.89	0.91	0.96
K (correction factor of Aida (1978))	0.95	0.97	0.89
k (fluctuation factor of Aida (1978))	0.12	0.10	0.07

3.2.4. Testing using LIDAR and Multibeam data sets.

Several model grids were used in defining the tsunami behaviour that needed to be resolved by 3DD during generation, propagation, and inundation. Ultimately a series of nested grids at progressively finer resolutions were applied to represent them, and define the model boundaries. This nested grid is applied to represent the necessary scenarios, starting from the regional behavior of tsunamis at the open ocean, to within bays, and then the finest resolution at the coast to resolve the mitigation measures for community, engineering design, and safety matters.

Topographic and bathymetric data for the model grid can be derived from several sources, including: GEBCO, ETOPO 2, SRTM, digitized navigational charts,

multi-beam data, and high-resolution digital terrain data (LIDAR data sets). The regional/wide area model grid was developed to incorporate all source scenarios that may significantly affect the coastal areas of interest. The grid size for regional/wide area models ranged from a few kilometers 1000 down to 500 m. Results from these models were used as initial condition for nested finer grids to model inundation. An important aspect of inundation modeling is the need to adequately represent coastal bathymetry and topography. High-resolution data sets are needed, and these can be derived from high-resolution bathymetric (multi-beam) survey, and topographic (LIDAR) survey, where the grid size can be made a maximum of 2 m resolution. LIDAR data consists of two types: ground striking and non-ground striking. Non-ground striking data consists of digital terrain data where all houses, structures and trees have not been removed, while ground striking data set was pure digital terrain data, where all structures, houses and trees have been removed.

Using LIDAR data set (ground and non-ground striking) of Whitianga Township, combined with high-resolution nearshore data from multi-beam surveys of Buffalo and Mercury Bays New Zealand (Prasetya et al. 2008), revealed that the 3DD tsunami model can handle highly non-linear bathymetric and topographic conditions, including all structures and vegetation covers, and produce a high accuracy result without having stability problem. The roughness length and horizontal eddy viscosity are varied according to the bathymetry and topography, as well as the type of land cover (building, structures and vegetations type). Standard values of roughness length used were 0.001 m for smooth and gently slooping topography, 0.01 m over rough irregular beds or topography, and 0.08 m for uneven random sea beds or topography. The horizontal eddy viscosity varies from 0.1 to 5 m^2/s. High eddy viscosity (in this case from 3 - 5 m^2/s) were set to the areas that had complicated geometry such as through the inlets or a complex of building or trees for inundation.

The model results using ground striking and non-ground striking of Whitianga Township, New Zealand, are illustrated in Figure 3.6 a-e. The ground striking data showed that the inundation flow interacted with the local topography condition which controls the maximum inundation distance inland, while the non-ground striking data sets show the interaction of the inundation flows with houses, structures, roading network, and vegetation, as well as the topographic condition that finally affects the pattern and maximum inundation distance inland.

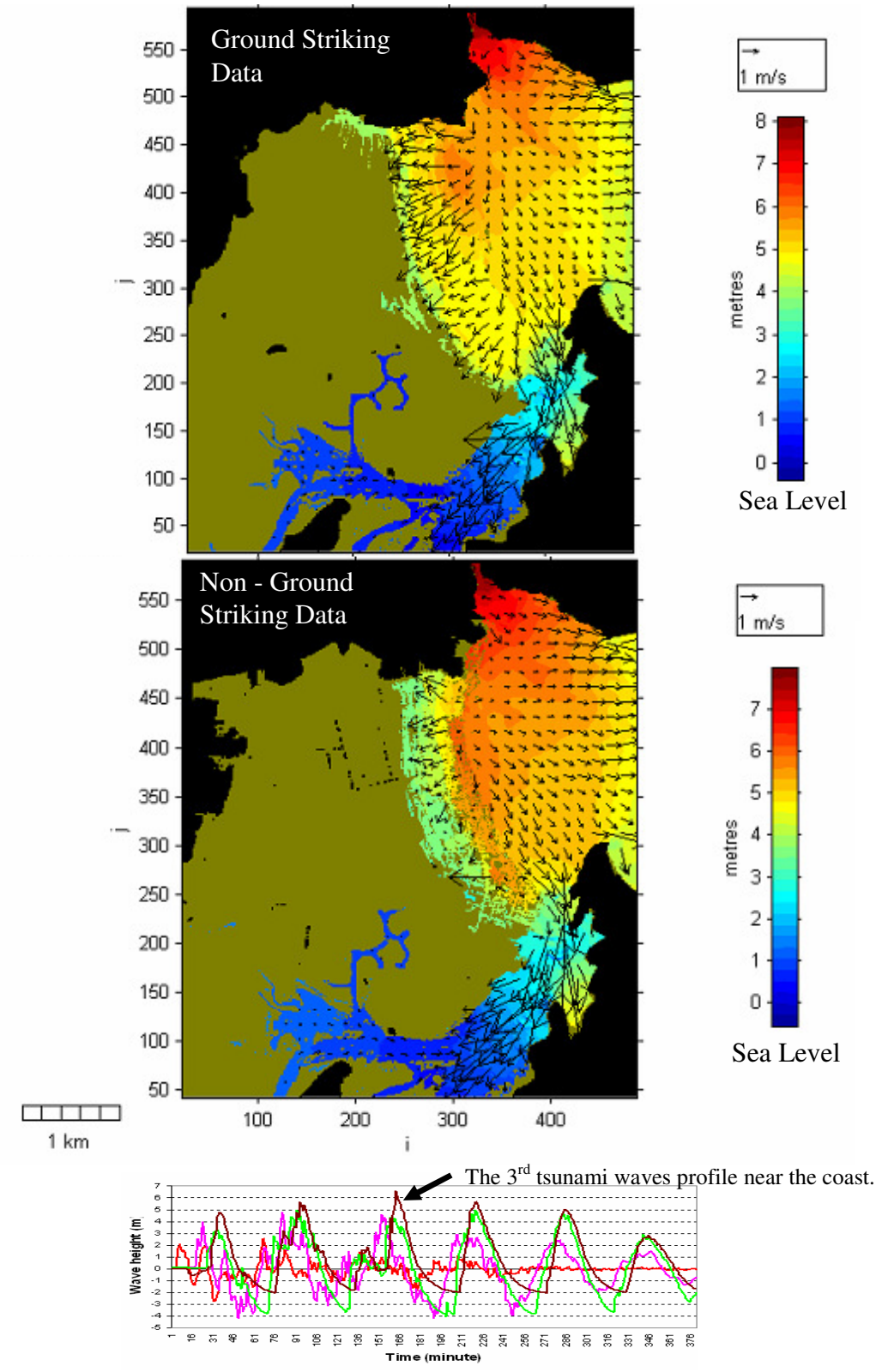

Figure 3.6.a. Different inundation dynamics are shown by ground striking and non-ground striking data at Whitianga, New Zealand during the third tsunami waves (black arrows on tsunami wave profile time series plot). For non- ground striking data, most of the flows are blocked and pass through the roads or between buildings and structures, while for ground striking data, the incoming inundation flows are almost uniform and only influenced by the local topography (source: Prasetya et al. 2008)

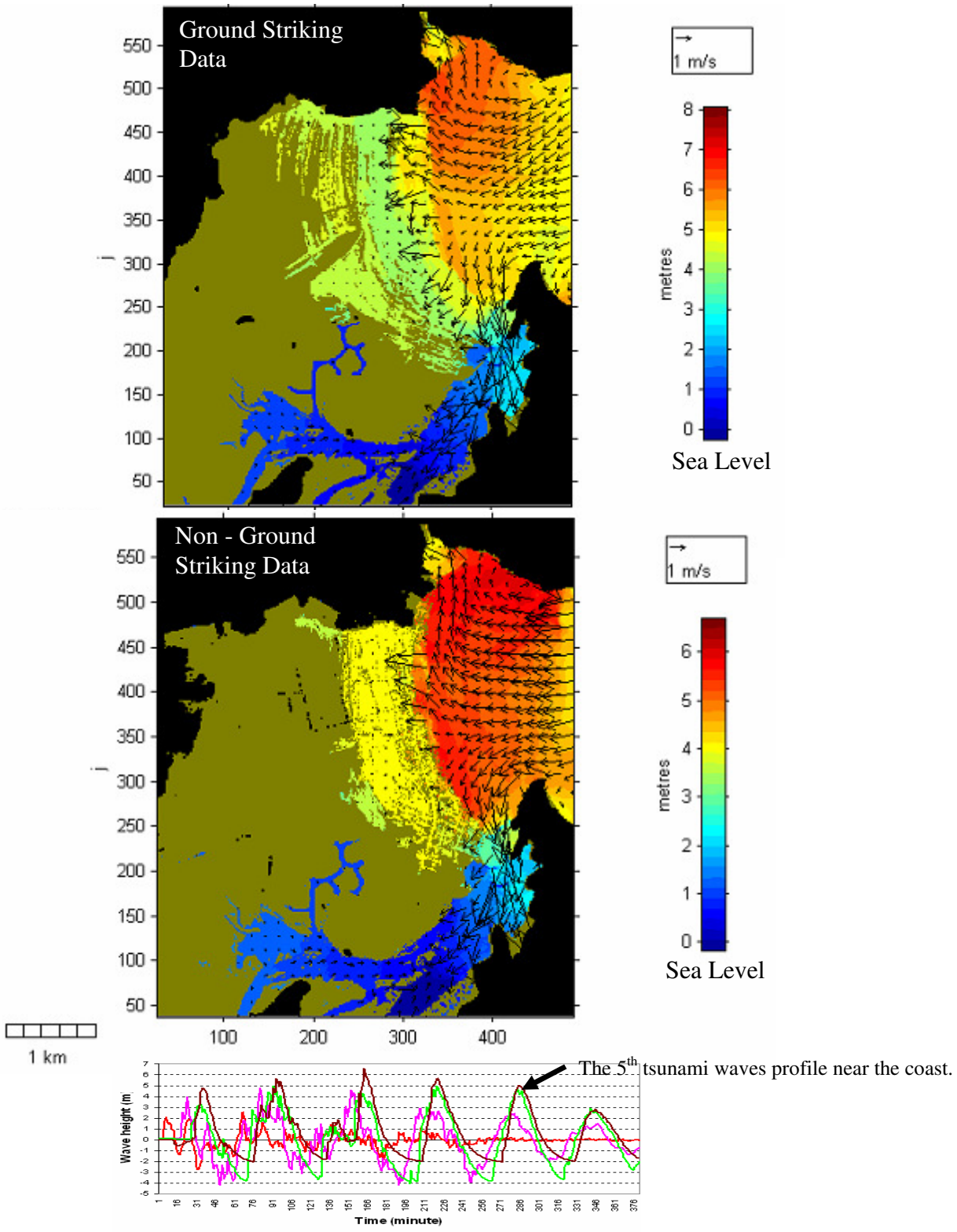

Figure 3.6.b. It's obvious that the inundation flow is influenced by the land cover condition. The extent of inundation flow inland is much shorter for non-ground striking data as shown after the fourth waves attacked. Further inland, the inundation flows prolong following the local terrain condition as gravity flows (source: Prasetya et al. 2008).

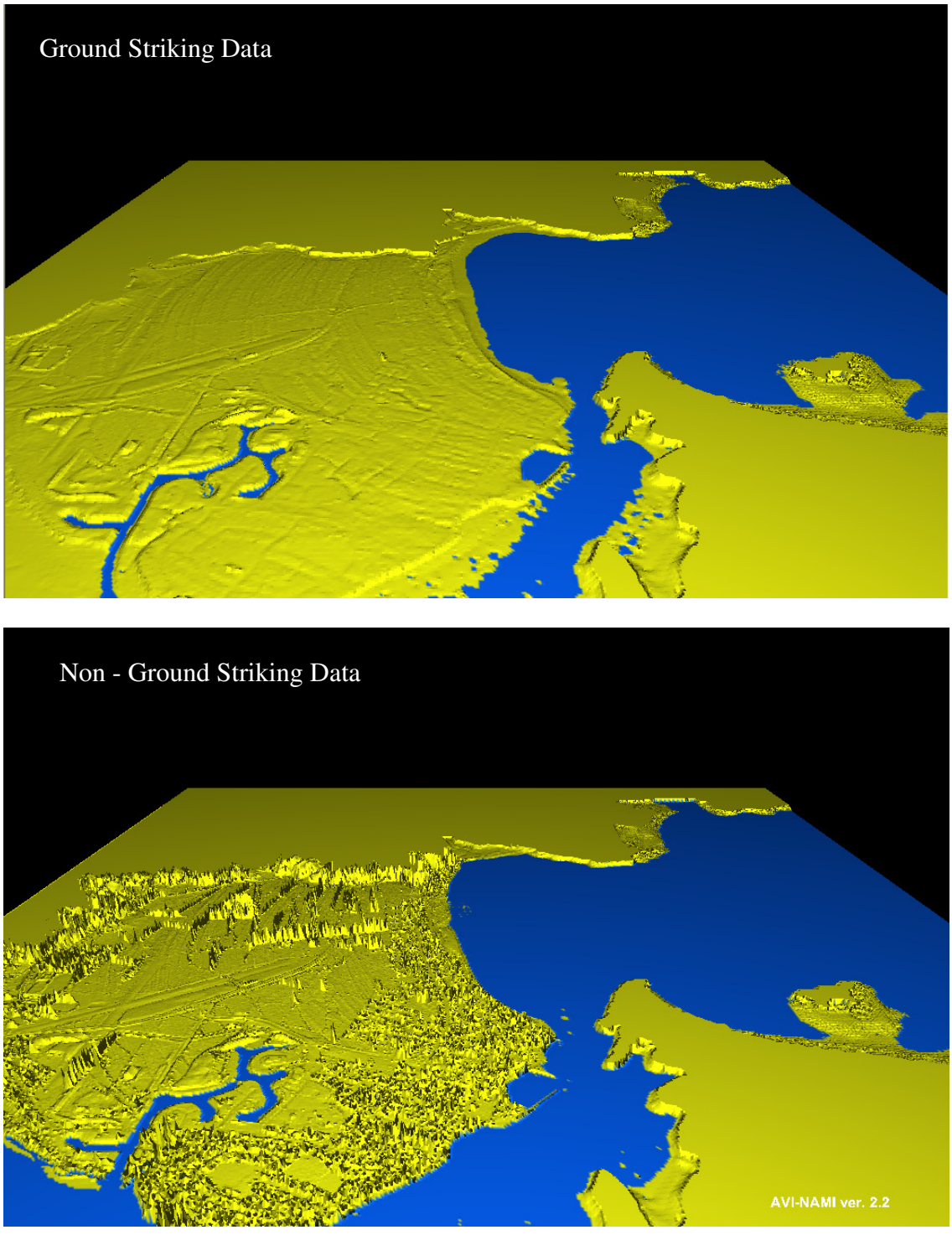

Figure 3.6.c. Example of three-dimensional plot of ground striking and non-ground striking data using Avinami ver.2.2 plotting tools.

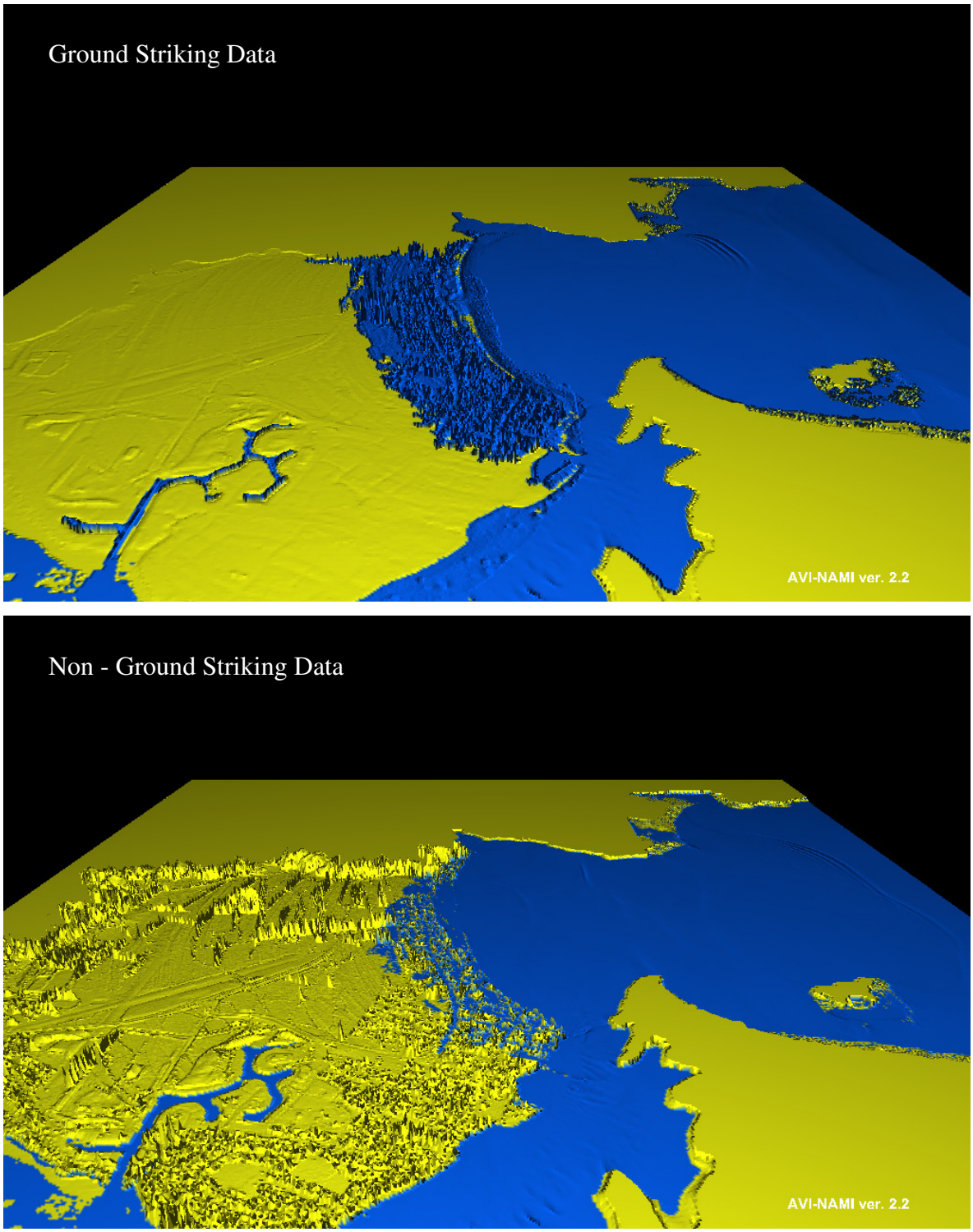

Figure 3.6.d Three-dimensional plot of 3DD model results using Avinami ver.2.2 plotting tools, shows different inundation pattern between ground striking and non-ground striking data from the same tsunami waves. On ground striking, tsunamis obviously penetrate further inland.

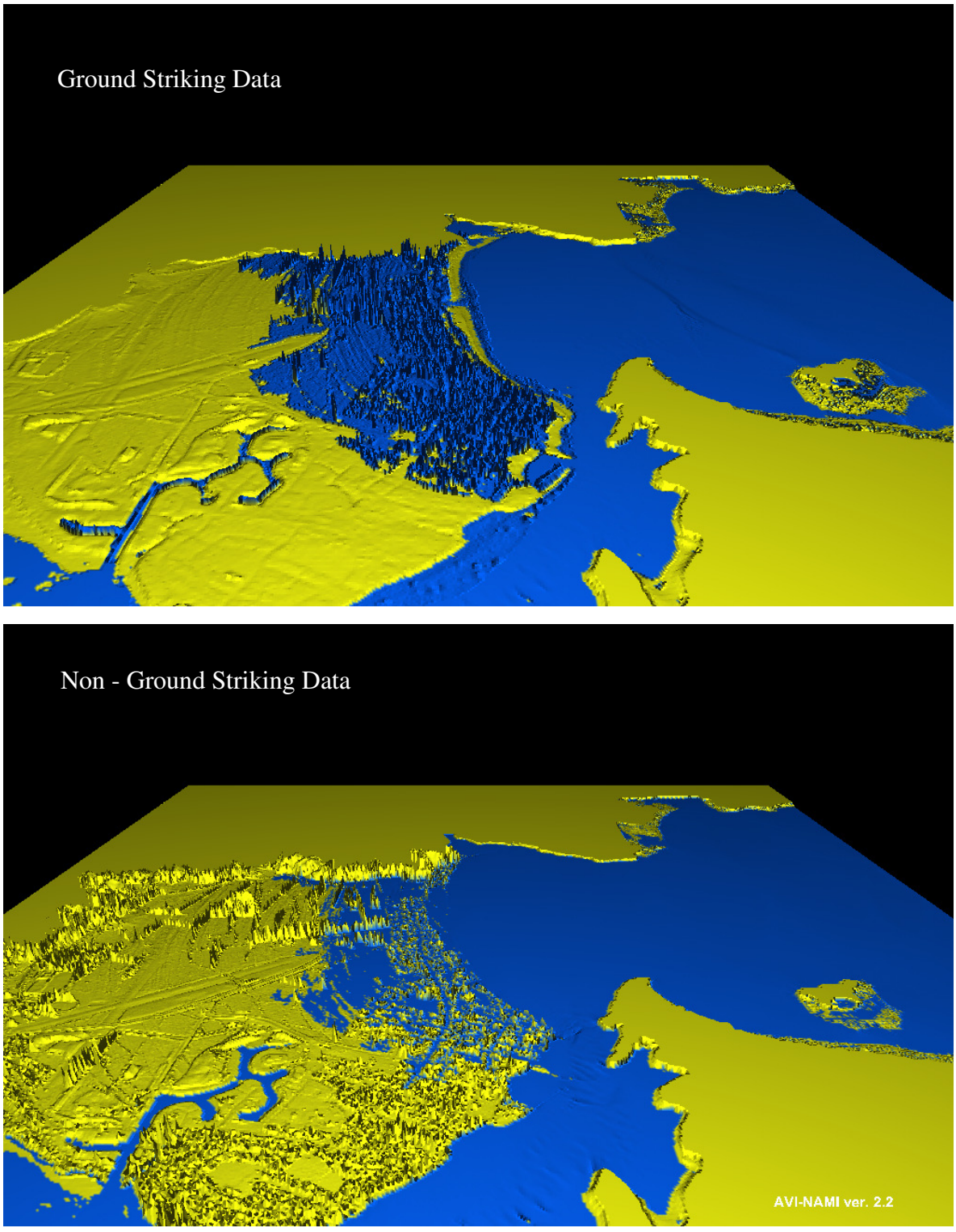

Figure 3.6.e. Inundation pattern after the 4th waves.

3.3. Modelling the 26 December 2004 Tsunami

The 3DD and POL3DD models were applied to the 2004 Tsunami event for the Banda Aceh region to investigate the inundation and debris dispersal dynamics. The results were written as papers that were submitted to the Journal of Natural Hazards (NHAZ 613 and NHAZ 899 - in review). The manuscripts for these papers form the rest of this chapter.

3.3.1. The Inundation Modelling

Results of inundation modelling of the 26 December 2004 Tsunami on Banda Aceh was written as a paper and submitted to Journal of Natural Hazards (NHAZ 613 – in review) as follow:

Modeling of Inundation Dynamics on Banda Aceh, Indonesia during the Great Sumatra Tsunamis 26 December 2004

Gegar Prasetya[1], Jose Borrero[2], Willem de Lange[1], Kerry Black[2], Terry Healy[1]

Abstract –The tsunami inundation flows on Banda Aceh, Indonesia reached 5 km inland during the 26 December, 2004 event and devastated most of the houses, buildings, and infrastructure along the coast, and killed more than 167,000 people. The overland flows from the northwest coast and the west coast collided at Lampisang village approximately 3.7 km from Ulee Lheue (northwest coast) and 6.8 km from Lhok Nga (west coast) as reported by survivors. Inundation modeling based on the nonlinear shallow-water wave equations reproduces the inundation pattern, and demonstrates a colliding of the overland flows. The model suggests that wave characteristics on the northwest coast of Banda Aceh were different from those on the waves that impacted upon the west coast. The areas, which experienced higher inundation levels, did not always experience greatest overland flow speeds, and the damage areas mostly coincide with the flow speed distribution rather than the runup and inundation depth.

Key words: Tsunami, Banda Aceh, inundation model

[1]Coastal Marine Group, Department of Earth and Ocean Sciences, University of Waikato, New Zealand. Email: gsp1@waikato.ac.nz
[2]ASR Ltd, Marine Consulting and Research, Raglan, New Zealand.

1. Introduction

The catastrophic tsunamis produced by the great Sumatra earthquake on December 26, 2004 inundated the coastal lowlands surrounding the Indian Ocean (Titov et al., 2005; Synolakis and Kong, 2006). The coastal area and offshore island of Aceh Province, Indonesia suffered the greatest devastation (Yalciner et al., 2005; Borerro et al, 2006; Jaffe et al., 2006). In Indonesia alone, more than 167,000 people perished and some 500,000 people were displaced (BRR, 2006).

The high velocities of the overland flows caused heavy casualties and extreme damage during the tsunami attack (Matsutomi et al., 2006; Synolakis and Bernard, 2006). In many coastal areas, the majority of the houses along the coast were completely destroyed. Only buildings made from reinforced concrete survived or were partially damaged. Floating debris such as fishing boats, damaged houses and other floating materials contributed to the damage.

Scour around man-made structures or trees were observed as well as large-scale erosion. At several river mouths, there was evidence of channel deepening, widening of the river mouth, enlargement of the estuaries and lagoons and sedimentation. These effects were not only observed along the coast of Banda Aceh Province, but at offshore islands Breuh and Simeulue. Inundation distances of up to 5 km led to salt-water contamination of the local freshwater supply.

To understand the patterns of tsunami inundation during the 26 December 2004 event, we conducted a detailed inundation modeling study using the two-dimensional hydrodynamic model 3DD (Black, 2001). Like most other hydrodynamic models used for tsunami propagation and inundation, it is based on the nonlinear shallow-water wave equations solved explicitly on an Eulerian grid with a flooding and drying scheme to simulate overland flows. This model was used by Borerro et al. (2007) to accurately reproduce tsunami hydrodynamics of propagation and runup for a standard benchmark problem used to validate numerical models (benchmark problem # 2 of the Third Workshop on Long Wave Runup Model, Liu et al., 2008). We used 3DD to simulate the patterns and extents of tsunami propagation throughout the Banda Aceh region.

2. Runup, flow depth and inundation

Our modeling results are compared to measurements of runup and inundation collected during post-tsunami field surveys conducted by the International Tsunami Survey Team (ITST) (Borrero, 2005; Yalciner et al. 2005; Borrero et al. 2006; Jaffe et al. 2006; Matsutomi et al. 2006) along the coastline of northern Sumatra and offshore islands (Nias, Banyaks, Babi, Simelue, Breuh and Weh Islands). Measured tsunami runup, flow depths and inundation distances are shown in Figure 1.

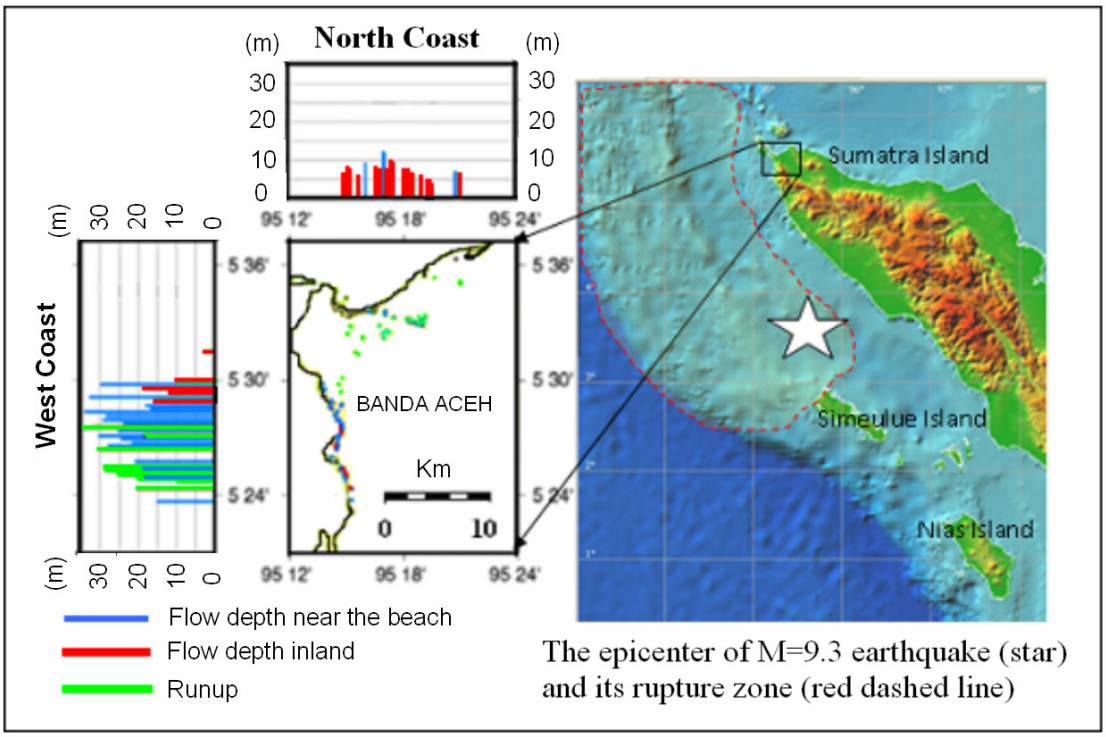

Figure 1. Measured values of tsunami runup, flow depth and inundation from field surveys carried out by the International Tsunami Survey Team (Borrero et al. 2006; Jaffe et al. 2006; Matsutomi et al.2006).

To avoid confusion between the terms *runup height*, *tsunami wave height* and *inundation* we used the definitions described in Synolakis and Okal (2005) as illustrated in Figure 2. The *flow depth* is measured from the ground level to the depth of the flow. This can be indicated by tsunami traces found on trees, walls of the buildings, and trim-lines on the hillsides. When referenced to mean sea level (MSL) this quantity is called the *tsunami elevation*. The *runup height* is the vertical elevation attained by the tsunami above MSL as measured at the limit of the inland flow. The corresponding horizontal distance measured from the shoreline is the *inundation distance*. The runup height depends upon the slope of the nearshore topography as well as the height of the incoming tsunami. For the same incident wave height, areas

with a gentle slope will experience lower runup heights but greater inundation distances as compared to the areas that have steeper slopes. Here usually, the largest maximum runup heights occurred in areas with steeper slopes at the shoreline.

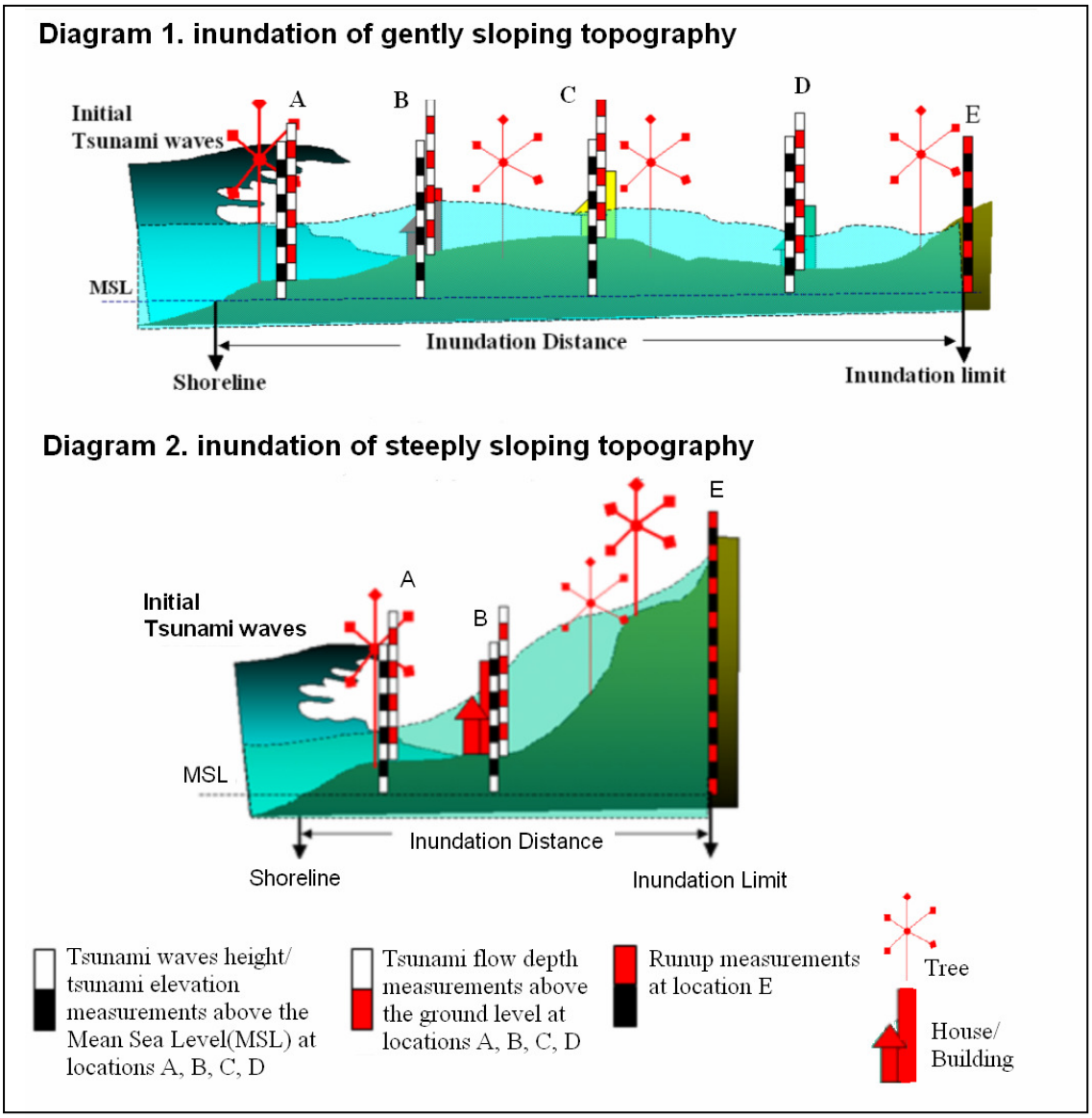

Figure 2. A schematic diagram defining the parameters of tsunami inundation (tsunami elevation, inundation, flow depth and runup). For tsunami waves of equal height along the coast, areas with steeper topography will experience higher runup heights and shorter inundation distance compared to the gentle slopes (Diagram 1 and 2). Flow depth usually measured from the traces found at trees or house/buildings that still stood after the tsunami attack.

Flow depths and runup heights were higher in the western part of Banda Aceh in comparison to the northern part. Along the northern shores of Banda Aceh, tsunami flow depths varied from 6 – 12 m and inundated the coastal plain up to 5 km inland. While on the west coast, flow depths were generally on the order of 15 – 25 m along the shores with extreme runup up to 35 m to the south of Lhok Nga. Nearshore

bathymetry, coastal topography, the type of ground cover and human land use significantly affected inundation distances. The effect of landforms on tsunami flows in the plains of Banda Aceh was studied by Umitsu et al. (2007). Using indicators of flow direction such as the orientation of broken fence posts, fallen trees and the columns of destroyed buildings, they showed that the inundation in the northern part of Banda Aceh was generally from the northwest, consistent with the early inferences of Borrero (2005).

The location where the northeastward propagating flows from the west coast penetrated the plain and met the flow from the north at the gap of the hills (Lampisang villages) is identified. A recent study by Paris et al (2007) at the west coast of Banda Aceh (Lhok Nga) documented the overland flow direction (indicated by tilted trunks and pillars, and debris wrapped around trees) as coming mostly from the west-southwest. In general, the overland flow direction based on the fieldwork (Borrero 2005, Borrero et al. 2006; Jaffe et al. 2006) and those by Paris et al. (2007) and Umitsu et al. (2007) has been inferred and indicated that, for the first 2 km from the shoreline, the inundation flow directions followed the direction of the incoming tsunamis. The land features on the coastal plain of Banda Aceh within this range did not affect the flow direction. The direction of the flow was changed when the inundation distance reached ~ 2.5 km inland. At this point, the flow depth reduced from 9 -10 m at the shoreline, to 2.5 – 3.5 m. Less information has been found on the tsunami backwash flow, since the indicators of these flows were hardly identifiable, indicating that the incoming flows were much stronger than the backwash flow. The return/backwash flow mostly was controlled by the topography and for the steep plane beaches; the backwash flow can be more energetic (Synolakis, 1986).

3. The Mathematical Model

The three-dimensional hydrodynamic model 3DD (Black, 2001) is used in depth-averaged, 2-dimensional mode (x and y directions) to simulate tsunami propagation, runup and inundation in Banda Aceh. The model uses a fully explicit time stepping solution with a robust flooding and drying scheme to simulate overland flows. Used extensively in modeling intertidal hydrodynamics of coastal estuaries (Black 1983, 1984; Black et al.1988, 1989; Lundquist et al. 2004), 3DD is ideal for simulating large wetting and drying zones, a feature which allows the model to reproduce the

inundation dynamics of the tsunami in Banda Aceh where the maximum inundation reached 5 km inland.

3.1. Model equations

Model 3DD solves the momentum and mass conservation equation given by:

$$\frac{\partial u}{\partial t} + u\frac{\partial u}{\partial x} + v\frac{\partial u}{\partial y} + w\frac{\partial u}{\partial z} - fv = -g\frac{\partial \zeta}{\partial x} - \frac{1}{\rho}\frac{\partial P}{\partial x} + A_H\left(\frac{\partial^2 u}{\partial x} + \frac{\partial^2 u}{\partial y}\right) + \frac{\partial}{\partial z}\left(N_Z\frac{\partial u}{\partial z}\right) \quad (1)$$

$$\frac{\partial v}{\partial t} + u\frac{\partial v}{\partial x} + v\frac{\partial v}{\partial y} + w\frac{\partial v}{\partial z} + fu = -g\frac{\partial \zeta}{\partial y} - \frac{1}{\rho}\frac{\partial P}{\partial y} + A_H\left(\frac{\partial^2 v}{\partial x} + \frac{\partial^2 v}{\partial y}\right) + \frac{\partial}{\partial z}\left(N_Z\frac{\partial v}{\partial z}\right) \quad (2)$$

$$w = -\frac{\partial}{\partial x}\int_{-h}^{z} u dz - \frac{\partial}{\partial y}\int_{-h}^{z} v dz \quad (3)$$

t is the time, u, v are horizontal velocities in the x, y directions respectively, w the vertical velocity (positive upward), h the depth, g the gravitational acceleration, ζ the sea level above a horizontal datum, f the Coriolis parameter, P the baroclinic component of the pressure, A_H the horizontal eddy viscosity coefficient, and N_z the vertical eddy viscosity coefficient. In this paper, the model is used in 2-dimensional mode.

As tsunamis propagate into shallow water, the forces acting on the water column must be considered to accurately model the inundation. The wavelength of the incident tsunami becomes shorter while the amplitude, steepness and curvature of water level increase. In this phase, factors such as the Coriolis force, the baroclinic component of the pressure, and the inertia force caused by the vertical acceleration of the water can be ignored. However, the bottom friction becomes increasingly important.

3.2. Bed Friction and Eddy Viscosity

At the sea bed, z = -h, the bottom stress represented by the last term in equation 1 and 2 becomes:

$$\rho N_z\frac{\partial u}{\partial z} = \tau_x^h \qquad \rho N_z\frac{\partial v}{\partial z} = \tau_y^h$$

where τ_x^s and τ_y^s denote the components of bottom shear stress, and can be represents by :

$$\tau_x^h = \frac{\rho g u_h \left(u_h^2 + v_h^2\right)^{0.5}}{C^2} \qquad \tau_y^h = \frac{\rho g v_h \left(u_h^2 + v_h^2\right)^{0.5}}{C^2} \qquad (4)$$

with u_h and v_h are the bottom water particle velocities and C is Chezy's coefficient which varies according to the bed type and depth (Black 1983).

This can be expressed as:

$$C = 18 \log_{10}(0.37\ h/z_o) \ ,$$

where z_o is the roughness length as defined in the Karman-Prandtl vertical velocity profile (Black, 1983). Typical values of z_o are of the order of 0.001 m for simulating the tidal hydrodynamics in estuaries, 0.01 m for rough irregular beds, and 0.08 m over very rough beds such as coral reefs (Black 1983). For our inundation modeling, we varied the bed friction throughout the model domain according to the roughness length, which represented different surface topography, or land cover types, as suggested by Black (2001) in modeling large intertidal areas, estuaries or over rough bed or boulders.

The horizontal eddy viscosity coefficient (ν) or A_H (on equation 1 and 2) is used to represent the formation of small-scale vortices ('eddies') in the flow (Black 1983). This value should be set with care, as excessive values will smooth out small-scale features in the flow. We used a value of 1 for offshore propagation and 5 nearshore and overland flows as the water mixed between mud, sand and other debris.

3.3. Flooding and Drying

The 3DD flooding and drying scheme (Black 1983, 2001) is designed to allow smooth transitions and reduced instabilities by avoiding sudden jumps in the current velocity during the drying and wetting processes. The model uses two parameters to control these: the *effective depth value* and *drying height*. The effective depth is used in the bed friction term (equation 4) to prevent this value from becoming too large in near zero depths. The 'drying' height is the depth when the model considers a cell to be 'dry' in flooding and drying zones. A 'dry cell' is denoted in the model as

$$D_t = D_w + \left(\varsigma_{i,j}^n + \varsigma_{i+1,j}^n\right)/2. < drying\_height \qquad (5)$$

D_t is the total water depth, D_w is the water depth below datum, ς is the average of the bounding sea levels.

The necessary value for these two parameters as threshold to control tsunami overland flow was obtained through model calibration. For this case, it was found that standard values of 0.3 m for the effective depth and 0.05 m for the drying height were acceptable.

4. Model Area

Model grids were produced by using bathymetry and topography data from several sources. The General Bathymetric Chart of The Oceans (GEBCO) Centennials Edition for deepwater bathymetry, and digitized navigational charts for nearshore bathymetry. For coastal topography we used a combination of 1:50,000 scale topographic maps of Banda Aceh and Shuttle Radar Topographic Mission (SRTM) 90 m resolution topography data (NASA). A set of three nested grids with resolutions of 1000 m, 200 m and 100 m was created to cover the regions of tsunami generation, propagation and coastal inundation.

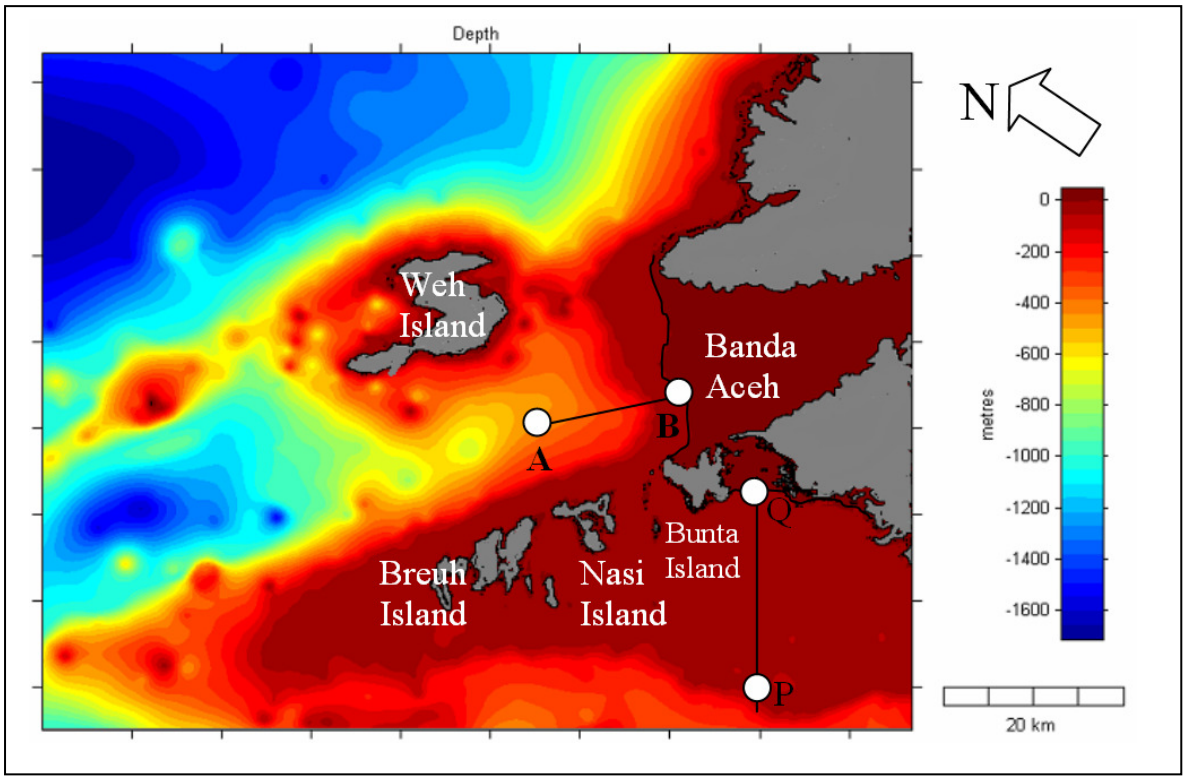

Figure 3. The 100 m model grid of Banda Aceh region including the offshore islands such as Weh, Breuh, Teunom, Bunta and Nasi Islands. A-B and P - Q are the transect line of the wave profile evolution over time in Figure 6a and 6b.

The fine scale (100 m) coastal grid (Figure 3) was refined with available aerial photographs and satellite imagery from 'before' and 'after' the event. Further

refinement incorporated field survey data collected by the International Tsunami Survey Team (ITST) and other institutions such as National Coordinating Agency for Survey and Mapping of Republic of Indonesia (Bakosurtanal). The 'before' and 'after' aerial imagery was used to identify different zones of land-use and coverage type as well as major changes in coastal landforms or features which may affect the tsunami flow. As described above, the landform information is very important in establishing the roughness length values for each grid node in the computational domain.

5. Model Setting

5.1. Model Parameters

A number of calibration runs were conducted to establish the best values for the various model parameters affecting the wave propagation and inundation flows over the model grid.

Roughness length: at water depths greater than 10 m, the roughness length value was set uniformly as 0.001 m. From 10 m to the shoreline a value of 0.01 m was adopted. From the shoreline further inland the values varied; from 0.01 m over flat regions including rice fields and fish/shrimp ponds to 0.08 - 0.2 m over dense vegetation, forests or built up areas.

Eddy viscosity: A value of 1 m^2s^{-1} was adopted over the large model grid during the tsunami generation and propagation phase with a value of 5 m^2s^{-1} during the overland flows and inundation phase.

Effective depth and drying height: 0.3 m and 0.05 m respectively.

The stability criterion for the explicit scheme, used the Courant, Friedrich and Levy condition as:

$$\frac{\Delta x}{\Delta t} \leq \sqrt{2gd_m},$$

where Δx is the grid cell size in x-direction in metres, Δt is the time step in seconds, g is gravity acceleration, and d_m is the maximum depth within the model domain. For 3DD, the Courant number should be less than 0.7 (Black, 1983; 2001).

5.2. Tsunami Source Model

The source model of this near field study on Banda Aceh region is based on the faulting scenario of Tanioka et al. (2006). Following Stein and Okal (2005), the

offshore Banda Aceh was the area where the fast slip and the highest vertical slips distributions occurred. This source area relates to the fault segment A to E of Tanioka et al (2006) and provide the biggest impact to Banda Aceh region which consistent with the directivity argument where tsunami amplitudes are largest when perpendicular to the fault. The global numerical model of tsunami propagation (Titov et al., 2005) also showed that Banda Aceh region (northern tip of Sumatra) was mainly affected by tsunamis that come from the source offshore Banda Aceh up to the southern part of Nicobar Island; while the source that extend to the north up to Nicobar Island with nearly N-S trending provide great impact to the East (Thailand) and to the West (Sri Lanka) as observed during the International tsunami Field Survey (ITST) (Jaffe et al. 2006; Synolakis and Kong, 2006; Yalciner et al. 2005).

On this study, we considered five fault segments (A to E) of Tanioka et al. 2006. We modified the fault length and orientation of segments A and C after calibrating the propagation model results with wave height attenuation observed south of Simeulue Island including the uplift and subsidence (Jaffe et al. 2006, Yalciner et al 2005), along the southwestern coast of Sumatra Island, and on the west and northwest coast of Banda Aceh including Simeulue Island. The initial surface displacements were assumed to match the sea floor deformation as computed using Okada's (1985) method with best modified fault segments (Table 1) and are illustrated in Figure 4. Comparison of tsunami elevation between original fault segments of Tanioka et al. 2006 with field observations (Jaffe et al, 2006, and Yalciner et al 2005) and modified fault segments at 6 locations are illustrated in Figure 5.a and 5.b.

Table 1. Fault parameters for seismic dislocation model modified from Tanioka et al. (2006)

Segment	L (km)	W (km)	Slip (m)	Depth (km)	Strike (degree)	Dip angle (degree)	Slip angle (degree)
A	109	100	15	10	350	10	110
B	160	100	0	10	340	10	100
C	246	120	29	27	340	10	110
D	159	100	5	10	340	10	110
E	159	100	10	27	340	10	110

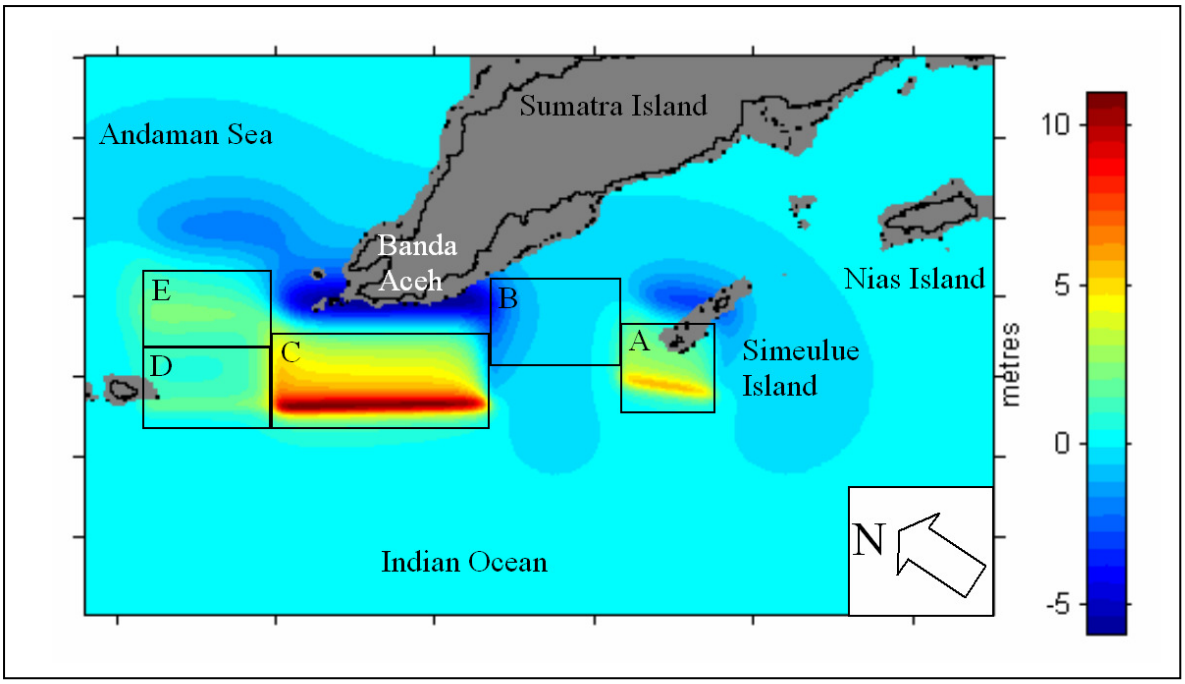

Figure 4. The initial waveform using modified fault segment A to E of Tanioka et al. (2006) scenario (Table 1) computed using the Okada (1985) methods.

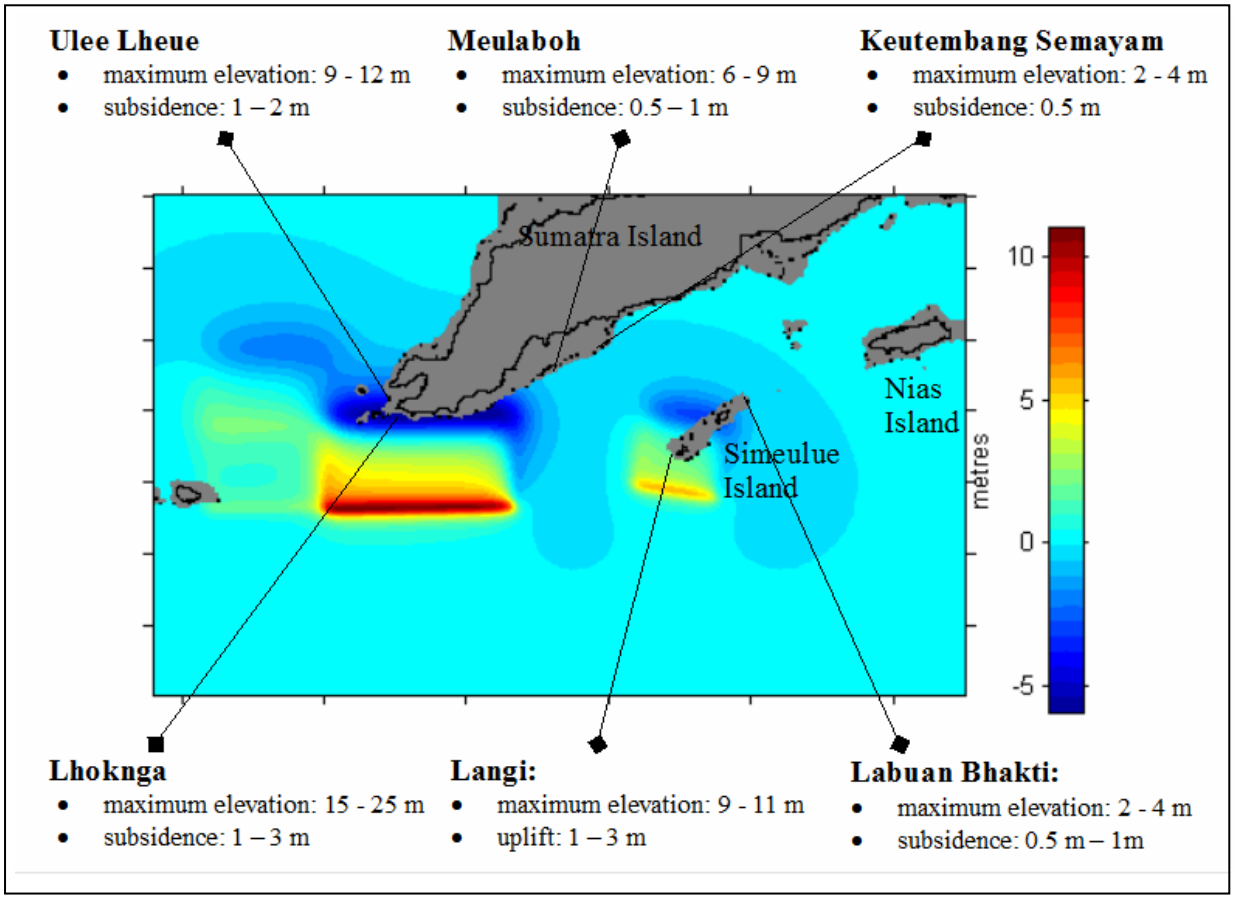

Figure 5 a. The locations of field observation (Jaffe et al.2006; Yalciner et al.2005) at six location that shows maximum tsunami elevation, uplift and subsidence that constraint the modification of Tanioka et al. (2006) fault segment A to C. The modified segment reproduce a better uplift and subsidence pattern at Simeulue Island as well as at Meulaboh and Ulee Lheue.

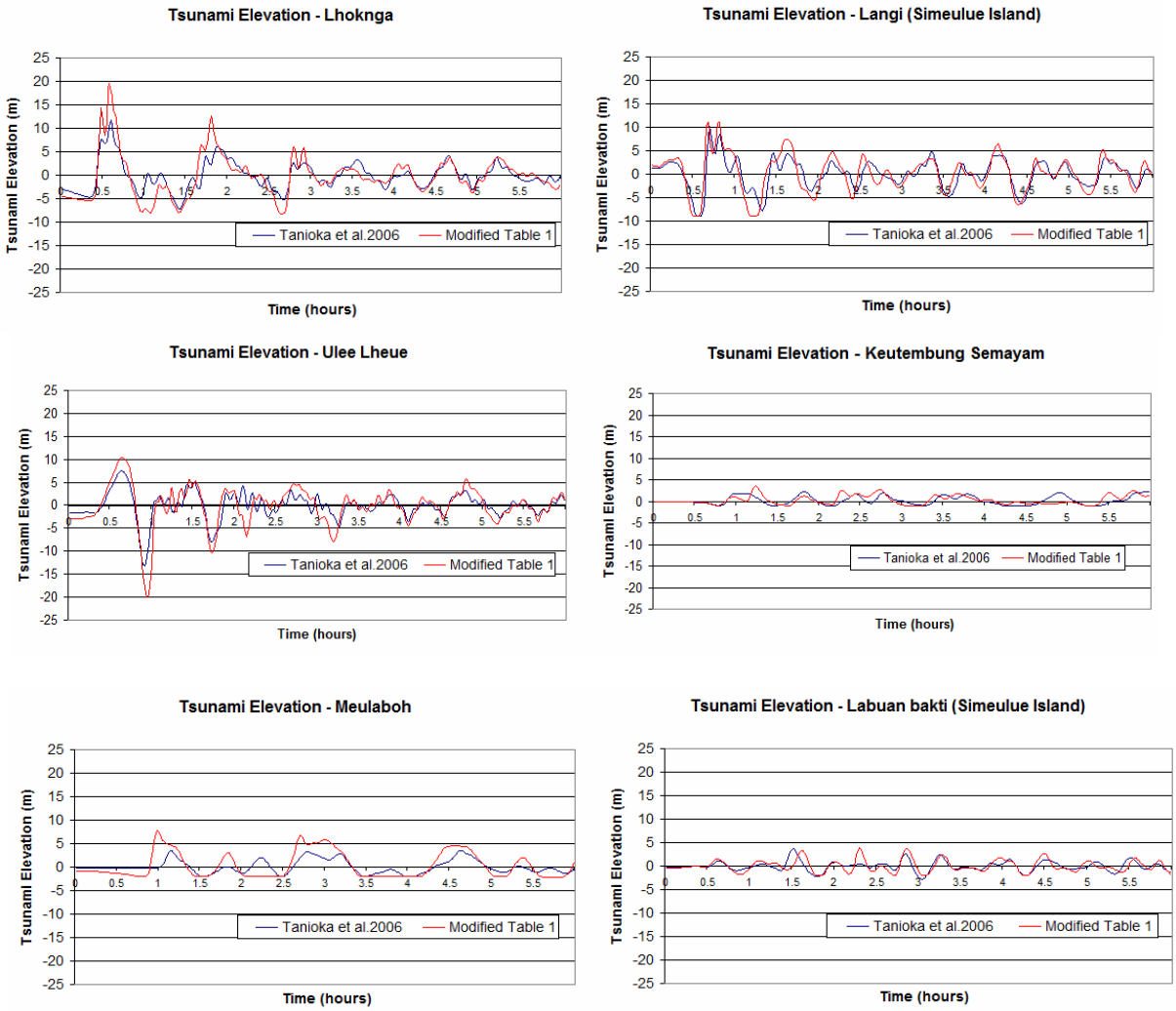

Figure 5 b. The tsunami elevation evolution over time at six (6) locations using original fault segment A to E of Tanioka et al. 2006 (dark blue) and modified fault segment (Table 1) (red). The modified fault segments provide a better tsunami evolution over time that consistent with most of field observations data. The segment A is critical to the tsunami distribution and uplift and subsidence patterns on Simeulue Island and the observed tsunami at Keutembang Semayam areas. Segment C was constraint by the observed tsunami elevation along the west coast of Sumatra Island from Keutembang Semayam up to Lhok Nga. The observed value of tsunami elevation at Keutembang Semayam and Meulaboh were critical in extending the fault segment C.

6. Model Results

6.1. Offshore-onshore Propagation

The initial condition of tsunamis waves as a result of fault rupture on segments A,B,C,D, and E as illustrated on Figure 4, shows that the western coast of Banda Aceh faces directly towards the area of greatest sea floor deformation (segment C), while the northern coast faces toward the Andaman Sea and is located behind a series of offshore islands (Bunta, Bate, Nasi, Teunom and Breuh Islands). It is apparent that the western coast was directly impacted by tsunami energy while the northwestern and eastern shores were affected by waves that had been refracted and diffracted from the Indian Ocean to the Andaman Sea through offshore islands, as illustrated in Figures 6.a and 6.b.

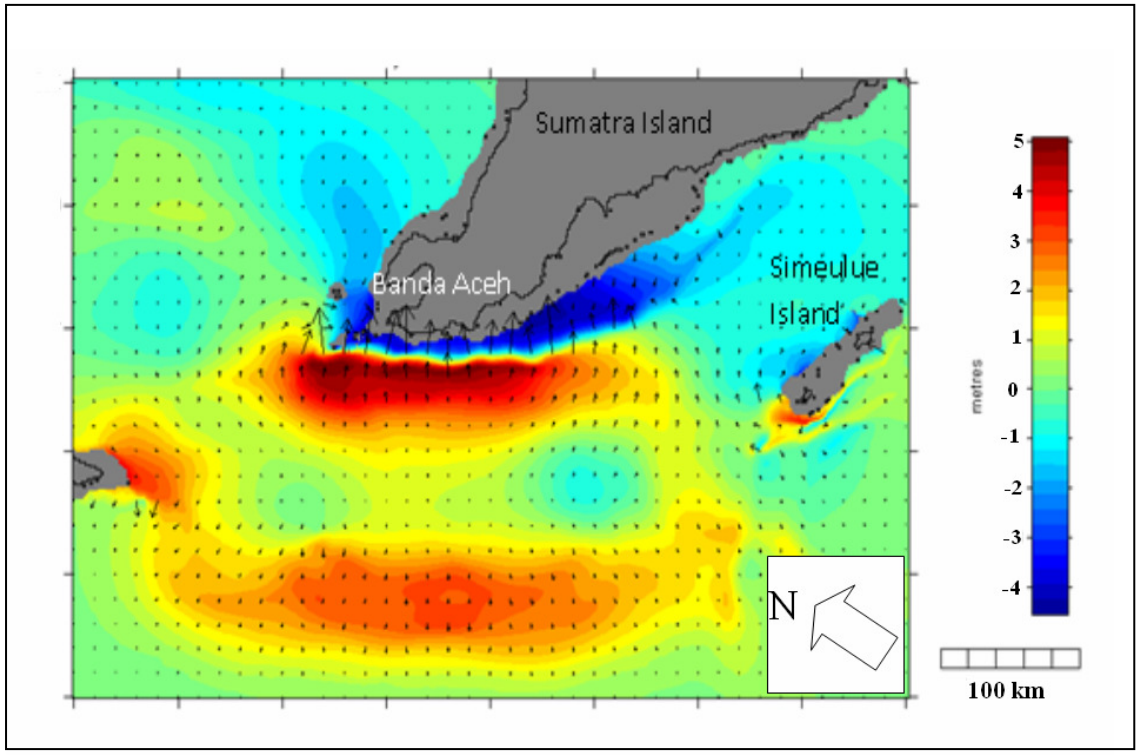

Figure 6.a. The wave propagation pattern towards Banda Aceh and adjacent coastline as well as to Simeulue Island 11 minutes after the fault ruptures. It's obvious that most of the western coast had suffered direct impact from tsunami energy arriving perpendicular to it, and less wave impact further to the south of Sumatra Island.

The shore perpendicular transects of wave height at different times for both the northern and western coasts are shown in Figures 7.a. and 7.b. Both areas experiences leading depression N-Waves (Tadepalli and Synolakis, 1994, 1996), however steeper waves within 100 – 300 m from the shoreline are evident along the west coast (Lhok

Nga). Tsunami elevations in the order of ~16 m are evident on the west coast as compared to ~10 m along the north coast (Banda Aceh city).

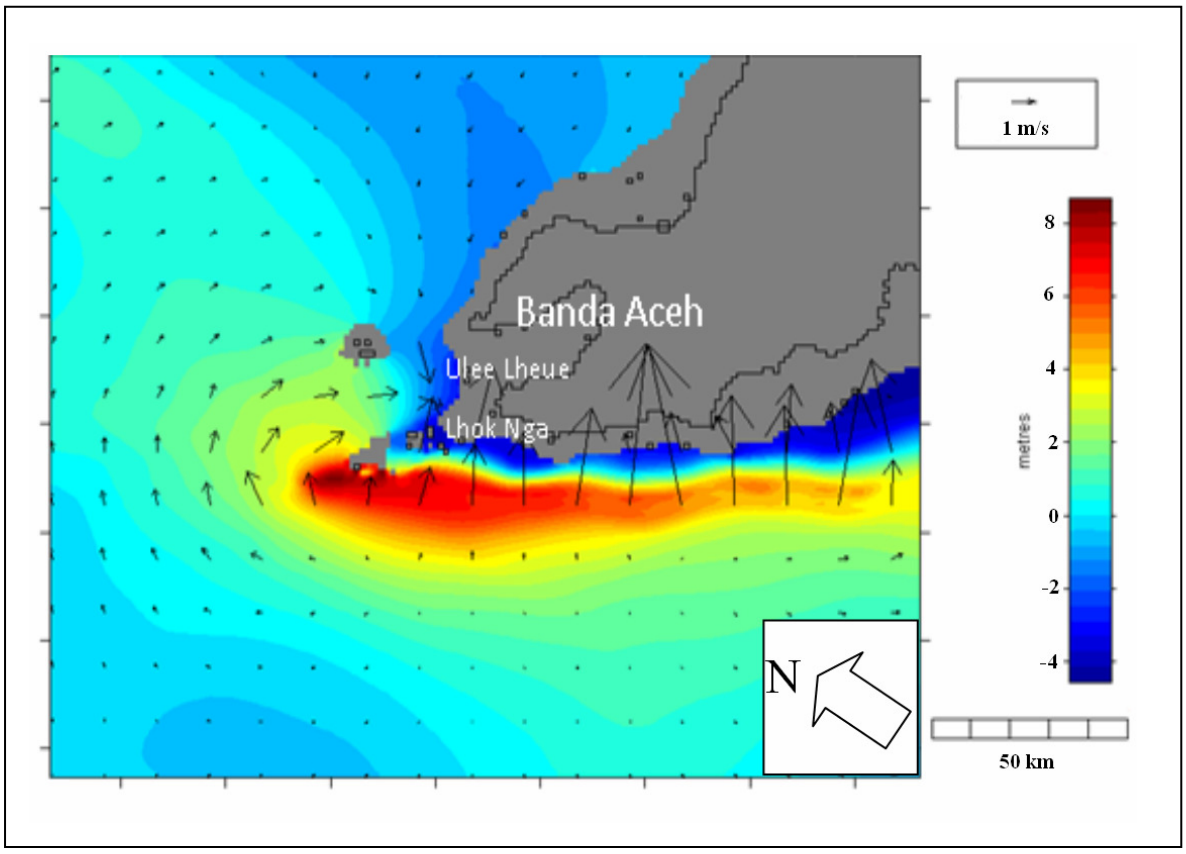

Figure 6.b. The northern coast of Banda Aceh was impacted by the tsunami after it refracted and diffracted around the offshore islands. Weh and Breuh Islands act like a gate and guide the waves perpendicular towards the northern coast.

These results reflects the effects of the nearshore bathymetry and geometric position of the areas in response to the waves that had been generated from the same source, and are consistent with the field observation of ITST. On the west coast, it appears that a wide continental shelf with a gentle slope is more dangerous since it could amplify the wave height ~ 3 times (3 x) close to the shoreline compared to the tsunami wave height in the middle of the continental shelf (Figure 7.b). On the other hand, the north coast had an impact from a smooth build up of tsunami wave as a result of refraction and diffraction by the offshore islands, and relatively deeper bathymetric conditions, as illustrated in Figure. 7.a.

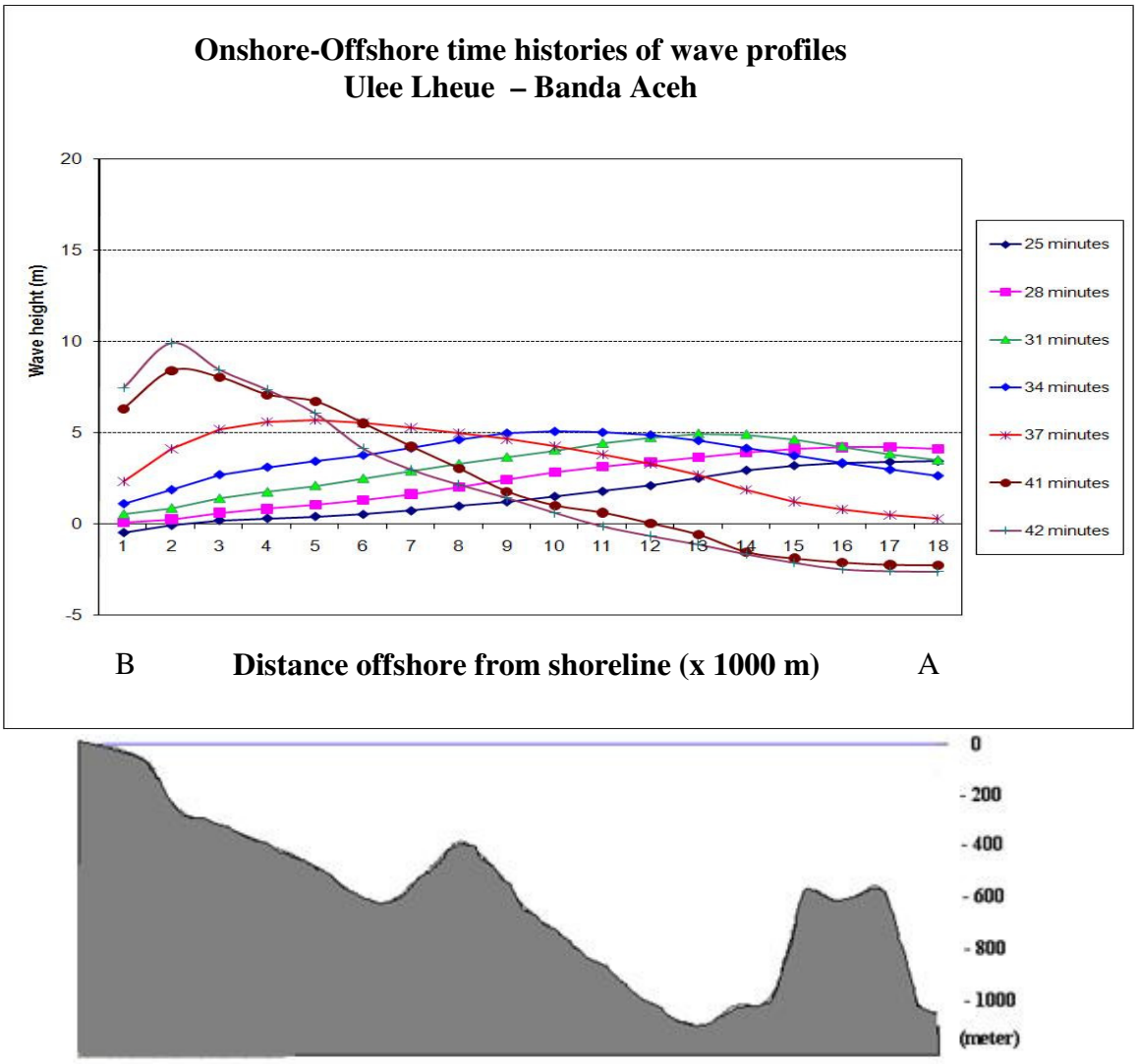

Figure 7.a. Time histories of modelled tsunami profiles at north-western Banda Aceh (Ulee Lheue) showing the smooth tsunami wave build up as it approaches the coastline.

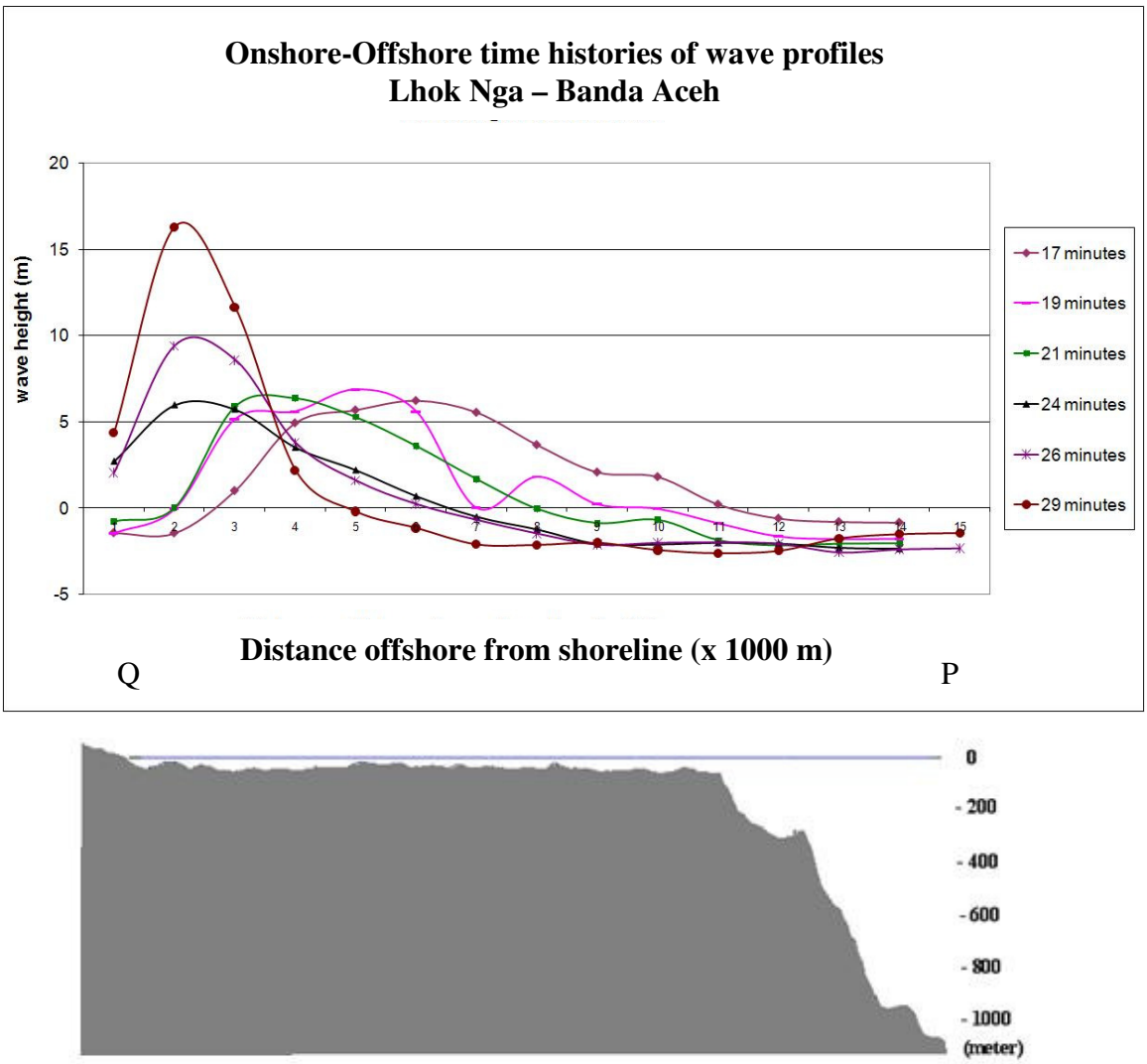

Figure 7.b. Time histories of modelled tsunami profile west of Banda Aceh (Lhok Nga) showing steep tsunami waves that builds up during propagation over the wide flat continental shelf. The maximum tsunami elevation at the coastline was about~ 17 m.

6.2. Runup and Inundation Flows

The distribution of maximum tsunami elevation and runup from the model accurately reproduces field survey data showing that the highest runup occurred along the coasts facing towards the tsunami source area as illustrated in Figure 8. Additionally, different types of wave reflection patterns and their interaction with subsequent incoming tsunami waves were also identified. Along the northwest coast, reflected waves collided with an incoming tsunami waves (fully opposite direction) to create a region of high tsunami elevation some 300 – 450m off the coast (F in Figure 8). On

the west coast, the reflected waves propagated offshore as well as alongshore with the alongshore component contributing to increased coastal inundation.

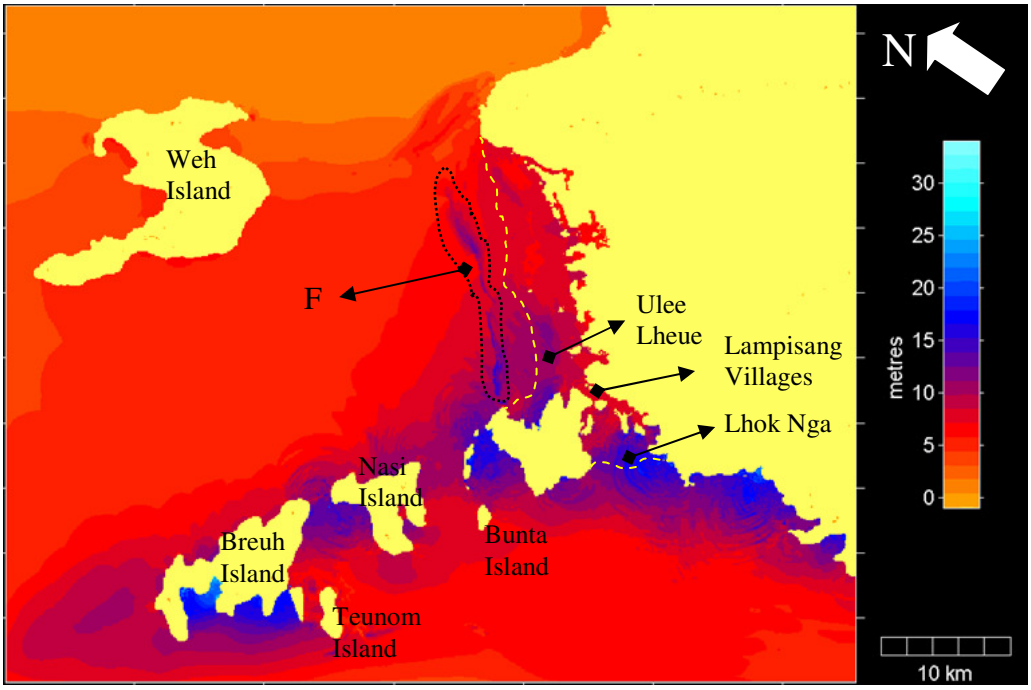

Figure 8. Maximum tsunami elevation and runup distribution on Banda Aceh including the offshore islands (Weh, Breuh, Teunom, and Nasi). Runup values range up to ~ 34 m on the west coast with flow depths of 15 – 30 m, while at the northwest coast flow depth ranges between 6 – 12 m. Flows from northwest coast collide with the flow from west coast at Lampisang Village. F (black dashed line) is a high tsunami elevation zone due to interaction of the reflection/high speed return flow and the following incoming tsunami waves.

6.2.1. Offshore islands

The model results show that the more exposed offshore islands of Breuh, Teunom, Nasi, and Bunta experienced runup that ranges up to 34 meters, which is in agreement with field survey measurements results and satellite imagery (Quickbird and Google Earth). On these islands, a trim line along the hillsides and tsunami-induced erosion inland were clearly identifiable.

On Weh (We) Island, however, its more protected location spared the full brunt of the tsunami waves, but was rather affected by waves that had been diffracted and refracted through the islands to the southwest. Both the field surveys and the model results show tsunami elevation and runup on this island varying from 2 – 5 m. The

highest runup occurred along the northwest and west coast, as illustrated in Figure 9. Most of the damage on Weh Island occurred along the northwest coast where there was a direct wave attack.

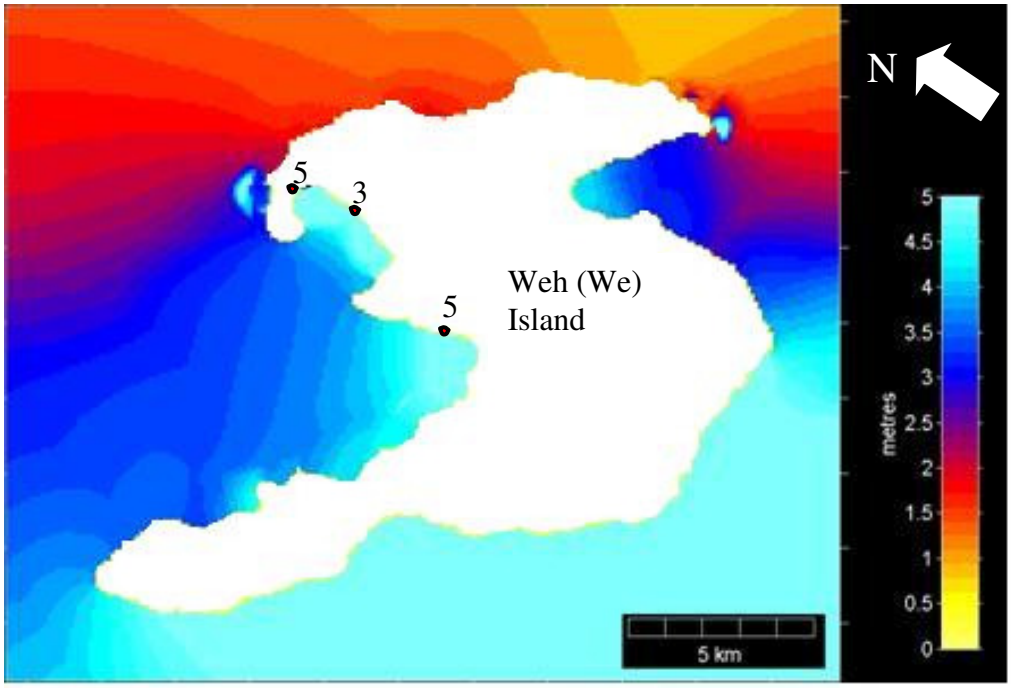

Figure 9. The maximum tsunami elevation and runup distribution around the coast of Weh Island ranged up to 5 m along the west and northwest coast (the numbers represent field measurements).

The western coasts of other offshore islands (Bunta, Nasi, Teunom and Breuh) faced directly towards the tsunami source areas. The tsunami from the west and southwest inundates the relatively low-lying areas of Breuh Island at Lambaro (A) and Lampuyang (B) and the flows continues overland to the Andaman Sea through these low-lying areas with speeds of up to 10 m/s, as illustrated in Figure 10. Modeled currents speeds between these islands reach ~15 m/s. The highest runup occurred in the area between Melingge and Blangujung (~34 m (C)). Satellite imagery shows the trace of the flow passing through a narrow gap in the hills on to the Andaman Sea. This was not reproduced in the model; however, the model grid resolution (100 m) is larger than the tsunami flow path, which was on the order of 80 m.

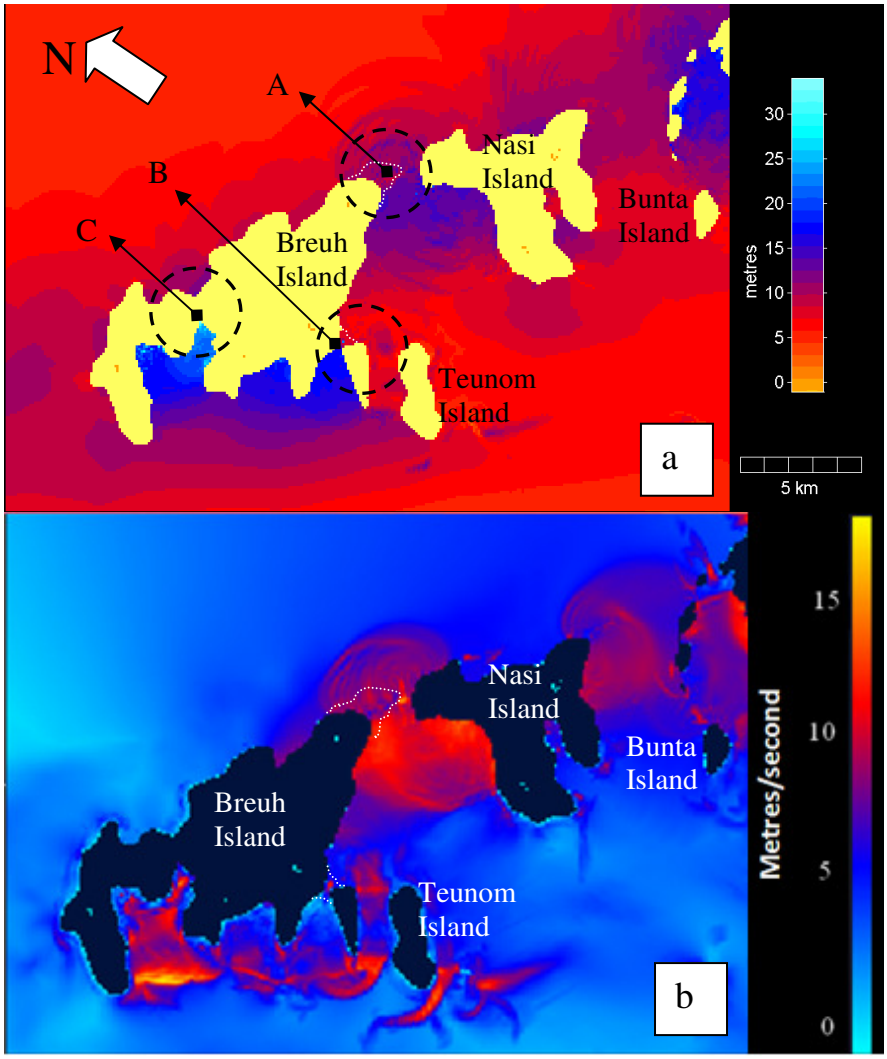

Figure 10. The maximum tsunami elevation and runup distribution on Breuh, Teunom, Nasi and Bunta Islands ranges up to ~ 34 m (a). Strong currents up to 15 m/s are generated between the islands, while overland flow speed ranges up to 10 m/s (b). A, and B are the locations where the flow overtopped the low-lying areas, and C is the location of the highest runup at Breuh Island.

While the west coast of Banda Aceh was directly impacted by tsunami waves propagating from the source region, the northwest coast however was impacted by refracted and diffracted tsunami waves through the offshore islands. Both areas were severely affected with inundation distance reaching more than 5 km inland. As reported by Borrero (2005), the tsunami overland flow from the Andaman Sea collided with overland flow coming from the Indian Ocean. The two flows met at Lampisang Village, located approximately 3.7 km from the northwest coast (Ulee Lheue) and 6.8 km from the west coast (Lhok Nga). This phenomenon is replicated in the model, as illustrated in Figure 8.

6.2.2. West coast – Banda Aceh

The model results show a non-uniform distribution of tsunami elevation and runup along the west coast, which agrees with the measurements of the field surveys. The model predicts a distribution of tsunami elevation and flow depths along the coast between 15 and 30 m, with runup ranging up to ~35 m on the hillside between Lhok Nga and the LaFarge Cement Factory with the nearshore bathymetry and topography condition as illustrated in Figure 11. Modeled overland flow speeds reach up to 22 m/s. The model results are illustrated in Figure 12.a to c.

Based on analysis of flow speed, depth, and direction, the low-lying areas are divided into three zones. First is the zone where flow speed and direction are solely determined by the incoming waves. In this area, landforms do not have a significant impact on overland flow. This zone is located near the shoreline and is characterized by high-speed, unidirectional flow, generally perpendicular to the shoreline with flow speeds and inundation depths decreasing landward. The second zone is a mixed zone where flows from Zone 1 converge due to local landforms causing increased flow depths and speeds. The third zone is the furthest inland where flow speeds and direction closely follows the low-lying terrain as gravity driven flow.

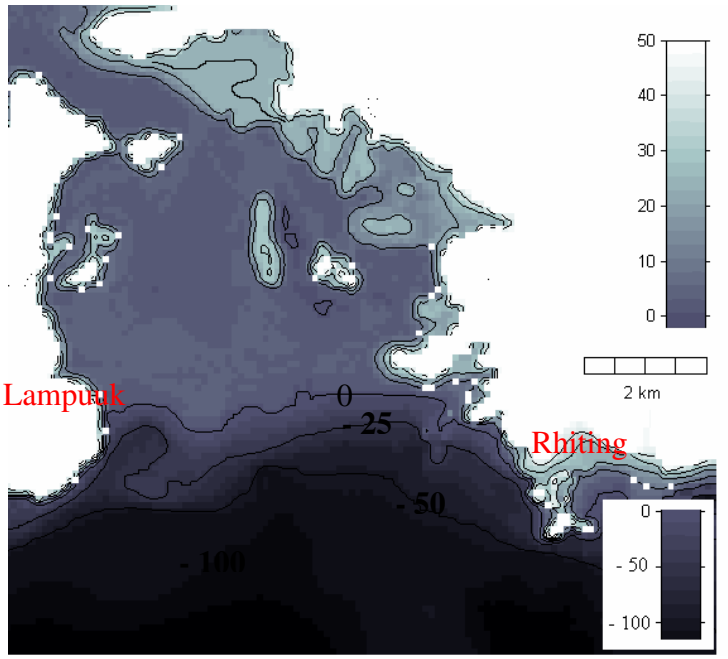

Figure 11. The nearshore bathymetry and topography condition of the areas between Lampuuk and Rhiting on the west coast.

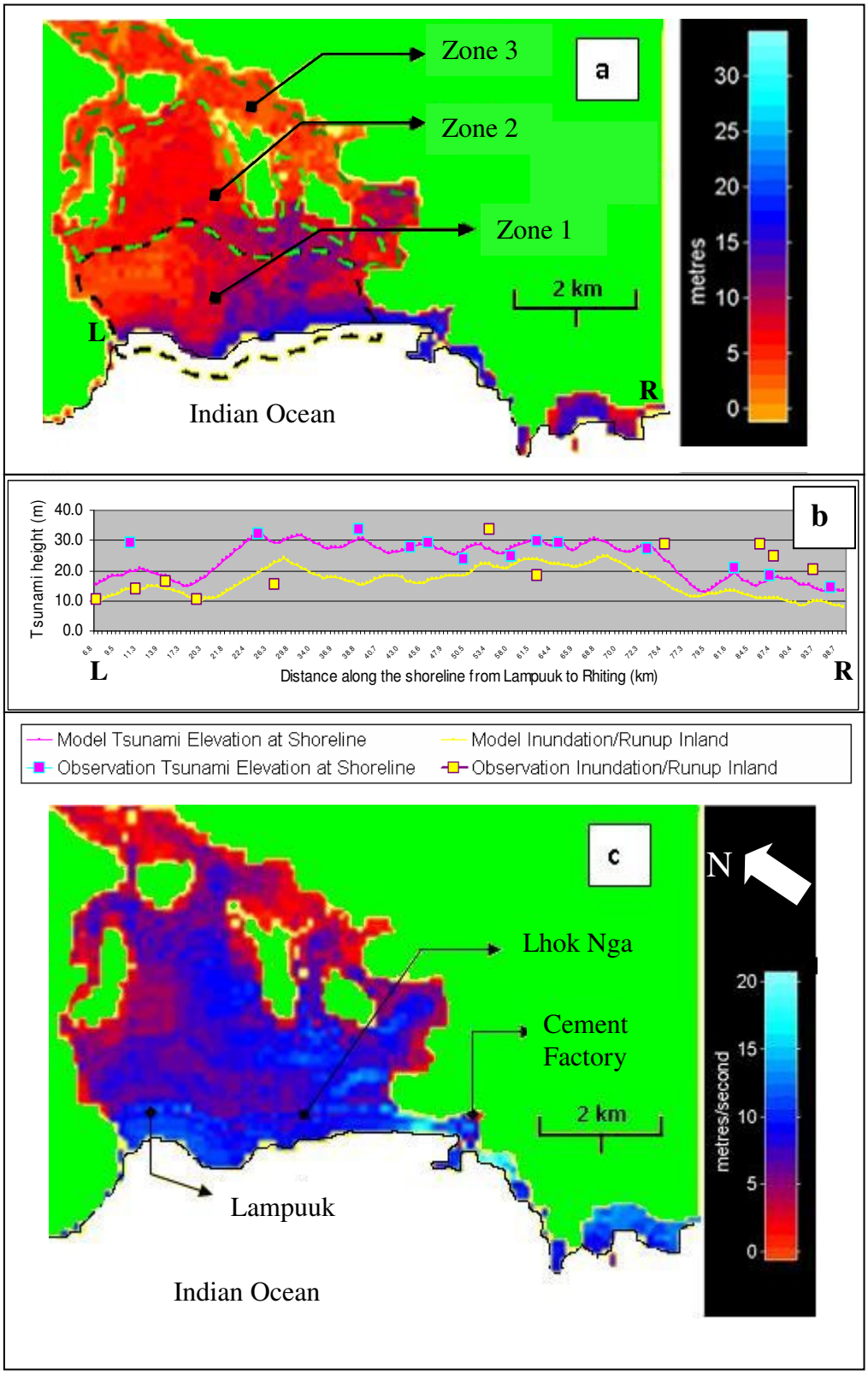

Figure 12. Distribution of maximum tsunami elevation from the shoreline to further inland (a) and its comparison with field data from Lampuuk (L) to Rhiting (R) (b) and maximum flow speed distribution (c). Zone 1 is the zone with high-speed flows at shoreline and same direction as the incoming waves. Zone 2 is the mixed zone where flows start to merge due to the terrain and flow speed increases again. Zone 3 is the zone where flow speed and direction are controlled by low-lying terrain conditions as gravity driven flows.

The three zones can be identified in vector plots of flow direction (Figure 13). These plots also show the dynamics of the incoming waves at the shoreline, the overland flow directions and speeds as well as the tsunami return flow. Figure 13.c shows the return flow beginning before the first tsunami waves reach the point of maximum inundation. The incoming and return flow follow different paths, clearly showing that the return flow is not as energetic as the incoming flow and is mostly control by the local terrain. It takes more than 12 hours for the seawater to drain from most land areas with the exception of the rice field, which remained inundated for more than 3 days.

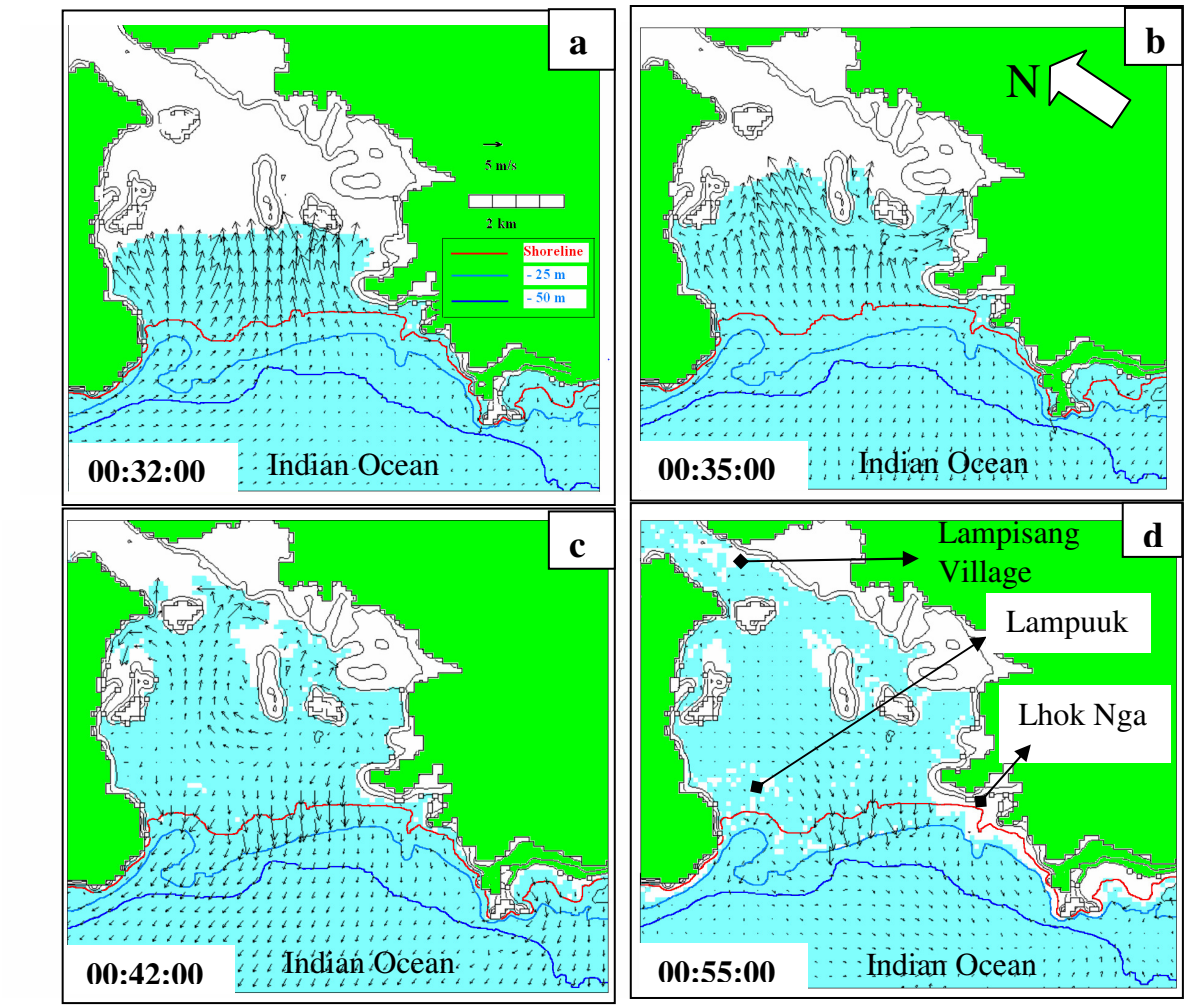

Figure 13. The vector plot of flow speed and direction shows the inundation dynamics on the west coast of Banda Aceh. The wave penetrates further inland where it meets with the flow from the northwest at Lampisang Village. (a) shows the initial stage when the flow penetrates inland (zone 1), and (b) when the flow converges identified as zone 2. The flow continues following the low terrain condition (c), which is identified as zone 3. The return flow clearly had different pattern, with slower velocity and was concentrated in the middle region (d). The number on the left corner show the time after the earthquake.

6.2.3. Northwest coast – Banda Aceh

The modeled extent of tsunami inundation over Banda Aceh is illustrated in Figure 14. Inundation distances reach up to 5.4 km inland, while flow depths and tsunami elevation range up to 12 m. This agrees with field measurements and satellite imagery (SPOT 2, Quickbird and Google Earth). The range of tsunami elevations and flow depths near the coast is between 6 to 12 m, with the highest occurring between Lampulo Market and Lam Badeuk. In this area, most of the houses were destroyed, and severe erosion occurred on the coastal plain. The model is consistent with these observations with modeled flow speeds over the area ranging up to 13 m/s (Figure 15).

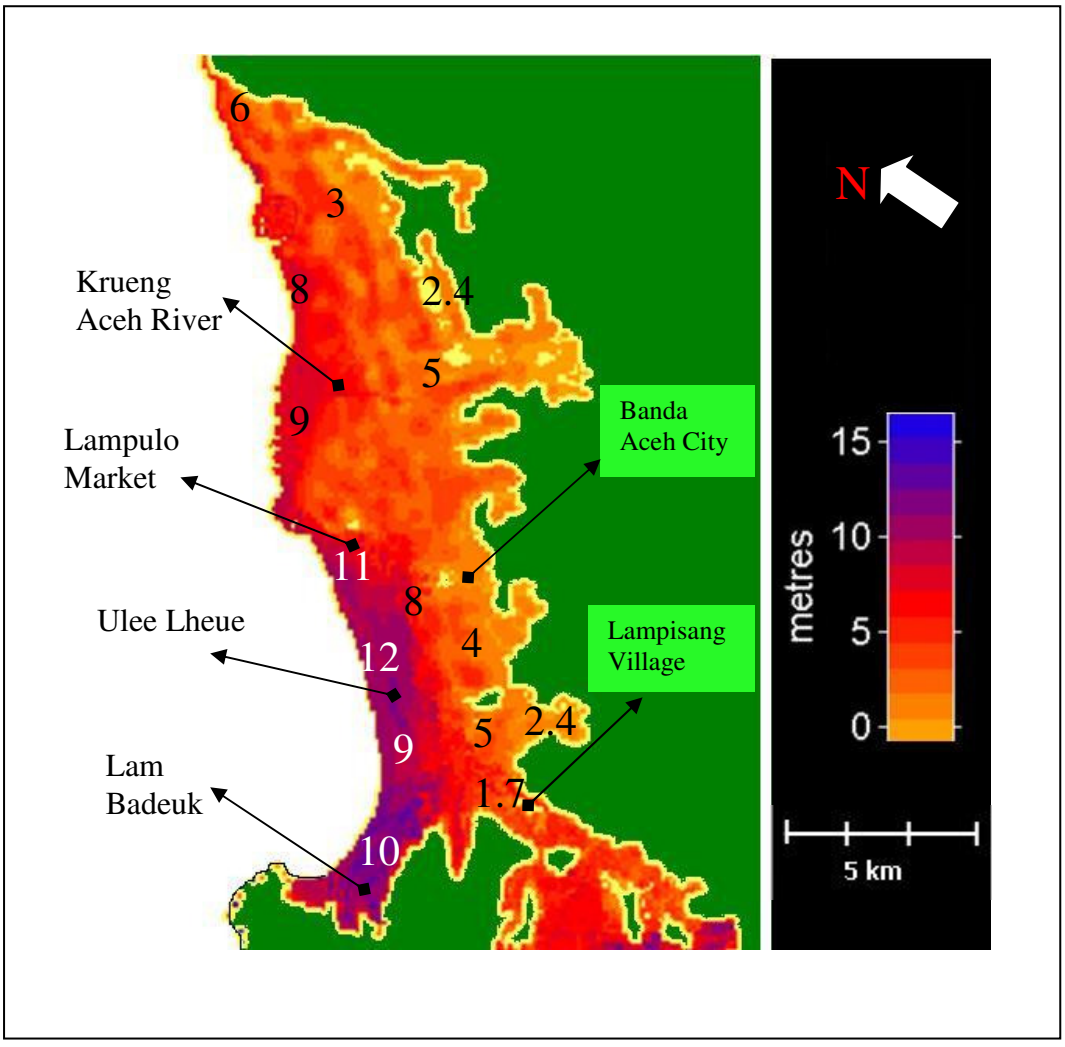

Figure 14. Distribution of maximum modeled overland flow depths compared with field measurements (the numerals) from various sources (ITST 1-2, Umitsu et al. 2007). The highest flow depths occurred between Lampulo Market and Lam Badeuk which is deltaic lowland coastal plain. The flow depth did not decrease significantly in this region as compared to adjacent areas where the landforms consist of dunes and beach ridges.

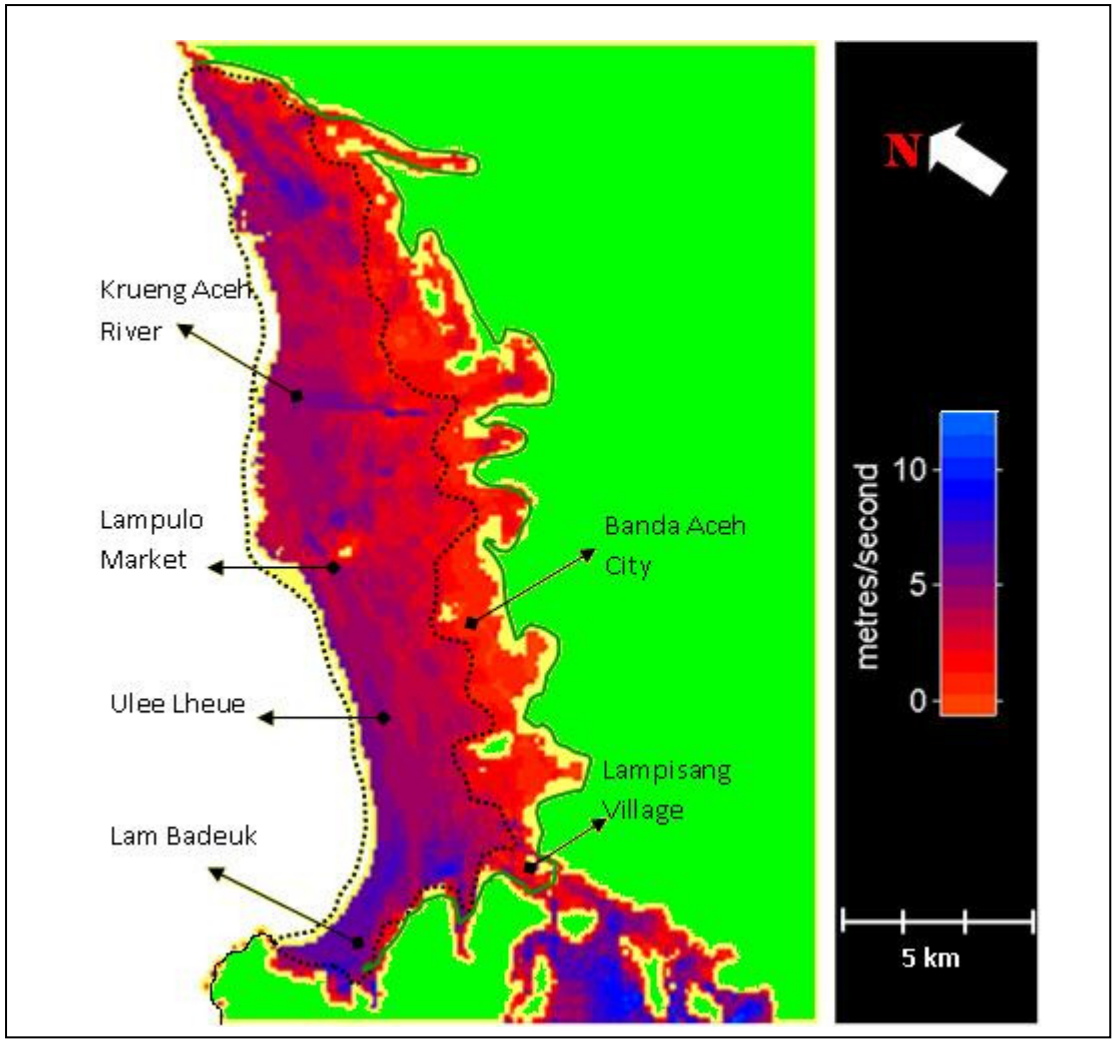

Figure 15. Distribution of maximum flow speed from the shoreline to the furtherest extent inland. The black dot line is the high-speed flow area with same direction to the incoming waves at the shoreline (same as Zone 1 at the west coast). The dark green line is the zone where flow speed and direction are controlled by terrain conditions (same as Zone 3 at the west coast). The yellow colour represents the inundation zone and the green color represents the un-inundation zone.

Due to the size, shape and type of the landforms in this region only two flow-zones are identified based on velocities distribution as illustrated in Figure 15. This region is characterized by deltaic lowlands with a broad coastal plain (Figure 16). Similar to our assessment of the west coast inundation patterns, nearshore flow speed and direction are determined primarily by the characteristics of the incoming waves with less influence from the landform. This region is indicated by the black dotted line in Figure 15. Further inland flow speed and direction follow the local terrain more closely. This region is inside the dark green line in Figure 15.

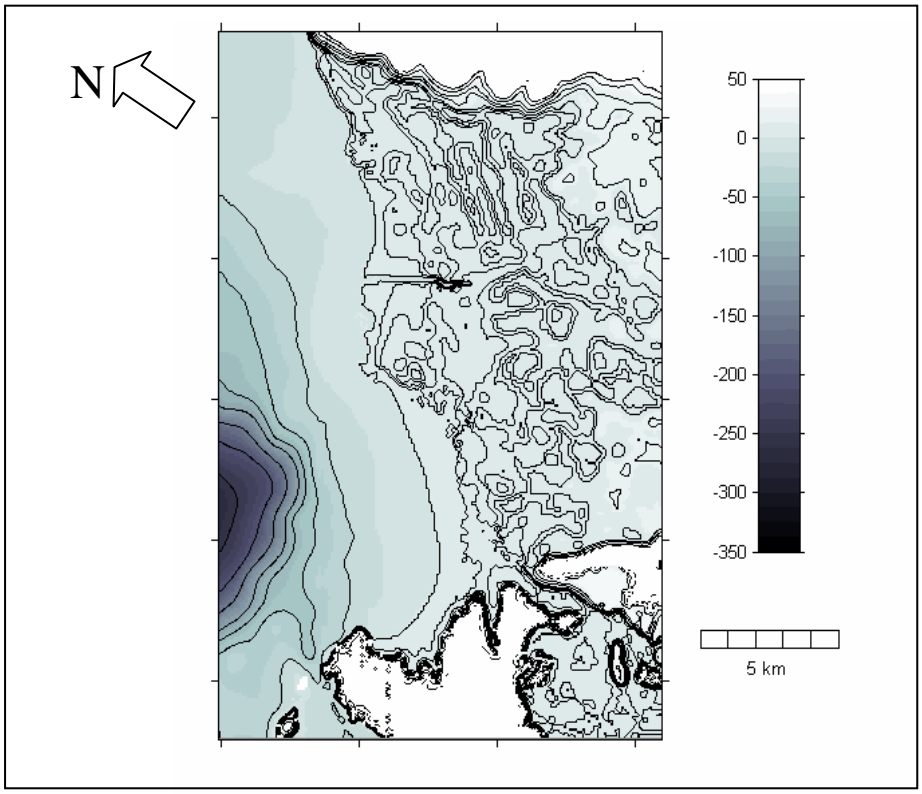

Figure 16. The deltaic lowland with a broad coastal plain is the characteristics of the northwest coast of Banda Aceh. Up to 5 km inland, the land level still less than 15 above the sea level.

It is obvious that at the end of the inundation zone, the flows follow the lower terrain while inundating the low-lying areas between beach ridges and natural levees as well as through drainages canals, small rivers and creeks. High-speed inundation flows reaching up to 10 m/s can be seen to extend significantly landward up through the Krueng Aceh River resulting in inundation distances on the order of 8 km.

From Figures 12 and 13, it is clear that the distribution of flow depth is not always in line with the distribution of the flow speed. The areas which experienced the deepest flooding do not necessarily experience the fastest flows. Therefore, in assessing tsunami hazard, and especially when making inundation maps, the overland flow speed should be taken into account.

A vector plot of the overland flow speeds (Figure 14) shows a generally unidirectional inundation flow, perpendicular to the coastline. This changes however to the east of Lampulo Market where overland flow direction oblique to the shoreline is modeled. Similar to the pattern modeled on the west coast, the tsunami return flow initiates

before the first surge reaches its maximum inland extent. This return flow interacts with the second incoming wave approximately 300 to 450 m offshore as illustrated in Figure 8. The second and third waves caused increased inundation as the sea levels also higher of 0.5 – 1 m as illustrated in Figure 17. Hence the flows penetrated further inland. Because this region is characterized by a broad low lying coastal plain, the return flow is also generally unidirectional. This is in contrast to the west coast where the return flows tended to follow the local topography. Similar to the west coast, however, the strength of the return flows was not as strong as the incoming flows.

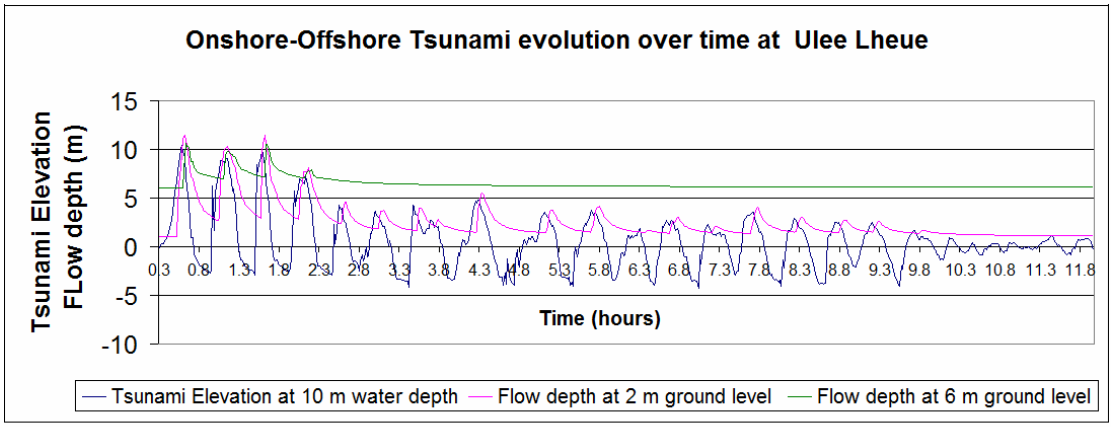

Figure 17. The onshore – offshore tsunami evolution over time shows the increasing of sealevel in the order of 0.5 – 1 m after the first wave attacked. The following waves were clearly propagated on the 'new' sealevel further inland as shown on the flow depth at 2 and 6 m above sea level (red and green) .

Our modeling also reproduces the collisions of the two flows that occurred at Lampisang Village in the gap between the hills that separate the northwest and west coast. The model results show the flow through the gap having speeds up to 5 m/s (Figure 15), and flow depth between 0.5 m - 4 m (Figure 14). The highest inundation levels of up to 6 m (the ground level is 2 m above MSL or flow depth of 4 m) but with lower speeds occur at this point as a consequence of the collision. According to survivor eyewitness account, the flows coming from the west coast were shallow but relatively high speed. After the first collision, most of the flow came from the northeast towards the southwest. Flow traces and indicators described in the field surveys agree with the model results as illustrated in Figure 18 (a,b,c,d) and 19 (a,b).

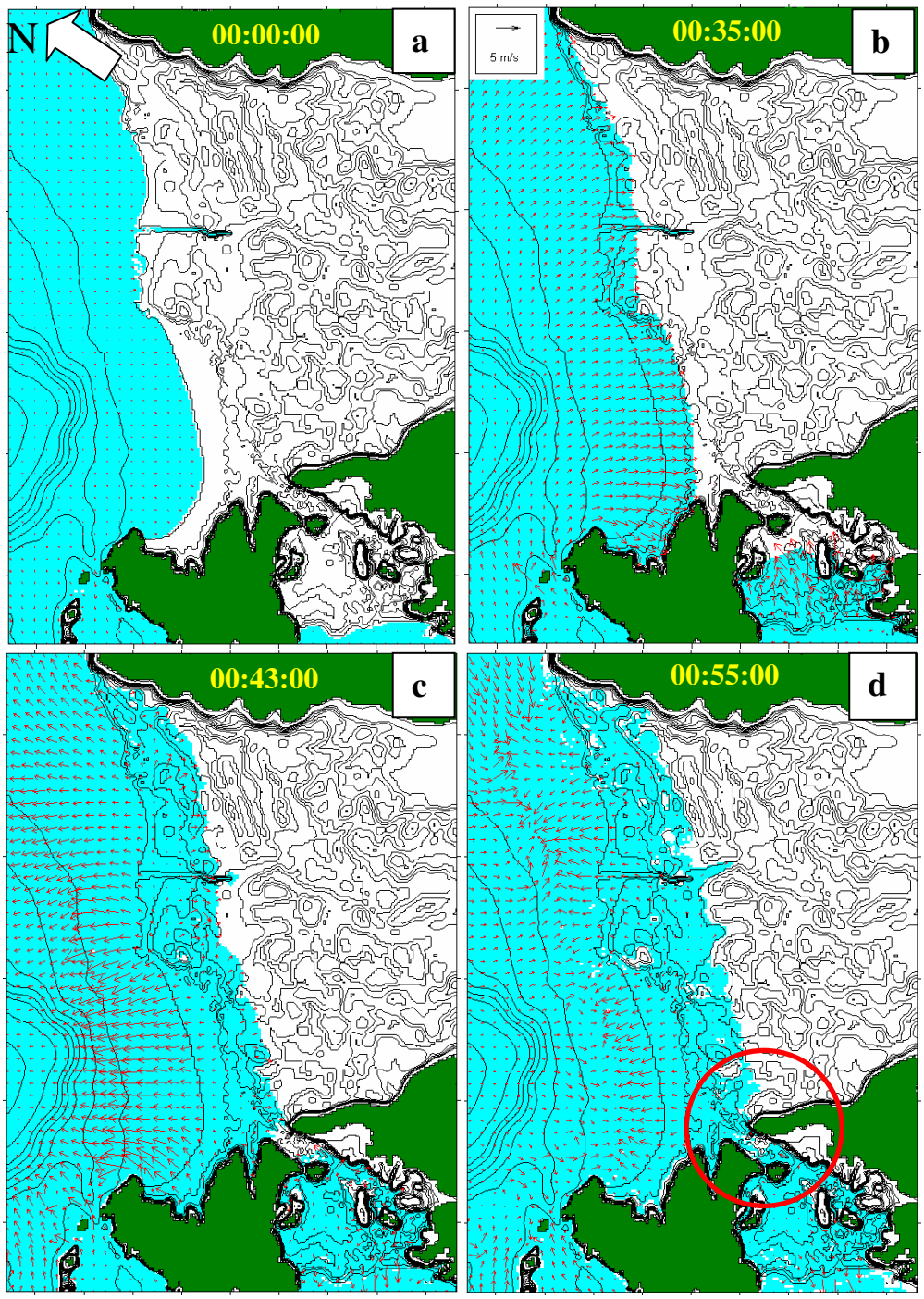

Figure 18. A vector plot of flow speed and direction showing the inundation dynamics on the northwest and west coast of Banda Aceh. The flow originating from the northwest penetrates the northwest coast further inland and meets with the flow from the west at Lampisang Village (red circle on d). (a) the initial stage where the shoreline position at Mean Sea Level, and (b) shows the initial stage when the flow penetrate the low-lying areas (mostly fish and shrimp pond areas at the northwest coast) inland. (c) the initiation of the return flow while the primary wave front continues landward, the return flow shows similar pattern to the incoming flow. (d) the second wave is approaching the coast and collided with returning flows at the nearshore zone. At this stage, the flows from the northwest start to collide with the flow from the west at Lampisang Village (red circle). The number on the top center of each figure show the time after the earthquake.

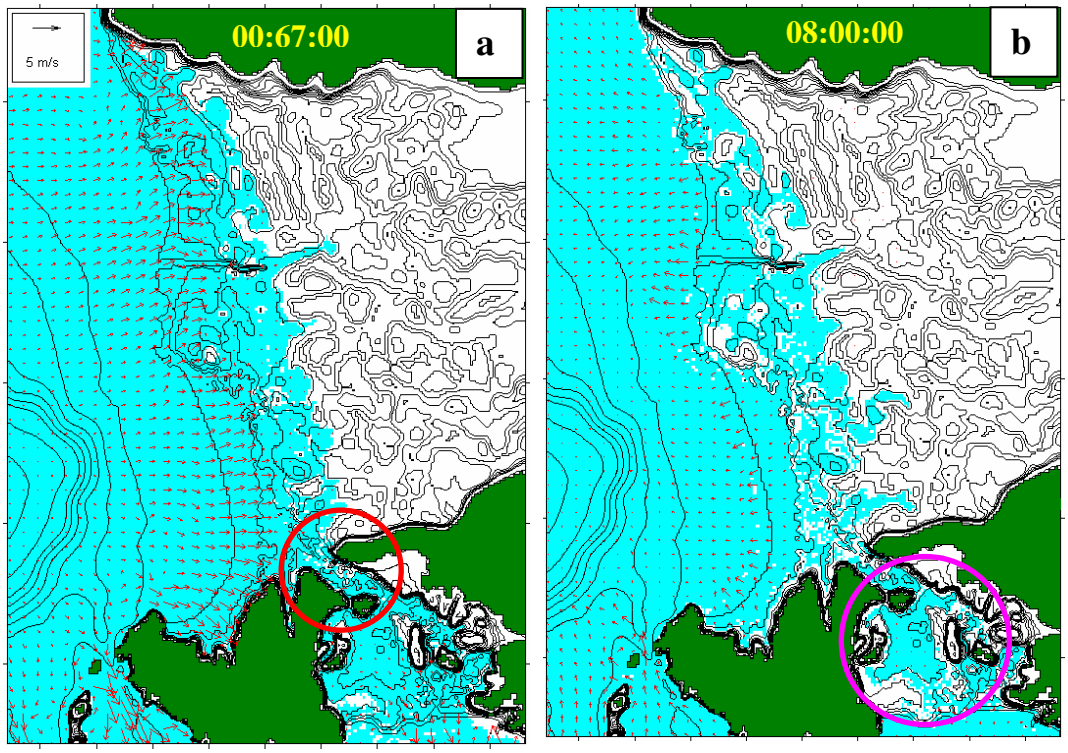

Figure 19. A vector plot of flow speed and direction showing the second wave on top of the first wave as it continues inland and follows the local terrain as a gravity driven flow. At this stage, the two flows completed inundate the Lampisang Village (red circle), (d) After 8 hours since the tsunami struck the areas, the return flow with lower velocity follow the terrain condition as gravity driven flows. At this stage, the model replicates the pattern of stagnant waters at most of the low-lying areas at the noethwest coast as well as at padi rice field (purple circle) on the west coast as observed by satellite image. The number on the top center of each figure show the time after the earthquake.

7. Discussion

Our modelling shows that areas, which experienced higher inundation levels, did not always experience greatest overland flow speeds. Areas on the broad coastal plain with low flat ground such as the region between Lampulo Market and Lam Badeuk show the greatest inundation distance and flow depth along the north coast and does not decrease significantly further inland as its overland flow speeds decreased (Figure 20. a). However, further to the east, where the coastal landforms consist of dunes and sand ridges, the overland flow speeds decrease initially, then increase as the flow interacts with the beach slope, as identified by Synolakis (1987) and Synolakis and Bernard (2006). This is shown in Figure 20.b (dot circle). A more typical flow depth and speed distribution during the runup processes is illustrated in Figure 20.c, taken from the west coast profile near Lhok Nga.

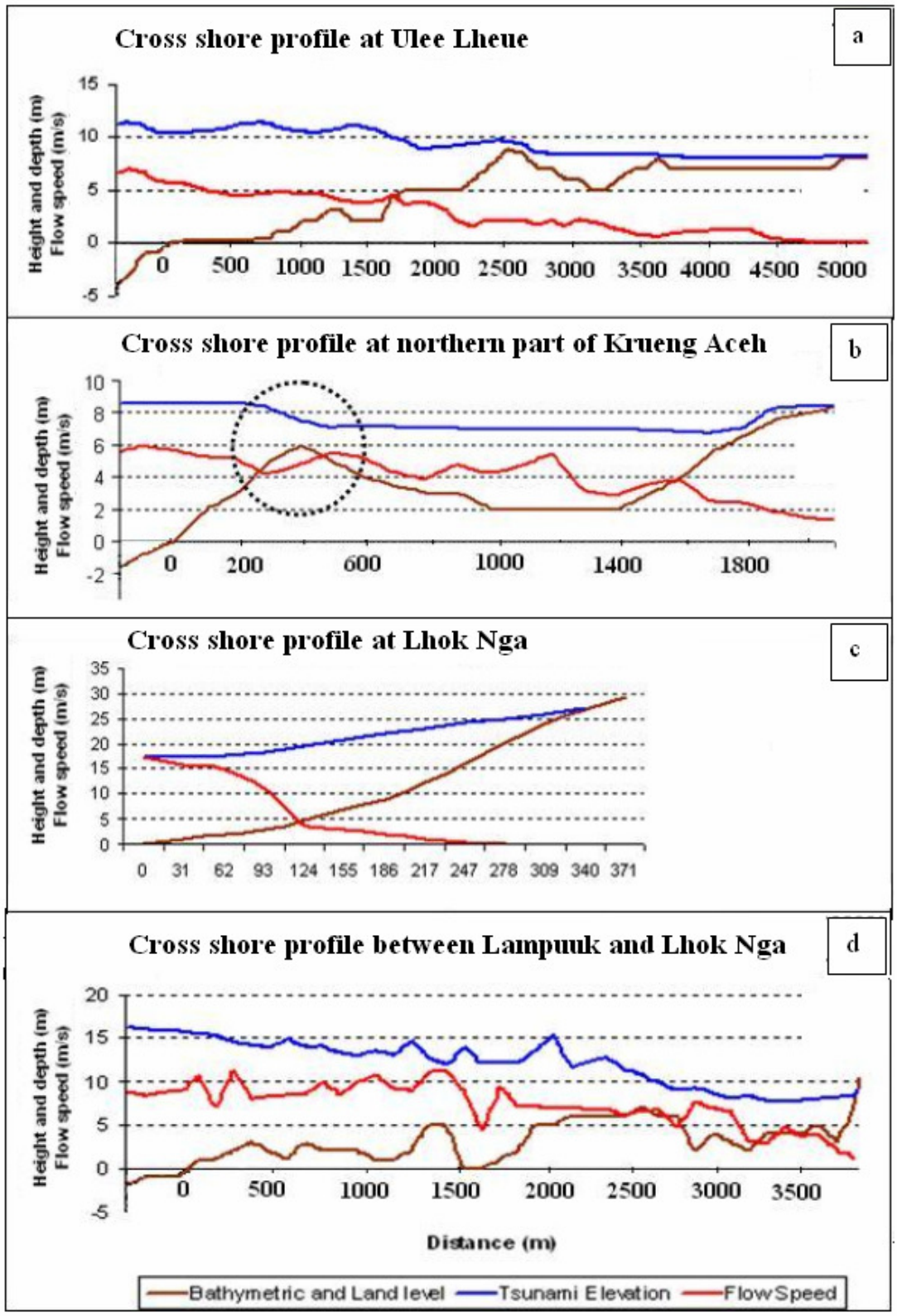

Figure 20. The variation of cross-shore profile plot of the tsunami elevation, flow depth and speed in response to the coastal landform of Banda Aceh. (a) shows the tsunami maintains its height for some distance inland before its decay on the broad coastal plain, (b) shows the flow speed decrease and then increase again at the dune and sand ridge zone (dot circle), (c) a classical example of the variation and (d) shows complex variations of tsunami elevation, inundation depth and flow speed. The axis number is the distance inland in metres.

The variable geomorphology of the west coast as compared to the broad and wide coastal plain of the northwest coast, provides a different distribution of inundation distance, and inland flow depths and speeds, as well as return flows. A pocket shape low-lying area of the west coast contributes to the increase of inundation level and flow speed in the middle of the inundation zone, as illustrated in Figure 20.d due to the convergence of the flows. This allowed the tsunami flows to propagate further inland, and collide with the flow from the north. The most dangerous returns flows were identified after the first and second waves attacked. During this period, the modeled unidirectional return flows reach maximum speed up to 20 m/s, and the flows maintain their speed up to 500 m offshore. Return flows follow the local terrain as a gravity driven flow, and a longer time is needed to drain the seawater from the land.

The zone where the flow speed and direction are primarily determined by the incoming waves (noted as Zone 1 Figure 12 and 15) coincide with the damage maps (UNOSAT, 2005) as illustrated in Figure 21. Regions of different levels of damaged areas (urban and rural/natural) correspond better to flow speed distribution inland rather than with the flow depth distribution. This implies that in assessing the tsunami hazard zone, information of the overland flow speed is very important. To date, most of the hazards maps only consider the flow depth and runup instead of the overland speed.

8. Conclusions

We modeled the tsunami propagation and inundation dynamics in Banda Aceh using the 3DD numerical model. Our modeling provides new insights into the overland flow dynamics that devastated Banda Aceh. The character of waves, which impacted the northwest and west coast, were different due to the interaction of the waves with the offshore islands, a wide flat continental shelf on the west coast and relatively steep bathymetric condition of the northwest coast. Tsunami elevations were on the order of 6 – 15 m on the northwest coast in contrast to 15 – 25 m along the exposed west coast. Our model results agree with field measurements collected in the months following the event.

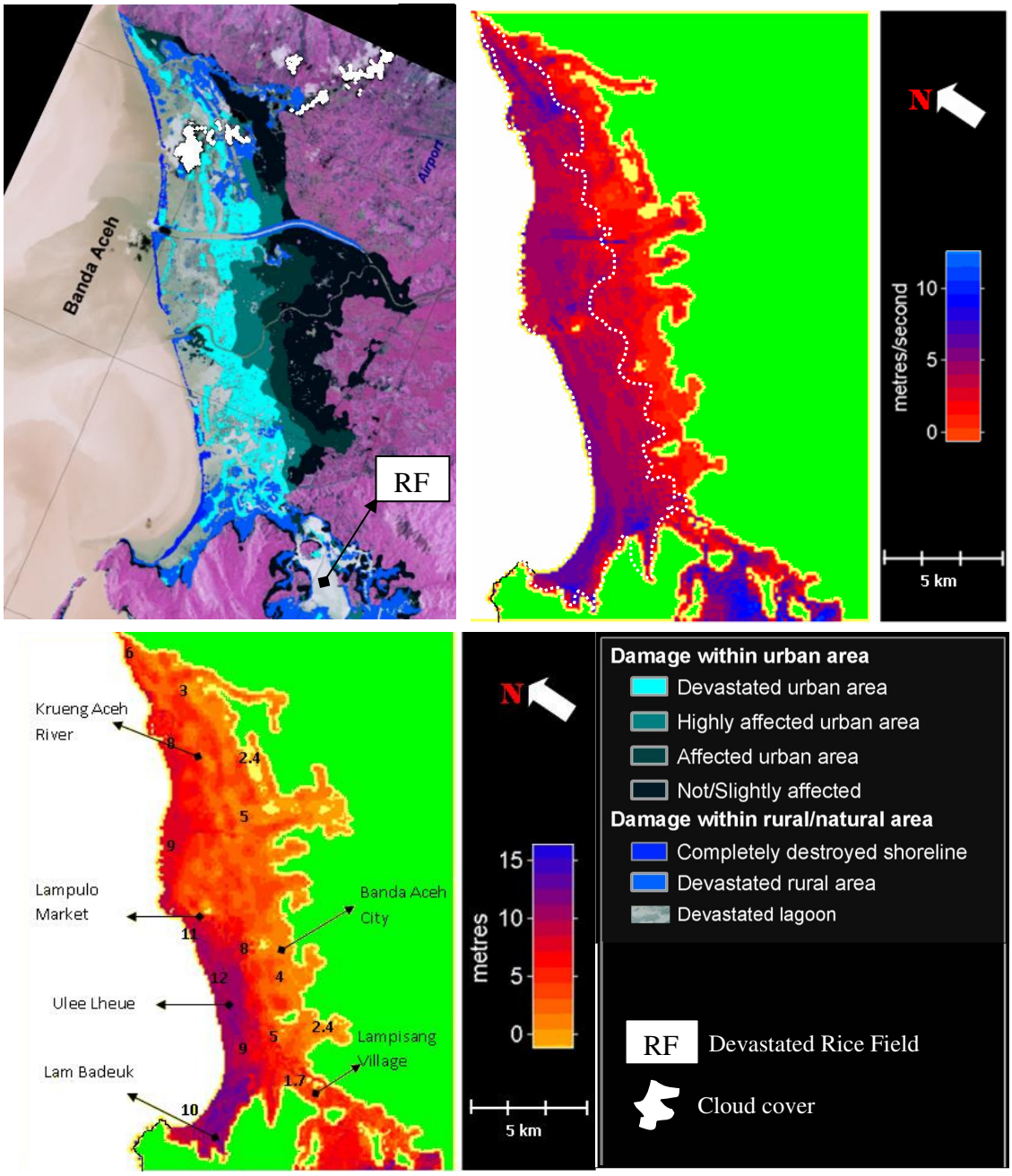

Figure 20. The damage maps (UNOSAT, 2005) derive from satellite imagery (SPOT 5 color – 2.5 m) and field measurements (a) shows that the damage within urban and rural or natural areas which mostly coincides with the flow speed distribution (b) rather than the runup and flow depth (c). The white dot-line (b) is the boundary of strong currents, which is in agreement with the boundaries of devastated urban and rural areas. The devastated rice field (RF) due to strong currents is easily identified on flow speed map (c), but hardly identified using the flow depth distribution maps (c). The yellow color on figure b and c represent the inundation zone and the green color represents the non-inundation zone.

Flow depth and flow speed distributions depend upon the nearshore topography and geomorphology. Broad coastal plains with low, flat ground allow of the tsunami waves to maintain their flow depth further inland as the overland flow speed decreased. Coastal topography consisting of dunes and sand ridges shows that overland flow speed decreases as the wave front approaches the shoreline, then increases. There is a more complicated distribution of tsunami elevation, flow depth and speed when the flow encounters irregular coastal topography. Rivers, drainage channels and creeks will extend the inundation further inland.

In deriving a hazard map from the numerical modeling results, it is necessary to carry out a simulation that covers the entire series of tsunamis that may be generated and which may consist of 3 to 5 waves. It is also important to incorporate modeled flow speeds in addition to the flow depth. To investigate the dynamics of the tsunami return flow, a longer simulation is also needed. Our modeling for the west coast of Aceh suggests that more than 12 hours are needed to drain the seawater from the land.

Acknowledgements

The numerical model research work had been funded through NZIDRS, New Zealand and the fieldwork funded partly by Tsunami Research Foundation – Indonesia, USGS – NOAA on ITST 1-2. Thanks to Drs. Rahman Hidayat, Dinar C Istiyanto, Widjo Kongko, Lukianto and all ITST Sumatra 2004 team for providing the fieldwork data.

References:

Black, K.P.:1983, Sediment transport and tidal inlet hydraulics. PhD thesis, University of Waikato, New Zealand, 331 p.

Black, K.P.:1984, Sediment transport, Tauranga harbor study, *Consulting Report to the Bay of Plenty Harbour Board*, New Zealand.1 and 2. 159 p.

Black, K.P., and Barnet, A.G.:1988, Sediment transport modelling under tidal flows with application in Natural Estuary, *IAHR Symposium on mathematical modeling of sediment transport in the Coastal Zone*, Copenhagen, Denmark. May/June 1988. 9 p.

Black, K.P., Healy, T.R., and Hunter, M.:1989, Sediment dynamics in the lower section of a mixed sand and shell –lagged tidal estuary, *Journal of Coastal Research*. **5(3)**, 503-521.

Black , K.P.: 2001, The 3DD Suite of Numerical Process Models , *ASR Ltd*., PO Box 67, Raglan, New Zealand. 90 p.

BRR, (Reconstruction and Rehabilitation Agency of Aceh and Nias).: 2006, Progres Report Aceh & Nias, *Two Years after the Tsunamis*, December 2006. 110 p.

Borrero, J.C.:2005, Field data and satellite imagery of tsunami effects in Banda Aceh, *Science* **308**, June 10, 2005.

Borrero, J.C., Synolakis, C.E. and Fritz, H.: 2006, Northern Sumatra field survey after the December 2004 Great Sumatra Earthquake and Indian Ocean Tsunami, *Earthquake Spectra, Special Issue III* **22**, pp. 93-104.

Borrero, J.C., Bosserelle, C., Prasetya, G., and Black, K.P.: 2007, Using 3DD to model tsunami inundation, *Proceedings of the Australasian Coast and Port Conference*, July 2007, Melbourne Australia, Paper 96, 6 p.

Fritz, H., Borrero, J.C., Synolakis, C.E., and Yoo., J.: 2006, 2004 Indian Ocean tsunami flow velocity measurements from survivors videos , *Geophysical Research Letters* **33**, pp. 1-5.

Jaffe, B.E, C. Borrero, J.C., Prasetya, G.S., Peters, P., McAdoo, B., Gelfenbaum, G., Morton, R., Ruggiero, P., Higman, B., Dengler, L., Hidayat, R., Kingsley, E., Widjo Kongko, Lukijanto, Moore, A., Titov, V., and Yulianto, E.: 2006, The December 26, 2004 Indian Ocean tsunami in Northwest Sumatra and Offshore Islands , *Earthquake Spectra, Special Issue III*, **22**, pp. 105 -135.

Liu, P.L.F, Yeh, H., and Synolakis, C.E .: 2008, Benchmark Problems in *Advance Numerical Models for Simulating Tsunami Waves and Runup*, In Liu, P.L.F, Yeh, H., and Synolakis, C.E (eds), Advance in Coastal and Ocean Engineering, Vol.10. pp. 223-230.

Lundquist , C.J., Thrush, F., Oldman, J.W., and Senior, A.K.: 2004, Limited transport and recolonization potential in shallow tidal estuaries. *Journal of Limnology and Oceanography* **49(2)**, pp. 386-395.

Matsutomi., H., Sakakiyama, T., Nugroho, S., and Matsuyama, M.: 2006, Aspects of inundated flow due to the 2004 Indian Ocean tsunami, *Coastal Engineering Journal* **48(2)**, pp. 167-195.

Okada, Y.: 1985, Surface deformation due to shear and tensile faults in a half space, *Bulletin of Seismological Society America* **5(4)**, pp. 1135-1154.

Paris, R., Lavigne, F., Wassmer, P., and Sartohadi, J.: 2007, Coastal sedimentation associated with the December 26, 2004 tsunami in Lhok Nga, west Banda Aceh(Sumatra, Indonesia), *Marine Geology* **238**, pp. 97-106.

Stein S., and Okal, E.A.: 2005, Speed and size of the Sumatra earthquake, *Nature* **434(7033)**, pp. 581-582.

Synolakis, C.E.: 1987, The runup of solitary waves, *Journal of Fluid Mechanics* **185**, pp. 523-545.

Synolakis, C.E., and Okal., E.A.:2005, 1992-2002: Perspective on a decade of post tsunami Surveys, *Adv.Nat.Technol. Hazards* **23**, pp. 1-30.

Synolakis, C.E., and Bernard, E.: 2006, Tsunami science before and beyond Boxing Day 2004, *Philosophical Transactions of The Royal Society. London,* **A 364**, pp. 2231-2265.

Synolakis, C.E. and Kong, L. (2006), Runup measurements of the December 2004 Indian Ocean Tsunami, Earthquake Spectra, 22(3), 67-91.

Tadepalli, S. and Synolakis, C.E.: 1994, The runup of N-waves, *Proceeding of the Royal Society, London*, **A 445**, pp. 99-112.

Tadepalli, S. and Synolakis, C.E.: 1996, Model for the Leading Waves of Tsunamis, Physical Review Letter 77, pp.2141 – 2144.

Tanioka, Y. Yudichara, Kasusose, T., Kathiroli, S., Nishimura, Y., Iwasaki, S., and satake, K :2006, Rupture process of the 2004 great Sumatra-Andaman earthquake estimated from tsunami waveforms, *Earth Planet Space* **58**, pp. 203-209.

Titov, V.V.,and Synolakis, C.E.: 1997, Extreme inundation flows during the Hokkaido-Nansei-Oki tsunami, *Geophysical Research Letters* **24(11)**, pp. 1315-1318.

Titov, V.V., Rabinovich, A.B., Mofjeld, H.O., Thomson, R.E., and Gonzalez, F.I.: 2005, The global reach of the 24 December 2004 Sumatra tsunami*, Science* **309**, pp. 2045.

Umitsu, M., Tanavud., C., and Patanakanog, B.: 2007, Effects of landforms on tsunami flow in the plains of Banda Aceh, Indonesia, and Nam Khem, Thailand. *Marine Geology* **242**, pp. 141-153.

Yalciner, A.C., Perincek, D., Ersoy, S., Prasetya, G., Hidayat, R., McAdoo B.G.: 2005, Report on December 26, 2004, Indian Ocean Tsunami, Field Survey on Jan 21-31 at North of Sumatra, *ITST of UNESCO IOC*, 18 p

3.3.2. The Debris Dispersal Modelling

Debris dispersal modelling is carried out to investigate the dynamic of waste and other debris during the great Sumatra Tsunamis 26 December 2004. The model results was written and submitted to Journal of Natural Hazards (NHAZ 899 - in review).

Debris **D**ispersal **M**odelling for the **G**reat **S**umatra **T**sunamis on Banda Aceh and Surrounding Waters.

GEGAR PRASETYA[1], KERRY BLACK[2], WILLEM de LANGE[1], JOSE BORRERO[2], TERRY HEALY[1]

Abstract – The Great Sumatra Tsunami on 26 December 2004 generated large amounts of debris and waste throughout the affected coastal region in Indian Ocean. In Banda Aceh - Indonesia, the tsunami flows were observed carrying a thick muddy sludge that mixed with all kinds of debris from the destroyed buildings, bridges and culverts, vehicles, fallen trees, and other flotsam. This waste and debris was mostly deposited inland, but traveled both onshore and offshore. Numerical dispersal modeling is carried out to simulate the transport of debris and waste produced by the tsunamis during the event. The model solves the Lagrangian form of the transport/dispersion equations using particle-tracking techniques. Model results show that understanding the pathway and distribution of the suspended materials and flotsam caused by tsunamis is important for a proper hazards mitigation plan and waste management action, and to minimize serious long-term adverse environmental and natural resources consequences.

Key words: Tsunami, Banda Aceh, debris and waste, dispersal model

[1]Department of Earth and Ocean Sciences, University of Waikato, New Zealand

[2]ASR Ltd, Marine Consulting and Research, Heaven on the Planet, Lombok, Indonesia www.asrltd.co.nz

Introduction

The Great Sumatra Tsunami on 26 December 2004 caused substantial environmental damage around the coastal areas of the Indian Ocean region. The areas to the northwest and west coast of Banda Aceh were hardest hit, and experienced almost total destruction. The disaster generated large amounts of debris and waste. The tsunami flows were observed carrying a thick muddy sludge that mixed with all kinds of debris and other floatsam during wave run-up and backwash. Some of the waste and debris was deposited inland, blocking rivers, channels and streams, and some was carried by the backwash flow into the sea. These solid waste materials included saline waters, sands and clay particles, that may contaminate, plus a mix of chemicals, oil, sewage, building materials and decomposing bodies, which could constitute a major environmental health problem.

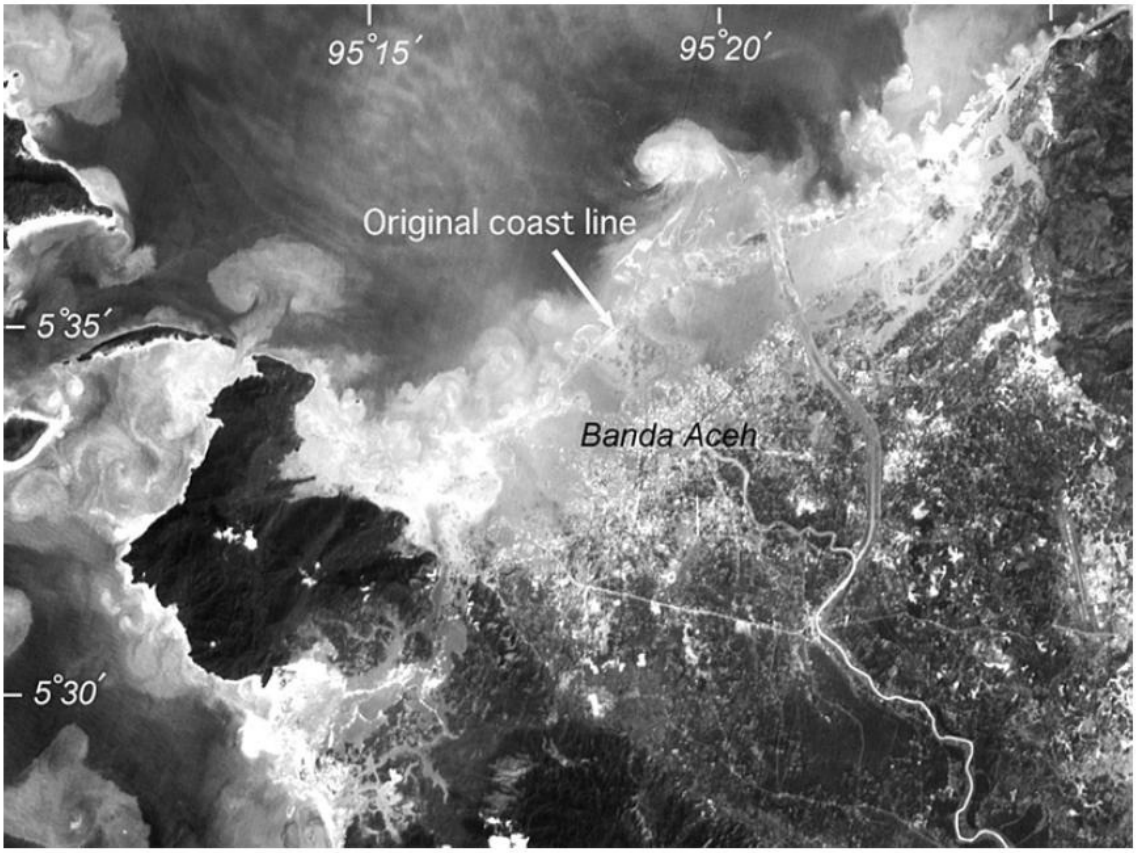

Figure 1. Satellite image showing a distribution of suspended materials in Banda Aceh 4 hours after the earthquake and tsunami. (Based on SPOT2 image, Umitsu et al. 2007). Highly turbid waters along the northwest and west coast, and the new formations from the backwash can be clearly identified extending offshore.

Aerial photographs and satellite imagery shortly after the event show the tremendous extent of the debris and waste that had been deposited inland and transported offshore, as illustrated in Figure 1. Black muddy sand that mixed with all kinds of debris were found everywhere inside the inundation zone in Banda Aceh, while most of the seawater close to the shore became highly turbid and was mixed with flotsam and other waste material from the land (Figure 2). It is necessary to identify the source of the materials and where they have been transported and deposited across the affected region in order to have a proper waste management action at sites, which are vulnerable to further contamination or spreading of contaminating substances and goods.

Figure 2. The tsunami flows appear as a thick muddy sludge that mixed with all kind of debris from the destroyed buildings, bridges and culverts, vehicles, fallen trees, and others flotsams as seen on photo (a) where deposited inland (b,c), and some of them were carried by the return flows offshore (d). Photo (d) taken 5 hours after the first wave inundated the City. (Photo d: courtesy Satgas Udara Sabang).

Rapid environmental assessment in and around Banda Aceh after the event (UNEP, 2005) shows it is necessary to have comprehensive information about the size and extent of the disaster, particularly with respect to the flow speed distribution and

pattern during the events, in order to identify and mitigate further adverse effects of the waste and debris on the environmental resources (Spaling and Vroom, 2007).

Numerical dispersal modeling can be used to simulate the transport of dissolved, passive and active material such as effluent, bacteria or sediment (Black 1996, Gomez-Gesteira et al. 1998, James, ID 2002). The model will provide valuable information for a proper mitigation plan and post-disaster waste management action. Lessons learned from the 26 December 2004 event reveal that the greatest impacts to the environment were not solely due to the tsunami itself, but also due to actions taken during the post-tsunami, as observed in Sri Lanka (Pilapitiya et al., 2006). In Japan, beside the debris and waste, a secondary post-tsunami disaster was oil fires (Iwabuchi and Imamura, 2005).

In this paper, numerical dispersal modeling is carried out to identify the pathway and distribution of the suspended materials and flotsam in Banda Aceh and surrounding waters. The distribution and the path of the flotsam and pollutant from possible sources identified by the International Tsunami Survey Team – ITST (Jaffe et al, 2006, Yalciner et al., 2005) as well as a Rapid Environmental Assessment of the United Nation (UNEP, 2005) are evaluated. Most of the possible sources of pollutants came from industrial sites, ports, urban areas (municipal solid waste), hospitals and reworking of marine sediment. The location of fertilizer, pesticides and oil depots at Krueng Raya Bay, the Cement Factory – La Farge/Andalas at Lhok Nga and Ulee Lheue port are investigated (Figure 3). For municipal solid waste, the locations are related to high-density populations, and mostly located along the coastal strip of the northwest coast (around Ulee Lheue Port) and the city of Banda Aceh. A general distribution of suspended materials and flotsam throughout the affected regions in Banda Aceh (inland, nearshore and offshore) will be assessed using multiple point sources at different locations along the coast.

Environmental Assessments

Rapid Environmental Assessments carried out by the United Nations Environmental Program in and around Banda Aceh (UNEP, 2005) found that a comprehensive audit of post tsunami environmental impacts is necessary to provide a sound knowledge base for medium-term planning and management of the environment and natural

resources. The preliminary findings reveal that for industrial sites and port, about 8,000 kilolitres of oil reportedly leaked from Banda Aceh facility at Krueng Raya Bay. The public port facility in Banda Aceh (Ulee Lheue port) was heavily damaged, as well as the Cement Factory La Farge/Andalas.

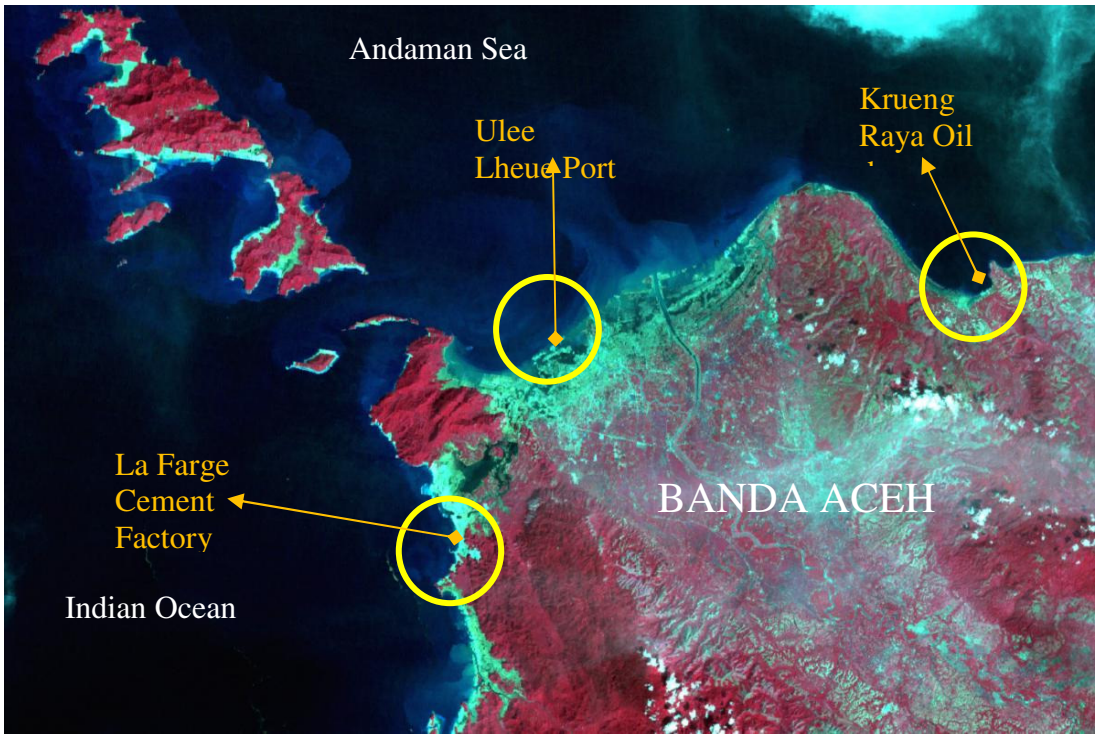

Figure 3. The false colour of Landsat image shows the inundation areas over Banda Aceh region. The image was acquired on December 29, 2004. The yellow circle shows the industrial sites that need further assessment using a dispersal model to see the size and extent of the possible pollutant distribution from these sources. (Image source: http://www.landsat.org/trfic/tsunami2004/picts/432_post.jpg)

There were high volumes of mud, sands and solid waste in order of 7 to 10 million tones in the city of Banda Aceh alone. The quantity of potentially hazardous waste created from household and small-scale chemicals industries and fertilizers were unknown, and need to be fully analyzed. Observations show the tsunami backwash dragged large amounts of material out to the sea. Nevertheless, the size and extent remains unknown. There is a need to identify the spread of the suspended materials and possible deposition areas, to account for potential damage to reefs and marine ecosystems.

Due to the size and extent of the disaster, freshwater quality and supply becomes a major concern. The water systems were badly affected, where thousands of wells and

boreholes were damaged, destroyed or contaminated. Post tsunami surveys carried out by the Ministry of the Environment (Government of Indonesia) showed high levels of faecal coliforms which was consistent with sewage contamination caused by a complex mixture of mud-laden residues which infiltrated natural and man-made water sources.

Industrial Sites and Port

Three areas are assessed using the numerical dispersal model. The areas are based on the Rapid Environment Assessment reports (UNEP 2005, Van Dijk 2005), and a series of International Tsunami Survey Team (ITST) reports for Banda Aceh. Each site (Figure 3) also represents three different tsunami waves characteristics. La Farge Cement Factory confronted a 15- 35 m tsunami on the west coast, while Ulee Lheue Port and Krueng Raya Oil depot to the northwest and east coasts were inundated with an 8-10 m and a 2-5 m of tsunami respectively.

The oil storage depots in Krueng Raya Bay consist of 8 tanks holding as much as 40.000 kilolitres of oil prior to the event. Some 8,000 kilolitres reportedly leaked during the event. Three of the tanks were transported a short distance within the plant, while one was moved into a village some 700 m away. Traces of oil were found amongst the waste and rubble in the proximity of the facility, and at the harbor about 2 km away. However, most of the oil was washed out and maybe diluted during the highly turbulent flows. It is essential to identify where the rest of the oil was transported during the event.

The Ulee Lheue port was completely damaged and washed away, including the oil retailing and fuel stations. The floating power generation unit was transported up to 3 km inland, surrounded by a massive accumulation of debris (Figure 4). No trace of oil spills or the buildings and facilities were found nearby. However, 2 km inland of the site, oil barrels and slick were found with mud and debris from houses.

The cement factory La Farge complex was damaged (Figure 5), and some parts of the factory structures were transported into the sea by the returning flows, and deposited around the port. Some of the tetrapods from the breakwater were found during seabed clearance operations of the port basin after the event. No hazardous raw materials in

substantial quantities from the cement factory were reported to have washed out into the sea (UNEP, 2005), although identification of these fine cements would be difficult.

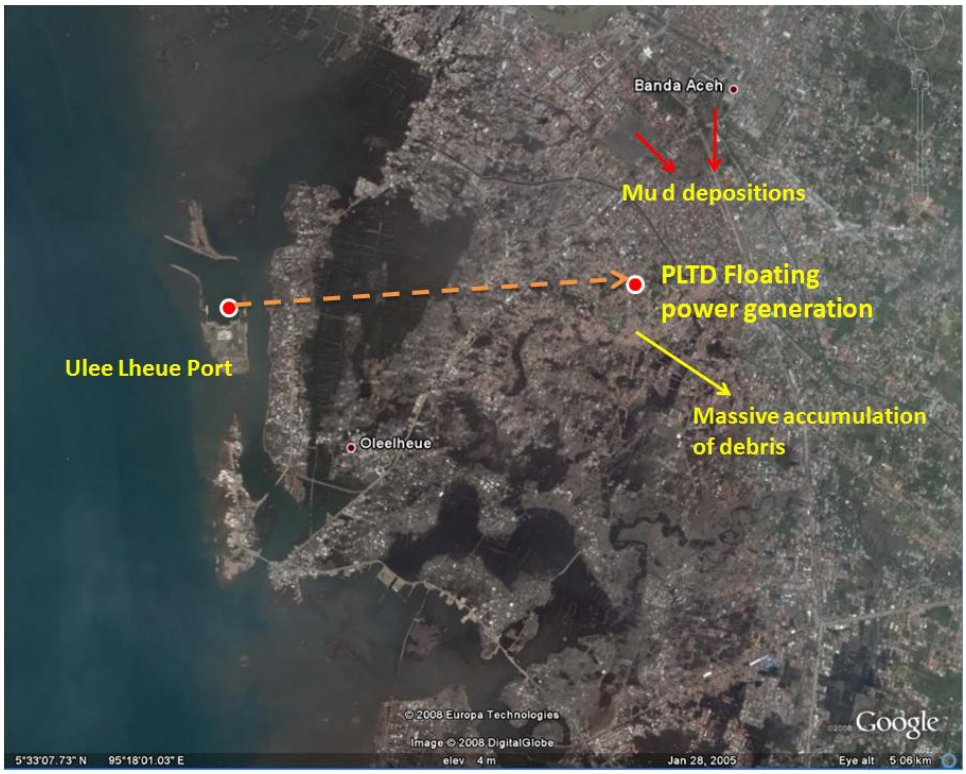

Figure 4. The distribution of floating debris and mud after the tsunami inundated the northwest coast. The floating power generation unit was transported up to 3 km inland from its original position at Ulee Lheue Port. (Map source: Google earth).

Hospital, Municipal Solid Waste and Sanitation.

The hospital at Banda Aceh city (Rapid Survey Assessment, UNEP, 2005) was inundated, but the hospital equipment and instruments were still in place, which minimized the possibility of scattering chemicals and other dangerous substances. Nonetheless, the organic waste distributed from the hospital needs to be investigated as well as the municipal solid waste disposal, which was located close to the shore, alongside waterways and wetlands (Figure 6). The wastes were mixed with the tsunami flows, and distributed within the affected region inland and offshore and could spread water-borne diseases, gastric complaints, typhoid and cholera as identified in the report. The same situation also occurred at the sanitation system areas.

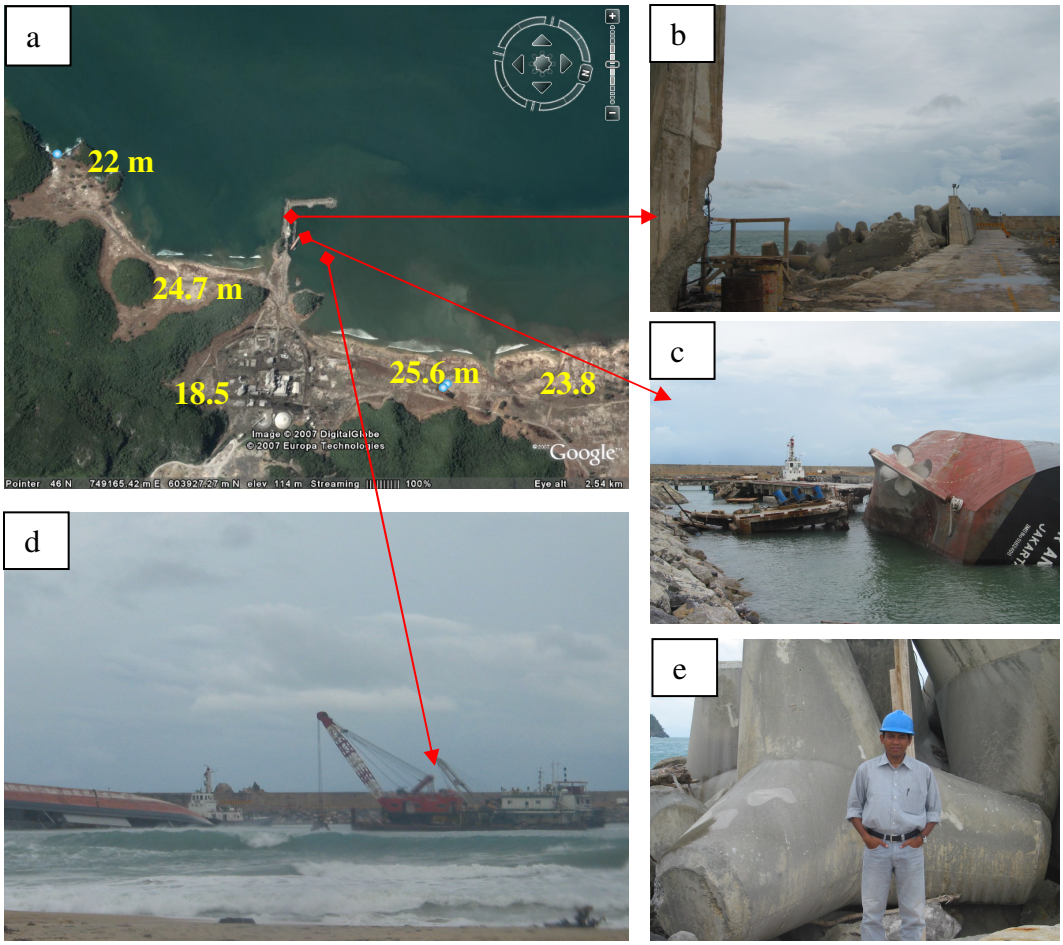

Figure 5 . The tsunami impact at the Cement Factory Port – Lhok Nga. (a) The breakwaters were overtopped by the tsunamis; (b) the ship was turned over behind the breakwater and (c) some of the tetrapods with sizes shown in the photo (e) had been scattered by the wave action. These were excavated during rehabilitation work (d). The numerals on photo (a) are the tsunami flow depth near the beach. (Photo 1 source from Google Earth, Photo 2,3,4,5 were taken by Lukianto).

Figure 6. Atypically, individual septic tanks (left) and sewage treatment facilities within the inundation zone were hardly disrupted by the tsunamis. (Photo source: USAID, 2005)

The mud and debris distributions.

As reported by the survivors, the tsunami flows appeared as a dark muddy color, which mixed with all kind of debris. The thickness of mud deposition varied from 1 m at the estuarine zone up to few centimeters at the end of inundation zone further inland (Figure 7), while onshore and offshore depositions of these fine materials were unknown.

Figure 7. Mud depositions ~ 1 m thick around the estuary areas appeared with black colors (left), while a few centimeters of mud with light-grey color deposited further inland (Photo courtesy of G.S. Prasetya)

The Model

Model Description

The models are from the 3DD Suite (Computational Marine and Freshwater Laboratory, Black, 2001), which consists of a series of coupled numerical models to simulate physical and biological processes in marine and freshwater environments. For this study, two modules are used: the 3DD hydrodynamic module and the POL3DD dispersal module. The 3DD hydrodynamic module had been used recently in studying tsunami generation, propagation and inundation dynamics for the Banda Aceh region (Borerro et al., 2007, Prasetya et al., 2008, Prasetya et al., (in press)). POL3DD (Black, 1996) is a Lagrangian 3-dimensional dispersal models that links to the 3DD hydrodynamics. The model has broad capabilities that can be used for transport of dissolved, passive and active material such as larvae, effluent, bacteria or sediment in homogenous and stratified ocean, continental shelf or shallow water environments. The model solves the Lagrangian form of the transport/dispersion equations using particle tracking technique (Black 1996, 2001).

The Eulerian governing equation of POL3DD for advection/diffusion is:

$$\frac{\partial C}{\partial t} = \frac{\partial}{\partial x}\left(E_x \frac{\partial C}{\partial x} - UC \right) + \frac{\partial}{\partial y}\left(E_y \frac{\partial C}{\partial y} - VC \right) + \frac{\partial}{\partial z}\left(E_z \frac{\partial C}{\partial z} + w_s C - WC \right) - kC + S_s$$

where C is the concentration, t is time, x,y,z are orthogonal spatial coordinates, E_x, E_y, and E_z are coefficients of eddy diffusivity, w_s is the still water fall velocity under gravity, and U,V,W are horizontal and vertical components of the fluid velocity, k is the decay coefficient for a non-conservative tracer (e.g. $k = 2.3/T_{90}$ for faecal indicator bacteria) and S_s is the tracer/effluent source term. Currents and sea level from 3DD hydrodynamic model results are used to specify the circulation in POL3DD. Currents derived from a hydrodynamic model firstly advect particles, and the diffusion is modeled as a random walk, with position increments proportional to horizontal and vertical eddy diffusivity (Black, 2001).

Conservative water-borne transport is often simulated to examine pollutant pathways, destination and residence times. Particles can be tracked until they all leave the model region as well as for chemical pollutants that relate to their own signatures, while E coli and faecal coliform depends on solar radiation levels and water clarity. Oil spills have many unique characteristics, including density of the oil, leakages, evaporations rates and vertical mixing into the water column which is considered inside the model. To investigate the distribution of the pollutant based on the identified source, four types of sub-models: conservative, chemical pollutants, E.Coli and oil spills within POL3DD are utilized. Details of the equations, treatment, and solutions used by the models in POL3DD are presented in Black (2001).

Model Setting

Prasetya et al. (2008, in press) established the hydrodynamic model of the 26 December 2004 tsunamis for Banda Aceh, covering the north, northwestern, and west coast including the offshore islands using the 3DD hydrodynamic module. The model was run for 12 hours, and produced current and sea level information every 1 minute. Current speed and direction from this model are used to specify the circulation in POL3DD.

Since the advection processes are straight forward, POL3DD gives several options for setting up the diffusion processes for horizontal and vertical diffusion. The horizontal diffusion (m^2s^{-1}) is modeled as a random walk with eddy diffusivities in two components: longitudinal (along the direction of flow) and lateral (across the flow). The longitudinal values is usually larger than the lateral to account for seabed and surface boundary layers, however, POL3DD directly accounts for boundary layers by tracking the particles in 3-dimensions at all times (Black, 2001). In this study, the longitudinal value ranges from 1 – 5 m^2s^{-1}, and 1 - 2 m^2s^{-1} for lateral. The vertical eddy diffusivity uses a standard linear mixing length formula with the gradient set to k_s=0.4, and minimum value of mixing length is set to 0.05 m to prevent the mixing going to zero at the seabed or surface as indicated in nature (Black, 2001). The aerial photo and satellite imageries are used to calibrate the pattern and extent of the model results.

To represent a general distribution of the suspended materials and flotsam, a particles were released from 20 positions along the northwest and west coast of Banda Aceh for the duration of inundation ~ 5 hours. Identification whether the suspended/floating materials from the northwest coast are transported into the west coast and vice versa were achieved by releasing particles from the northwest coast alone without any particle being released from the west, and vice versa.

In simulating the E.Coli distribution from the sites (Ulee Lheue and Banda Aceh City), the suggested T90 values are 2-4 hours during the day at the water surface (Black, 2001). T90 is primarily indicative of bacterial sensitivity to solar radiation, with lowest values during mid-day and highest during hours of darkness. It is defined as the time during which the original organism population would reduce by 90%, or concentration decays to 90% of its initial value. The oil spreading at Krueng Raya oil depots with total amount of leakages of 8000 kilolitres is investigated as well as from the port facilities at Ulee Lheue. Standard oil specifications were used for both sites since there is no data available.

Results and discussions

The suspended/floating materials pathways and distributions

Three different models run were used to investigate the pattern of suspended/floating material pathways during 12 hours of simulations. The first model run assessed the dynamics of suspended/floating materials from the west coast, including the possibility of the particles to be transported up to the east coast through Lampisang village; the place where two flows collided (Prasetya et al. 2008). The second model run assessed the dynamics of suspended/floating materials from the east coast, including the possibility of the particles to be transported up to the west coast through the collision zone, and the third model run assessed the general distribution of the suspended material or flotsam from west and east coast in Banda Aceh and surrounding seas during the 26 December 2004 event.

West Coast Sources

The sequences of particle pathways from the west coast are illustrated in Figure 8 a-f. The straight-line particle pathways of Figures 8c and 8d show the strong inundation flow where the flows pass through the sand ridges and coastal plain without changing their directions up to 4 km inland. The particles moves very quickly from the release point along the shoreline and takes 10 minutes to reach ~ 4 km inland across the rice field behind the sand ridges and coastal plain (Figure 8c). The particles continue to move to the collision zone where the flow is mostly controlled by the landform features. At this stage, the flow speed is decelerated and the returning flow has started. The particles need ~ 5 minutes to travel 1 km through the low-lying areas to reach the perimeter of collision zones.

Some of the particles remain in the middle of the inundation zone at the rice field where the return flows are weakening, and becomes stagnant, as shown by the satellite images and identified during field surveys. The model shows most of the returning flow passes through the narrow low lying areas between Lamphuuk and Lhok Nga, and distributes the particles along the shore (Figure 8f). Most of the particles accumulate on both sides of the nearshore zone at Lamphuuk and Lhok Nga. The particles move further along the shore and offshore through those two areas.

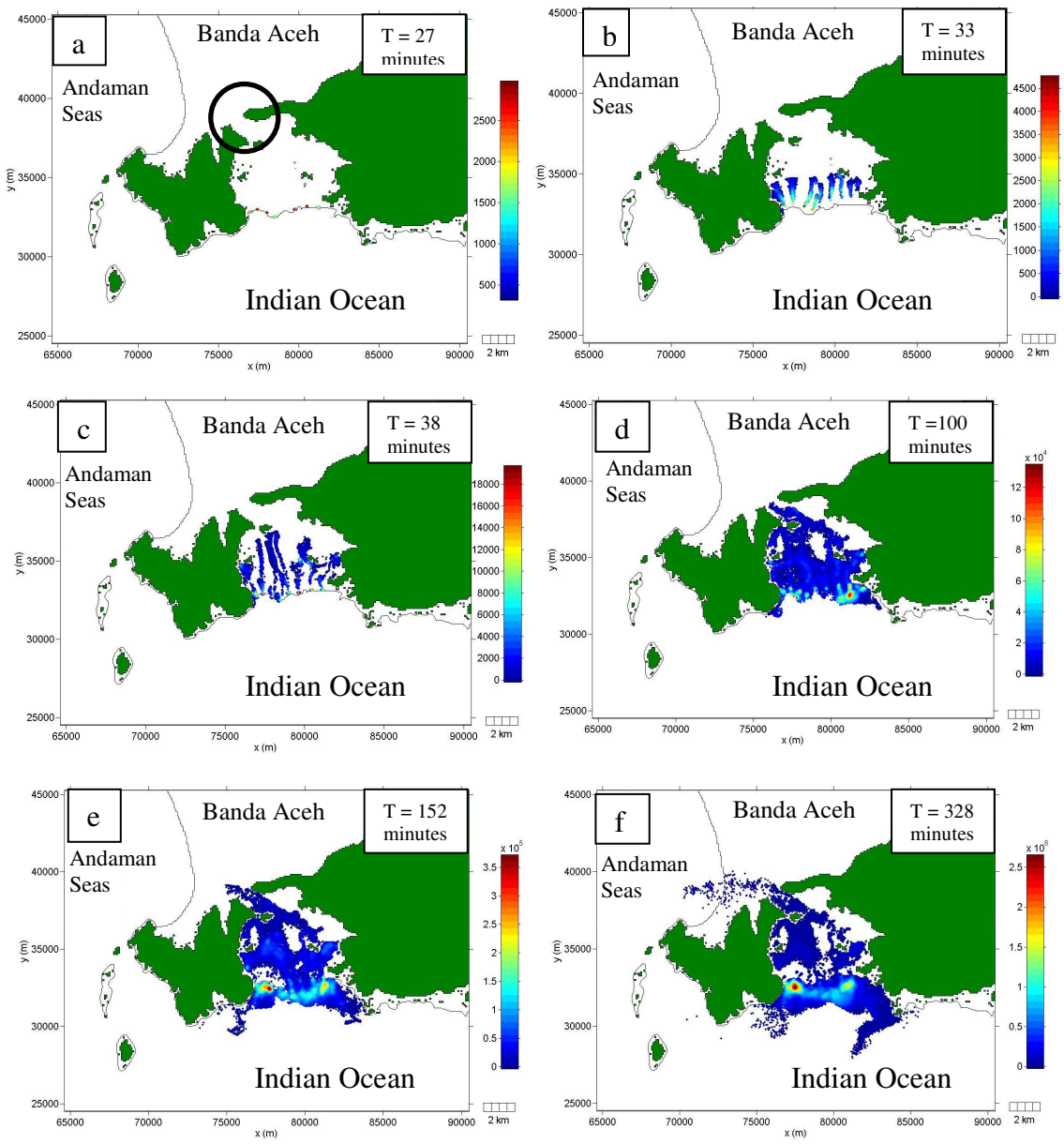

Figure 8. A sequence of particles pathways from west coast of Banda Aceh to the northwest coast. The particles move fast in straight-line inland. The black circle is Lampisang village (a) where the flow from the northwest collided with the flow form the west

Northwest Coast Sources

The sequences of particle pathways for the north-west coast are illustrated in Figure 9a-d. For the first 7 minutes after the tsunami hit the shoreline, the particles along the northwest coast of the eastern Krueng Raya River were transported inland by unidirectional flows up to 1.5 km, and ~ 3 km for most of the coastal plain area below the Krueng Raya River, such as Ulee Lheue (Figure 9b). The particles still move further inland when the returning flows started, similar to the occurrence on the west coast. The decelerating flows inland advect the particles at a slower rate and

movement is controlled by the local coastal landforms, as gravitational flows through the coastal ridges (Figure 9d).

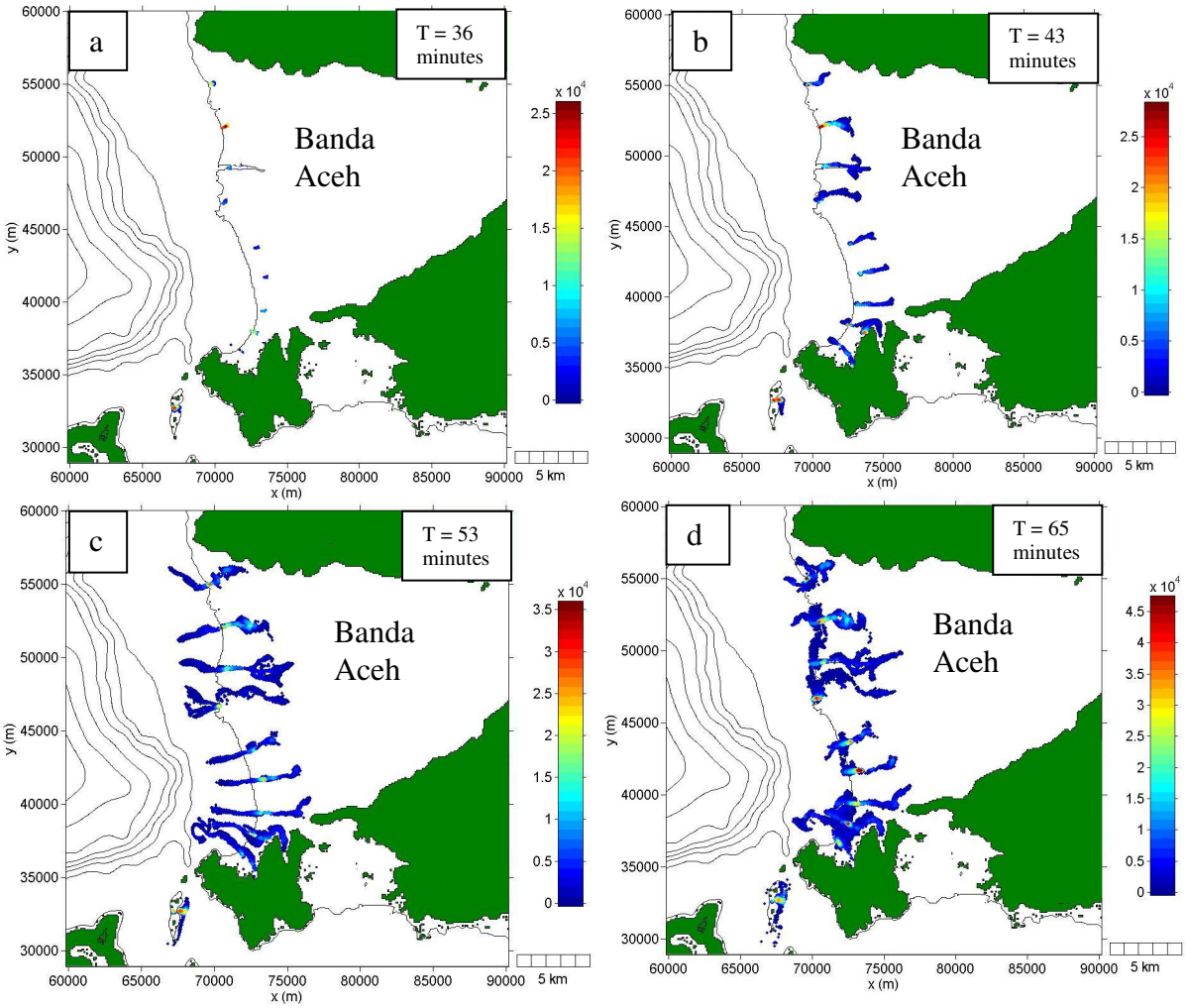

Figure 9. A sequence of particles pathways from northwest coast, during the first inundation, the particles moves inland and washed back inshore through almost the same pathways (b,c). The influence of second waves on particles pathways is shown on (d) where further up, the particles pathways controlled by the local coastal landform.

The returning flows carried some of the particles inshore through the same pathways as it transported inland. This unidirectional flow carried the particles up to 2 km offshore (Figure 9c) and particularly occurred on large and wide coastal plain compare to the areas where the beach face were characterized by sand ridges such as those areas above Krueng Raya River. At this location, most of the returning flows are controlled by topographic conditions. The flow pathways become more complex on the nearshore zone when the return flows interact with the following incoming waves.

Most particles from the western part of Ulee Lheue pass through the collision zone and accumulated at the end of the collision zone (Figure 9b and c). Some particles are transported further west and become trapped within the stagnant water at the rice field. Only few particles reach the shoreline of the west coast; much less than the number of particles transported to the northwest coast from the west coast.

The offshore particles (due to the returning flows) are distributed mostly within the nearshore zone. However, some of the particles drifted up to 5 km offshore, induced by the large eddy formations (Figure 10d). These eddy formations are shown on an aerial photograph taken 6 hours after the earthquake (Figure 2d) and on the satellite imagery SPOT2 taken 4 hours after the quake (Figure 1). An inland distribution of particles shows that the particles were trapped at the stagnant water as illustrated in Figure 10c and d, which also shows on satellite images (Figure 1), and was observed during field surveys (2c, 2d). To the northeast of Krueng Raya River, stagnant waters occur within swales, while to the west, it is observed on the wide coastal plain, especially at the shrimp ponds and rice fields.

General distribution of particles

Twelve hour simulations of the particles released on both northwest and west coasts show a distribution of the particles within the region both inland and offshore (Figure 11a-f). Most of the particles were transported to the sea; however, some of them were left inland on the stagnant waters. To the northeast of Krueng Raya River, the particles were trapped at the stagnant water between the sand ridges, while to the west, the particles were trapped at the stagnant waters on the rice field, and also to the areas within the proximity of the collision zone. The nearshore accumulations of the particles were clearly identified with extensions to the offshore through eddy formations on most of the northwest coast. On the west coast, high accumulation of particles also occurs at the nearshore zone. These accumulations were separated into two areas on both sites of the return flows at the middle of these regions. The particles are distributed further along the shore and offshore through both sides of the inundation zone, where cliffs are located.

Assessment of the model results from the particles released at the northwest coast alone shows that the contribution of the particles from the northwest coast to the west coast region is less than the particles from the west coast to the northwest, hence any contaminant from the northwest, especially in those areas west of Ulee Lheue, are minimal. We identified that due to high-speed flows during runup most of the particles are moved or transported further inland with the longitudinal direction being more dominant than the lateral direction. This straight line (unidirectional) transport of particles was confirmed by the evidence of the floating power station (barge) and most of the fishing boats that had been transported 3 km inland from their positions at Ulee Lheue port (Figure 4). With this evidence, identifying the origin of the floating materials found inland is uncomplicated, but not for the materials found offshore.

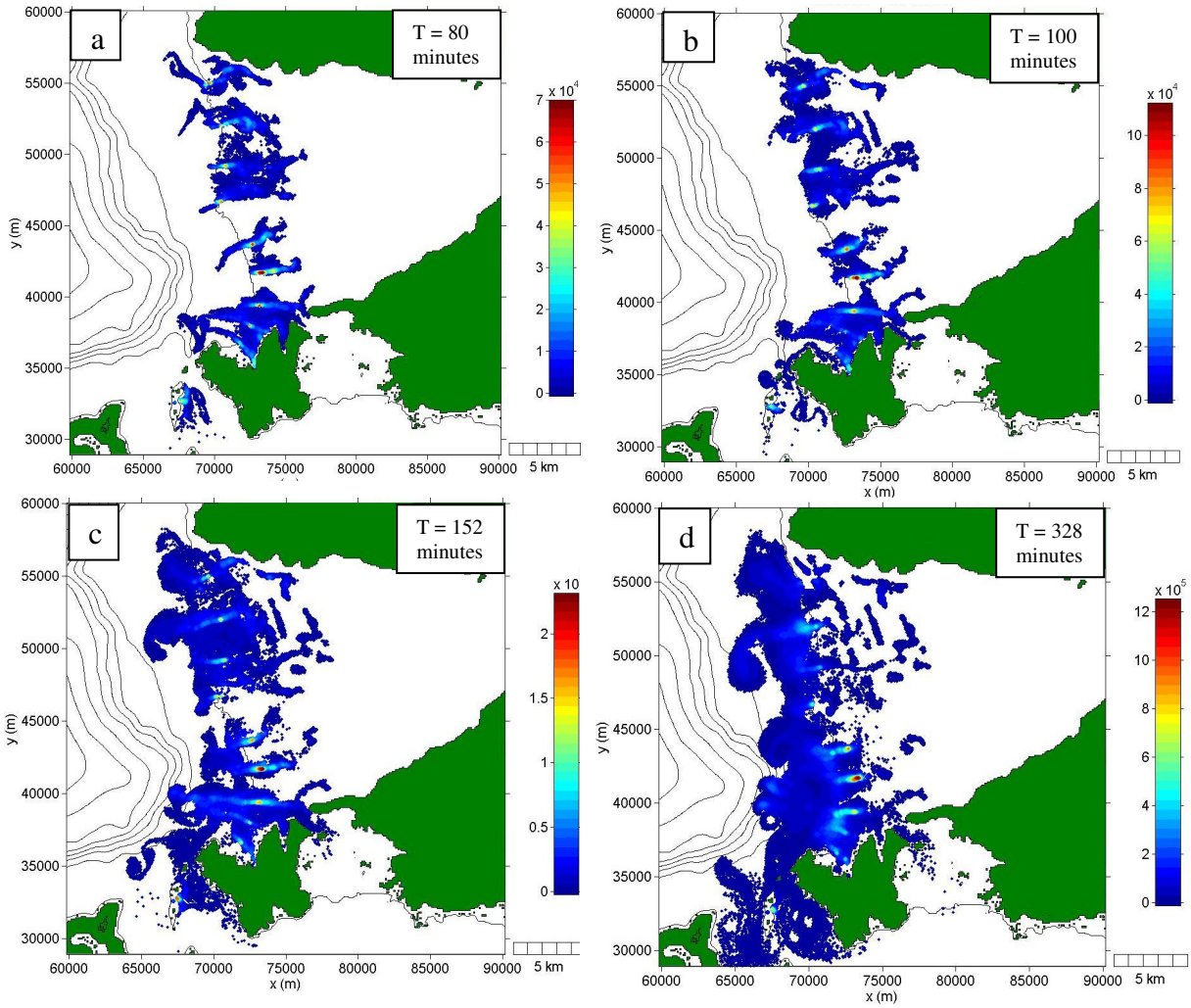

Figure 10. The following waves (second waves) transport most of the particles that had been washed offshore during the returning flows back inshore and further inland (a,b). The returning flows carry the particles back to inshore and offshore after maximum inundation is reached (c). The eddies are formed and transport the particles further offshore (d).

Distributions of the particles further offshore from the northwest coast are to the west (Figure 10 e). The particles pass through the areas between Nasi Island and Bunta Island to Indian Ocean, while the particles that travel along the shore between Bunta Island and the mainland to the west are merged with the particles that come from the west coast. These particles are transported along the shore to the northwest. The satellite imagery shows similar features where the eddy formations were further offshore and high turbidity occurs along the shore due to returning flows of suspended material from the land, as identified on both satellite imagery and model results (Figure 11c, d, e and f).

The oil distribution from Krueng Raya Depot facilities

The tsunami waves that hit the Krueng Raya region were smaller, and the depot is located in 'the shadow zone'. The runup ranges from 2 to 5 m. The eight tanks of oil storages/depots in Krueng Raya Bay were hit, four of them were transported and 8,000 kilolitres of oils were reported leaked. The model shows the particle trajectories of the oils as illustrated in Figure 12a-d, where it is confirmed that the tanks were transported into a former village inland (b), and the prevailing propagation of the oils was eastwards along the shore where its traces were found at the harbour (d).

The oil distribution from the Ulee Lheue Port Facilities

The model shows that the oil spreading from the port facilities follows the direction of the flows up to 3 km inland from the shore (Figure 13a-d). The lateral spreading of the oils is minor due to the high-speed flows in longitudinal directions as illustrated in Figure 13b. The returning flows bring back the oils inshore which follow almost the same path as it was transported inland (Figure 13c). After 5 hours of tsunami attack, the model shows that the oils that had been transported inland were already returned back to the seas, and only small traces were left inland (Figure 13d). At this stage, the lateral transport starts to be more dominant and eddies were formed.

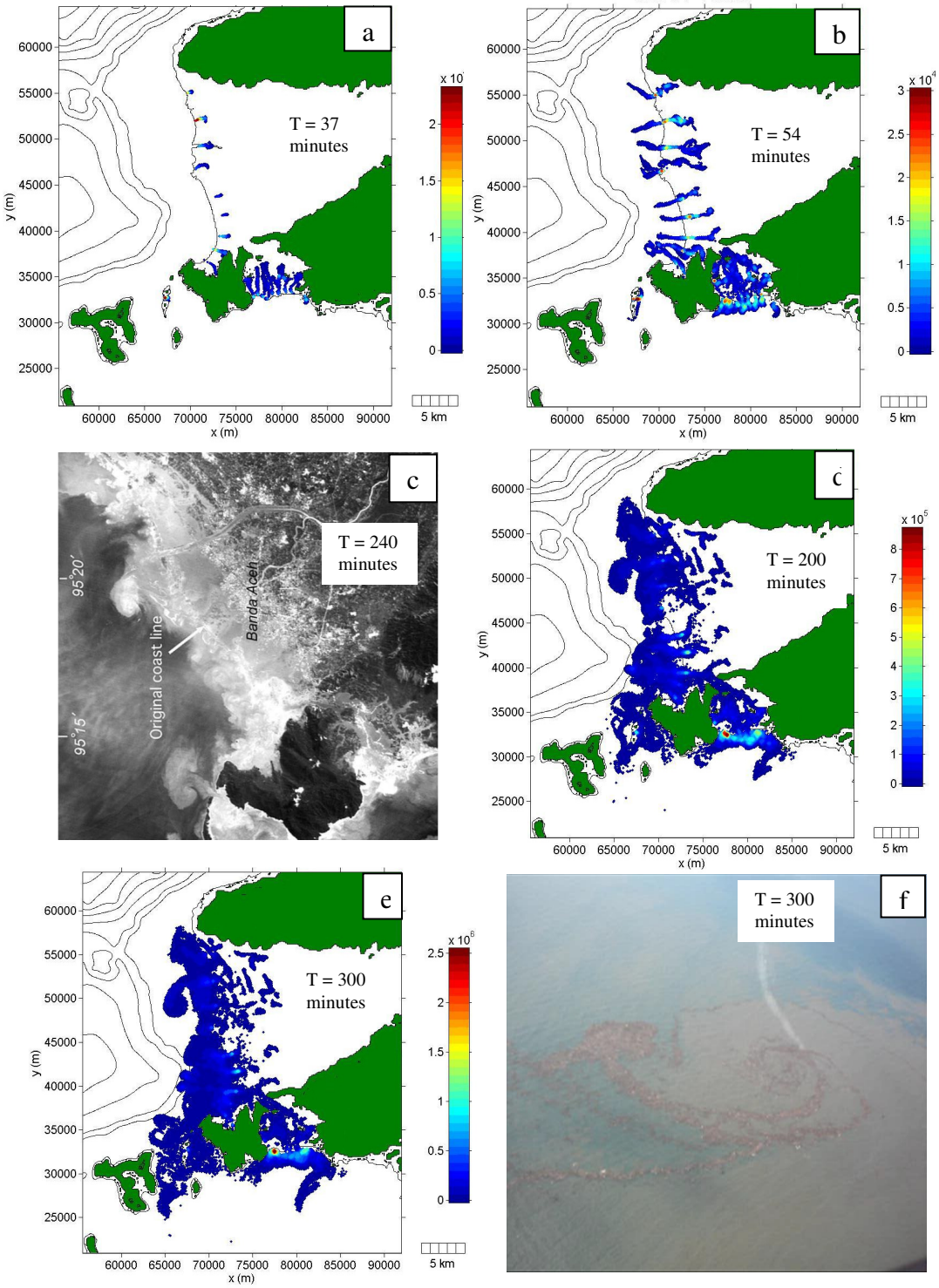

Figure 11. A sequence of general distribution of particles through Banda Aceh region from the particles that had been released from northwest and west coast shows an agreement with the SPOT2 images (Umitsu et al. 2007) taken 4 hours after the event (c) and with the aerial photo taken 5 hours after the event (f) with corresponding simulation results (d,e) (Photo source: Satgas Udara Sabang).

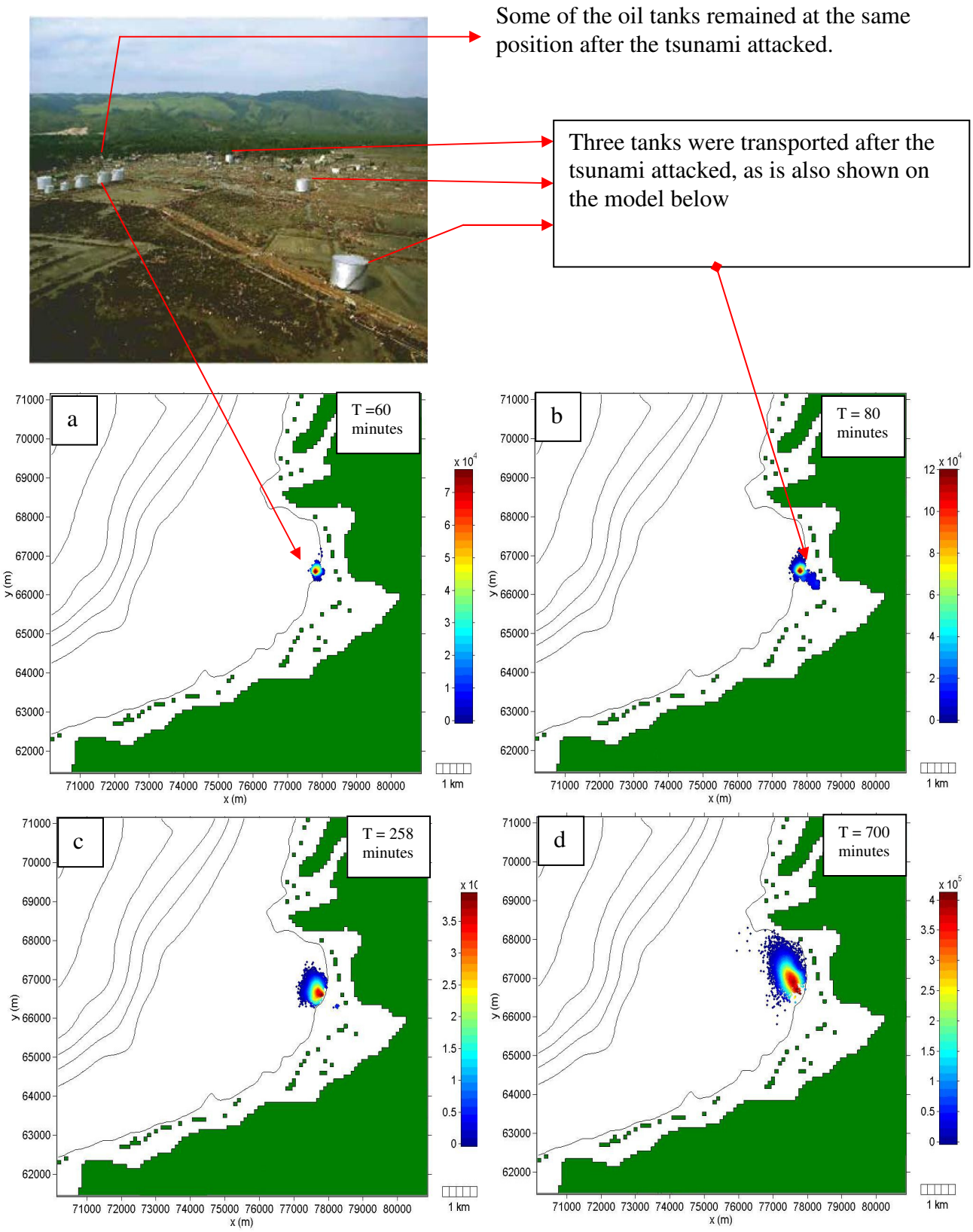

Figure 12. A sequence of the oil spills distributions at Krueng Raya Bay where three tanks were transported as seen in Photo on the top of Figure (a). The oils distributed further along the shore to the east, where its traces were found in harbour (d) (Photo source: GS.Prasetya)

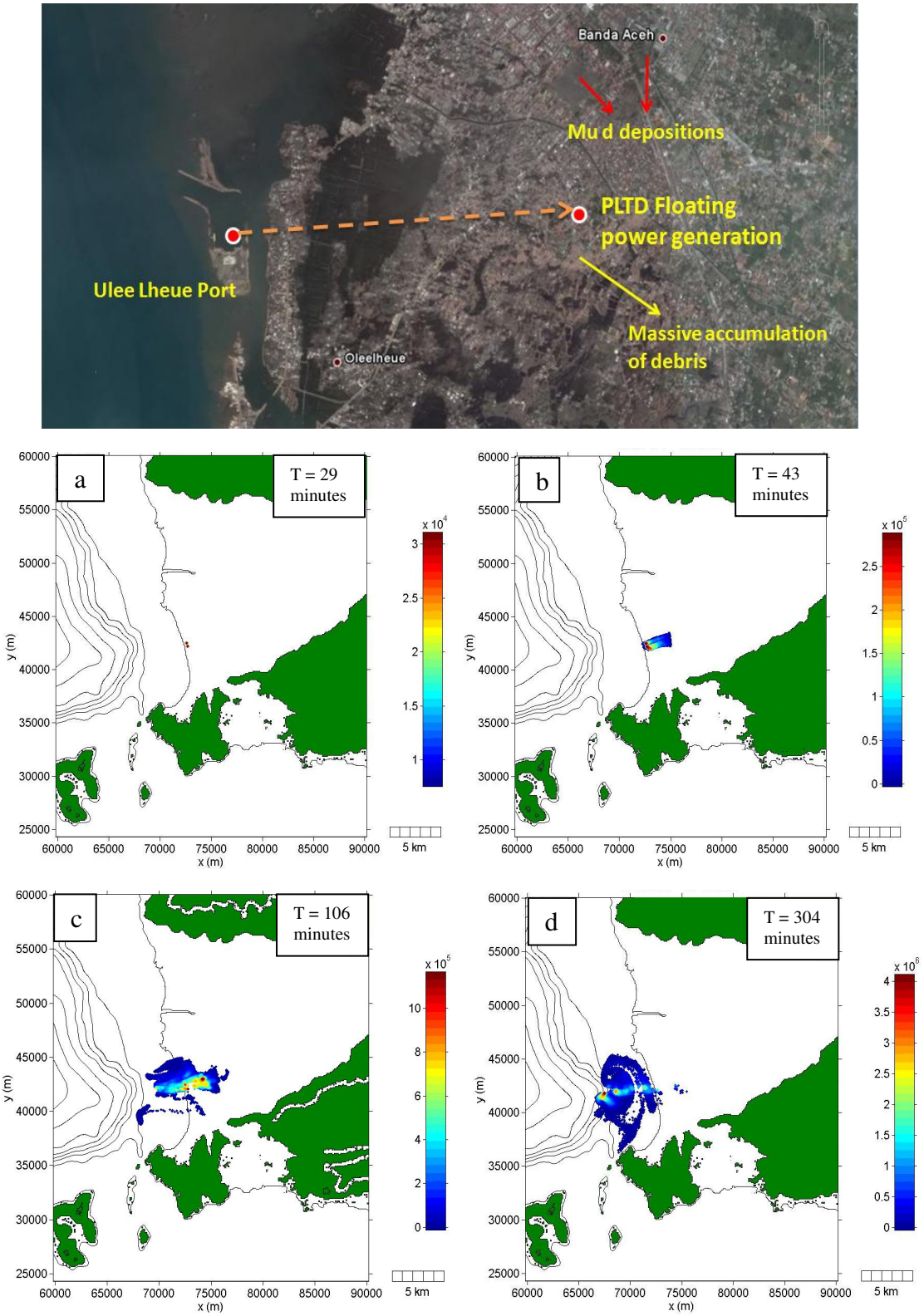

Figure 13. An assessment of oil and debris pathways from the Ulee Lheue port shows that most of the oil has been transported inland (b) and carried back offshore by return flows (c) and left small traces inland (d). The floating power generation pathway is replicated and illustrated in Figure b, where most of the particles were transported by the unidirectional flow inland (Image source: Google Earth)

The model results confirmed the rapid survey assessment results (UNEP, 2005) where further away from the site, oil barrels and slick was found in the stagnant water and mud between the rubble and debris from houses, and nothing was close to the source.

The E.coli distribution assessment.

Several factors may influence the populations of the organisms in water body such as sunlight intensity and duration, salinity and temperature and suspended particulate matter concentrations. The Faecal Coliform bacteria group is an indicative organism from the intestinal tract of humans and other animals (Kashefipour et al. 2002), where during the tsunamis, most of the municipal solid waste disposal site and treatment plan as well as individual septic tanks were completely destroyed, and carried by the tsunami flows. The model results for Ulee Lheue and Banda Aceh city are illustrated in Figure 14.

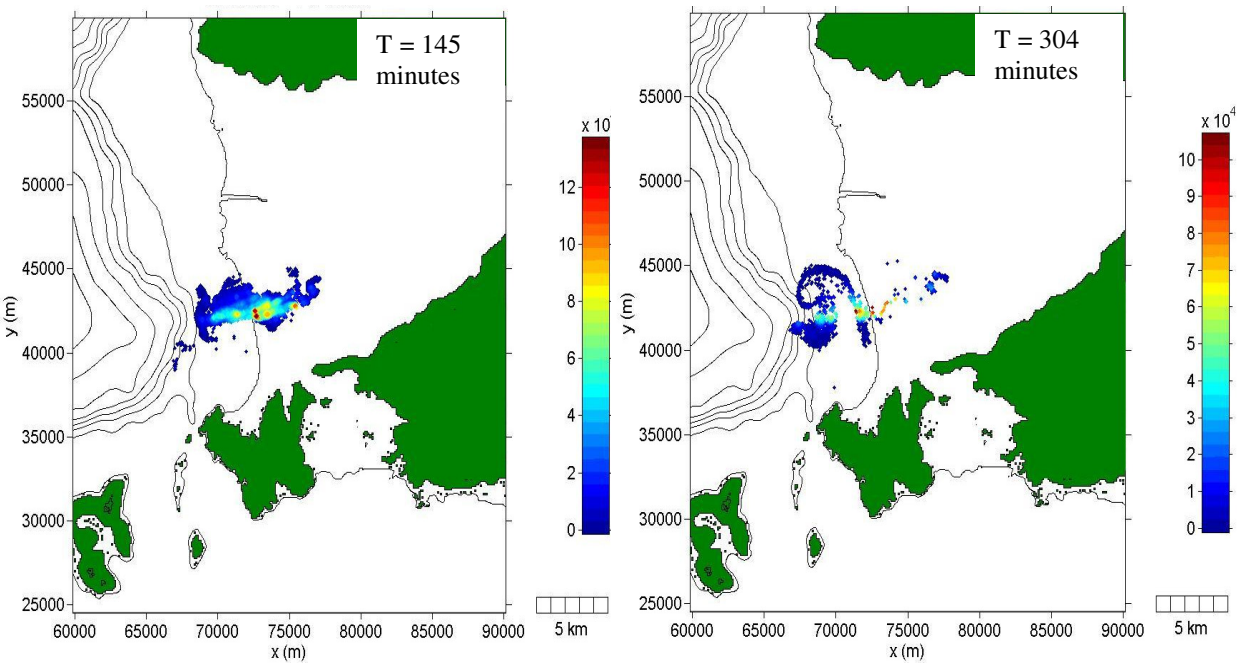

Figure 14. An assessment of E.coli from Ulee Lheue and Banda Aceh City with T90 ~ 2 hours shows that most of the E.coli were carried back inshore and left few of it inland (right) after 5 hours.

Several factors may influence the population of the coliform remaining in the water body, such as sunlight intensity and duration, temperature and salinity levels, and suspended particulate matter concentrations. Given that the tsunami occurred during the day, the T90 is set to 2 hours (Black, 2001) but the intense turbidity of the water may increase this value up to 5 hours as a daily average in turbid muds. For the first

2.5 hours, the coliform distribution is still high both inland and offshore. However, after 5 hours, the concentration of the coliform inland was reduced, and mostly accumulated in the stagnant waters, while relatively high accumulation was still present inshore and offshore was still present.

Assuming that the sources of the Coliform existing along the coast are both northwest and west, the general distribution of the coliform after 5 hours is illustrated in Figure 15, and has a similar characteristic as before (Ulee Lheue and Banda Aceh E.coli assessment). Most of the high concentrations of coliform were found along the shore, while inland, the coliform are represented by small amounts of particle remains, mostly in the stagnant water of low-lying areas, former rice fields and the lagoon.

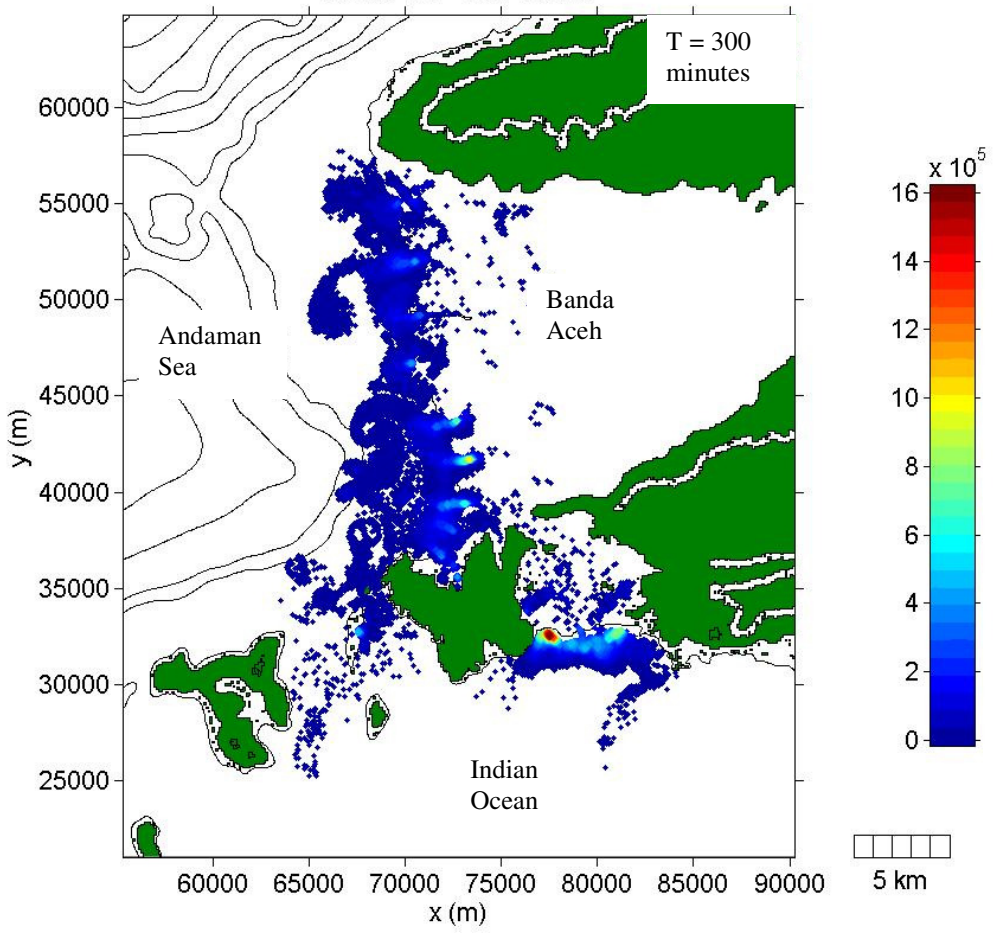

Figure 15. The general distribution of the E.coli where most of the coliform were accumulated back along the shore after being transported inland. Small amounts of coliform represented by a number of particles remained in stagnant waters.

Conclusion

Understanding the pathway and distribution of the suspended materials and flotsam caused by tsunamis is important for a proper hazards mitigation plan and post-disaster waste management action, to minimize serious long-term environmental and natural resources consequences. This can be done using numerical modeling of pollutants, known as dispersal modeling. The model shows that most of the floatsam had been transported inland through unidirectional pathways up to 3 km inland before it was transported by the gravitational flows, controlled by the local topography. The return flows had the same characteristic for the first and second waves that dragged some of the flotsam inshore through almost the same pathways, and transported further offshore through advection and eddy formation.

The particle pathway analysis (on the evidence of the collision of two flows from northwest and west coast at Lampisang villages) shows that the amount of suspended material transported from the northwest coast to the west coast was less than the reverse. This implies that pollutants from the most developed region in the northwest coast did not affect the environment of the west coast. However, it is necessary to remember that any development on the west coast could influence the environment of the northwest coast.

The pathways of the floating power generation unit (PLTD) that was transported inland from its location at Ulee Lheue Port was identified, and verified the unidirectional characteristic of the flows at some extent inland. In this case, the flows were up to 3 km inland before returning as gravitational flows mostly controlled by the local coastal landforms and topography. The oil spill from this location also verified the rapid environment assessment of UNDP (2005) at Ulee Lheue and oil depot at Krueng Raya Bay. With these results, the numerical model can be used to investigate the origin of material found inland, by using the model in "reverse tracking" mode.

This Study shows that it is useful to include information into tsunami hazard maps about where materials actually come from, and where they will be transported to and deposited. A better plan would be to relocate possible dangerous flotsam/pollutant sources, at the same time developing a proper post-disaster waste management action

that should start immediately at sites after an event, which are vulnerable to further contamination or spreading of contaminating substance and goods.

Acknowledgements.

The numerical model research work had been funded through NZIDRS, New Zealand and the fieldwork funded partly by Tsunami Research Foundation – Indonesia, USGS – NOAA on ITST 1-2. Thanks to Dr. Umitsu for permission to utilize the material for Figure 1, Drs. Rahman Hidayat, Dinar C Istiyanto, Widjo Kongko, Lukianto and all ITST Sumatra 2004 team for providing the fieldwork data.

References:

Black K.P.: 1996, Lagrangian Dispersal and Sediment Transport Model and Support Software. Occasional report no. 20. *Department of Earth Sciences*. University of Waikato and NIWA, Hamilton . New Zealand.60 p.

Black, K.P.: 2001, The 3DD Suite of Numerical Process Model – a digital manual. *ASR Ltd*. PO Box 67, Raglan, New Zealand.

Borrero, J.C., Bosserelle, C., Prasetya, G., and Black, K.P.: 2007, Using 3DD to model tsunami inundation, *Proceedings of the Australasian Coast and Port Conference 2007*, July 2007, Melbourne Australia. Paper 96, 6 p.

Gomez-Gesteira, M., Montero, P., Prego, R., Taboada, J.J., Leitao, P., Ruiz-Villarreal, M., Neves, R., Perez-Villar, V.: 1998, A two dimensional particle tracking model for pollution dispersion in A Coruna and Vigo Rias (NW Spain). *Oceanologica Acta* **22**, pp. 167-177.

Iwabuchi, Y., and Imamura, F.: 2005, Study on the Oil Spread and Fire caused by a Tsunami, *Proceeding of the Third International Conference on Asian and Pacific Coasts Asian and Pacific Coasts 2005*, pp. 471-474.

Jaffe, B.E, C. Borrero, J.C., Prasetya, G.S., Peters, P., McAdoo, B., Gelfenbaum, G., Morton, R., Ruggiero, P., Higman, B., Dengler, L., Hidayat, R., Kingsley, E., Widjo Kongko, Lukijanto, Moore, A., Titov, V., and Yulianto, E.: 2006, The December 26, 2004 Indian Ocean tsunami in Northwest Sumatra and Offshore Islands, *Earthquake Spectra, Special Issue III* **22**, pp. 105 -135

James, I.D.: 2002, Modelling pollution dispersion, the ecosystem and water quality in coastal waters: a review. *Environmental Modelling and Software* **17**, pp. 363 - 385.

Kashefipour, S.M., Lin, B., Harris, E., Falconer,R.A.: 2002, Hydro-environmental modeling for bathing water compliance of an estuarine basin, *Water Research*. **36**, pp. 1854-1868.

Prasetya, G.S., Healy, T.R., DeLange, W.P., Black, K.P.: 2008, Extreme tsunami run-up and inundation flows at Banda Aceh, Indonesia: are there any solutions to this type of coastal disaster?. *American Society of Civil Engineers*, pp.14-28.

Prasetya, G.S., Borrero, J.C., DeLange, W.P., Black, K.P., Healy, T.R. (submitted), Modelling of Inundation Dynamic on Banda Aceh, Indonesia during the great Sumatra Tsunamis 26 December 2004.Submitted to *Journal of Natural Hazard*.

Pilapitiya, S., Vidanaarachchi, C., Yue, S.:2006, Effects of the tsunami on waste management in Sri Lanka, *Guest editorial. Waste Management*, **26**, pp. 107-109.

Spaling, H., and Vroom, B.: 2007, Environmental assessment after the 2004 tsunami: a case study, lessons and prospects. *Impact Asssessment and Project Appraisal*, **25(1)**, pp. 43-52.

Umitsu, M., Tanavud, Ch., Patanakanog, B.: 2007, Effects of landforms on tsunami flow in the plains of Banda Aceh, Indonesia, and Nam Khem, Thailand, *Marine Geology* **242**, pp. 141-153.

Van Dijk, S.: 2005, Environmental Impact Assessment Tsunami Indonesia. *UNDAC environmental impact assessment*, Banda Aceh. 17 p.

United Nation Environmental Program (UNEP).: 2005, After the tsunami: Rapid Environmental Assessment. 35 p.

USAID.: 2005, Aceh Assessment Report. *Environmental Service Program*, March.2005. 31 p.

Yalciner, A.C., Perincek, D., Ersoy, S., Prasetya, G., Hidayat, R., McAdoo B.G.: 2005, Report on December 26, 2004, Indian Ocean Tsunami, Field Survey on Jan 21-31 at North of Sumatra, *ITST of UNESCO IOC*, 18 p.

3.4. Discussions

- **Model Performance**

Model performance statistics that are applied for the benchmark test show the 3DD model has a skill to reproduce comparable time histories of wave height up to 95 %. This result is consistent with the Aida (1978) correction factor (K) and fluctuation factor (k) (Table 3.2). The model provides the best replicate of the time histories of wave height at Gauge 7 with Brier Skill Score (BSS) (Sutherland et al. 2004) of 0.97, and less on Gauge 5 (BSS of 0.89). The model also replicates the highest runup of 31.7 – 32.0 m (Shuto, 1994) measured on a steep slope at the small valley located on the small pocket beach between Gauge 5 and 7 (Figure 3.2) (Borerro et al., 2007).

Modelling of the real world scale of the 26 December 2004 event on Banda Aceh shows the 3DD model successfully reproduced most features of the tsunami dynamics during the events on both northwest and west coasts such as the maximum inundation distance inland, the collision of the two flows at Lampisang Village, the inundation flow speed, tsunami elevation and inundation distribution, and the highest runup at Lhok Nga. The model performance statistic provides a BSS of 0.965 on tsunami elevation along the shoreline and inundation and runup height inland for the northwest coast, which covered the areas from Lam Badeuk to Krueng Raya including the Banda Aceh city and Ulee Lheue. However, the BSS was lower for the west coast from Lampuuk to Rhiting, being 0.84 for tsunami elevation along the shoreline and 0.85 for inundation inland, even though the model successfully replicated some of the highest runups between Lampuuk and Rhiting such as at the Cement Factory.

The difference on a skill score test for tsunami elevation along the shoreline and inundation height or flow depth inland and runup on both coastal areas shows the importance of the grid size of the model used in relation to the coastal bathymetry and topographic features of the areas. The northwest coast, which is characterized by deltaic lowlands with broad coastal plain, shows that a 100 m grid size was sufficient, but apparently not for the west coast with coastal features such as sand dunes, steep cliff, and a pocket shape of low lying areas between two steep hills. A comparison between observation and the model shows clearly those effects of the tsunami elevation at the coastal areas as well as the runup and inundation distance further inland (Figure 3.8).

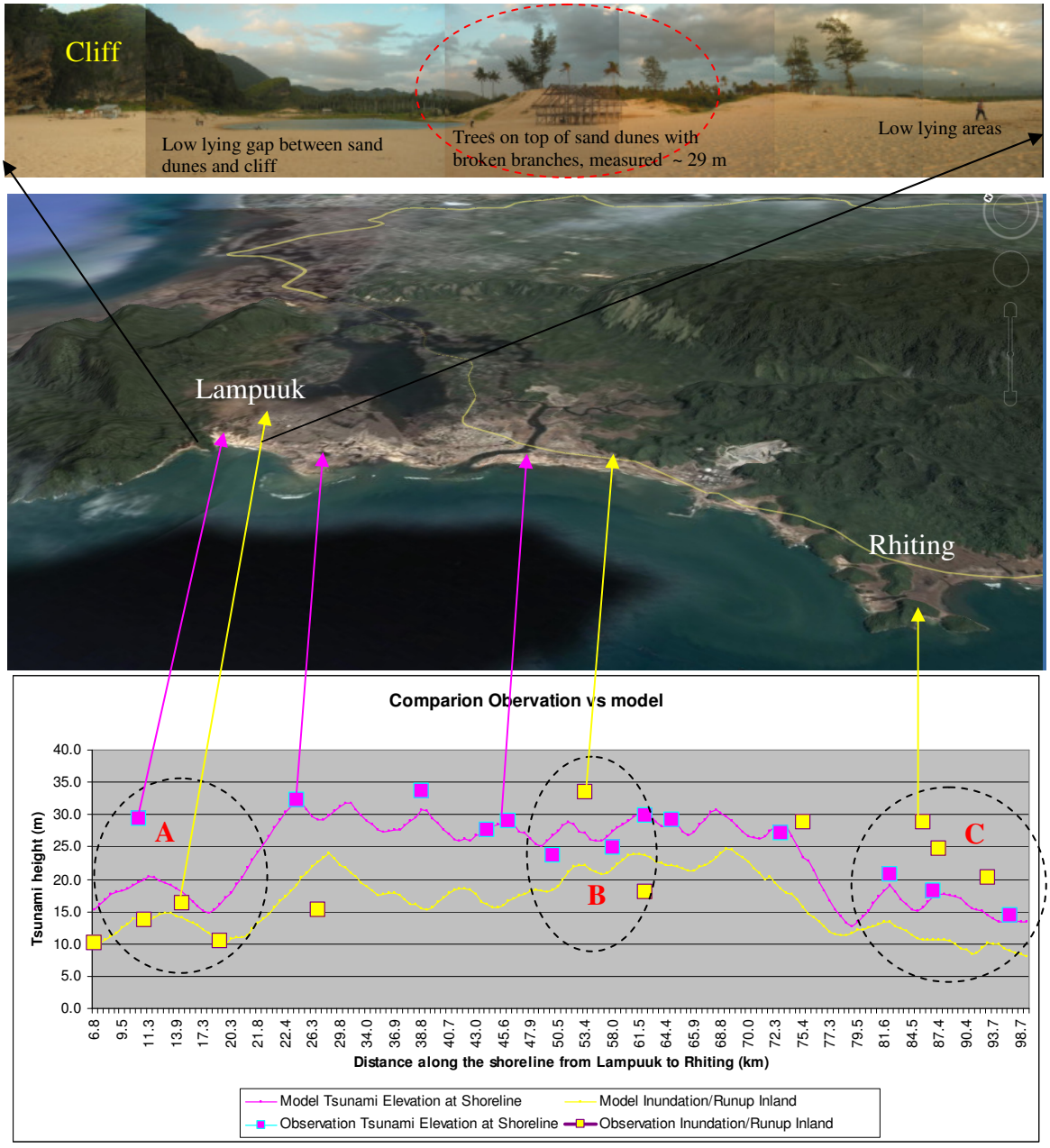

Figure 3.7. Comparison of tsunami elevation, inundation depth and runup between observation and model on the west coast from Lampuuk to Rhiting. Region A is the area where the observation of tsunami at the areas close to the shoreline had a big discrepancy from the model, while the inundation depth behind this point from the model was reasonably consistent with the observations. The 100 m grid apparently smoothes the topography data since the sand dunes located in between low lying areas have horizontal dimensions less than 100 m^2. Region B and C is where the tsunami elevation at the shoreline is reasonably consistent between model and observation, but not for inundation depth and runup due to complex coastal topography that can not be represented by the 100 m grid resolution. The skill score (BSS) for the tsunami elevation along the shoreline is improved to 0.99 when the tsunami elevation measurement at Region A is not considered in the calculation (Photo: GS Prasetya, Image: Google Earth).

The highest tsunami elevation based on field observation was ~ 30 m at region A as measured on the trees that still stand on top of sand dune, which is not represented on the model grid due to sand dune size less than 100 m^2. Excluding this measurement from the skill score computation improved the BSS to 0.99 with bias only 0.09 for all the data set. However, the runup and inundation distribution inland was under-predicted as shown with a bias of ~ -5.2 and BSS of 0.85. Almost 2/3 of the observation data of the flow depth and runup inland were above the modelled values.

In modeling the inundation for a hazard map, the requirement of high resolution data for both onshore-offshore bathymetry and coastal land terrain is critical since it determines the quality of hazard maps produced. This was demonstrated using a LIDAR data set. The differences of the inundation modelling results using the non-ground striking and ground striking data (Figure 3.6 a-e) shows the inundation processes must be taken into account in preparing hazard mitigation measures, not just the end results i.e. maximum inundation distances and flow depth. The inundation flow speed information is especially critical.

- **The diffusion term and debris dispersal model**

Since the 3DD model utilizes the nonlinear shallow water equation with a complete advection and diffusion term, the flow patterns are well presented especially when the wave attacks subside. At this stage, the flow is no longer dominated by the advection processes. The study of tsunami debris dispersal on Banda Aceh based on the 26 December 2004 event shows the importance of incorporating the diffusion term into the tsunami model. The model shows that some of the waste and other flotsam were carried further offshore through the onshore-offshore flow pattern with large eddy formations after the tsunami attacks, while during the tsunami attacks most of the flow inland and offshore were uni-directional flows where the advection processes were dominant. Tracking the transport mode of the floating power generation from Ulee Lheue Port inland clearly shows the uni-directional flow path. The debris dispersal model is the next modelling step after the inundation model that needs to be incorporated in making a hazard map.

3.5. Summary

- The numerical model known as 3DD modeling suites (Black 2001) are able to reproduce tsunami hydrodynamics during propagation and runup at both laboratories (replicate the benchmark problem #2 from the 3rd international Workshop on Long Wave Runup in 2004), and the real world scales (the 26 December 2004 Tsunami). The benchmark model output from 3DD shows the same accuracies as the popular MOST models of PMEL NOAA. While on the real world scale, it shows well agreement with field survey data of coordinated International Tsunami Survey Team. The model performance measures further provides the skill score (BSS) of 0.89 to 0.97 which consistent with correction factor (K) and fluctuation (k) of Aida (1978). The inundation model results showed the important of tsunami wave shape in relation to the coastal damage, maximum runup and inundation and the effect of the onshore island and the geometry of the coastal areas on tsunami wave characteristics. Steeper waves provide more devastating impact as shown on Lhok Nga – Lampuuk.

- An important aspect of inundation modeling is the need to adequately representing coastal bathymetry and topography. The 3DD model had been applied to the area where the high-resolution LIDAR data sets (ground striking and non-gound striking), and nearshore data from multibeam survey are available. Model results show that 3DD can handle highly non-linear bathymetric and topographic conditions, including all structures and vegetation covers without a model stability problem.

- In deriving an inundation map from the numerical modeling results using LIDAR data sets, it is necessary to carry out a simulation that utilized both ground and non-ground striking data, and covers the entire series of tsunamis that may be generated. It is also important to incorporate modeled flow speeds in addition to the inundation depth. Based on the inundation model in Banda Aceh, the devastations that occurred during the 2004 Tsunami are best explained by the flow speed distribution instead of the inundation height.

- Understanding the pathway and distribution of the suspended materials and flotsam caused by tsunamis is important for a proper hazards mitigation plan and post-disaster waste management action, to minimize serious long-term environmental and natural resources consequences. This can be done using numerical modeling of pollutants, known as POL3DD dispersal modeling. Model application for the Banda Aceh region shows that most of the flotsam had been transported inland through unidirectional pathways up to 3 km inland before it was transported by the return gravitational flows, controlled by the local topography. The return flows had the same characteristic for the first and second waves that dragged some of the flotsam inshore through almost the same pathways, and was subsequently transported further offshore through advection and eddy formation.

- It is useful to include information about where materials actually come from, and where they will be transported and deposited into tsunami hazard maps. A better plan would be to relocate possible dangerous flotsam/pollutant sources, while developing a proper post-disaster waste management action that should start immediately after an event at sites, which are vulnerable to further contamination or spreading of contaminating substances.

3.6. Additional References

Aida, I.: 1978, Reliability of a tsunami source model derived from fault parameters, *Journal of Physic of The Earth* **26**, pp. 57 – 73.

Black K.P.: 1996, Lagrangian dispersal and sediment transport model and support software, Occasional report no. 20. Department of Earth Sciences. University of Waikato and NIWA, Hamilton . New Zealand, 60 p.

Black, K.P.: 2001, The 3DD Suite of numerical process models, ASR Ltd., PO Box 67, Raglan, New Zealand. www.asrltd.co.nz.

Black, K.P. and Vincent, C.E.: 2001, High-resolution field measurements and numerical modelling of intra-wave sediment suspension on plane beds under shoaling waves. *Coastal Engineering* **42**, pp.173-197.

Borrero, J.C., Bosserelle, C., Prasetya, G., and Black, K.P.: 2007, Using 3DD to model tsunami inundation, *Proceedings of the Australasian Coast and Port Conference*. July 2007, Melbourne Australia. Paper 96, 6 p.

Gonzalez, F.: 1999, Tsunami: Predicting destruction by monster waves, *Scientific American,* May 1999, pp.56-55.

Goto, C., and Shuto, N.: 1983, Numerical simulation of tsunami propagation and runup, in Iida and T.Iwasaki (eds.), *Tsunamis: Their Science and Engineering,* Terra Science Pub.Co., pp. 439-451.

Imamura, F., Shuto, N. and Goto, C.: 1988, Numerical simulation of the transoceanic propagation of tsunamis, *Proceeding 6th Congress Asian and Pacific Regional Division*, IAHR, Japan, pp. 265-272.

Imamura, F.: 1996, Review of tsunami simulation with a finite difference method, *In Long wave Runup Models*, edited by H.Yeh, P.Liu, and C.Synolakis, World Scientific, pp. 25-42.

Kawahara, M., Takeuchi, N., and Yoshida, T.: 1978, Two step explicit finite element method for tsunami wave propagation analysis, *International Journal of Numerical Methods in Engineering* **12**, pp. 331-351.

Kennedy, A.B., Chen, Q.m Kirby, J.T. and Dalrymple, R.A.: 2000, Boussinesq modeling of wave transformation, breaking, and runup. 1: 1D, ASCE, *Journal of Waterway, Port, Coastal, and Ocean Engineering* **126**, pp. 39-47

Liu, P. L.-F., Synolakis, C.E. , and Yeh, H.: 1991, A report on the international workshop on long wave runup, *Journal of Fluid Mechanic* **229**, pp. 678-688.

Liu, P.L.F , Cho, Y.S, Yoon.S.B and Seo, S.N. (1995), Numerical Simulations of the 1960 Chilean Tsunami Propagation and Inundation at Hilo, Hawaii, in : Tsuchiya.Y and Shuto.N, (eds), *Tsunami: Progress in Prediction, Disaster Prevention and Warning*, Kluwer Academic Publication. Netherland, pp.99 - 116

Lynett, P.J. and Liu, P.L.-F.: 2002, A numerical study of submarine landslide generated waves and runups, *Proceeding of Royal Society London*, **A 458**, pp. 2885-2910.

Middleton, J.F. and Black, K.P.: 1994, The low frequency circulation in and around Bass Strait: a numerical study. *Continental Shelf Research* **14**, pp. 1495-1521.

Prasetya, G.S., Healy, T.R., de Lange, W.P.: 2008, Hydrodynamic modeling of tsunami overwash of Whitianga Township and Harbour, Department of Earth and Ocean Sciences, Report prepared for *Environment Waikato*, 92 p.

Priest, G.R., Baptista, A.M., Fleuks, P., Wang, K., Kamphaus, R.A., Peterson, C.D.: 1997, Cascadia Subduction Zone Tsunamis: Hazard Mapping at Yaquina Bay,

Oregon, Final Technical Report to the National Earthquake Hazards Reduction Program, *DOGAMI Open File Report* **0-97-34**, 143 pp.

Shuto, N.: 1994, Surveyed Data, *Tsunami Engineering Technical Report 11*, Disaster Control Research Center, Tohoku University, 120 pp.

Shuterland, J., Peet,A.H., Soulsby, R.L.: 2004, Evaluating the performance of morphological models, *Coastal Engineering* **51**, pp. 917 – 939.

Synolakis, C.E., and Bernard, E.: 2006, Tsunami science before and beyond Boxing Day 2004, *Philosophical Transactions of the Royal Society*, **A, 364**, pp. 2231-2265.

Titov, V.V. and Synolakis, C.E.: 1998, Numerical modeling of tidal wave runup, *Journal of Waterway, Port, Coastal and Ocean Engineering, ASCE* **124(4)**, pp.157-171.

Yeh, H, Liu, P.L.F., Synolakis, C. E. (ed).: 1996, *Long-wave Runup Models*, World Scientific, 403 p.

Chapter 4
Simulation of Historical and Potential Catastrophic Tsunami Events

4.1. Introduction

Historical records within the Indonesian Archipelago suggest that the region is very susceptible to tsunamis from both earthquake and volcanic sources. Most of the potential catastrophic tsunami sources are identified by this study is along the Sunda Arc subduction zone. A few have also been identified for the eastern Indonesian Archipelago along the Banda Arc, Halmahera, Molluca Collision Zone, and the North Sulawesi Subduction Zone (Figure 4.1).

In this chapter, historical and potential catastrophic events from earthquake sources, based on the scenarios defined in Chapter 2, are assessed. Fault parameters are derived using the McCaffrey (2008) method as shown on Table 2.1, with slip angles varying from 90^o to 110^o. Initial conditions are computed using the Okada (1985) method, and numerical simulation is carried out using 3DD software. Volcanic sources, other than Anak Krakatau, Tambora and Banda Api, are not considered in this chapter, since most of the baseline data in relation to volcanic activities and their physics are still poorly understood.

4.2. The Model Grids

Bathymetric and topographic data at the resolution necessary for meaningful inundation mapping was not available for the entire coastal area of the Indonesian Archipelago. Therefore, the SRTM 90 (Space Radar Topography Mission) and GEBCO (General Bathymetric of The Oceans) data, as well as the Nautical Charts of Indonesian Archipelago produced by Indonesian Navy Hydrographic office, were mostly utilized in constructing the model grid. The model grid size is the maximum size that still well represents the hydrodynamic behaviour of tsunamis.

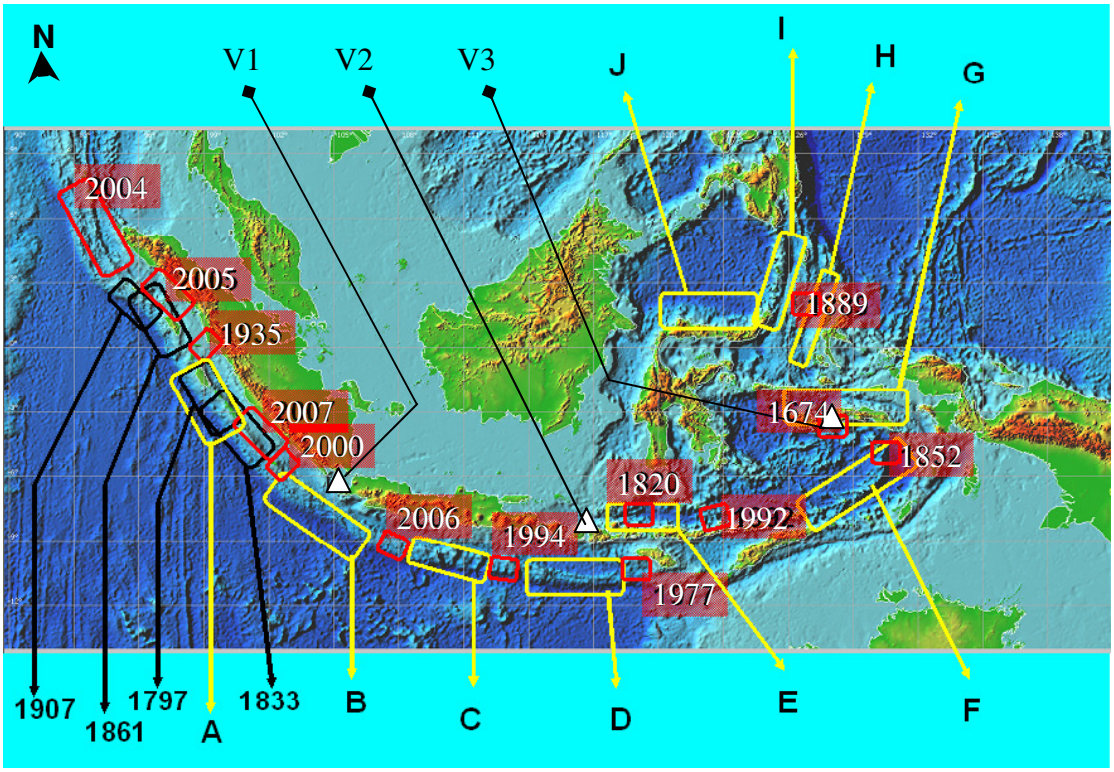

A = seismic gap after series of large earthquake in 2004, 2005 and 2007. (Possible for a return period of 1797 or 1833)

B = seismic gap, no historical record for the last 300 years.

C = seismic gap on south of Java Island

D = seismic gap on south of Bali and West Nusa Tenggara

E = potential large earthquake on north of Sumbawa-Flores Island

F = potential large earthquake on Banda arc

G = potential large earthquake on Seram subdcution zone

H = potential large earthquake on Halmahera – Molluca subduction zone

I = potential large earthquake on Halmahera – Sangihe subduction zone

J = potential large earthquake on North Sulawesi subduction zone

V1 = Anak Krakatau Volcano

V2 = Tambora Volcano

V3 = Banda Api Volcano

Figure 4.1. Seismic gaps and potential large tsunamigenic earthquakes within the Indonesian archipelago based on the historical record, possible maximum rupture length and basin tectonics. The number inside the red boxes is the year when the last earthquakes associated with tsunamis occurred, except for the 2000 event. Other numbers represent historical catastrophic events.

4.3. Earthquake Source

4.3.1. The 1797 Events

A large earthquake, followed by numerous aftershocks (Newcomb and McCann, 1987), occurred in the Indian Ocean off the west coast of central Sumatra Island in 1797. With a sparse historical record, damage on the mainland due to the earthquake and tsunami was difficult to quantify. Tsunami impacts had been observed at ports and a settlement (known as Padang City now) along the coast. Many fishing boats were destroyed and drifted inland. There was no information about the earthquake magnitude, until paleogeodetic studies (Natawidjaja et al. 2006) suggested the uplift was around 6-10 m with a fault length of 350-400 km. These correlate with a moment magnitude Mw = 8.0 – 8.4, and a return period of ~ 230 years, based on micro-atoll dating (Natawidjaja et al. 2006). Coral data uplift of the 1797 event is illustrated in Figure 4.2, while the available historical record of the event follows (Natawidjaja et al. 2006):

114.0 The strongest earthquake in the memory of the people in Padang, happened on February 10, 1797 around 10 p.m. The moon which was full shone brightly but darkened at the first quake and stayed so during the night - the first shock lasted for about one minute - the waves of the sea ran with fury up the river by which the whole place was flooded. Next, all the water ran out the river, which was suddenly dry; this repeated itself three times; the river banks were covered with fish; a sailing ship of 150 tons which was moored to a tree near the mouth of the river, broke loose when the sea entered and was driven to behind the then fort, a distance of 3/4 Eng. miles; on the way the vessel hit a stone house and two wooden ones which were demolished. Several smaller vessels, which were moored in the river, were also dislodged and moved off by the sea; some of these were later found behind the great pasar [market in Indonesia storage building in front of the house of the Resident at the river bank was lifted by the rushing waves and put down in the Chinese kampong - all of Aijermanies [Air Manis, a village name meaning "Sweet Water"], a seaside village at the corner opposite the Padang harbor is flooded and many houses flushed away - the next day one found several of the unfortunate inhabitants dead on the tree branches, where they had climbed to save themselves.

The inhabitants of Padang left their houses and fled to the square outside the city; they saw the ground break open at some places some 3-4 inches wide, and then in further shaking close again.

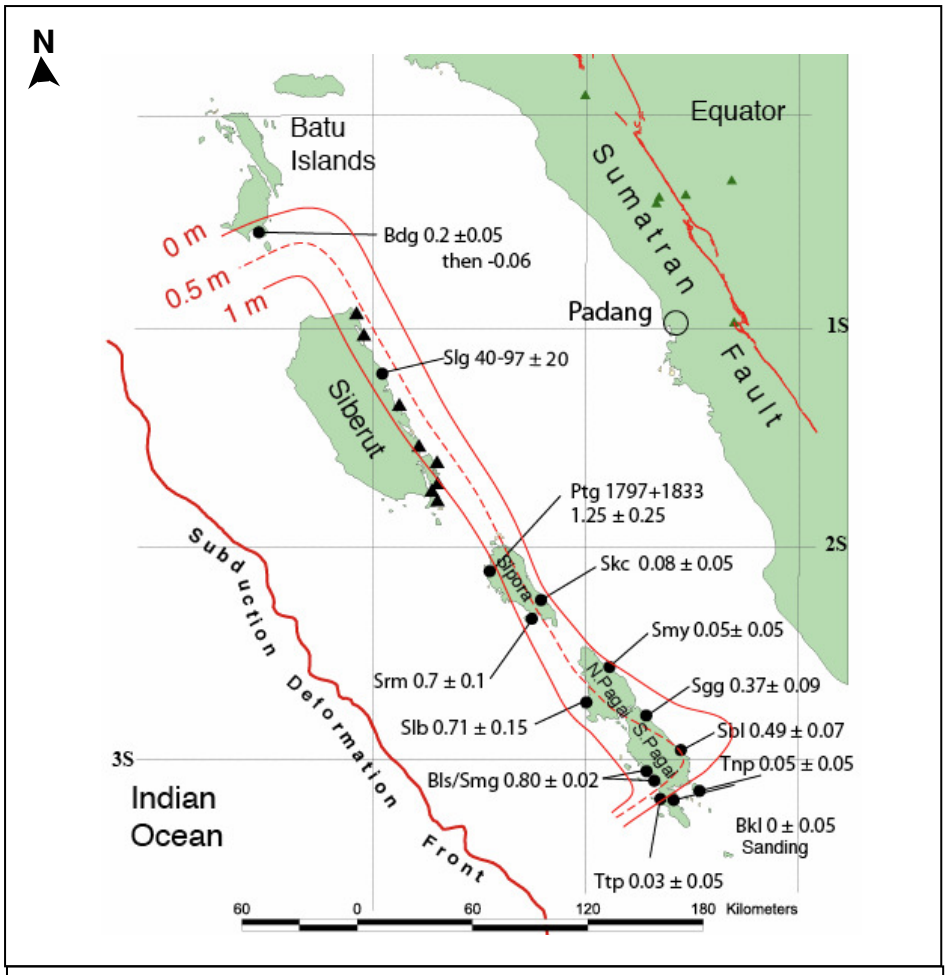

Name of station observations: Badgugu (Bdg), Silogui (Slg), Teluk Salibi (Tsb), Sikici (Skc), Simanganya (Smy), Pitogat (Ptg), Siruamata (Srm), Singingi (Sgg), Silabu(Slb), Bulasat (Bls), Saomang (Smg), Tiop bay (Ttp), Siatanusa (Stn), Bangkaulu (Bkl), Tinopo (Tnp), Sibelua (Sbl).

Figure 4.2. Coral data up-lift of the 1797 (Natawidjaja et al. 2006) event shows the slip extends to the trench (subduction deformation front).

Fault Parameters

In simulating this event, the fault plane is considered to consist of two segments, in order to take into account the irregularities of rupture zone along the subduction deformation front. Combining with the paleogeodetic data, and possible maximum length of fault rupture following McCaffrey (2008), the fault parameters for the 1797 event are defined (Table 2.1). This approach gives a maximum length of ~ 389.57 km and average slip of ~ 9.74 m. With a dip angle = 10^{o}, and depth = 10 km, the computed maximum moment magnitude (M_{wmax}) is 8.47.

Initial Condition

Based on the fault parameters, the initial condition for a tsunami is computed using the Okada (1985) methods that provide a negative leading wave (Figure 4.3).

The pattern of initial conditions shows that most the offshore islands experienced uplift. The maximum uplift was located on the offshore side of the forearc islands of Siberut, Sipora and Pagai, as suggested by the micro-atoll data.

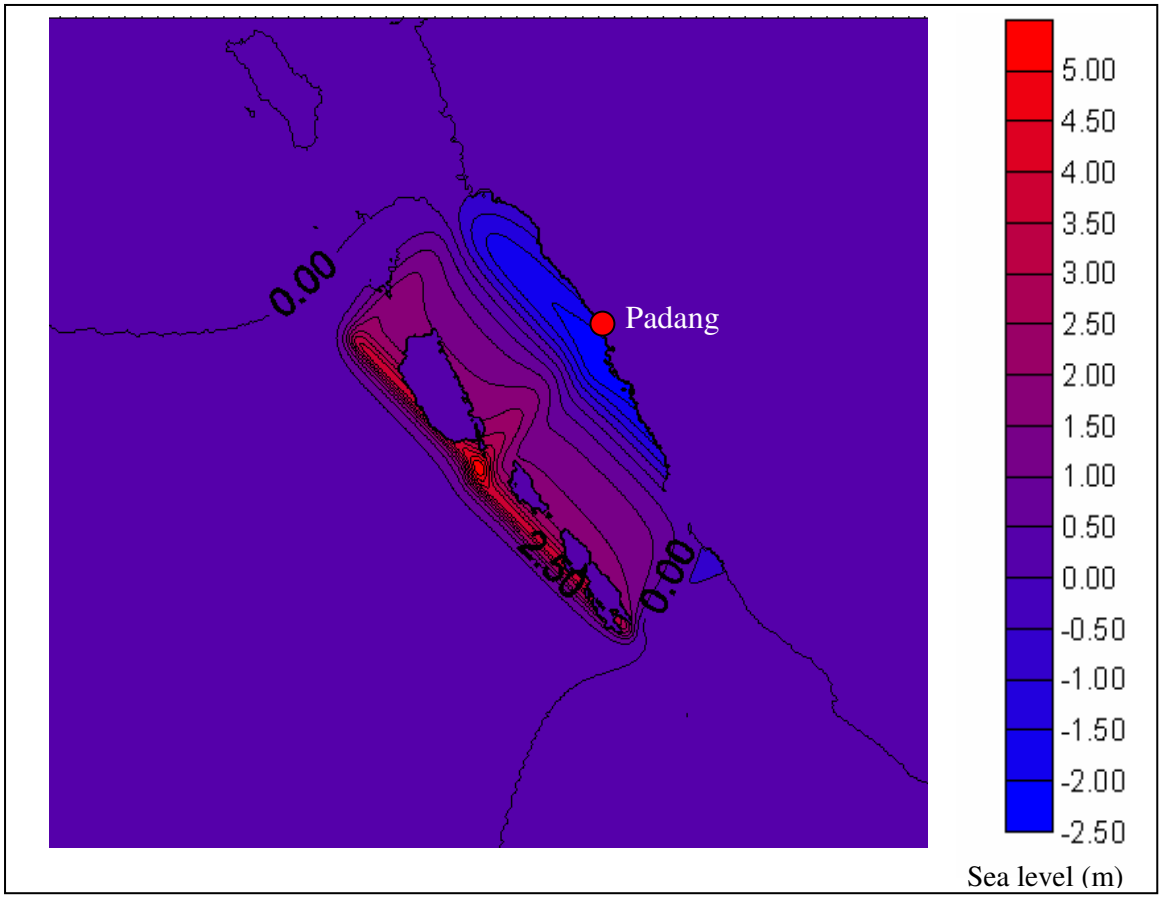

Figure 4.3. Initial tsunami condition based on the Okada (1985) method.

Numerical Modelling Results

The maximum distributions of tsunami elevations along the coast of Sumatra, and offshore islands during three hours of simulation are illustrated in Figure 4.4. The modeled tsunami results show > 770 km of the west coast of Sumatra Island is affected. High tsunami elevations occurred along the coast of West Sumatra Province (Padang City) up to the Batu Islands. The presence of offshore islands, such as Batu Islands which are located immediately to the north of the source area, reduce the impact of tsunami waves further north, but amplify the wave heights along the nearby coastline (Figure 4.4). The arrival time of the first waves is between 15 – 20 minutes after the fault rupture.

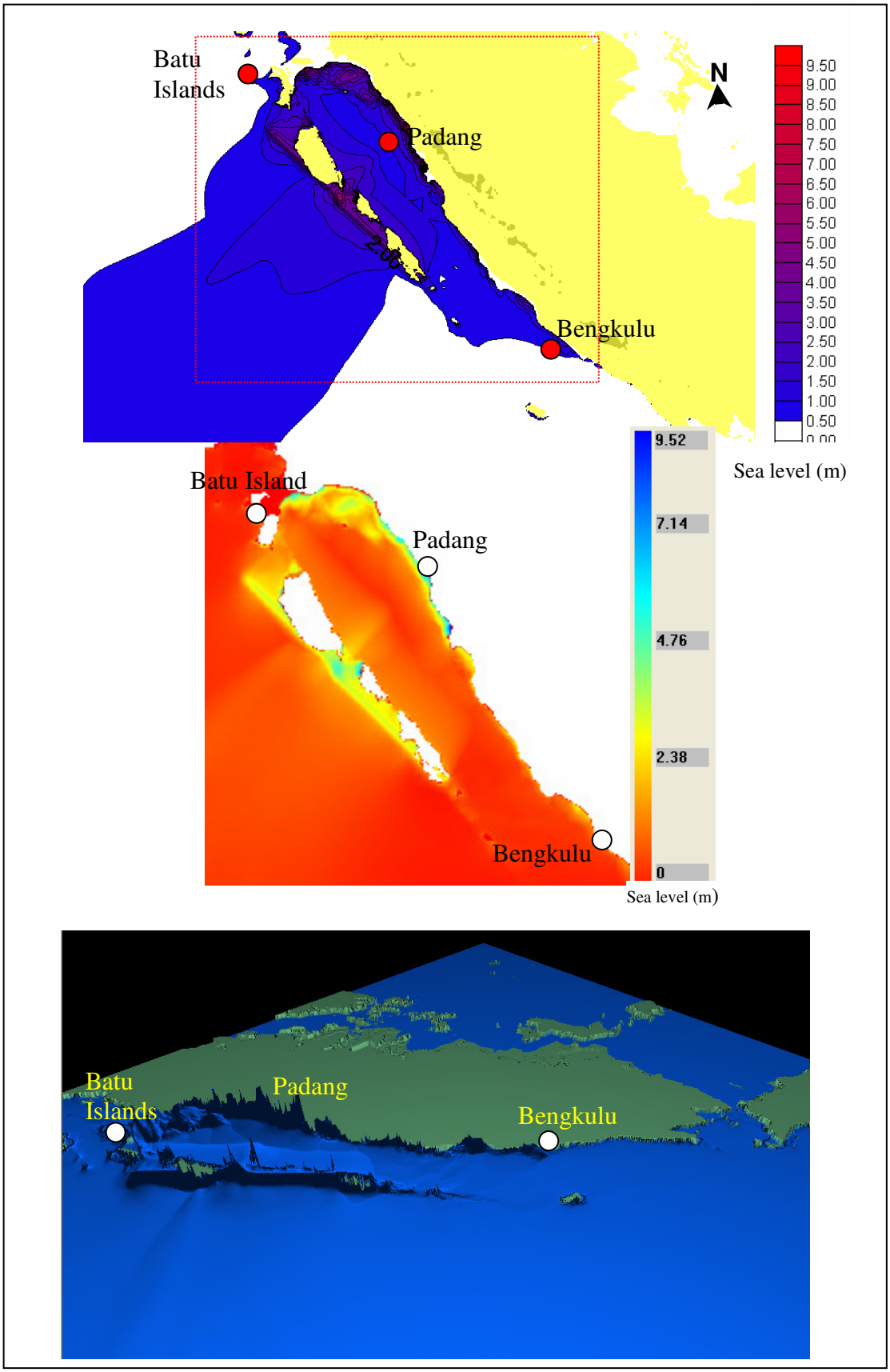

Figure 4.4. Maximum tsunami elevation along the west coast of Sumatra Island shows that a maximum height of 9.5 m occurred along the coast of Padang City (Top and middle figures). Over 770 km length of coastline is affected, from Batu Islands to further south near Bengkulu as shown on 3 dimensional plots.

The configurations of offshore islands and bathymetric features within this region clearly determined the characteristic and level of tsunami impacts along the coast of Siberut basin regions, as was also identified by McClosky et al. (2008). Wave amplification, due to resonance caused by the geometry of the basin, increases the vulnerability of these areas to tsunami hazards. Hence the location of the highest uplift for initial condition needs to be assessed carefully: is it between the offshore Islands (Siberut-Sipora-Pagai) and the west coast of west Sumatra, or does it extend to the trench?

Choosing an appropriate initial condition based on 'correct' source mechanism is crucial for making inundation maps or hazard and risk assessments for this region. According to the micro atoll studies this event re-occurs every ~ 230 years.

4.3.2. The 1833 event

Newcomb and McCann (1987) considered the 1833 event one of the 10 largest events for the past two centuries. This event generated tsunami along >550 km of the south central coast of Sumatra. Many buildings collapsed and two-foot-wide (60 cm) cracks in the ground were observed. Micro-atoll data (Natawidjaja et al. 2006), as illustrated in Figure 4.5, suggested that the moment magnitude of the earthquake was about 8.6 – 8.9, with uplift from 10 – 15m. Natawidjaja et al. (2006), based on a sparse historical record, summarized the event as follow:

> 25.5 Earthquakes are often felt at Padang, but rarely of such intensity that they endanger inhabitants. The most powerful eartquake since many years occurred on November 24, 1833, just after 8 p.m., for about 2 minutes. The air was damp, quiet and humid, in moonlight. The oscillating movement of the earth, together with underground shocks and a rattling sound that clearly came from the S.E., made everybody rush out of their houses and created fear in all. One heard everywhere a hard stomping of "rijstblokken" (rice blocks?) and people yelling. Along the river fissures had opened here and there, which then closed again. The sea had repeatedly run up the sloping beach, up to 10 to 12 "voet" (feet?) high. All wooden houses creaked and shook enormously; but the stone houses fared worse, with damaged walls, some fell over, and some roofs that collapsed. In some houses, furniture had been thrown from one corner to the other. There was considerable damage but few accidents.

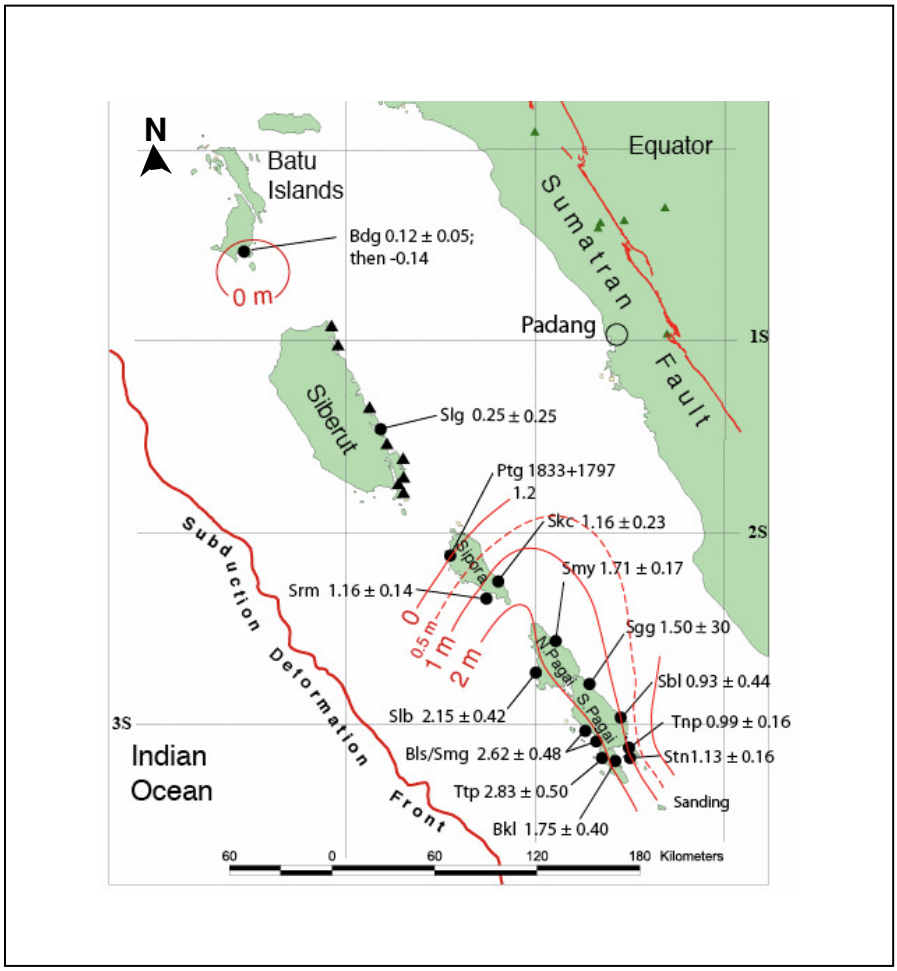

Figure 4.5. Coral data up-lift for 1833 (Natawidjaja et al. 2005) event showed the slip extends to the trench (subduction deformation front).

Fault Parameters

Using the McCaffrey method (2008), fault parameters were calculated (Table 2.1). The fault plane is divided into three segments following the geometry of the trench and interpretation of micro-atolls studies (Natawidjaja et al. 2006). The exact location of the southeastern-end of the fault rupture is unknown. Estimated of total length of fault rupture is 424 km, with the southeastern-end of fault rupture located immediately to the north of Enggano Island. The average slip of 10.5 m, width of 150 km, dip angle of 10^{o}, and depth = 10 km provide a maximum moment magnitude M_{wmax} = 8.5. These parameters suggest a return period between 177 to 265 years with the convergence rate between 40 – 60 mm/year (Table 2.1).

Initial Condition

Based on the computed earthquake and fault parameters, the initial condition for tsunami was calculated using the Okada (1985) method (Figure 4.6). The calculated uplift distribution at the northern end of the rupture zone at Sipora and Pagai Islands, replicates the uplift distribution determined by micro-atoll studies.

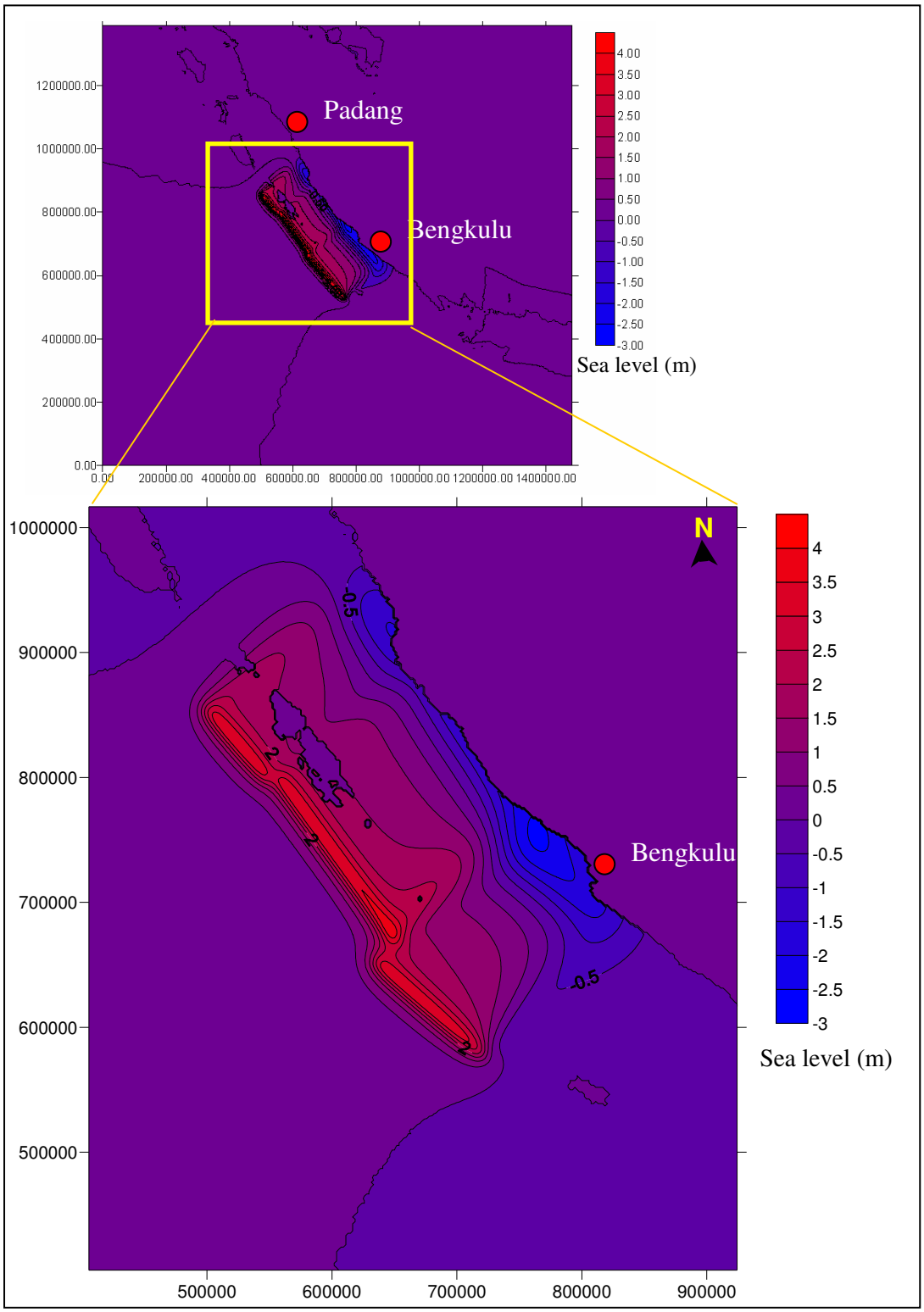

Figure 4.6. Initial condition of the 1833 tsunami computed by the Okada (1985) method. Scale bar unit is in metres.

Numerical Modelling Results

The modeled tsunami elevation after 3 hours simulation shows the tsunami impacts over 900 km of the west coast of Sumatra Island from Batu Islands up to Sunda Straits, as well as the offshore islands (Siberut, Sipora and Pagai) (Figure 4.7). The arrival time of the first waves is between 12 – 20 minutes along the coast of west Sumatra (Padang to Bengkulu).

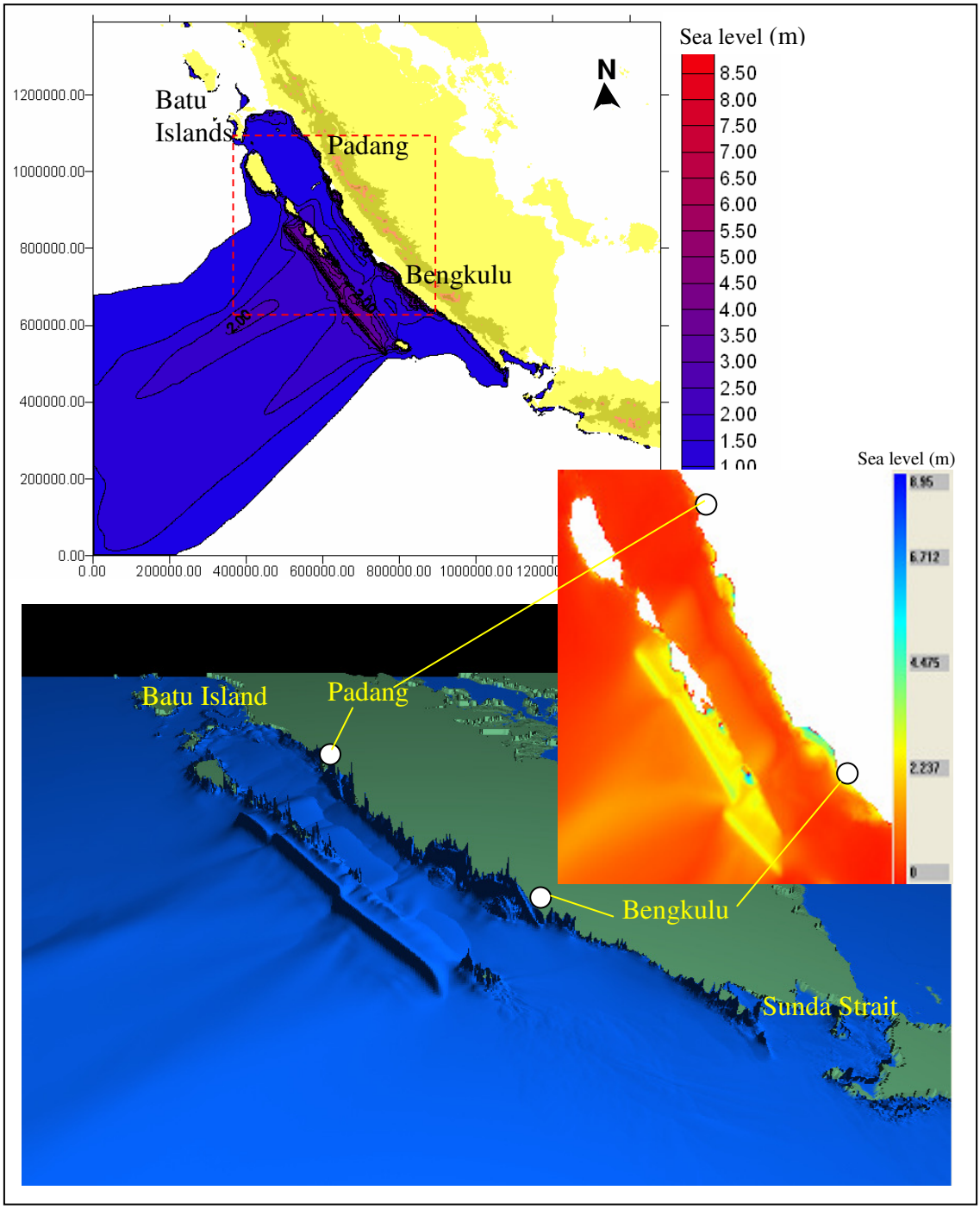

Figure 4.7. Maximum tsunami elevation distributions show the maximum height of > 8.5 m occurs along the Bengkulu coastal areas (top and middle figures). Over 900 km lengths of coastline from Batu Islands to further south in Sunda Strait are affected by tsunami as also shown on 3 dimensional plot (bottom figure).

The highest tsunami elevation occurred along the Bengkulu coast, that has a direct impact from the source region (Figure 4.8). There are no offshore islands that could act as a barrier, such as the forearc islands of Siberut, Sipora and Pagai.

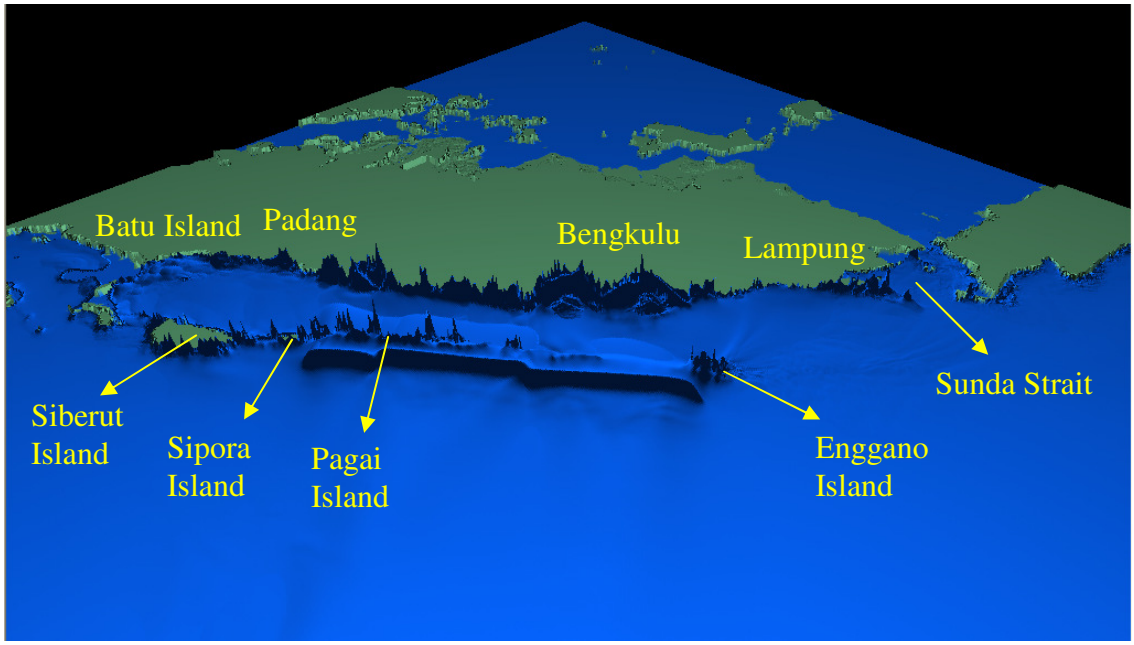

Figure 4.8. Maximum tsunami elevation distribution shows that, the Bengkulu coastal areas experience the highest tsunami elevations, since it has a direct impact from the source region. Enggano Island is clearly providing protection to the coastal areas between Lampung and Bengkulu, while Pagai and Sipora Islands provide protection to the areas between Bengkulu and Padang, except the localities along Padang coast, where tsunami elevations are considerably higher than the neighboring coastline.

4.3.3. The 1861 Event

This great event, according to Newcomb and McCann (1987), occurred in February 1861 at a major segment of the plate boundary in northern Sumatra. It appears to have taken place between the trench and the islands of the trench slope break. The quake was felt from the Malay Peninsula to central and eastern Java, with the highest intensities extending for 300 km along the coast nearby the epicenter. Tsunami impacted over 500 km of the northern Sumatra west coast, and devastated towns on the seaward side of the Batu Islands, and at the southwest shore of Nias with a tsunami height of 7 m. There is an evidence of coseismic uplift at the north and west coast of Nias, where piers of rock and reefs become exposed, and small islands become connected to Nias (Newcomb and McCann, 1987).

Fault Parameters

Taking into account the historical record for delineating the source boundaries, the uplift data from micro-atoll studies at South Simeulue Island (Meltzner et al., 2008), as well as the geometry of the subduction deformation front (the trench), the major fault segment is located between the trench, and the islands on the trench slope break. The fault parameters were calculated using the McCaffrey method (2008), which gives the total length of fault rupture of 400 km with an average slip of 10.1 m, and dip angle of 12^{o}. These parameters give the maximum moment magnitude of the earthquake (M_{wmax}) = 8.49, and with a convergence rate between 40 – 60 mm/years this correspond to a return period between 192 and 250 years (Table 2.1).

Initial Condition

Based on the fault parameters, the initial condition of tsunami is calculated using the Okada (1985) method. The results as illustrated in Figure 4.9 showing that negative leading waves are formed. The highest uplift located seaward of the offshore Islands of Nias and Batu, and extending to the trench.

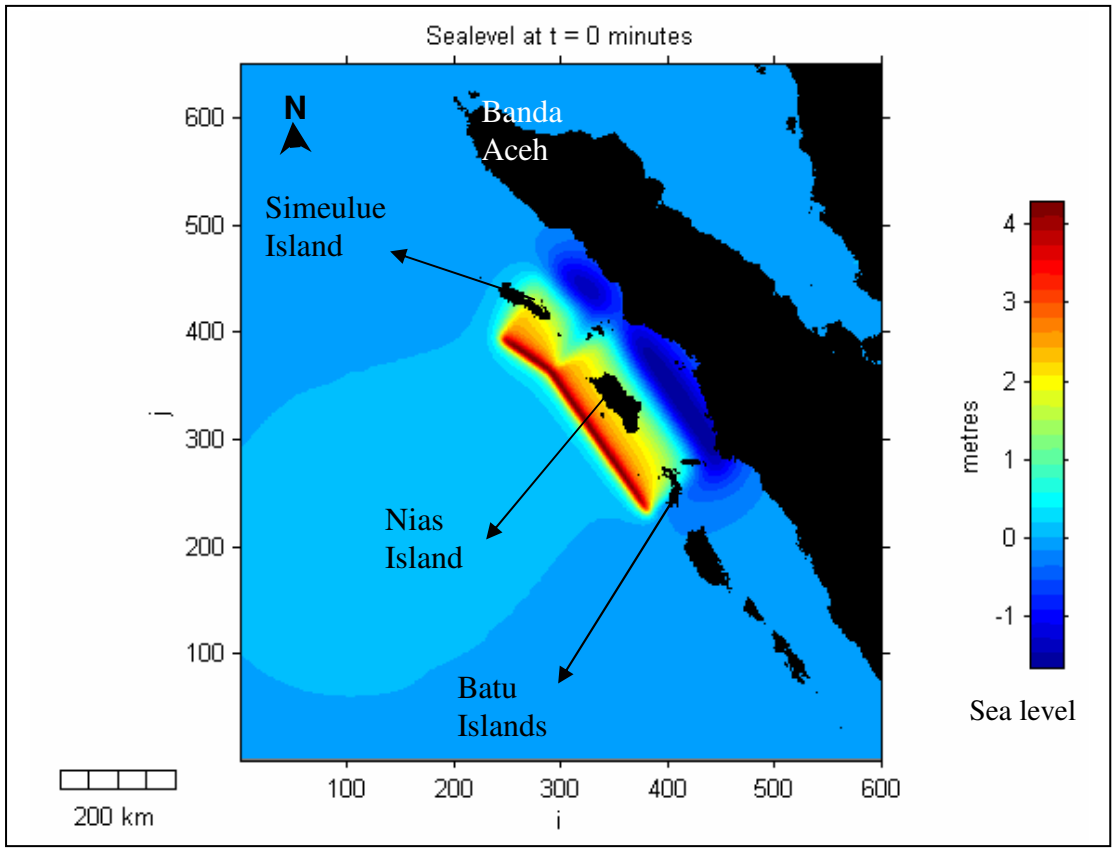

Figure 4.9. Initial condition for the tsunami computed using the Okada (1985) method shows the uplift region covered the Nias Island and half of the Batu Islands.

Numerical Modelling Results

The tsunami elevations after 3 hours of simulation, shows that the waves impacted over 700 km of the northwestern coast of Sumatra Island, from Batu Islands to Banda Aceh (Figure 4.10). The highest tsunami elevations occurred along the seaward side of the Nias, south Simeulue and Batu Islands, as recorded in the historical report. Tsunami elevations reach a maximum height of ~ 9 m along the seaward coast of Nias Island facing to the source. Arrival time of the first waves is 10 minutes at Banyak and Batu Islands, and around 20 minutes along the coastal areas between Singkil and Batu Islands.

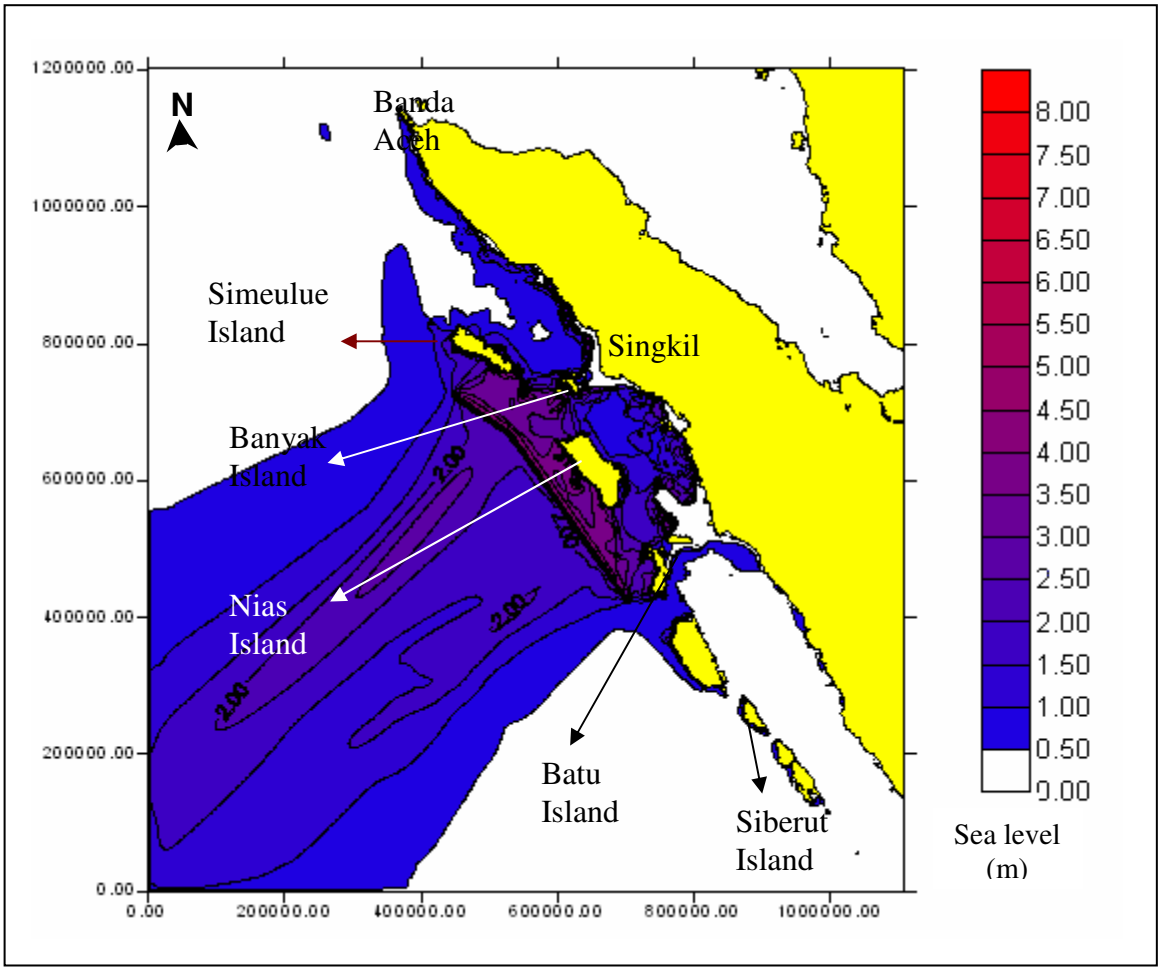

Figure 4.10. Maximum tsunami elevation distribution along the coasts of offshore islands and the northwestern coast of Sumatra Island shows, the worst affected are Nias Island, South Simeulue, Banyak and Batu Islands.

According to Newcomb and McCann (1987), seiches were reported on Java Island where the quake also was felt. The model showed the offshore propagation of the tsunami into the Indian Ocean, but further southeastward to Java Island is not

covered by the model, given that southeast boundary is limited to the areas of Bengkulu and Enggano Island (Figure 4.11).

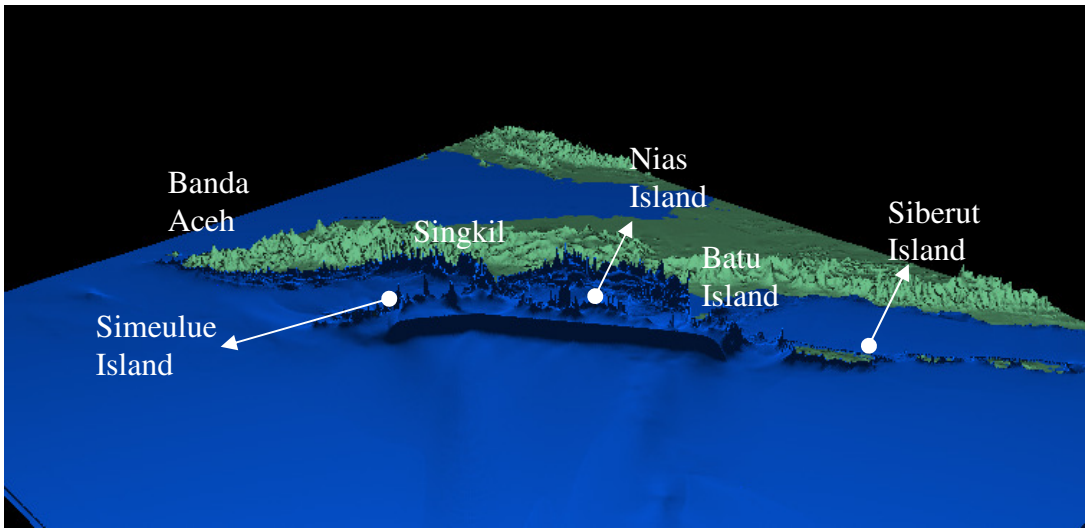

Figure 4.11. Three-dimensional plot of the maximum tsunami distribution as illustrated in Figure 4.10 shows the seaward side of south Simulue, Nias and Batu Islands were hardest hit by tsunamis as well as along the coastline of the mainland between Batu Islands and Singkil.

4.3.4. The 1907 Event

The 1907 event was a special event for people who lived in Simeulue Island, and become well known after the 26 December 2004 event. The 1907 event devastated the coastal area of Simeulue Island where almost 2/3 of population who lived along the coast perished, and some of the dead bodies were found on top of the trees (McAdoo et al. 2006). 'Smong', the oral history of the 1907 event that passed down from generation to generation, help saved lives of people who lived on this island during the great 26 December 2004 tsunami.

Newcomb and McCann (1987) indicated that the 1907 event appears to be greater than 1861 event only because tide gauges were already in use. However, the earthquake magnitude M = 7.6 as assigned by Gutenberg and Richter (1954) for this event is too small to generate tsunamis that affected over 950 km along the coast of Sumatra from Banda Aceh to Batu Islands.

According to Newcomb and McCann (1987), the location of the epicenter is on the seaward of the trench slope break, but landward of the trench based on the extent of moderate intensities in the interior of Sumatra. The aftershocks were reported for 8 days, and only caused localized damaged.

Fault Parameters

Newcomb and McCann (1987) noted, that a strong earthquake had been felt on Nias Island, as well as devastation of the seaward coast of Nias and Batu Islands. Considering the geometry of the trench, the tsunami impacts along the coast with leading depression waves, paleo-tsunami deposit evidence at northwestern coast of Sumatra (Meulaboh) (Monecke et al. 2008), and along the west-southwestern coast of Simeulue Island, as well as coral data (Meltzner et al. 2008), the fault parameters were derived and calculated using the McCaffrey (2008) method that suggesting 3 segments with variable slip. This gives a total length of the fault segment as 360 km, with variable slip from 6 to 9 m. With focal depth = 10 km, and dip = 8-10^{o}, the maximum moment magnitude (M_{wmax}) is 8.4. Considering the convergence rate between 40.0 to 66.9 mm/year, the return period for this event is between 173 to 225 years (Table 2.1).

Some other scenarios can be seen in Appendix 1.

Initial Condition

Based on the fault parameters, the initial condition is calculated which results in a leading depression wave on the seaward side of Simeulue Islands (Figure 4.12).

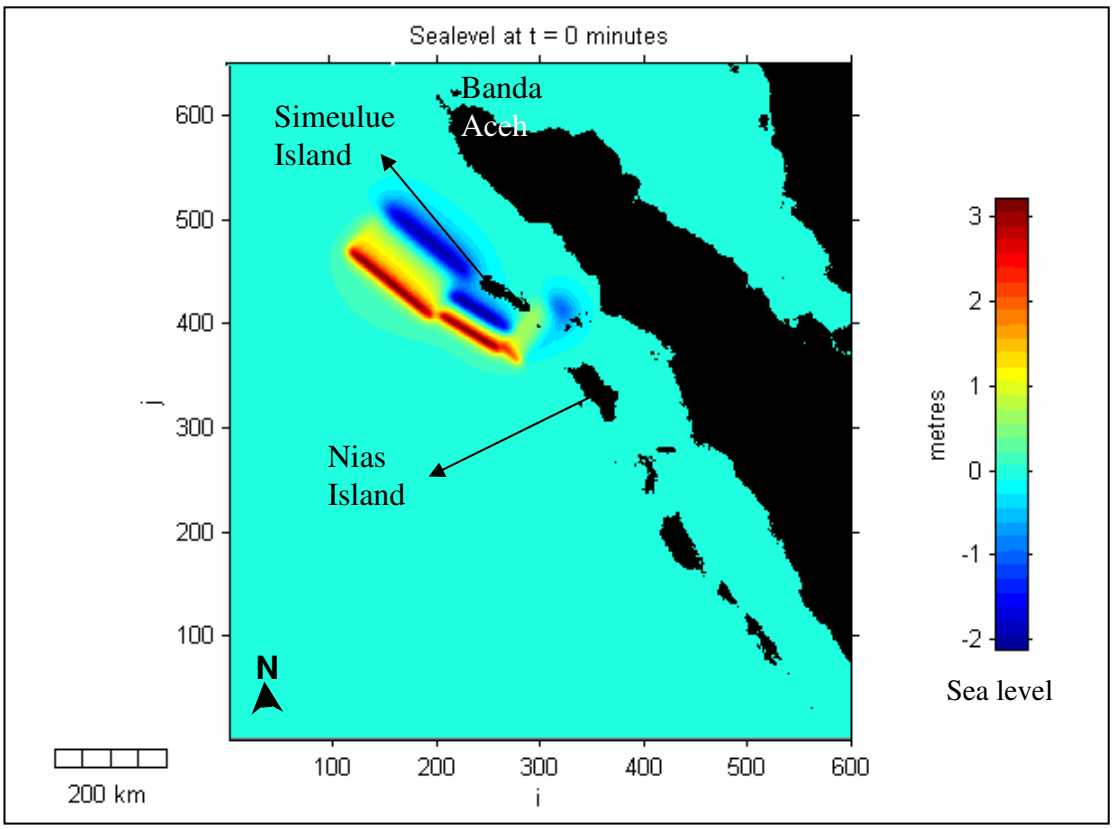

Figure 4.12. Initial condition of tsunami computed using Okada (1985) method. The leading depression wave is consistent with eyewitness accounts.

Numerical Modelling Results

The model result shows that the tsunami impacted most of the coastal areas along the Simeulue, Banyak, and northern Nias Islands, as well as to the northwestern part of Sumatra Island (Meulaboh). With this fault configuration, the tsunami impact towards Batu Islands was minimal. Maximum tsunami elevation up to 11 m occurred along the seaward side of Simeulue Island as eyewitness reproted, where some of the dead bodies were found on top of the trees (McAdoo et al. 2006) (Figure 4.13). The arrival time of the first waves at Simeulue Island is 10 minutes after the fault rupture.

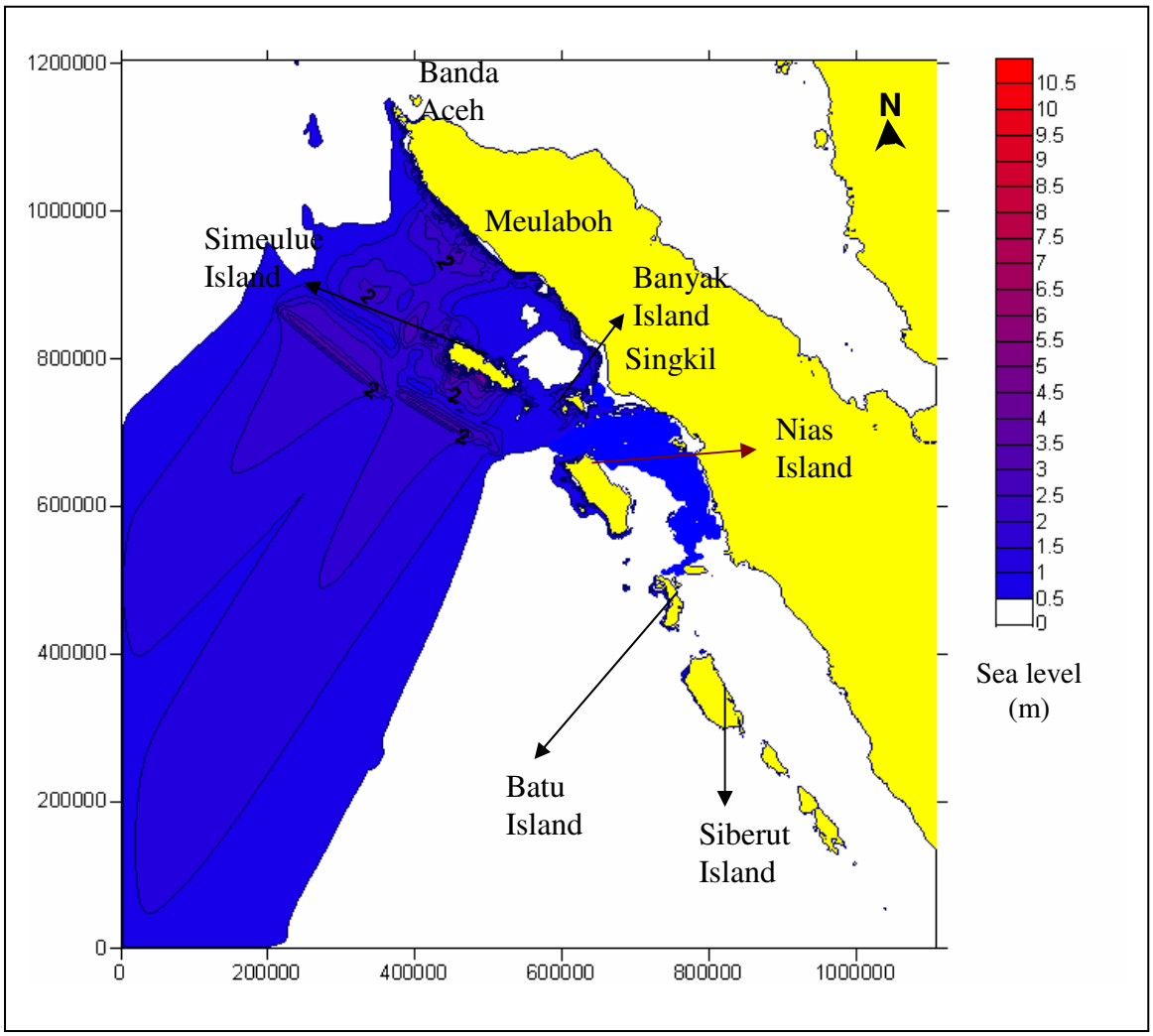

Figure 4.13. Maximum tsunami elevation distribution along the coasts of offshore islands, and the northwestern coast of Sumatra which shows the extent of the tsunami propagation further north to Banda Aceh.

The three-dimensional plot of the simulation results (Figure 4.14 - 15) shows that the maximum tsunami elevations occurred along the seaward side of Simeulue Island. Maximum tsunami elevations along the shoreline are between 7 – 11 m. This

is consistent with eyewitness accounts, where the tsunami came on shore like a wall, and many dead bodies were found stranded at the top of the trees.

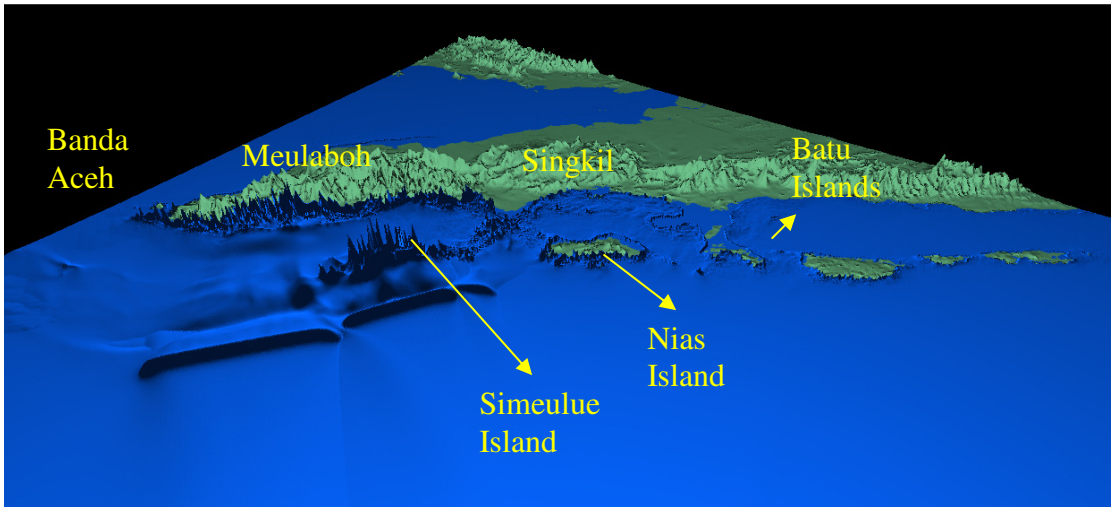

Figure 4.14. Three-dimensional view of maximum tsunami runup is showing major impact on the seaward side of south Simulue, northern Nias and Banyak Islands. The tsunami height distribution refers to Figure 4.13.

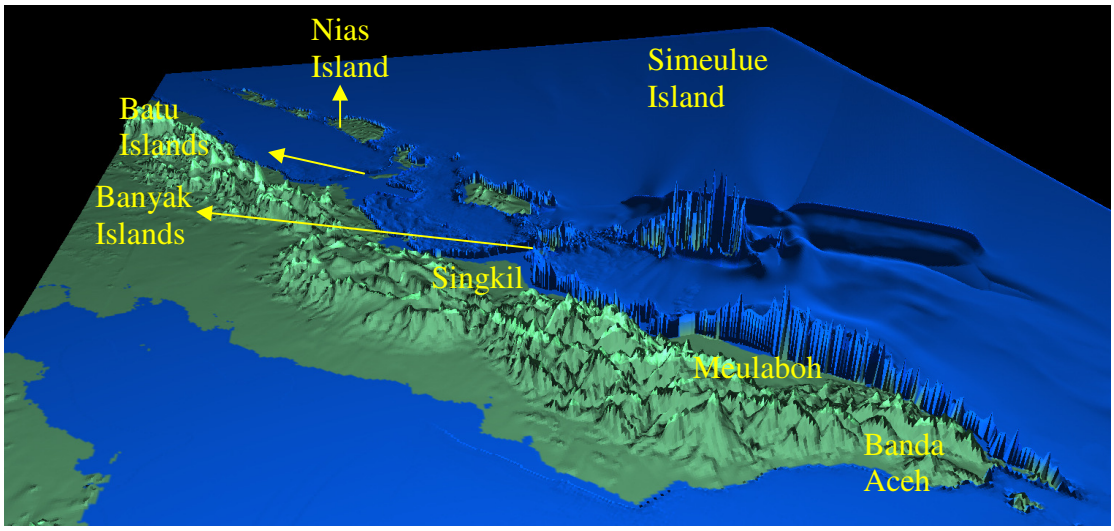

Figure 4.15. High tsunami elevation focuses on Simeulue Island, and gradually decreases from Banyak Islands – Singkil, and Tapak Tuan to Banda Aceh. The tsunami height distribution refers to Figure 4.13.

Paleotsunami studies which were carried out after the 26 December 2004 event, provide evidence for tsunami wave impacts along the seaward side of Simeulue Island (Figure 4.16), from the northern tip (Langi, A) to the central (Teupah, B) and south (Busung Bay, C) as well as to the northwest of Sumatra (Meulaboh). At Busung Bay (south Simeulue), several layers were found which are possibly related to the 1861 and other events. In contrast, the northern tip of the island (Langi) showed only one layer below the 2004 deposit which possible of the 1907 event. At northern Meulaboh, Monecke et al. (2008) identified the tsunami deposits at a distance of up to 1 km inland.

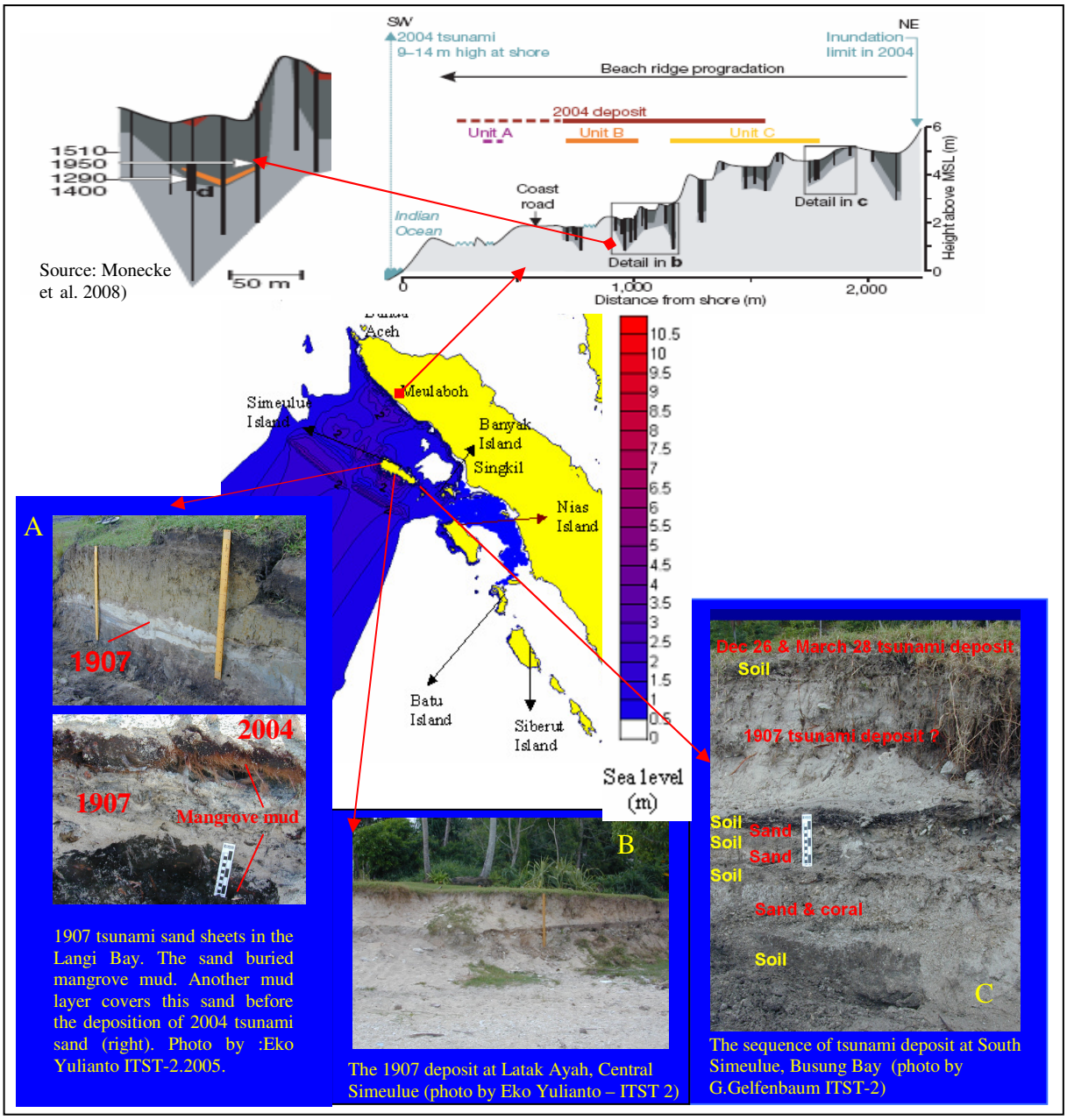

Figure 4.16. Plot of maximum tsunami distribution shows relatively uniform distribution of the tsunami elevation along the seaward side of the Simeulue Island with height between 7 – 11 m, and along the northwestern coast of Meulaboh between 4 – 8 m. This produced the tsunami deposit that had been preserved along the coast. The deposits clearly show the evidence of the 1907 events, and also some other events that affected the southern end of the Island (Busung Bay, C). At this southern end (C), there are at least 3 other events identified from the sand layer before 1907 event. They possibly are the 1861, 1833 or 1797 and the 1600s' events which occurred further southeastward. The same evidence was also found by Monecke et al. 2008 at Meulaboh (Sumatra Island)

4.3.5. Sunda Gap

The Sunda Gap is located between Enggano Island and West Java, as a transition from a frontal type subduction zone along Java Island into the oblique zone along Sumatra Island. For more than 300 years, no large shallow earthquake has been reported and the gap seems quiet. A potential future large earthquake is calculated

based on the McCaffrey (2008) method. The length of rupture zone is determined from the largest earthquakes that occurred either side of the gap.

Fault Parameters

Considering the geometry of the deformation zone, the fault plane is divided into three segments. Using the McCaffrey (2008) method, the fault parameters were calculated, giving a total length of the fault plane = 624 km, and average slip = 15.6 m. With a dip angle = 10^{o}, focal depth = 10 km, provides a maximum moment magnitude (M_{wmax}) = 8.75. The convergence rate between 40.0 – 66.9 mm/year, gives a return period between 233 to 390 years (Table 2.1).

Initial Condition

The initial condition for tsunami generation for this subduction zone type of earthquake produce a negative leading wave. Maximum initial tsunami elevation offshore is 6.0 m above sea level with the leading depression of – 4.5 m (Figure 4.17).

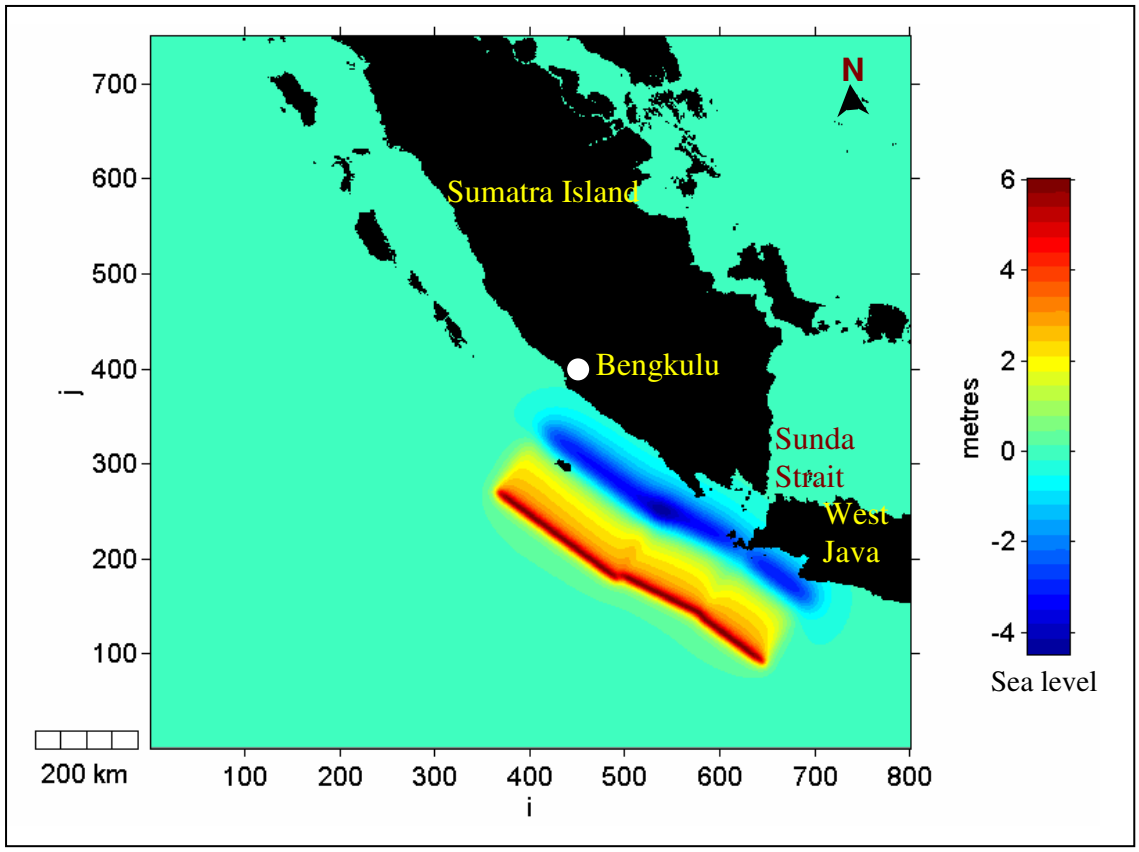

Figure 4.17. Negative leading waves of a potential tsunami initial condition computed using Okada (1985) method.

Numerical Modelling Results

Maximum tsunami elevations along the coast after 3 hours of simulations, show the areas between Bengkulu and West Java have a high impact from tsunamis (Figure 4.18). A maximum 16 m tsunami elevation, with an average height between 8 to 10 m, occurs along the coast. The modeled tsunami also shows a considerable tsunami elevation inside the Sunda Strait. Tsunami elevations on both sides of the Strait have an average height between 6 to 10 m. The model did not show the effect of the tsunami propagating further into the Java Sea. A detailed model is needed to assess the extent of tsunamis into the Java Sea. Arrival time of the first waves after the quake is 15 minutes on the west coast of Java, to 20 minutes on the southeast coast of Sumatra Island.

Tsunami impact along the Coast of Sumatra Island was identified as far as Batu Island, with possible seiches further away to the north. The extent of tsunami impact to the east along the south Java coast was limited by the model boundary at the Central Java coast.

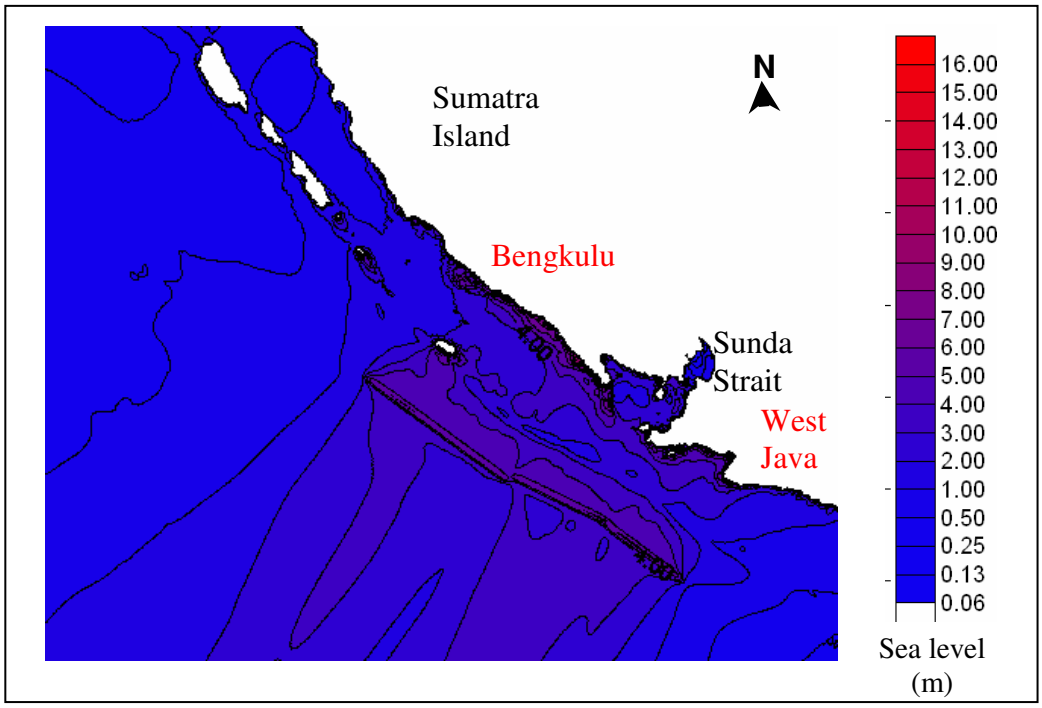

Figure 4.18. Maximum tsunami elevation distribution along the coasts of Sumatra and offshore Islands, Sunda Strait, and West Java. Tsunami is concentrated on the areas between Bengkulu and West Java, which are perpendicular to the source region.

A three-dimensional plot of the event is illustrated in Figure 4.19 showing clearly the distribution of maximum tsunami elevation along the Coast of Sumatra Island and West Java. Tsunami elevations subsided further away along the coast of

Sumatra Island to the northwest, as well as to the east of West Java. The highest tsunami elevation of ~16 m occurs in the bay close to Tjimaja –Tjikadu on the southern coast of West Java. While along the southwestern coast of Sumatra Island from Sunda Strait to Bengkulu, a maximum tsunami elevation ranges from 8 - 12 m.

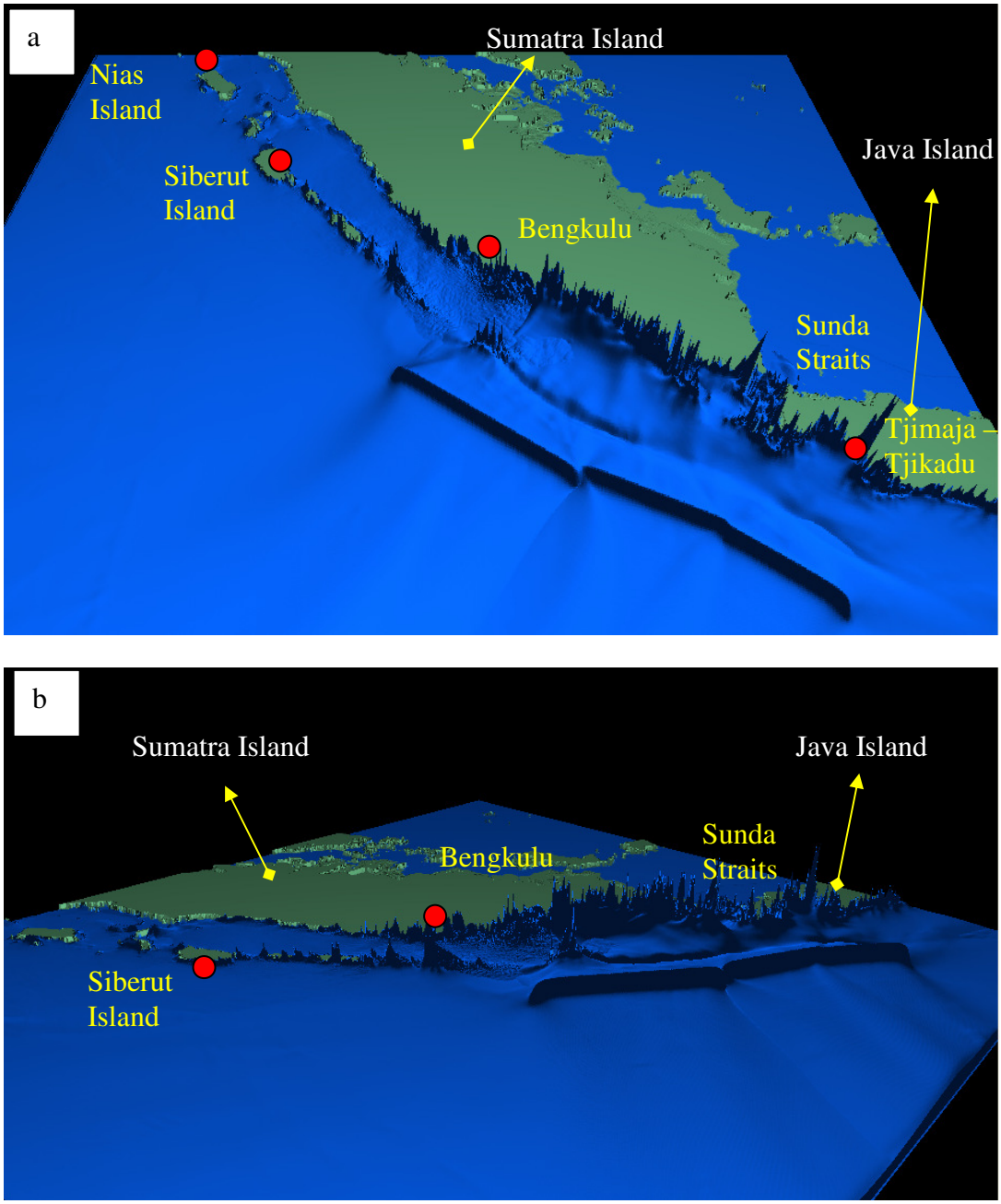

Figure 4.19. Maximum tsunami elevation along the coasts of Sumatra and Java Island. Figure (a) shows the maximum elevations occurred at the bay of Tjimaja- Tjikadu West Java as well as inside the Sunda Strait, and continue along the Sumatra coast up to Bengkulu. Tsunami elevation reduced further away from the source as shown on Figure (b). Tsunami height scale refers to Figure 4.18.

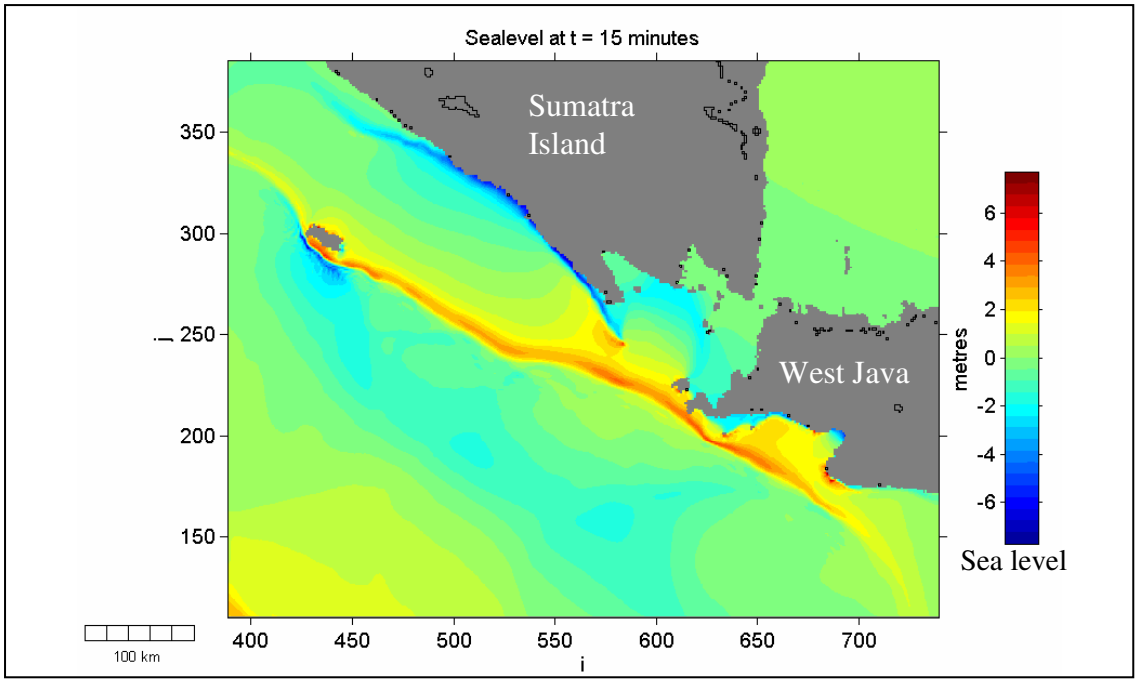

Figure 4.20. Within 15 minutes after fault rupture, tsunami elevations along the southern coast of West Java already reach 6-7 m. Concurrently on the Sumatra coast, within this time, the sea levels are still receding due to the negative wave.

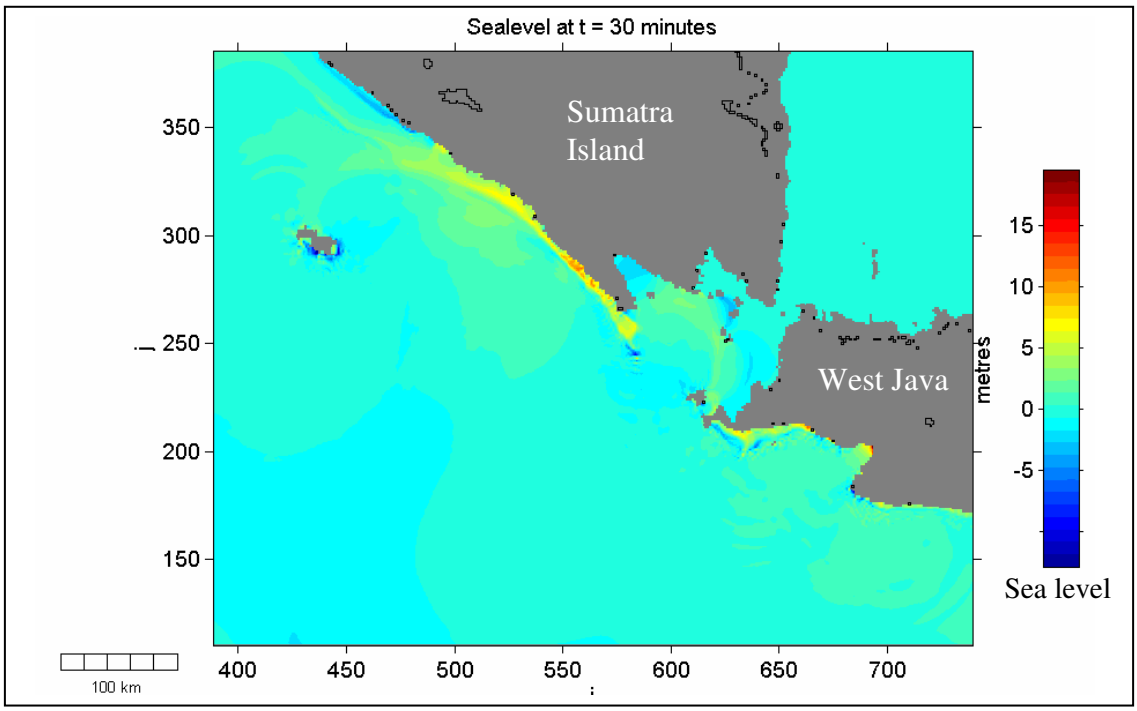

Figure 4.21. Most of the southern coast of West Java and Sumatra were hit by tsunamis with elevations > 15 m.

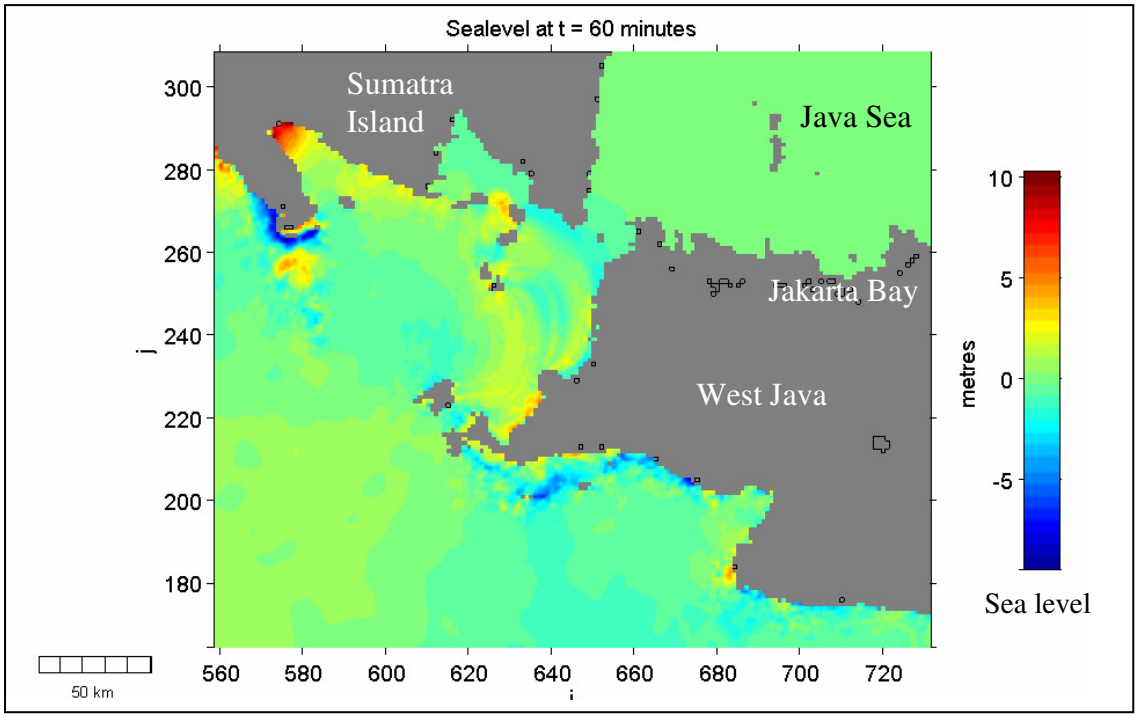

Figure 4.22. Tsunami wave behaviour inside the Sunda Strait shows the coastal areas on both sides of the strait experienced considerable tsunami elevation. Within this time (60 minutes after fault rupture), the tsunami penetrates to the Java Sea.

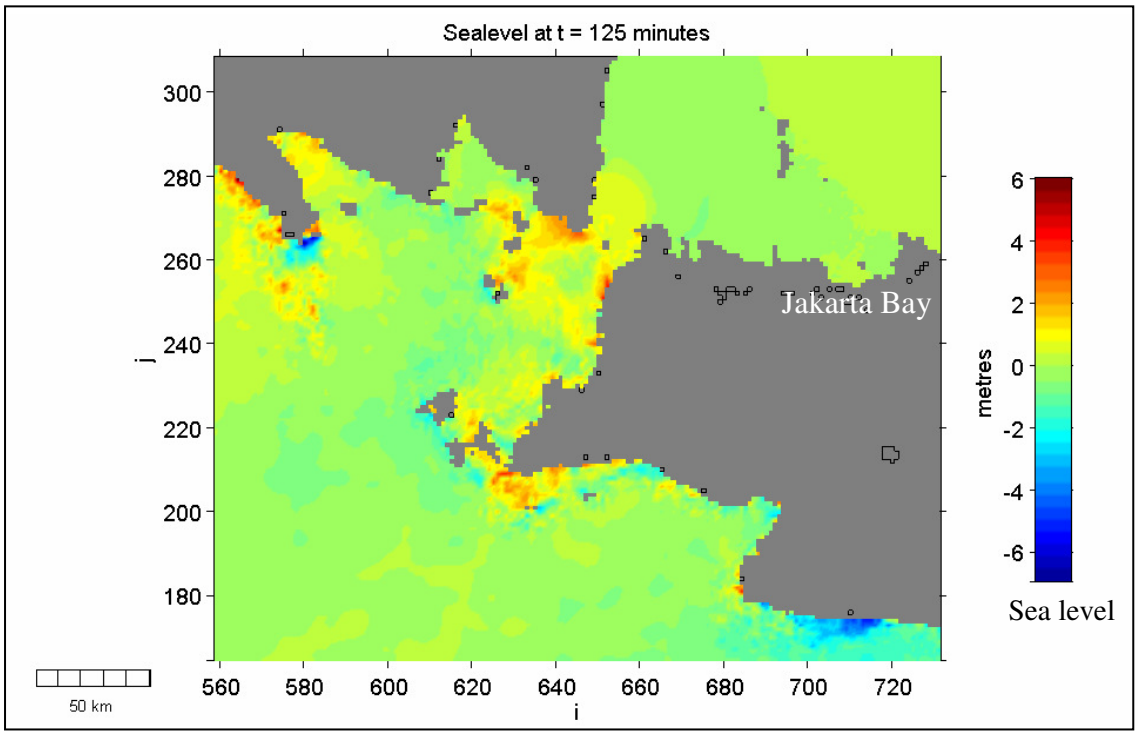

Figure 4.23. Two hours after the fault rupture, tsunami waves affect the coastal areas in the Java Sea. Tsunami elevation within Jakarta Bay varies between 1 – 2 m.

4.3.6. West-Central Java Gap

The West-central Java Gap is the area between the active zone to the west of Java, and the central area of Java around the Roo Rise. Not much information is available on the seismic activities for shallow events larger than M_w = 8.0 (ITDB/Pac2004). Most of historical large events since the 1600s occurred at the boundaries of the gap (NewComb and McCann, 1987).

Fault Parameters

A total length of 446 km of fault rupture is estimated for the gap. The fault parameters were computed using McCaffrey (2008) method, with a focal depth = 15 km, and dip angle of 20°, providing an average slip of the fault rupture of 11 m, and maximum moment magnitude (M_{wmax}) = 8.5 (Table 2.1). The convergence rate between 40.0 – 66.9 mm/years provides a recurrence interval for this gap between 167 to 279 years.

Initial Condition

With these fault parameters, the initial condition for tsunami generation is computed using the Okada (1985) method. The maximum initial tsunami elevation is 5.0 m above sea level, with leading a depression of – 2.0 m as illustrated in Figure 4.24. This source is perpendicular to the coastline of south Java Island.

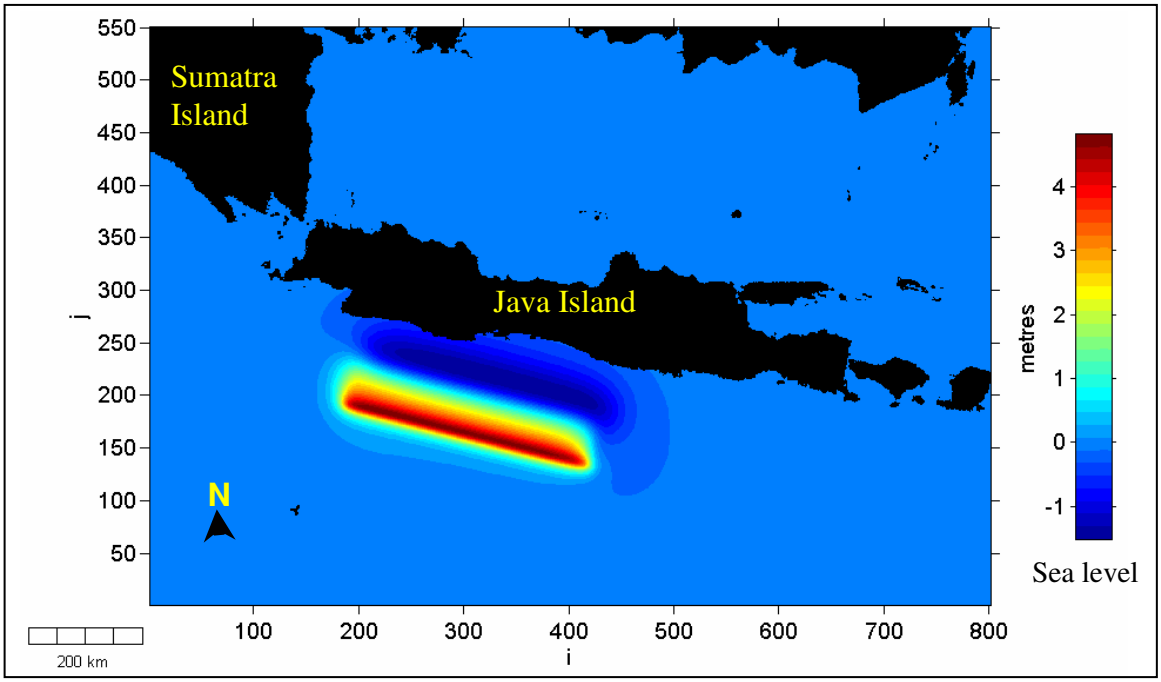

Figure 4.24. Initial condition of tsunami generation computed using Okada (1985) method form the leading depression waves.

Numerical Modelling Results

The maximum distribution of modelled tsunami elevation after 3 hours of simulation (Figure 4.25.a), show most of the areas from Sunda Straits, to Lombok Strait were affected by tsunami. Wave focusing occurs for the area between Sukabumi and Pacitan. This causes higher elevations at the center of the area perpendicular to the fault plane, and provides a maximum elevation of up to 13 m. The three-dimensional plots (Figure 4.25.b) show this effect clearly. The first waves arrive 15 minutes after the fault rupture.

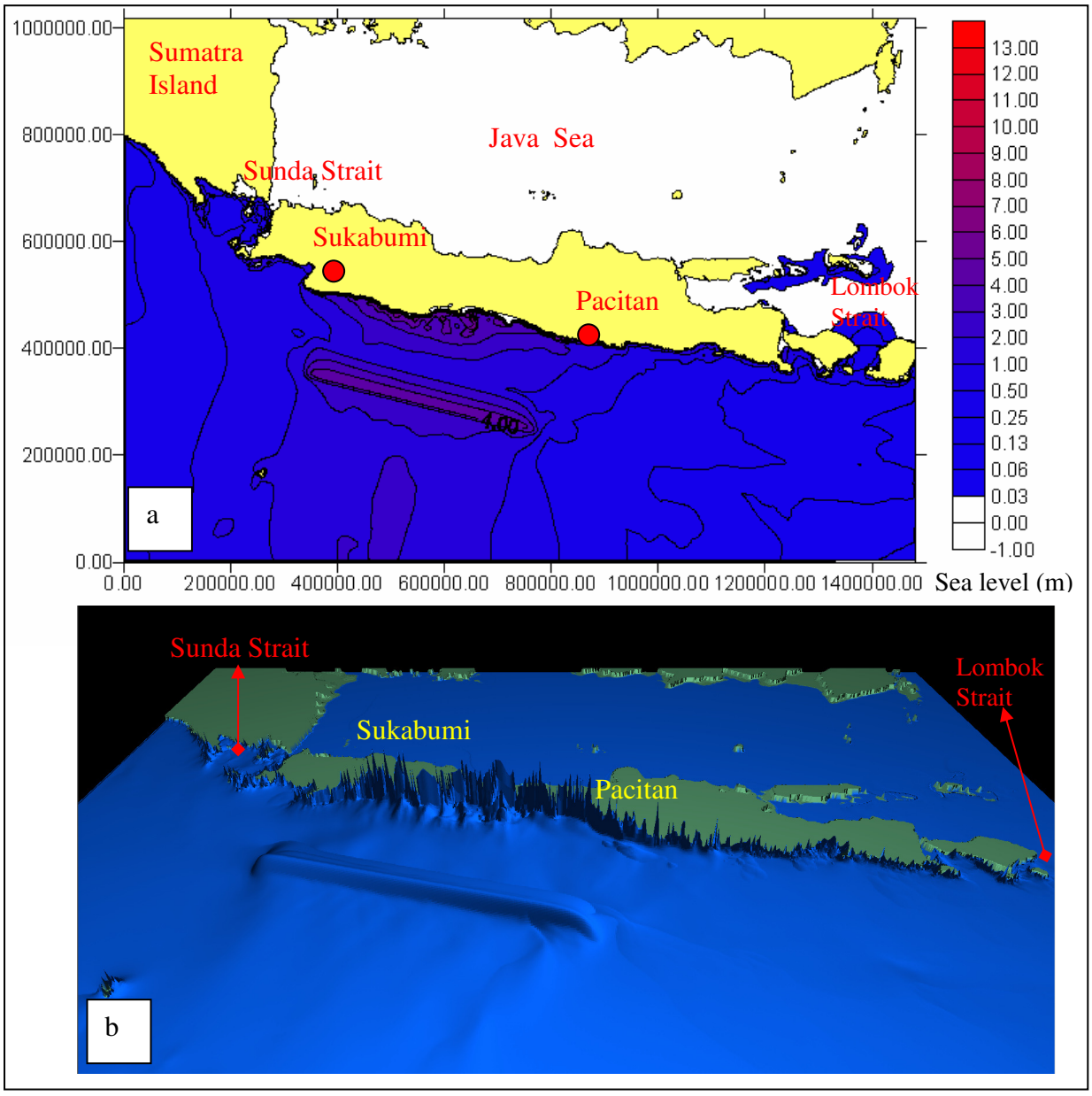

Figure 4.25. Maximum tsunami elevation distribution along the coasts of Sumatra, Java, Bali and Lombok Islands. Figure (a) shows the maximum elevation occurs between Sukabumi and Pacitan, and subsides further away from the source as is clearly evident on the 3-dimensional plot (b).

4.3.7. Central-East Java Gap

The central-east Java gap is the area between the active zone of Central Java (Roo Rise) and East Java, where the 1994 events occurred. Not much information is available for the seismic activities of this gap for shallow events larger than $M_w = 8.0$.

Fault Paramaters

A total length of 279 km of fault rupture is estimated for the gap. Fault parameters are assessed as focal depth =15 km and dip angle = 20^o, the calculated average slip of the fault rupture and maximum moment magnitude ($M_w$max) are 7 m and 8.2 respectively (Table 2.1). Considering the convergence rate between 40.0–66.9 mm/years, the recurrence interval for this gap is 104 to 175 years.

Initial Condition

With these fault parameters, the initial tsunami generation is computed producing a negative leading wave as for the west-central Java gap. Maximum initial sea level at the source region is 5.0 m, and minimum sea level depression is – 2.0 m (Figure 4.26).

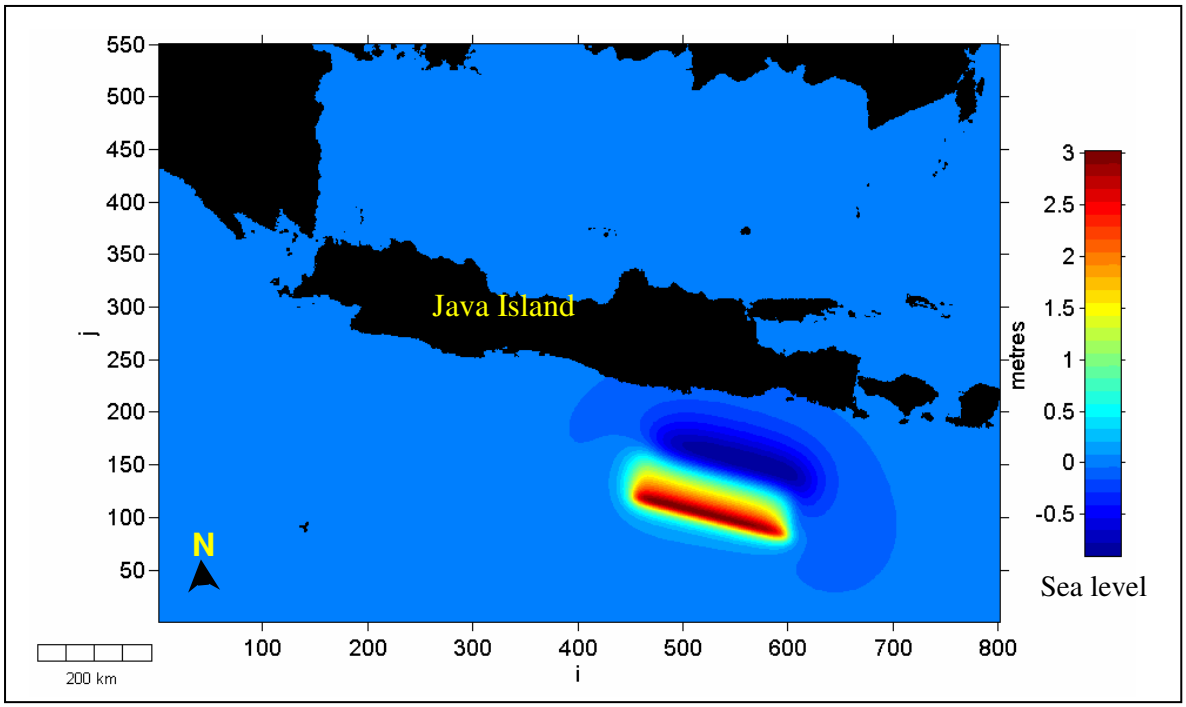

Figure 4.26. Initial condition of tsunami generation for the central-east Java gap with leading wave depression computed using the Okada (1985) method.

Numerical Modelling Results

The distribution of maximum tsunami elevations shows that the hardest hit areas are perpendicular to the fault plane along the southern coast of East Java (Figure 4.27.a.and b). Maximum elevations of up to 8.5 m occur at the center of the areas between Pacitan and Meru Betiri National Park (MBNP). The tsunami propagates to the Java Sea through Lombok Strait, and hits Pagerungan Islands and Madura Island. The first waves arrive between 12 – 15 minutes after the fault rupture at the southern coast of Java Island between Pacitan and Meru Betiri National Park.

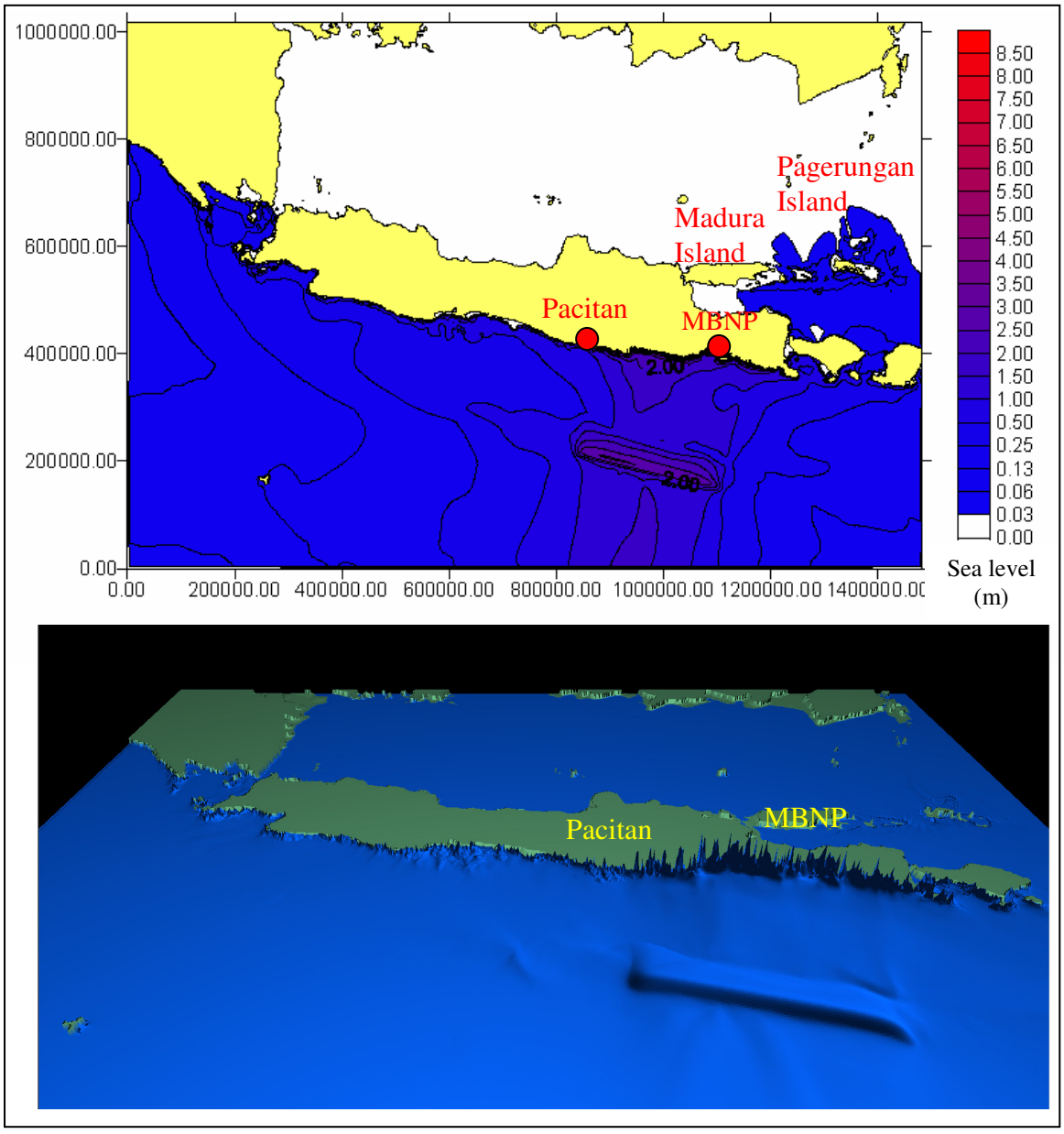

Figure 4.27. Maximum tsunami elevation distribution along the coast clearly shows the areas between Pacitan and Meru Betiri National Park experience the highest tsunami elevation. Tsunami elevation subsided further away from the source along the coast in both directions as clearly evident on 3-dimensional plot.

4.3.8. Sumba Gap

This gap is located between two events, which occurred at the edge of Lombok Basin: the 1994 East Java Tsunami, and the 1977 Sumba Tsunami event. Of interest, the mechanism of the 1977 Sumba Tsunami was not typical of the subduction zone earthquakes; instead it was due to a normal faulting mechanism (Newcomb and McCann, 1987). However, there is no historical record for shallow earthquakes greater than $M_w = 8$ for this gap (ITDB/Pac2004).

Fault Parameters

The fault parameters are derived for a single segment along the fault plane. The length of segment along the gap is 504 km, providing an average slip = 12.6 m. By considering the dip angle = 10^o, and the focal depth = 10 km, these predict the maximum moment magnitude ($M_w$max) = 8.6 (Table 2.1). With the convergence rate between 40 to 78 mm/years, the recurrence interval of this scenario is from 161 to 315 years.

Initial Condition

The initial condition of tsunami generation is computed with a maximum elevation above sea level of 5 m, and below sea level of –3 m (Figure 4.28). The source alignment is perpendicular to the Islands of Bali, Lombok and Sumbawa.

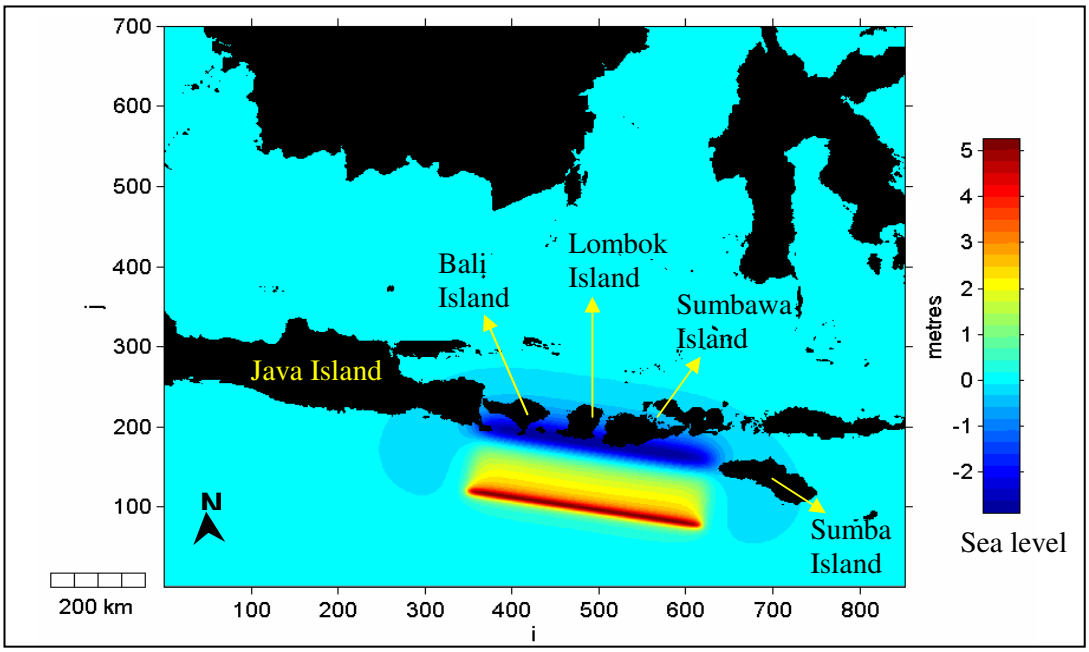

Figure 4.28. Initial condition of tsunami computed using Okada (1985) method produces a leading depression wave.

Numerical Modelling Results

Most of the coast perpendicular and nearby to the source regions were heavily affected by tsunamis, as shown by the distribution of maximum tsunami elevation (Figure 4.29-30). The highest tsunami elevation of 14 m occurred along the southern coast of Bali, Lombok and Sumbawa Islands, and the eastern part of Java Island, and western coast of Sumba Island. Tsunami elevation gradually subsides along the southern coast for both sides of the hardest hit region.

The first waves arrive within 10-15 minutes after the fault rupture, and penetrate to the Java Sea through the straits between the islands (Bali, Lombok and Alas Straits). The tsunami affects the small islands in the Java and Flores Seas, such as Pagerungan Island and some other offshore islands further north, close to Sulawesi Island.

Bathymetric features between the source area and Sumba Island to the east caused the western coast of Sumba Island to experience high tsunami elevation, as occurred for the areas that are perpendicular to the source region. Maximum tsunami elevations within this region also reach 14 m.

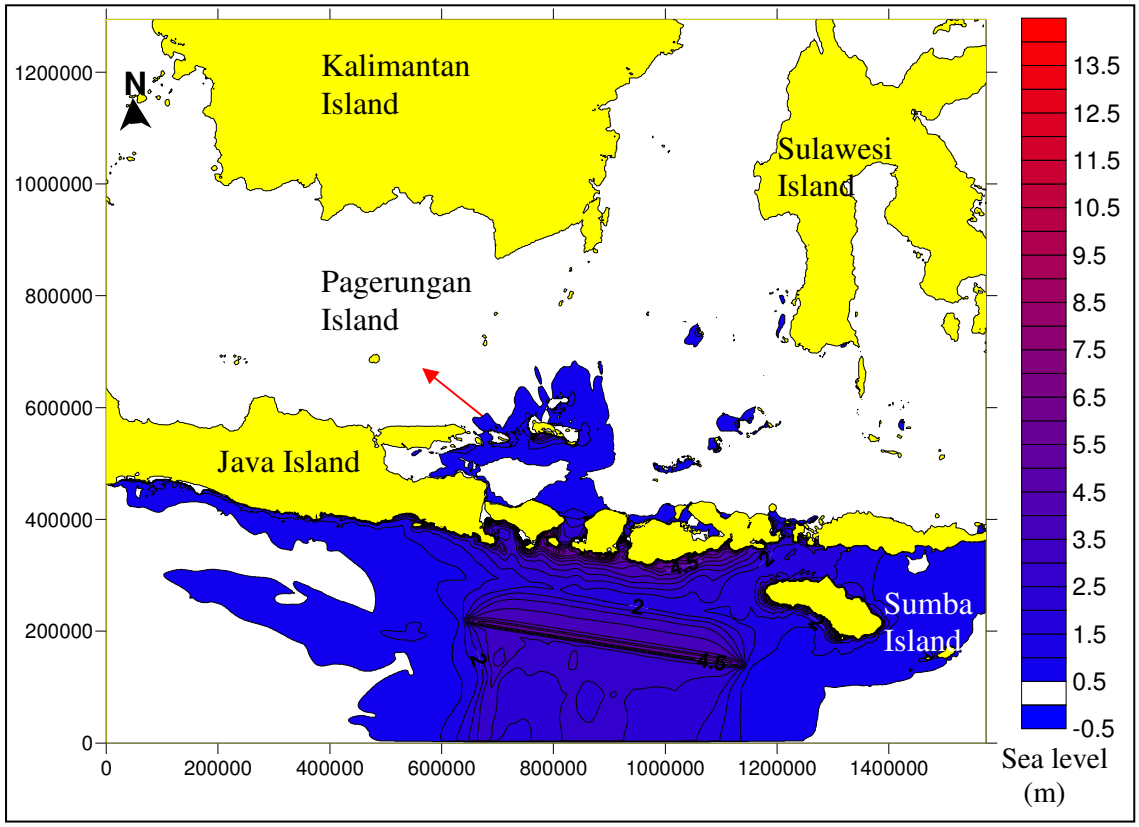

Figure 4.29. Maximum tsunami elevation distribution shows the hardest hit areas are located perpendicular to the fault plane. However, the western coast of Sumba Island also experienced high tsunami elevation due to the bathymetric features and the geometry of the island.

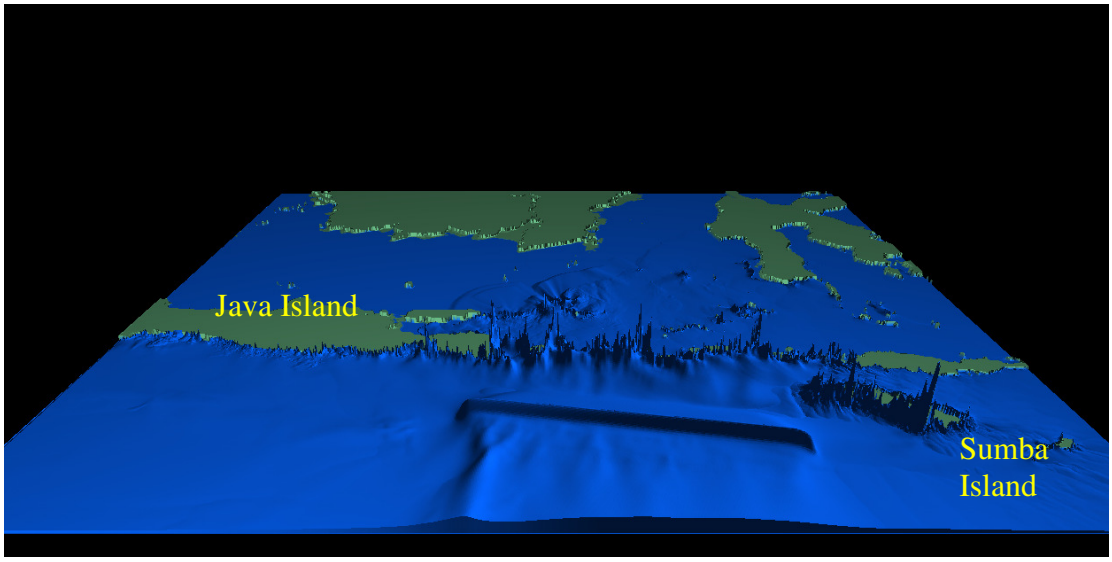

Figure 4.30. Three-dimensional plot of maximum tsunami elevation distribution shows the areas with highest tsunami elevation along the southern coast of Java, Bali, Lombok, Sumbawa and Sumba Islands. The tsunami elevations distributions refer to Figure 4.29.

4.3.9. Banda Arc Gap

No large shallow earthquakes have occurred along the Banda Arc segment since the last event in 1852 (Ms = 8.0, H_{max} = 8.0 m) that occurred in the Southern Banda Arc Basin. The rupture zone of the 1852 event is still poorly understood. Therefore, the gap is defined as the area from the Southern Banda Arc Basin (the suggested epicenter location of the 1852 event) to the Ombai Straits, following the curvature of the subduction zone.

Fault Parameters

Three segments are considered along the defined rupture zone, with a total length of 390 km. With this length, an average slip of 9.75 m is calculated. Furthermore, considering the focal depth = 20 km, and dip angle = 10^{o}, the maximum moment magnitude ($M_w$max) is calculated using the same method as $M_w$max = 8.68 (Table 2.1). The recurrence period of this event with a convergence rate of 20 to 50 mm/y is 195 to 487 years.

Initial Condition

The initial tsunami generation is calculated, and produces a leading negative wave towards the Banda Sea, and positive leading waves to the areas around Aru and

Timor Seas as well as to the northern coast of Australia (Figure 4.31). The maximum elevation of positive leading wave is 3.8 m, while the leading depression is –2.2 m.

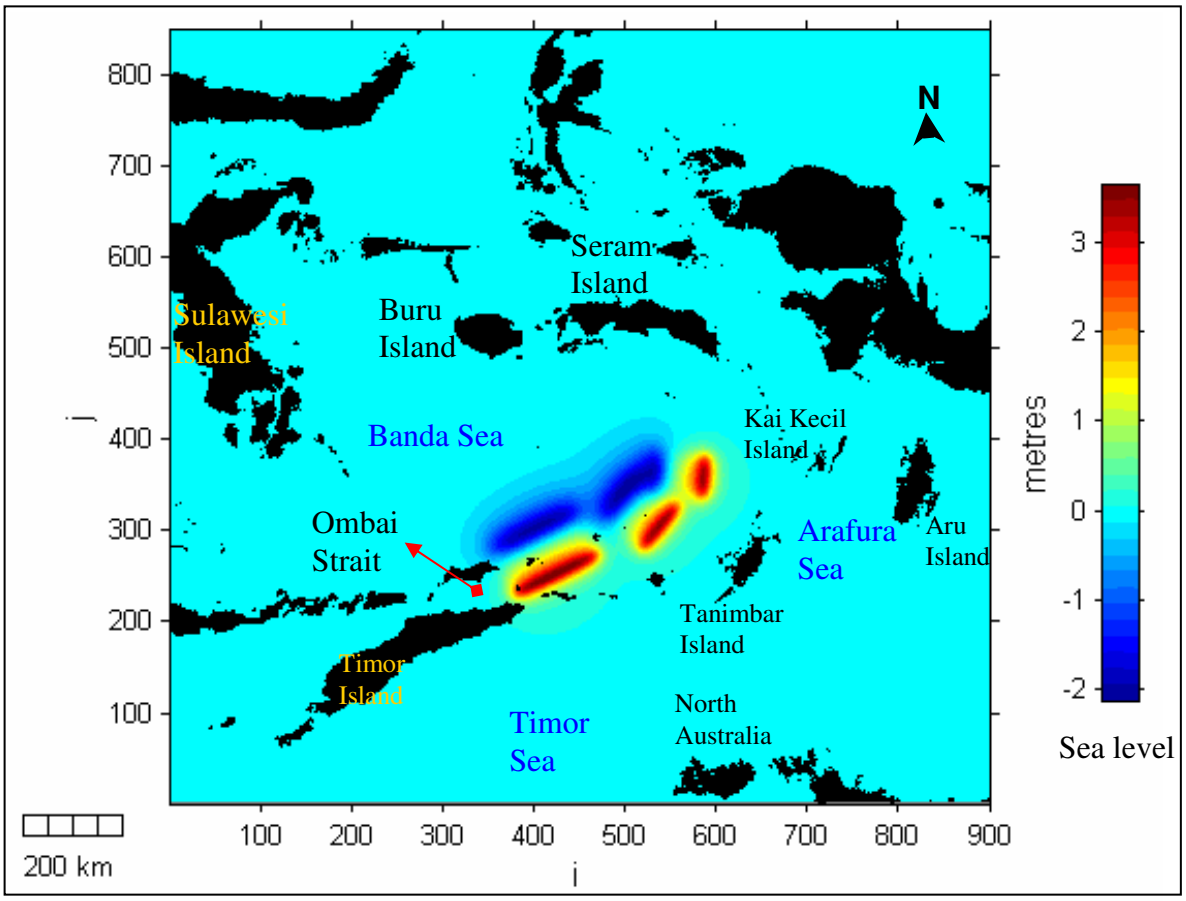

Figure 4.31. Initial condition of tsunami computed using the Okada (1985) method with three segments along the rupture zone from Timor (Ombai Strait) to southern Banda Basin.

Numerical Modelling Results

The tsunami propagates towards Banda and adjacent seas from the source region, and affects most of the coastal areas around the Banda, Arafura (Aru) and Timor Seas. The waves are concentrated towards Buru and Seram Islands in the Banda Sea, Tanimbar Islands and north of Australia in the Arafura and Timor Seas, as they are perpendicular to the rupture zone (Figure 4.32.a). The three-dimensional plot of maximum tsunami elevation shows the highest tsunami elevation occurs along the northwest coast of Tanimbar Islands, and Kai Kecil Island as well as the northern part of Australia (Figure 4.32.b).

Tsunami that impacted on Tanimbar and Kai Kecil Islands are positive leading waves, and provide a maximum elevation of 11.5 m on this region. Arrival time of the first tsunami waves varies from 5 minutes close to the source, up to 30 minutes along the eastern coast of Sulawesi Island.

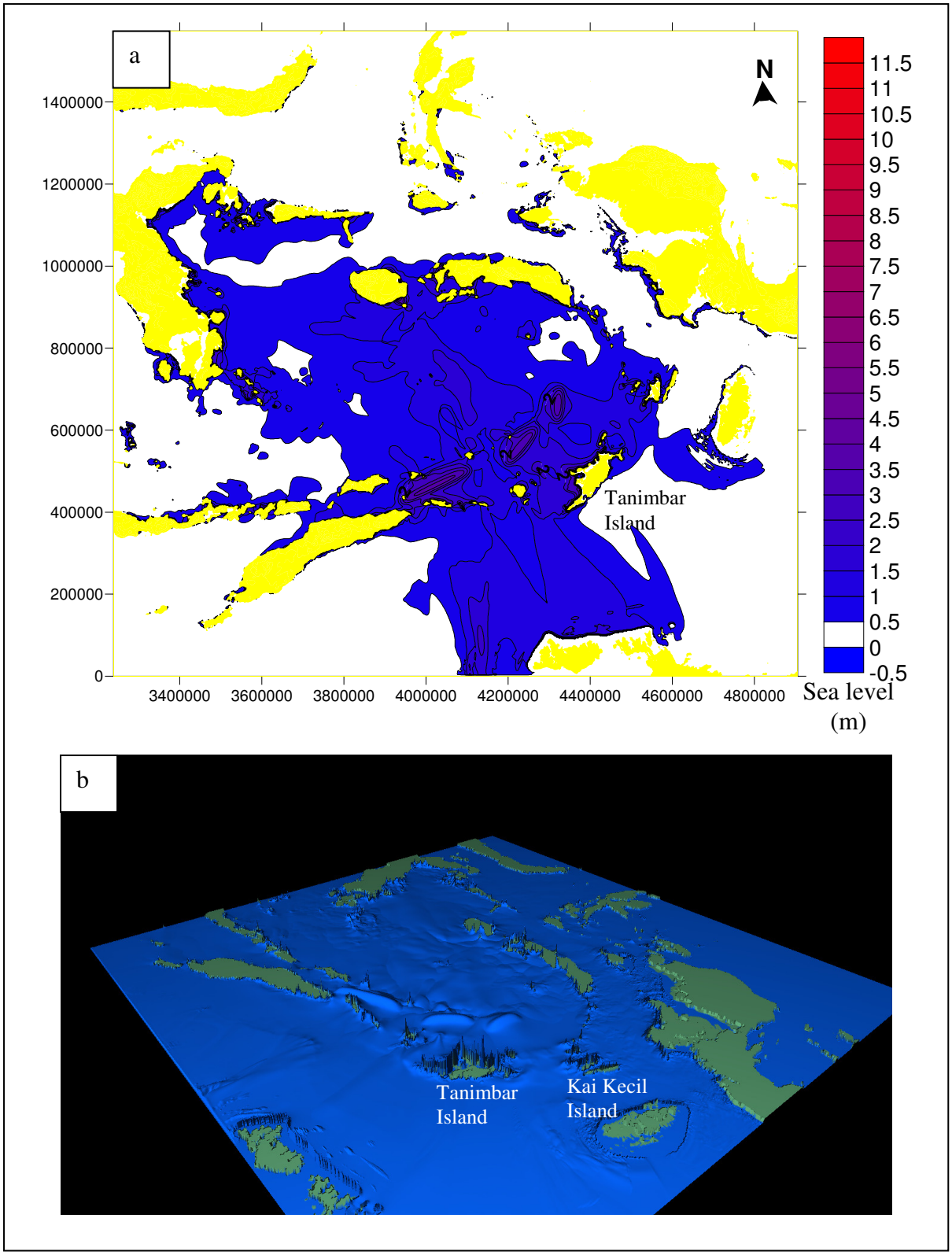

Figure 4.32. Distribution of maximum tsunami elevation shows the affected areas around Banda, Timor and Aru seas (a). The highest tsunami elevation occurs along the northwestern coast of Tanimbar Island facing the source region, as well as the Kai Kecil Island which is shown on 3-dimensional perspective plot (b).

4.3.10. Seram Trench

Seram Trench is located between Seram - Buru Islands and the Bird Head of Irian Jaya to the east, Halmahera Island to the north, and Sulawesi Island to the west. There is no historical record of shallow earthquakes associated with tsunamis along this Trench since 1600. The historical record showed that the 1674 (M_s = 8.0) event occurred on the other side (northern) of Seram Island, even though it is quite obvious that high seismicity occurred between Buru and Seram Islands.

Fault Parameters

Based on the geometry of the trench, the fault plane is represented by three segments with total length of 797 km. An average slip of 19.95 m is calculated, and considering the dip angle of 15^o, and earthquake depth = 15 km, the calculated maximum moment magnitude (M_{wmax}) is 8.89 (Table 2.1). With a convergence rate between 20 – 50 mm/year, the recurrence period of this event ranges from 399 – 997 years.

Initial Conditions

The computed initial tsunami generation produces an initial uplift for most of the Islands (Buru and Seram). Positive elevation occurred along the trench, which makes a positive leading wave toward the Molluca Sea, Halmahera Island, and Birds Head in the north, while negative leading waves propagate toward the Banda Sea (Figure 4.33).

Numerical Modelling Results

Tsunamis from this source affect most of Eastern Indonesia (Figure 4.34). Maximum tsunami elevations up to 24 m occur at some places along the coast of northern Buru and Seram Islands, as well as the Birds Head, and the southern coast of Halmahera, and other islands in the north. High tsunami elevation also occurred along the northern coast of Flores, Tanimbar and Kei Kecil Islands in the south. The three-dimensional plot of maximum tsunami elevation distribution clearly shows the areas that have a high impact from tsunamis (Figure 4.35). This result showed that the great event could occur within this region, as occurred during the 1674 event. The first wave arrives immediately after the fault ruptures along the northern coast of Seram and Buru Islands.

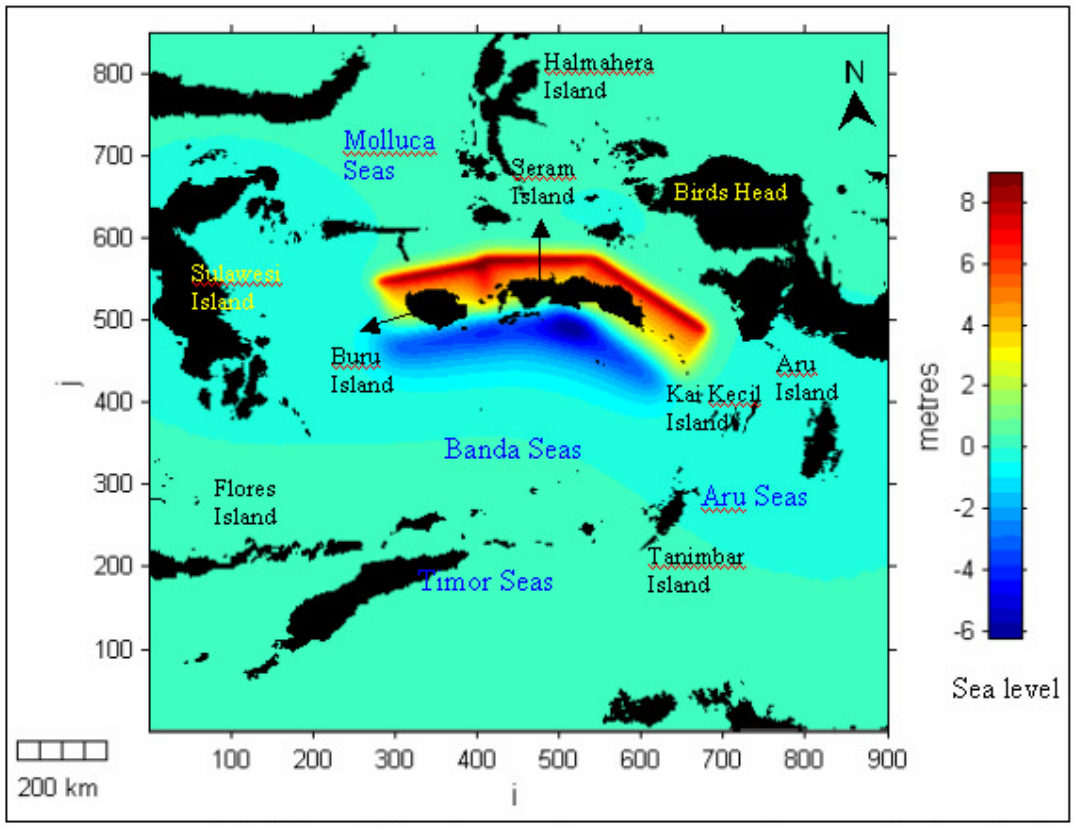

Figure 4.33. The initial tsunami generation from Seram Trench computed using the Okada (1985) method. The positive leading waves head to the north, and the negative leading waves towards areas in Banda, Timor, Aru (Arafura), and Java Seas. Scale bar unit is meters.

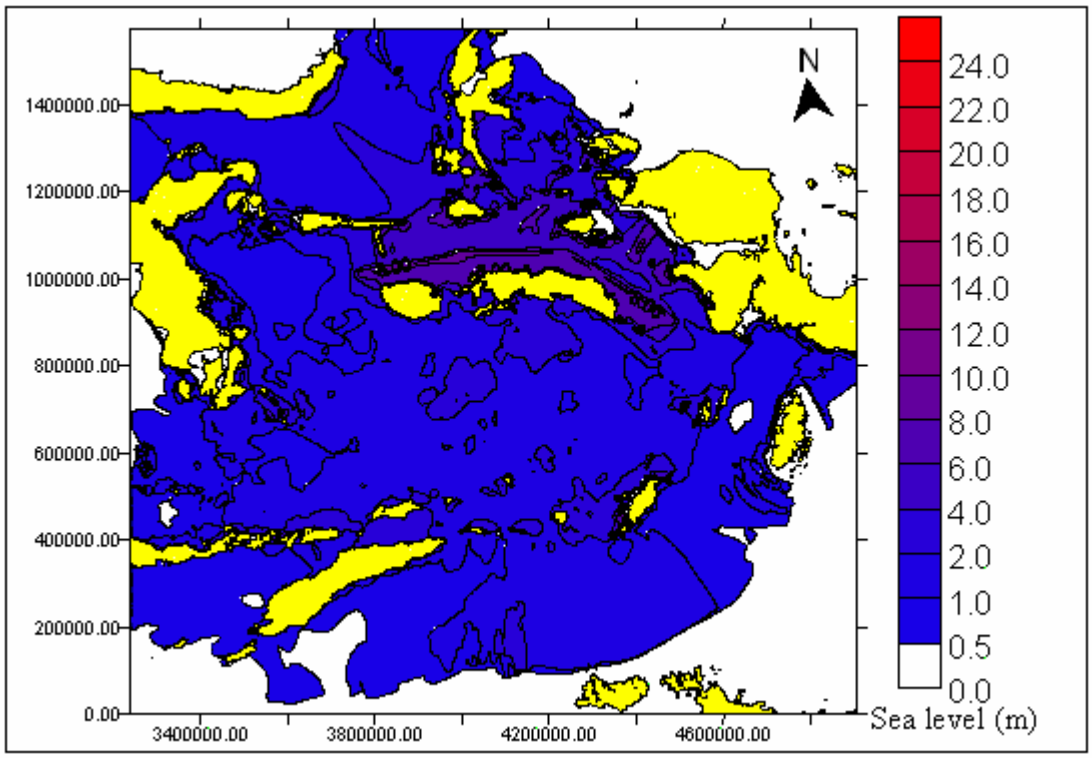

Figure 4.34. Distribution of maximum tsunami elevation shows most of the eastern Indonesian archipelago was affected by tsunamis from this source. The highest tsunami elevation occurs at some places along the coast of northern Buru and Seram Islands as well as the Birds Head and southern coast of Halmahera Island.

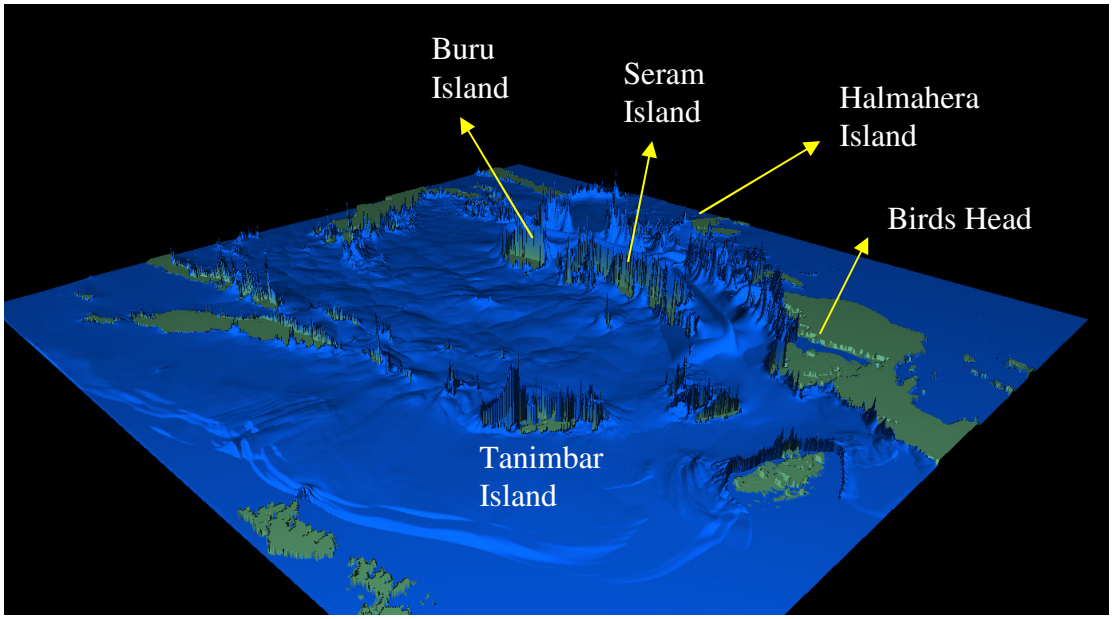

Figure 4.35. Three-dimensional perspective plot of maximum tsunami elevation distribution from Figure 4.34 shows most of the eastern Indonesian archipelago was affected by tsunamis. The coast along northern Buru and Seram Islands, as well as the Birds Head and southern coast of Halmahera, and other islands in the north were hardest hit. To the south, Tanimbar, Kai Kecil and Aru Islands also experiences with relatively high tsunami elevations.

4.3.11. Molluca Trench

The Molluca Trench is located at a unique and complex subduction zone, called the Molluca Collision Zone (McCaffrey, 1988; Katili, 1989). The historical record shows that this region is seismically active with both shallow and deep large earthquakes. However, not all of them are associated with damaging tsunamis. There was one event in 1889 along the Molluca Trench with M_s = 8.0 that generated tsunamis with a height (H_{max}) ~ 15 m.

Fault Parameters

Considering the maximum length of Molluca Trench as the potential tsunami source, gives a total length = 534 km. Following the McCaffrey (2008) method, the average slip becomes 13.37 m, and with focal depth = 10 km, dip angle = 10^o, the computed maximum moment magnitude ($M_w$max) is 8.66, which is higher than the historical event. With the convergence rate of 20 – 50 mm/year, it corresponds to a recurrence period of 267 to 668 years (Table 2.1).

Initial Condition

The initial tsunami generation from this source is computed and produces a positive leading wave towards the Sulawesi and Molluca Seas. The west coast of the northern part of Halmahera Island experiences uplift, while the middle of the island mostly experienced subsidence (Figure 4.36).

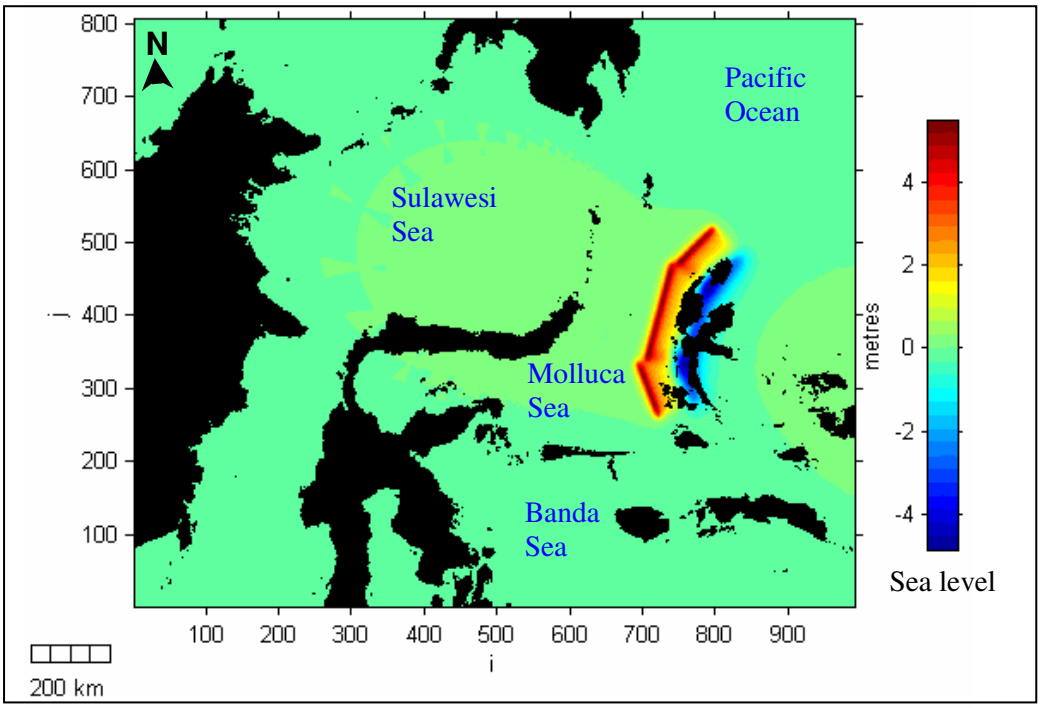

Figure 4.36. Initial tsunami generation along the Molluca Trench computed using the Okada (1985) method.

Numerical Modelling Results

After three hours of simulation, the distribution of maximum tsunami elevations within the model region is shown in Figure 4.37.a-b. The highest tsunami elevation is 13 m, and occurs along the western coast of Halmahera Islands, eastern coast of Northern Sulawesi Peninsula (Manado), and the offshore islands of Sangihe and Central Sulawesi (Banggai and Taliabu Islands). Most of these regions face towards the subduction zone. The waves propagate further to the northwest, and affect the coastal areas around Sulawesi Sea. A series of offshore islands between Molluca and Banda Seas prevent the tsunami from propagating further towards Banda Sea; hence the impacts further south are minimized. Within 5 – 10 minutes after the fault rupture, the first waves hit the western coast of Halmahera Island.

The highest tsunami elevation produced by the model with these fault parameters (M_{wmax} = 8.66) is 13.0 m, which is less than the historical record of the 1889 event (M_s = 8,0 with H_{max} = 15 m). Many factors may to contribute to this

discrepancy including local amplifications, shoaling and refraction. However, a more detailed bathymetry and topography data are needed to simulate these in order to better replicate the tsunami elevation data from historical record.

This simulation is based on a 1 arc minute grid and, in general, provides tsunami characteristics and distribution pattern for elevation for source scenarios that might cause severe impact to the coastal areas around the Mollluca Sea.

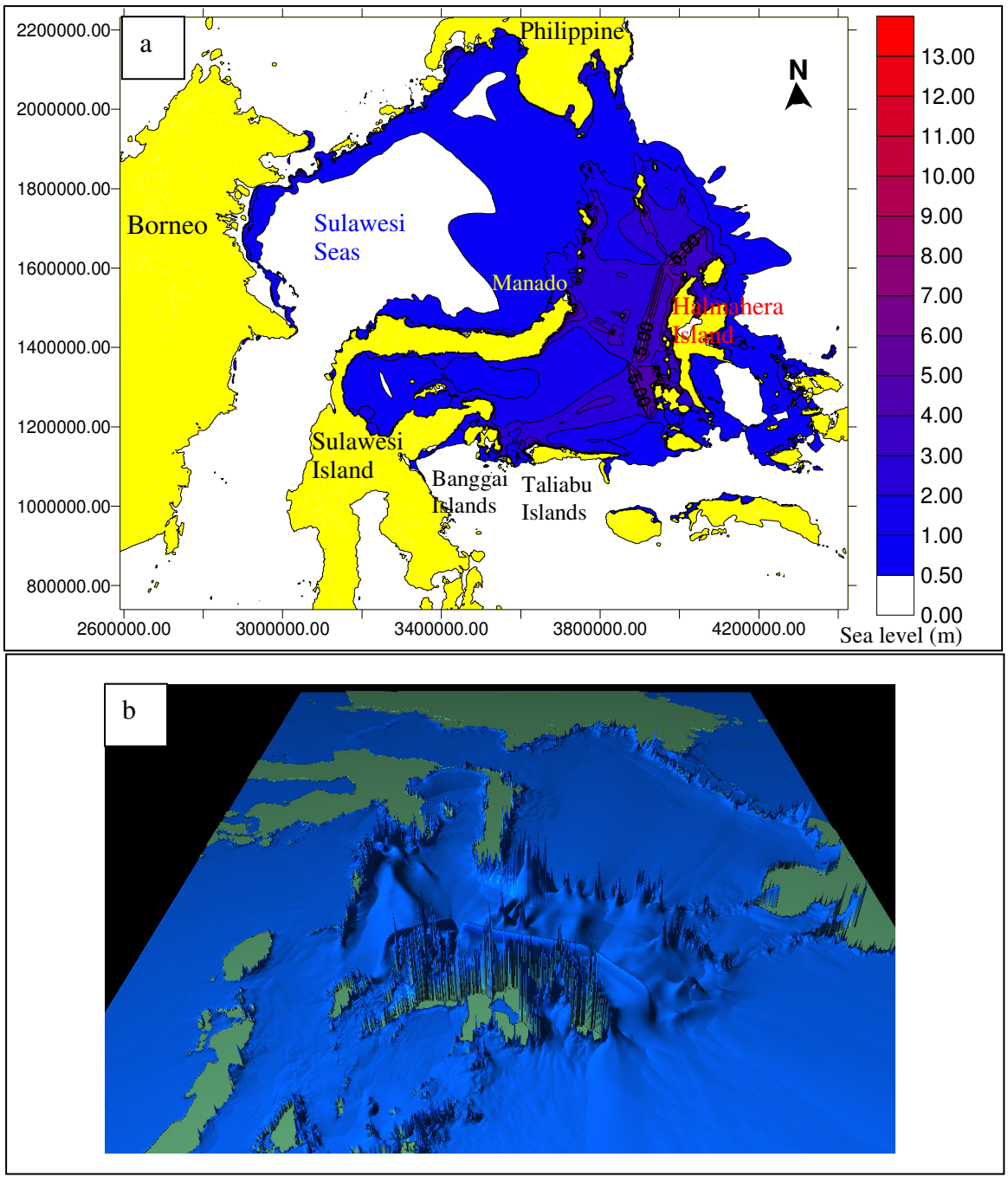

Figure 4.37. Maximum tsunami elevation distribution from a Molluca Trench event shows the distribution of tsunami elevation in a two dimensional plot (a), and perspective three-dimensional plot (b).

4.3.12. Sangihe – Talaud Trench

The historical record for the Molluca Sea Collision zone revealed only one large event associated with a damaging tsunami that occurred in 1889. This event is recorded as having occurred within the Molluca Trench system (ITDB/PAC2004). However, also it may have occurred in the Sangihe – Talaud Trench system since there was no instrumentally recorded data during that period of time that can be used to locate the earthquake source precisely.

Fault Parameters

Assuming all segments of the Sangihe-Talaud Trench have the potential to be a tsunami source, it gives a fault plane with total length of 591 km. This consists of two main segments following the alignment of the deformation zone. The average slip, and maximum moment magnitude ($M_w$max) were computed with a focal depth = 10 km, and dip angle = 10^o. This gives an average slip of 14.8 m, and the maximum moment magnitude (M_{wmax}) = 8.7. With a convergence rate between 20 – 50 mm/year, the recurrence period for this event is between 295 to 739 years (Table 2.1).

Initial Conditions

An initial condition for the tsunami generation were computed and produces a positive leading wave towards Halmahera Island and the Pacific Ocean, and negative leading waves will propagating towards the Sulawesi Sea (Figure 4.38). The highest positive leading wave is 6.0 m, and a deepest leading depression wave is – 4.5 m.

Numerical Modelling Results

Maximum tsunami elevation after 3 hours of simulation is 19.0 m, and occurs at some places along the coast of western Halmahera, Sangihe and Talaud Islands. It is obvious that the waves affect the coastal area around the Sulawesi Sea, and penetrate to the Makassar Strait (Figure 4.39). However, tsunami impacts are minimal in the Banda Sea and the areas around Tomini Bay. Most of the waves are blocked by the Sula Islands (Taliabu Island and other small islands). The three-dimensional perspective plot (Figure 4.40) shows the areas that have suffered the largest impact from this scenario.

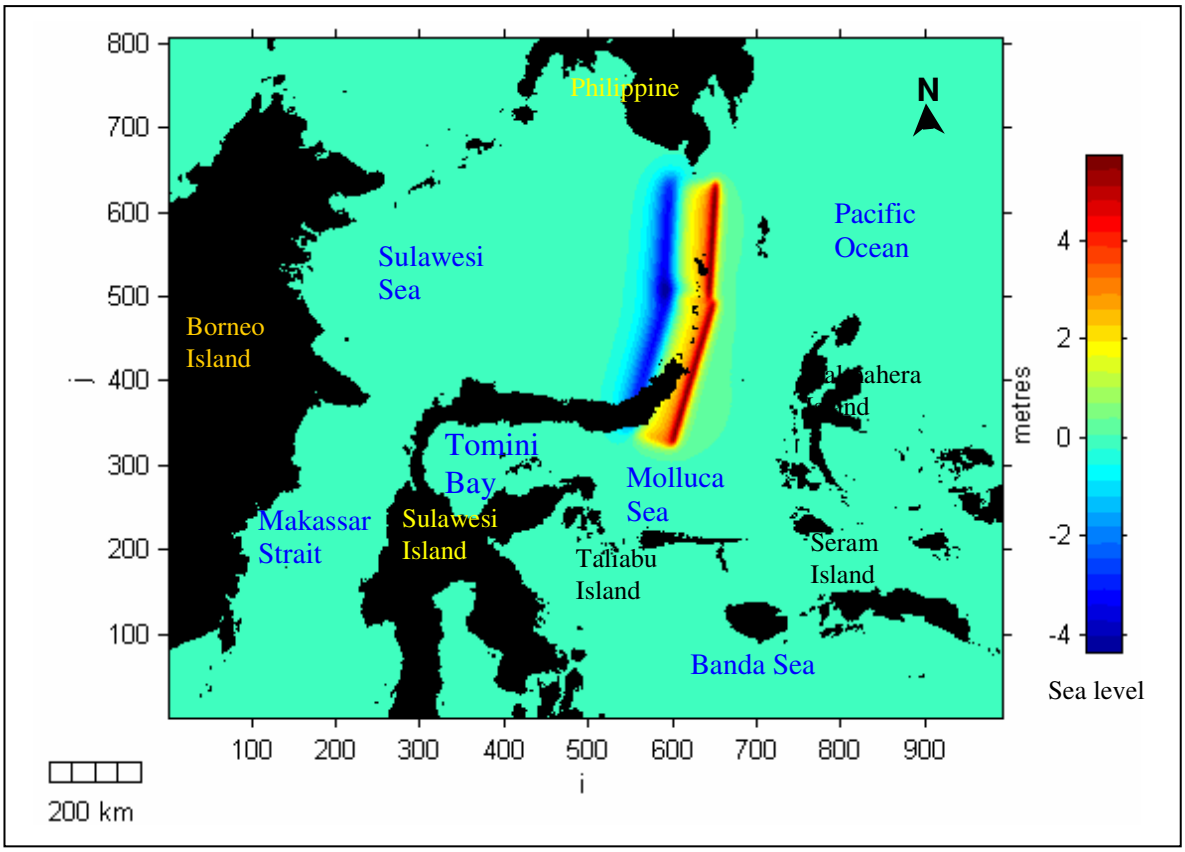

Figure 4.38. Initial conditions of tsunami generation along the Sangihe-Talaud Trench were computed using Okada (1985) method, predicting both positive and negative leading waves.

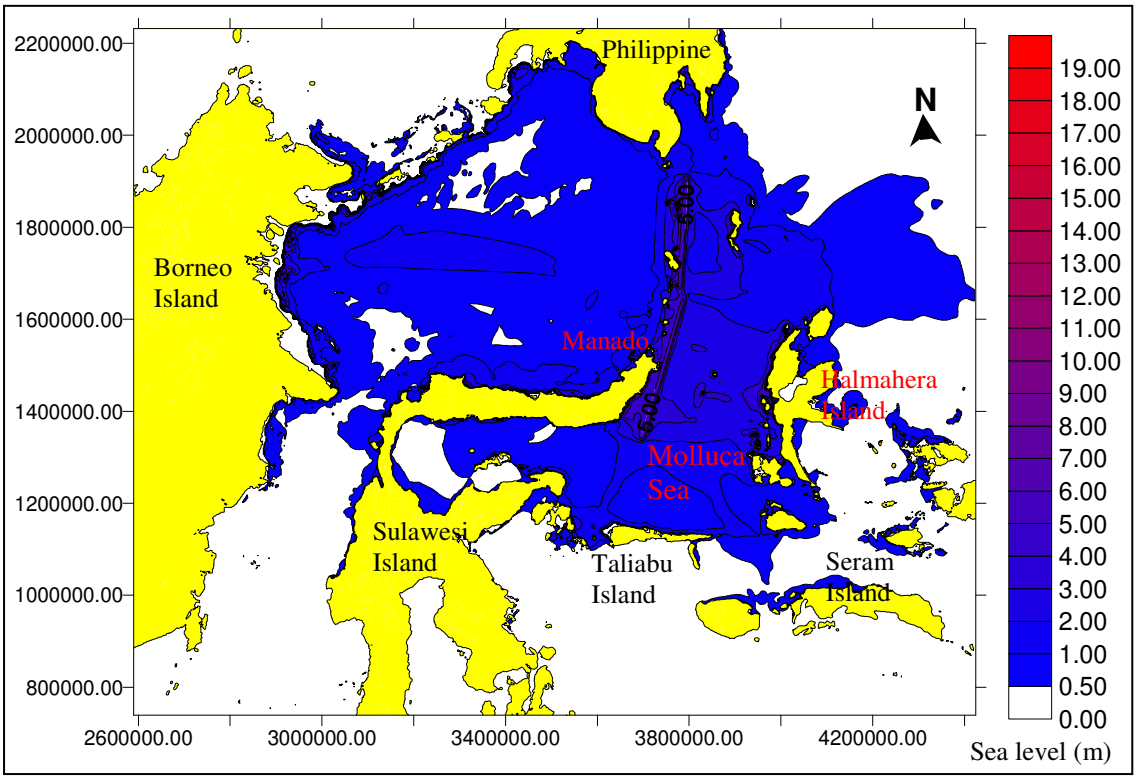

Figure 4.39. Distribution of maximum tsunami elevation shows the maximum tsunami elevations occur mostly in areas perpendicular to the rupture zone.

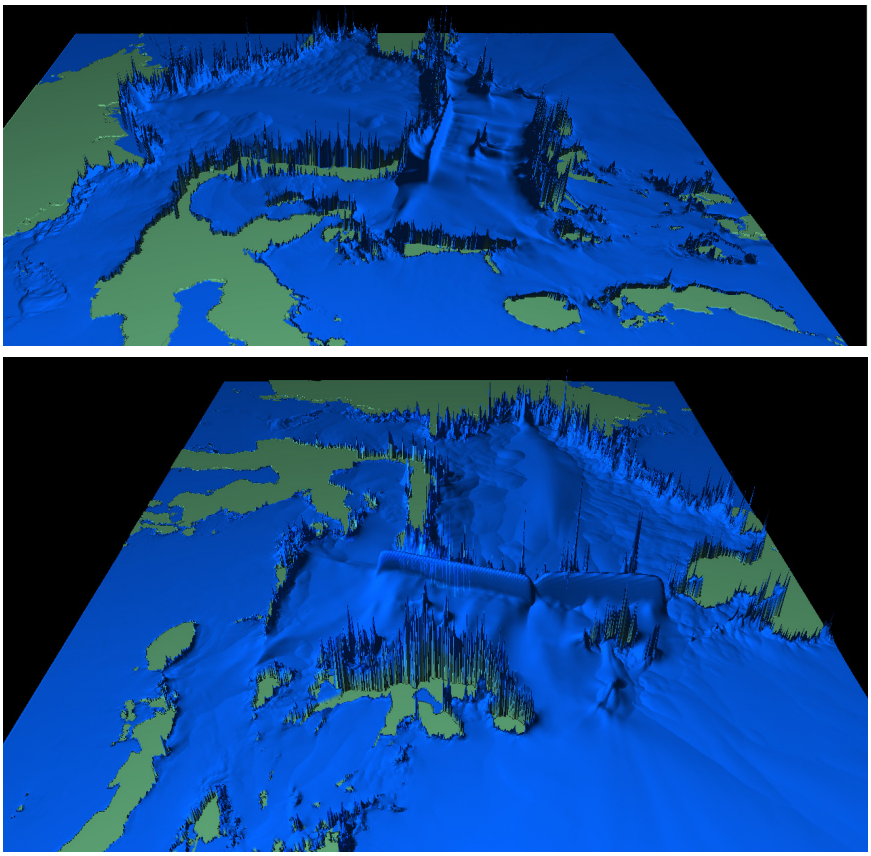

Figure 4.40. Three-dimensional perspective plot of the maximum tsunami elevation showing that the largest tsunami occurs mostly in areas perpendicular to the rupture zone, such as along the western coast of Halmahera Island. The northern arm of Sulawesi Island and eastern coast of Borneo experience the same height of tsunami elevation. The tsunami elevation scale refers to Figure 4.39.

4.3.13. Northern Sulawesi Trench

There is no historical record of large shallow earthquake events associated with damaging tsunamis in the northern Sulawesi Trench. This subduction-zone mostly produces shallow thrust earthquakes orientated perpendicular to the structural trend of Sulawesi Island. Therefore, damaging tsunamigenic earthquakes are possible.

Fault Parameters

The total length of potential fault rupture along the trench is 422 km. The computed average slip is 10.57 m. Considering a focal depth of 15 km, and dip angle = 15^{o}, the computed maximum moment magnitude (M_{wmax}) is 8.64 (Table 2.1). With a convergence rate of 20 – 50 mm/year, the recurrence period of this scenario event is between 211 to 528 years.

Initial Conditions

The initial conditions of tsunami generation were computed using those fault parameters. A negative leading wave was predicted towards the northern arm of Sulawesi Island, with a leading depression of – 3 m, and positive leading waves of 5 m towards the Sulawesi Sea (Figure 4.41).

Numerical Modelling Results

The distribution of maximum tsunami elevations after three-hours of simulation shows that the largest waves occurs perpendicular to the rupture zone along the northern arm of the Sulawesi Island for the near field, and along the coastal areas of the South Philippines for the far field (Figure 4.42). The maximum tsunami elevation along the northern coast of Sulawesi is 15 m. The tsunami propagates into the Makassar Strait and the Molluca Sea, producing a maximum tsunami elevation ranging from 0.5 to 3 m. The impacts around the coastal areas of the Sulawesi Sea are less (Figure 4.43). The first waves arrive along the northern arm of Sulawesi Island within 10 – 15 minutes, and to the southern Philippines it takes between 30 – 45 minutes.

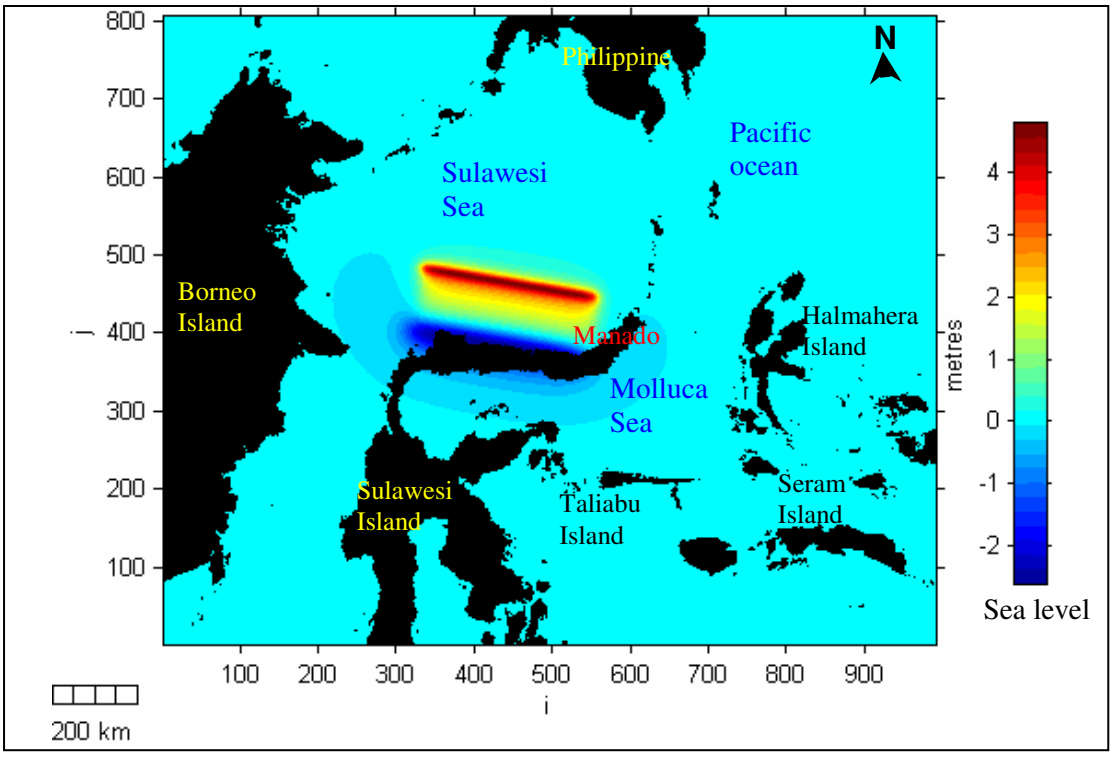

Figure 4.41. Initial conditions of tsunami generation computed by the Okada (1985) method. Negative leading waves are propagating towards the northern arm of Sulawesi Island.

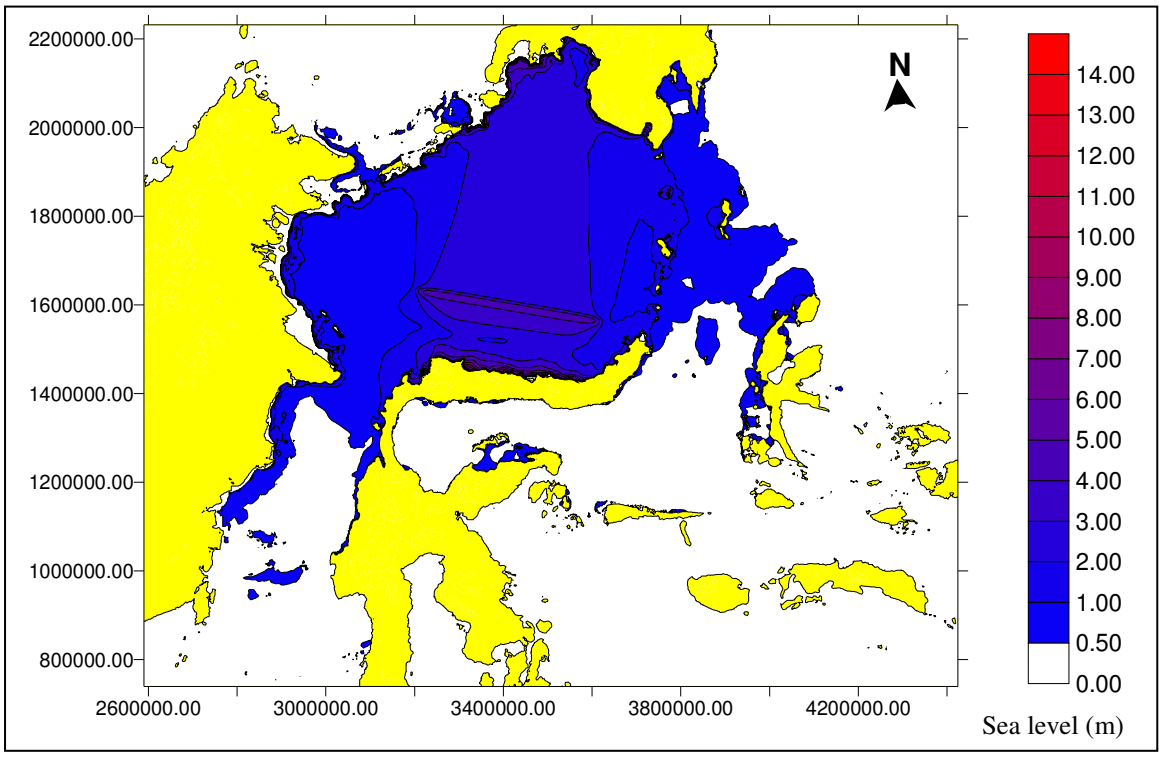

Figure 4.42. Maximum tsunami elevation occurs mostly to the areas that are perpendicular to the rupture zone.

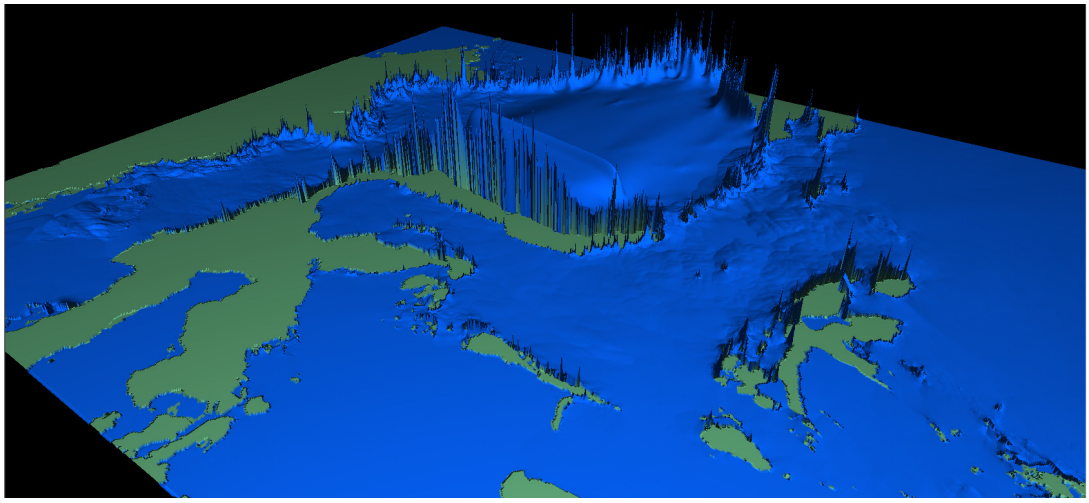

Figure 4.43. Three-dimensional perspective plot of maximum tsunami elevation showing that the northern arm of Sulawesi Island, which is close to the source, experiences the highest tsunami elevation. Slightly lower waves affect the coastal areas of the Southern Philippines. The tsunami elevation scale refers to Figure 4.42.

4.3.14. Northern Sumbawa Trench

The Northern Sumbawa Trench had one notable historical event in 1820, with magnitude M_s =7.5, and tsunami height (H_{max}) = 24 m. After this event, no further large shallow earthquake has been associated with a damaging tsunami within this region, and the region seems to be seismically quiet.

Fault Parameters

The total length of the back-arc subduction zone is 340 km, and giving an average slip of 8.5 m. Maximum moment magnitude (M_{wmax}) = 8.3 was calculated using the focal depth = 15 km, and dip angle = 20°. With the convergence rate between 20 – 50 mm/years, the recurrence interval is between 170 to 425 years (Table 2.1).

Initial Conditions

Using these fault parameters, the initial tsunami generation was computed and produces a maximum elevation of 4 m, and a minimum of -2 m (Figure 4.44). The leading positive waves propagated towards the coastal areas of the northern coast of Sumbawa and Flores Islands, as well as the coastal areas of Java, Kalimantan, Sulawesi and Sumba Islands.

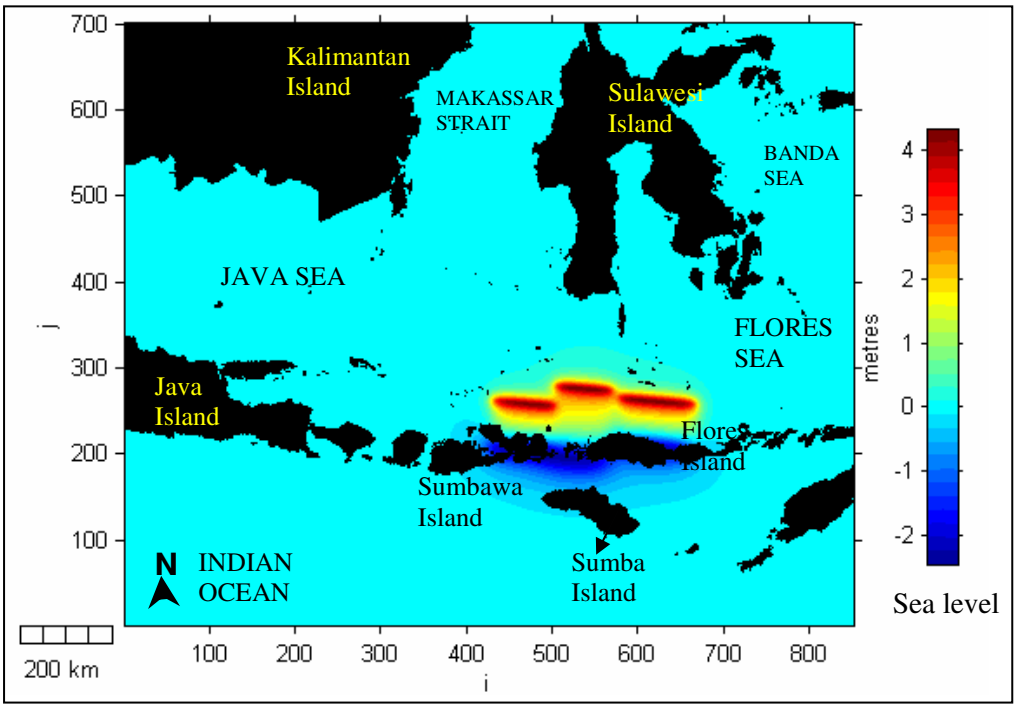

Figure 4.44. The initial tsunami generation along the northern Sumbawa trench is computed by the Okada (1985) method and provides a predictive initial tsunami elevation.

Numerical Modelling Results

Three hours of simulation was carried out to assess the tsunami impact from the source scenario. The model results show the affected coastal areas are located around the Java and Flores Seas, as well as the northern part of Sumba Island (Figure 4.45).

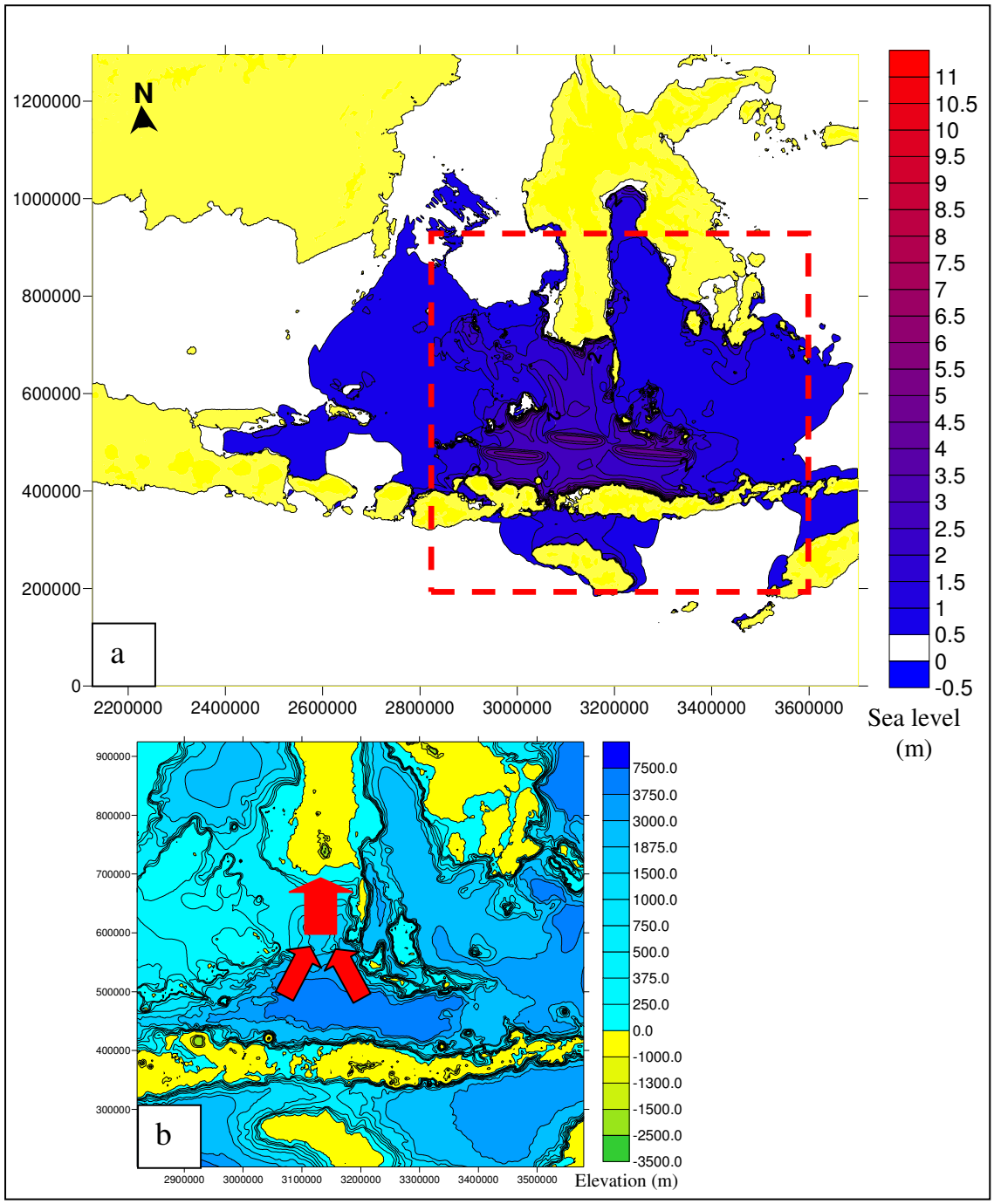

Figure 4.45. Maximum tsunami elevation occurred mostly in the areas facing perpendicular towards the rupture zone (a). Wave focusing (red arrows) towards South Sulawesi Island was caused by the bathymetry features of the region (b).

The maximum tsunami elevation of 11 m occurs along the northern coasts of Sumbawa and Flores Island. While along the south coast of Sulawesi Island, the maximum tsunami elevation varies between 5 – 9 m (Figure 4.45). The propagation pattern of tsunamis to the north was affected by the configuration of offshore islands, as well as bathymetry features that focused the waves into the south coast of Sulawesi Island.

Compared to the 1820 event (maximum wave height (H_{max}) = 24 m), the maximum modelled tsunami elevation is half that recorded in the historical record. This evidence suggests that a secondary mechanism such as landslide or submarine slumping should be considered, as occurred during the 1992 and 1998 of Flores and Biak tsunamis. There is no historical record of tsunami earthquakes within this zone as identified at the southern coast of Java Island.

The three-dimensional plot of the near-field and far-field pattern of maximum tsunami elevations along the northern coast of Sumbawa and Flores Islands, and along the southern coast of South Sulawesi, clearly shows the effect of the offshore islands, and bathymetry features on the wave propagation in Java and Flores Seas (Figure 4.46).

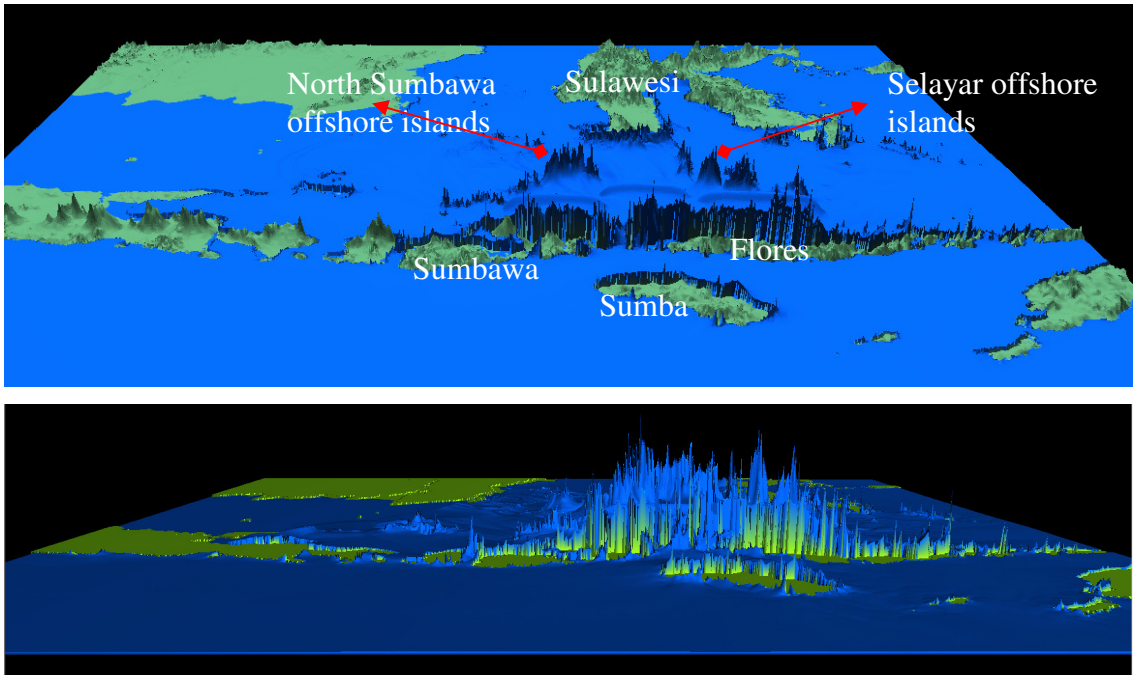

Figure 4.46. Three-dimensional perspective plot of maximum tsunami elevation distribution shows the maximum tsunami elevations occurred mostly to the areas that perpendicular to the rupture zone. Wave focusing towards South Sulawesi Island was obvious, caused by the bathymetry features of the region and the presence of offshore islands.

4.4. Volcanic Tsunami Sources

Volcanic activities and the processes of volcanic tsunami generation within the Indonesian Archipelago are still poorly understood; mostly due to the lack of baseline data for volcanic tsunami research activities. From 18 volcanoes that have been identified as potentially generating tsunamis in the future (Chapter 2), only three are assessed based on the availability of baseline data, historical record, and their current activities. The 3 considered are Anak Krakatau in Sunda Strait with a historical event in 1883, Tambora Volcano on Sumbawa Island following the historical event in 1815, and Banda Api Volcano located in a former 7 km wide of caldera in the Banda Sea.

4.4.1. Anak Krakatau

Physical and numerical modeling of the 1883 Krakatau event (Prasetya, 1998; Prasetya et al., 2000; de Lange et al., 2001) revealed that a single large explosion could not produce the observed waves of the Krakatau 1883 event (Figure 4.47). Instead a sequence of one or more pyroclastic flows associated with a collapsing column in and around the Krakatau Volcanic Complex is the most likely mechanism causing the largest tsunami. The steep entry angle ($\geq 60^{o}$) of pyroclastic flows were shown experimentally with a mixture of coarse sand and mud, explained the occurrence of the Calmeyer and Steers shallow areas, and the bathymetry changes associated with the eruption.

The experiments showed waves are easily generated by gravity flows entering the water, regardless of the slope. The wave properties depend on the relative densities of the flow and the receiving body, and the velocity of the flow. These findings were confirmed by Freundt (2003) who used hot materials in his physical model. Caldera collapse is considered also potentially capable in generating tsunamis; however, their efficiency in generating large waves required sudden or fast processes as identified during the physical model experiments (Prasetya, 1998; Prasetya et al., 2000). Usually caldera collapse is associated with large column collapse, so it is difficult to distinguish between the two processes for large historical eruptions.

Anak Krakatau is growing in the middle of the former Krakatau Volcano between the former Danan and Perboewatan vents (Figure 4.48), with the first eruption in 1927 (Simkin and Fiske, 1983). In 2008, the diameter of Anak Krakatau was 4 km with a height ~ 273 m. The potential scenario for tsunami generation from Anak Krakatau simulated involved caldera formation following an explosive eruption.

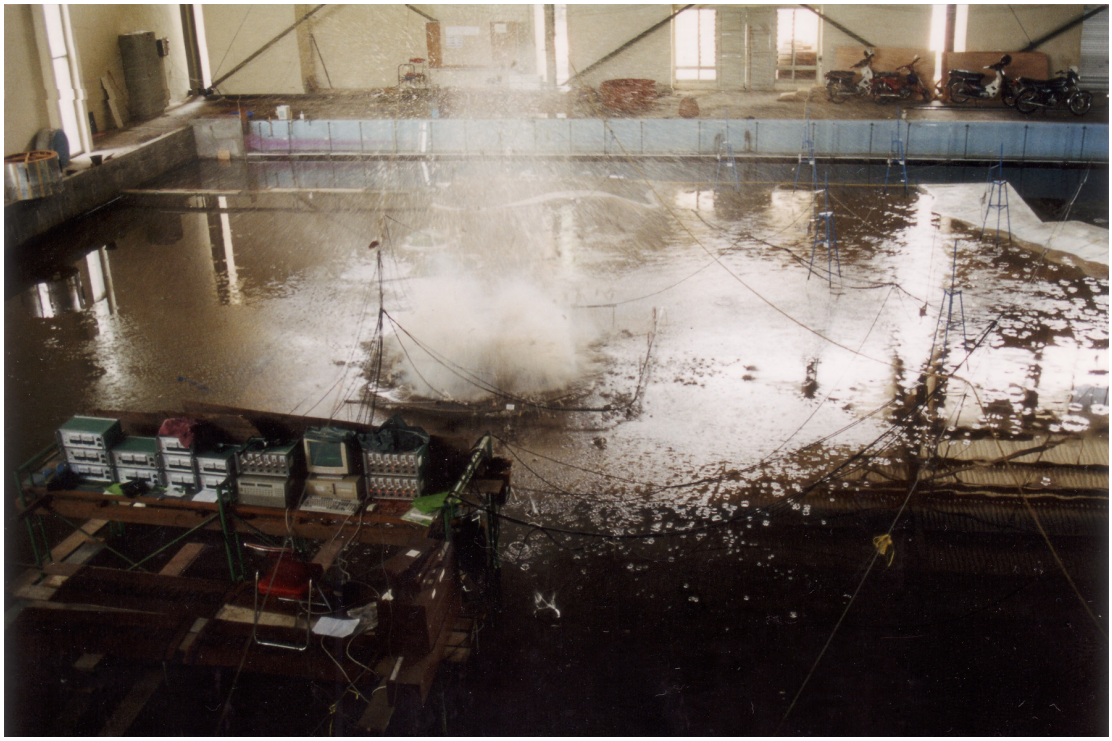

Figure 4.47 Physical modeling experiment of a high intensity explosion suggested the areas surrounding the volcano became dry and no waves were generated by the direct transfer of explosive forces (Prasetya, 1998)

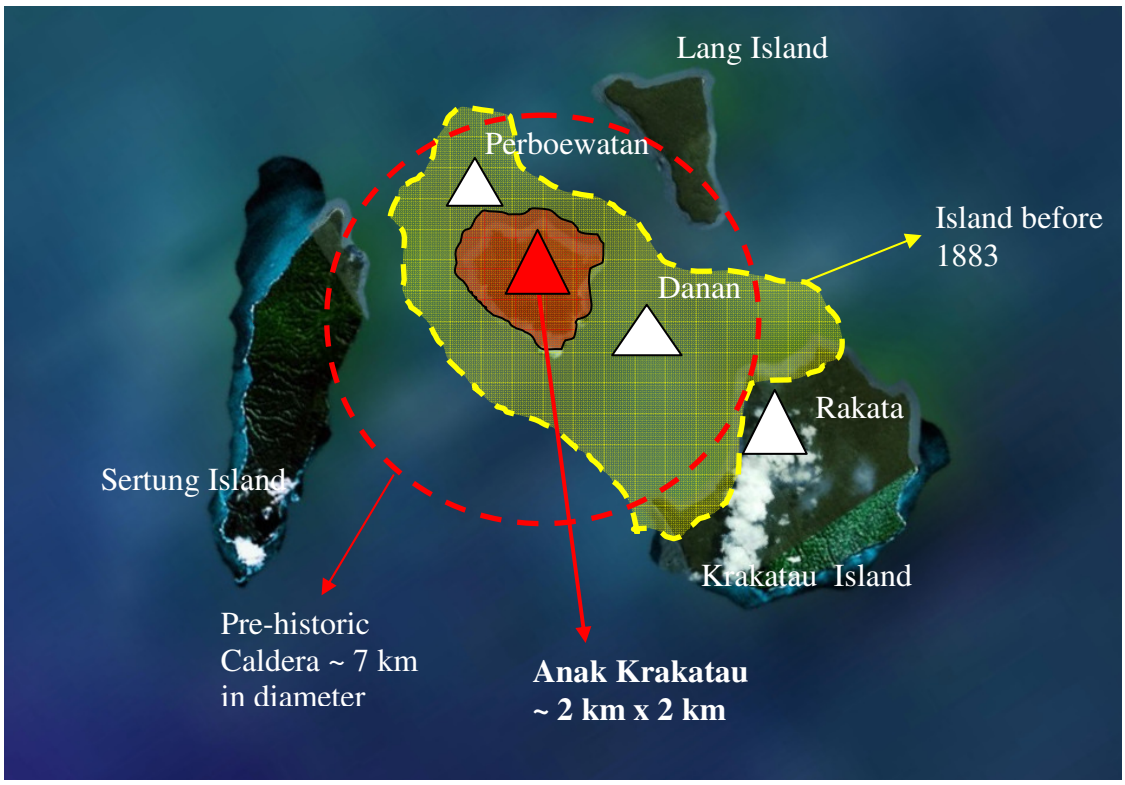

Figure 4.48. The dimensions of Anak Krakatau in 2008 (2 km x 2 km with a height ~ 273 m). It is located between the former Danan and Perboewatan vents of Krakatau.

Initial Condition

The observation that the entire Krakatau volcano disappeared and formed a caldera during the 1883 events was adopted as the basic scenario. Case 4 of the initial disturbance defined by Le Mehaute and Wang (1996) to simplify complex explosion wave generation processes with crater formation, was applied as illustrated in Figure 4.49. This case satisfies continuity when the free surface disturbances are defined by a free surface elevation, and is consistent with the results of the physical modeling experiments of Prasetya (1998) as illustrated in Figure 4.50.

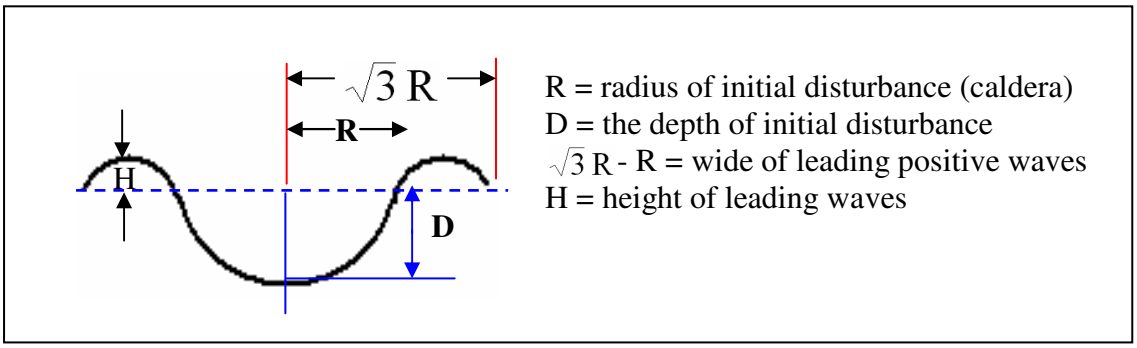

Figure 4.49. Schematic of the initial condition for a simplified complex explosion wave generation process with crater formation, following case 4 of Le Mehaute and Wang (1996).

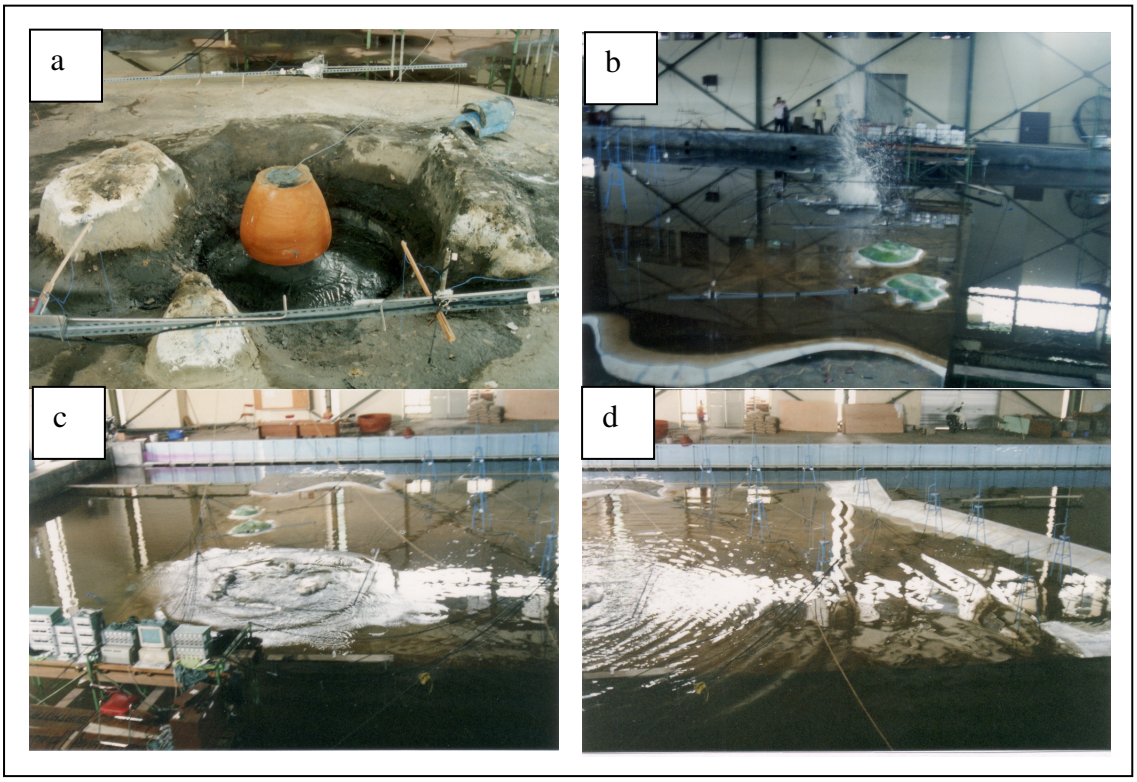

Figure 4.50. Sequence of physical modeling experiments (Prasetya, 1998) of the volcanic explosion of Anak Krakatau: (a) the model setup, (b) during explosion, (c) wave pattern near to the source after explosion, and (d) wave trains approaching the shore.

The diameter of the caldera, or the initial disturbance (2R), is 4 km with depth = 200 m, and an initial leading positive wave = 10 m as illustrated in Figure 4.51 and 4.52. The model grid resolution for this simulation is 200 m, as derived primarily from the map produced by the Navy Hydrographic Office of the Republic of Indonesia, and the National Coordinating Agency for Survey and Mapping (BAKOSURTANAL).

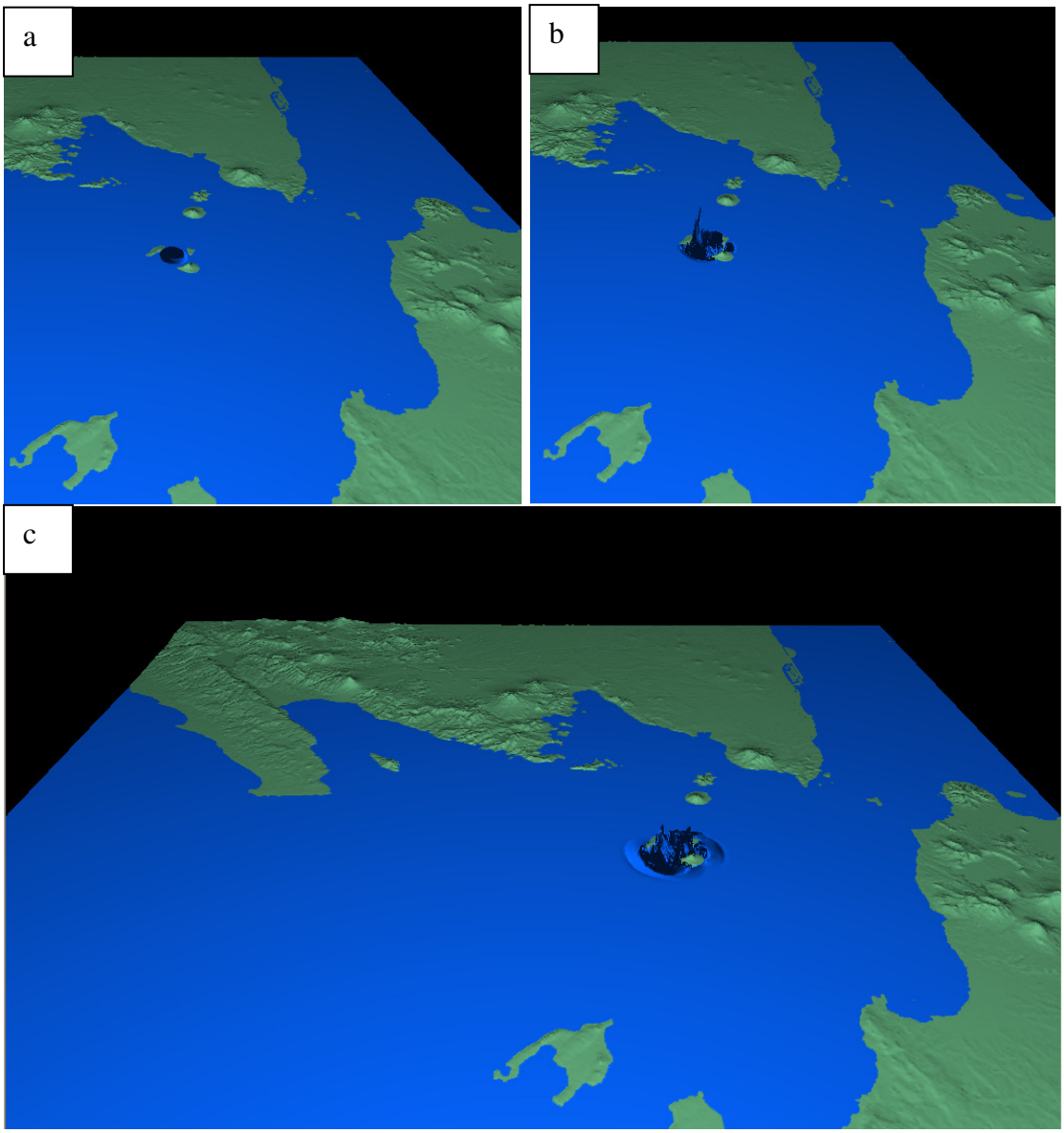

Figure 4.51. Initial condition for a tsunami generated by an eruption of Anak Krakatau using Le Mehaute and Wang (1996) case 4 model at (a) t= 0, (b) during the first 2 minutes, and (c) 5 minutes after the caldera collapse.

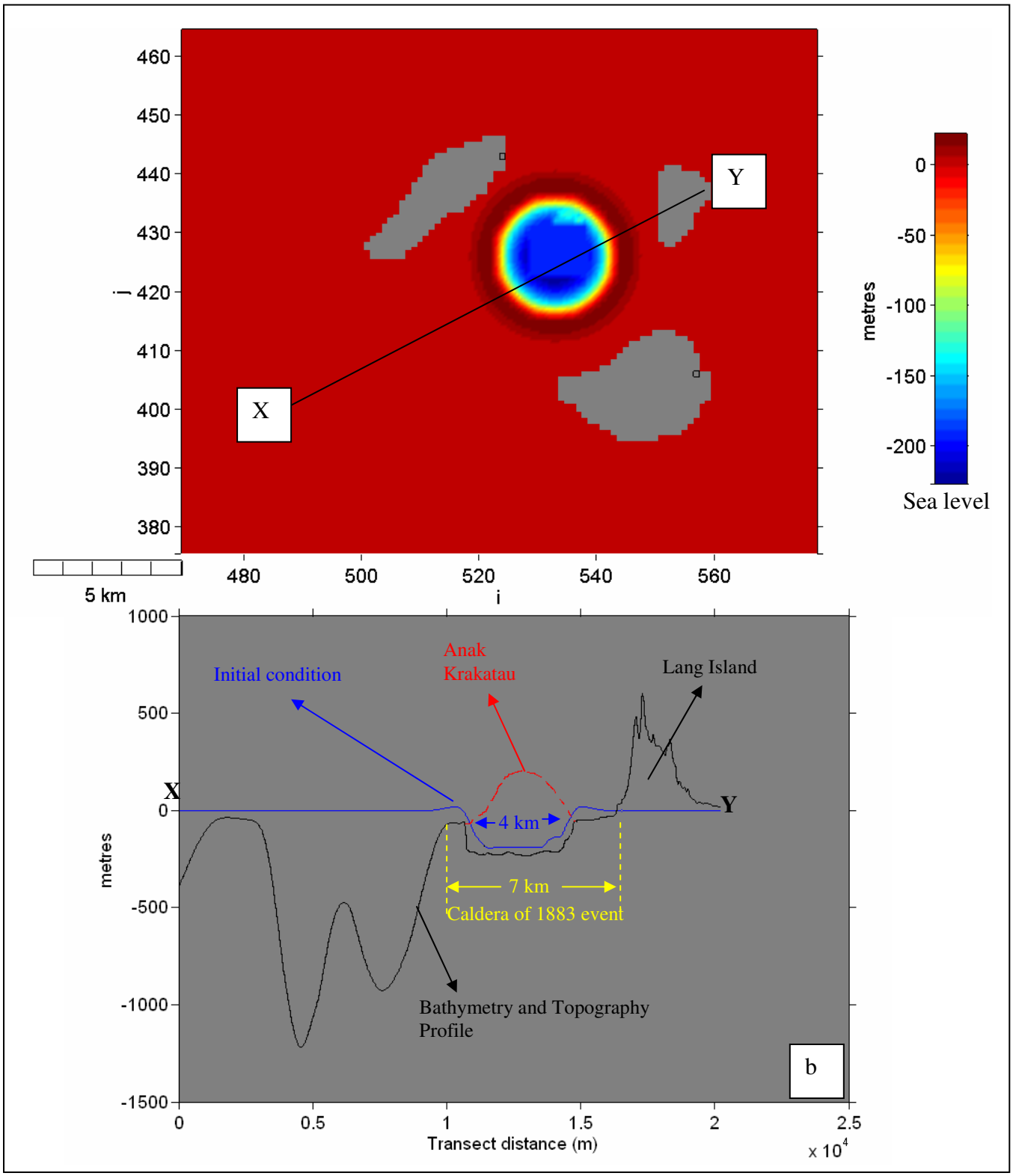

Figure 4.52. Plan view of the initial condition (a) and its cross-section computed using Le Mehaute and Wang (1996) with diameter of 4 km. The 1883 event had a diameter of 7 km.

Numerical Model Results

With a 2 km caldera radius from the center of the island, the initial disturbances are located inside the Krakatau Volcanic Complex as shown in Figure

4.51 and 4.52. The waves propagate outwards from the source through the gaps between Sertung and Krakatau Islands, Krakatau and Lang Islands, and Lang and Sertung Islands (Figure 4.53).

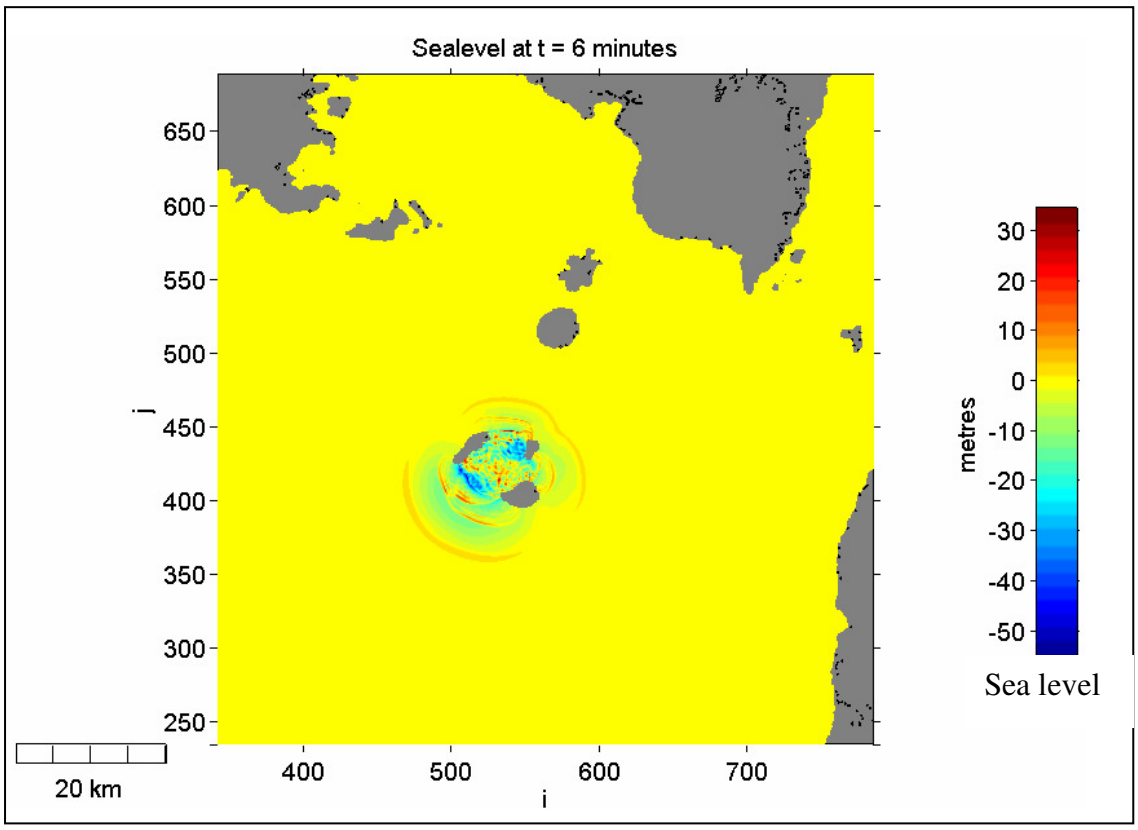

Figure 4.53. The tsunami propagates outwards from the generating area through the gaps between Sertung, Krakatau and Lang Islands with positive leading waves. The second and third waves have clearly formed at 6 minutes and starting to leave the generating area.

Wave oscillations inside the Krakatau Volcanic Complex create complex dispersive wave pattern. The waves propagate faster in the deeper regions to the southwest, west and northwest directions (Figure 4.54) and reach Sebuku Island in the northeast at the same time as they reach the southern tip of Teluk Betung Bay of Sumatra Island, twice (2x) the distance from the source to Sebuku Island.

Within 45 minutes, most of the waves reach the coastal areas surrounding the Sunda Straits, and enter the Java Sea. It is clear that towards the coast of West Java, leading negative waves are dominant (Figure 4.55), except towards Sebuku Island (including Kalianda and Radjabasa at the Sumatra Coast), and to the tip of Ujung Kulon, where the leading waves are still positive. Time histories of wave profiles show these evidences as illustrated in Figure 4.56 and Appendix 2.

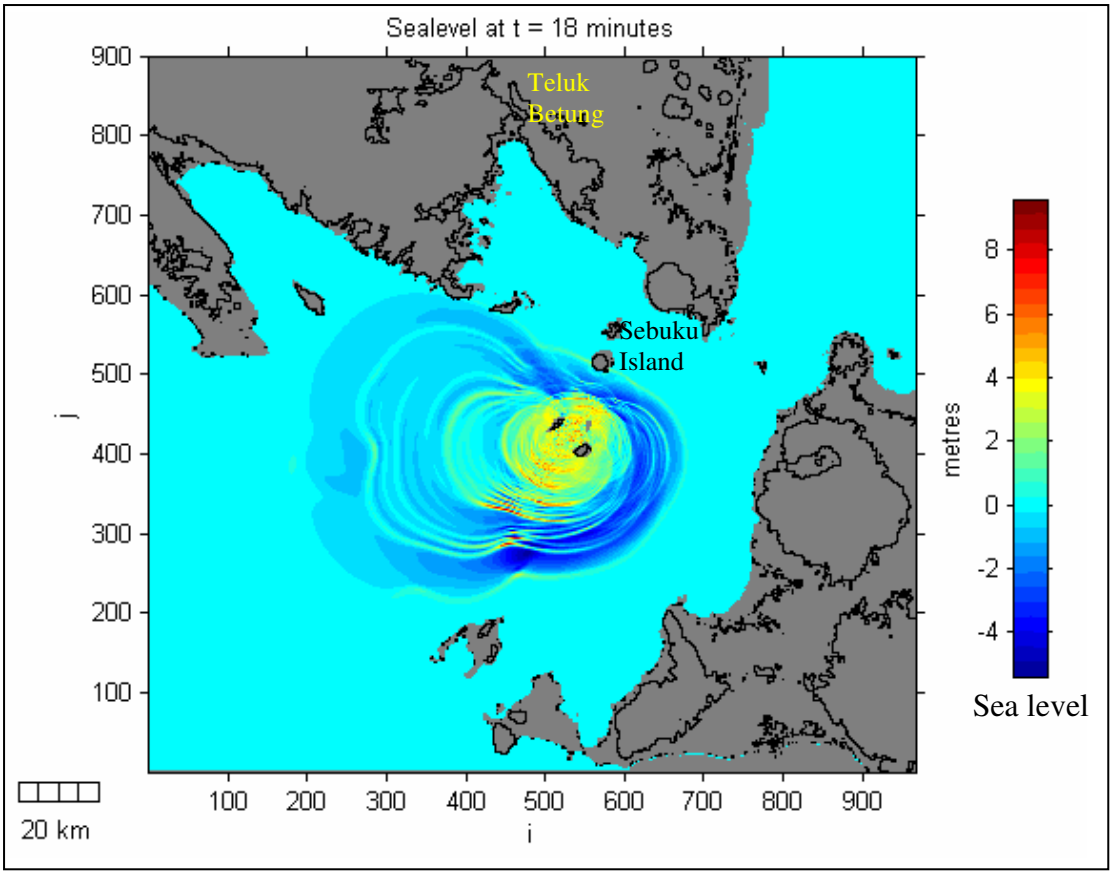

Figure 4.54. The simulated tsunami from Anak Krakatau propagates faster to the northwest, west and southeast, as these regions are deeper than the rest of the Sunda Straits.

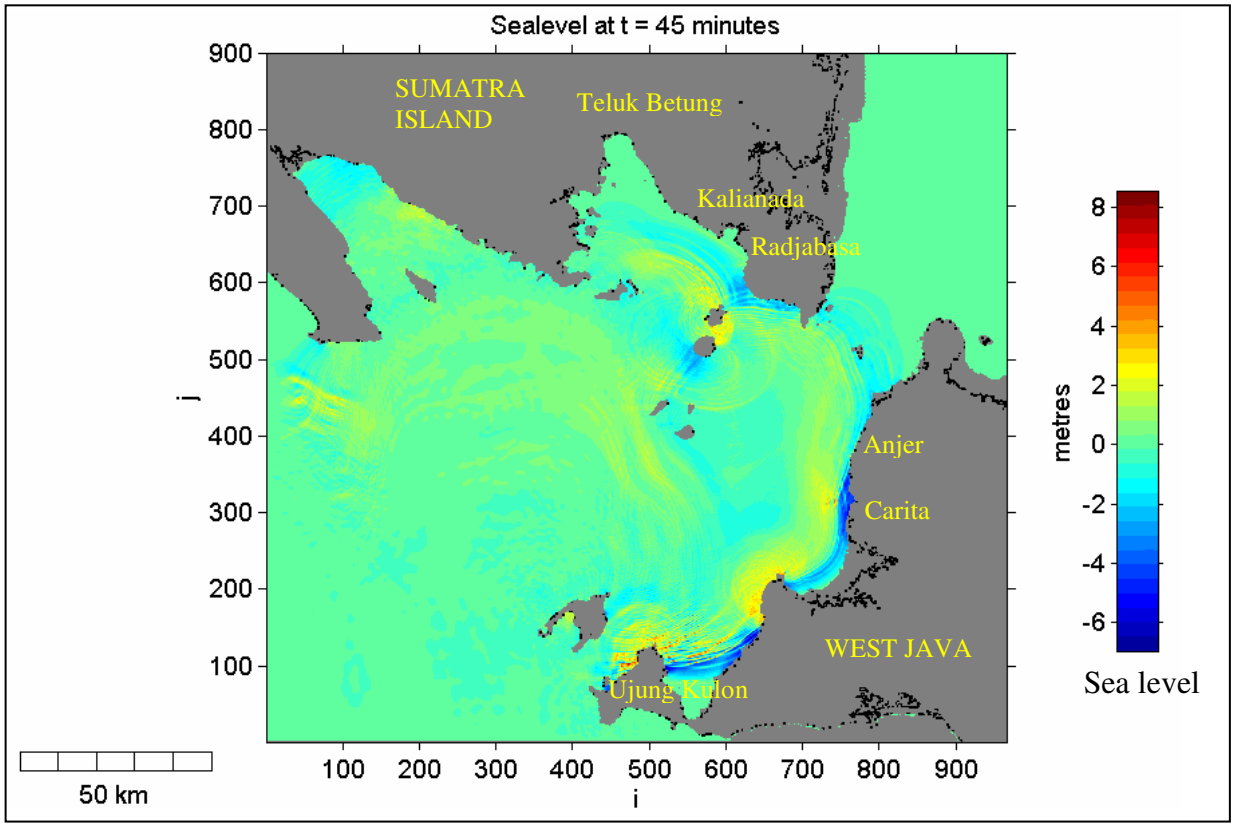

Figure 4.55. Within 45 minutes, tsunamis reach most of the coast around the Sunda Strait with leading negative waves propagating towards the West Java coast.

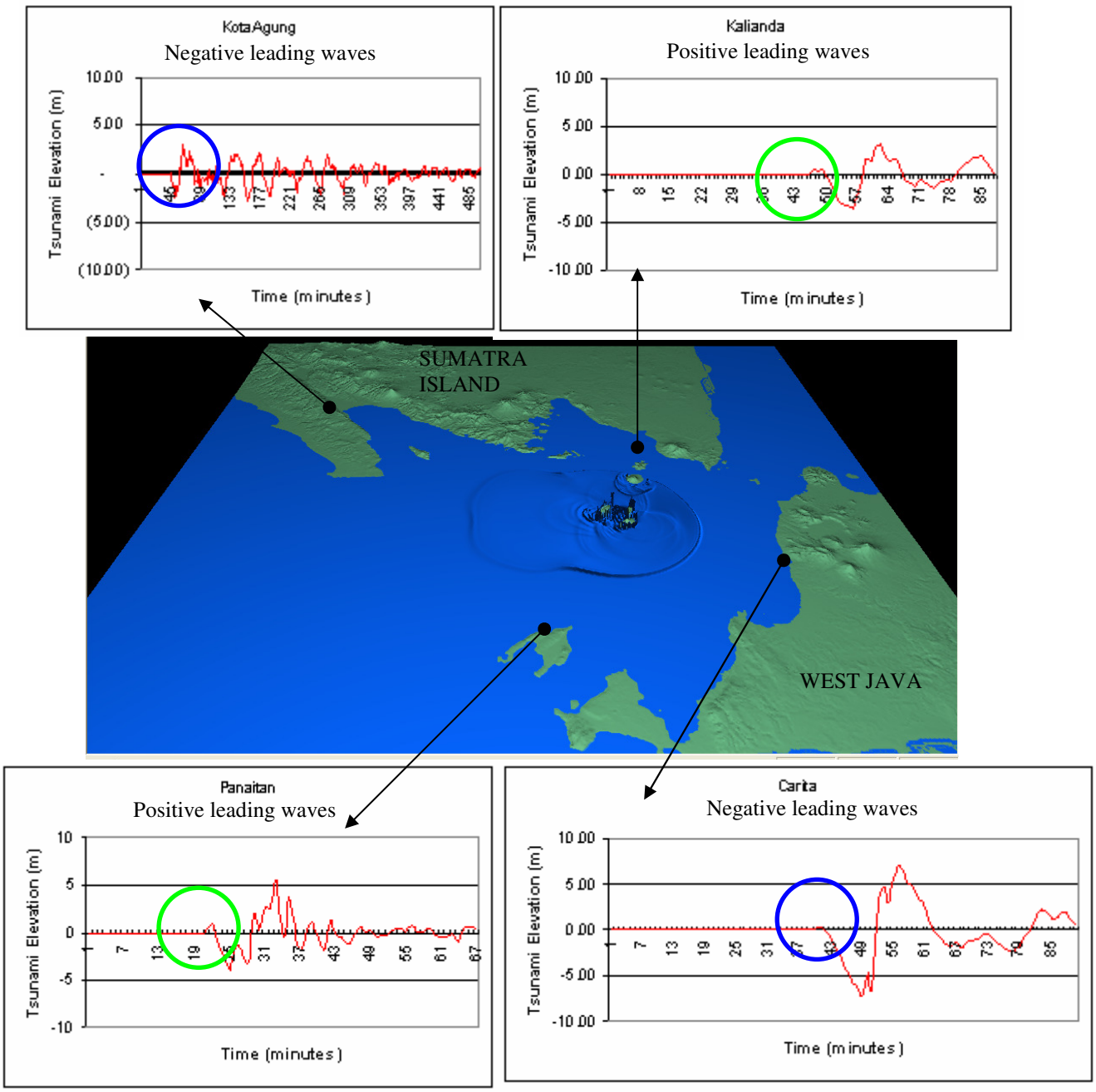

Figure 4.56. A time series of tsunami elevations show different leading waves around the coasts of Sunda Strait. The blue circles show negative leading waves, while the green circles show positive leading waves.

The highest tsunami elevation of nearly 9 m occurs at the tip of Ujung Kulon, and 4 -7 m along Anjer – Carita and Labuan coastal areas. The arrival time of the first waves is between 28 – 60 minutes. Along the Sumatra coast, the tsunami elevation varies from 1.5 to 4 metres. The arrival time of the first wave ranges from 18 to 66 minutes. The distribution of maximum tsunami elevation and the arrival time of the first waves are illustrated in Figure 4.57.

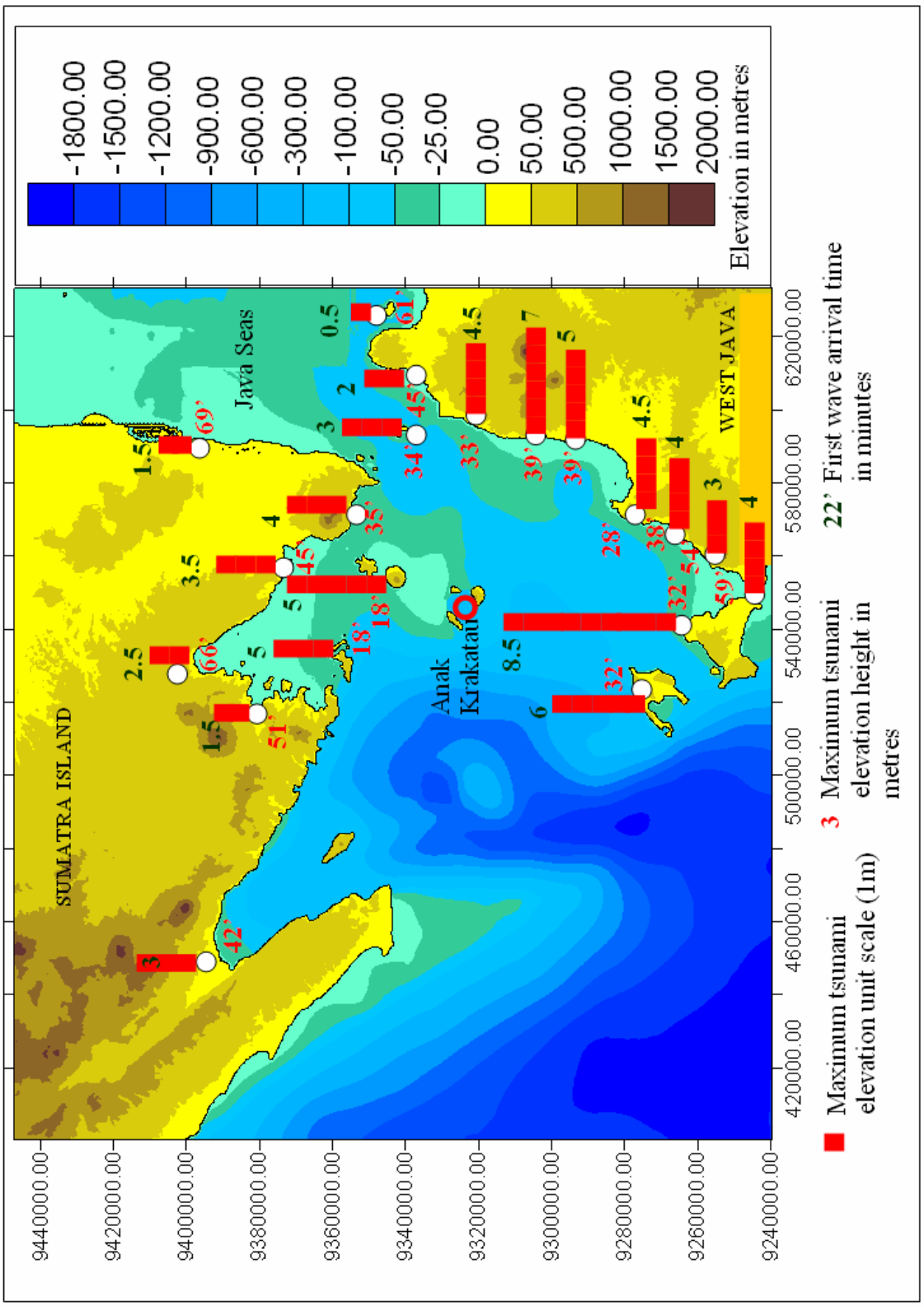

Figure 4.57. Maximum tsunami elevation around the coastal areas in the Sunda Strait (number in black), and the arrival time of the first tsunami waves reaching the coast (number in red).

4.4.2. Tambora Volcanic Tsunami Scenario

Slothers (1984) noted that tsunamis were observed during the Tambora eruption of 10 and 11 April 1815. Tsunami elevations between 1 – 2 m were reported at Besuki (East Java), and at several coastal areas of the nearby islands, such as Madura Island, and along the northern coast of Sumbawa, Lombok, Bali Islands, and as far as Maluku (Molluca) Islands to the east. Further evidence of tsunamis during the Tambora eruption was the presence of high salinity in the lake on Satonda Island, which was interpreted as due to being overtopping by tsunamis (Figure 4.58).

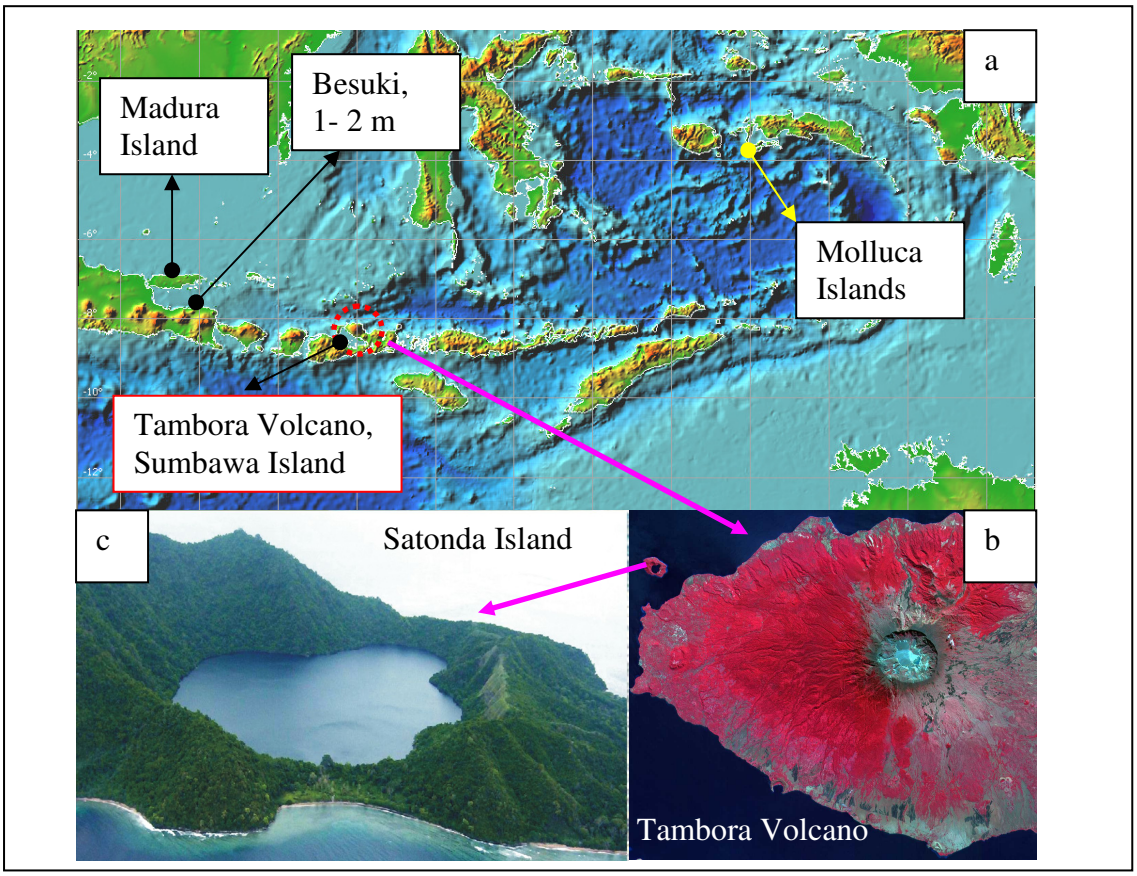

Figure 4.58. Tambora Volcano is located on Sumbawa Island (a), occupying the whole Sanggar Peninsula (b). Tsunami were observed at Besuki, Madura Island and Molluca Island (Slothers, 1984) during the 1815 eruption (a). The high salinity water in the lake on Satonda Island was thought to come from the ocean during the tsunami event of 1815 (Sutawidjaja et al., 2006).

Sigurdsson and Carey (1989) identified that at least 7 pyroclastic flows were generated during the event, which spread over most of the volcano and the entire peninsula (Sanggar Peninsula). Pyroclastic flows entered the ocean in all directions around the volcano, extending the coastline seaward to an unknown extent, and generating tsunamis (Sutawidjaja et al., 2006).

The volume of pyroclastic flow deposits on land was estimated as 2.6 km^3 DRE (Dense Rock Equivalent) area of with the total deposition area on the slopes of Tambora about 820 km^2, and for the surges about 874 km^2. The flows exceed a total thickness of 20 m, with an average thickness of 7 m, which indicates a minimum sub-aerial volume of 5.7 km^3 (Sigurdsson and Carey, 1987; Sutawidjaja et al., 2006). The size of the caldera is 7 km, with a depth of 1,100 m after the 1815 eruptions.

Initial Conditions

A single pyroclastic flow is modelled. This flow extends for 40 km from the caldera, as occurred during the 1815 event and is radially uniform with the subaqueous portion extending a further 15 km offshore. The initial profile was calculated using simple circular deformation with a leading positive wave. This replicated the wave profiles from a flume experiment of a single pyroclastic flow (Prasetya, 1998), as illustrated in Figure 4.59, that produced a leading positive waves with a trough behind it.

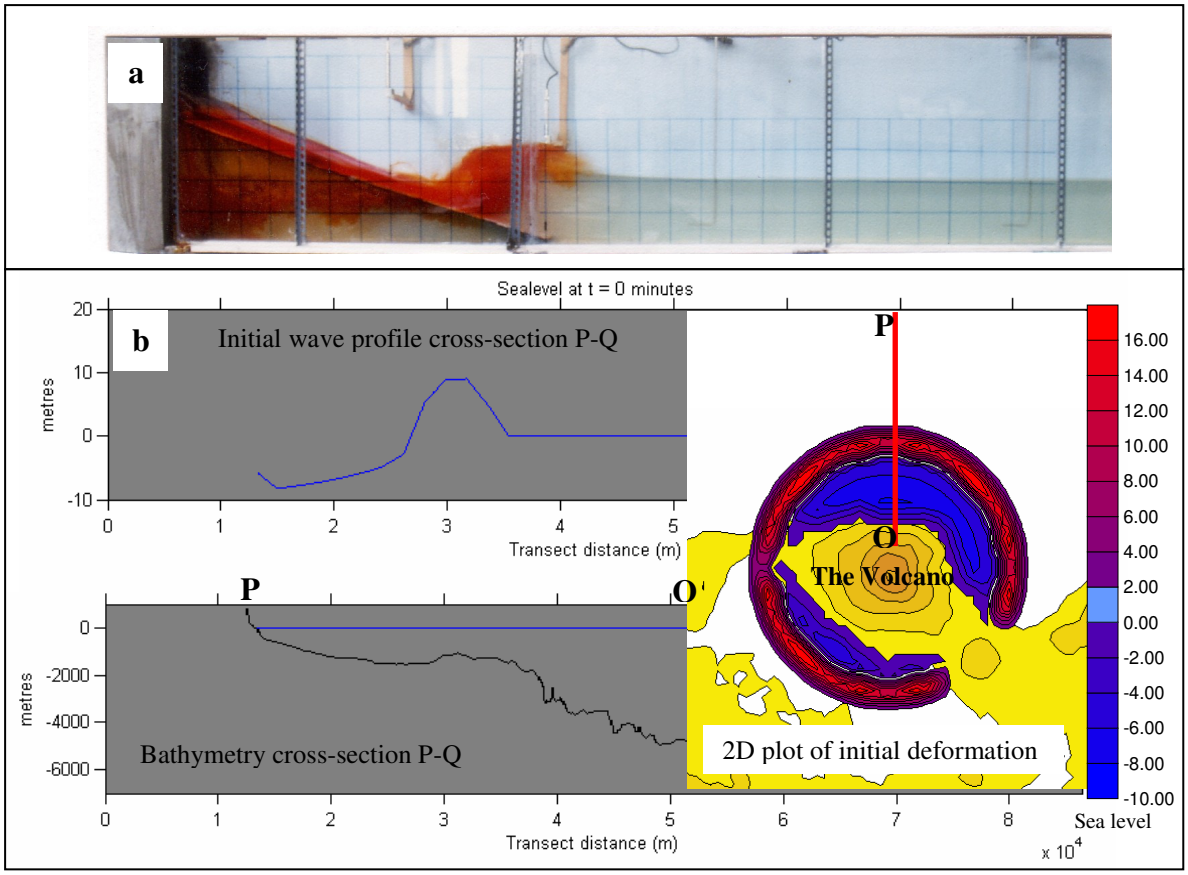

Figure 4.59. Initial condition of the tsunami caused by a pyroclastic flow with leading positive waves. The computed profiles (b) replicate the experimental profile (a). Scale bar unit is in metres.

The trough behind the leading positive waves within the generating area also occurs for sub-aerial landslides that generate tsunamis, as was demonstrated by Fritz et al., 2001. The experiments show that the presence of a water level depression (trough) behind the positive leading waves propagating offshore creates other wave that rushes back towards the coast. This possibly will cause high runup, depending on the beach slope, while the positive leading waves propagate offshore.

Numerical Model Results

The pyroclastic flow mechanism generates a leading positive wave towards the Java and Flores Seas, and also inside Saleh Bay (Figure 4.60). Time histories of wave profiles from the coastline to offshore, show that the waves are gradually dispersed when they propagates into deeper water. Meanwhile, the waves that rushing back towards the coast produces a high runup along the coast (Figure 4.61 and Appendix 3).

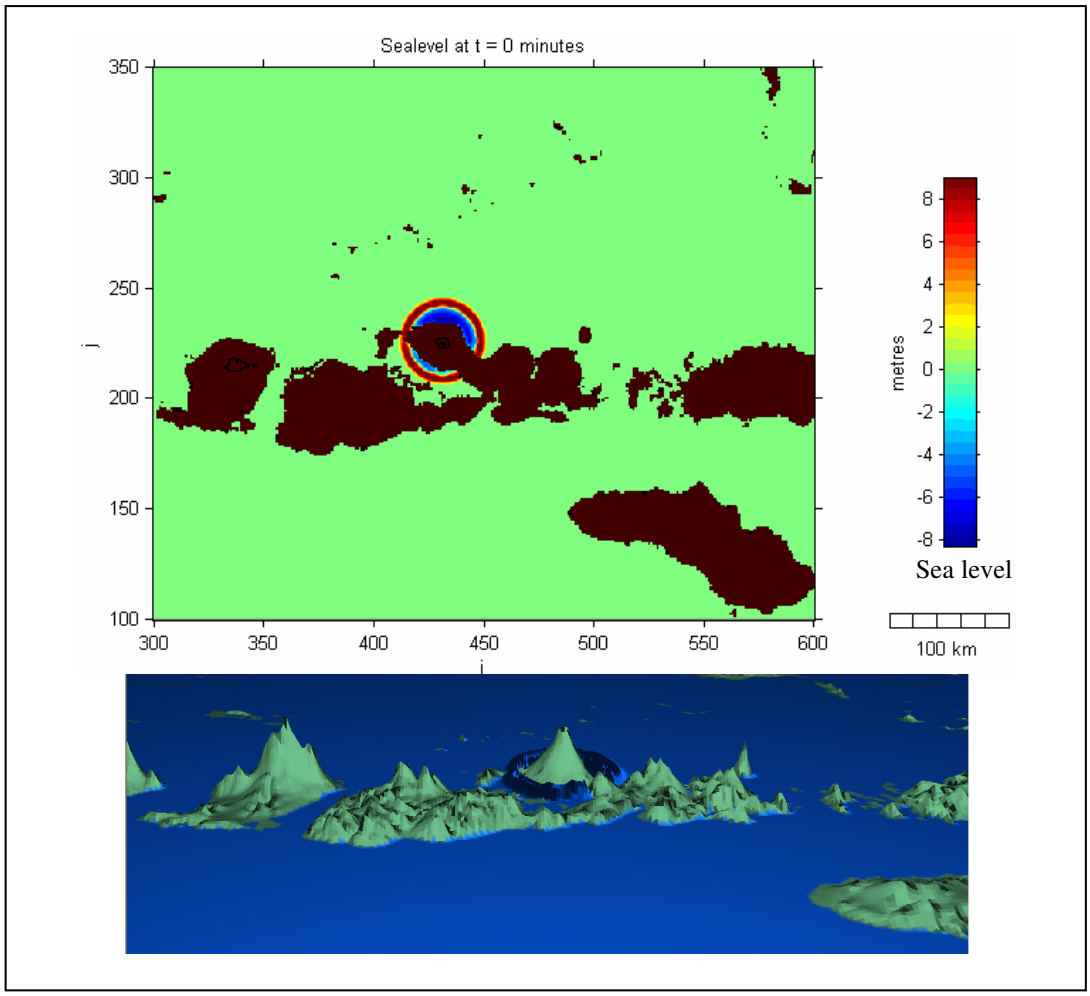

Figure 4.60. Initial conditions for tsunami generated by pyroclastic flows calculated using a symmetrical flow distribution around the volcano as occurred during the 1815 event. The flow is assumed enter to the sea at 40 km from the center of the volcano, and subaqueously propagates a further 15 km offshore.

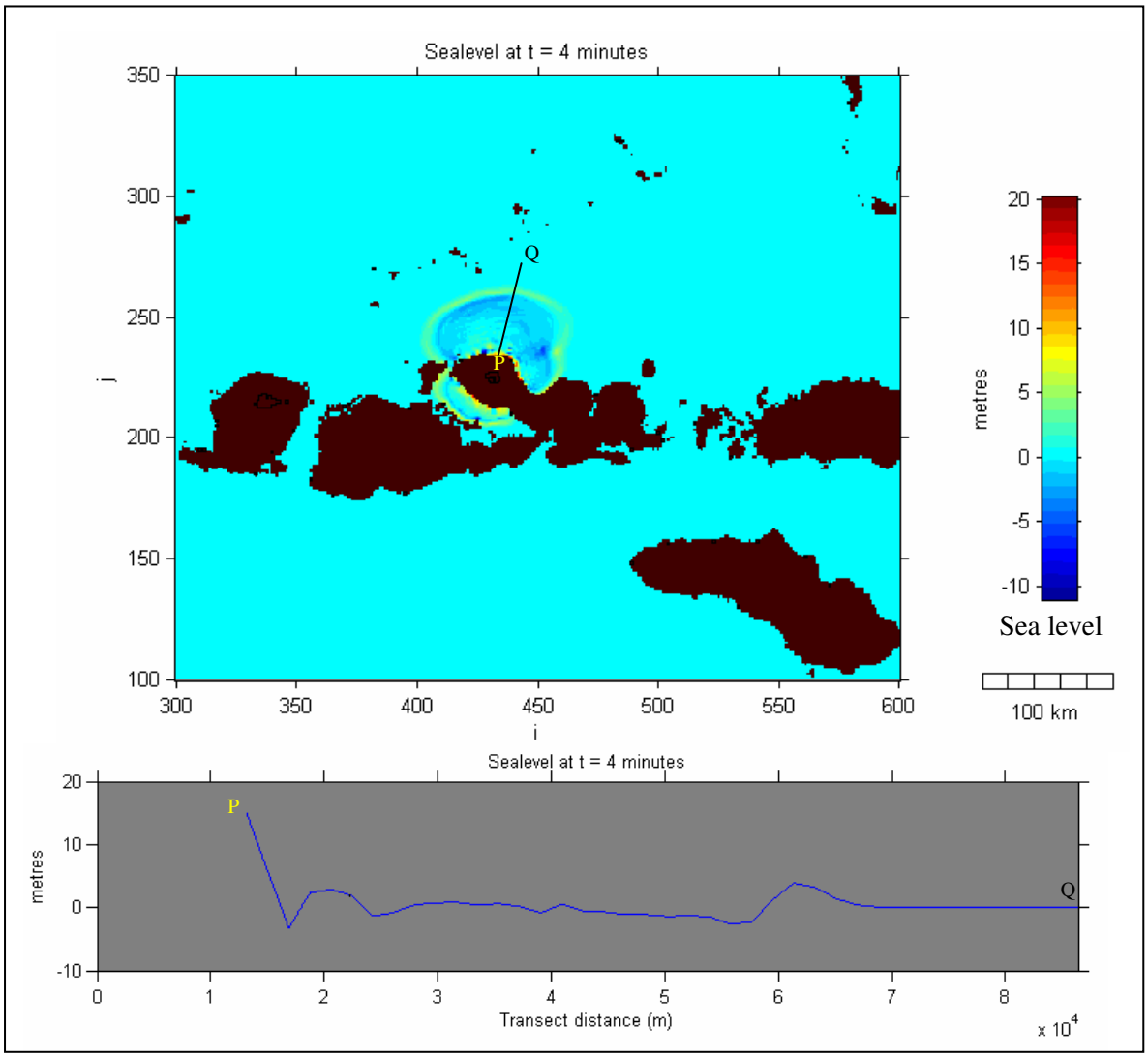

Figure 4.61. Pattern of tsunami propagation after 4 minutes showing waves rushing back to the coast to produce a high tsunami runup along the Sanggar Peninsula, while the leading positive waves, that propagate further offshore are dispersed rapidly.

With the existence of offshore islands, wave propagating to the north is slower than those heading east towards the Flores Sea, and to the west along the northern part of Lombok Island (Figure 4.61). Within 23 minutes, the tsunami elevation at offshore islands varies between 1.5 to 3.5 m, while larger tsunami from 4 – 8 m still occur inside Saleh Bay due to wave resonance (Figure 4.62 and 4.63).

The forced wave oscillations inside Saleh Bay occur because the Bay is connected to the Java Sea by two narrow straits between Moyo Island and the main land. The model also shows the distribution of tsunami elevation outside the Bay along the northeast coast of Sanggar Peninsula in Java Sea have same magnitude with what observed inside the Bay.

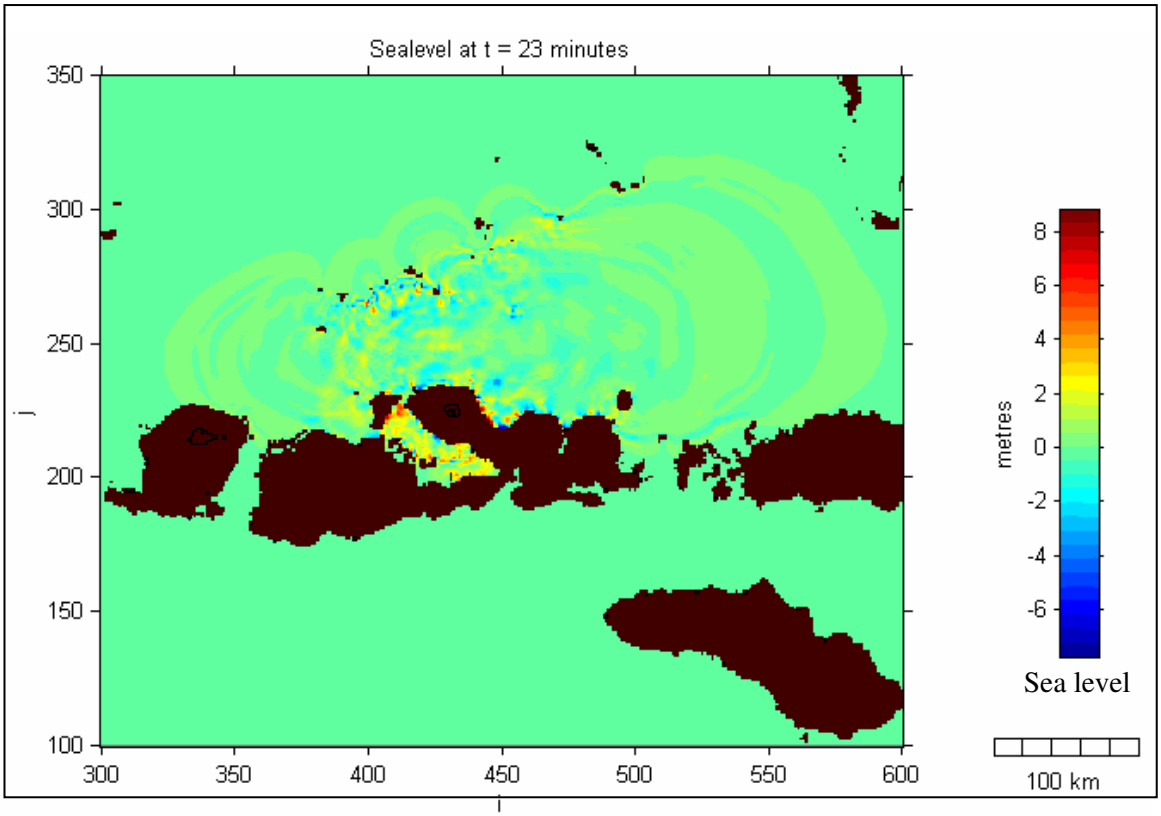

Figure 4.62. The tsunami waves propagate faster to the east into deeper water regions, compared to the north and west. The offshore islands to the north slow down tsunami propagation and also cause complex wave pattern within this zone.

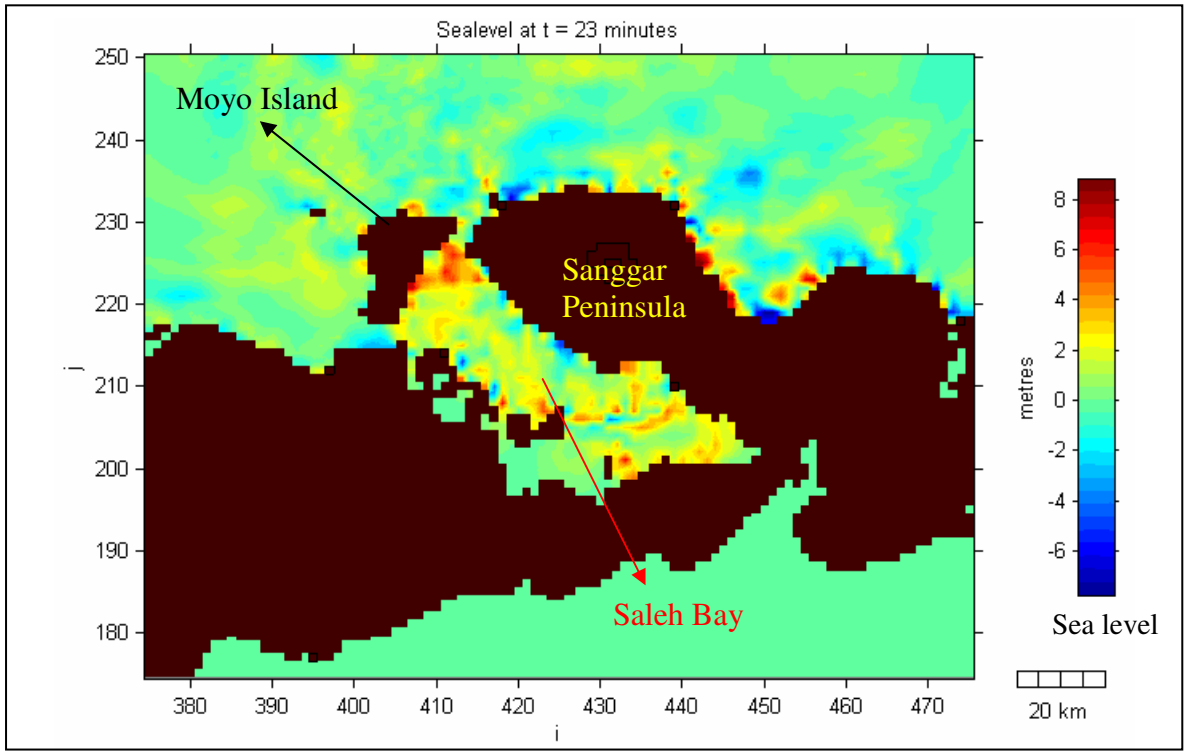

Figure 4.63. Saleh Bay with two narrow straits experienced wave resonance that creates a high sea level within the entire Bay.

Within 1.5 hours, tsunamis reach the northern coast of the East Java coast with heights between 0.5 to 1 m (Figure 4.64). As noted by Slothers (1984), during the 1815 event, this region experienced a tsunami of 1 – 2 m. The model also shows that tsunamis reach the southern coast of Sulawesi Island, and propagate further to the Makassar Strait and Flores Sea. Within 5 hours, most of the regions were affected by tsunamis (Figure 4.65).

The maximum tsunami elevation distribution shows that most of the region nearby the source experiences the highest tsunami elevation including along the northern coast of Sumbawa, Flores, Lombok and Bali, as well as to the offshore islands (Figure 4.66). The maximum tsunami elevation of 27 m occurs at the northern coast of Sanggar Peninsula, within the perimeter of the volcano, and elevations gradually decrease further away from the source to the east and the west. Inside the Saleh Bay, the maximum tsunami elevation is 20 m, with an average high of 7 m throughout the Bay (Figure 4.67).

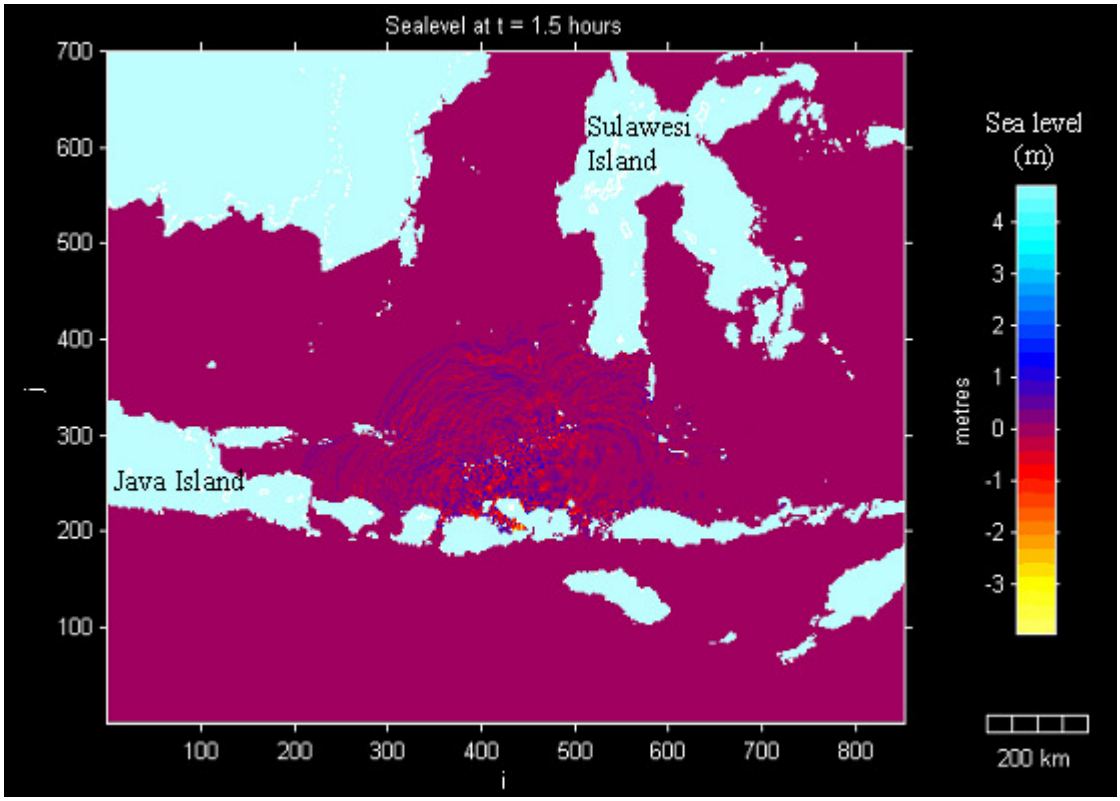

Figure 4.64. The tsunami reaches South Sulawesi Island and East Java within 1.5 hours. The tsunami elevation at the northern coast of East Java is between 0.5 to 1 m.

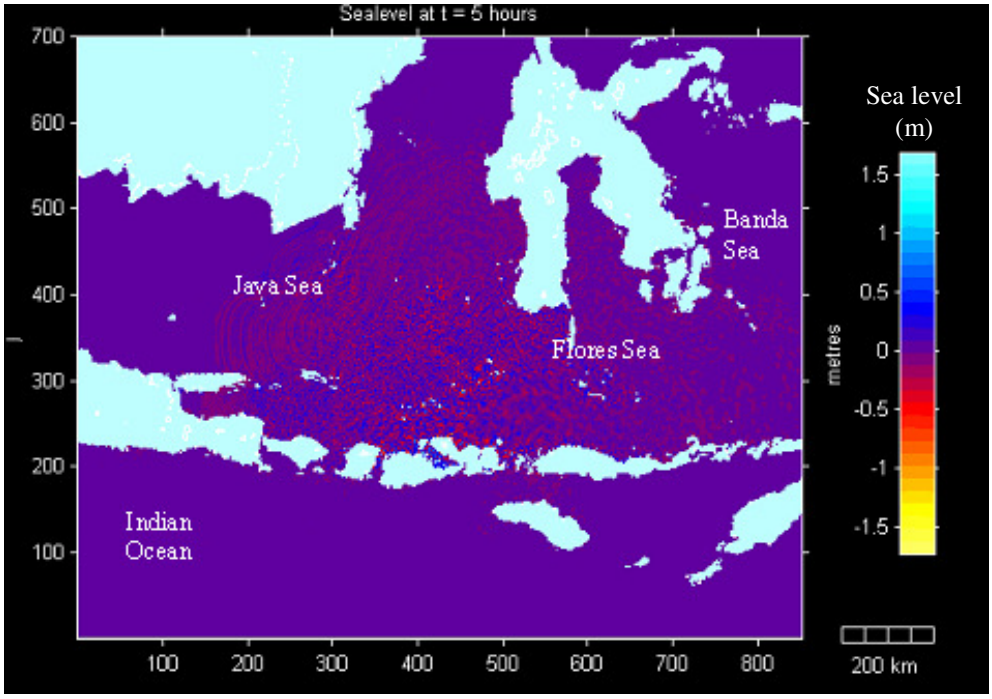

Figure 4.65. Within 5 hours, tsunamis affect most of the region around Java, Flores and Banda Seas, and also penetrate to the Indian Ocean through the straits between the islands.

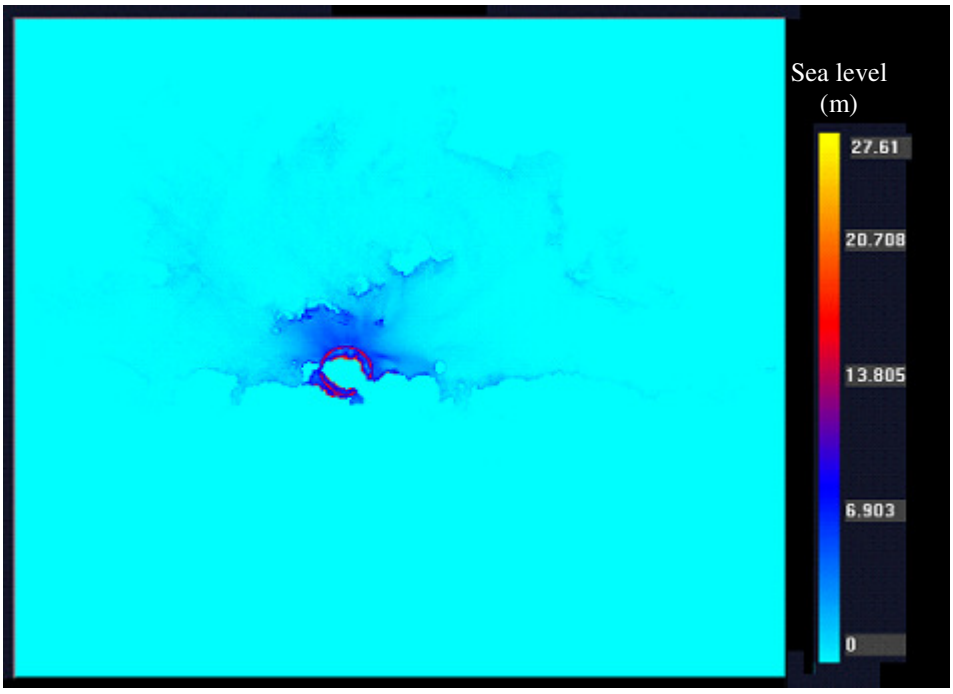

Figure 4.66. The maximum tsunami elevation distribution shows that most of the region close to the source experiences high tsunami elevation.

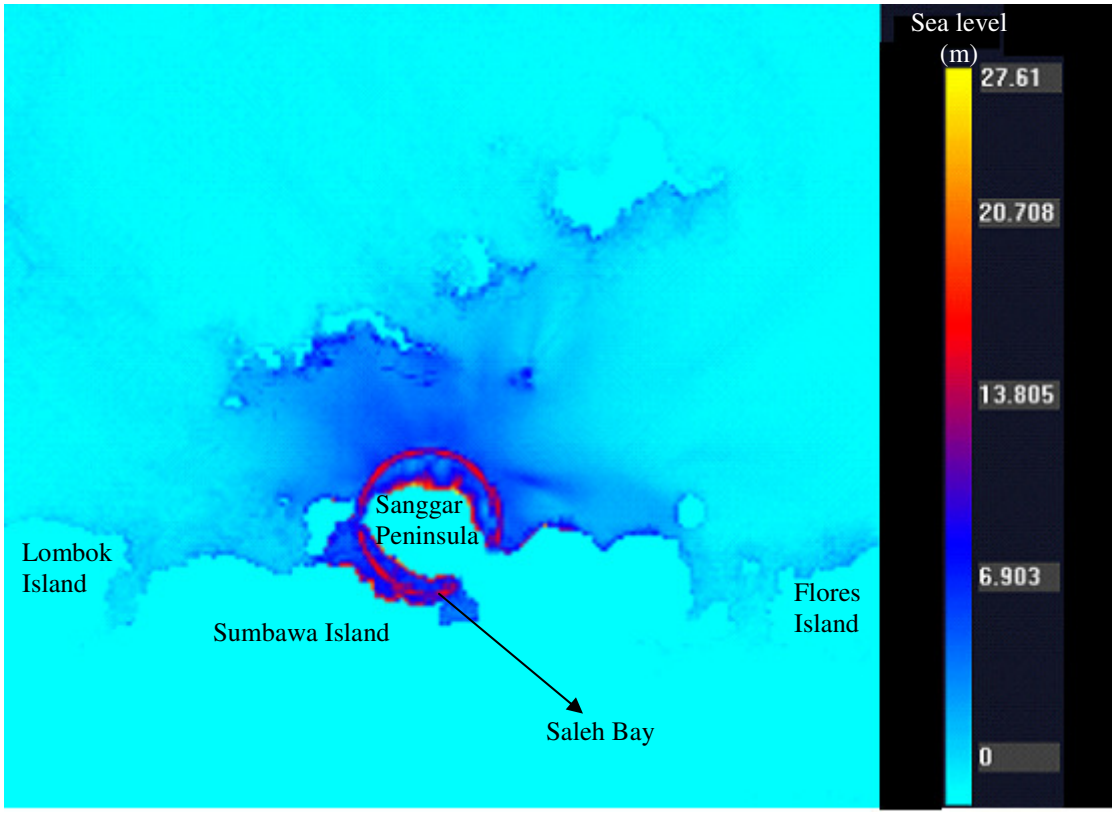

Figure 4.67. The highest tsunami elevation occurs along the coast of Sanggar Peninsula (flanks of the Tambora Volcano) due to the waves that rush back to the coast where the pyroclastic flows enter to the sea, as also occurs inside the Saleh Bay.

4.4.3. Banda Api Volcano

Banda Api volcano forms a conical peak rising to 640 m at the center of a 3-km wide island in a 7 km wide caldera. This caldera also has three islands along the margins of the southern and eastern walls: Lonthor, Pisang and Kapal. The three islands are considered as a remnant of the pre-caldera volcano (Figure 4.68). Since 1586, Banda Api volcano has erupted 26 times, consisting of strombolian eruptions with occasional lava flows that reached the sea. However, no tsunamis have been reported. The most recent eruptions occurred from 9 - 17 May 1988.

Numerical modeling of possible tsunamis during the formation of a 7 km wide caldera was carried out. The model grid resolutions (bathymetry and topography) were not adequate to assess the potential tsunami generated by the present day Banda Api Volcano (diameter of 3 km), given that the resolution of the grid is 1.852 km. No bathymetry data are available for a finer grid resolution.

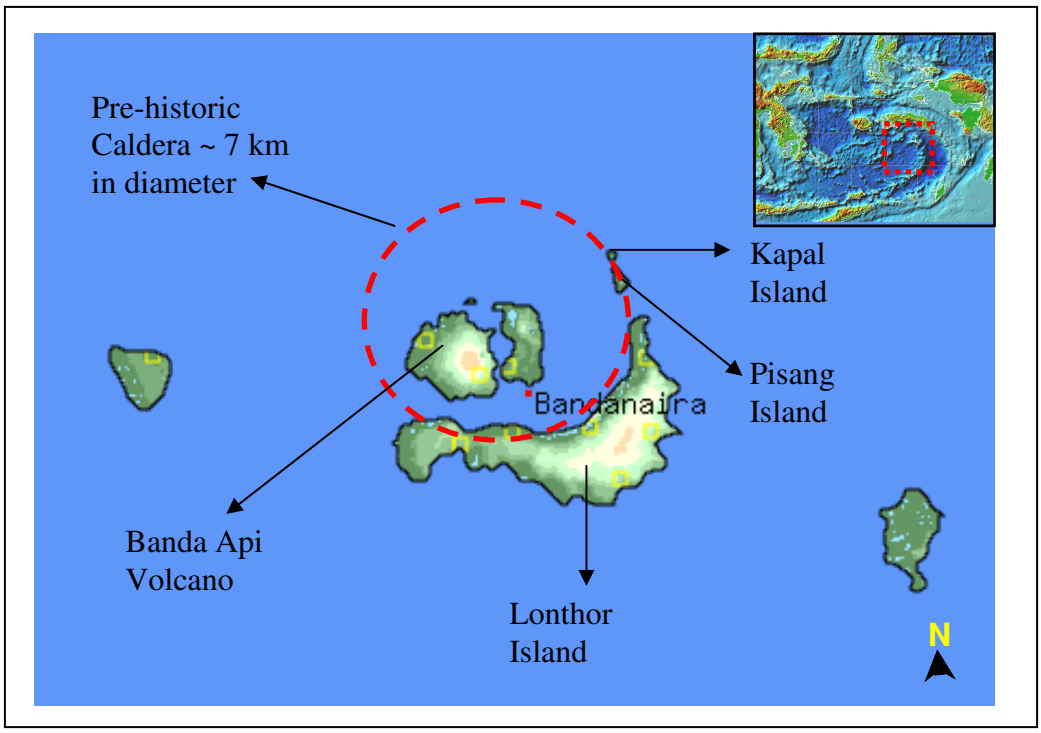

Figure 4.68. Banda Api volcano located within a 7 km wide caldera that has three islands on the southern and eastern walls: Lonthor, Pisang and Kapal. These three islands are considered as a remnant of the pre-caldera volcano.

Numerical Model Results

A seven (7) km wide caldera with depth = 240 m, and an initial leading waves height = 3 m, provides the initial tsunami conditions as illustrated in Figure 4.69. This initial disturbance formed radial impulsive waves with a diameter ~ 20 km and a maximum height ~ 60 m. This wave occurs 5 minutes after the caldera collapse, and during this time negative leading waves become dominant (Figure 4.70). Most of the waves propagate to the north, west and east, since the remnant of the pre-caldera volcano at the southern walls obviously affects propagation to the south and southeast. Within 12 minutes, the first leading negative waves reach the south coast of eastern Seram Island.

Three minutes after the first leading negative waves reach the shore, tsunami elevations up to 40 m occur along the southern coast of eastern Seram Island. Four minutes later, the southern coast of central Seram Island experiences > 40 m of waves in a large pocket bay perpendicular to the source. Tsunami waves continue to propagate westward to Seram and Buru Islands, and produces high tsunami elevations along the southern coast ranging from 20 – 50 m (Figure 4.71).

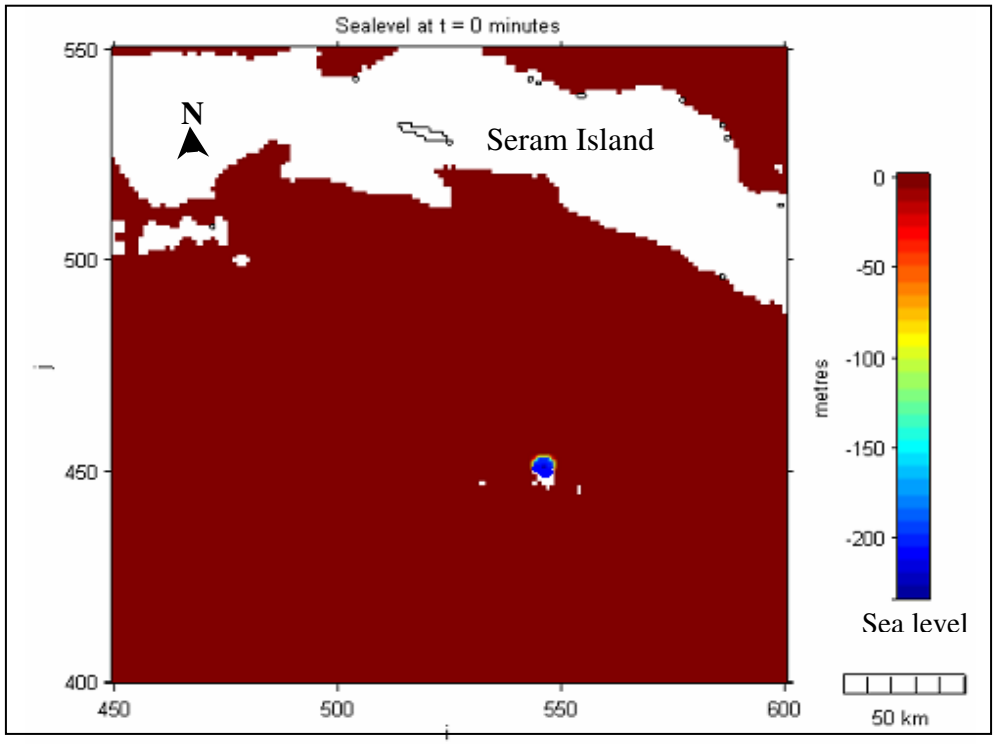

Figure 4.69. Initial conditions of a tsunami produced by the pre-historic caldera with diameter = 7 km, and depth = 240 m.

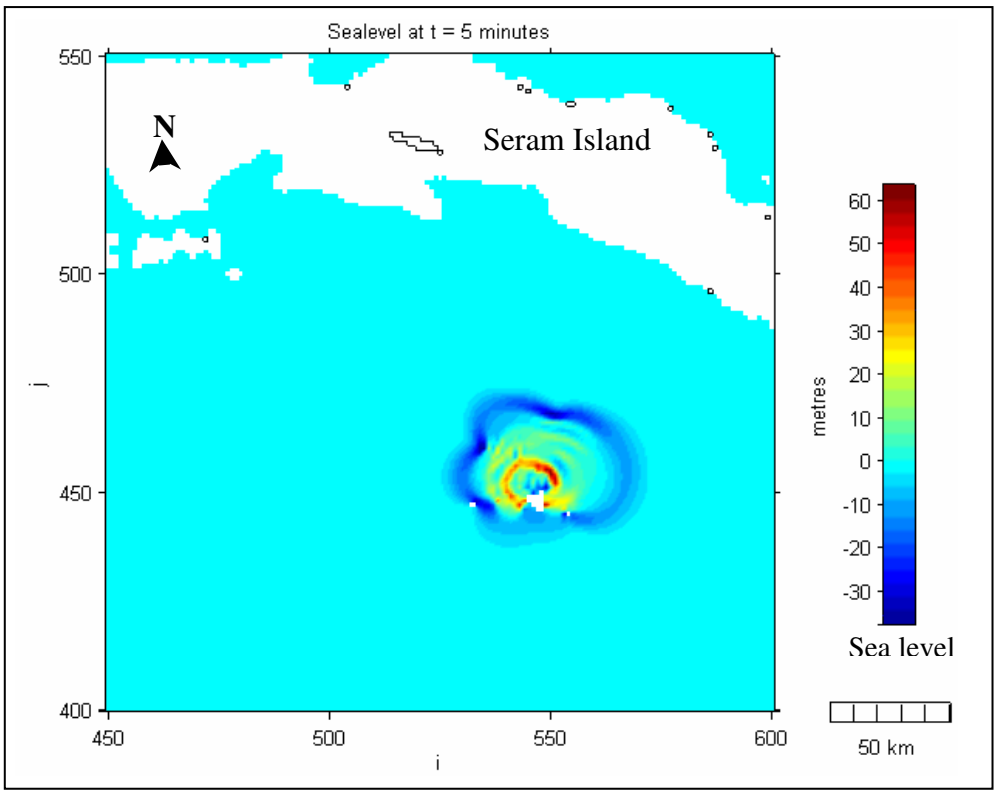

Figure 4.70. Radial impulsive waves are formed with a diameter ~ 20 km within 5 minutes after caldera collapse. A negative leading wave is obvious and becoming dominant and the remnant of the pre-caldera volcano affects southward wave propagation.

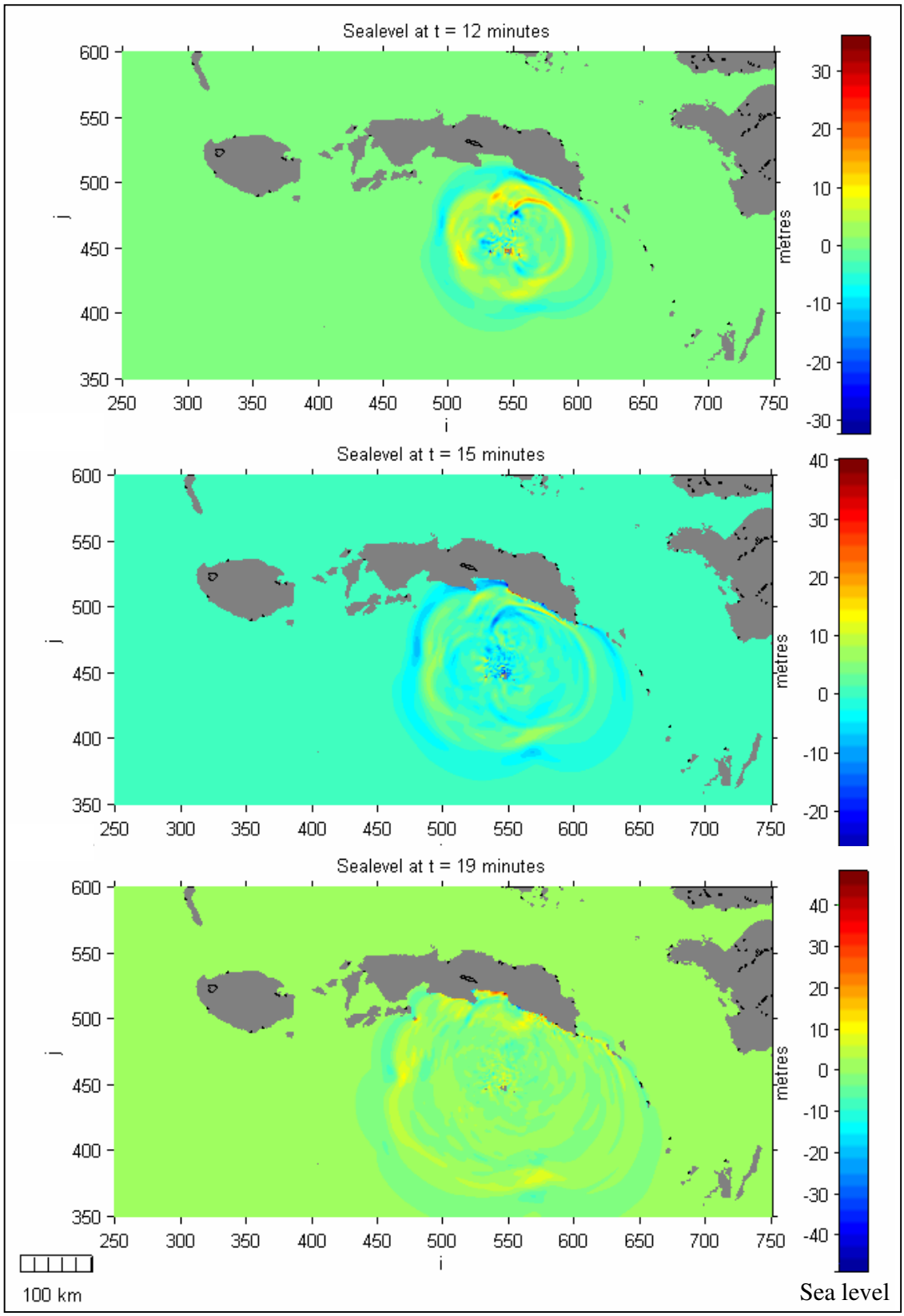

Figure 4.71. Sequences of wave propagations that shows a tsunami is affecting the southern coast of Seram, Buru and the neighbouring offshore islands.

After 43 minutes, the tsunami affects a wider region in the Banda Sea, such as the west coast of Papua Province below Bird Head, Kei Kecil Islands, and further south to Tanimbar and Ombai Islands (Figure 4.72). The effect of the remnant pre-caldera volcano (Lonthor, Pisang and Kapal Islands) on the wave propagation to the south and southeast is less evident then during the first 5 minutes after caldera collapse.

Tsunamis did not propagate much to the north, since Seram and Buru Islands blocked most of the waves (Figure 4.72 and 4.73). However, this caused the tsunami elevation along the southern coast of Seram and Buru Islands to be higher compared to other areas surrounding the Banda Sea. After 120 minutes, tsunamis affect most coastal areas around the Banda Sea and propagate further to Arafura (Aru), Timor, Flores and Java Seas (Figure 4.73).

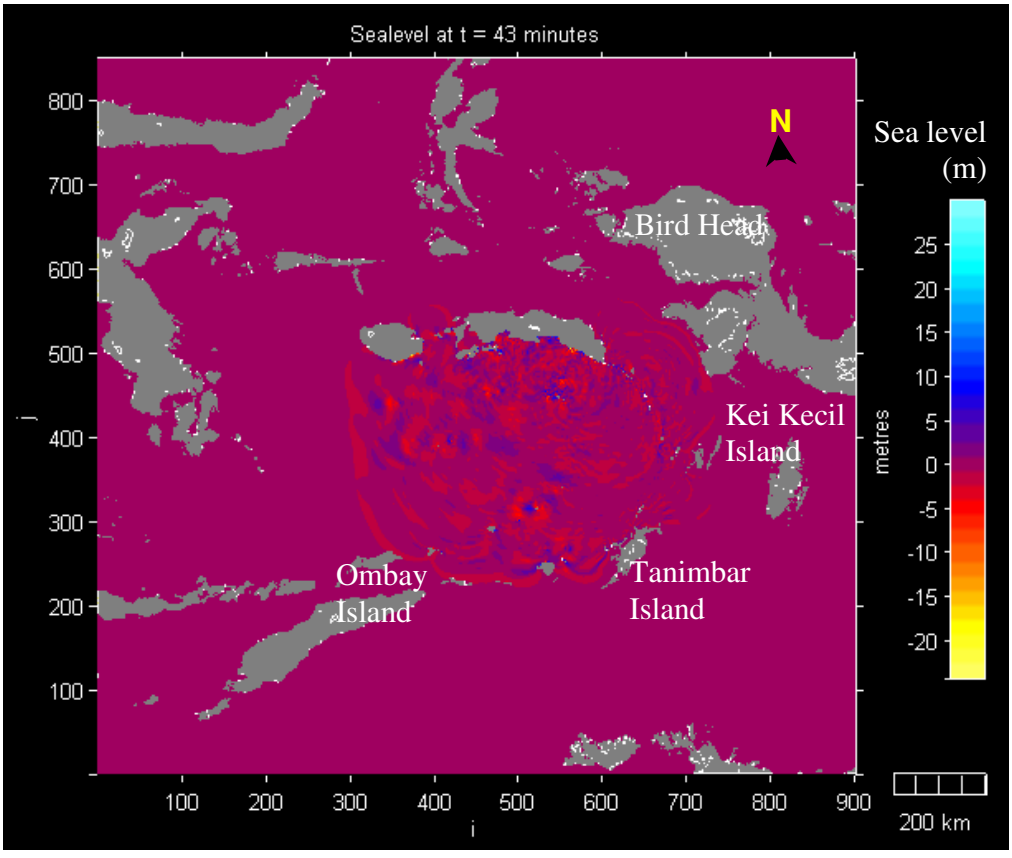

Figure 4.72. Tsunami propagation pattern after 43 minutes shows the affecting areas along the southern coast of Seram, Buru and the neighbouring offshore islands.

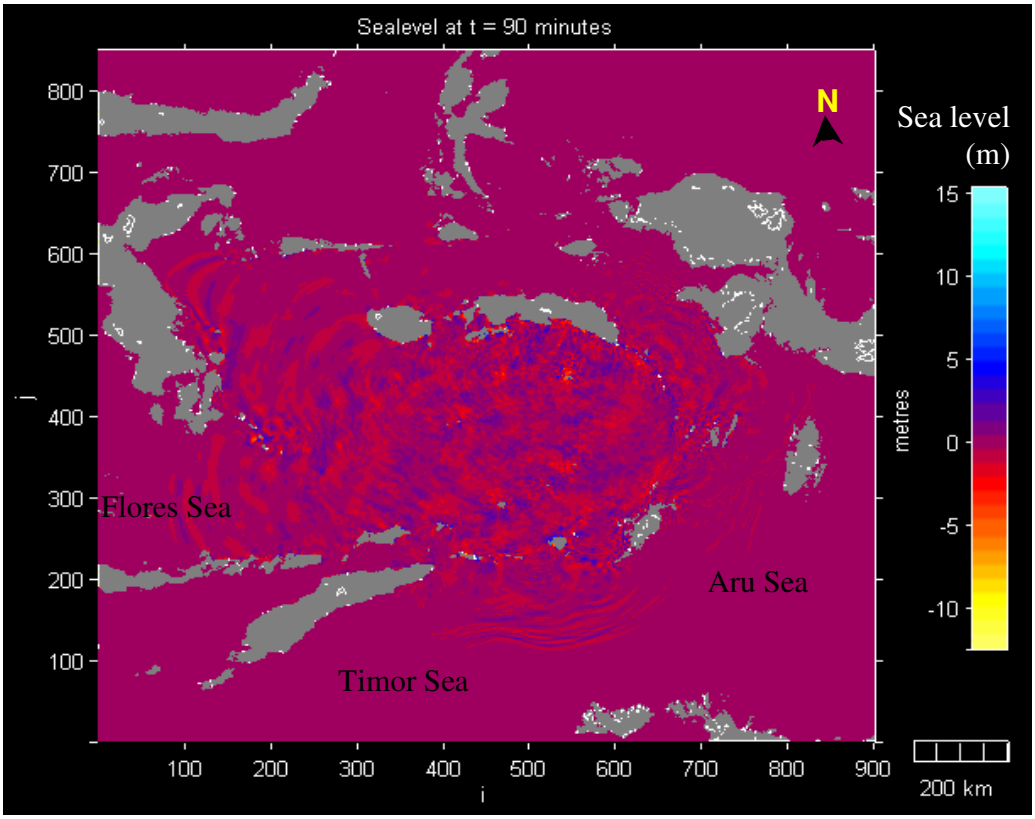

Figure 4.73. The tsunami propagates further to the Aru (Arafura), Timor and Flores Seas but not to the north since Buru and Seram Islands block most of the waves. As a consequence, tsunami elevations along the southern coast of Buru and Seram Island are higher compared to other affected coastal areas.

The maximum tsunami elevation distribution plot shows that tsunami wave focusing mostly occurs towards the southern coast of Seram Island, and to the west (Figure 4.74). While to the south, there is only one wave-guide along ridges of the island volcanic arc. No wave focusing occurs to the east, since most of the bathymetric conditions within this region are uniform, gradually shoaling towards Papua Island through the chain of offshore islands.

The highest tsunami waves occur along the southern coast of Seram Island, where they reach as high as 78 m. Historical records within this region for a 1674 for earthquake source (M_s = 8.0) report a maximum wave height (H_{max}) of 80 m. This may be correct but

the source was probably not a fault mechanism, but a secondary mechanism such as submarine landslide or slumping.

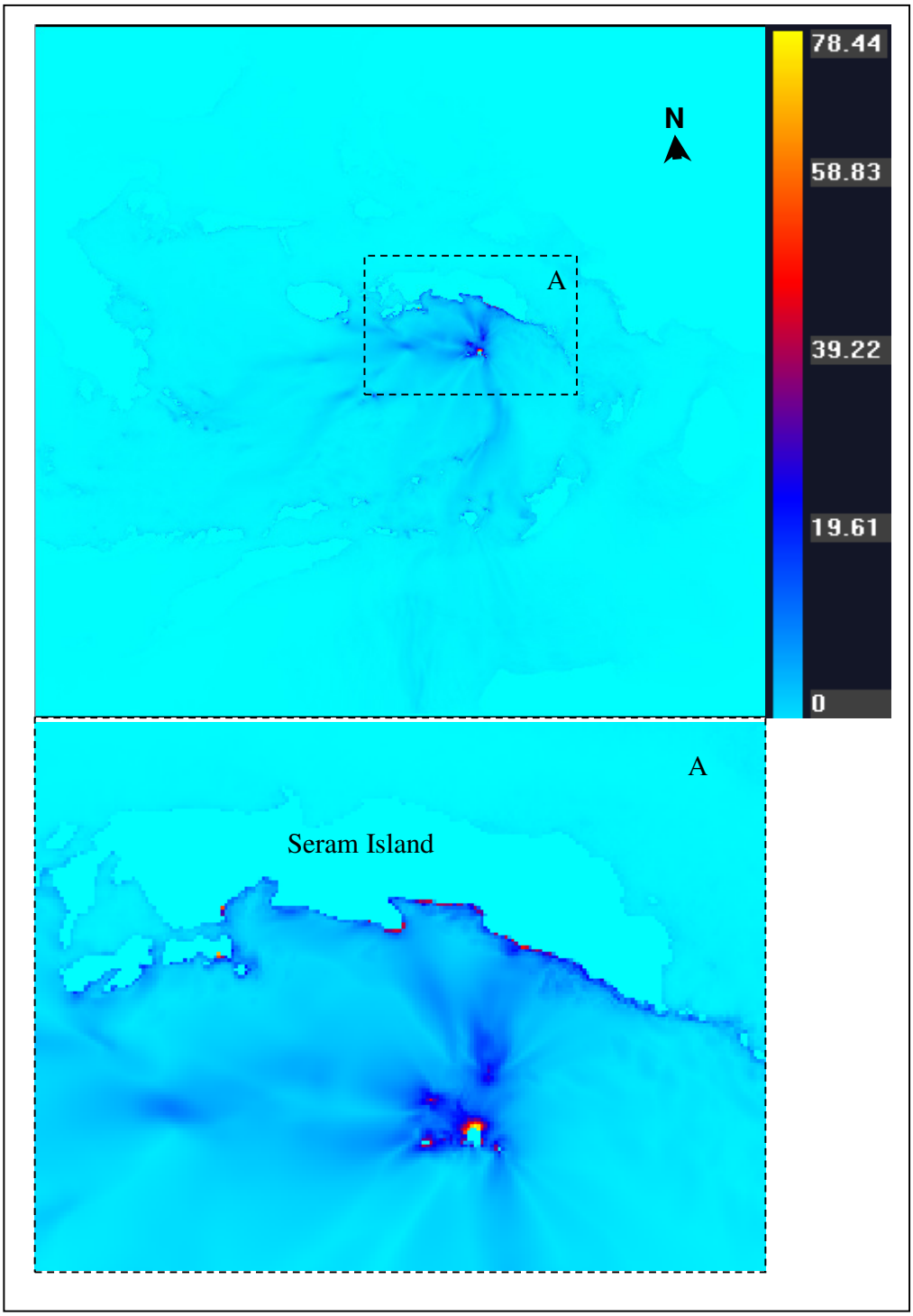

Figure 4.74. The maximum tsunami elevation distribution around the Banda Sea, shows that most of wave focusing occurs toward Seram Island and to the west. As a consequence of these, most of the highest tsunami elevation occurs along the southern coast of Seram Island (A).

4.5. Discussion

Numerical model simulations of historical and potential tsunami sources show that most coastal areas of the Indonesian Archipelago are susceptible to tsunamis from earthquake and volcanic sources. This must be considered in future re-development and coastal hazard management along the Indonesian coast. Further, it is important to understand the characteristics for each tsunami from each source in order to define a tsunami hazard zone. Tsunami hazard mitigation should consist of at least (Cox, 1979; NTHMP, 2001):

- A tsunami warning system to indicate where and from which coastal areas people should be evacuated;
- A land-use management system to designate coastal areas were usage should be restricted, construction should be prohibited, or specific design criteria should pertain, and designated evacuation routes and site for refuges should be established; and
- An insurance system based upon coastal areas of risk.

Numerical modelling results show that tsunami generated by earthquake sources posses different characteristics to those generated by volcanic sources, as identified previously by de Lange et al. (2001). Tsunami from earthquake sources usually consist of 3 to 7 waves; and in most cases, the 2nd or 3rd wave is the most dangerous both in the near and far field. For the volcanic sources, it depends on the source mechanism. If it is generated by a single mechanism, such as caldera collapse, pyroclastic flows or submarine explosion, in most cases the first wave is the most dangerous in the near field. But, for the far field, each source had its own characteristics. For example, the scenario of caldera of collapse for Banda Api volcano where tsunami arrived at the east coast of Sulawesi Island as a wave packet (Figure 4.75), comparable to the far-field tsunamis from earthquake sources (in this case the Northern Sulawesi Trench scenario) (Figure 4.76) that propagate for a long distance without losing their characteristic (non-dispersive). Numerical modelling results shows that maximum tsunami elevations at the coastline range from 8 – 25 m for most of the earthquake sources, and more than 40 m for the volcanic sources.

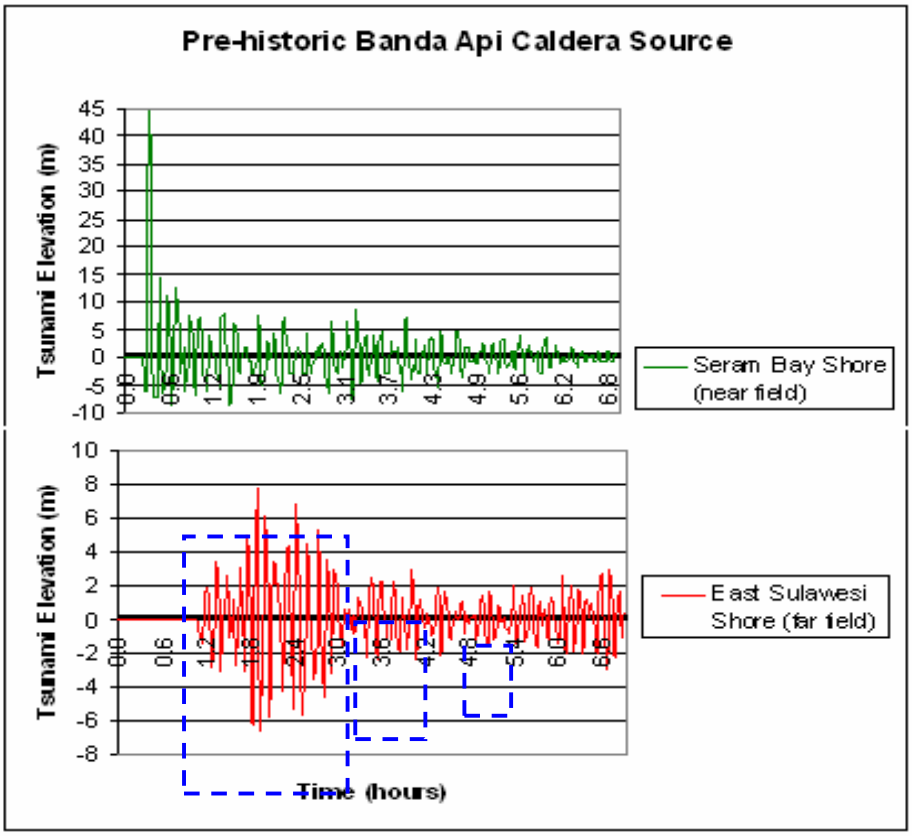

Figure 4.75. Time histories of a tsunami generated by caldera collapse at Seram Bay shore (near field), and East Sulawesi Island shore (far field) shows that tsunami arrive as wave packets (dark blue dashed line).

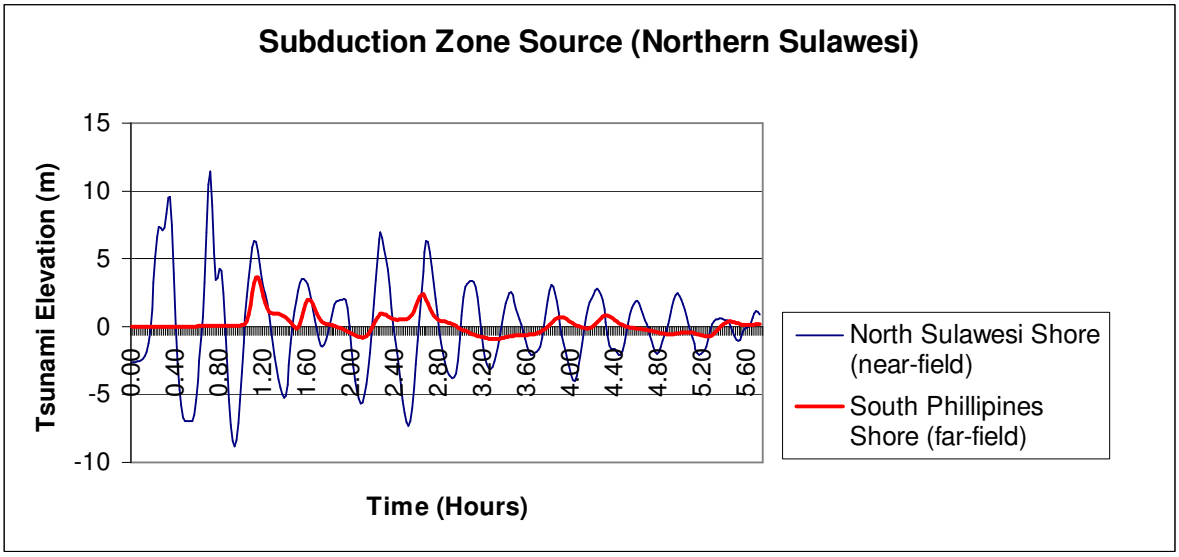

Figure 4.76. The difference of time histories of a tsunami generated by a subduction zone earthquake mechanism at North Sulawesi shore (near field with leading negative waves), and South Philippines shore (far field with positive leading waves).

4.6. Summary

The general characteristic of tsunami leading waves along the coastline of the Indonesian Archipelago was derived based on the scenarios of each event simulated. It takes 10 to 30 minutes for the first wave to attack the coastal areas for most of identified sources along the subduction zone within the region. A negative leading wave is typical for tsunamis that arrive along the southern coast of Sumatra, Java Bali and Nusa Tenggara Islands, which facing to the subduction zone. Negative waves also occurred along the northern part of Sumbawa and Flores Island, east coast of Sulawesi and south coast of Seram and Buru Islands, and northern arm of Sulawesi Island. Areas within the Molluca Collision Zone will experience either negative or positive leading waves, depending from which subduction zone the tsunami approaches from.

The initial leading waves from volcanic sources are difficult to determine, since it depends on the generating mechanism involved. In the case of a pyroclastic flow source, mostly the leading wave is positive. While submarine explosions involve leading positive waves, and a deep trough due to the crater formation depending on the bathymetric features of the region, such as for the Anak Krakatau scenario. At some places the leading wave is positive (i.e. Kalianda and Panaitan) and other places it is negative (i.e. Kota Agung and Carita).

Numerical modeling results show that for all potential sources are capable of generating catastrophic tsunamis for the coastal zones of the Indonesian Archipelago. With maximum tsunami elevations along the coastline comparable to the 26 December 2004 Tsunami event, their impact on the coastal area will be as great as the 2004 Tsunami event, which raised the question whether there are any solutions for this type of coastal disaster. The 2004 event was modelled and analysed to address this question. The results were presented as a paper during the Solutions to Coastal Disaster 2008 Conference on April 13 – 16, 2008 in Hawaii, USA. The manuscript of this paper forms the rest of this chapter.

Paper submitted and presented on Solutions to Coastal Disaster 2008

April 13 –16, 2008
Turtle Bay, Oahu, Hawaii. USA.

EXTREME TSUNAMI RUN UP AND INUNDATION FLOWS AT BANDA ACEH, INDONESIA: ARE THERE ANY SOLUTIONS TO THIS TYPE OF COASTAL DISASTER?

Gegar S. Prasetya[1], Terry .R. Healy, Willem P.de Lange[1], Kerry P. Black[2]

1. Coastal Marine Group, Department of Earth and Ocean Sciences, The University of Waikato, Hamilton, New Zealand, gsp1@waikato.ac.nz
2. ASR Ltd, Marine Consulting Research, Raglan, New Zealand.

Abstract: Almost 3 years after the extreme 26 December 2004 tsunami event, which devastated the Banda Aceh region of Sumatra, certain coastal protection works have been planned and implemented. They comprise mainly of seawalls, breakwaters, and planting forest trees and mangroves as a wave-absorbing greenbelt. Numerical modeling of this catastrophic event was established to investigate the processes of tsunami propagation and inundation flows over the Banda Aceh coastal region, identify zones that had escaped devastation (as identified during the post event field survey) and assess possible types of coastal protection along the affected coasts. Results of the modeling showed that for protection against such a 2004-type event, huge structures ~ 15 m high would be required, but are not economically feasible. However, mature mangroves stands may offer reasonable protection, and this option shows greater promise as an affordable solution.

INTRODUCTION

The most powerful earthquake of the last 40 years struck the Indian Ocean on 26 December 2004 and generated massive tsunamis that had wide impact along the coastlines of the Indian Ocean (Geist et al., 2006). The Aceh province of Indonesia, 150 km from the source of the earthquake, suffered the greatest. Some 130,000 people were confirmed dead, more than 37,000 people missing and 500,000 people were displaced (BRR, 2006) along 800 km of devastated coastline. Most of the infrastructure, houses, school, hospitals, and coastal environment were damaged. An initial estimate of the cost to rebuild Aceh and Nias, according to the Reconstruction

and Rehabilitation Agency of Aceh and Nias (2006) was USD 6.1 billion, while the human cost can not be calculated.

The extreme run up and inundation flows that devastated the coastal areas during this event were recorded and documented by eyewitnesses and the International Tsunami Survey Team (ITST). This precious data set has provided a new insight into tsunami dynamics and characteristics, as well as their impact on the coastal areas. These data demonstrated that the most severe impact on the coast of Aceh Province and its offshore islands occurred within 15 to 45 minutes after the quake. Some 4 hours later, the reflected waves, with considerable height, struck the coast again, and wave activity continued for some time afterwards. The global numerical model of tsunami propagation (Titov et al., 2005) demonstrated these reflections were consistent with eyewitness accounts at the southern tip of Simeulue and Nias Islands. Here, people observed the high waves around noon (local time 12.00) and observations from some other islands further south reported that these waves were higher than the original tsunami. The resonating wave activity continued until evening. There are no eyewitness observations of these reflective tsunamis on the west and north coast of Banda Aceh, possibly because the first series of tsunamis had already devastated and killed most of the people along the coast.

Most of the coastal structures in Banda Aceh existing at the time were completely devastated except for those buildings that contained reinforced structures, and of specific shape, such as Mosques, which allowed most of the tsunami energy to pass around them (Synolakis and Kong, 2006). However, adjacent scouring was a common phenomenon, as well as undercuting and collapsed walls. Wooden structures were completely swept away by the tsunami and its backwash, and the resulting flotsam created dangerous projectiles. Infrastructure, such as the bridge at Gleerbuk, was transported up to 500 m from its original position, while the floating-anchored barge providing electric power generation drifted as far as 3 km inland in Banda Aceh, a situation observed in earlier tsunamis (Imamura et al., 1995). The palm oil tank in Suak Timah Meulaboh drifted as far as 2 km inland. The effect was even

greater for vessels; some were transported up to 3.5 km inland. Floating debris projectiles became the most dangerous to human life and very destructive.

Existing coastal protection structures such as breakwaters, seawalls and armoured units (tetrapods) were not effective, due to the massive size of the tsunamis. However a coastal forest did provide evidence of reducing the tsunami impact. To the south, at Lhok Nga, tetrapods at the cement factory port were scattered adjacent to the port due to tsunami action. During the rehabilitation of the port, part of the cement plant structure had been excavated from the bottom of the port basin, showing that return flows were very strong in this area. The highest tsunami run up of ~ 35 m was measured in this area with flow depths of 15-30 m, yet the cement factory survived with damage to the building platform. In comparison, on the north coast, most of the coastal protection structures at Ulee-Lheue and around the port were damaged and transported away, even though the flow depths here as measured were far less, i.e. between 6-12 m. In Simeulue and Babi Islands, the undisturbed mangroves and coastal forest caught a considerable sized block of hard coral measuring ~3 x 5 m washed up by the tsunamis, and the landward impact of the tsunami was minimized. Obviously, the practice of utilizing mangroves and/or coastal forest as tsunami protection warrants further investigation.

In this paper, extreme run up and inundation flows based upon the post event field survey and numerical model results are investigated in relation to the coastal protection and management of low-lying areas. Discussion is also presented on the various types of coastal protection solution optimal for this type of coastal disaster.

THE RUN UP AND INUNDATION FLOWS

The media coverage of the 26 December 2004 tsunami event illustrated the need for the general public to understand tsunami terminology used by scientists. Confusion about the terms *run up height*, *tsunami wave height* and *inundation* resulted in misleading information about what happened. In Banda Aceh, this situation had an impact on the subsequent rehabilitation, reconstruction and future mitigation efforts.

The *run up height* depends upon the slope of the ground inland, and the ability of the topography to concentrate the wave energy or reflect it. For the same incoming tsunami waves, those areas with a gentle slope inland will experience lower run up heights but longer inundation distances compared to the areas that have steeper slopes. Therefore, in reporting the properties of tsunamis, the location of measurements should be mentioned, as is standard practice in tsunami surveys (Synolakis and Okal, 2005). The *flow depth* is the depth of water under the tsunami wave as it flows inland, and if already referenced to Mean Sea Level (MSL), it is termed *tsunami elevation*. At the inland limit of the flow, the vertical elevation from mean sea level is termed the *run up height,* and the horizontal distance from the shoreline is the *inundation distance*. The *run up height* was frequently confused with the *tsunami wave height* in the media coverage, but we accept the public observations that the *tsunami elevation* is equal to the *tsunami wave height*.

Results of the December 2004 post-tsunami field survey carried out by the International Tsunami Survey Team along the west, north and northeastern coasts of Sumatra and the offshore islands of Aceh Province, showed that the tsunami run up, flow depth and inundation distance were highly variable (Figure 1). The tsunami flow depth and run up were typically 15 m in most cases along the west coast, but ranged up to 35 m in Lhok Nga. However along the northern coast of Banda Aceh, the flow depth varied from 6 – 12 m and inundated most of the coastal area up to 5 km inland due to the low topography. On the west coast, maximum inundation occurred between Lampuuk and Lhok Nga where the waves penetrated further inland. According to survivor eyewitness accounts, at Lampisang, waves from the west (Indian Ocean) collided with waves from the north (Andaman Sea) approximately 6.8 km from Lhok Nga and 3.7 km from the northern shoreline perpendicular to it. This situation showed the flow speed from the west was faster, flow depth was greater, and travel distance almost twice as far as from the north. Due to the topographic and landform configuration, run-up along the west coast was higher than the tsunami wave itself at the coast. Maximum run up of nearly 35 m was measured at a site close to the cement factory in Lhok Nga.

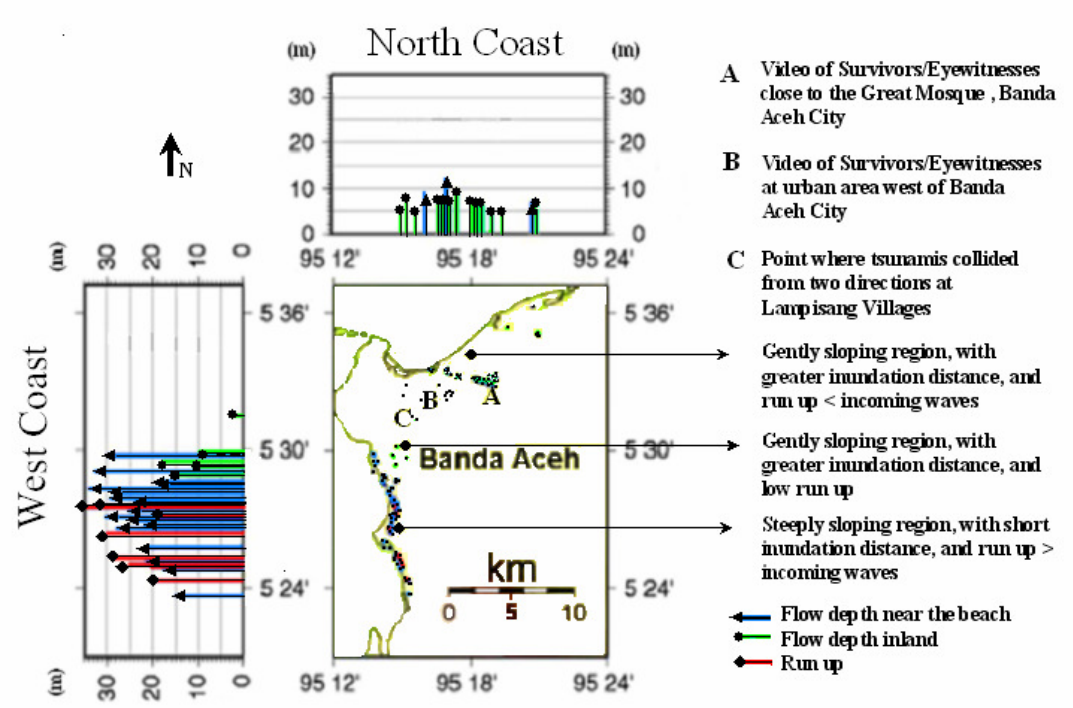

Figure 1. Run up, flow depth and inundation distances are highly variable on Banda Aceh. (Base map source and data: Yalciner et al., 2005, Jaffe et al., 2006, Borrero et al., 2006, Matsutomi et al., 2006, ITDB/PAC 2004, Http://walrus.wr.USGS.gov/tsunami/Sumatra)

Two videotapes of inundation flows made by eyewitnesses nearly 2.5 km from the shoreline make it possible to calculate the current velocity and the floating debris speed through the City of Banda Aceh close to the Great Mosque (A) and at major inundated areas to the south (B) on Figure 1 and 3. Fritz et al. (2006), based on particle image velocimetry (PIV) analysis, measured the flow velocities as between 2 – 5 m/s which confirmed the calculation of maximum flow rates made by Matsutomi et al. (2006) of ~ 5.2 m/s. Based upon a video tape at Site A, the street acted as a channel and the leading tsunami front with depth 10 cm propagated at low speed until 40 s later, the flow speed become 4 m/s with increasing flow depth up to 2 m as shown on Figure 2.a.

The flow carried all kinds of debris, and the water was dark and muddy. At the second video (position B), the flow depth reached a maximum ~ 3 m, approximately

10 minutes after the tsunami fronts arrival. From a simple calculation, and using the satellite imagery for the limit of inundation inland, the average velocity from this point to the maximum inundation distance 1.3 km inland is 2.1 m/s. The video also shows that at this point, it took ~ 3 hours for the water level to subside from ~ 3 m to ~ 1.5 m as shown on Figure 2.b. It took more than a day for the water to entirely recede from this site. Another possible cause of this slow return flow is land subsidence.

Figure 2.a. The Video at location A showed the leading initial tsunami wave with leading flow height of 20 cm, followed 40 seconds later by high speed flows with depths of 2-3 m; which carried all kind of debris.

Figure 2.b. At location B, the video showed the leading turbulent fronts (left), and 10 minutes later when the water became stagnant (center). The water subsided with debris trapped around the house (right).

THE COASTAL IMPACT

The extent and size of coastal damage due to tsunami action onshore and further inland was extensive, and included, but was not limited to, erosion, scouring and sedimentation, contamination of groundwater and freshwater wells during the inundation and saltwater stagnant period, and its impact on coastal structure, terrestrial vegetation and organisms. The size and extent of coastal impact in west and

northern Banda Aceh City can be seen in Figure 3. The wetland areas were particularly affected. Typical features of these impacts were large-scale erosion and scouring, channel deepening, widening of the river mouth, enlarging the estuaries and lagoons, and sedimentation over the land. Many of these features are visible on Quick Bird Satellite Images. Up to 1 m thick of mud had been deposited at Suak Timah villages north of Meulaboh.

In analyzing the structural damage from this event, it is evident that contributions came from both the earthquake and the tsunami wave forces. The floating debris projectiles carried by tsunamis flows are an additional consideration. Very strong ground shaking had been felt by all survivors in Banda Aceh, some buildings already collapsed or partially damaged along the coast were swept out by the tsunami waves as flotsam. Reinforced concrete structures may withstand the quake, but had damaged walls, leaving intact roofs and columns and had scouring at their base. Those buildings were partially damaged due to the tsunami wave action. A good example of the scale of tsunami and some earthquake forces can be seen in Figure 4, where typical damage to a house due to the tsunami wave (photo1) and due to the earthquake (photo 2) at Lagundri Bay, Nias Island is illustrated. Photos 3 and 4 show the response from different types of houses to the same size of tsunami wave. The second storey of the house in photo 3 is partially damaged due to a 10 m tsunamis flow depth, but the simple houses (photo 1 and 2) were completely swept away as shown on photo 4. Photo 5 and 6 show the type of house that typically survived the extreme tsunami flow depth. Most of the Mosque (photo 6) in Lhok Nga survived even though the flow depth reached >20 m and the 3-storey building, which had a structure similar to the mosque, also survived in Banda Aceh with a flow depth > 12 m.

Due to the size and extent of the tsunamis, none of the coastal protection structures were effective. The breakwater at the cement factory port in Lhok Nga, as well as at Ulee Lheue Port, had been designed to protect against storm waves and not extreme tsunamis. The coastal structures at the cement factory port extended nearly 3 m above

mean sea level with 2 m tetrapods at the base. Interestingly, the majority of the tetrapods still maintained their position, and only some of them were entrained and scattered around the port basin even though the flow depth measured at the cement plant was 18.9 m (Jaffe et al., 2006, Matsutomi et al, 2006).

Natural on-shore barriers such as mangroves and other coastal forest provided some protection from tsunami impact. A mangrove forest at Babi Island (offshore Sumatra Island) that had been conserved for more than 50 years without any human intervention provided good protection. However most of the mangrove stands along the Sumatra mainland coast were under stress due to land use changes, and did not.

THE NUMERICAL MODEL

Detailed simulation of tsunami behavior at Banda Aceh in this study utilized the 3DD suites of numerical model based on non-linear shallow water wave equations (Black, 2001). The model was initially developed and applied for simulating the physical processes from micro-scale circulation over sand beds (Black and Vincent, 2001) to continental circulations (Middleton and Black 1994). The model can be set into 'two-dimensional' (2D) and 'three-dimensional' (3D) modes with capabilities in simulating the flooding and drying for large intertidal zones (Black, 2001). 3DD uses a fully explicit time stepping solution and its flooding and drying scheme is designed to allow smooth transition and reduced instabilities by avoiding a sudden jump of the current velocity during drying and wetting processes in simulating large intertidal zones. This feature allows the model to simulate the inundation dynamics accurately. Benchmarking to a standard benchmark problem # 2 of third workshop of Long Wave Run up Model workshop (held on June 17-18 2004 on Catalina Island) and real world scales using the 26 December 2004 events demonstrated the ability of 3DD to accurately reproduce tsunami hydrodynamics during propagation and run up (Borrero et al., 2007).

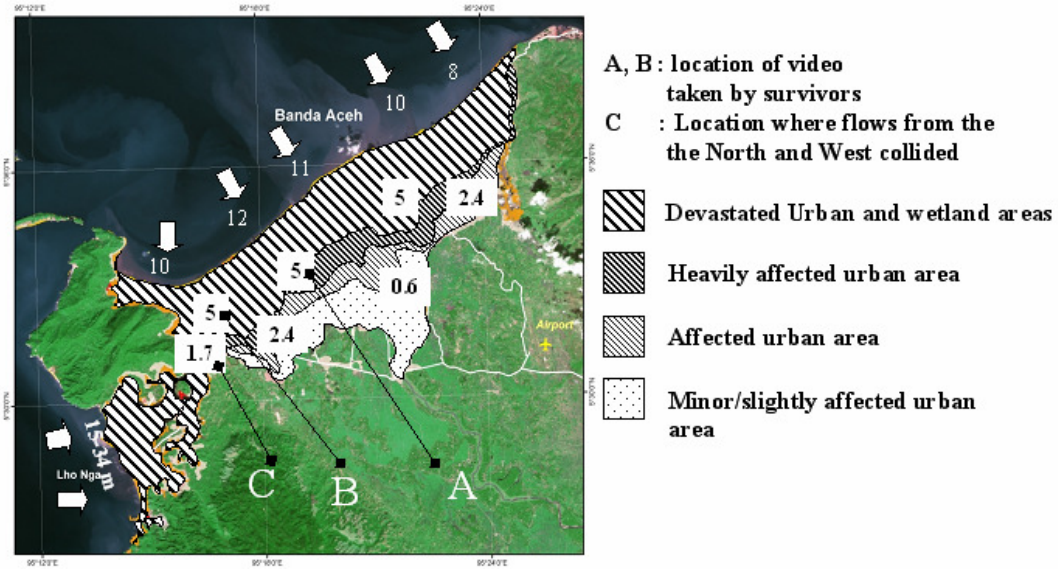

Figure 3. Damage map of Banda Aceh showing the impact of tsunamis wave fronts from two directions. The numerals indicate the tsunami elevation in meters near the beach (white) and flow depth inland (black). (Damage map source: UNOSAT, Tsunami data: Borrero et al. 2006, Jaffe et al., 2006, Matsutomi et al., 2006).

Model Results of 26 December 2004 events

Using a 100 m grid for simulation of the wave at Banda Aceh, the flow depth, run up, and maximum inundation measurement were compared to data from the field survey (Yalciner et al., 2005; Borrero et al., 2006; Jaffe et al, 2006; and Matsutomi et al., 2006). The tsunami source model used the fault scenario proposed by Tanioka et al., (2006) after Stein and Okal (2005). The simulation was run for 12 hours to obtain detailed information on inundation flow behavior. The run up distribution at the west coast varied from 12 – 30 m (cf. 15 to ~35 m: from survey observations) and at the northern coast from 9 – 12 m (cf. 6 -12 m: from survey observations). The model showed the colliding of the two flows with a depth of between 2 – 4 m at Lampisang village. This is close to the survivor accounts and observation of ~1.7 – 3 m (Borrero et al, 2006). Figure 5 shows a time histories of the tsunami when it reaches maximum inundation and the times series of water elevations.

Modelling Application to Coastal Protection

Some new coastal protection works have been planned and implemented at the Banda Aceh site. These comprise a greenbelt of coastal forest, and structures including breakwaters and a seawall along the coastal area of Banda Aceh Province. In this study, the model was used to test the effectiveness of various combinations of soft and hard protection measures.

Hard Structure Scenarios

Effectiveness of various coastal protection structures was tested. A combination of seawalls were placed along the coast with 5 m height to test against the 6-12 m of tsunami elevations observed on the north coast of Aceh, and 8 m height to test against the 15 - 35 m of tsunami elevations.. In both cases the structures had 100 m width. A second combination used a 10 m high seawall at the north coast, and 15 m protection structures along the west coast just behind the existing 5 m and 8 m seawall, giving a total width of 200 m. The modeling results are shown in Figure 6.a-c after 1 hour of simulation, where Figure 6.a is the inundation pattern without any structures, 6.b is the inundation pattern with 5 and 8 m structures, and 6.c is the inundation pattern with 8 and 15 m structures.

The scenario of a 5 m height seawall along the northern coast and 8 m at the western coast was unable to prevent tsunami inundation of these areas inland of the structures. There is almost no effect on minimizing the tsunami inundation, and in fact the structures exacerbated the situation since the backflows were mostly blocked along the coast, and water could escape only through rivers. This caused a longer inundation period of the northern area, as shown on Figure 6.b-c.

By increasing the seawall height (second combination), most of the incoming tsunami waves are blocked, and hinterland inundation occurs only through rivers. Most of the low-lying coastal areas at the north coast become inundated from the channels and rivers. At the west coast, because only one river exists, the extent of inundation was not severe, even though during the 26 December 2004 events, these areas were

heavily damaged. The model results show the 15 m height wall at the west coast and 8 m height at the north coast could minimize the inundation and tsunami flow depths inland. The time histories plot can be seen on Figure 7.

Figure 4. Damage to different types of houses due to different impact scales of the tsunami wave height and flow depth and earthquake.

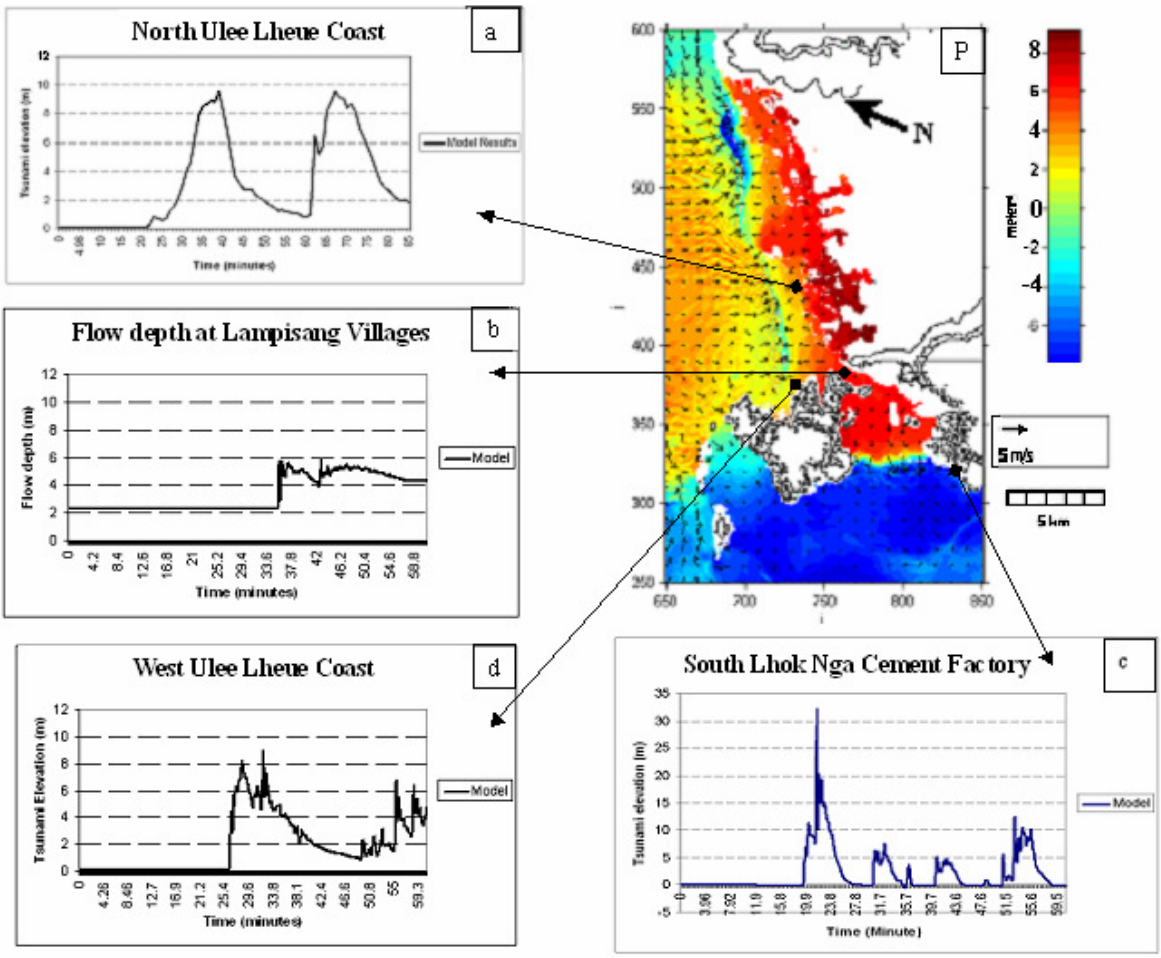

Figure. 5. Tsunami elevation and flow depth evolution over time, extracted from the model simulation (a-d) with maximum inundation distances (P) up to 5 km inland.

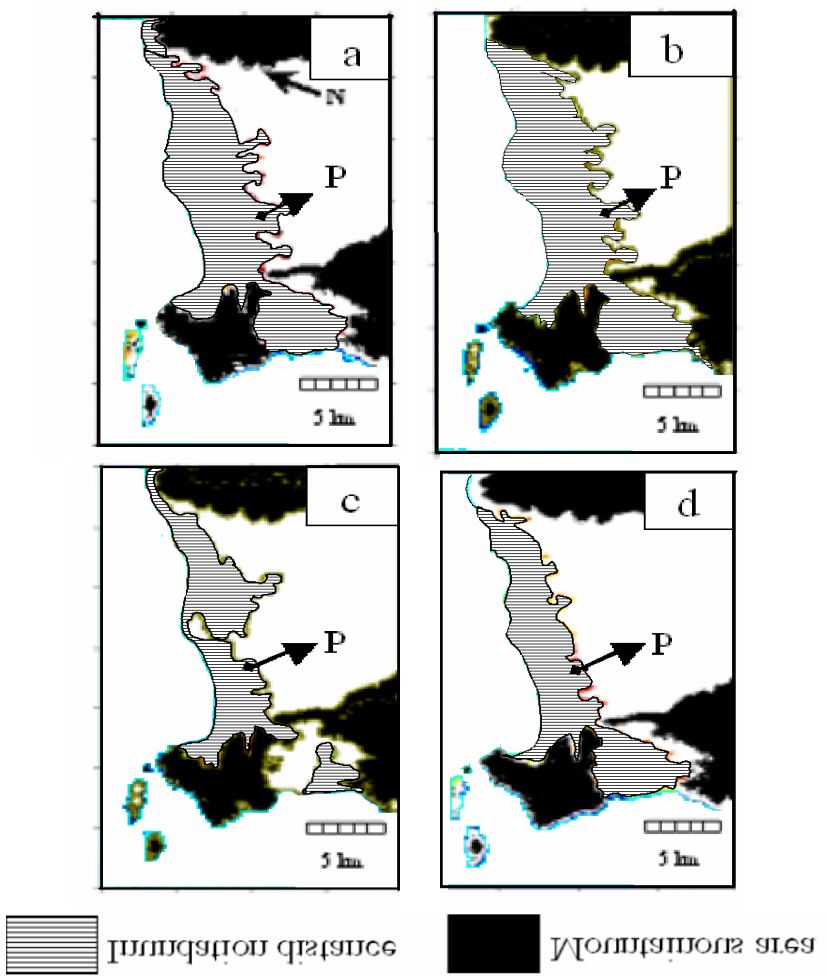

Figure 6. a-d. Modelling results showing the comparison of original inundation distance without structure (a), structures 5 and 8 m (seawall1); 10 and 15 m (seawall 2) to the north and west respectively (b,c) and coastal forest (d).

Coastal Forest Scenarios

In simulating the densities and resistance of the trees, a two-dimensional bed roughness (roughness length) was estimated by taking into account the topography, and the width, height and extent of mangroves and coastal forest. As proposed by the Department of Forestry (BPDAS Krueng Aceh, 2006), along the northern coast of Banda Aceh City, the mangroves and coastal forest will be planted back 3.5 km from the coastline. However to the west where the highest tsunami flow depth occurred, the wide of the greenbelt was only up to 500 m inland. With a value for roughness

length of between 0.08 to 0.2, the model results show that the coastal forest can reduce the tsunami elevation and inundation further inland at the northern coast, but not along the western coast, where the width was less. The forest did not substantially reduce the tsunami height at the shoreline, but as the wave penetrates further inland, the forest represented with high roughness length, induces a reduction in tsunami flow speed, and therefore inundation distance, as shown on Figure 6.d, and its time histories on Figure 7.

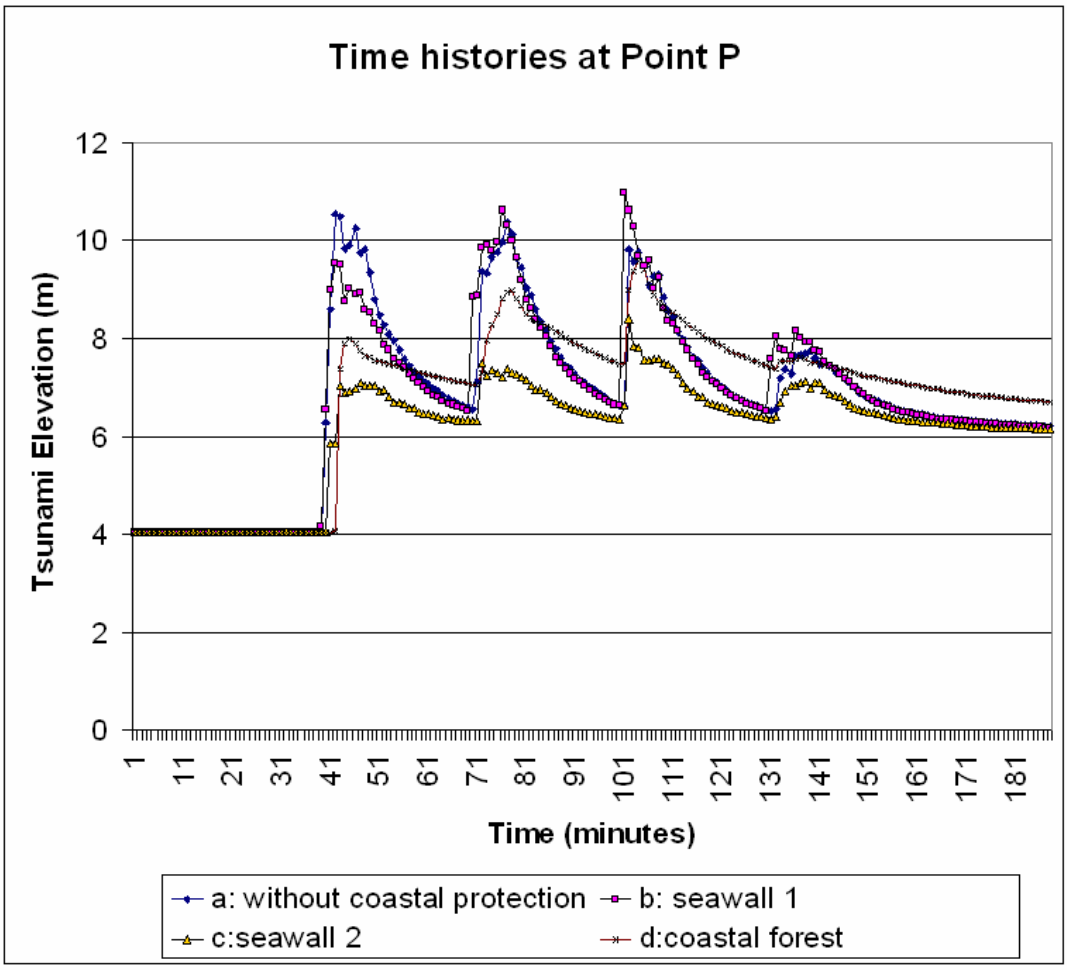

Figure 7. The time histories at point P on Figure 6.a-d showing the effect of coastal protection measures on the tsunami elevation height.

DISCUSSION

The field surveys of the Sumatran coastline following the December 2004 tsunami has provided valuable data sets that can be used effectively to model efforts to mitigate a similar disaster in future. The height, flow depth, run up and inundation distance along the coastline were highly variable and very site specific depending upon the bathymetry and onshore topography, as well as the vegetation and land use. Insufficient knowledge of the onshore bathymetry and topography, as well as land use make for difficulties in assessing and quantifying the impact of the tsunami, and may lead to inappropriate conclusions on how to mitigate the impact from a similar sized event in the future. Further research is needed on the kind of protection, which should be put in place for effective prevention of loss of life, as well as reducing the economic impacts through structural and non-structural mitigation measures.

For preventing loss of live, it is clear that preparation of coastal resilient community is essential, as is an early warning system. There is need for integration of life-long effort to educate the population about the hazards and preparedness for an extreme event. McAdoo et al. (2006) identified that "oral history" that had been passed on from generation to generation evidently saved thousands of people who lived on Simeulue Island, which is just 50 km from the epicenter of the earthquake in the Indian Ocean where, the northern tip of the island experienced the same wave height as at Banda Aceh. This phenomenon was observed in earlier tsunamis by Caminade et al., (2000) in Vanuatu, and recent tsunamis in the Solomon Island by Fritz and Kalligeris (In press). However, since the oral history tradition as in Simuelue, Vanuatu, and Solomon Islands no longer exists in the towns/cities due to their modern life style, educational material should be designed alternatively through a combination of numerical modeling, field survey results, and eyewitness accounts of the December 2004 catastrophic event. It is obvious that with good community preparedness, all individuals will know what to do upon warning of a pending tsunami.

In reducing the economic impact, the usual response is to opt for structural mitigation measures. However, the size and extent of the December 2004 event showed that traditional coastal protection structures are not economically feasible. Alternatively the idea of a suitably wide band of healthy mangroves and coastal forest that could provide a significant protection is another option, but it needs careful design and implementation. Not all types of mangroves and coastal forest can withstand extreme events. Possibly, criteria for 'healthy' mangroves and coastal forests is exemplified by the mangroves and coastal forest at Babi Island, which is naturally conserved and had not suffered intervention by human activities for more than 50 years.

CONCLUSION

The numerical model studies undertaken here suggest that coastal protection structures are only effective against a tsunami if their height is at least ¾ of the highest tsunami elevation height. However, to protect more than 800 km of coastline with huge structures is economically not feasible. Any long coast structures must be designed carefully where there are rivers or canals since the flows that come from the rivers could flood the area behind the structures, and create strong currents upon incoming surge and withdrawal of the waves. Specific design may need a barrier or gate across a river mouth, but such a scheme would need a guarantee that the gates still work during an extreme event.

The model results on mangroves and coastal forest impacts shows that a greenbelt scenario could give protection to some extent, but more research is required to quantify the forest characteristics. Also the use of a greenbelt in combination with other soft options such as a dune system to increase their functions as a natural coastal protection should be investigated. However, planting mangroves and coastal forest is a desirable affordable response because they function not only as a coastal protection system for tsunamis, but also as nursery ground for many coastal wetland habitats.

As the devastation of the 26 December 2004 tsunami demonstrated, it is critical to plan carefully what kind of coastal protection optimizes effective prevention against loss of life, as well as reducing the economic impacts on future generations. It is important not to rush into implementing any coastal protection system before quantitative and systematic assessment has been carried out.

ACKNOWLEDGEMENT

Prof. Costas Synolakis and an anonymous reviewer provided valuable comments that improved the paper. The numerical model research work had been funded through NZIDRS, Ministry of Education, New Zealand. Thanks to Drs. Rahman Hidayat, Dinar C Istiyanto, Widjo Kongko, Lukianto and all ITST Sumatra 2004 Team for providing the fieldwork data.

REFERENCES

Black , K.P. (2001). "The 3DD Suite of Numerical Process Models", ASR Ltd., PO Box 67, Raglan, New Zealand. 90 p.

Black , K.P. and Vincent, C.E.(2001). "High-resolution field measurements and numerical modeling of intra-wave sediment suspension on plane beds under shoaling waves", Coastal Engineering Vol. 42: 173-197.

Borrero, J.C., Synolakis, C.E. and Fritz, H. (2006). " Northern Sumatra Field Survey after the December 2004 Great Sumatra Earthquake and Indian Ocean Tsunami", Earthquake Spectra, Special Issue III, Vol 22: 93-104.

Borrero, J.C., Bosserelle, C., Prasetya, G., and Black, K.P. (2007). "Using 3DD to model tsunami inundation", Proceedings of the Australasian Coast and Port Conference. July 2007, Melbourne Australia. Paper 96. 6 p.

BPDAS Krueng Aceh. (2006). " Map of Mangroves and Coastal Forest Cultivation Plan (Post Tsunami) on Aceh Besar District and Banda Aceh". Forestry Office of Banda Aceh Province. 1 p.

Caminade, J.P., Charlie, D., Kanoglu, U., Koshimura, S., Matsutomi, H., Moore, A., Rsucher, C., Synolakis, C. and Takahashi, T.(2000). "Vanuatu Earthquake and Tsunami cause much Damage, Few Casualties, EOS, Transactions American Geophysical Union, 81 (52) 64: 646-647.

Fritz, H., Borrero, J.C., Synolakis, C.E., and Yoo., J. (2006). "2004 Indian Ocean tsunami flow velocity measurements from survivors videos", Geophysical Research Letters Vol.33: 1-5.

Fritz, H. M., and N. Kalligeris. (In press). "Ancestral heritage saves tribes during 1 April 2007 Solomon Islands tsunami". Geophysical Research Letters (accepted, in press).

Geist, E.L., Titov, V.V., and Synolakis, C.E. (2006). "Tsunami Wave of Change", Scientific American, 294: 56-63.

Imamura, F., Synolakis.C.E., Gica, E., Titov.V.V., Listonco, E., Lee., H.L.(1995). "Field Survey of the 1994 Mindoro, Phillipines Tsunami, Pure and Applied Geophysics, 144(3-4): 875-890.

ITDB/PAC. (2004). "Integrated Tsunami Databases for the Pacific", version 5.1.1.2004.CD ROM, Tsunami Laboratory, ICMMG SD RAS, Novosibirks, Russia.

Jaffe, B.E, C. Borrero, J.C., Prasetya, G.S., Peters, P., McAdoo, B., Gelfenbaum, G., Morton, R., Ruggiero, P., Higman, B., Dengler, L., Hidayat, R., Kingsley, E., Widjo Kongko, Lukijanto, Moore, A., Titov, V., and Yulianto, E.(2006). "The December 26, 2004 Indian Ocean tsunami in Northwest Sumatra and Offshore Islands", Earthquake Spectra, Special Issue III, vol 22: 105 -135.

McAddo, B.G., Dengler, L., Titov, V., and Prasetya, G.S. (2006). " Smong: How an oral history saved thousands on Indonesia's Simeulue Islands", Earthquake Spectra, Special Issue III, Vol 22: 661-669.

Matsutomi., H., Sakakiyama, T., Nugroho, S., and Matsuyama, M. (2006). " Aspects of inundated flow due to the 2004 Indian Ocean tsunami", Coastal Engineering Journal Vol. 48(2): 167-195.

Reconstruction and Rehabilitation Agency of Aceh and Nias. (2006)."Progres Report Aceh & Nias, Two Years after the Tsunamis. December 2006. 110 p.

Stein S., and Okal.E.A. (2005). "Speed and Size of the Sumatra earthquake", Nature, 434(7033): 581-2.

Synolakis, C.E., and Kong, L. (2006). "Run up Measurements of the December 26, 2004 tsunami", Earthquake Spectra, 22 (S3): 67–91.

Synolakis, C.E., and Okal., E.A. (2005). "1992-2002: Perspective on a Decade of Post tsunami Surveys, Adv.Nat.Technol. Hazards, 23: 1-30.

Tanioka, Y. Yudichara, Kasusose, T., Kathiroli, S., Nishimura, Y., Iwasaki, S., and satake, K (2006). "Rupture process of the 2004 great Sumatra-Andaman earthquake estimated from tsunami waveforms", Earth Planet Space, 58: 203-209.

Titov, V.V., Rabinovich, A.B., Mofjeld, H.O., Thomson, R.E., and Gonzalez, F.I. (2005). "The global reach of the 24 December 2004 Sumatra tsunami", Science, 309: 2045.

Yalciner, A.C., Perincek, D., Ersoy, S., Prasetya, G., Hidayat, R., McAdoo B.G. (2005). "Report on December 26, 2004, Indian Ocean Tsunami, Field Survey on Jan 21-31 at North of Sumatra", by ITST of UNESCO IOC. 18 p.

4.6. Additional References

Cox, D.K.: 1979, Local tsunamis in Hawaii – implications for hazard zoning, *Hawaii Institute of Geophysics*, University of Hawaii, 46 p.

de Lange, W.P., Prasetya, G.S., Healy, T.R.: 2001, Modelling of tsunamis generated by pyroclastic flows (Ignimbrites), *Natural Hazards* **24,** pp. 251 – 266.

Fritz, H.M., Hager, W.H., Minor, H.E.: 2001, Lituya Bay case: rockslide impact and wave runup, *Science of Tsunami Hazards* **19 (1)**, pp. 3-22.

Le Mehaute, B. and Wang, S.: 1996, *Water waves generated by underwater explosion*: Singapore, World Scientific, 367 p.

McCaffrey, R.: 2008, Global frequency of magnitude 9 earthquakes, *The Geological Society of America* **36 (3)**, pp. 263 – 266.

Natawidjaja, D., Sieh, K., Chlieh, M., Galetzka, J., Suwargi, B., Cheng, H., Edwards, R.L., Avouac, J.-P., Ward, S.: 2006, Source parameters of the great Sumatran megathrust earthquakes of 1797 and 1833 inferred from coral microatolls, *Journal Geophysical Research* **111, B06403**, pp. 1-37.

Newcomb, K. R, and McCann, W.R.: 1987, Seismic history and Seismotectonic of the Sunda Arc, *Journal Geophysical Research* **92**, **B1**, pp. 421-439.

Okada, Y.: 1985, Surface deformation due to shear and tensile faults in a half space, *Bulletin of Seismological Society America* **74 (4)**, pp. 1135-1154.

Prasetya G.S., De Lange, W.P., and Healy, T.R.: 2000, Volcanic tsunami generations mechanism based on Krakatau event 1883 and future mitigations in *Regional Report on Tsunami Research*, Shuto. F (ed), Japan, pp. 31-45.

Prasetya, G.S.: 1998, Modelling of volcanic tsunamis, M.Sc.thesis, The University of Waikato, Hamilton, 282 p.

.Sigurdsson, H. and Carey, S.: 1996, Plinian and co-ignimbrite tephra fall from the 1815 eruption of Tambora volcano, *Bulletin Volcanology* **51**, pp. 243 – 270.

Simkin, T., and Fiske, R.: 1983, Krakatau, 1883 - the volcanic eruption and its effects, *Smithsonian Institutions Press*, Washington D.C, 464 p.

Slothers, R.B.: 1984, The great Tambora eruption in 1815 and its aftermath, *Science* **224**, pp. 1191-1198.

Sutawidjaja, I.G., Sigurdsson, H., Abrams, L.: 2006, Characterization of volcanic deposits and geoarcheological studies from the 1815 eruption of Tambora volcano, *Journal Geologi Indonesia* **1 (1),** pp. 49 - 57.

_____, National Tsunami Hazard Mitigation Program (NTHMP).: 2001, Designing for tsunamis, Seven principles for planning and designing for tsunami hazards, NOAA, USGS, FEMA, Alsaka, California, Hawaii, Oregon, and Washington, 60 p.

Chapter 5
Tsunami Hazard Maps, Early Warning and Education Program

5.1. Introduction

The seismotectonic assessment of the Indonesian Archipelago identified previous and potential tsunamigenic earthquakes and volcanogenic tsunamis, which provided scenario for numerical modeling of tsunami. The results provide the necessary information to permit the construction of tsunami hazard maps, and designing an early warning system and public education programme. Tsunami hazard maps developed in this chapter define the level of hazards that may affect coastal areas around the Indonesian Archipelago. The maps will be based on the maximum tsunami elevation value at shoreline due to the lack of detail nearshore bathymetry and topographic data at the resolution needed to represent the nearshore and overland dynamics of tsunamis. Less than 100 m resolution is needed to realistically represent the inundation dynamics and velocity distributions. Ideally LIDAR data and high-resolution multibeam survey are needed for engineering design and preparedness (Prasetya et al., 2008[a]).

Using the hazard maps, and considering the calculated arrival times of tsunami waves, an effective early warning system and necessary education programme will be discussed. The potential risk based on return period assessments for each of the sources identified will also be discussed.

5.2. Tsunami Hazard Map

This map summarises the potential catastrophic tsunamigenic earthquake and volcanogenic tsunami sources within the Indonesian Archipelago, and defines the potential tsunami hazards affecting the coastal areas as determined by numerical modeling based on scenario developed previously. It provides basic information for decision makers considering development of the coastal areas in the region, and prioritizes the regions required detailed inundation maps.

The ranges of tsunami elevations at the shoreline have been correlated to the hazard level, as determined by field surveys along the west coast of northern Sumatra (including Banda Aceh city) and offshore islands after the 26 December 2004 and 28 March 2005, and South Java Tsunami 17 July 2006 events. Five colour scales are used, these are:

- Red, for very high hazard zone with tsunami elevation at the shoreline greater than 9 m,
- Orange, high hazard zone with tsunami elevation at shoreline between 5 – 9 m,
- Yellow, for medium hazard zone with tsunami elevation at shoreline from 2 – 5 m,
- Green, for low hazard zone with tsunami elevation less than 2 m, and
- Dark blue, for no tsunami hazard zone.

Red: Very high hazard zone (tsunami elevation at the shoreline > 9 m)

The damaged areas are very extensive for gently sloping topography, and high runup occurs for steeply sloping topography. During the 26 December 2004 event, at Lhok Nga and Meulaboh, most of the buildings were completely destroyed, with only substantial buildings like mosques surviving. Most of the inhabitants perished. Heavy scouring and erosion on the riverbank, river mouth and beach face occurred, and only a few trees were not broken or uprooted (Figure 5.1). Tsunami penetration further inland maybe as far as 5 km for low-lying topography.

Figure 5.1. Very high hazard zone (tsunami elevation at the shoreline between > 9 m). Examples from Lampuuk – Lhok Nga Banda Aceh (right, photo courtesy BRR Aceh Nias), and Meulaboh (left, photo courtesy International Tsunami Survey Team (ITST)-2 team) after the 26 December 2004 event.

Orange: High hazard zone (tsunami elevation at the shoreline between 5 – 9 m)

An example of this zone during the 26 December 2004 Tsunami event was the northern-end of Banda Aceh and Meulaboh. Most of the one-storey buildings were destroyed. The two-storey buildings that survived mostly had broken walls. In general, only a few inhabitants survived. The damaged area was extensive, and scour and erosion occurred at river mouths and beaches. Some trees survived. Tsunami inundation for low-lying areas penetrated 1 – 3 km inland (Figure 5.2).

Figure 5.2. High hazard zone (tsunami elevation at the shoreline between 5 – 9 m). Examples from North Banda Aceh (right) and Meulaboh (left) after the 26 December 2004 event (photo (right) courtesy Satgas Udara Belawan TNI –AU, and (left) courtesy of International Tsunami Survey Team (ITST)-2 team).

Yellow: Medium hazards zone (tsunami elevation at the shoreline from 2 - 5 m)

An example of this zone is from the South Java 17 July 2006 Tsunami. Most two-storey buildings survived, and some one-storey buildings had broken walls or completely collapsed (Figure 5.3). The casualties are relatively high (in this case ~ 600 people perished), however, most vegetation survived. Tsunami on low-lying areas penetrated inland up to 600 m. Scour and erosion occurred along the beach face and river mouths.

Figure 5.3. Medium hazard zone (tsunami elevation at the shoreline from 2 – 5 m). Examples from Pangandaran West Java on 17 July 2006. Damage situation taken from the plane (right, photo courtesy Reuters) and on the ground (left, photo courtesy of Disaster Prevention Research Center (DPRI) Kyoto University).

Green: Low hazard zone (tsunami elevation at the shoreline less than 2 m)

Most one-storey buildings with good construction survived for this zone, as happened after the 28 March 2005 event at southern end of Nias Island. A simple brick house will experience broken walls if the tsunami strikes perpendicular to it. Almost no casualties occur, and most vegetation still stands. Small-scale scour and erosion still occurs and the tsunami penetrates up to 300 m inland in low-lying areas (Figure 5.4).

Figure 5.4. Low hazard zone (tsunami elevation at the shoreline less than 2 m). Examples from Nias Islands after the 28 March 2005 event. Damage on the wall of a simple house (left) and traces of tsunami height on the trees are identified within the areas (red circle on photo right). (Photo courtesy of International Tsunami Survey Team (ITST)-2).

Blue: No hazard zone

This zone is where there is no tsunami impacted along the coast.

Figure 5.5. Typical areas that had no impact by tsunamis. Photos are in Bali beach areas.

The resulting tsunami hazards maps are illustrated in Figure 5.6.a-c.

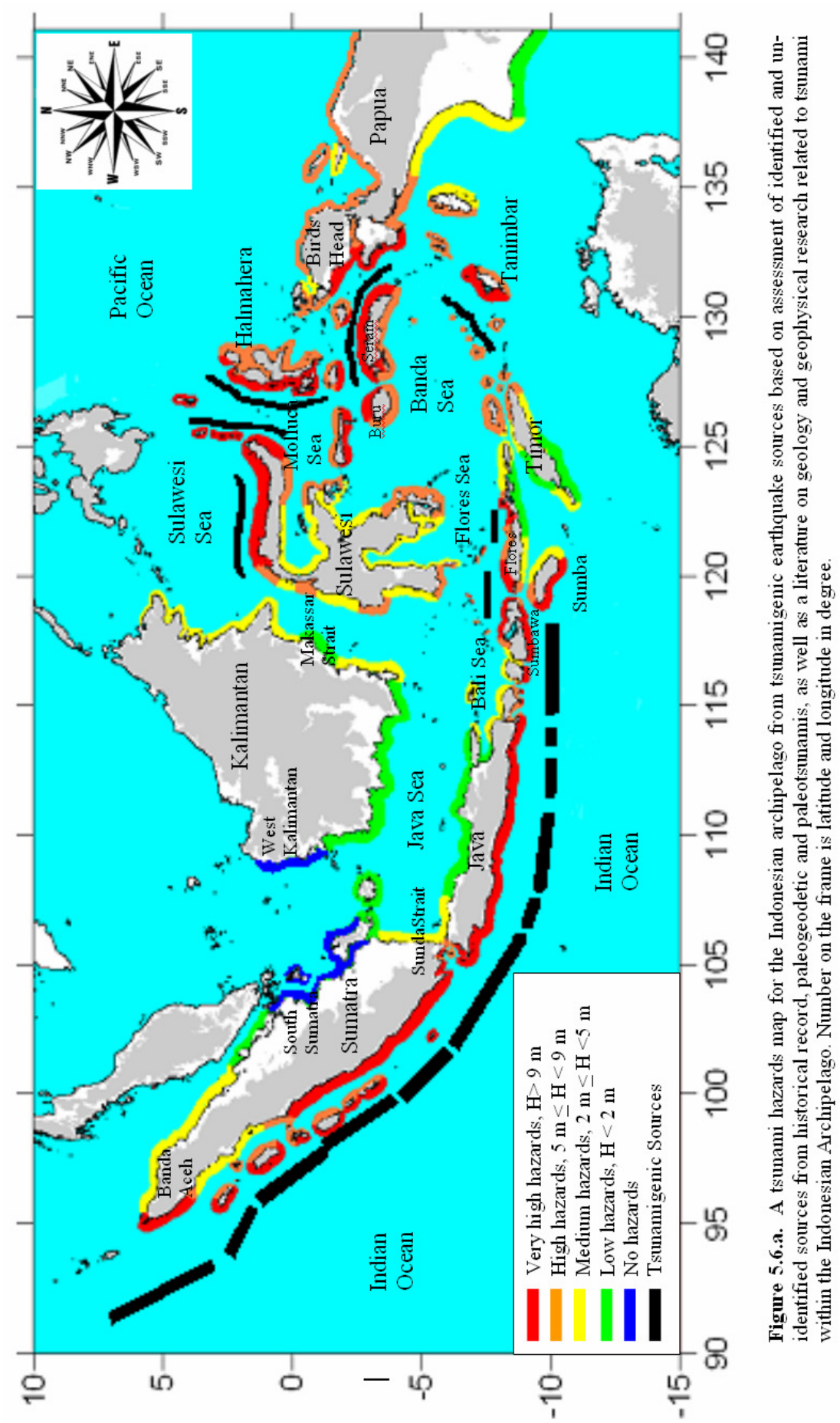

Figure 5.6.a. A tsunami hazards map for the Indonesian archipelago from tsunamigenic earthquake sources based on assessment of identified and unidentified sources from historical record, paleogeodetic and paleotsunamis, as well as a literature on geology and geophysical research related to tsunami within the Indonesian Archipelago. Number on the frame is latitude and longitude in degree.

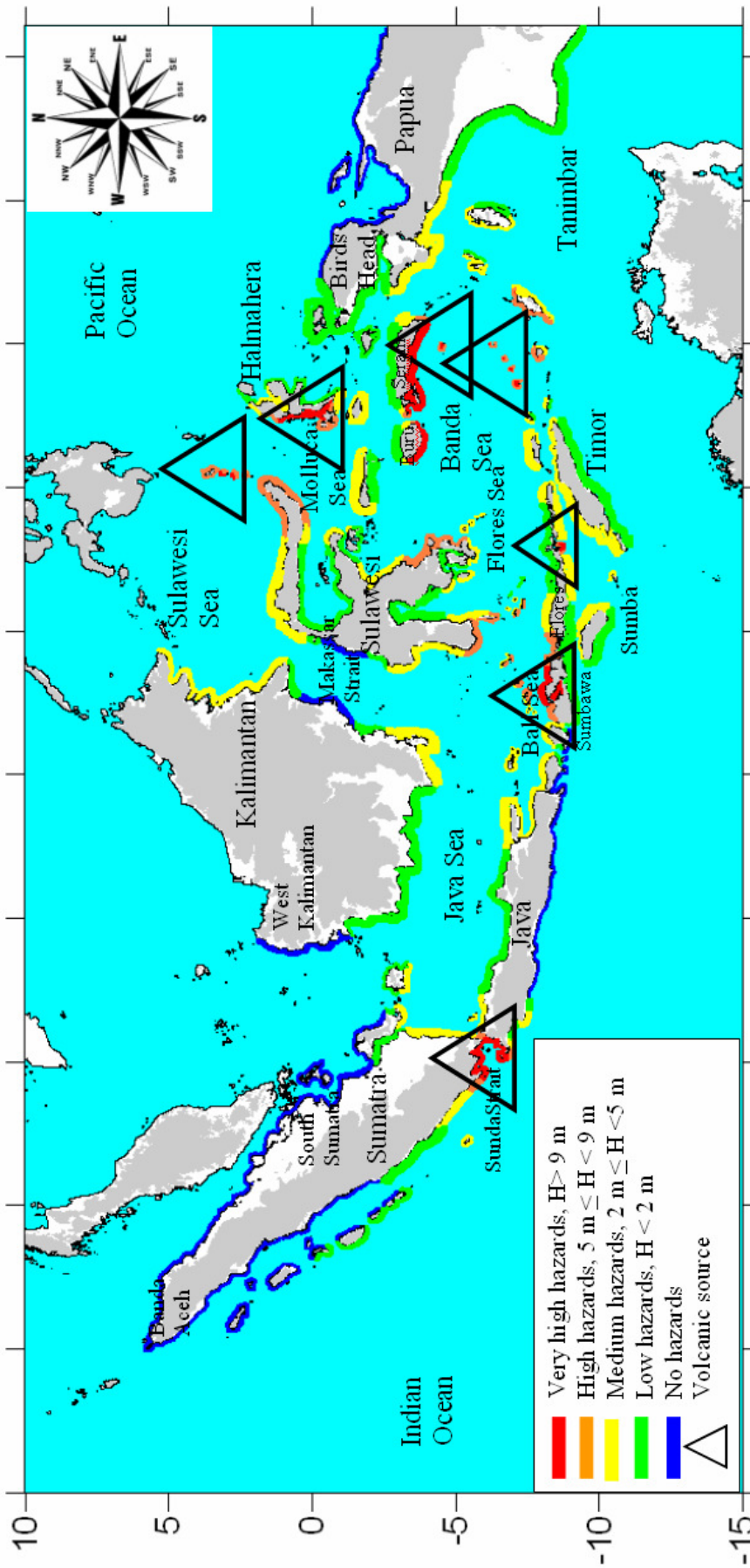

Figure 5.6.b. Tsunami hazard map from volcanogenic tsunami sources based on assessment of identified and un-identified sources from the historical record, paleogeodetic and paleotsunamis, as well as a literature on geology and geophysical research related to tsunami within the Indonesian Archipelago. Number on the frame is latitude and longitude in degree.

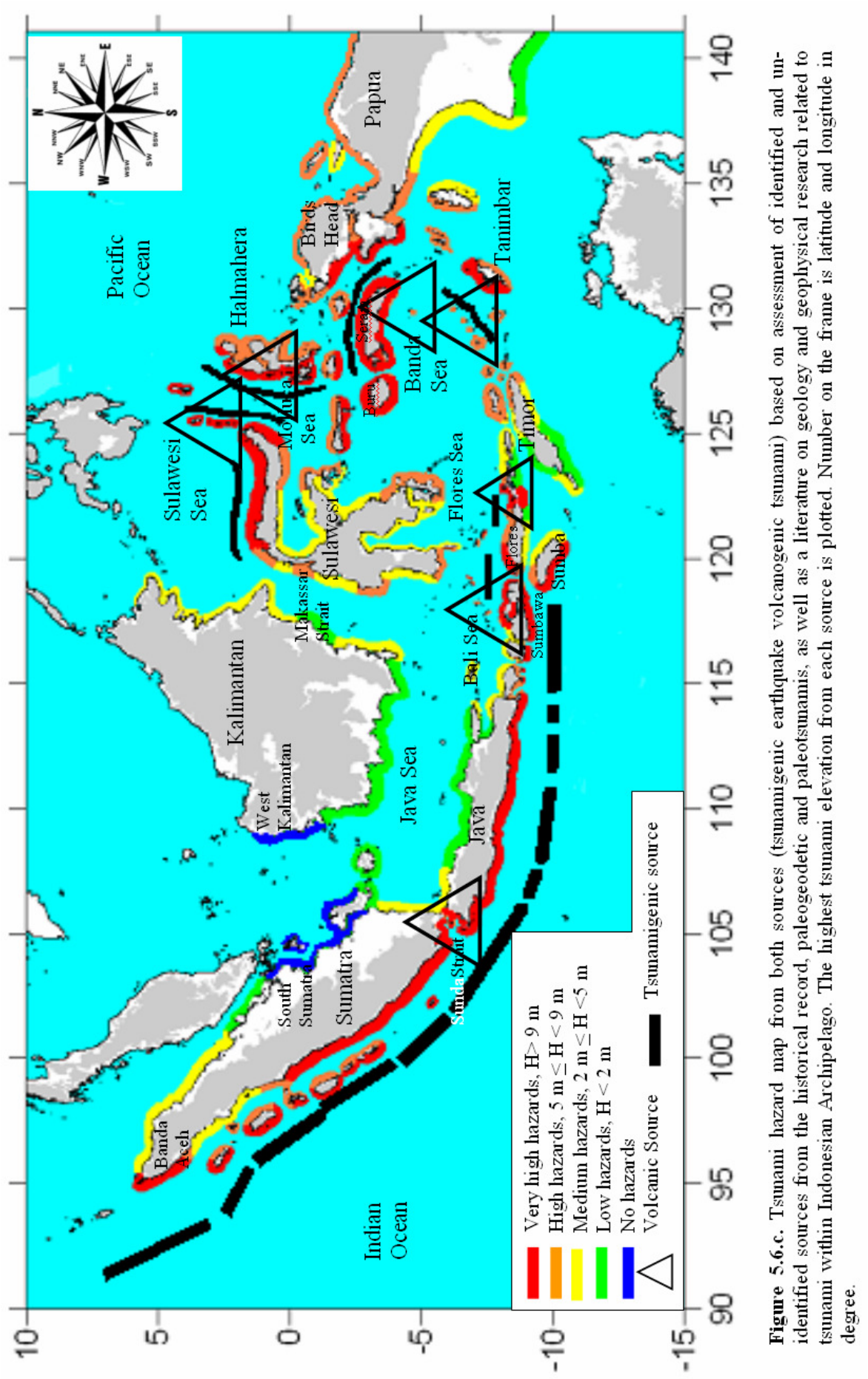

Figure 5.6.c. Tsunami hazard map from both sources (tsunamigenic earthquake volcanogenic tsunami) based on assessment of identified and unidentified sources from the historical record, paleogeodetic and paleotsunamis, as well as a literature on geology and geophysical research related to tsunami within Indonesian Archipelago. The highest tsunami elevation from each source is plotted. Number on the frame is latitude and longitude in degree.

5.3 Early Warning

Numerical modelling showed that the arrival time of the first simulated tsunami wave ranges from 10 to 30 minutes. The challenge in designing an effective Early Warning System for the whole archipelago is obvious. McAdoo et al. (2006), after the 26 December 2004 Tsunami event, identified the need for a combination of high-tech tsunami warning systems, including a full of network of satellite-linked tsunameters (that measure small changes in pressure at the seafloor) along with local, grassroots education. Local knowledge and wisdom that passed on from generation to generation at Simeulue Island (located 40 km from the source of the 26 December 2004 Tsunami event) saved thousands of people who lived at the north end of the Island. Here the maximum wave height exceeded 10 m (McAdoo et al., 2006). People felt the ground shaking, and used that as the first natural warning for the impending tsunamis, evacuating before the tsunami struck.

After the 26 December 2004 event, a number of countries indicated their great interest in the development of an early warning system in the Indian Ocean. In 2005, the Government of Republic of Indonesia committed itself to establishing such an early warning system, and prepared the Grand Scenario of Indonesian Tsunami Early Warning System (Indonesian – TEWS) report. The system consists of two main components: the upstream component where most of the technology involved; and a downstream component, which involves increasing public awareness and the dissemination of information.

Upstream Component

The Upstream Component comprises high technology, starting with earthquake (seismic) monitoring, oceanographic (sea level) monitoring, tsunami modelling, crustal deformation monitoring, and an information and communication system that covers the whole Indonesian Archipelago. Realizing that the arrival time of tsunami is within 10 – 30 minutes of generation, the system is designed that within 5 – 10 minutes a warning should be disseminated to authorized parties and communities at local, regional and a national level.

The Geophysical and Meteorological Agency (BMG) is responsible for the Early Warning System and to provide warnings. The schematic diagram of the system (Figure 5.7) shows how the data one gathered from the field, processed, analysed, integrated and

disseminated through automatic and interactive flow processes, and the time line of processing is illustrated in Figure 5.8.

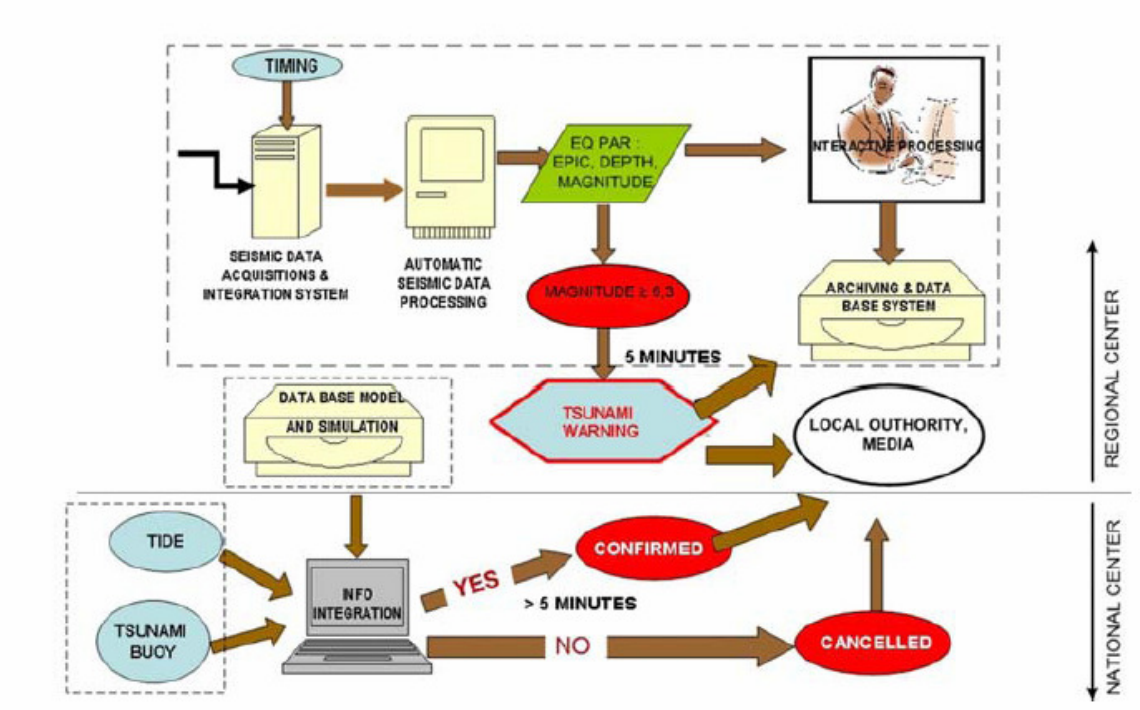

Figure 5.7. Schematic diagram of the Early Warning System (Source: BMG).

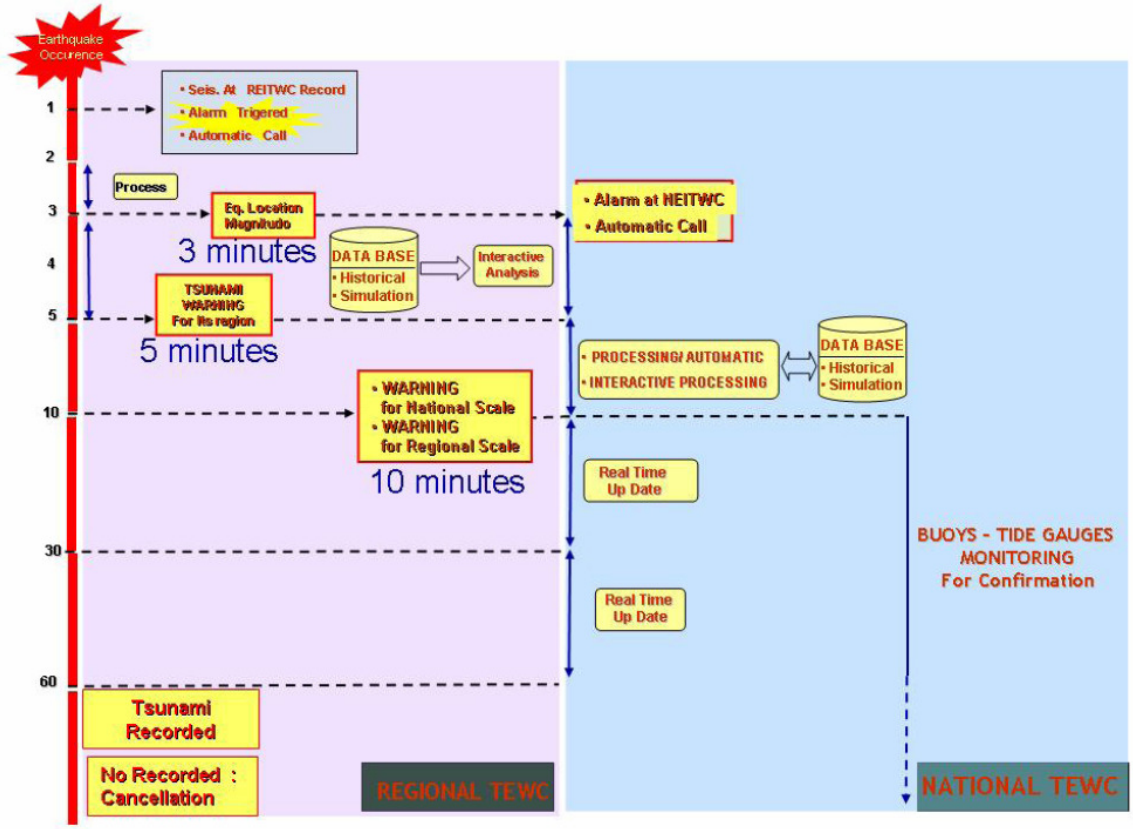

Figure 5.8. Time line for processing the warning (Source: BMG).

As illustrated in Figure 5.8, within 3 minutes of an earthquake, the seismic monitoring system will determine the earthquake parameters from the network stations, and if it meets the characteristics of a tsunamigenic earthquake, tsunami information (elevation and arrival time) will be retrieved from a database of tsunami simulations (pre-calculated models). These processes, according to the design, will take 2 minutes. Overall, within 5 minutes the warning can be issued and disseminated to the authorities, media and communities at the regional level closest to the source. While at the National level, the information will be issued within 10 minutes after the earthquake occurrence. A confirmation or cancellation will be given when sea level monitoring stations provide the field data measurement.

Downstream Component

Downstream components are the complementary part of the Tsunami Early Warning System, and includes the dissemination of early warnings to authorized parties and communities. The central and local governments roles in early warning dissemination and the required level of community preparedness, response and capacity building (institution, community, and individuals), is in accordance with the stipulated Standard Operating Procedure (SOP) of the Early Warning System. Community preparedness is an important factor because a successful Early Warning System depends on how people react to the warning.

According to the Country Report presented during the Intergovernmental Oceanographic Commision (IOC) meeting on the Indian Ocean Tsunami Warning and Mitigation System IV (ICG/IOTWS) in Mombasa, February 28 – March 2, 2007, interface-institutions for dissemination has already been established for several institutions (Figure 5.9). The current system dissemination to the public is based on several methods, from simple to more sophisticated and complicated. So far, the most effective is via the short messages (sms) by mobile phone. The 'five and one system' that disseminates the information from the Geophysical and Meteorological Agency through several telecommunication systems such as VPN-MPLS, internet, RANET, leased channel, and VSAT has been installed in more than 15 locations in Indonesia. A siren system has also been installed at many places in the coastal areas that prone to the tsunamis, and it is planned to install more in the future (Harjadi, 2007).

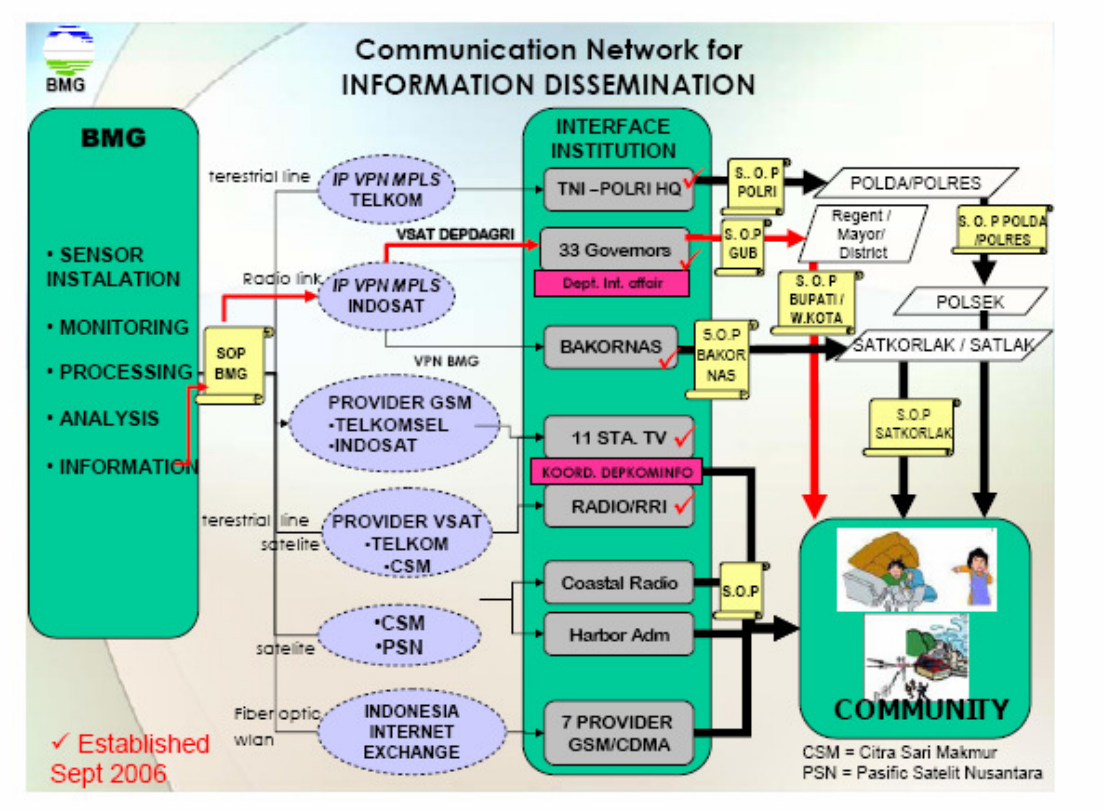

Figure 5.9. Schematic diagram of the communication network for information dissemination established in 2006 for the Early Warning System (Source: BMG).

The Network Stations

To implement a system that can achieve the goal of issuing a warning within 5 – 10 minutes after the quake, for very vast areas and a long coastline, Early Warning System requires a large seismic, tide and crustal deformation station network operating in the real time mode. There is 1 national center, and 10 sub-national or regional stations for seismic monitoring that will be equipped with 160 broadband seismic networks, and 500 accelerometers by the target completion date in 2009 (Figure 5.10). The tide network will consist of 80 tide gauges (realtime) for tsunami in addition to the existing tide station (Figure 5.11), and 78 GPS stations will be installed (Figure 5.12) in addition to the seismic and tide network. These GPS stations were very crucial in detecting pre-seismic strain a deformation.

There are 21 offshore buoys; 10 from Germany in the Indian (4 offshore Sumatra) and Pacific Oceans (6 offshore Sulawesi and Papua), 3 DART buoys from USA (1 in offshore Sumatra, and 2 in offshore Java), 1 from Malaysia (offshore Banda Aceh) and 9 from Indonesia (Figure 5.13). All buoys from Germany, USA and Malaysia are dedicated

to the tsunami detection and working in the same way as the well-known DART buoys from the USA. The Indonesian buoys are oceanographic buoys (multipurpose) that can measure other oceanographic and meteorology parameters. These buoys are an upgrade of those previously installed in the 1990s, and are known as Seawatch Buoys for real time oceanographic and meteorology monitoring. The real time data measurements from the Buoys had been designed to contribute to modelling of the marine environment, including tsunamis (Prasetya, 1994).

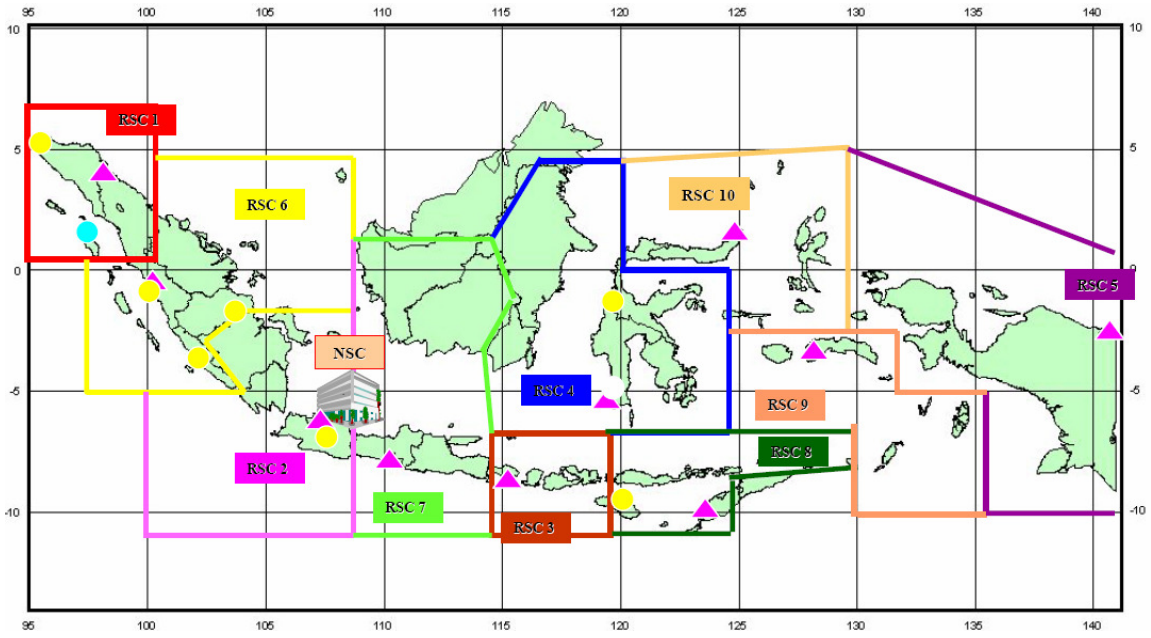

Figure 5.10. Seismic network comprising 1 National Seismic Center (NSC) and 10 Regional Seismic Center (RSC) equipped with 160 broadband seismometers and 500 accelerograph (Source: BMG).

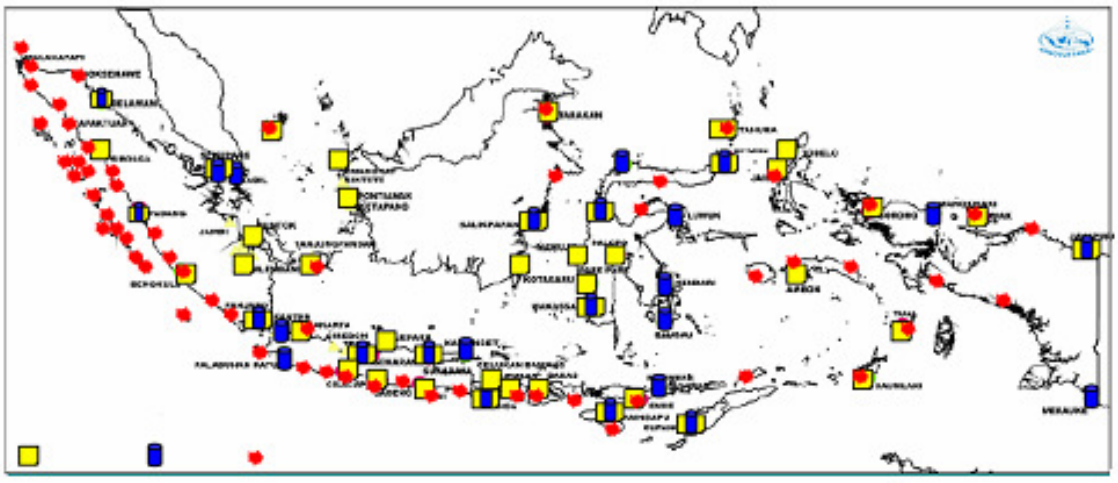

Figure 5.11. Tide network consisting of 40 analogue (yellow) and 20 digital (blue) gauges with additional 60 digital tide gauges (red) that measured the sea level in real time (Source: Bakosurtanal).

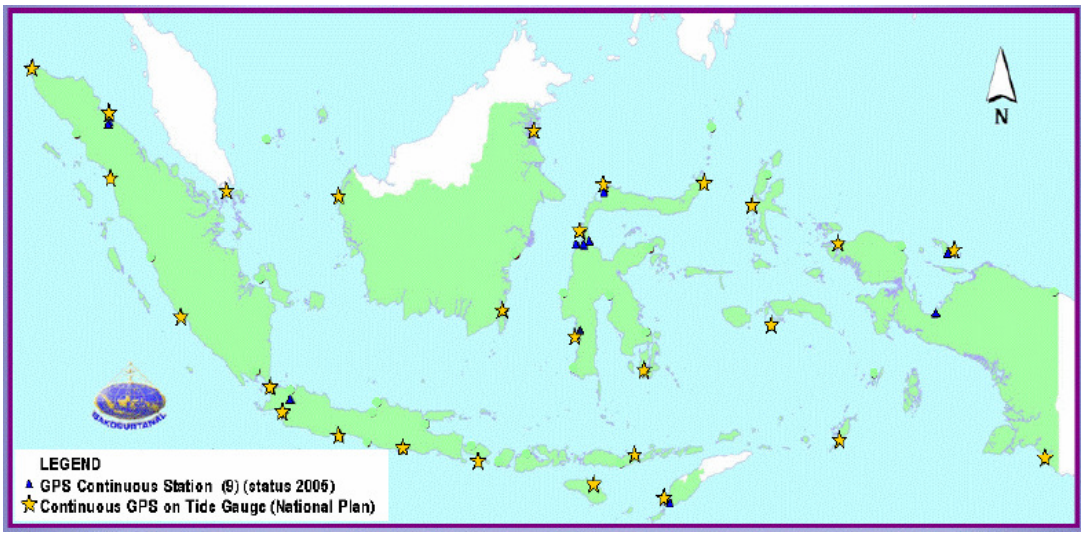

Figure 5.12. The GPS station for crustal deformation monitoring (Source: Bakosurtanal)

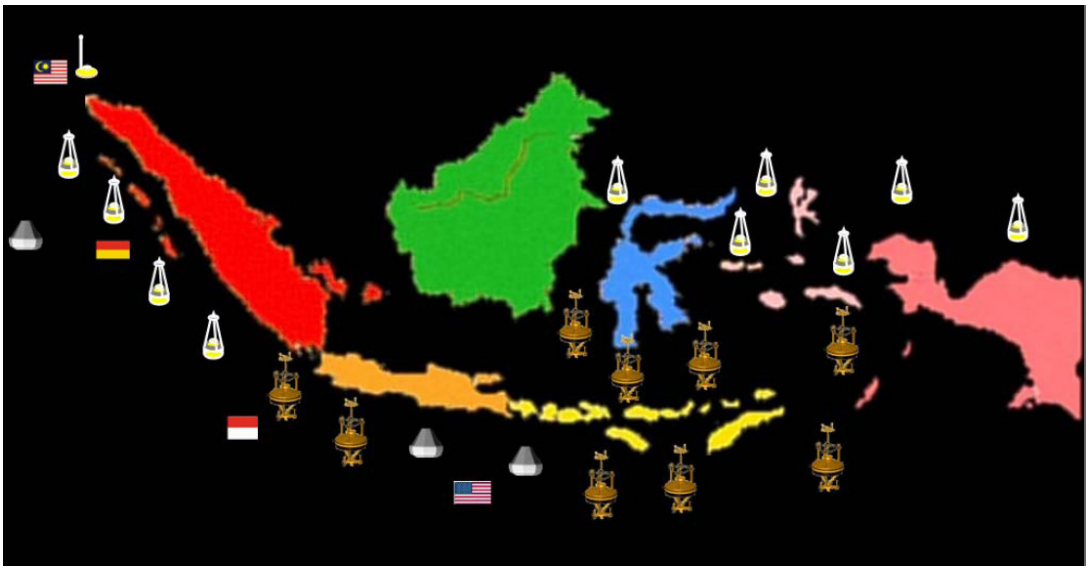

Figure 5.13. Offshore buoy arrays across the Indonesian Archipelago (Source: Harjadi, 2007)

5.4 Education Program

Most of the casualties during the 26 December 2004 event occurred because people didn't have enough knowledge about earthquakes and tsunami, and did not know how to react when they occurred. People along the west coast from Meulaboh up to Banda Aceh on Sumatra Island felt the earthquake, but did nott know how to respond and evacuate to safe places from the impending tsunamis. On the contrary, people on Simeulue Island, that preserved their ancestral knowledge, as a part of day-to-day life, survived. The message is clear and simple: after significant shaking (earthquake) run to higher ground (McAdoo et al., 2006). This type of community warning and self-evacuation are a challenge for the

modern life style in cities, where people less aware of nature and each other. Further, most of the earth science education within Indonesia concentrated on how to explore and exploit the natural resources, and less on natural hazards because there were less job opportunities.

In response to the challenge, a public education and community preparedness programme as part of the early warning system has been implemented intensively through various media such as; brochures, posters, stickers, comics, books, articles in newspapers, TV talkshows, radio broadcastings, games and simulations, trainings (including educating trainers) and community tsunami drills. This program is led by the Indonesian Institute of Sciences, in cooperation with non-government, people-centred, community-based organizations, international organizations and institutes, and other stakeholders, in tsunami prone areas. More than 80,000 printed books/material; 60 trained volunteers; 630 teacher and community trainers; 25,000 children exposed in children and community science support, and more than 8000 people attended a national exhibition on disaster preparedness have been involved (Harjadi, 2007). Due to the long return period of earthquakes and tsunamis, efforts to include earthquake and tsunami hazards and preparedness as part of educational curricula taught in schools are stillin preparation. Examples of the education material developed so far are illustrated in Figure 5.14.

Numerical modelling results of the 26 December 2004 Tsunami on Banda Aceh, combined with video taken by the survivors, and fly through satellite images processed by the European consortium on Satellite Remote Sensing (such as CNES and SERTIT) are integrated as educational outreach materials. The three-dimensional view (Figure 5.15 a) of the model results processed using ARC-GIS by Brinkmann F, von Halem G and Kellerman M (MSc student at Department of Earth and Ocean Science University of Waikato) have been combined with the video of survivors at Banda Aceh City and Meuraxa (Figure 5.15 b), to provide a comprehensive view on how tsunami propagated and inundated Banda Aceh. The fly through of satellite images shows the extent of the impacts after the event, which can be combined with photos of destruction on the ground (Figure 5.15 c). This type of media provides knowledge on the complete processes of nearshore tsunami propagation and inundation behaviour, as well as the extent of the impacts based on the real events. The results are saved in .wmf format and can be viewed using a basic multimedia viewer (Appendix 4).

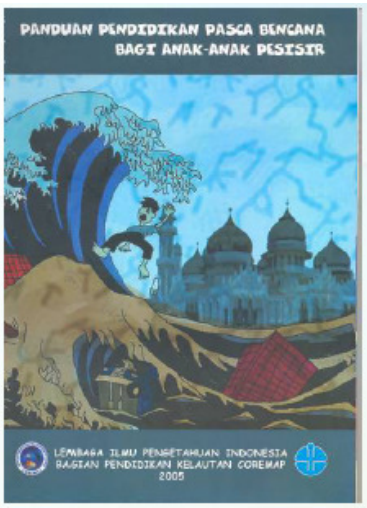

- Books

- Posters

- Comics

- Stickers

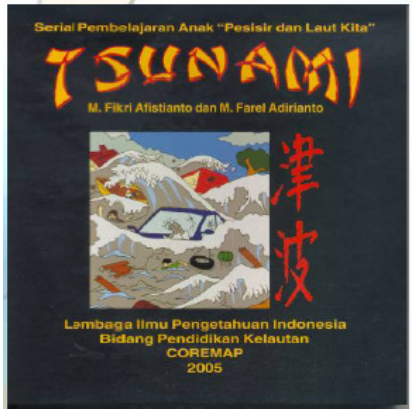

Figure 5.14. Examples of education materials such as books, comics, brochures and stickers, that have already been produced for the community.

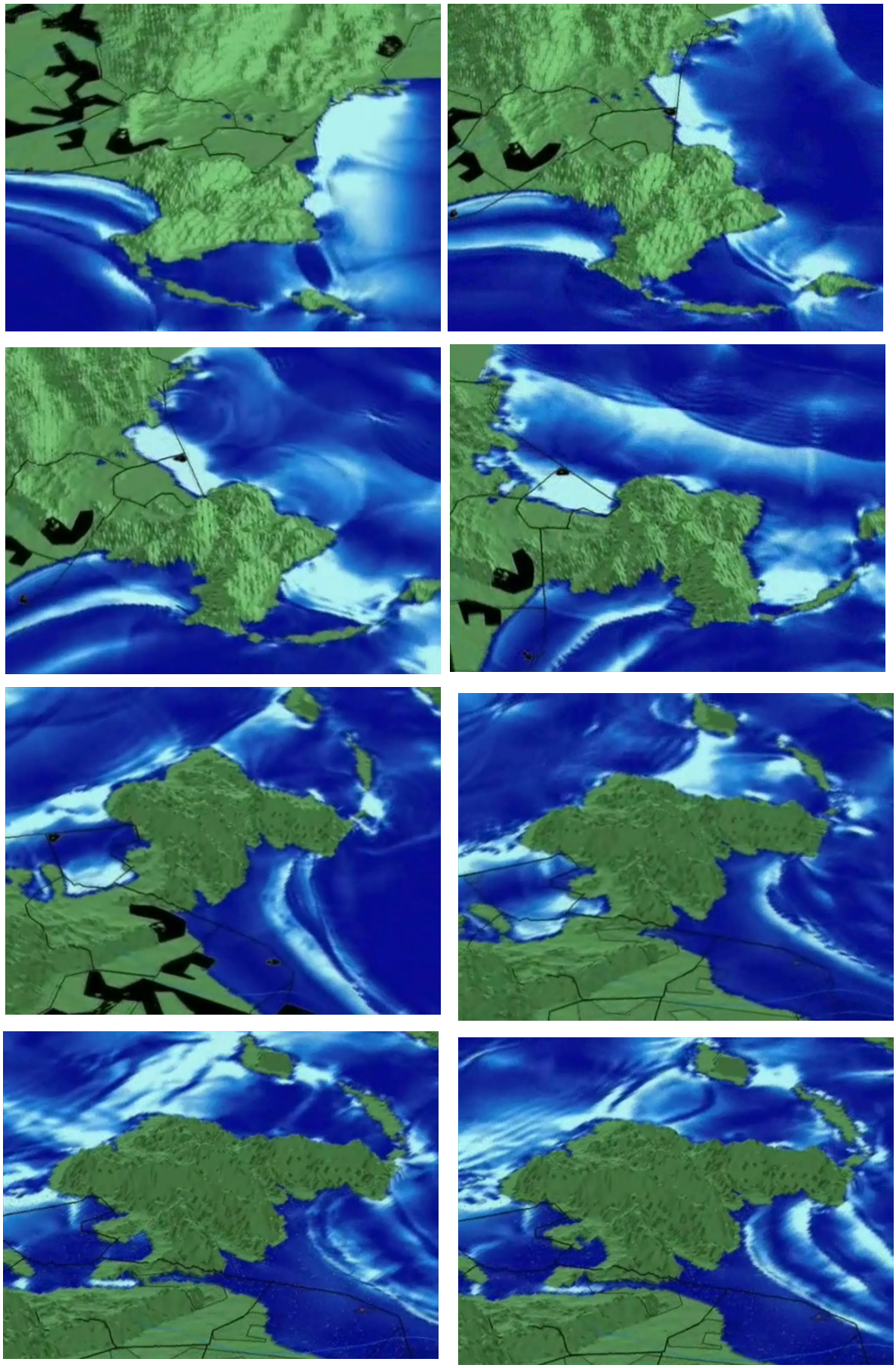

Figure 5.15 a. Three-dimensional view of tsunami behaviour movie based on numerical modelling results, which have been integrated with satellite images and video of the survivors.

Figure 5.15 b. Video taken by tsunami survivors at two locations in Banda Aceh, the first 4 snapshots at Banda Aceh City, and the rest at Meuraxa, southern Banda Aceh City.

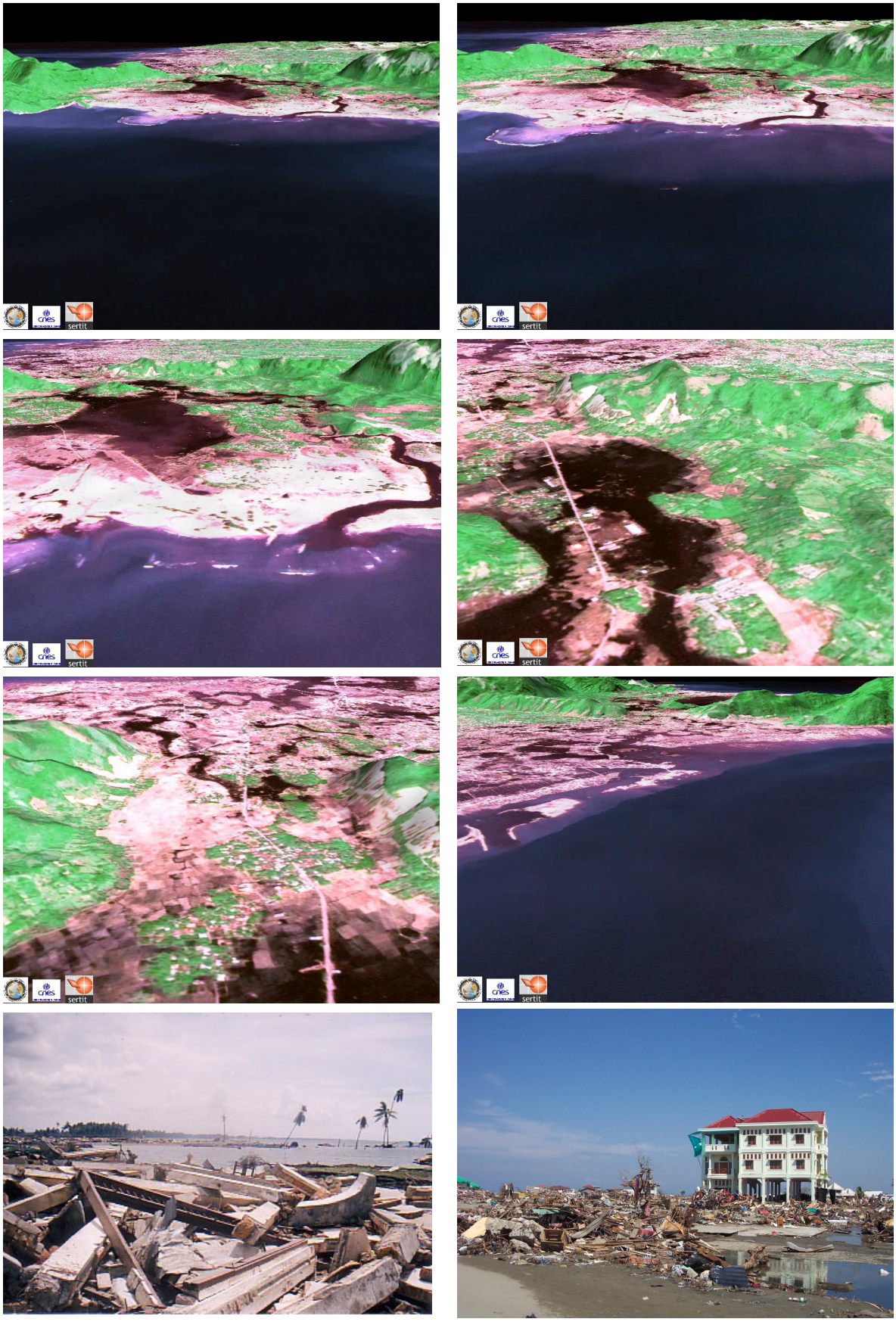

Figure 5.15 c. Three-dimensional view of tsunami impacts with fly through satellite images showed the affected areas, and integrated with pictures of the impacts on the ground (Image source: ESA-SERTIT-CNES, Photo source: GS Prasetya)

The creation of these types of education materials was inspired by people who stayed at sheltered places in Simeulue Island as reported during the field survey conducted by the International Tsunami Survey Team (ITST-2), after the 26 December 2004 and 28 March 2005 events. People in Simeulue who had local knowledge and a way to evacuate themselves into a safe places were genuinely enthusiastic to share their knowledge, and discuss the differences between the two events (Figure 5.16). After the 28 March 2005 event, the villagers occupied their shelter up to 8 April 2005 as the residents had witnessed the sea receding (actually the seafloor was exposed due to uplift) and were waiting for the water to return as a tsunami (McAdoo et al., 2006). During the discussion at the shelter, their argument was that on 26 December 2004, the sea receded only a few minutes then huge waves came. While during the 28 March 2005 event, the sea had receded for 3 days so they were afraid of bigger waves than those of 26 December 2004 (Figure 5.16).

Figure 5.16. The International Tsunami Survey Team (ITST-2) arrived shortly after the 28 December 2005 event on Simeulue Island, and had discussion with local people at shelter/ evacuation place. Most of them had a happy face and took the event as part of their daily life as shown by kids that bring fishes on his hand based on his catch of the day (Photo: ITST-2)

5.5. Discussion

For the constructed hazards map, tsunami information at shoreline was used to derive the hazards level, since detailed nearshore bathymetry and topography data were not available at the resolution needed for inundation modelling. In determining the hazards level, the observations of recent events such as the 26 December 2004, 28 March 2005, 17 July 2006 and 12 September 2007 were used to describe the level of possible damage that might occur. The 26 December 2004 event in Banda Aceh represented a catastrophic event with tsunami elevations exceeded 9 m at the shoreline and also provided data for tsunami elevations between 5 – 9 m. The 28 March 2005 and 12 September 2007 events represent tsunami impact to coastal areas with elevations up to 2 m. The 17 July 2006 event represented tsunami impact with elevations between 2 to 5 m. This approach is very useful, since many areas around the Indonesia Archipelago, and most of other parts of the world, lack detailed nearshore bathymetric and topographic data.

The precious data sets of coastal damage and tsunami elevation at shoreline measured during post-event surveys provide better evaluations of tsunami inundation. When the model grid resolution is too coarse for inundation model, the predicted tsunami elevation at shoreline can be used for constructing the hazards map when combined with coastal damages data, and allows managers to prioritize the areas that really need to have a detailed inundation mapping, whenever data are available.

The hazards map developed for tsunamigenic earthquakes, shows most of the southern coast of the Indonesian Archipelago will potentially experience tsunami elevations exceeding 8 m. The same situation also occurs for the northern arm of Sulawesi Island, west coast of Halmahera Island, northern coast Seram Island, west coast Birds Head, northern Tanimbar Island, northern coast of east Sumbawa Island and west Flores Island. The lowest hazard areas are the South Sumatra Province, Bangka Island and West Kalimantan Province. Coastal areas surrounding the Java Sea have potential hazard levels of green and yellow, while surrounding Bali and Flores Seas are yellow and orange, and surrounding the Banda Sea are yellow, orange and red for the Molluca and Sulawesi Seas. The Makassar Strait has hazard levels from green to orange.

The hazard map for volcanic sources shows the highest hazard zones are relatively localized and close to the sources. These are coastal areas surrounding the Sunda Strait, Sanggar Peninsula and Saleh Bay in Sumbawa Island, the southern coast of Flores Island, and coastal areas surrounding Banda Sea, especially the southern coast of Seram and Buru

Islands. Coastal areas surrounding the Molluca Sea have the highest hazard zones, especially those that are close to the source areas along the western coast of Halmahera Island. While the northern arm of Sulawesi Island potentially has the highest impact from an offshore volcanic sources (Sangihe and Talaud, as well as from the sources on the western coast of Halmahera Island). Most of the areas along the southern coast of the Indonesian Archipelago facing to the Indian Ocean will experience less impact from the volcanogenic tsunamis, except for the areas close to the Sunda Strait.

Combining the tsunami hazards maps for tsunamigenic earthquake and volcanogenic sources indicates the areas that are highly affected by tsunamis from both sources. These are the coastal areas surrounding the Sunda Strait, Bali, Flores, Banda, Molluca and Flores Seas. As a consequence of this situation, these regions should be prioritized for any mitigation measures, and detailed inundation models are really needed.

- **Return Interval and Early Warning System**

Considering at the recurrence interval for both sources, tsunamigenic earthquakes are more frequent then volcanogenic tsunamis. The recurrence interval for potential catastrophic tsunamigenic earthquakes (Table 2.1) is between 155 and 997 years for the minimum convergence rate, while using a maximum convergence rate predicts between 93 to 398 years. Coral reef data show that giant earthquakes at Mentawai Islands re-occurred every 230 years or so (Natawidjaja et al., 2006), while the McCaffrey (2008) method using the minimum convergence rate predicts 223 to 248 years (average ~ 235 years). However, when the maximum convergence rates are used, the calculated values are far below the coral reef data. This result suggest the importance of crustal deformation studies using continuous GPS measurements to determine an exact value for convergence rate in order to predict more accurately the recurrence interval for each source.

Coral reef data suggest that both the 1833 and 1797 events are due to re-occur. Another segment that needs to be considered to the north of these two events is the 1907 event, which larger than had been though so far. It is uncertain if this is a concern after 26 December 2004 event, since most earthquake stresses are propagating to the south but along the Mentawai fault as revealed by the 28 March 2005 event (Mw = 8.5) with an epicenter around Banyak Islands (between Simeulue and Nias Islands). The 12 September 2007 event (Mw = 8.5) occurred further south (offshore Bengkulu) leaving a gap along the previous 1797 and 1833 segment. It is not clear whether event on 28 March 2005 was a repeat of the 1861 or 1907 events, since both were located on a different segment. The 12

September 2007 event may be a repeat of 1833 event as well. Nevertheless, it is obvious that tsunami threats along the Sumatra segment are still there, with two events approaching their dormant period: 1797 and 1833.

For the seismic gaps that have already been identified, the absence of historical data before AD 1800 makes it difficult to predict future events. Particularly it is difficult to determine the convergence rate required to calculate the return interval, especially for the eastern Indonesian Archipelago where measurements are sparse. For this region most of the data used were from published literature (Newcomb and McCann, 1987; Malod et al., 1995; Rangin et al., 1999; Natawidjaja, 2003; Kopp et al., 2006; McCaffrey, 2008), which shows a number of gaps that have had no large event since AD 1800. Therefore, 2008 years has been subtracted from the calculated return period to estimate when the next event will occur (Table 5.1).

Table 5.1. Defining the future event from the return intervals

FAULT SEGMENT	Return Period	Historical Event	Next Event	Years from 2008	Standard deviation
	(years)	(AD)	(AD)	(years)	(years)
1907	173.46 - 225.5	1907.00	2080.46 - 2132.50	72.46 - 124.50	25.06
1861	192.44 - 250.18	1861.00	2053.44 - 2044.97	45.44 – 103.18	27.80
1797	162.32 - 243.48	1797.00	1959.32 - 2040.48	32.48	27.05
1833	148.68 - 223.01	1833.00	1981.68 - 2056.01	3.41 - 48.01	24.78
SUNDA GAP	233.20 - 390.03	There is no historical for these gaps, and since **AD1800** there has been no large shallow earthquake occurring in these gaps		25.2 - 181.02	28.37
West- Central JAVA GAP	161.90 - 279.28			71.28	31.03
East JAVA GAP	101.40 - 174.91			overdue	19.43
SUMBA GAP	161.55 - 315.01			5.57 - 107.01	35.00
BANDA ARC	195.08 - 487.71			70 - 278.71	97.54
SERAM FAULT	398.91 - 997.27			190.9 - 788.27	199.45
MOLLUCA	267.43 - 668.57			59.43 - 459.57	133.71
SANGIHE	295.75 - 739.38			87.75 - 530.38	147.88
NORTH SULAWESI	211.33 - 528.33			3.33 - 319.33	105.67
NORTH SUMBAWA	170.19 - 425.47			35.13 - 216.47	85.08

Table 5.1 shows that along the Sumatra segment, potential catastrophic tsunamis associated with large shallow earthquake are likely to occur within a few decades, while for the eastern Archipelago, they will be 70 to 700 years later. An exception is the East Java gap where the return period calculation shows there is an event in 1901, 1928 and 1974 but nothing on the historical record. This result demonstrates that, even if the return interval is already passed, there is still a possibility that the earthquake will not occur. This happened with the predicted big earthquake in Tokai district central Honshu Island, Japan that had

been expected to occur in 1993 – 1998 (Mogi. K., 1986; Rikitake, T., 1999). The reason why is still unclear.

- **Network station prioritizing and the Early Warning System**

Most potential tsunami sources that might impact on the coastal areas of the Indonesian Archipelago can be categorized as "near field" tsunami, where the travel time of the tsunami waves to reach the coasts are between 10 to 30 minutes. Hence, the Indonesian Tsunami Early Warning System (InaTEWS) needs to arrange the network stations based on not only the arrival time of tsunamis, but also the characteristic of the source.

Lessons learnt from the Pacific Tsunami Warning Center (PTWC) in Hawaii, and the National Oceanographic and Atmospheric Administration (NOAA), development of an early warning system in the Pacific using a real-time tsunami monitoring system called DART, the Deep-ocean Assessment and Reporting of Tsunamis (Titov et al., 2005), shows the system was most effective at providing warnings for Pacific Rim countries, that is mostly for far field tsunamis. Therefore, most of the buoy arrays along the Sunda Arc are mostly useful for the wider Indian Ocean, where tsunamis will take at least 2-3 hours to reach Sri Lanka and India. However, they will not provide much warning of tsunami that arrives within 10 to 30 minutes for the southern coast of the Indonesian Archipelago.

Considering the source mechanism of tsunamigenic earthquakes along the Sunda Arc, it is clear that any potential catastrophic tsunamigenic earthquake causes subsidence along the coast and leading negatives waves for the tsunamis. This information can be captured immediately after the earthquakes by crustal deformation monitoring system, as well as tidal stations that installed along the coast. Further, a crustal deformation monitoring system can detect any unusual pre-seismic condition. For an early warning system within this region, no offshore buoys are needed except for the wider Indian Ocean. The situation are different for the southern Java Island, where from the historical record, tsunami earthquakes are more frequent, such as the 17 July 2006 event. People along the Pangandaran coast did not feel any ground shaking before the tsunami came, nor was there subsidence along the coast following the earthquake. For tsunami earthquakes it is necessary to detect the sudden change of sea level offshore after the earthquake and therefore a combination of offshore buoys, and tide stations is useful. For an early warning system within the Indonesian Archipelago, tide stations installed close to the shore are easier to maintain, and more cost effective compared to operating the offshore deep-water buoys.

For the volcanic sources, it is not critical to have a complete early warning system as a volcanic eruption takes several days or weeks to develop. The most important factor for volcanic sources is to recognize which generating mechanisms are likely to generate tsunamis that could cause devastating impacts to the surrounding areas. Once the source mechanism of the tsunami is clear, then mitigation measures can be optimally planned.

- **Mitigation Measures**

The hazard maps provide the information necessary for designing long term mitigation measures for reducing the economic impacts, as well as to prevent loss of life, in addition to the early warning system and preparedness and awareness programs. The usual mitigation response for reducing the economic impact is to opt for structural measures such as building seawalls, dykes or breakwaters. Horikawa and Shuto (1983), based on experiences in Japan, stated that it is quite dangerous to believe that the violent attack of tsunami can be completely prevented by man-made structures, and it is incorrect to depend too much on the functioning of coastal defence structures.

Generally, a coastal defence structures could minimize the possible impact when they are designed properly, and involve a combination of soft (non-structural) and hard (engineering/structural) solutions. Lessons learnt from the 26 December 2004 event (Prasetya et al., 2008[b]) show that for the extreme run up and inundation flows in Banda Aceh, huge structures ~ 15 m high would be required, but are not economically feasible. However, mature mangrove stands may offer reasonable protection, and this option shows greater promise as an affordable solution, especially if implemented in combination with sand dunes and coastal forest, but this also needs careful design and implementation. Not all types of mangroves and coastal forest can withstand extreme events. The mangroves and coastal forest at Babi Island (Figure 5.17) exemplify criteria for healthy mangroves and coastal forests, where its naturally conserved, and has not suffered from intervention of human activities for more than 50 years (Prasetya et al., 2008[b]). Shuto (1993) recognized this previously with positive views of the function of coastal forest if it is carefully designed. He reported that forests:

- stop floating debris;
- reduces water flow velocity and inundation height;
- provides a life-saving means by catching people carried off by tsunamis; and
- collects wind-blown sands and raises dunes that act as a natural barriers against tsunamis.

However, some trees could still be up-rooted by tsunamis and become destructive floating debris for extreme events such as the 26 December 2004. Further research should be done, and careful design should be considered before it comes into practice. Need deep-rooted trees and a wide enough forest strip.

Figure 5.17. The healthy mangroves in Babi Island offshore Simeulue that have been preserved for the last 50 years. All debris including blocks of coral were, caught by the trees.

For large low-lying areas, where there are no hills nearby, vertical evacuation structures should be provided, either by using an existing building or newly constructed structures, such as those now built in Banda Aceh. Five vertical evacuation buildings (Figure 5.18) have been constructed. The first tsunami drills were carried out on November 2, 2008 to test the structures, and involved more than 8000 people in Meuraxa district. The evacuation buildings are multifunctional and can be utilized for daily activities and community meeting inline with tsunami preparedness and awareness activities. One building is also used for the Tsunami Research and Disaster Mitigation Centre (Figure 5.19).

Figure 5.18. Two evacuation buildings (black arrows) are constructed within a new housing complex. Photo is taken from another evacuation building (Photo source: GS.Prasetya).

Figure 5.19. Vertical evacuation buildings in Banda Aceh that have a multifunction design. One of them is the Tsunami Reseach and Disaster Mitigation Centre Building (Photo source: GS.Prasetya).

- **Challenge in sustaining public education, preparedness and awerness program.**

Given the long return periods for catastrophic tsunami events, it is a challenge to sustain all mitigation activities (upstream and downstream) within the system until the next event occurs. There is need to develop life-long efforts to educate the population about the hazards and preparedness for an extreme event. Especially, it is important that preparedness and awareness should be practiced on a routine basis. The most successful approach is to

include earthquake and tsunami hazards, and preparedness, as part of educational curricula taught at schools, especially for those regions that have high probability of suffering extreme damage by the tsunamis. Programs such as an annual in remembrance of the 26 December 2004 event are likely to be effective (Figure 5.20).

Figure 5.20. Tsunami drills in Banda Aceh on November 2, 2008, utilizing vertical evacuation buildings such as the Tsunami Research and Disaster Mitigation Center Building, and one of the community buildings in Meuraxa district (b) (Photo source: GS.Prasetya).

5.6. Summary

- A tsunami hazards map for the Indonesian Archipelago has been constructed based on numerical modelling results of tsunami from potential tsunamigenic earthquakes and volcanogenic sources. Five levels of hazards were defined, based on modeled and historical tsunami elevation at the shoreline and its correlation with the extent of damage and destruction from recent events. These are: red for very high hazards

with tsunami elevation at the shoreline greater than 9m, orange for high hazards with tsunami elevation from 5 to 9 m, yellow for medium hazards with tsunami elevation from 2 – 5 m, and green for low hazards with tsunami elevation at shoreline < 2 m. These maps provide basic information to decision makers considering development of coastal areas, as well as prioritizing detailed inundation map.

- Most tsunamigenic earthquakes identified potentially produced tsunami elevations > 8 m along the coastline that perpendicular to the fault plane. Hence, almost all of the southern coast of the Indonesian Archipelago is categorized very high risk. Likewise is the situation for the northern arm of Sulawesi Island, west coast of Halmahera Island, northern coast of Seram Island, west coast of Birds Head, northern Tanimbar Island, northen coast of east Sumbawa Island and west Flores Island. Similarly, the simulated volcanogenic tsunami events show that they produce greater tsunami elevations in the near field, and accordingly the coastline surrounding the Sunda Straits, southern coast of Seram and Buru Island and northern coast of Sumbawa are categorized as a high to very high risk zone. Most of the areas that had less impact from both sources (tsunamigenic earthquakes and volcanic sources) are South Sumatera Province and Bangka Island, and the areas that had highest impact from both sources are Sunda Strait, West Halmahera and northern arm Sulawesi Islands, North Sumbawa and Flores Islands, South Seram and Buru Islands, eastern Sulawesi and West Tanimbar Islands.

- For the high and very high-risk zones there are no structural mitigation measures that are economically feasible; so the first one (1) kilometer from the shoreline should be a sacrificial zone. Only substantial structures, like mosques have survived. Vertical evacuation is one of the solutions to prevent the loss of live and for the long run, planting mangroves and coastal forest combine with sand dunes will be the appropriate choice, but should be implemented through careful design.

- The hazards map and recurrence interval for each potential tsunamigenic earthquakes zone identified, provide useful information in prioritizing the Early Warning System implementation, as well as the preparedness and awareness

programs. The need to install more seismic monitoring, tidal station along the coastal region and continuous Global Positioning System (GPS) is obvious, combined with earthquake monitoring and calibrating the recurrence interval computation, as well as the tide station on coastal region. Development of life–long efforts to educate the population about the hazards and preparedness for an extreme event, into educational curricula taught at schools are the obvious most favorable ways. The tsunami drills should be carried out annualy and be part of activities during the remembrance of the 26 December 2004 events, not only for Banda Aceh, but for most of the tsunami prone areas identified by the hazards map.

- The natural warning is the earthquake. If the ground shaking is felt long enough (up to 1 minute), never wait until warning from the authorities is sent out, but immediately find higher ground before it is too late! In case the earthquake was not felt, then wait the information and warning from the authorities.

5.7. References

Harjadi, P.J.:2007, National report establishment of Indonesia Tsunami Early Warning System (InaTEWS), Intergovernmental Coordination Group for The Indian Ocean Tsunami Wanring and Mitigation System (ICG/IOTWS), Mombassa, 28 Feb-2 March 2007, Kenya. 70 p.

Horikawa, K and Shuto, N.: 1983, Tsunami disaster and protection in Japan, in K.Iida and T.Iwasaki (eds), *Tsunamis - Their Science and Engineering*, Terra Scientific Publisher Co., Tokyo, pp. 9 -22.

McAddo, B.G., Dengler, L., Titov, V., and Prasetya, G.S.: 2006, Smong: How an oral history saved thousands on Indonesia's Simeulue Islands, Earthquake Spectra, Special Issue III, **22**, pp. 661-669.

McCaffrey, R.: 2008, Global frequency of magnitude 9 earthquakes, *The Geological Society of America* **36 (3)**, 263 – 266.

Mogi, Kiyoo.: 1986, Recent earthquake prediction research in Japan, *Science* **233 (471)**, pp. 324 – 330.

Natawidjaja, D., Sieh, K., Chlieh, M., Galetzka, J., Suwargi, B., Cheng, H., Edwards, R.L., Avouac, J.-P., Ward, S.: 2006, Source parameters of the great Sumatran megathrust earthquakes of 1797 and 1833 inferred from coral microatolls, *Journal Geophysical Research* **111, B06403**, pp.1-37.

[a]Prasetya, G.S., Healy, T.R., de Lange, W.P.: 2008, Hydrodynamic modeling of tsunami overwash of Whitianga Townships and Harbour, Department of Earth and Ocean Sciences, prepared for *Environment Waikato*, 92 p.

[b]Prasetya, G.S., Healy, T.R., de Lange, W.P.: 2008, Extreme tsunami runup and inundation flow at Banda Aceh, Indonesia: Are there any solution to this type of coastal disaster? in Wallendorf, L., Jones, C., Eing, L., Jaffe, B (eds): Solution to Coastal Disaster 2008 Tsunamis, , ASCE, pp.13-26.

Prasetya G.S.: 1994, Contribution of Oceanographic Data Buoys in Numerical Modelling of Marine Environments in Indonesian Waters, in Proceedings of Joint Cooperation Norwegian - Indonesia in Marine Science and Technology, December 1994, Jakarta, pp. 64-74.

Rikitake, T.: 1999, Probability of great earthquake to recur in the Tokai district, Japan: Reevaluation based on newly-developed paleoseismology, plate tectonic, tsunami study, micro-seismicity and geodetic measurements, *Earth Planet Space* **51**, pp.147 – 157.

Shuto, N.: 1993, Tsunami intensity and disaster, in S.Tinti (ed). Tsunami in the world, Advances in Natural and Technological Hazards Research, Kluwer academic Publishers, Dordrecht, pp.197 – 216.

_____, Expert mission to Indian Ocean Countries to assess requirements and capacity for an effective and durable National Tsunami Warning and Mitigation System, Indonesia, 29 August – 2 September 2005, Intergovernmental Oceanographic Commission, 60 p.

_____, Report of Intergovernmental Coordination Group for The Indian Ocean Tsunami Warning and Mitigation System (ICG/IOTWS), Proceeding of the IOTWS meeting, Mombasa.

Chapter 6

Major Research Findings and Conclusions

6.1. Introduction

The Indonesian Archipelago is the place where four (4) major plates (the Eurasian, Indo-Australian, Caroline and Philippines Sea plates) meet and collide, and form a complex region containing a subduction-zone, collision zone, fault zone, forearc basin, backarc thrusting and spreading zone, and a volcanic chain along an island arc. This geologic setting has made the region an active seismic zone, richly endowed with natural resources that made the region important for trade since at least the seventh century. It possesses vast areas of wilderness that supports the world's second highest level of biodiversity, in line with a distinct ethnic, linguistic and religious groupings that made the region the world's fourth most populous, and hence the most vulnerable from the geologic hazards.

The 26 December 2004 event followed by the 28 March 2005 event, were the defining moments for the population in reassessing the existing philosophy that purely concentrated on exploration and exploitation of natural resources, into a new paradigm of natural hazards based development programme. Change from response into mitigation actions lead to assessment of all the potential geologic hazards that may impact and disrupt the life and welfare of people who live in the region. These two events were also a turning point in studying a subduction zone earthquake generated tsunamis (Synolakis and Bernard, 2006; Geist et al., 2007). Scientists have urged the public and policy makers to consider all subduction-type tectonic boundaries to be "locked, loaded and dangerous zones that possess potential tsunami threats". Reliable and comprehensive databases for past and recent events, and subsequent scientific analysis to define potential threats, are needed in mitigating the tsunami hazards.

Results of assessment on seismotectonic characteristic of the Indonesian Archipelago in conjunction with identification of previous and potential tsunamigenic earthquakes and volcanogenic tsunamis, as well as numerical modeling of tsunamis based

on scenarios developed, shows the region is very susceptible to tsunamis from subduction zone earthquakes and volcanic eruptions.

6.2. Tsunamigenic Region

The historical record shows that most of the catastrophic tsunamis have occurred along the Sunda Arc subduction zone up to Lesser Sunda, including the Krakatau volcano. Fewer events have occurred in the eastern part of the Archipelago along the Banda Arc, Halmahera and Molluca Collision Zones, northern Sulawesi Island, and the Makassar Straits. Along the Sunda Arc, most tsunamis are from earthquake sources and only three from the volcanic sources (Weh Island, during Pleistonce, Krakatau in 1883, and Tambora Volcano in 1815). While in the eastern part of the archipelago, the size and extent of the earthquakes and associated tsunami impacts were less but more frequent due to the complex tectonic structure. Within this region, volcanic tsunamis are more likely with 18 sources compared to the western Archipelago.

The potential catastrophic tsunamigenic region has been determined using seismic gap analysis based on historical records, geometry and dimension of basin configuration, major active thrusting faults, the nature of the subduction zone geometry, and the activity of a major volcanic arc along the Indonesian Archipelago. Fourteen (14) segments of catastrophic tsunamigenic earthquakes and 21 potential volcanogenic tsunami sources were identified. These are: the return period of the 1907, 1861, 1797 and 1833 events on the west coast of Sumatra Island, Sunda Gap at the offshore of Sunda strait from Enggano Island to West Java, West-Central Java Gap, East Java Gap, Sumba Gap, Banda Arc Gap, Seram Trench, Molluca Trench, Sangihe Trench, North Sulawesi Subduction Zone, and North Sumbawa Subduction Zone. For the volcanic sources, there are 3 volcanoes along the Sunda Arc (Weh Island, Anak Krakatau, and Tambora), and 18 volcanic island arcs on the eastern Archipelago, which is around the Banda and Molluca Seas, and offshore of the northern arm of Sulawesi Island (Sangihe- Talaud Islands arc).

Using McCaffrey (2008) methods and convergence rate from the published literature (Newcomb and McCann, 1987; Malod et al., 1995; Natawidjaja, 2003; Kopp et al., 2006, McCaffrey, 2008), the recurrence interval of each source was calculated, and showed that tsunami threat on the west coast of Sumatra remains, and has nearly reached the dormant period. The micro atoll data for recurrence interval of the Mentawai Islands is about 200 - 240 years (Natawidjaja et al., 2006 and Sieh, 2006), which is consistent with

calculations using the minimum value of the convergence rate (40-45 mm/years) i.e. between 223 to 243 years. Using the maximum convergence rate, which is gives a minimum recurrence interval, most of the historical events and the gaps identified (ie., Sunda, West-Central Java, East Java, and Sumba Gaps, as well as Banda Arc and North Sumbawa Trench) were overdue, except for the 1907, Sangihe, Molluca and Seram Trenches (Table 6.1).

The minimum convergence rates that provide maximum recurrence interval show only that the East Java Gap is overdue, and was supposed to occur in 1974. Using an average value of convergence rates, the 1797 event is overdue and was supposed to occur in 1991, the West-Central Java Gap in 2004, and East Java gap in 1901. However, the historical record shows that there was no tsunami within the identified gap since AD1800. Overall, the near future event that falls within the period less than 50 years from now (2008) are West Sumatra segment (1861, 1797, 1833) as well as for North Sumbawa Trench and above 50 years for the 1907 and most of tsunamigenic sources around the Banda Sea except the northern Sulawesi Trench and Sumba Gap that might be possible occurred within 3 – 5 years from 2008 according to recurrence interval based on maximum and average convergence rate respectively.

The calculation of recurrence intervals shows that the East Java Gap is overdue for a large event using either maximum, minimum or average convergence rates. The situation for the East Java Gap is comparable to the expected earthquake in the Tokai district of central Honshu Island, Japan, that was expected to occur 10 – 15 years ago, but has still not occured yet (Mogi, K., 1986; Rikitake, T., 1999). Nevertheless, it is clear that continuous Global Positioning System (GPS) measurements are needed that will give an accurate convergence rate to improve earthquake prediction, as well as in refining calculation of the recurrence interval. Paleotsunami data along the coast, on the other hand, will be very useful in providing the evidence of tsunami events in the past to refine the recurrence interval calculation using empirical method, as has been applied on Simeulue Island.

There is an indication that most rupture propagation of the large tsunamigenic earthquakes nucleated close to the trench along the Sumatra segment is to the northwestward (e.g., the 26 December 2004 and 12 September 2007). This is consistent with the direction of the Indo-Australian plate movement along the oblique subduction zone. For those earthquakes, which are generated further away from the trench along the Mentawai Fault Zone such as the March 28, 2005 (and also the 2002 and 1935), their aftershocks were distributed equally on both sides of the epicenter and did not generate

large tsunamis. This implies better relocation of the 1861 and 1907 segment. Any sequence of earthquakes nucleated at the southeastern end of each segment boundary and located close to the trench, is a warning for the possible generation of damaging tsunamis.

Unlike the tsunamigenic earthquake sources, the volcanogenic tsunami sources are better defined in terms of their position, but difficult to predict when the volcano will erupt. Among the 21 identified volcanogenic sources, three of them were definitely potentially generated catastrophic tsunamis at regional scales. These are the Anak Krakatau Volcano in the Sunda Straits with the historical event in 1883, Tambora Volcano at Sanggar Peninsula Sumbawa Island with the historical event in 1815, and the Banda Api Volcano in Banda Seas with a pre-historic caldera that had the same size as the pre-historic Krakatau Caldera.

6.3. Tsunami Behaviour and their Impacts

Numerical modelling results from an identified tsunamigenic earthquake and volcanogenic sources show the different behaviour of tsunami and their impact on the coast in the near field and far field. Tsunami from earthquake sources provides almost the same impacts both on near field and far field, while the volcanic sources depend on the generating mechanism. In most cases, they are either generated by pyroclastic flow, submarine explosion, or caldera collapse; the first wave is the most dangerous for the near field. However, for the far field, the most dangerous is not always the first wave as shown by the caldera collapse mechanism for the pre-historic Banda Api volcano, where the waves approaching the far field coast as a wave packet.

The initial leading waves for earthquake sources in most cases were consistent either for near field or far field, and become an indication of the incoming tsunami to the coast. This characteristic had been used as an early warning for impending tsunami by the people in Simeulue Island who evacuated to a safe place during the 26 December 2004 event. However, the initial condition for volcanic sources depends on the generating mechanism. In the case of pyroclastic flows, mostly of the leading wave is positive, while for a submarine explosion which involves a positive leading wave and deep trough due to the crater formation, it is not always the same. At some places along the coast, the leading wave is positive and in other places it is negative. There is no clear generalization for this type of event.

Table 6.1. The earthquake parameters, recurrence interval, and future events based on the McCaffrey (2008) method.

FAULT SEGMENT	Total Length of Segment	SLIP	Mo	M_{wmax}	Convergence Rate (mm/years)			Recurrence Interval (years)			Historical Event (year)	Potential Next Event (year)			Standard Deviation (+/-)
					Min	Max	Avg	Max	Min	Avrg		Max	Min	Avrg	
	(km)	(m)	(Nm)	(Nm)											(years)
1907	360.8	9.02	5.622E+21	8.43	40	52	46	225.50	173.46	199.48	1907	2133	2080	2106	25
1861	400.28	10.01	6.92E+21	8.49	40	52	46	250.18	192.44	221.31	1861	2111	2053	2082	29
1797	389.57	9.74	6.555E+21	8.48	40	60	50	243.48	162.32	194.79	1797	2040	1959	1992	27
1833	356.82	8.92	5.499E+21	8.42	40	60	50	223.01	148.68	178.41	1833	2056	1982	2011	25
SUNDA GAP	624.04	15.60	1.682E+22	8.75	50	66.9	58.45	312.02	233.20	266.91	No historical record since AD1800	2112	2033	2067	28
West-Central JAVA GAP	446.85	11.17	6.568E+21	8.48	40	69	54.5	279.28	161.90	204.98		2079	1962	2005	31
East JAVA GAP	279.85	7.00	2.576E+21	8.20	40	69	54.5	174.91	101.40	128.37		1975	190	1928	19
SUMBA GAP	504.02	12.60	1.097E+22	8.62	40	78	59	315.01	161.55	213.57		2115	1962	2014	35
BANDA ARC	390.17	9.75	1.315E+22	8.68	20	50	35	487.71	195.08	278.69		2288	1995	2079	98
SERAM FAULT	797.82	19.95	2.767E+22	8.89	20	50	35	997.27	398.91	569.87		2797	2199	2370	199
MOLLUCA	534.86	13.37	1.236E+22	8.66	20	50	35	668.57	267.43	382.04		2469	2067	2182	134
SANGIHE	591.50	14.79	1.511E+22	8.72	20	50	35	739.38	295.75	422.50		2539	2096	2223	148
NORTH SULAWESI	422.66	10.57	1.157E+22	8.64	20	50	35	528.33	211.33	301.90		2328	2011	2102	106
NORTH SUMBAWA	340.38	8.51	3.811E+21	8.32	20	50	35	425.47	170.19	243.13		2225	1970	2043	85

Mo = moment magnitude
M_{wmax} = maximum moment magnitude
Red box = event that overdue
Yellow box = event that nearly approaching the dormant period < 40 years (from 2008)
Green box = event that > 50 years (from 2008)

Nearshore bathymetry and geometry position of the coastal region will determine the tsunami characteristic and their impact on the coast even though they come from the same source. Wide continental shelves with gentle slopes on an exposed coast that lie perpendicular to the source, provide steep waves, while coast that is located not perpendicular to the source region and laid on the lee side of offshore islands with relatively steep bathymetry will experience a tsunami that smoothly builds up a kind of symmetric sine wave through refraction and diffraction processes. Numerical modelling results of the 26 December 2004 Tsunami (Prasetya et al., [c] Chapter 3) shows results that are consistent with field measurements of the tsunami, and damage characteristics of the region reported by the International Tsunami Survey Team (ITST).

The steepest waves with highest elevation along the coast ranged from 15 m to 30 m and occurred on the west coast of Banda Aceh (Lhok Nga – Lampuuk) that lies perpendicular to the source. The waves wiped out all buildings and vegetation, left bare coastal areas up to 3 km inland and caused heavy erosion and scour at the beach front and the river mouth. The waves penetrated the largest distances inland on gently sloping topography as far as 6.8 km, and runup on steeply sloping topography as high as 35 m. To the northwest, the coast that represents a smoothly build up of a symmetric sine wave with tsunami elevation along the shoreline ranged from 6 to 12 m, shows the devastating effects to the buildings and coastal landforms due to broad coastal plains with low, flat ground that allowed the tsunami waves to maintain their flow depth up to 5 km inland as the overland flow speed decreased.

For coastal topography with dunes and sand ridges, the overland flow speeds decrease as the wave front approaches the shoreline, and then increase again before it slows further inland. There is a more complicated distribution of tsunami elevation, flow depth and speed when the flow encounters irregular coastal topography. Rivers, drainage channels and creeks extend the inundation further inland. Mostly, the overland flow directions are determined by the incoming tsunami wave direction up to certain distance from the shoreline until the flow speed decreases, and the flow follows the low-lying terrain as gravity driven flow. The high-speed unidirectional flows were obvious up to 2 – 3 km from the shoreline on gently sloping topography, as shown by the model results of the 26 December 2004 event, where tsunami elevation at the shoreline was > 10 m.

The modelled tsunamis of the 26 December 2004 event also show that the distribution of the flow depth is not always consistent with distribution of the flow speed. The areas that experienced the deepest flooding do not necessarily experience the fastest

flows, while the damage within urban and rural or natural areas mostly coincide with the flow speed distribution rather than runup and inundation depth distribution. Consequently, in assessing the tsunami hazards, especially when making inundation maps, the overland flow speed should be taken into account or incorporated into the inundation map as an addition to inundation depth information.

The availability of high resolution topography and bathymetry data sets such as from LIDAR (Light Detecting and Ranging) and multibeam survey provide an opportunity for detailed modelling of inundation behaviour for hazard mitigation, such as in designing evacuation sites, buildings and routes, as well as city planning and preparedness. The two types of LIDAR data sets were useful in analysing the flow field, and help to minimize possible impacts of tsunamis through careful designing and placing vital infrastructure or life line facilities, and avoiding the most dangerous places, or preventing the existing places through designing necessary mitigation measures (Prasetya et al., 2008a).

Extreme runup and inundation flow during the 26 December 2004 event raised the question as to whether there is any solution for this type of coastal disaster. The study of Prasetya et al., (2008[b] Chapter 4) suggested that coastal protection structures are only effective against a tsunami if their height is at least ¾ of the highest tsunami elevation height. To protect a long coastline with rivers or canals, specific design may need a barrier or gate across a river mouth with guarantee that the gates will work during extreme event. Another solution is to use "vegetation greenbelts" that usually consist of mangroves and coastal forest. The greenbelt could provide protection to some extents, but needs careful design and implementation as well as in combination with a dune system. Not all mangroves and coastal forest could withstand extreme event. Possibly, the mangroves and coastal forest at Babi Island, offshore Simeulue, which is naturally conserved and had not suffered intervention by human activities for more than 50 years, exemplify a criterion for healthy mangroves and coastal forest. Planting mangroves and coastal forest is a desirable affordable response, because they function not only as a coastal protection system for tsunamis, but also as nursery ground for many coastal wetland habitats. If the choice is to use a hard structure, it must be designed as a multipurpose structure since the return period of tsunamis maybe very long.

The impacts of tsunami on the coastal areas include not only the destruction of the infrastructure, buildings, housing, coastal landforms, as well as massive casualties, but also generate resulting waste and debris that mixed with other flotsam during wave runup and backwash, that creates another huge problem leading to serious long term adverse

environmental and natural resources consequences. The 26 December 2004 event demonstrated that the extent of works for the clean up operation in Banda Aceh took more than 4 months after the event. Understanding the pathway and distribution of the suspended materials and flotsam caused by tsunamis is important for a proper hazards mitigation plan, and waste management action that can be assessed through debris dispersal model (Prasetya et al.[d], Chapter 3). The model results show that most of the flotsam was transported inland through unidirectional pathways up to 3 km inland before it became transported by the gravitational flows controlled by the local topography. The first and second flows dragged back some of the flotsam inshore through almost the same pathways, and became transported further offshore through advection and eddy formation as revealed on satellite images 4 hours after the event.

Input from the dispersal modelling results can be added into the hazard maps in conjunction with the inundation height and flow speed information, and can be used to develop a scenario for the existing infrastructure in the tsunami prone areas. A better plan would be to relocate possible dangerous flotsam or pollutant sources, while developing a proper post-disaster waste management plan that should start immediately at sites which are vulnerable to further contamination or spreading of contaminating substance and goods. Reconstruction work for the destroyed infrastructure and buildings can be done rapidly, but environmental rehabilitation and remedy will take a longer time.

6.4. Hazards Map, Early Warning and Education

- **Hazards Map**

A tsunami hazard map for the Indonesian Archipelago has been constructed based upon numerical modelling results of tsunami from identified potential tsunamigenic earthquakes and volcanic sources. Nearshore tsunami behaviour can be accurately reproduced using available numerical codes of tsunami generation, propagation and inundation. However, the results strongly depend on detailed information about the source mechanism and local bathymetry and topography of the region. The lack of detailed nearshore bathymetry and topography at a resolution needed to represent the nearshore and overland flow dynamic of tsunamis within the Indonesian Archipelago are obvious. Therefore, the hazard levels are defined based on tsunami elevation at a shoreline, and its correlation with the level of damage and destruction derived from the recent events using four different colours. These are: red for very high hazards with tsunami elevation at a

shoreline greater than 9 m, orange for high hazards with tsunami elevation from 5 to 9 m, yellow for medium hazards with tsunami elevation from 2 – 5 m, and green for low hazards with tsunami elevation at shoreline below 2 m (Table 6.2). This hazard map provides basic information for decision makers in considering the development of the coastal areas and prioritizing the necessary detailed inundation map.

Table 6.2. Hazards level classification in relation with possible destruction or damage

Hazards Level	Red	Orange	Yellow	Green
Description:	**Very high hazards zone**	**High hazards zone**	**Medium hazards zone**	**Low hazads zone**
Tsunami				
Elevation at shoreline	> 9 m	5 < H ≤ 9 m	2 < H ≤ 5 m	H ≤ 2 m
Damages areas:				
Gently sloping topography	2 - 7 km	2 - 5 km	1 - 2 km	up to 1 km
Steeply sloping topography	≥ 35 m	up to 20 m	up to 10 m	up to 5 m
Damage to the buildings within 1 km from the shoreline:				
Reinforced 2 - 3 level of concrete structure with open floor	Survived, damage on the first and second floor, broken /collpase wall	Survived, damage on the first and second floor, broken /collpase wall	Survived, damage on the first floor, collapsed broken wall	Survived
Reinforced 1 level of concrete structure	Complete destruction	Complete destruction	minor to heavy destruction, partially collapse/broken wall	Survived, minor damage mostly on the wall
Brick house without reinforced	Complete destruction	Complete destruction	heavy destruction, partially collapse/broken wall	Survived but partially damaged or collapsed
Simple house	Complete destruction	Complete destruction	Complete destruction	mostly damaged on the wall
Casualties	Most inhabitants perished	Massive casualties, and injured people	Some casualties, and injured	Mostly people get injured, minor casualties
Environmental changes:				
beach front	Heavy erosion/scour	Heavy erosion/scour	erosion/scour	small erosion
river mouth	widen	widen	change	small change
trees	most uprooted, few survived.	mostly uprooted, some survived.	most survived, some uprooted	mostly survived

For the high and very high-risk zones, there are no structural mitigation measures that are economically feasible, and the first 1 km from the shoreline is the “sacrifice zone”. Only buildings with advances design structures such as mosques will be survived. Vertical evacuation is one of the solutions to prevent the loss of life and for the long term, planting mangroves and coastal forest combined with sand dunes should be the appropriate choice.

Most of tsunamigenic earthquakes identified potentially produced tsunami elevation greater than 8 m along the coastline when located perpendicular to the fault plane, hence, almost all of the southern coasts of Indonesian Archipelago along the Sunda Arc are categorized high and very high hazard zone. Likewise, for the northern arm of Sulawesi Island, west coast of Halmahera Island, northern coast of Seram Island, west coast of Birds

Head, northern Tanimbar Island, northen coast of east Sumbawa Island and west Flores Island.

The volcanogenic tsunamis events simulated show that they produce greater tsunami elevation in the near field; therefore, the coastline surrounding the Sunda Straits, southern coast of Seram and Buru Island, and northern coast of Sumbawa are categorized as a high to very high hazard zone. Most of the areas that had less impact from both sources (tsunamigenic earthquakes and volcanic sources) are South Sumatera Province and Bangka Island. The areas that had highest impact from both sources are Sunda Strait, West Halmahera and northern arm Sulawesi Islands, North Sumbawa and Flores Islands, South Seram and Buru Islands, eastern Sulawesi and West Tanimbar Islands. As a consequence, these regions should be prioritized in any mitigation efforts.

- **Early Warning**

The Indonesian Tsunami Early Warning System (InaTEWS) that is already in place needs to evaluate most of their offshore buoys located in the Indian Ocean, unless they are dedicated for and as a contribution to wider Early Warning System in the Indian Ocean. Considering the source mechanism of tsunamigenic earthquakes along the Sunda Arc, any potential catastrophic tsunamigenic earthquake will provide the initial information of subsidence along the coast, and leading negative waves for the tsunamis. This information can be captured immediately after the earthquakes by the crustal deformation monitoring system as well as tidal stations that are installed along the coast. The crustal deformation monitoring system can also detect any unusual pre-seismic condition.

For the southern coast of Java Island, from the historical record, tsunami earthquakes are more frequent such as occurred during the 17 July 2006 (M_w = 7.6). People along the Pangandaran coast had not felt any ground shaking before the tsunami arrived, nor observed subsidence along the coast following the earthquake. The need to detect the sudden change of sea level offshore after the earthquake is important, and combination of the offshore buoys, and tide stations along the coast will be helpful. In terms of maintaining the long term sea level monitoring system for the early warning system within the Indonesian Archipelago, utilizing the tide stations installed along the coast are more cost effective compared to operate the offshore buoys.

- **Education Program**

The general population does not have enough knowledge about earthquakes and tsunamis, and how to react when they occur was a major cause of massive casualties during

the 26 December 2004 event. People along the west coast from Meulaboh up to Banda Aceh on Sumatra Island felt the earthquake, but didn't know how to respond and evacuate to safe places from the impending tsunamis. On the contrary, people in Simeulue Island that preserved their ancestral knowledge, which is passed down to the younger generation, survived. The message is clear and simple: after significant shaking (earthquake) and observing the sea receding, run to higher ground (McAdoo et al., 2006). However, this type of community warning and self-evacuation is a challenge for modern a lifestyle in the city. Morover, most of the earth science education in Indonesia, mostly concentrated on how to explore and exploit the natural resources, and less on natural hazards.

People who relocated to tsunami shelter area following the 28 March 2005 even suggested the idea to reproduce education material combining numerical model results based on the real events, eyewitness video during the tsunami attack, and their impact on the coastal areas during the post-event field survey. This education material was designed as a short movie to provide knowledge on how tsunami impacted on the coastal area, as revealed during the discussions. Most of the people occupied the shelter zone for almost three days after the 28 March 2005 event, while during the 26 December 2004, they stayed only 1 day. The reason is that they were worried that bigger waves than the 26 December 2004 will come, since the sea still receding, while actually the sea floor exposed due to uplift.

To sustain all activities in regard to keeping the Early Warning System running as part of community preparedness and awareness until the next event occurs, integration of life-long efforts to educate the population about the hazards and preparedness for an extreme event is needed. The most favorable way is to a put earthquake and tsunami hazards, and preparedness as part of educational curricula taught at schools especially for those regions that have high possibility to be attacked by catastrophic tsunamis. Still, the earthquake is the natural warning. If the ground shaking is felt long enough (up to 1 minute), find a safety on higher ground before it is too late. In case the earthquake is not felt, then wait for the information and warning from the authorities.

6.5 Remarks on Future Research

Some research identified by Synolakis and Bernard (2006) is still key issue that requiring solution for each region, where each source is unique and provides distinct impact for a particular coastal region.

- **Research on tsunamigenic region**

There is still more research required to identify the tsunamigenic processes within the Indonesian Archipelago at a regional and local level. The secondary generating mechanism from the earthquake and volcanic sources, such as submarine or subaerial-landslides is even more dominant compared to the impact from the main source. In identifying this source, detailed bathymetry data and seismic profiles or side scan sonar are needed, which is hardly available within the region. Collecting these data is very important, as the sea floor images have proven to be very useful in studying volcanic edifice failures as well.

Further research on deciphering the patterns of great earthquake associated with damaging tsunamis along the subduction zone within the Indonesian Archipelago needs to be refined. There are still uncertainties on the empirical methods that have been used due to the very short record to observe the process as identified by McCaffrey (2008). Some results of this research are consistent with the results of other methods applied on the Sumatra segment, especially research on the great earthquake on Mentawai's Islands Arc that used micro-atoll data and continuous GPS measurements, but not along the Java segment where the empirical method used to calculate the recurrence interval from identified possible sources suggest that events are mostly overdue. To solve these uncertainty, the paleotsunamis studies through identifying the tsunami deposits along the southern coast of Java becomes an alternative to be used as a proxy, as on Mentawai Islands with micro-atoll data, to attempt to define past tsunamis and their recurrence interval.

Details and continuous crustal deformation monitoring are also needed since the empirical calculation is sensitive to the convergence rate. This is not only for the Sunda Arc, but also for the eastern Archipelago along the Banda Arc where the plate convergences are complex and still poorly understood.

The directionality of fault rupture along the Sumatra segment that had been identified needs to be further investigated using near future events, as the rupture propagation data are limited for the past event. Determination of the segment boundaries of each event is extremely important, since directionality of fault rupture propagation shows that most of the large shallow earthquakes associated with devastating tsunamis were nucleated at the southeastern-end of fault segments close to the deformation front (trench). The rupture propagated to the northwest direction as a consequence of the Indian Ocean

plate movement to the north along the southeast-northwest lineaments of the collision zone. The question as to whether the same segment will be ruptured exactly at the same place, is still unresolved until the next event occurs.

- **Research on source mechanism**

Unlike the earthquake sources that are already established using Manshina and Smyle (1971) and Okada (1985) type solution, more research is needed for the landslides and volcanic sources mechanism. The volcanic source processes involves more than one mechanism through sequences of eruption processes. The question of whether one mechanism is applicable to another still needs to be resolved, since each volcano possesses its own characteristics. It is necessary to assess, which generating mechanism is responsible for the main cause of the largest tsunami, or whether a sequence of single mechanisms or combination of mechanism cause the tsunami through the eruption processes for each volcano. Assessment of the far field impacts of each volcanogenic tsunami generating mechanism also needs further investigation since the caldera collapse mechanism for the pre-historic caldera of Banda Api shows tsunami approaching the southeast coast of Sulawesi as a wave packet, while for the same type of mechanism for the Anak Krakatau scenario did not.

- **Research on tsunami propagation, runup and inundation**

Identifying tsunami wave characteristic during propagation from the source to the coast, and during runup and inundation for each region are important in assessing and quantifying the impact of tsunami as well as for the mitigation measures that should be put in place. The role of specific bathymetric features (such as a wide continental shelf with gentle slope versus steep slope) to the waves shape in relation with a damage level, runup height, distribution of overland flow velocities, duration of the event, and inundation distance are crucial in designing mitigation measures in preventing the loss of life as well as economic loss. Insufficient knowledge may lead to inappropriate conclusions on how to mitigate the impacts.

- **Research on mitigation measures**

Structural or non-structural mitigation measures need to be investigated carefully, such as the application of mangrove and other coastal forest that need careful design and

planning during implementation. Not all mangroves and coastal forest survived during the 26 December 2004 event, and neither did the coastal protection structures that had been design to prevent storm waves. Specific designs are needed to reduce the possibility of the structure to amplify the tsunami impacts rather than reduce them, and still withstand the tsunami attack. Research on hydraulics performance and impact loading of man-made structures or natural barriers such as vegetation, trees, and sand dunes are needed. Research on debris flows and impact loading by floating debris during overland flows will provide information in relation to the secondary hazards that may be impacted.

- **Multi-discipline and Integrated research**

Finally, multi-discipline research is needed in regard to the uncertainties of the source region, preventing loss of life and economic loss through structural or non-structural mitigation measures as well as developing tsunami-resilient communities with education as the core of effective tsunami mitigation efforts. For example, research on tsunami deposits is necessary to fill the gap of un-identified large earthquakes and their recurrence interval in the historical record, and provide evidence to the coastal communities of the possible threat in the future. The deposits can also be used to verify the uncertainties of other methods in determining a potential large earthquake associated with the devastating tsunamis.

6.6. References

Geist, E.L., Titov, V.V., Arcas, D., Pollitz, F.F., and Billek, S.L.: 2007, Implications of the 26 December 2004 Sumatra-Andaman earthquake on tsunami forecast and assessment model for great subduction-zone earthquakes, *Bulletin of the Seismological Society of America* **97** (1A), pp. S249-S270.

Manshina, L., and Smylie, D.E.: 1971, The displacement fields of inclined faults, *Bulletin of the Seismological Society of America*, **61** (5), pp. 1433-1440.

McAddo, B.G., Dengler, L., Titov, V., and Prasetya, G.S.: 2006, Smong: How an oral history saved thousands on Indonesia's Simeulue Islands, *Earthquake Spectra, Special Issue* III, **22**, pp. 661-669.

McCaffrey, R.: 2008, Global frequency of magnitude 9 earthquakes, *The Geological Society of America* **36 (3)**, pp. 263 – 266.

Mogi, Kiyoo.: 1986, Recent earthquake prediction research in Japan, *Science* **233 (471)**, pp. 324 – 330.

Natawidjaja, D., Sieh, K., Chlieh, M., Galetzka, J., Suwargi, B., Cheng, H., Edwards, R.L., Avouac, J.-P., Ward, S.: 2006, Source parameters of the great Sumatran megathrust earthquakes of 1797 and 1833 inferred from coral microatolls, *Journal Geophysical Research* **111, B06403**, pp.1-37.

Okada, Y.: 1985, Surface deformation due to shear and tensile faults in a half space, *Bulletin of Seismological Society America* **74 (4)**, pp. 1135-1154.

[a]Prasetya, G.S., Healy, T.R., de Lange, W.P.: 2008, Hydrodynamic modeling of tsunami overwash of Whitianga Townships and Harbour, Department of Earth and Ocean Sciences, Report prepared for *Environment Waikato*, 92 p

[b]Prasetya, G.S., Healy, T.R., de Lange, W.P.: 2008, Extreme tsunami runup and inundation flow at Banda Aceh, Indonesia: Are there any solution to this type of coastal disaster? in Wallendorf, L., Jones, C., Eing, L., Jaffe, B (eds): *Solution to Coastal Disasters 2008 Tsunamis*, ASCE, pp. 13-26

[c]Prasetya, G.S., Borrero, J., de Lange, W.P., Black, K.P., Healy, T.R.:(Submitted to Natural Hazards), Modelling of Inundation Dynamic on Banda Aceh, Indonesia during the Great Sumatra tsunamis, 26 December 2004. 30 p (in review).

[d]Prasetya, G.S., Black, K.P., de Lange, W.P., Borrero, J., Healy, T.R.:(Submitted to Pure and Applied Geophysics), Debris dispersal modelling for the Great Sumatra tsunamis on Banda Aceh and surrounding waters. 27 p (in review).

Rikitake, T.: 1999, Probability of great earthquake to recur in the Tokai district, Japan: Re-evaluation based on newly-developed paleoseismology, plate tectontic, tsunami study, micro-seismicity and geodetic measurements, *Earth Planet Space* **51**, pp. 147 – 157.

Sieh, K.: 2006, Sumatran Megathrust – from science to saving lives, *Philosophyical Transactions of the Royal Society,* **A, 364**, pp.1947 - 1963.

Synolakis, C.E., and Bernard, E.: 2006, Tsunami science before and beyond Boxing Day 2004, *Philosophical Transactions of the Royal Society*, **A, 364**, pp. 2231-2265

APPENDICES

APPENDIX 1. Numerical Modelling Results from Tsunamigenic Earthquake

1907 Fault Scenario	Segment 1	Segment 2	Segment 3	Moment Magnitude (Mw)
Scenario A				
Length (km)	249.5			8.28
Width (km)	100			
Focal depth (km)	10			
Dip Angle (km)	10			
Slip angle (degree)	110			
Displacement (degree)	6.24			
Fault axis angle (degree) relative to the North	300			
Scenario B				
Length (km)	45.7	124.5	190.65	8.49
Width (km)	120	60	100	
Focal depth (km)	10	10	10	
Dip Angle (km)	8	8	8	
Slip angle (degree)	110	90	100	
Displacement (degree)	6	9	8.5	
Fault axis angle (degree) relative to the North	315	302	310	
Scenario C				
Length (km)	45.7	124.5	190.65	8.49
Width (km)	120	40	100	
Focal depth (km)	10	10	10	
Dip Angle (km)	8	8	8	
Slip angle (degree)	110	90	100	
Displacement (degree)	6	9	8.5	
Fault axis angle (degree) relative to the North	315	302	310	

SCENARIO A

Initial condition (deformation) shows the entire region of Simeulue Islands experience with subsidence from 0.3 – 1 m.

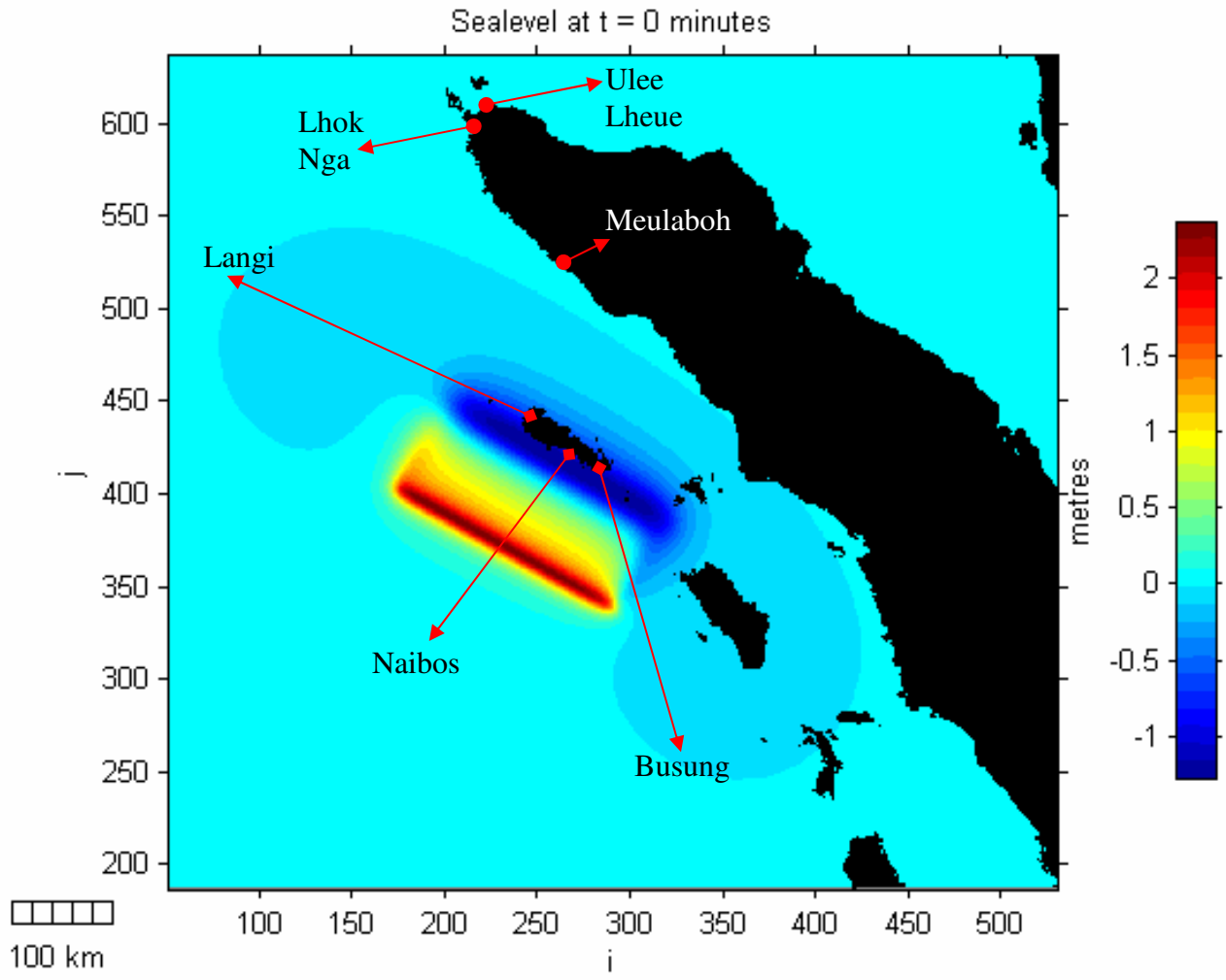

SCENARIO B

Initial condition (deformation) shows a half of the northern part of Simeulue Island on the seaside experience with subsidence from 0.1 – 0.5 m, and at the south end experience with uplift from 0.1 – 1m.

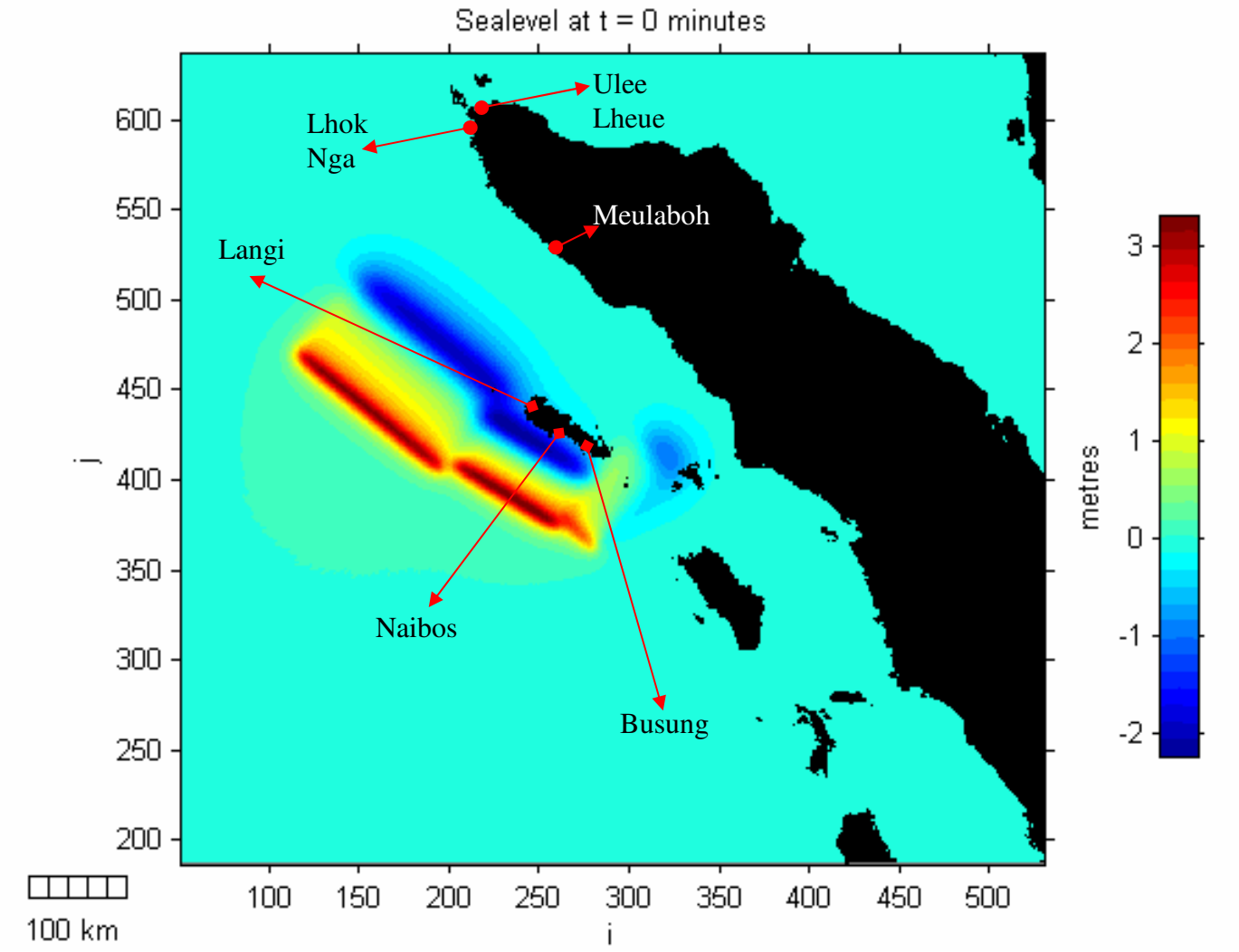

SCENARIO C

Initial condition (deformation) shows most of Simuelue Island on the seaside experience with minor subsidence up to 0.2 m, and at the south end experience with uplift from 0.1 – 1m.

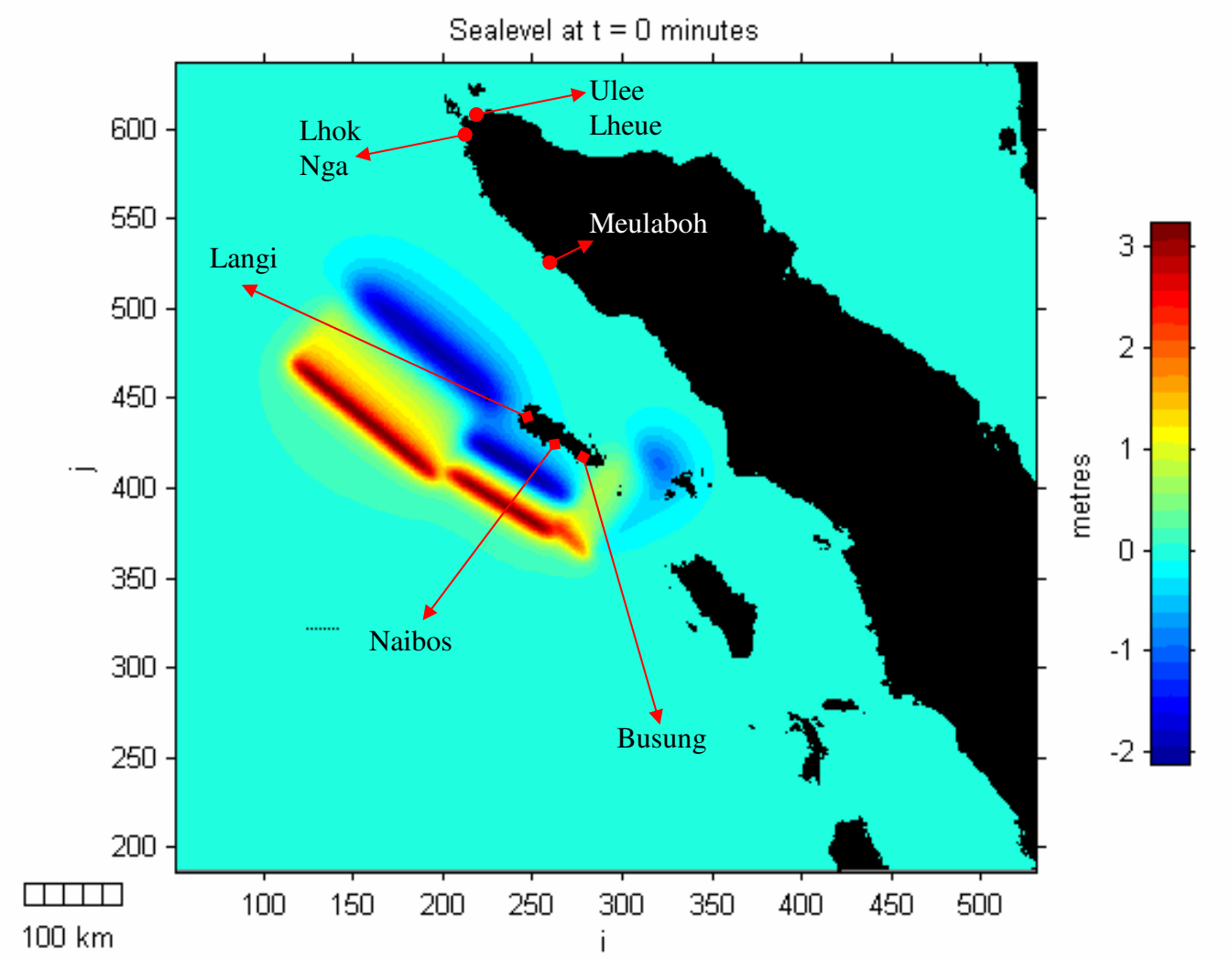

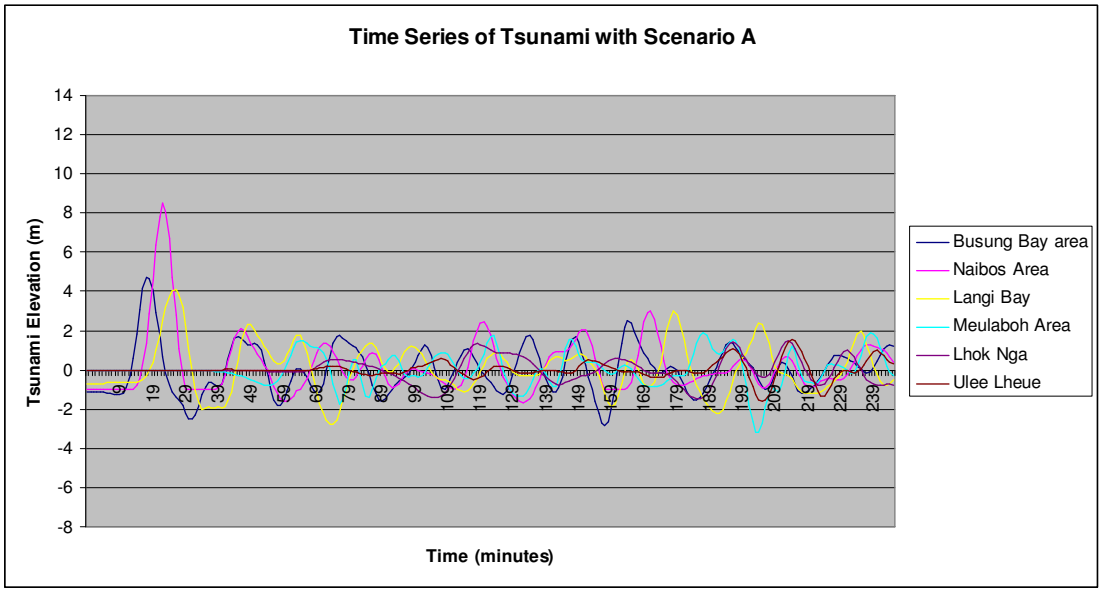
Time Series of Tsunami with Scenario A
Tsunami Elevation (m)
Time (minutes)
Busung Bay area
Naibos Area
Langi Bay
Meulaboh Area
Lhok Nga
Ulee Lheue

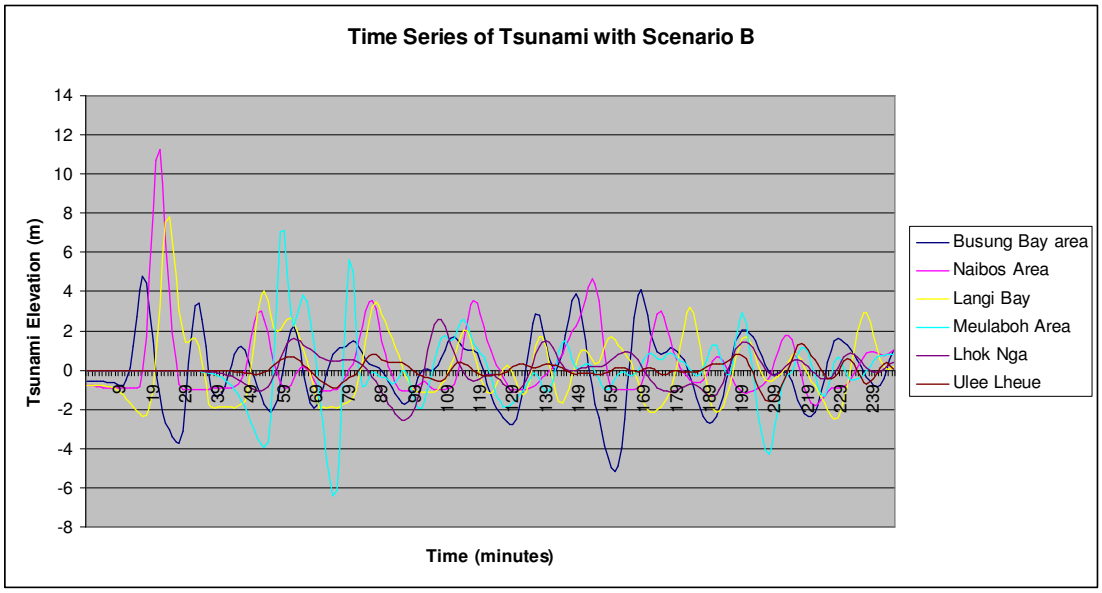
Time Series of Tsunami with Scenario B
Tsunami Elevation (m)
Time (minutes)
Busung Bay area
Naibos Area
Langi Bay
Meulaboh Area
Lhok Nga
Ulee Lheue

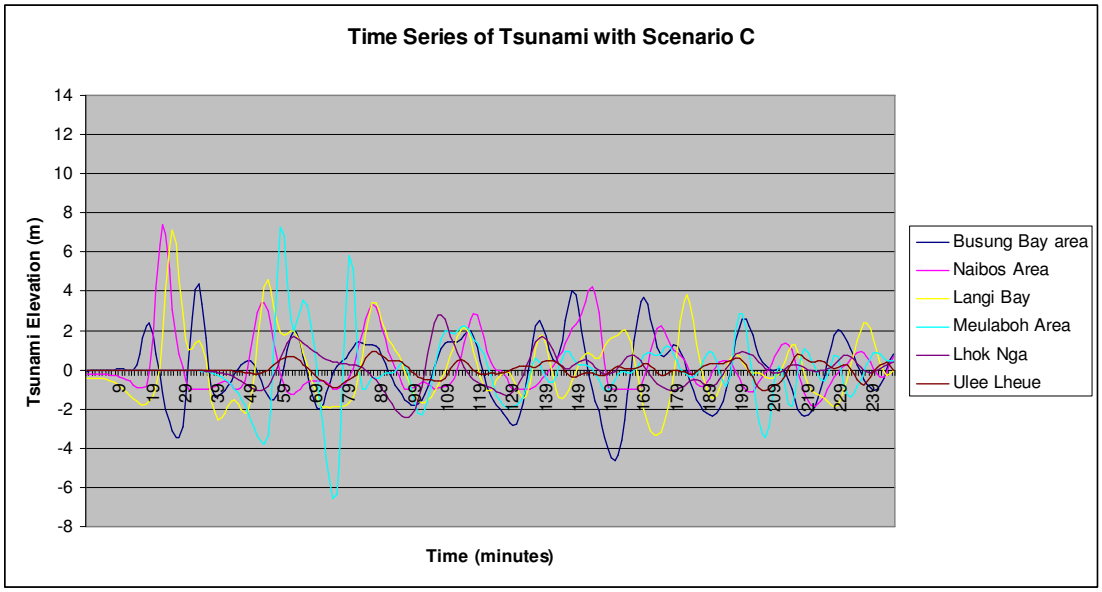
Time Series of Tsunami with Scenario C
Tsunami Elevation (m)
Time (minutes)
Busung Bay area
Naibos Area
Langi Bay
Meulaboh Area
Lhok Nga
Ulee Lheue

Scenario A model Results

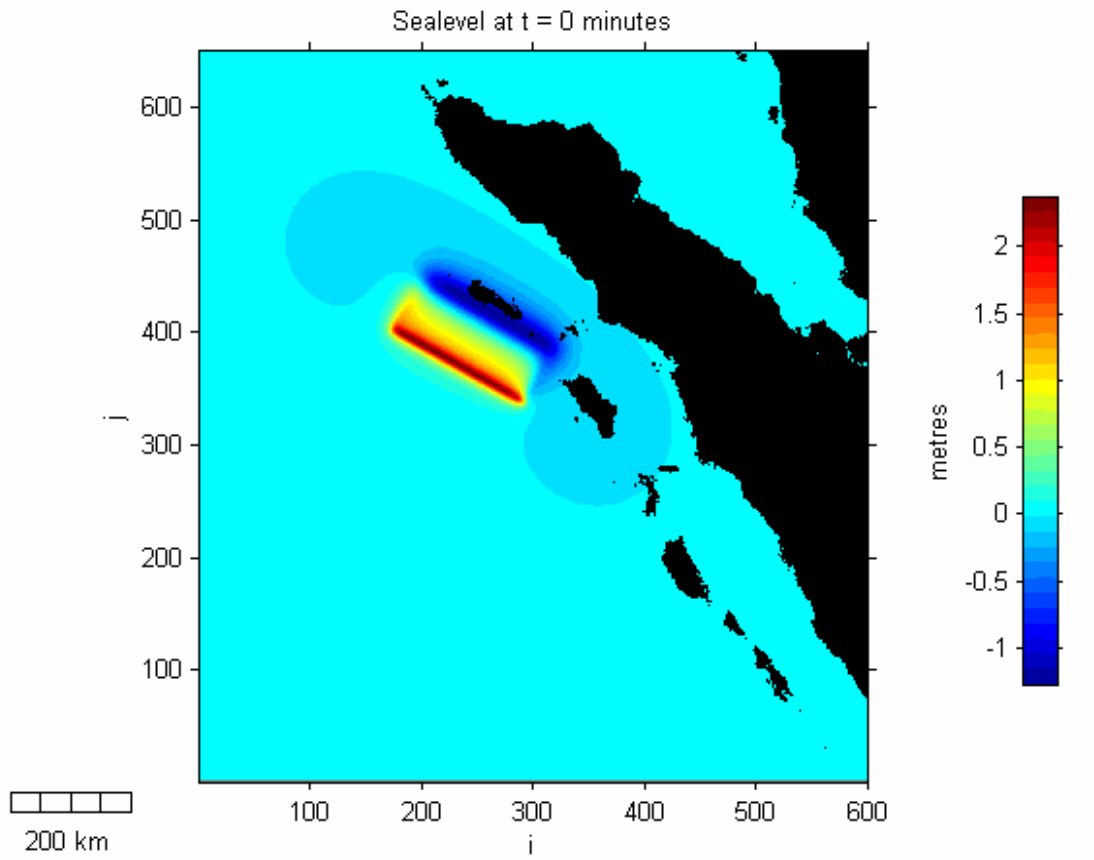

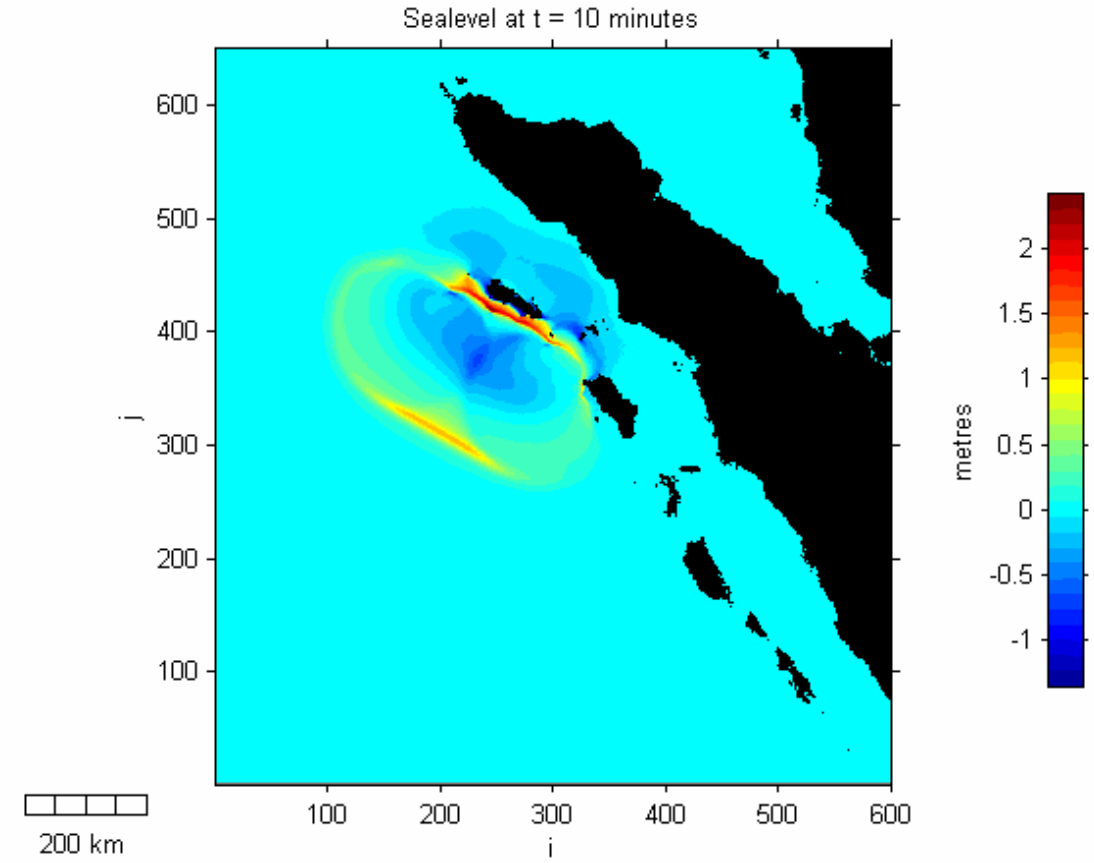

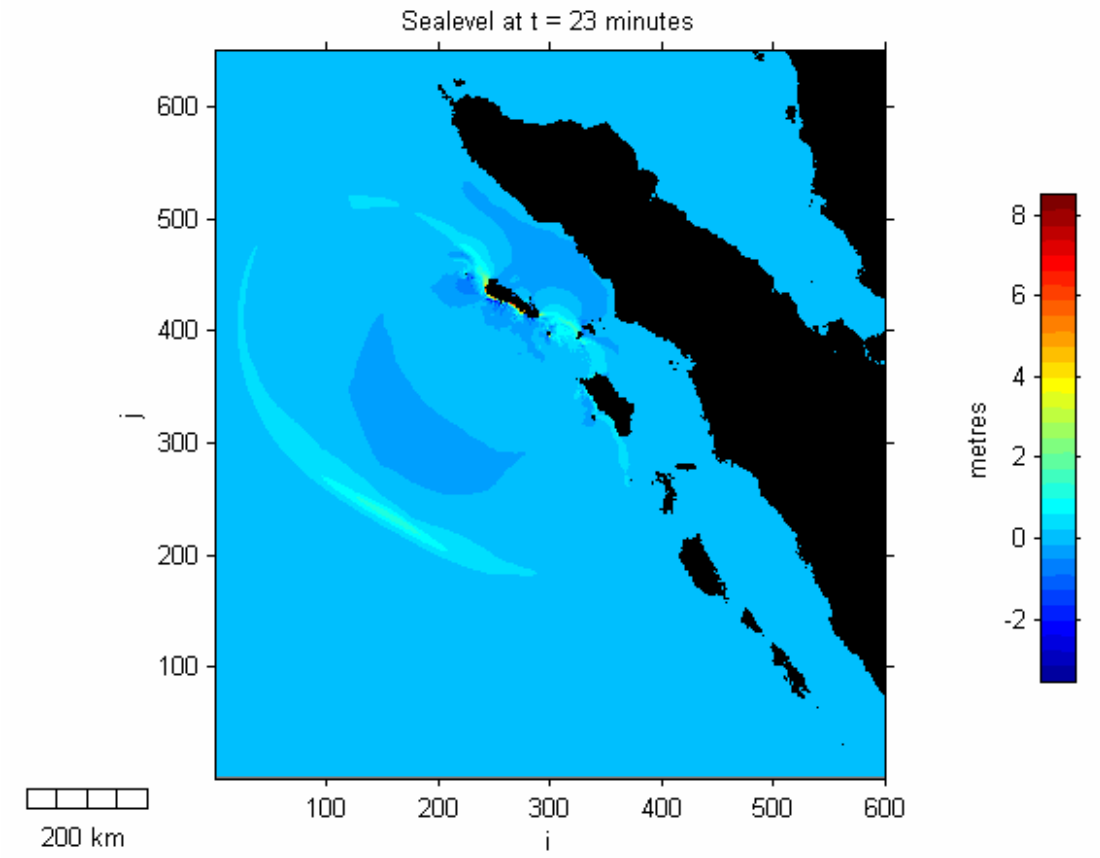
Sealevel at t = 23 minutes
600
500
400
300
200
100
j
100
200
300
400
500
600
i
200 km
8
6
4
2
0
-2
metres

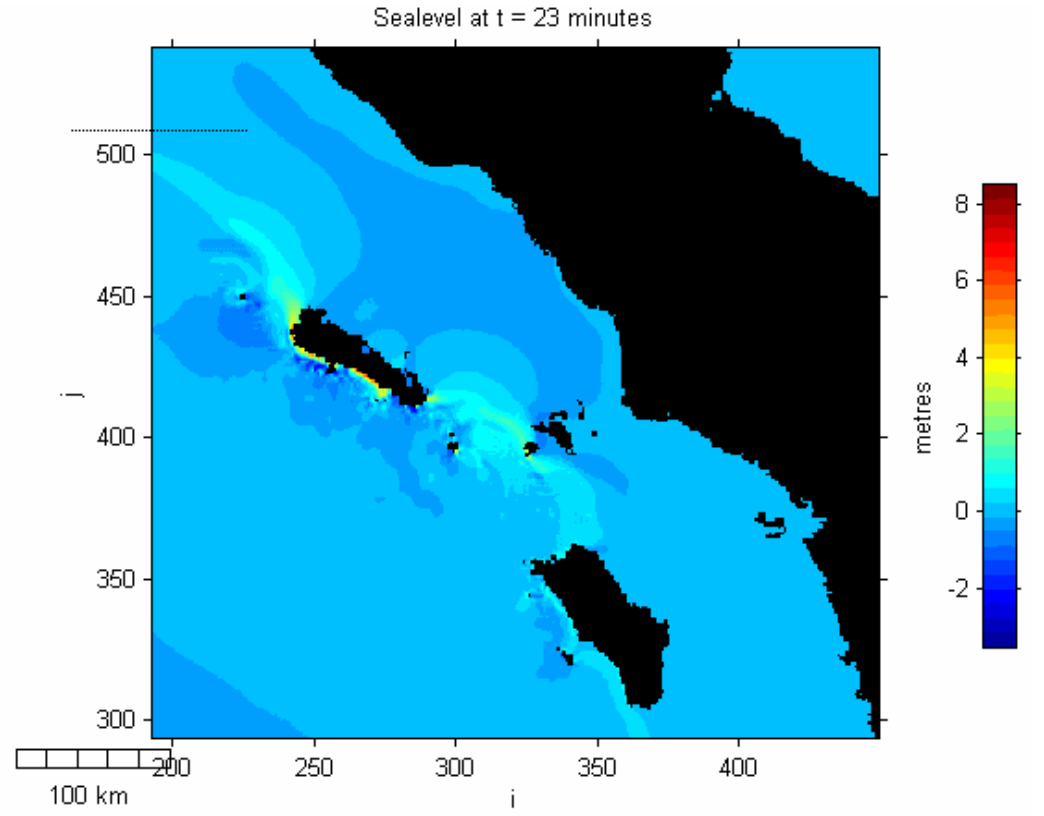
Sealevel at t = 23 minutes
500
450
400
350
300
j
200
250
300
350
400
i
100 km
8
6
4
2
0
-2
metres

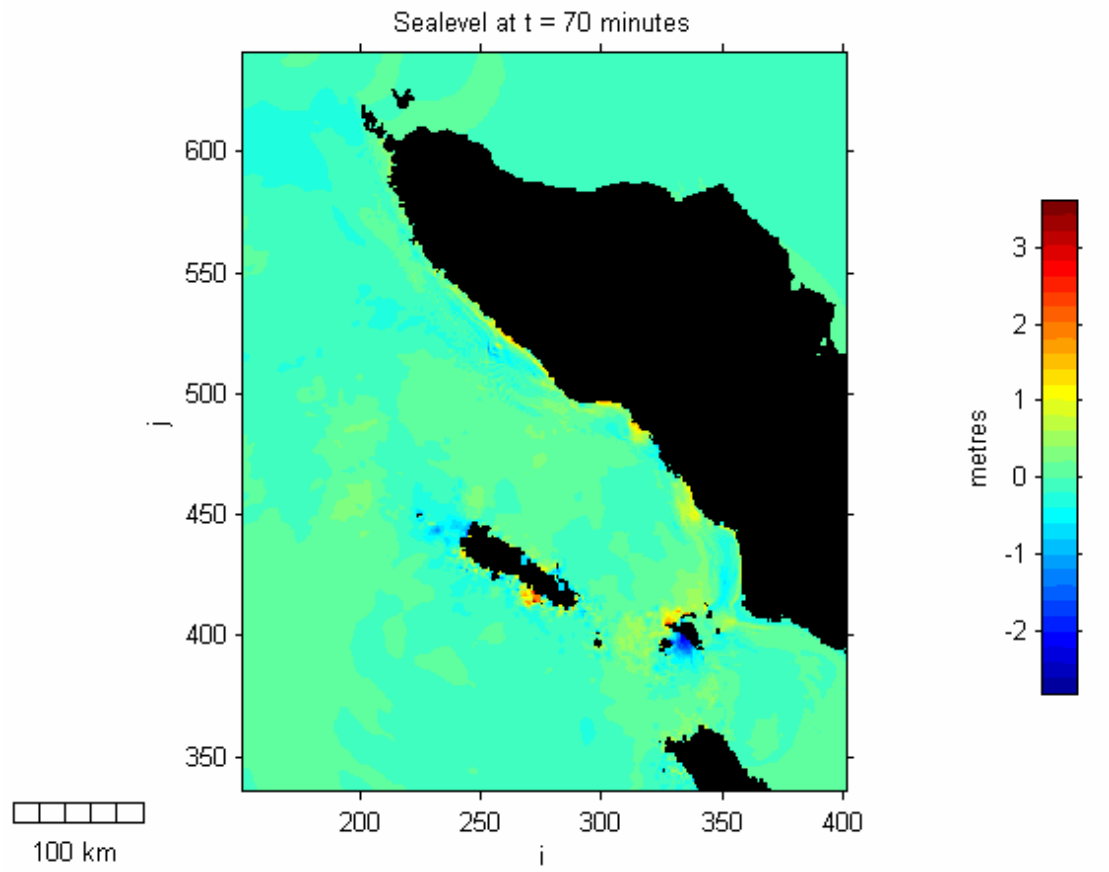
Sealevel at t = 70 minutes
600
550
500
450
400
350
j
200
250
300
350
400
i
100 km
3
2
1
0
-1
-2
metres

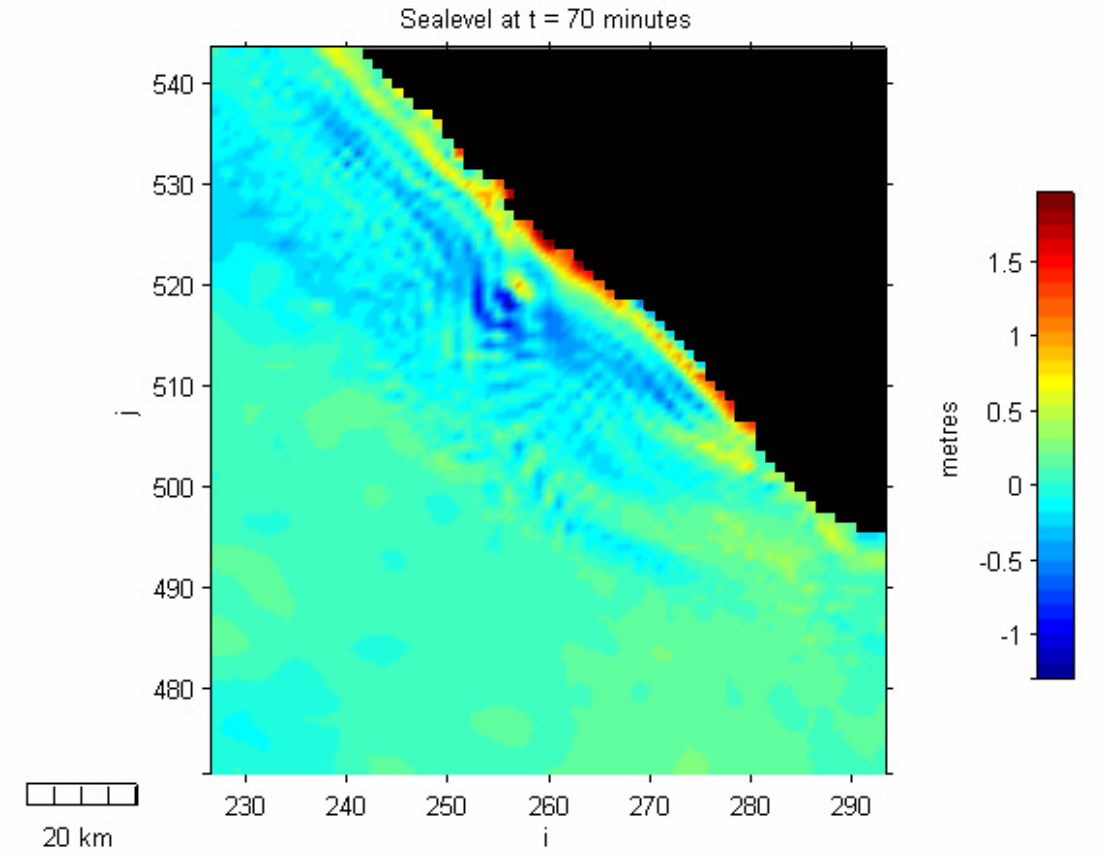
Sealevel at t = 70 minutes
540
530
520
510
500
490
480
j
230
240
250
260
270
280
290
i
20 km
1.5
1
0.5
0
-0.5
-1
metres

Scenario B model Results

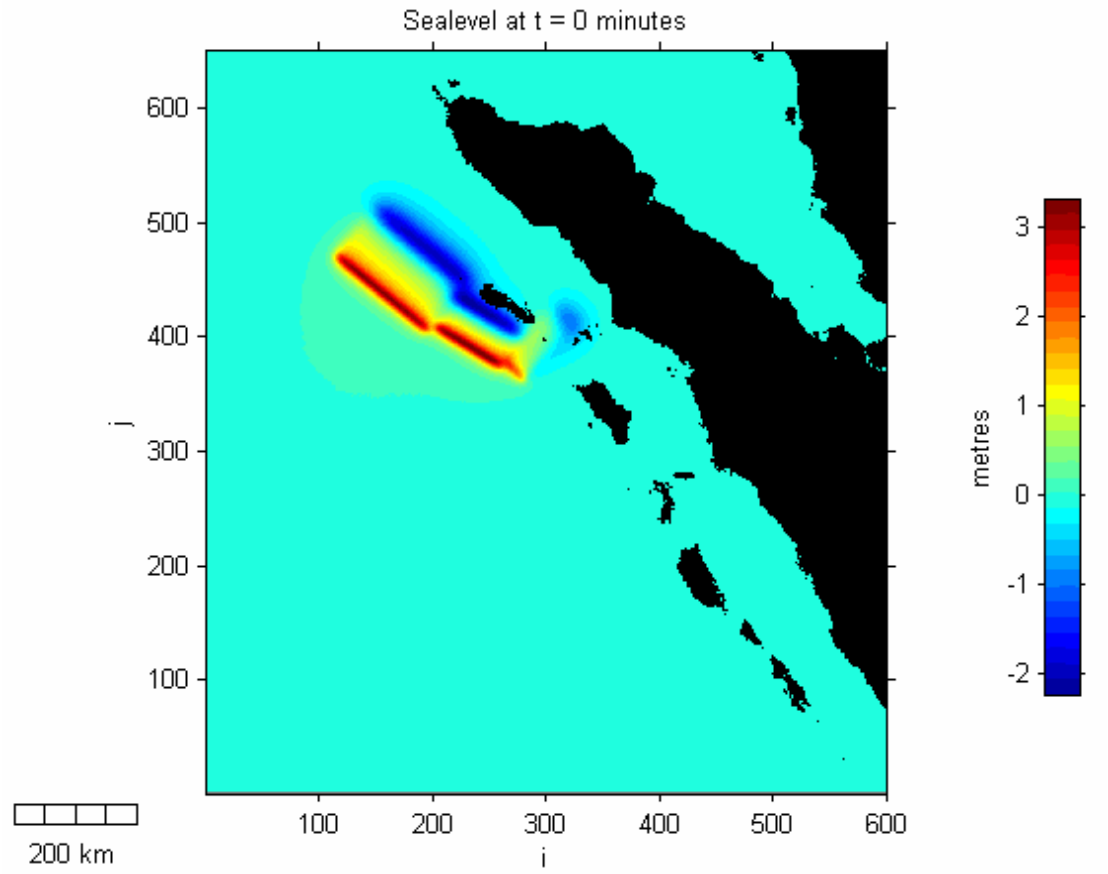

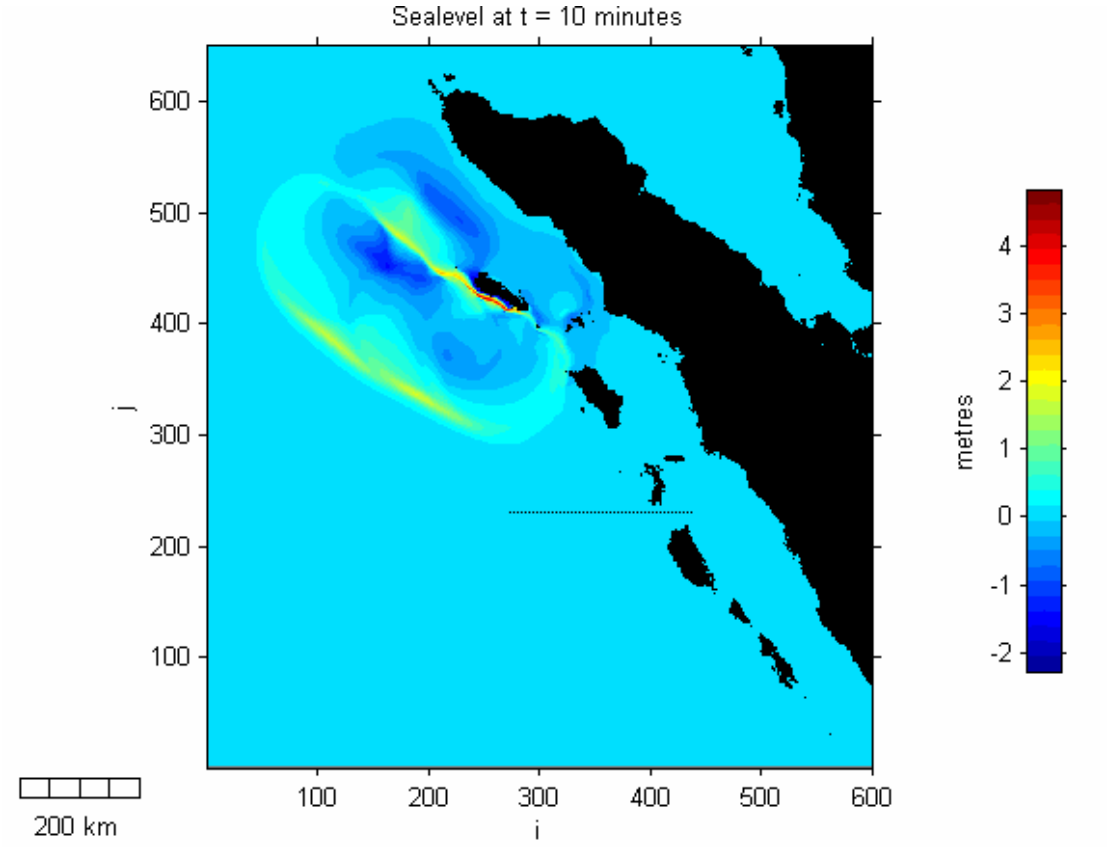

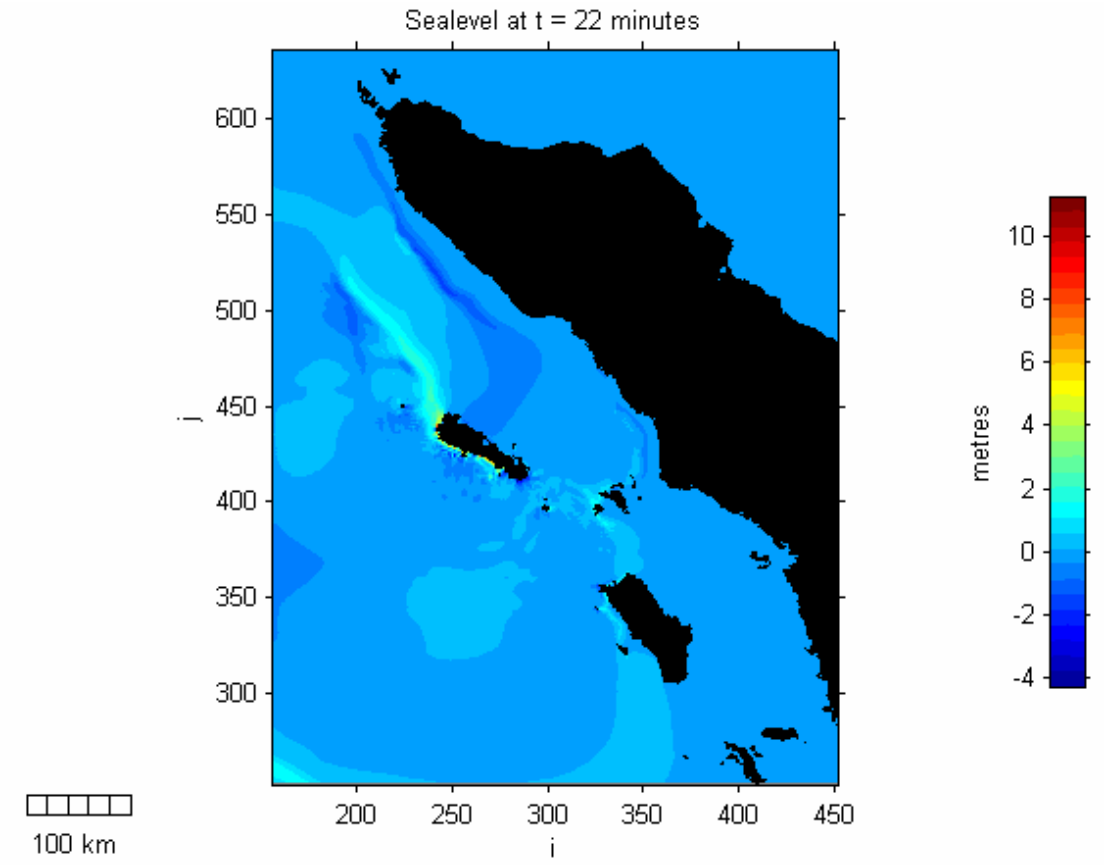
Sealevel at t = 22 minutes
600
550
500
450
400
350
300
j
200
250
300
350
400
450
i
10
8
6
4
2
0
-2
-4
metres
100 km

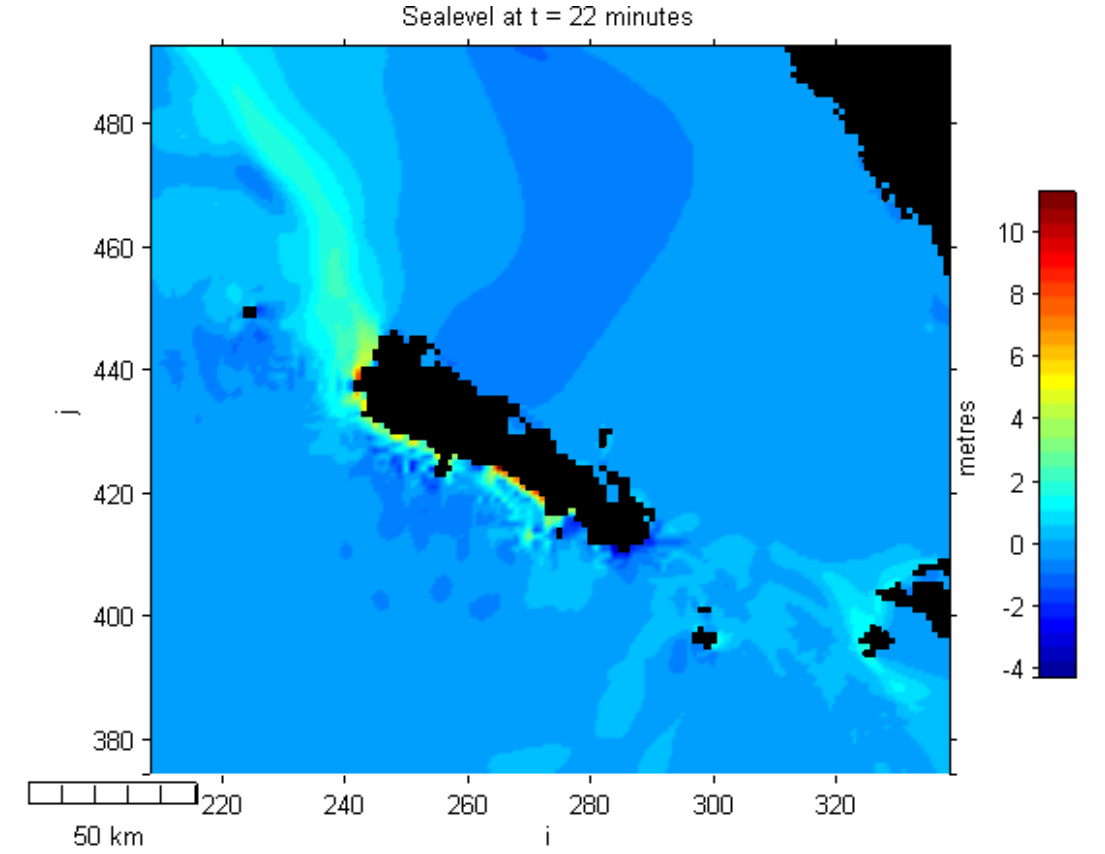
Sealevel at t = 22 minutes
480
460
440
420
400
380
j
220
240
260
280
300
320
i
10
8
6
4
2
0
-2
-4
metres
50 km

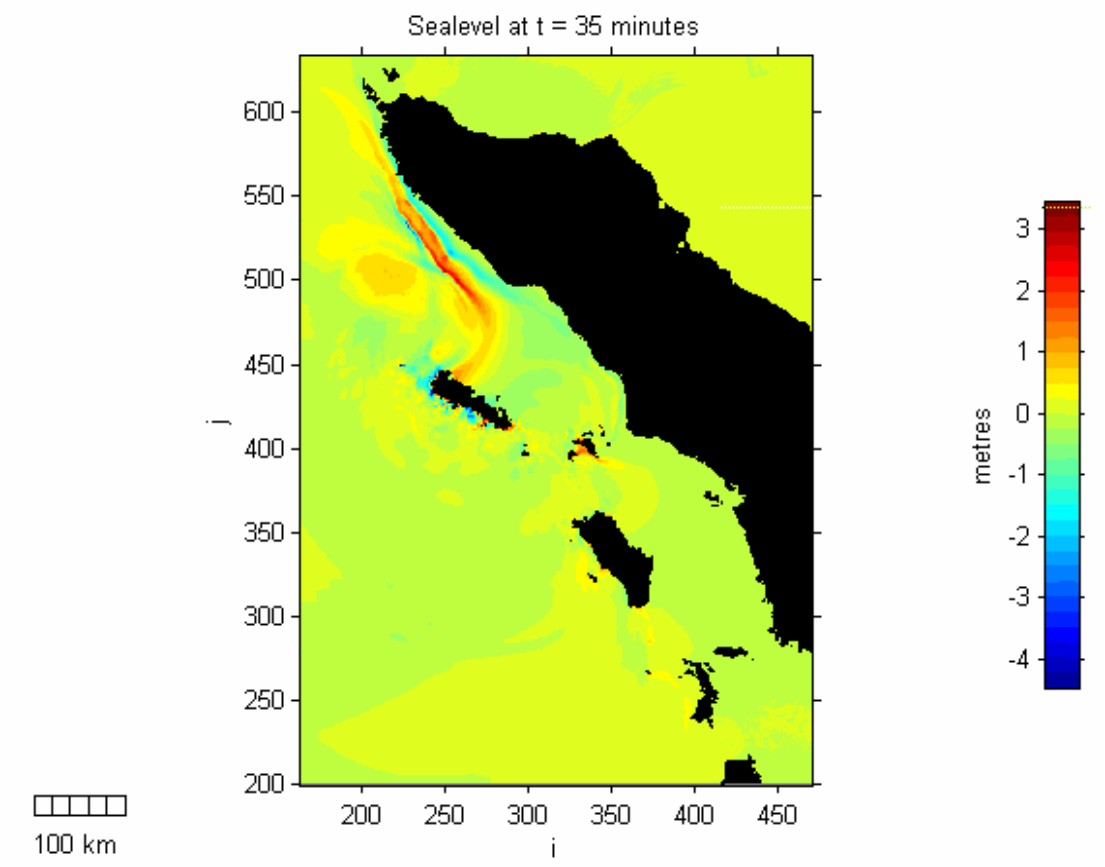
Sealevel at t = 35 minutes
600
550
500
450
400
350
300
250
200
j
200
250
300
350
400
450
i
3
2
1
0
-1
-2
-3
-4
metres
100 km

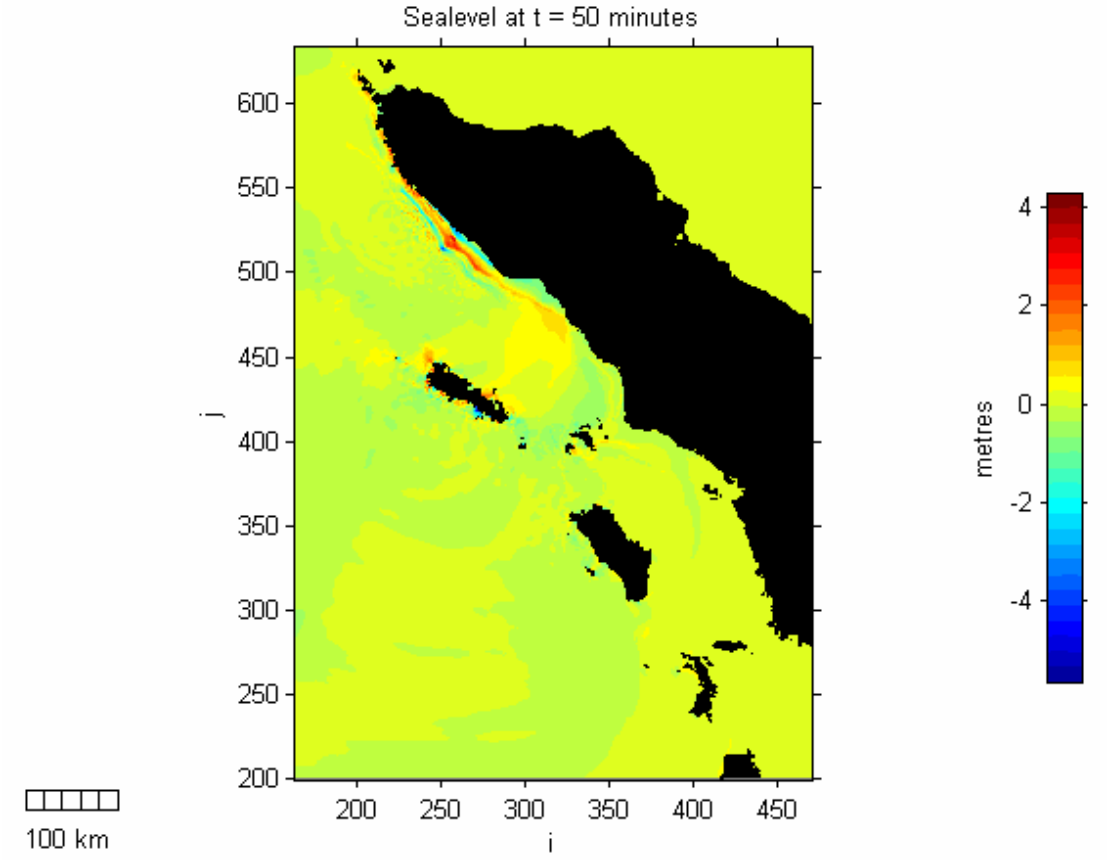
Sealevel at t = 50 minutes
600
550
500
450
400
350
300
250
200
j
200
250
300
350
400
450
i
4
2
0
-2
-4
metres
100 km

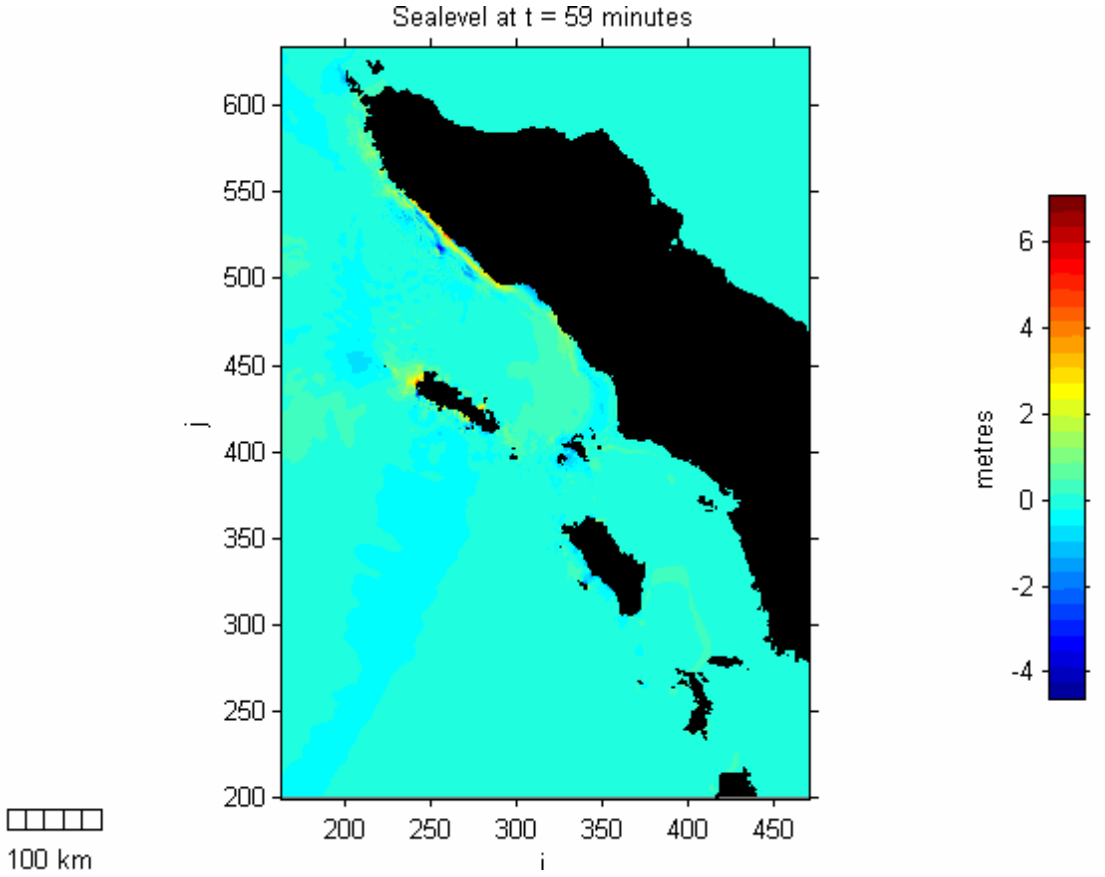
Sealevel at t = 59 minutes
600
550
500
450
400
350
300
250
200
j
200
250
300
350
400
450
i
6
4
2
0
-2
-4
metres
100 km

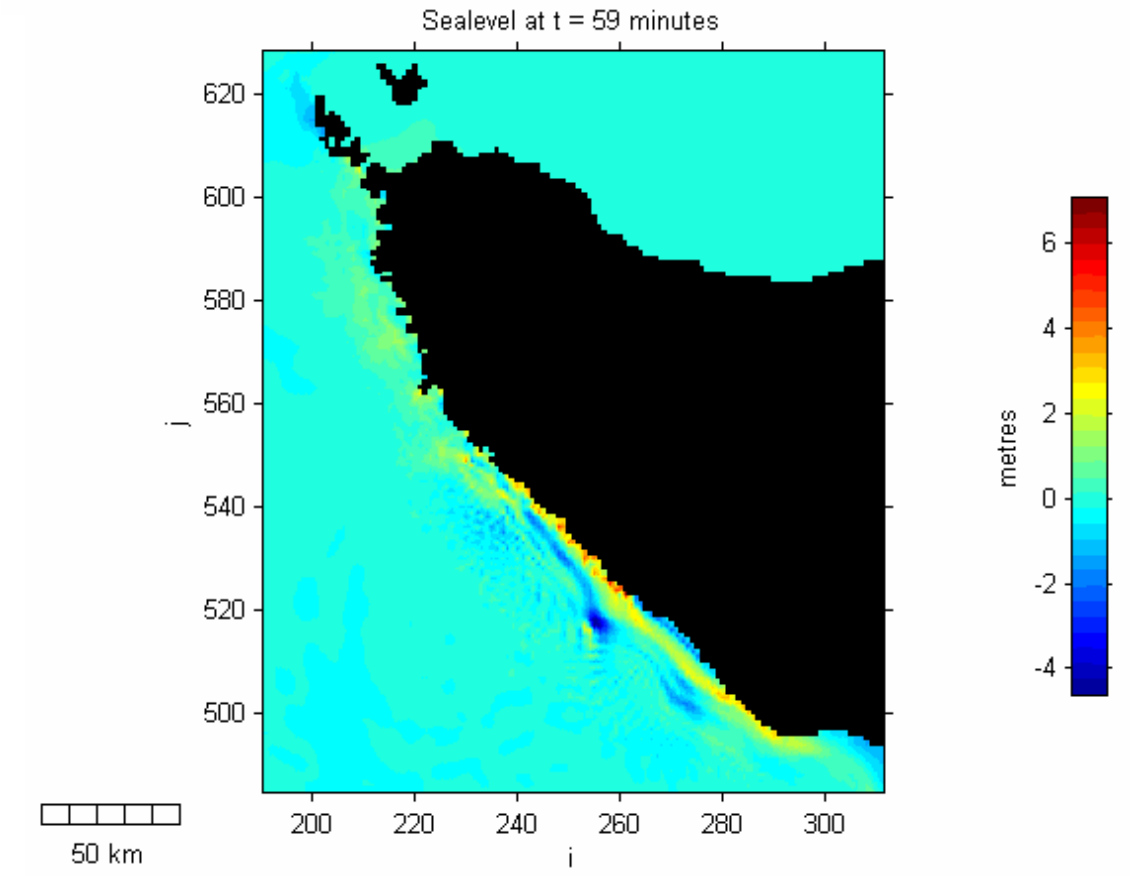
Sealevel at t = 59 minutes
620
600
580
560
540
520
500
j
200
220
240
260
280
300
i
6
4
2
0
-2
-4
metres
50 km

Scenario C model Results

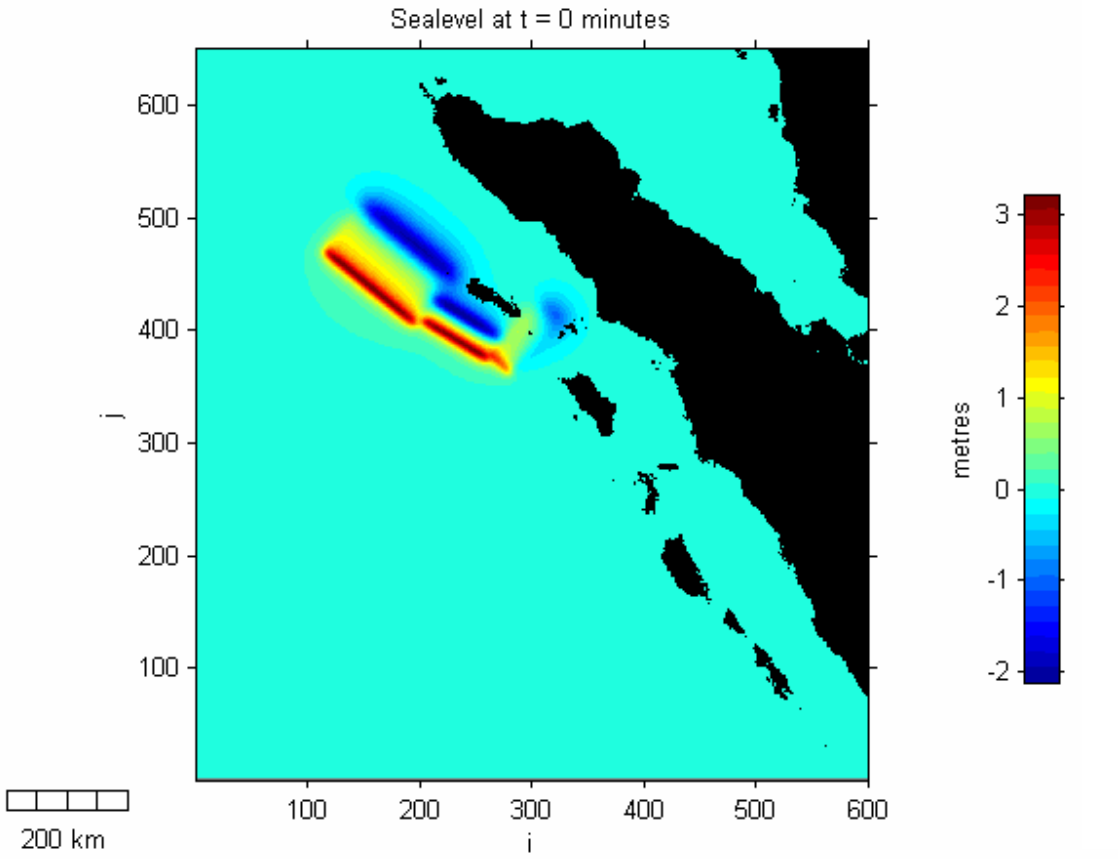

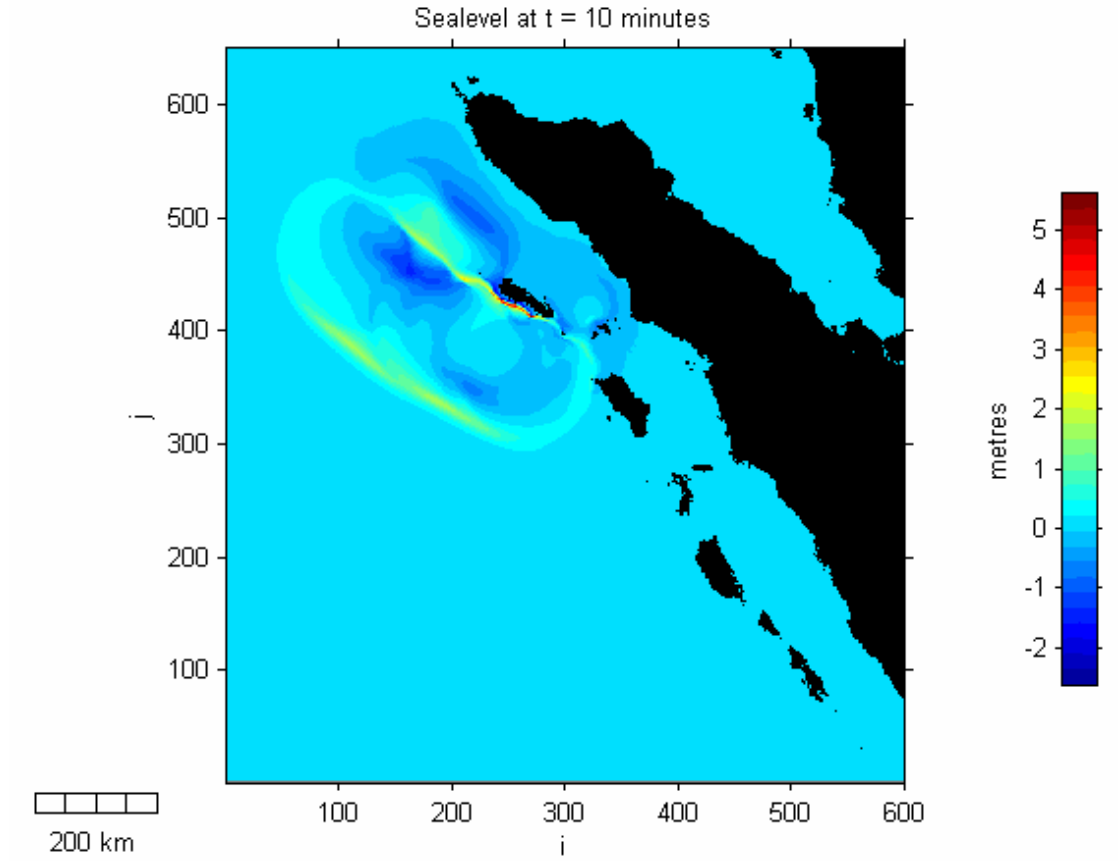

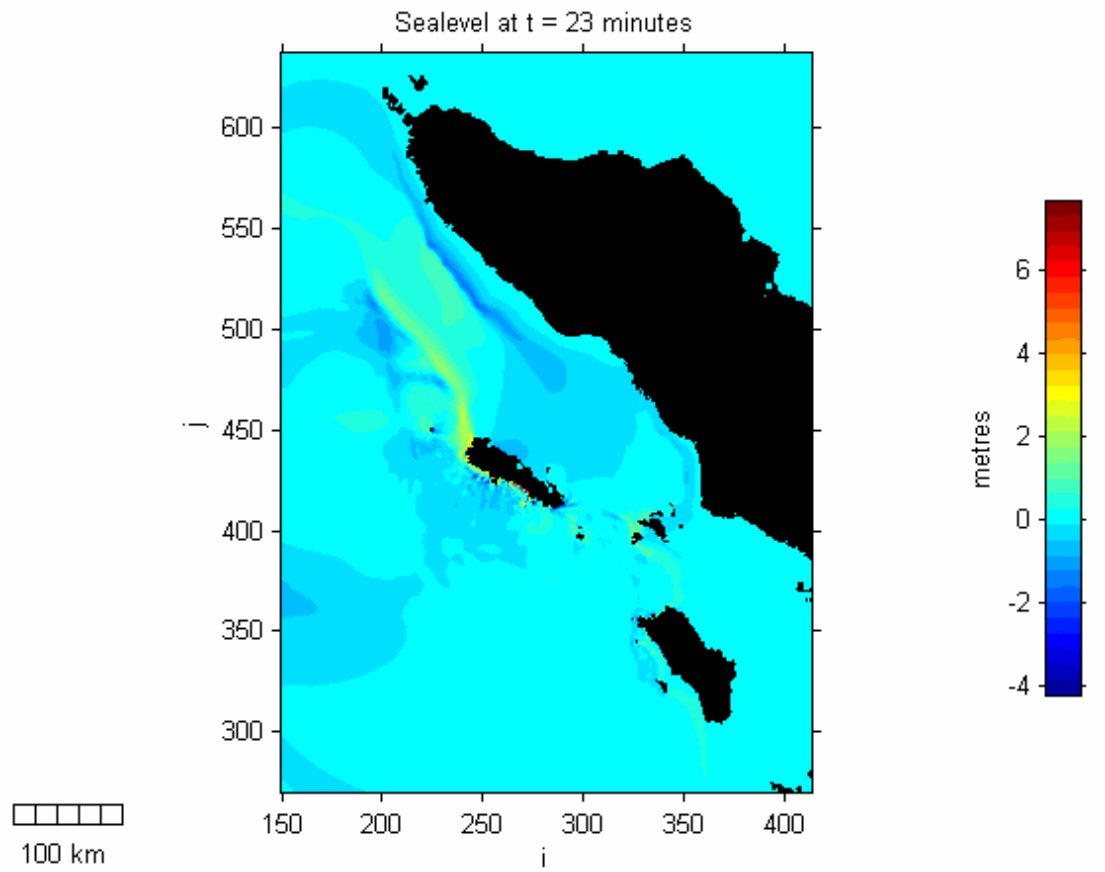
Sealevel at t = 23 minutes
600
550
500
450
400
350
300
j
150
200
250
300
350
400
i
6
4
2
0
-2
-4
metres
100 km

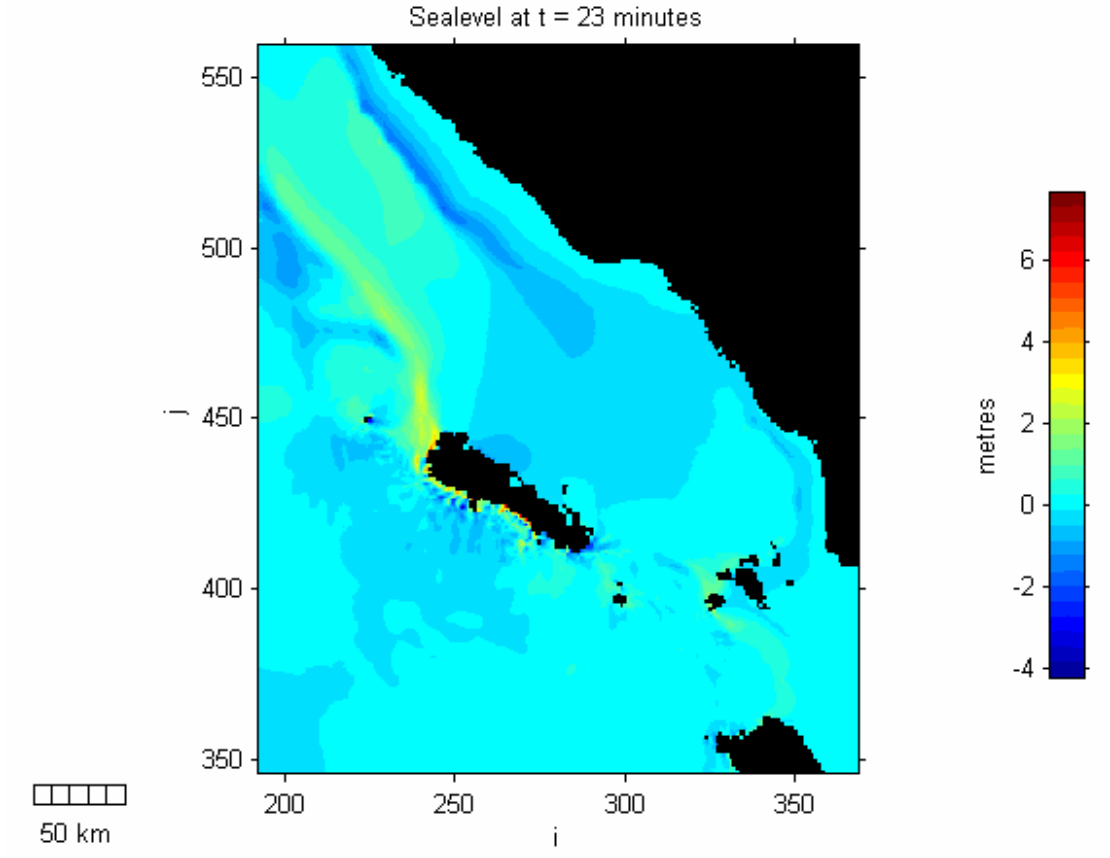
Sealevel at t = 23 minutes
550
500
450
400
350
j
200
250
300
350
i
6
4
2
0
-2
-4
metres
50 km

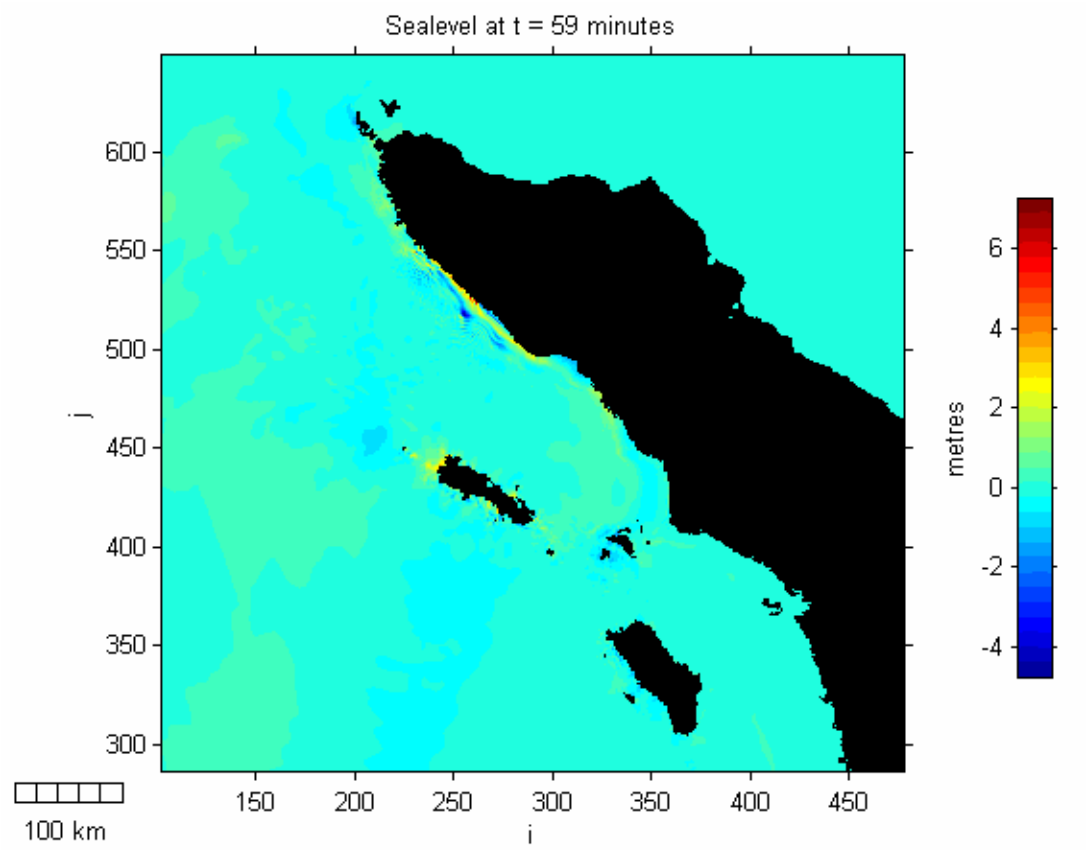
Sealevel at t = 59 minutes
600
550
500
450
400
350
300
j
150
200
250
300
350
400
450
i
6
4
2
0
-2
-4
metres
100 km

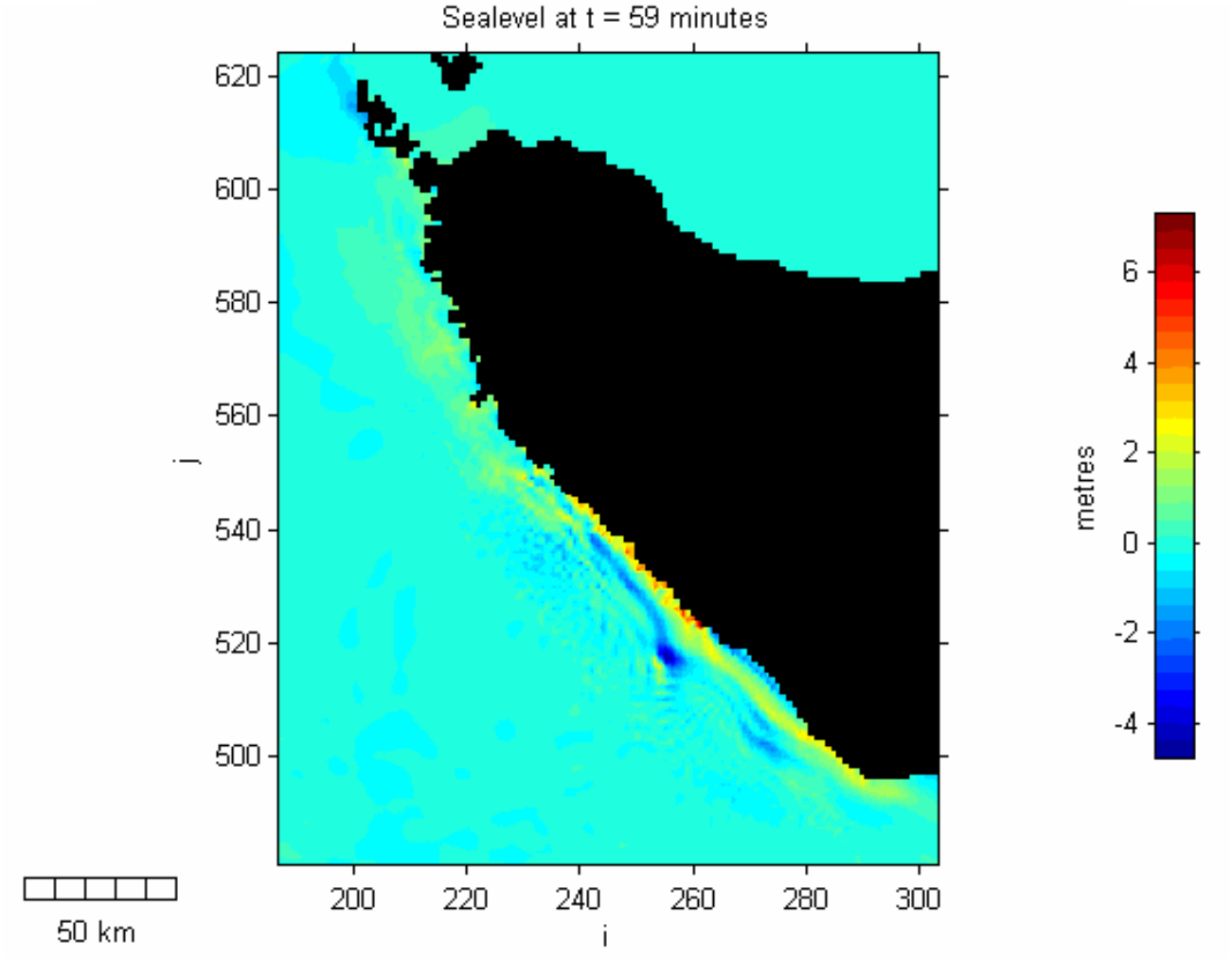
Sealevel at t = 59 minutes
620
600
580
560
540
520
500
j
200
220
240
260
280
300
i
6
4
2
0
-2
-4
metres
50 km

Summary of the 1907 Modelling Scenario.

Newcomb and McCann (1987) suggested the location of the epicentre is on the seaward of the trench slope break, but landward of the trench. With the fault parameter derived for scenario A, the initial deformation shows that the entire island experienced with subsidence, which is inconsistent with micro-atolls data (Meltzner et al., 2008 ~ cited reference in Chapter 4), where during the 1907 the south end of the island was uplifted. However, the resulting tsunami elevation (8 – 9 m) at the central Simeulue Island could explain the eyewitnesses account of the sea that receding first before huge waves comes, and where some of the dead bodies are found on top of the three. Small tsunami that propagates towards Meulaboh area from this source scenario is not consistent with tsunami deposit identified by Monecke et al. 2008 (cited reference in Chapter 4) at the northern Meulaboh that preserved between 1 – 3 m above sea level, and up to 1.2 km inland while the tsunami elevation at the coast is between 1 – 2 m. Therefore, another scenario is designed (Scenario B and C) that incorporated the variation of the accretionary wedges as well as variable slip distribution in addition to that eyewitnesses accounts, micro-atolls studies results, and tsunami deposit at north Meulaboh and along the west coast of Simeulue Island. Scenario B results show the initial condition where there is still small subsidence occurred along the west coast within a range of 0.2 – 0.5 m. However, the tsunami elevation up to 7 m that produce tsunami deposit at north of Meulaboh are achieved, as well as the tsunami elevation at central Simeulue that reach 11 m as potentially what eyewitnesses account during the 1907 event. With this scenario most of the wave phenomena are consistent with other data, except the subsidence that occurred along the west coast. However, if the uplift before the 1907 event were high enough that make most of the coral exposed, than small subsidences within a range of 50 cm maybe doesn't effect to much on the previous uplift plus the possible rebounding mechanism shortly after the event that lead to most of the coral still stay at the same level as what occurred during the 28 March 2005 event. Otherwise the scenario C where the width of the central segment is reduced as minimum width of the accreationary wedge that shows the initial deformation did not create subsidence on the islands as what expected by micro-atoll studies. The resulting tsunami waves along Meulaboh area are still the same as scenario B, however, the high of tsunami elevation at the central Simelue is reduced to 7 m compare to 11m of the scenario B. With 7 m of tsunami elevation at shoreline maybe is too low compare to the eyewitnesses account where the dead bodies are found on top of the tree at some distance from the shore. The high of the tree are usually between 9 – 12 m. To accommodate this, a second generating mechanism from submarine landslide is favourable as the bathymetry at the trench shows really steep slope at the central part of Simeulue Island. Detail bathymetry data and seismic profiles are needed to further justify the possibility of the second generating mechanism during the 1907 on central Simeulue Island.

APPENDIX 2. Numerical Modelling Results of Anak Krakatau scenario

Ap1.1. Two-dimensional plot (2D) of tsunami dynamic

Anak Krakatau eruption on November 2007 (Photo courtesy of Tom Pfeiffer of Volcano Discovery)

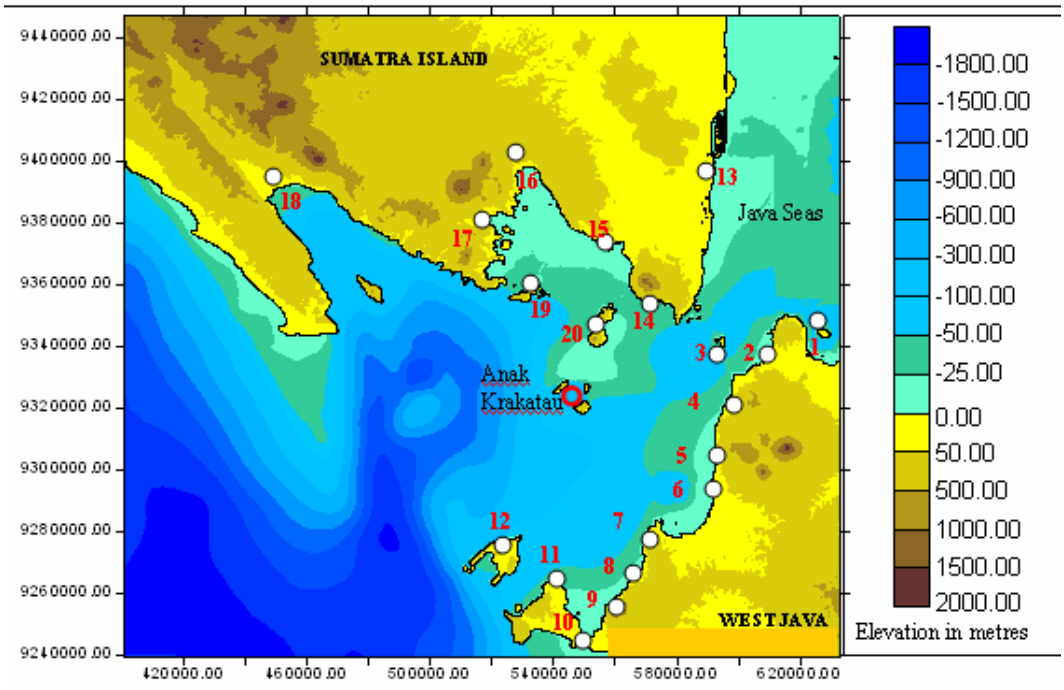

1. **Banten Bay**
2. **Merak**
3. **P. Sangeang**
4. **Anjer**
5. **Carita**
6. **Labuan**
7. **Kalitjaah**
8. **Sumur**
9. **Tjikawung**
10. **UjungKulon Bay**
11. **Tj,Ujung Kulon**
12. **Panaitan**
13. **Lampung**
14. **Radjabasa**
15. **Kalianda**
16. **Teluk Betung**
17. **Menango**
18. **Kota Agung**
19. **P.Legundi**
20. **P.Sebsi**

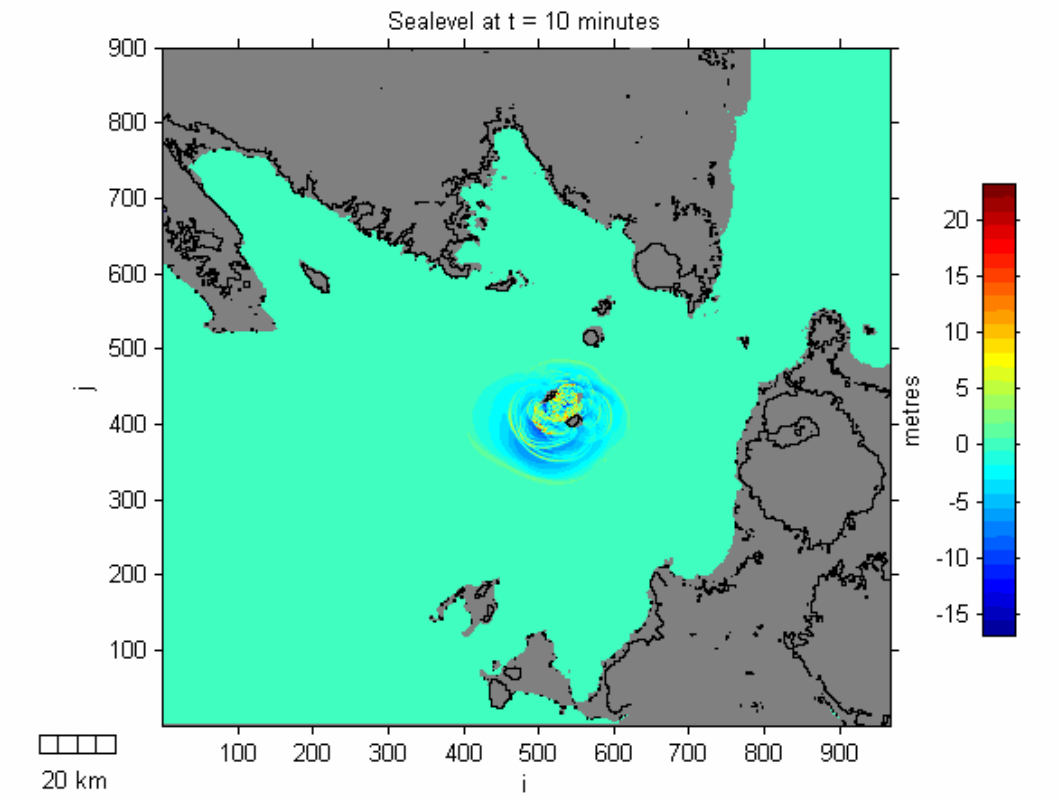
Sealevel at t = 10 minutes
900
800
700
600
500
400
300
200
100
j
100 200 300 400 500 600 700 800 900
i
20 km
20
15
10
5
0
-5
-10
-15
metres

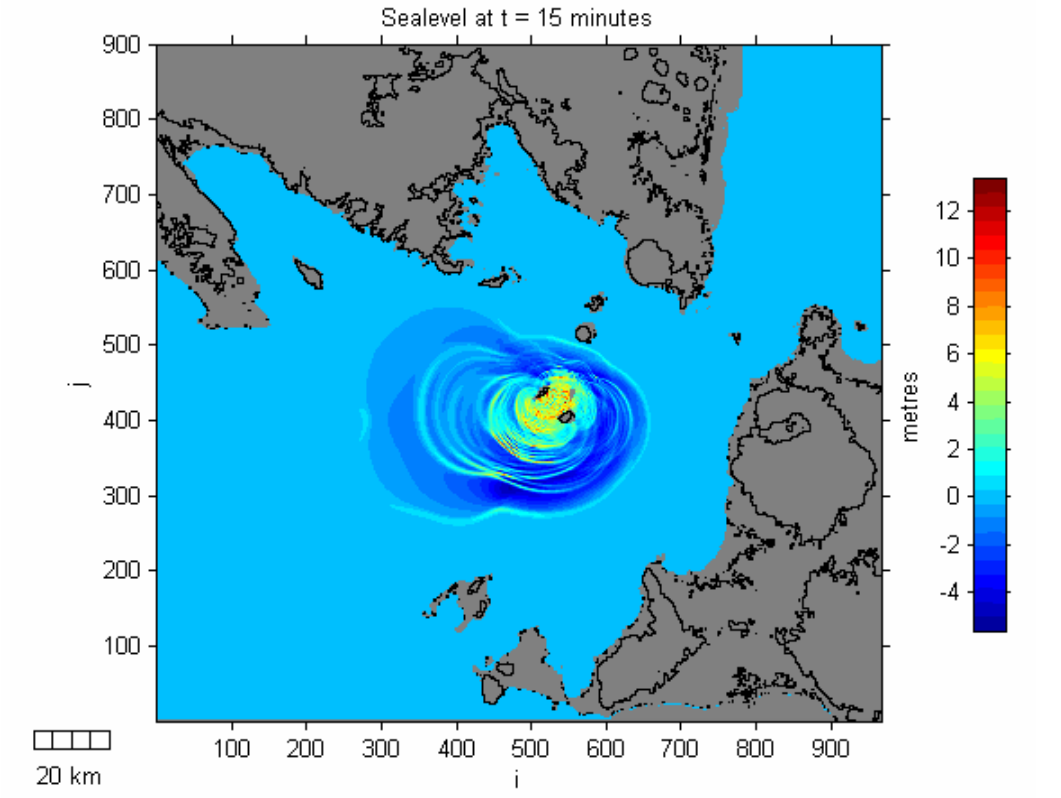
Sealevel at t = 15 minutes
900
800
700
600
500
400
300
200
100
j
100 200 300 400 500 600 700 800 900
i
20 km
12
10
8
6
4
2
0
-2
-4
metres

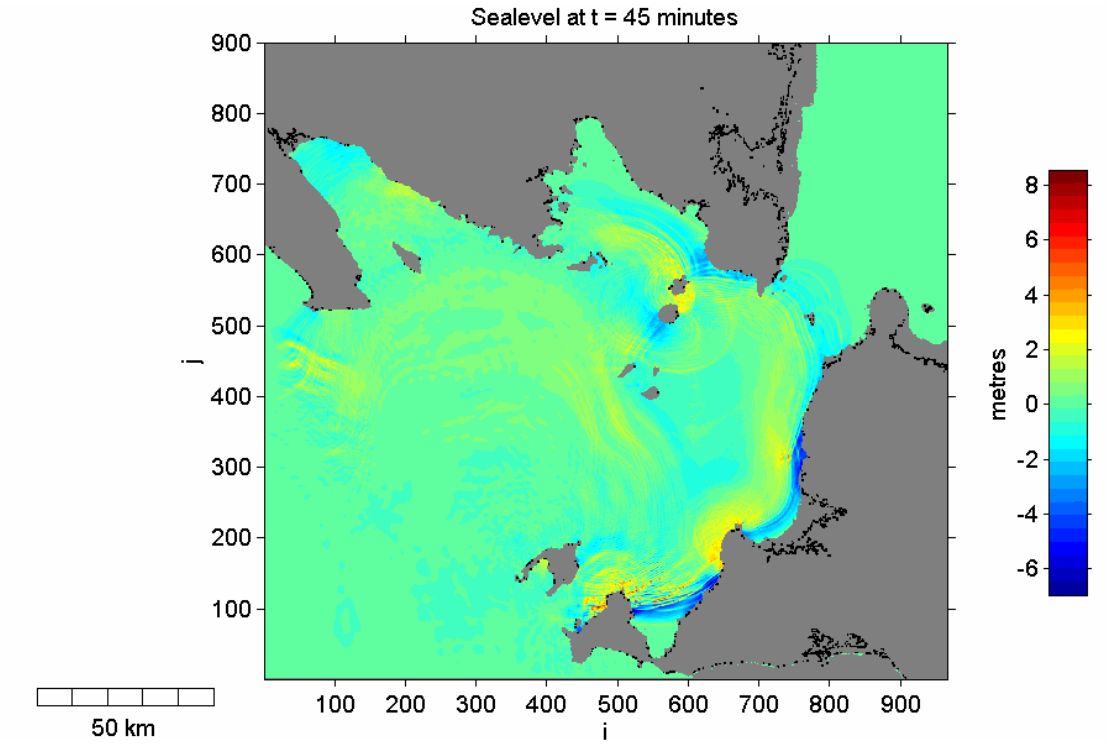
Sealevel at t = 45 minutes
900
800
700
600
500
400
300
200
100
j
100 200 300 400 500 600 700 800 900
i
8
6
4
2
0
-2
-4
-6
metres
50 km

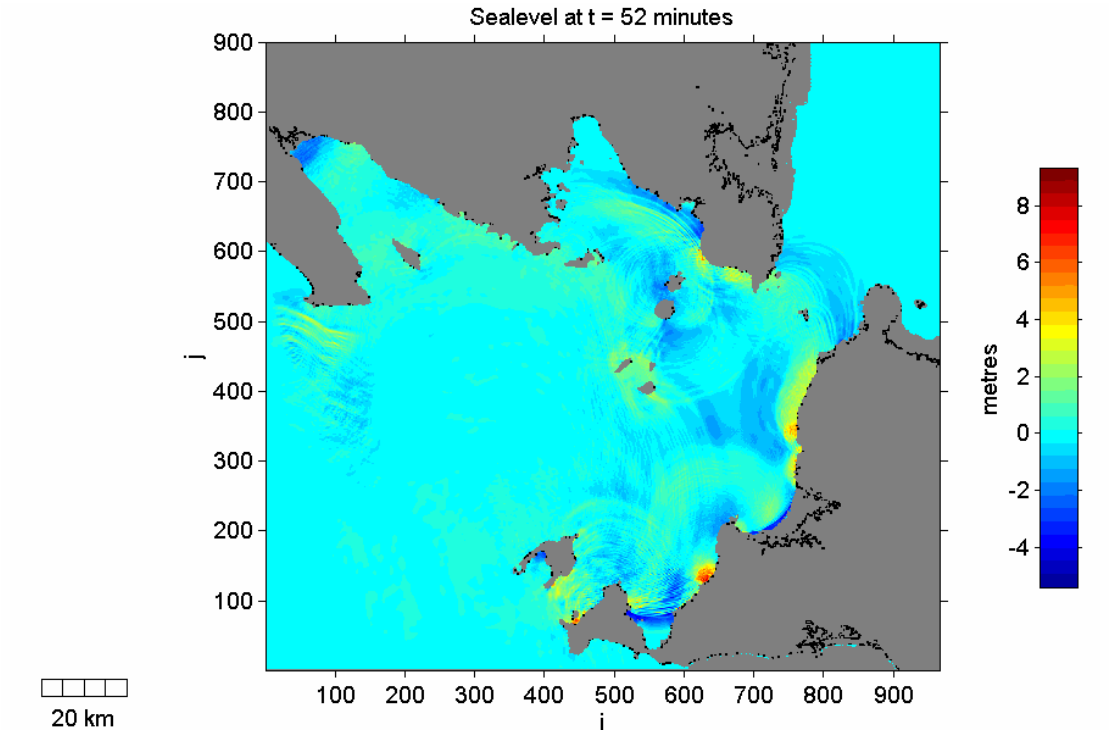
Sealevel at t = 52 minutes
900
800
700
600
500
400
300
200
100
j
100 200 300 400 500 600 700 800 900
i
8
6
4
2
0
-2
-4
metres
20 km

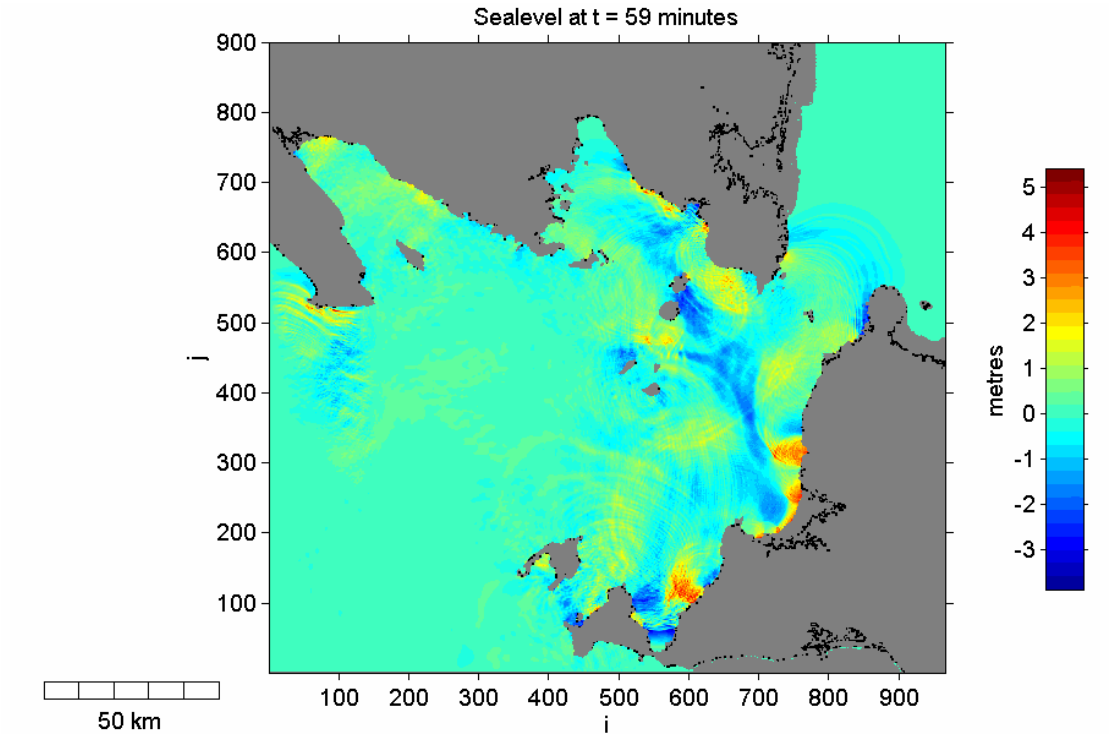
Sealevel at t = 59 minutes
900
800
700
600
500
400
300
200
100
j
100 200 300 400 500 600 700 800 900
i
5
4
3
2
1
0
-1
-2
-3
metres
50 km

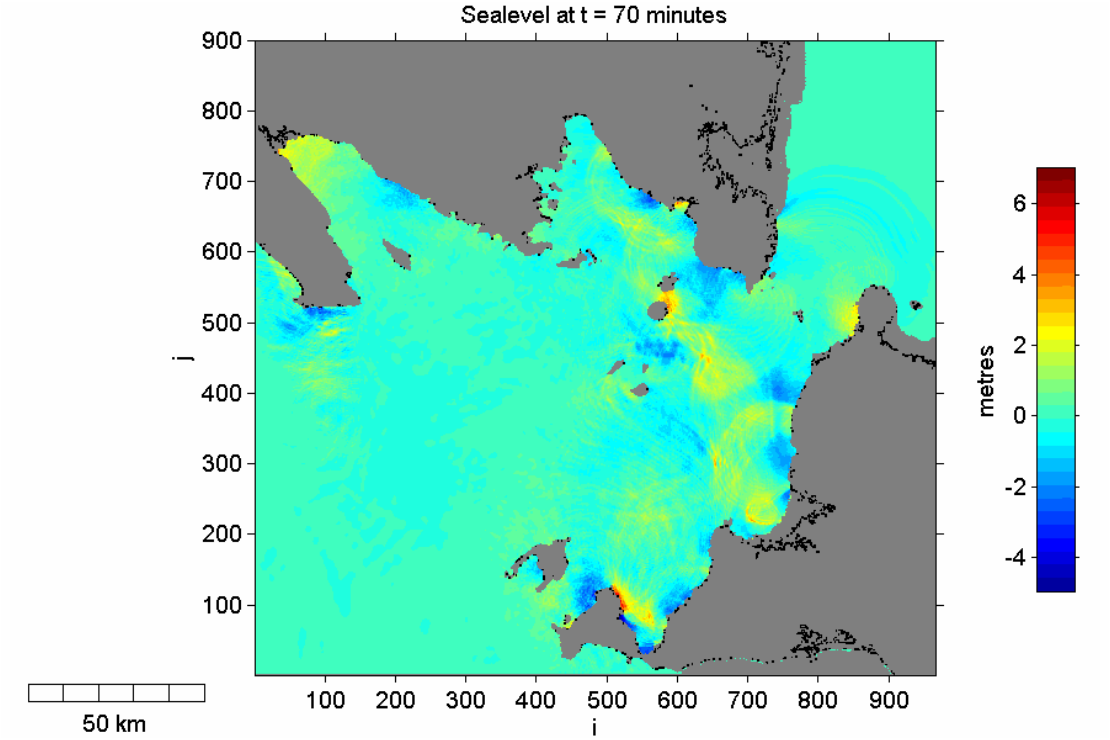
Sealevel at t = 70 minutes
900
800
700
600
500
400
300
200
100
j
100 200 300 400 500 600 700 800 900
i
6
4
2
0
-2
-4
metres
50 km

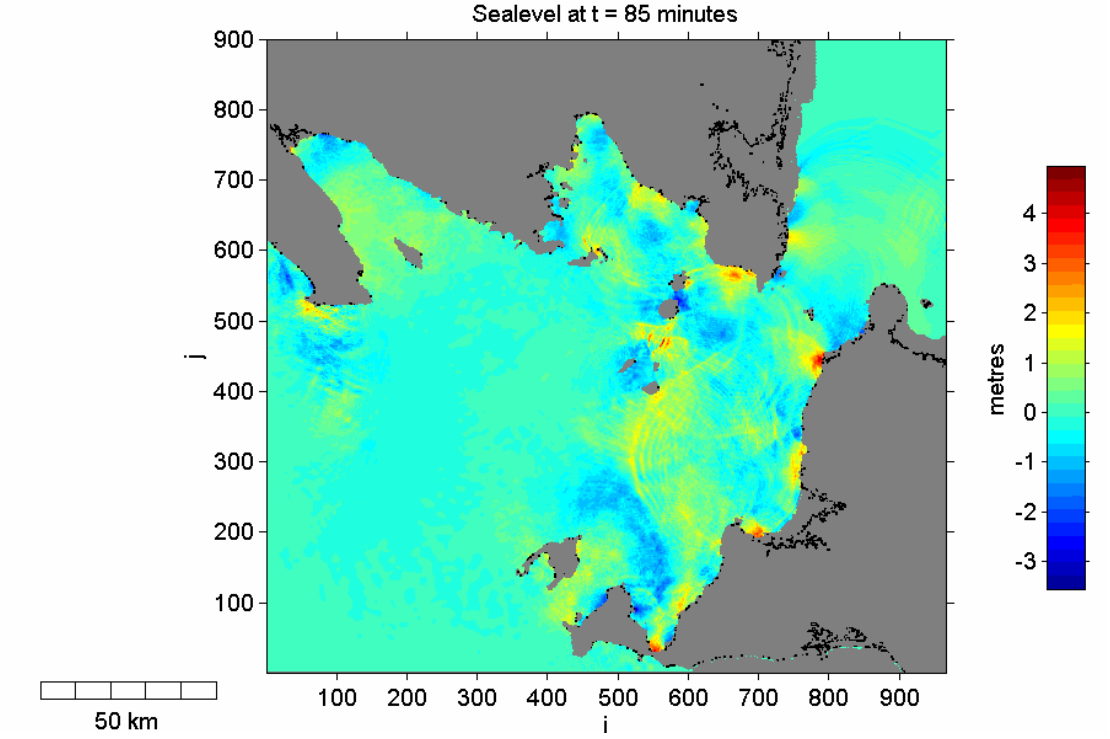
Sealevel at t = 85 minutes
900
800
700
600
500
400
300
200
100
j
100 200 300 400 500 600 700 800 900
i
4
3
2
1
0
-1
-2
-3
metres
50 km

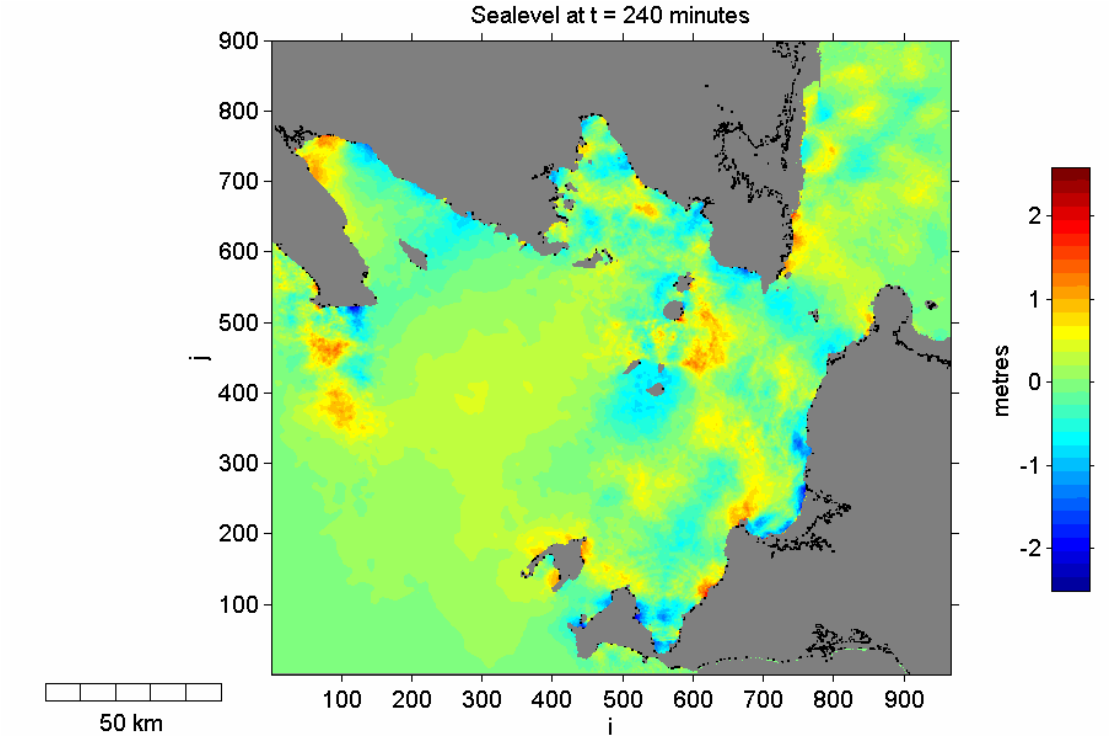
Sealevel at t = 240 minutes
900
800
700
600
500
400
300
200
100
j
100 200 300 400 500 600 700 800 900
i
2
1
0
-1
-2
metres
50 km

Ap1.2. Time histories of tsunami dynamic at some places around Sunda Straits

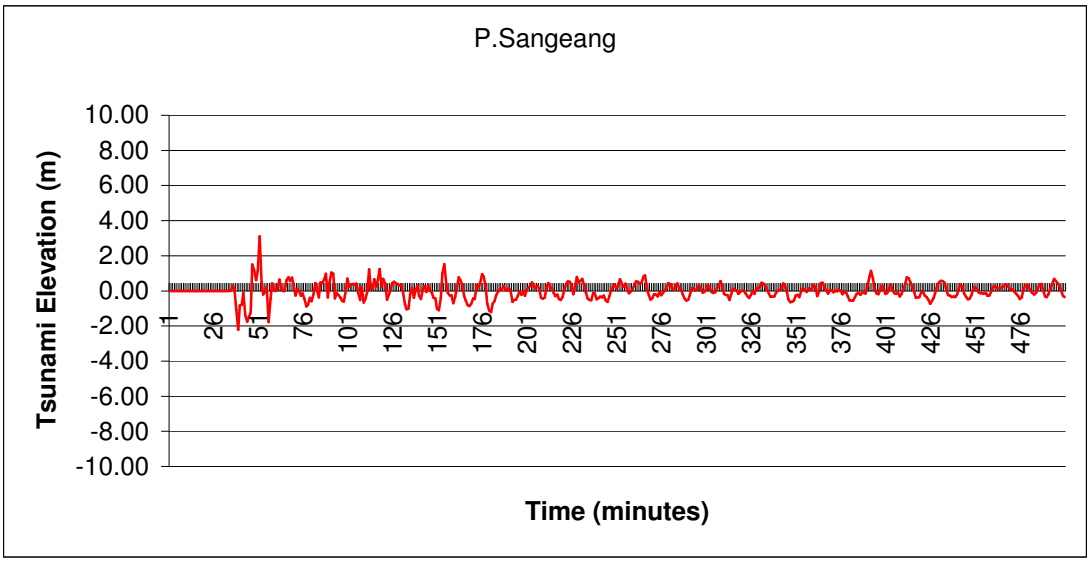

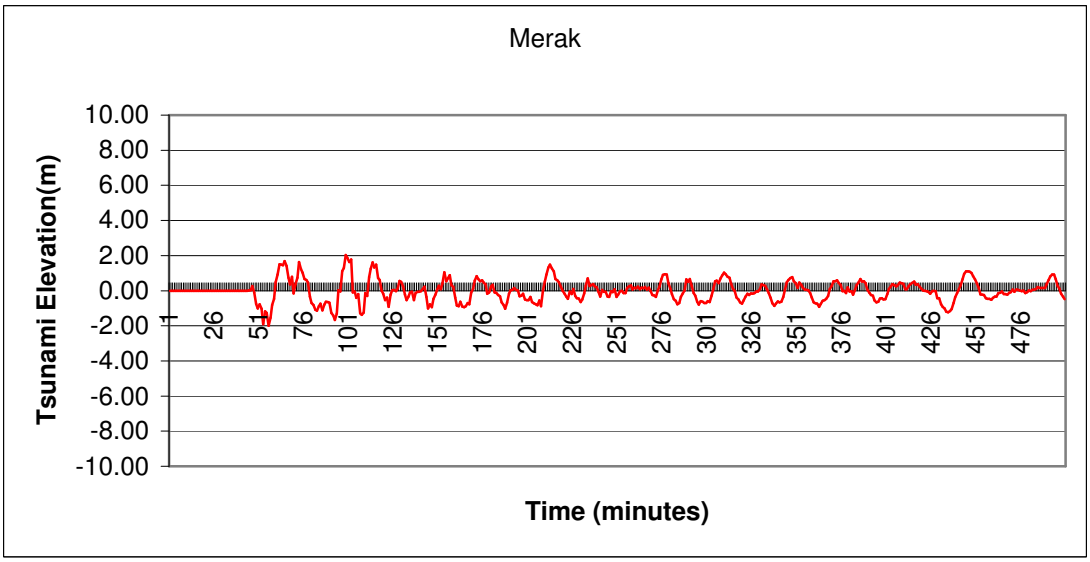

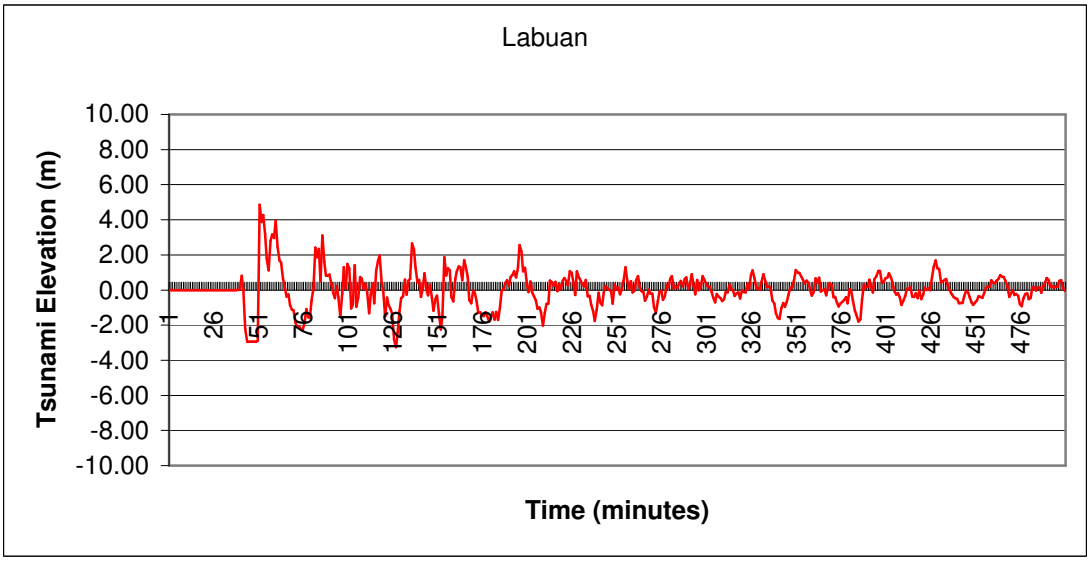

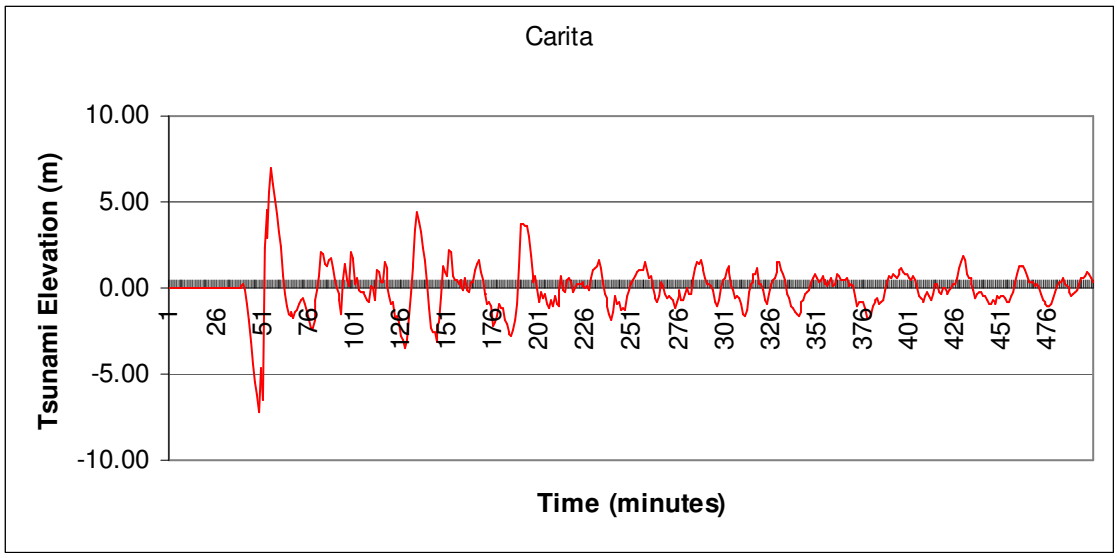
Carita
Tsunami Elevation (m)
10.00
5.00
0.00
-5.00
-10.00
1
26
51
76
101
126
151
176
201
226
251
276
301
326
351
376
401
426
451
476
Time (minutes)

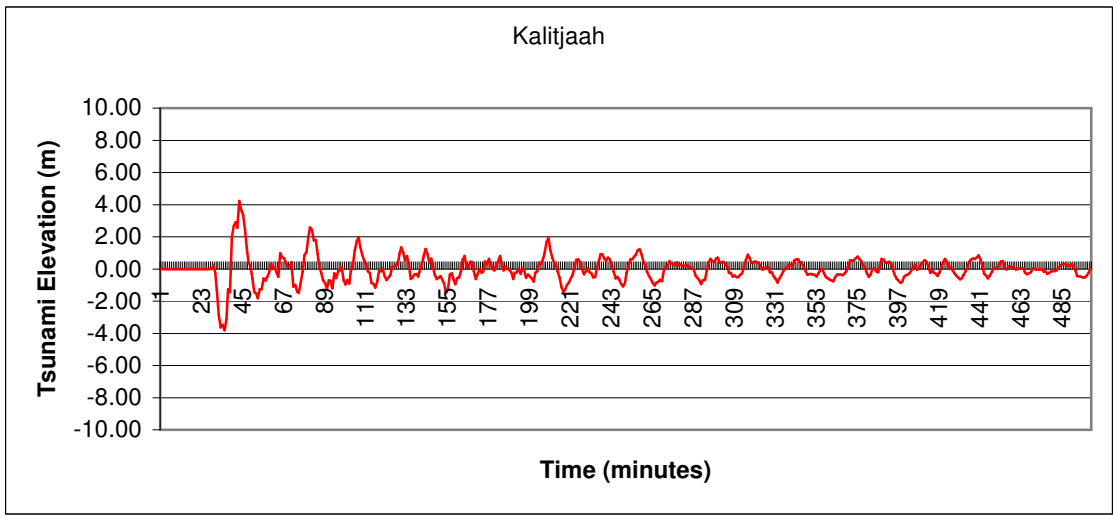
Kalitjaah
Tsunami Elevation (m)
10.00
8.00
6.00
4.00
2.00
0.00
-2.00
-4.00
-6.00
-8.00
-10.00
1
23
45
67
89
111
133
155
177
199
221
243
265
287
309
331
353
375
397
419
441
463
485
Time (minutes)

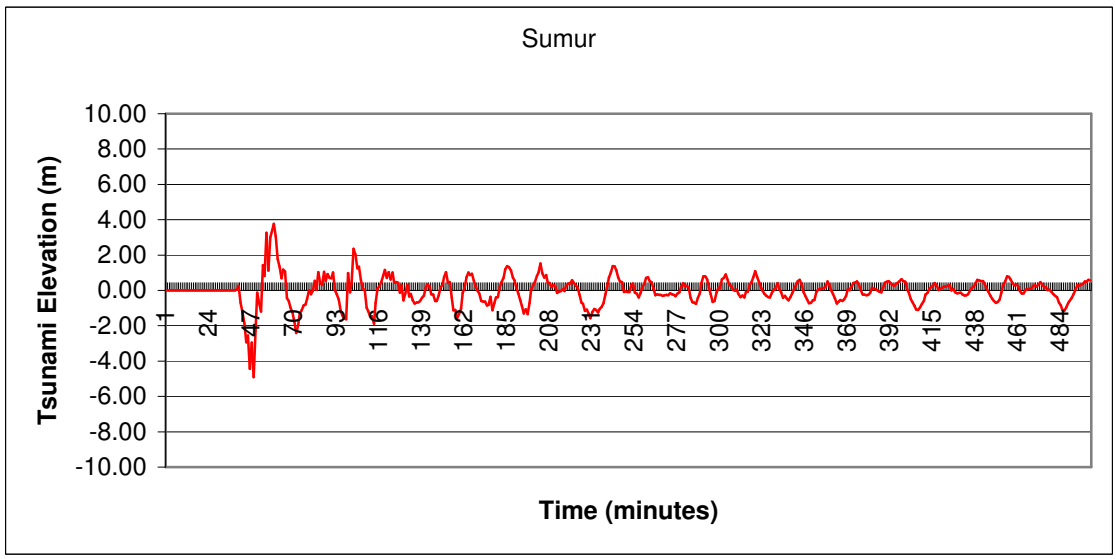
Sumur
Tsunami Elevation (m)
10.00
8.00
6.00
4.00
2.00
0.00
-2.00
-4.00
-6.00
-8.00
-10.00
1
24
47
70
93
116
139
162
185
208
231
254
277
300
323
346
369
392
415
438
461
484
Time (minutes)

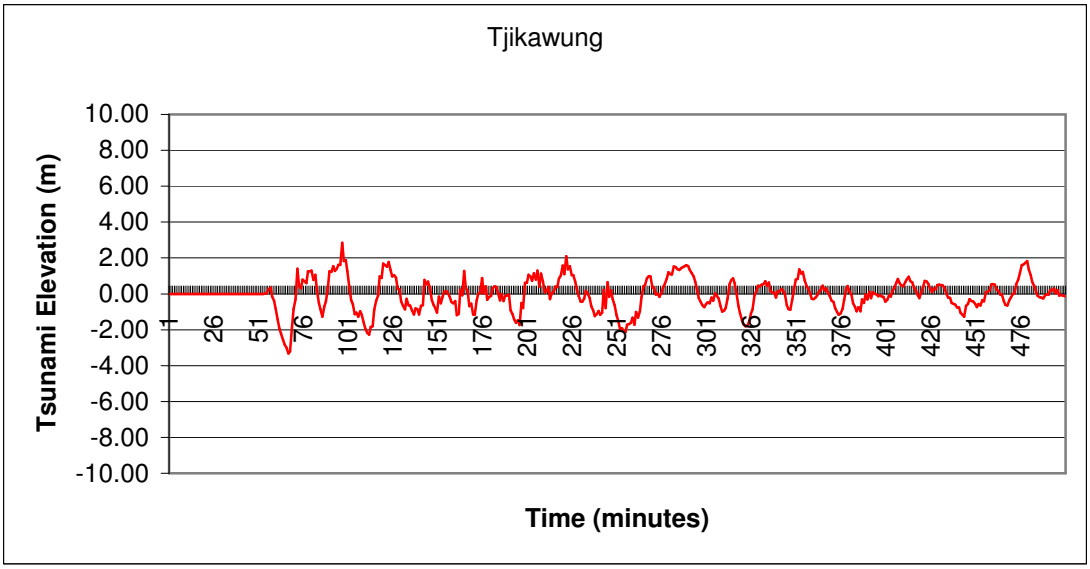
Tjikawung
Tsunami Elevation (m)
10.00
8.00
6.00
4.00
2.00
0.00
-2.00
-4.00
-6.00
-8.00
-10.00
1
26
51
76
101
126
151
176
201
226
251
276
301
326
351
376
401
426
451
476
Time (minutes)

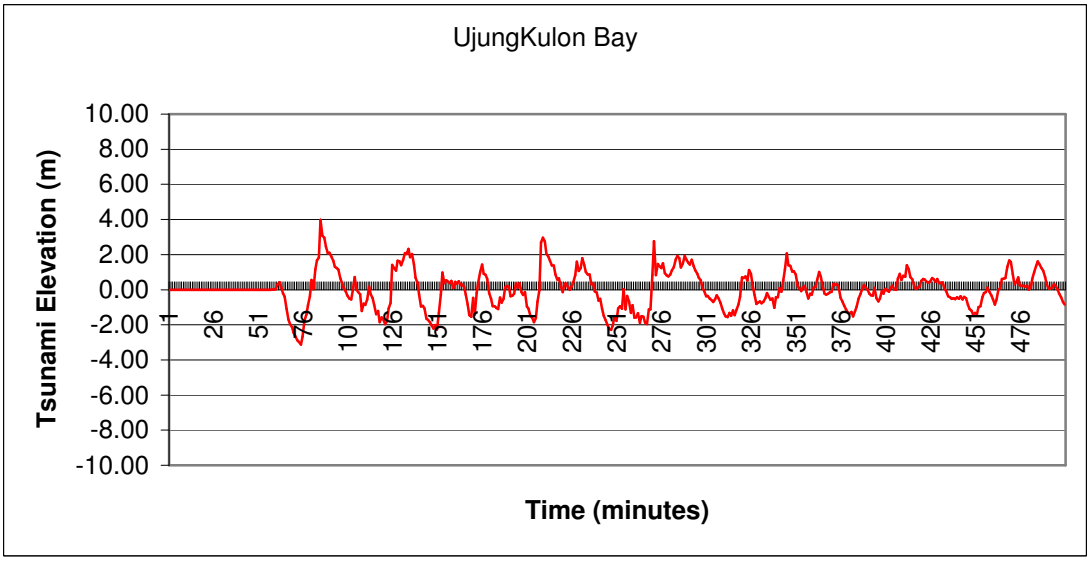
UjungKulon Bay
Tsunami Elevation (m)
10.00
8.00
6.00
4.00
2.00
0.00
-2.00
-4.00
-6.00
-8.00
-10.00
1
26
51
76
101
126
151
176
201
226
251
276
301
326
351
376
401
426
451
476
Time (minutes)

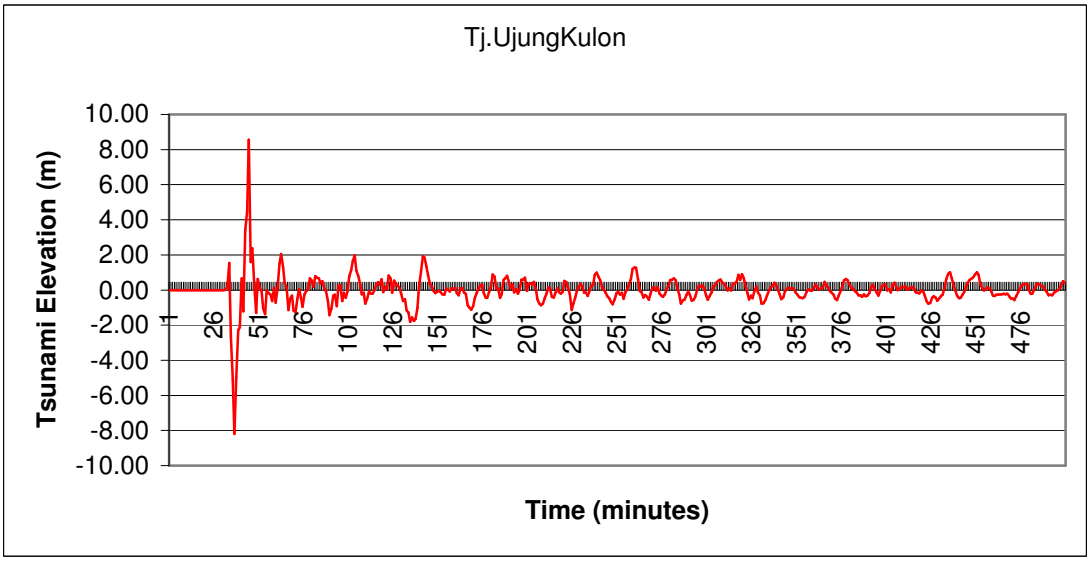
Tj.UjungKulon
Tsunami Elevation (m)
10.00
8.00
6.00
4.00
2.00
0.00
-2.00
-4.00
-6.00
-8.00
-10.00
1
26
51
76
101
126
151
176
201
226
251
276
301
326
351
376
401
426
451
476
Time (minutes)

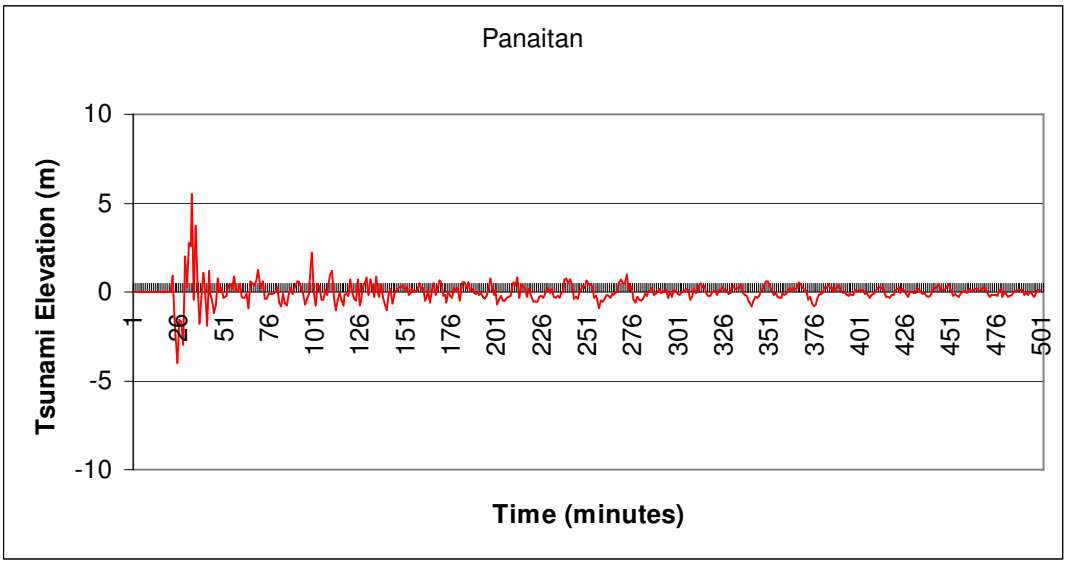
Panaitan
Tsunami Elevation (m)
10
5
0
-5
-10
1
26
51
76
101
126
151
176
201
226
251
276
301
326
351
376
401
426
451
476
501
Time (minutes)

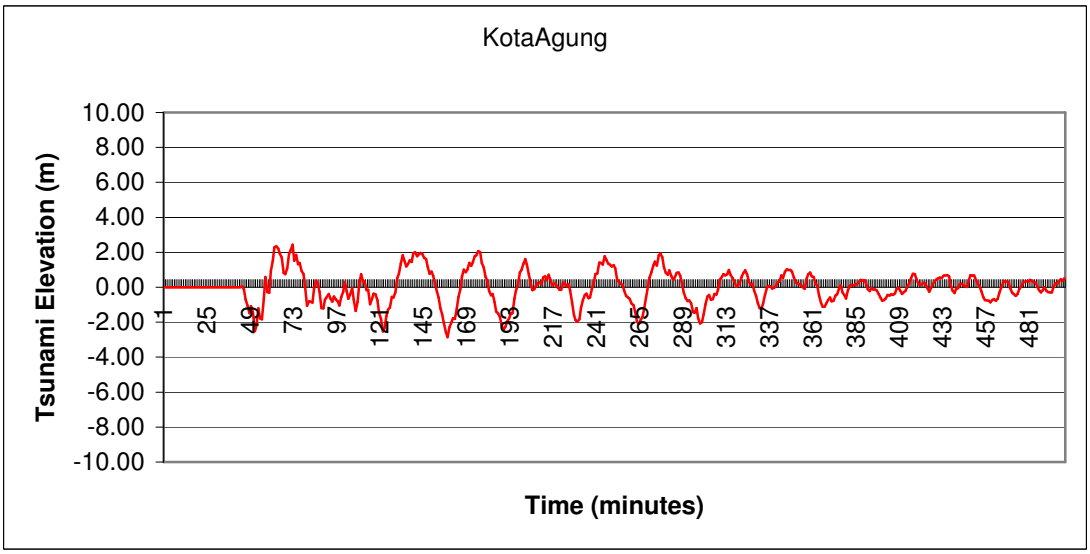
KotaAgung
Tsunami Elevation (m)
10.00
8.00
6.00
4.00
2.00
0.00
-2.00
-4.00
-6.00
-8.00
-10.00
1
25
49
73
97
121
145
169
193
217
241
265
289
313
337
361
385
409
433
457
481
Time (minutes)

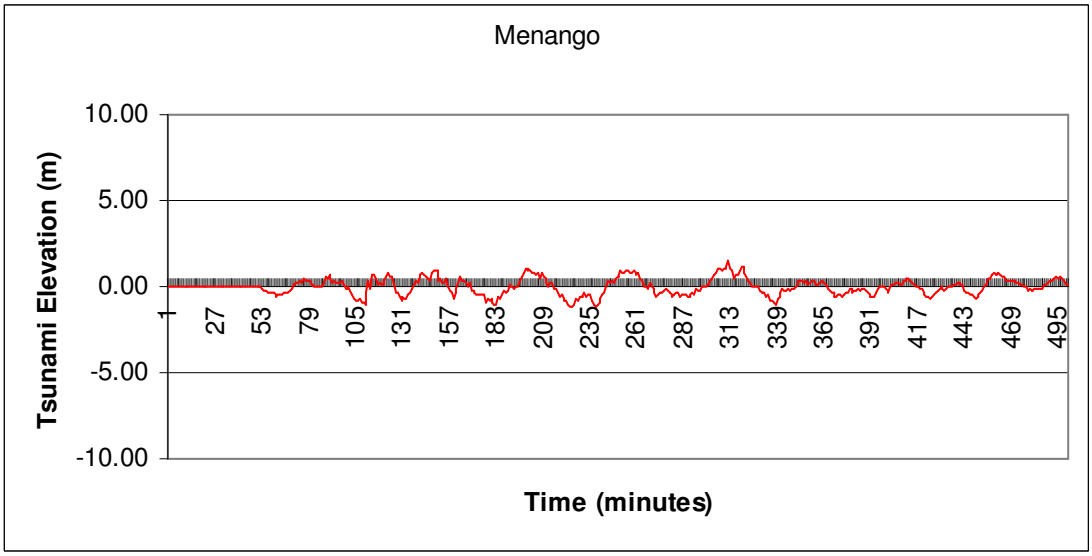
Menango
Tsunami Elevation (m)
10.00
5.00
0.00
-5.00
-10.00
1
27
53
79
105
131
157
183
209
235
261
287
313
339
365
391
417
443
469
495
Time (minutes)

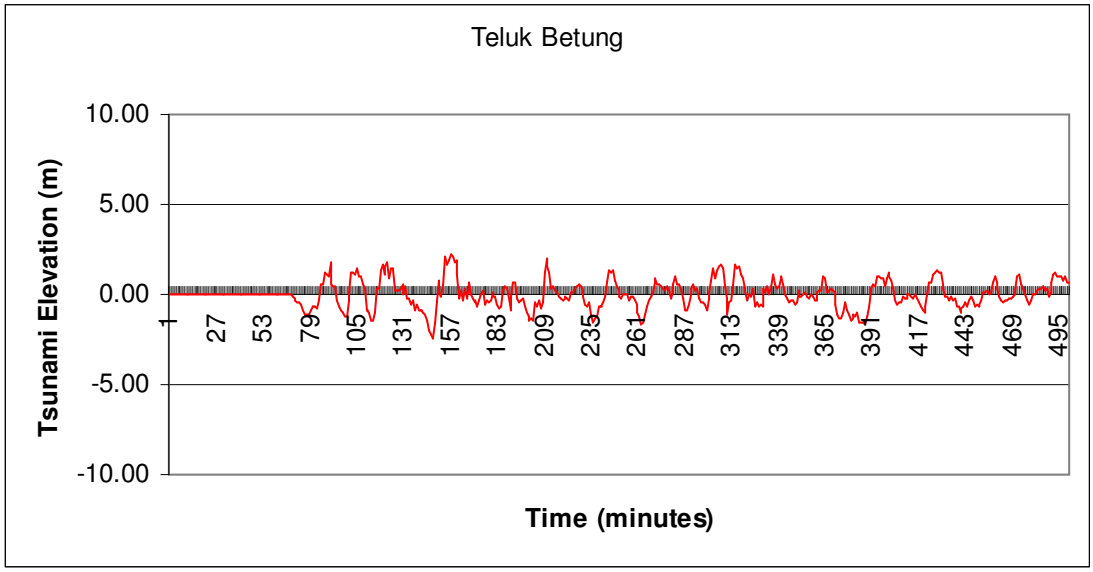
Teluk Betung
Tsunami Elevation (m)
10.00
5.00
0.00
-5.00
-10.00
1
27
53
79
105
131
157
183
209
235
261
287
313
339
365
391
417
443
469
495
Time (minutes)

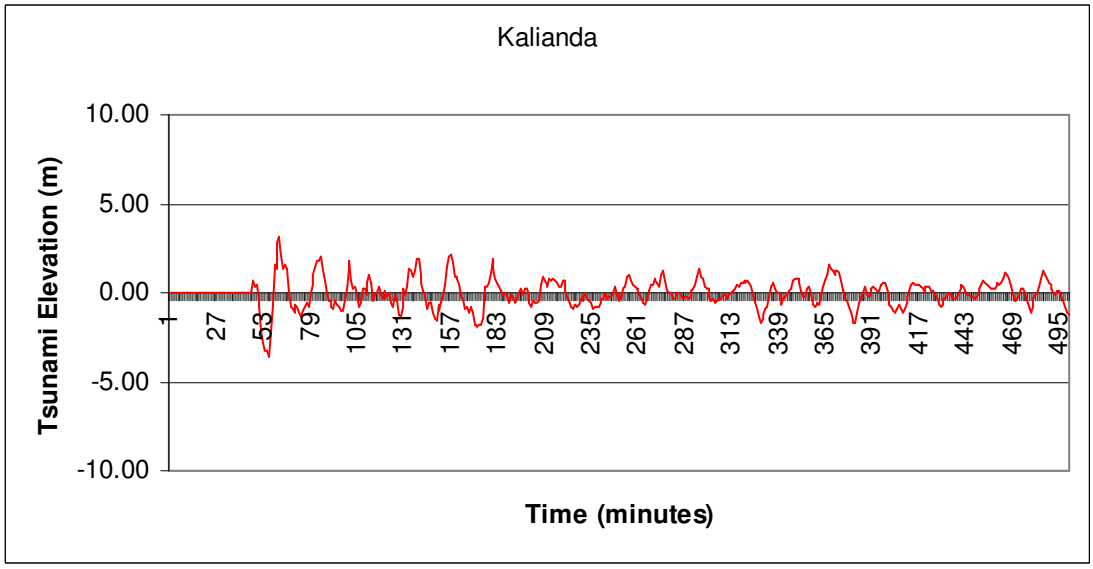
Kalianda
Tsunami Elevation (m)
10.00
5.00
0.00
-5.00
-10.00
1
27
53
79
105
131
157
183
209
235
261
287
313
339
365
391
417
443
469
495
Time (minutes)

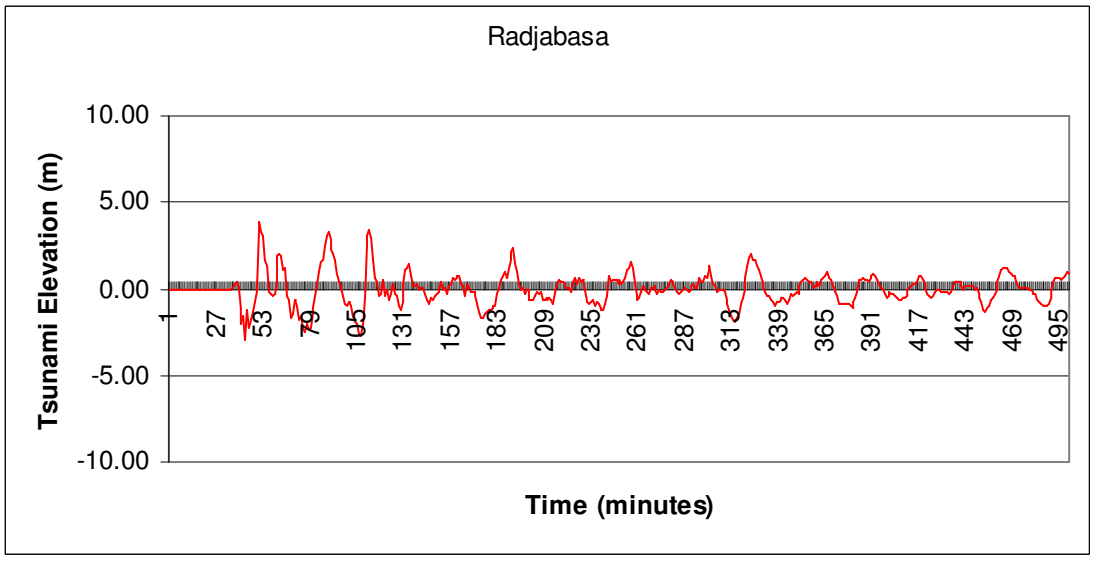
Radjabasa
Tsunami Elevation (m)
10.00
5.00
0.00
-5.00
-10.00
1
27
53
79
105
131
157
183
209
235
261
287
313
339
365
391
417
443
469
495
Time (minutes)

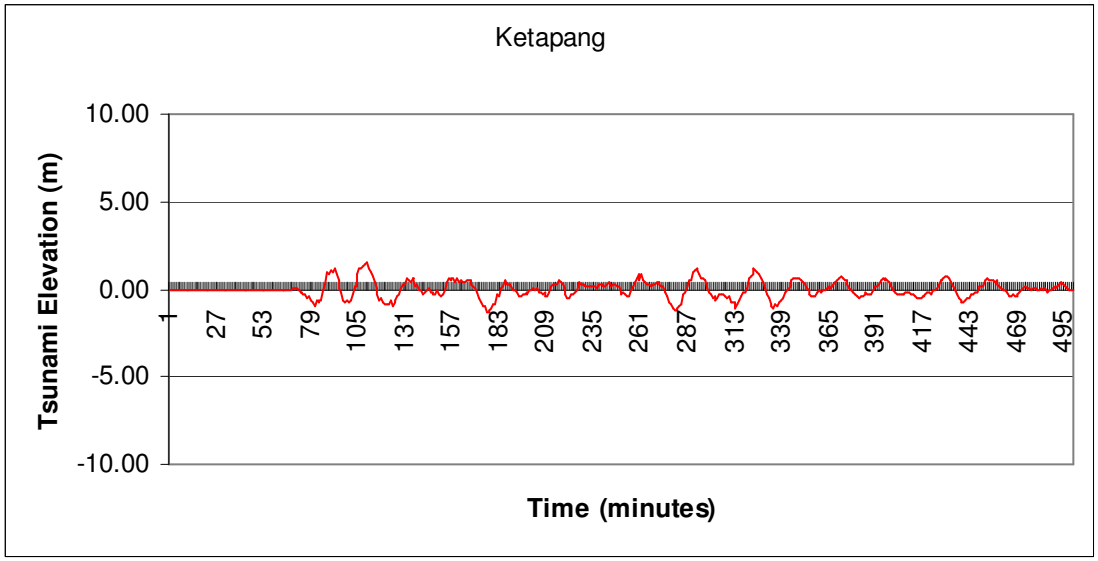
Ketapang
Tsunami Elevation (m)
10.00
5.00
0.00
-5.00
-10.00
1
27
53
79
105
131
157
183
209
235
261
287
313
339
365
391
417
443
469
495
Time (minutes)

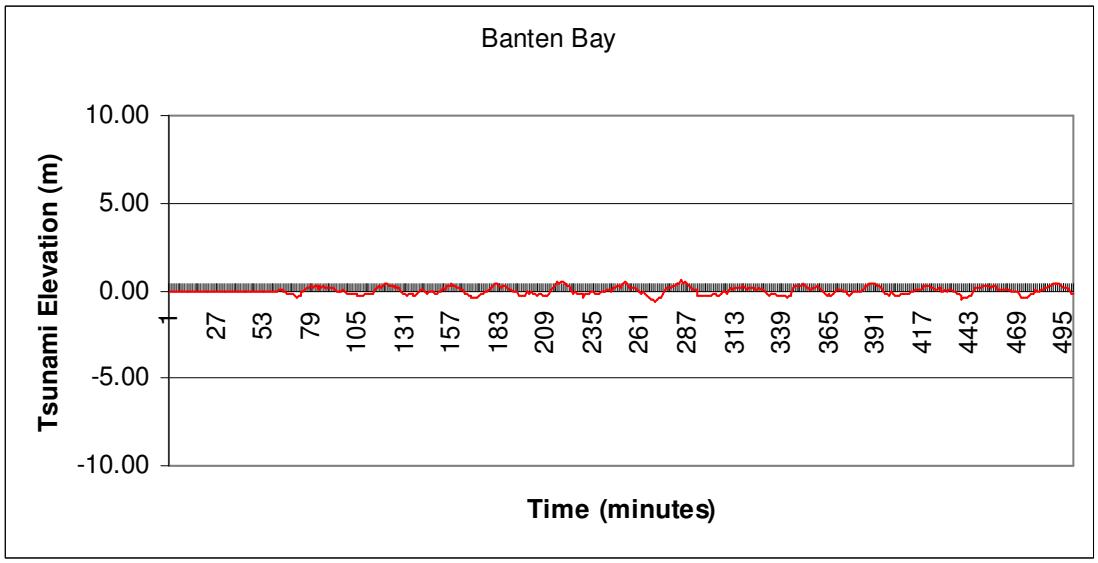
Banten Bay
Tsunami Elevation (m)
10.00
5.00
0.00
-5.00
-10.00
1
27
53
79
105
131
157
183
209
235
261
287
313
339
365
391
417
443
469
495
Time (minutes)

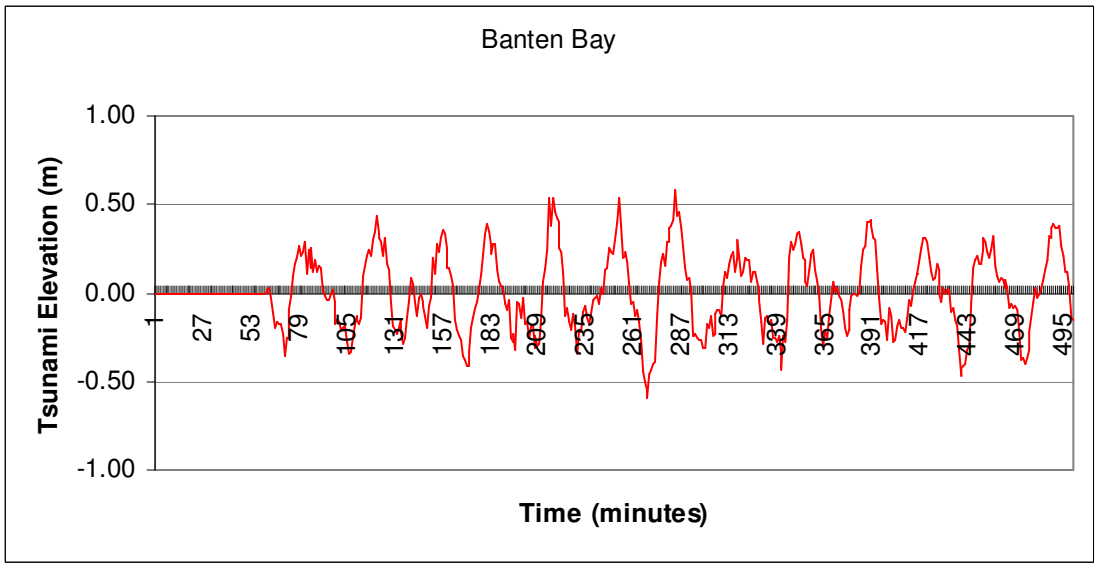
Banten Bay
Tsunami Elevation (m)
1.00
0.50
0.00
-0.50
-1.00
1
27
53
79
105
131
157
183
209
235
261
287
313
339
365
391
417
443
469
495
Time (minutes)

APPENDIX 3. Numerical Modelling Results of Tambora Volcano Scenario (Pyroclastic Flows).

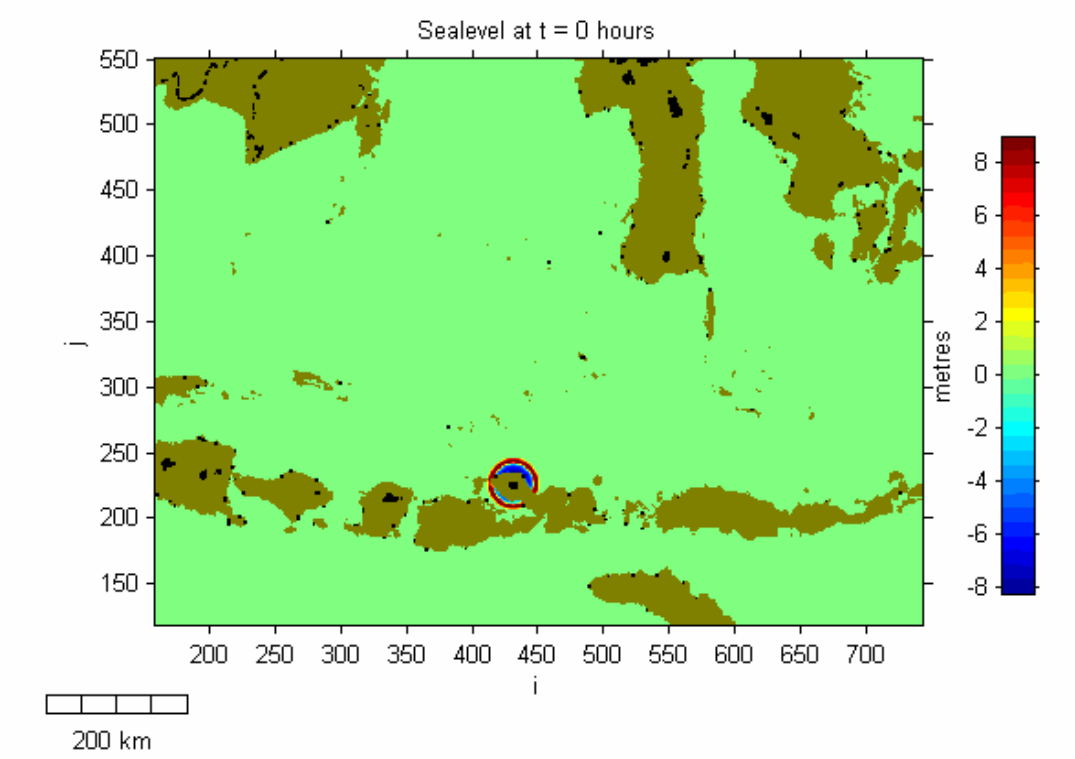

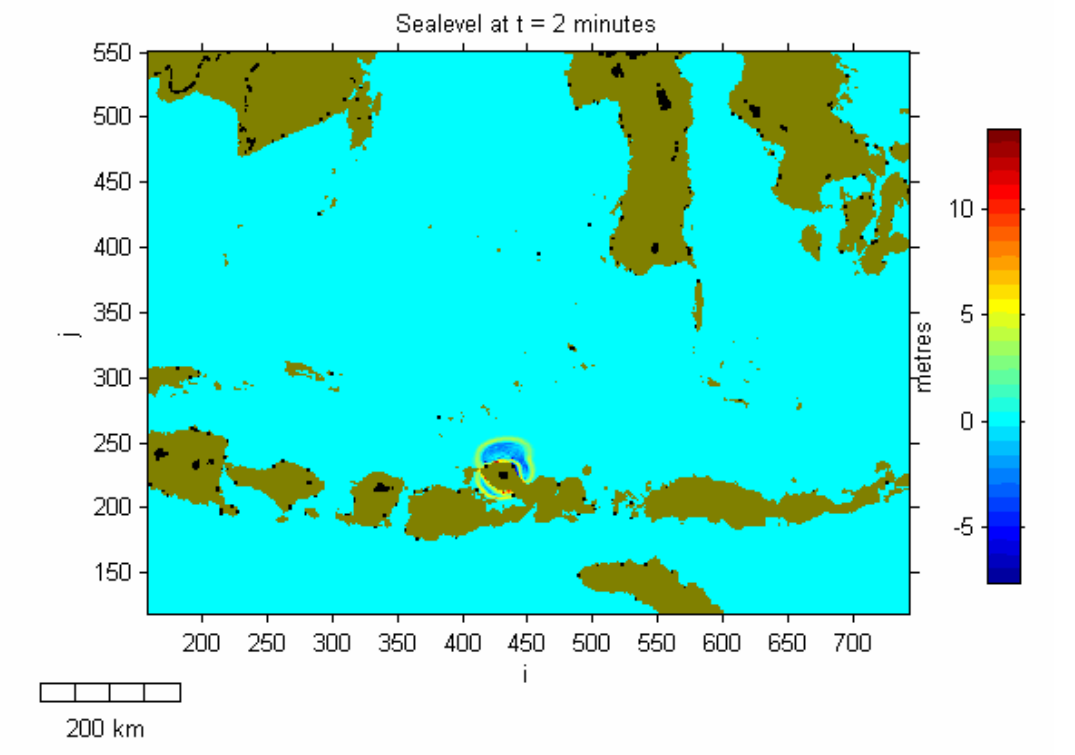

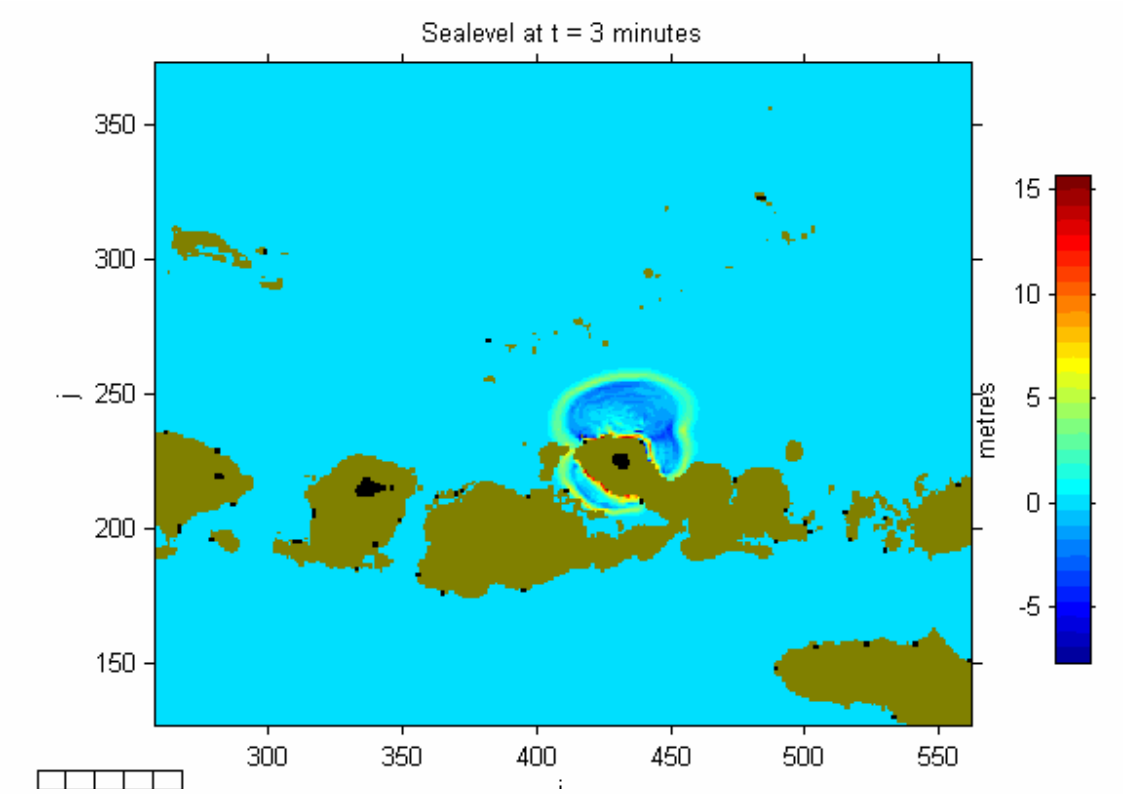
Sealevel at t = 3 minutes
350
300
250
200
150
300
350
400
450
500
550
15
10
5
0
-5
metres

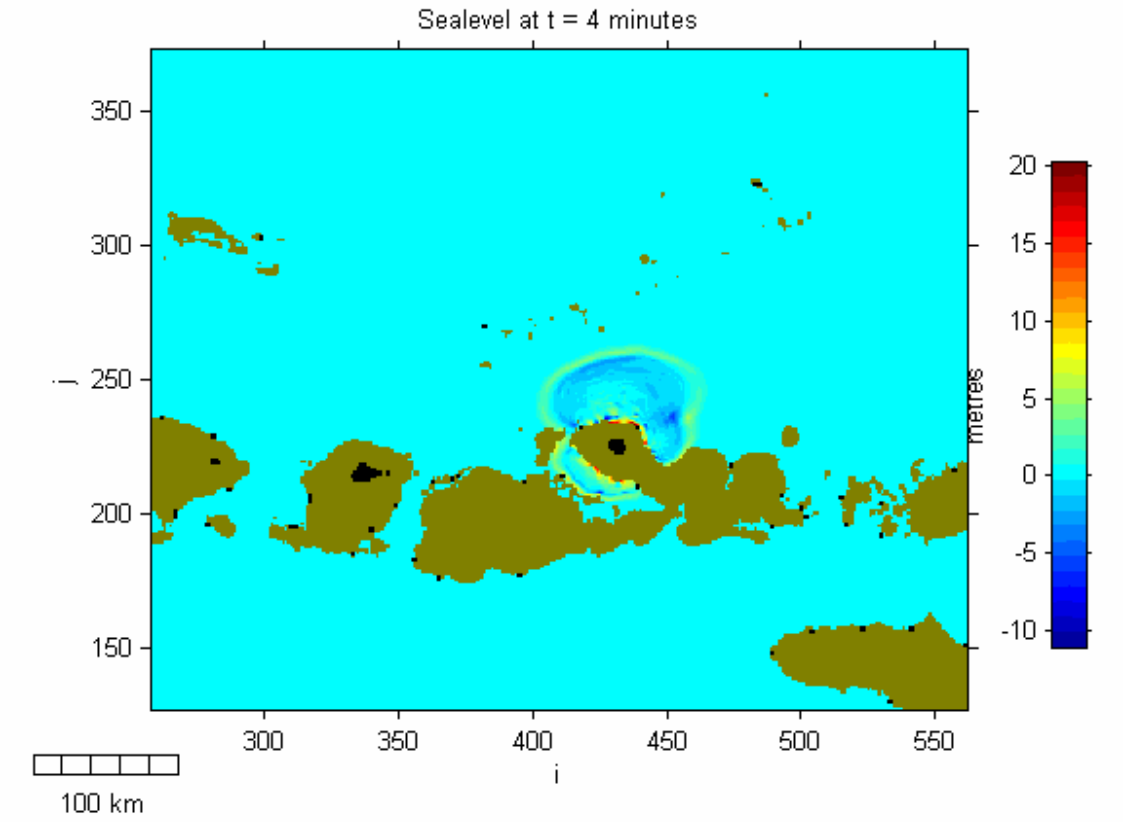
Sealevel at t = 4 minutes
350
300
250
200
150
300
350
400
450
500
550
i
20
15
10
5
0
-5
-10
metres
100 km

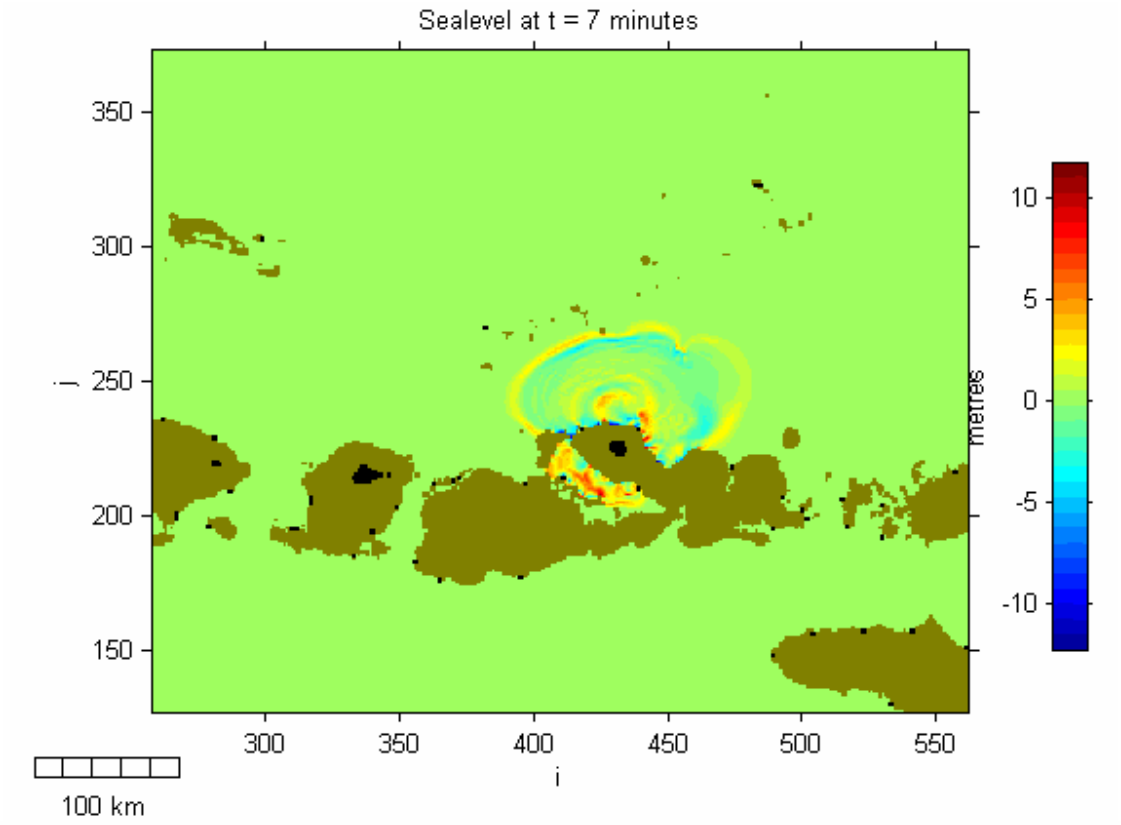
Sealevel at t = 7 minutes
350
300
250
200
150
j
300
350
400
450
500
550
i
10
5
0
-5
-10
metres
100 km

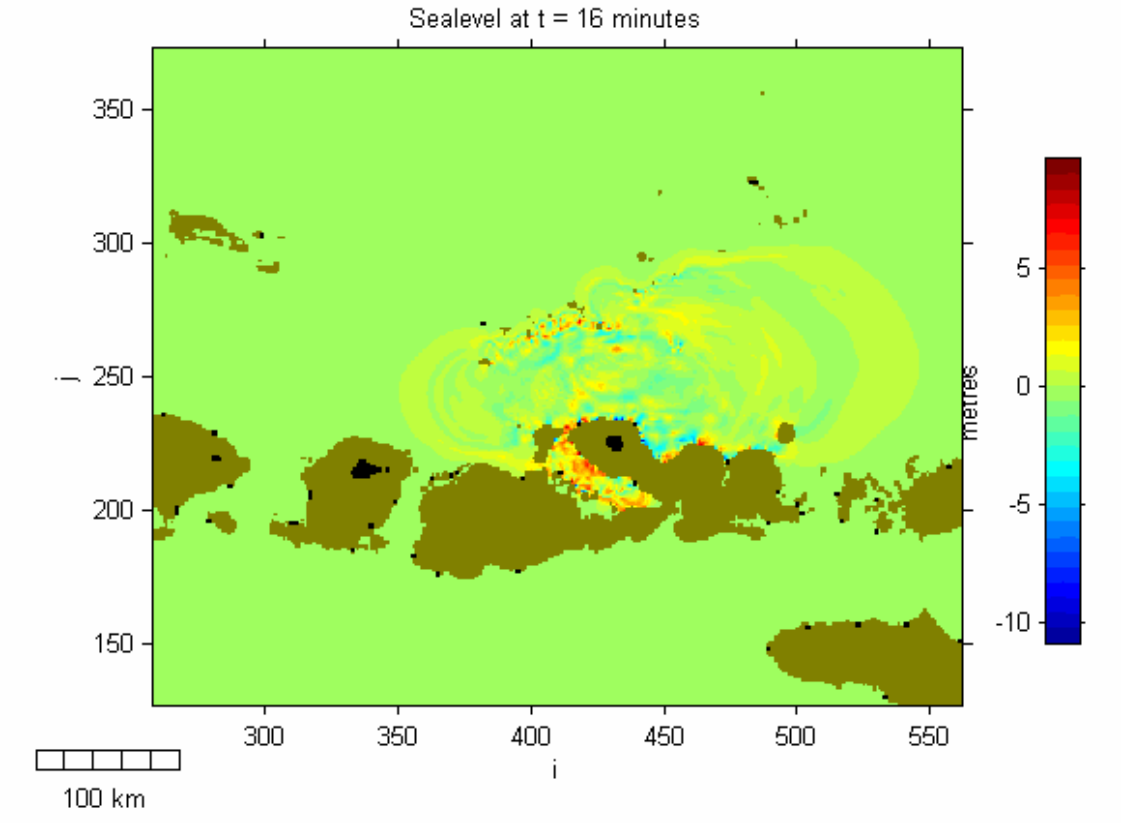
Sealevel at t = 16 minutes
350
300
250
200
150
j
300
350
400
450
500
550
i
5
0
-5
-10
metres
100 km

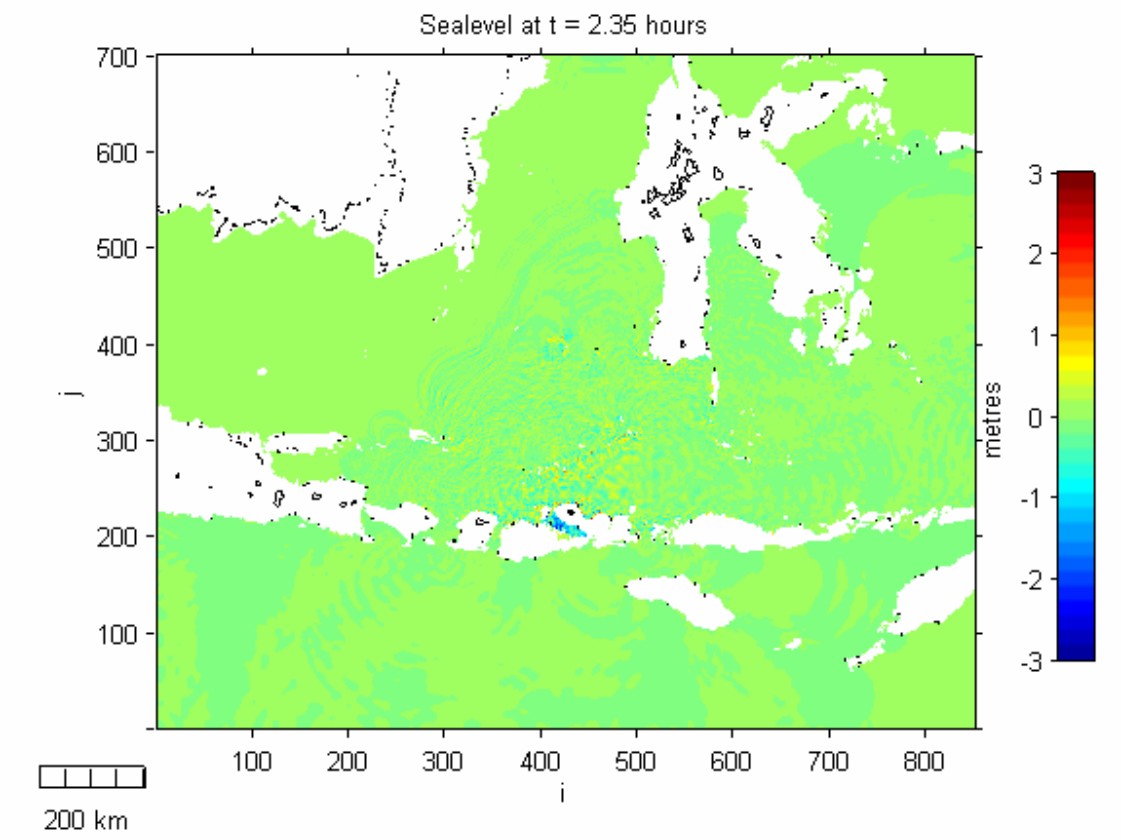

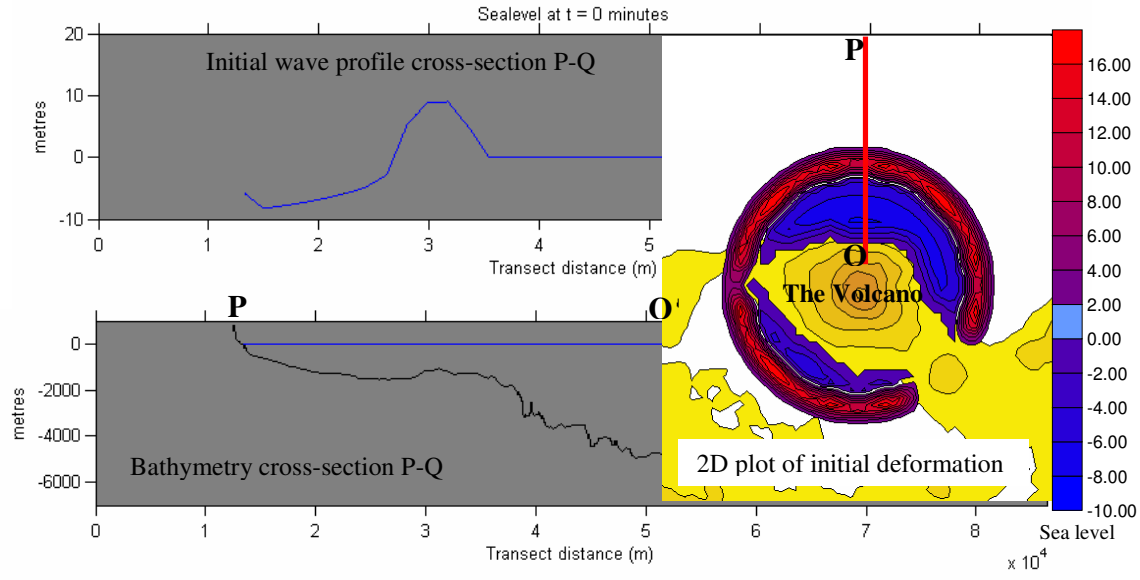

Tranasect of the sea level profile location (P-Q)

Ap.2.2. Time histories of Profil P - Q

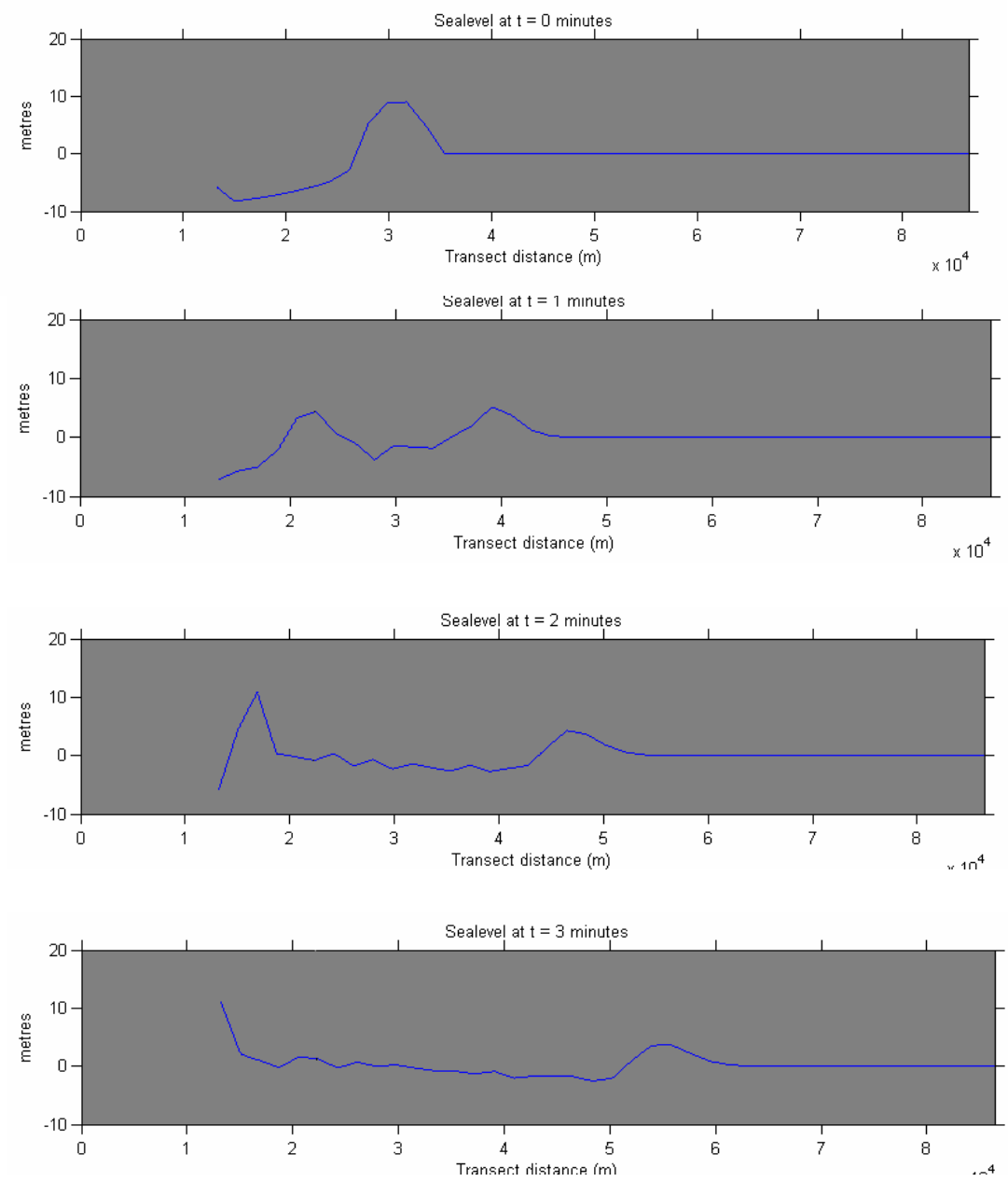

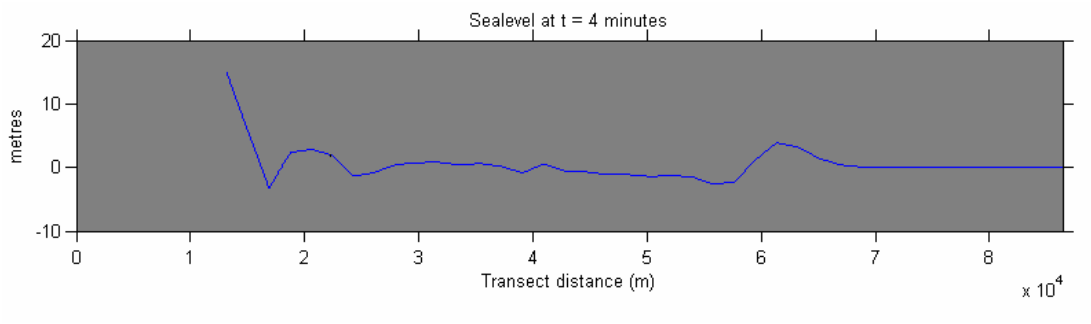
Sealevel at t = 4 minutes
metres
20
10
0
-10
0
1
2
3
4
5
6
7
8
Transect distance (m)
x 10^4

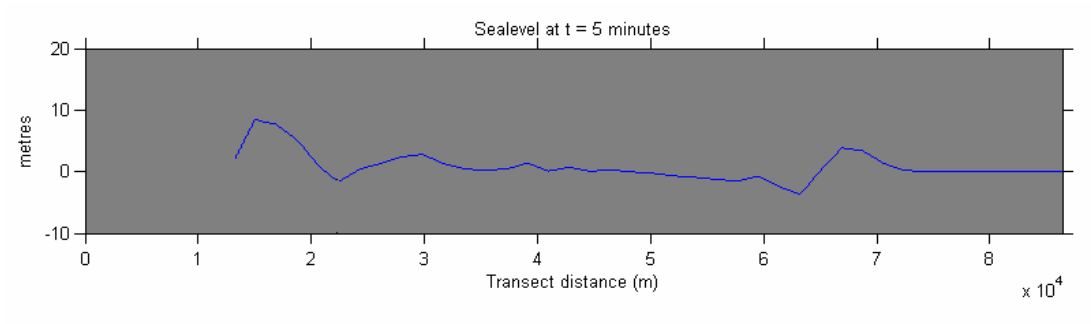
Sealevel at t = 5 minutes
metres
20
10
0
-10
0
1
2
3
4
5
6
7
8
Transect distance (m)
x 10^4

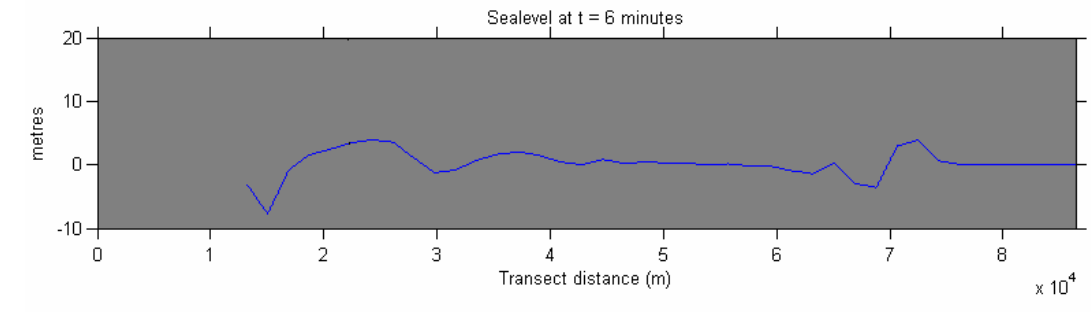
Sealevel at t = 6 minutes
metres
20
10
0
-10
0
1
2
3
4
5
6
7
8
Transect distance (m)
x 10^4

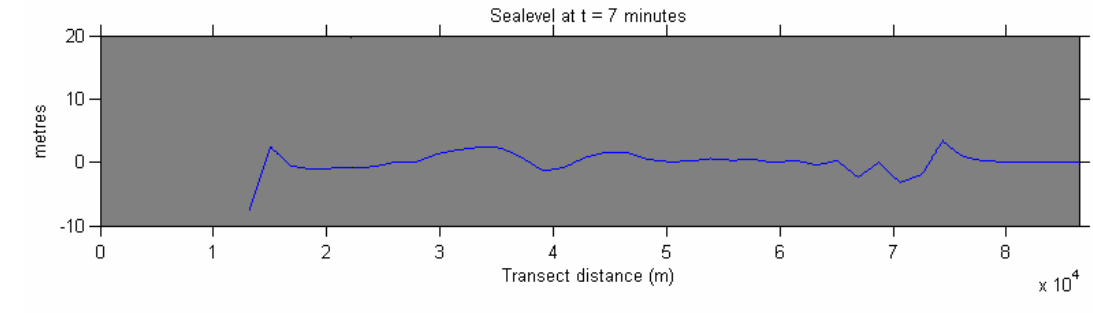
Sealevel at t = 7 minutes
metres
20
10
0
-10
0
1
2
3
4
5
6
7
8
Transect distance (m)
x 10^4

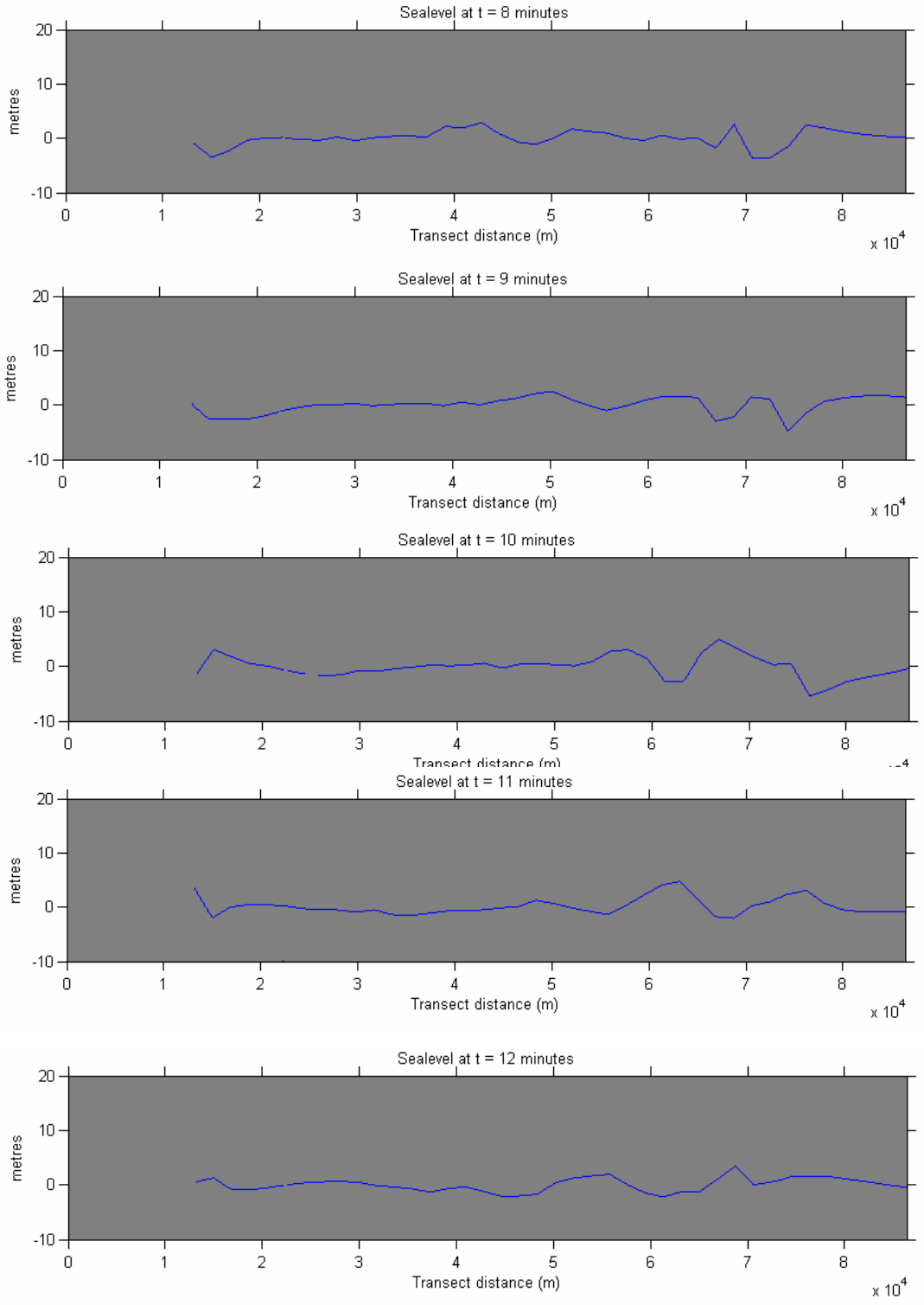
Sealevel at t = 8 minutes
metres
Transect distance (m)
x 10^4
Sealevel at t = 9 minutes
metres
Transect distance (m)
x 10^4
Sealevel at t = 10 minutes
metres
Transect distance (m)
Sealevel at t = 11 minutes
metres
Transect distance (m)
x 10^4
Sealevel at t = 12 minutes
metres
Transect distance (m)
x 10^4

APPENDIX – 4. EDUCATIONAL OUTREACH MATERIAL

This educational outreach material in the form of short movie is developed based on the 26 December 2004 event, and utilizing the movie/animation from:

- the fly through of satellites images over Banda Aceh (CNES, SERTIT, ESA),
- the 3-dimensional view of the numerical modelling results that shows the tsunami inundation and the colliding of the two waves at Lampisang villages (GS Prasetya, Brinkman F, von Halem G, and Kellerman M),
- the ocean wide propagation based on V.Titov model (NOAA),
- the survivor video